An Activity-Based Proteomics Approach for Identifying Ajoene's *S*-thiolation Protein Targets in Blood and Cancer Cells

Thesis presented for the degree of

DOCTOR OF PHILOSOPHY

Department of Chemistry

Faculty of Science

University of Cape Town

DANIEL ANDREAS KUSZA

SUPERVISORS

Professor Roger Hunter and Doctor Catherine H. Kaschula

July 2021

Declaration

"An Activity-Based Proteomics Approach for Identifying Ajoene's *S*-thiolation Protein Targets in Blood and Cancer Cells"

I, **Daniel Andreas Kusza**, declare the following:

1. That the above-titled report is my own work, both in concept and execution, apart from the normal guidance of my supervisors;

2. That in cases where others' work has been cited, this has been acknowledged and referenced;

3. That no part of this work has been, is being, or is to be submitted for another degree at this or any other university;

4. That I grant the University of Cape Town free licence to reproduce this work, in whole or in part, for the purpose of research.

I hereby present this report in fulfilment of the requirements for the degree of **Doctor of Philosophy** in the Department of Chemistry at the University of Cape Town.

Daniel Kusza
1st of July 2021

Abstract

Garlic has been used as a medicinal plant since ancient times and is well-documented to produce several organosulfur compounds (OSCs) that show promising chemopreventative and therapeutic properties. The vinyl disulfide sulfoxide garlic rearrangement product, ajoene, is one of the phytochemicals in garlic that possesses a broad spectrum of biological activities against a variety of cancers both *in vitro* and *in vivo*. Our group's previous investigations into ajoene's cytotoxicity have shown that it modifies proteins by *S*-thioallylating redox-sensitive cysteine residues through a thiol-disulfide exchange reaction. Further investigations into this exchange have been the primary aim of this PhD thesis using a biotinylation protocol for trapping out the said protein targets of ajoene to link them to anticancer signalling pathways.

The thesis begins in **Chapter One** with an overview of the chemopreventative and antitumour activity of OSCs from garlic in which a particular emphasis is placed on OSC structure and mechanistic aspects of their cancer biology.

Chapter Two discusses the various aspects of ajoene as the target natural product of the thesis. These include its biosynthesis and synthesis, in both native form and as derivatives, for SAR studies, for which a UCT synthesis is described. Mechanistic aspects of ajoene's cytotoxicity towards cancer cells in terms of *S*-thioallylation via disulfide exchange are then discussed at length. Of crucial importance for the chemical biology studies to follow was the conclusion that *S*-thioallylation by ajoene is regioselective at the vinyl sulfur, as well as effectively irreversible with suitably reactive cysteine thiol groups.

Chapter Three presents an in-depth Chapter on the metabolism and pharmacokinetic properties of ajoene and selected derivatives in a murine xenograft model for human oesophageal cancer (WHCO1). This concluded, disappointingly, that no significant differences in terms of tumour volume, mass and growth rate were observed compared to an untreated control. A follow-up study using a small library of eight ajoene derivatives varying ajoene's different functional groups in a blood stability study, revealed a proportional relationship between the *in vitro* half-life in blood and the IC_{50} value for WHCO1 cancer cells. This led to mass spectrometry studies showing that ajoene *S*-thioallylates the βCys-93 residues in haemoglobin, a chemical modification that most likely explains both ajoene's blood instability and its lack of antitumour activity *in vivo*.

Chapter Four describes the organic synthesis and characterisation of four biotin-ajoene chemical biology probes for chemical biology investigation of *S*-thiolation in which the background theory of activity-based protein profiling and biotin affinity purification is presented. In the synthesis of these probes, chemical stability emerged as a major stumbling block. Gratifyingly, after several trials, the fourth probe designed and constructed, using a simplified tether involving a convergent "Click"-strategy, turned out to be chemically stable. Subsequent biological validation studies confirmed that the probe retained cytotoxicity against cancer cell lines *in vitro* (human epithelial mammary gland adenocarcinoma cancer cells (MDA-MB-231) and WHCO1) and shared the same compound–target interaction as its parent ajoene; namely, the regioselective *S*-thiolation of cellular proteins.

Chapter Five constitutes a proteomics study into ajoene's primary protein targets in the MDA-MB-231 cell line using our biotin-ajoene probe. Streptavidin-coated magnetic beads in conjunction with an affinity purification mass spectrometry protocol allowed the isolation and identification of 633 protein targets for ajoene in the MDA-MB-231 proteome. Pathway analyses revealed that ajoene interacts with several targets involved in the control of cell cycles (G_2/M cell cycle checkpoint), energy metabolism (glycolysis and pentose phosphate pathway) and the regulation of protein metabolism (translation, folding, quality control and degradation), which supports previously reported cytotoxic modes of action for ajoene against MDA-MB-231 cancer cells. Importantly, we have validated that ajoene *S*-thioallylates glutathione *S*-transferase (GSTP1), which is a known cancer-therapy target in breast cancer.

Overall, this study complements findings on the cancer-cell protein targets of allicin from crushed garlic, by identifying proteins regulating apoptotic and antiproliferative signalling pathways. These findings support the hypothesis that the anticancer activity of ajoene is due to its *S*-thioallylation of proteins essential to cellular functions.

The thesis concludes with comprehensive experimental and reference sections.

Publications and Conference Proceedings

Publications

Kaschula, C. H., Tuveri, R., Ngarande, E., Dzobo, K., Barnett, C., **Kusza, D. A.**, Graham, L. M., Katz, A., Rafudeen, M. S., Parker, M. I., Hunter, R., Schäfer, G., Ngrellmyuctacza, E., (2019) The garlic compound ajoene covalently binds vimentin, disrupts the vimentin network and exerts antimetastatic activity in cancer cells. *BMC Cancer 19*, 248.

Kaschula, C. H., Hunter, R., Cotton, J., Tuveri, R., Ngarande, E., Dzobo, K., Schäfer, G., Siyo, V., Lang, D., **Kusza, D. A.**, Davies, B., Katz, A., and Parker, M. I. (2016) The garlic compound ajoene targets protein folding in the endoplasmic reticulum of cancer cells. *Mol. Carcinog. 55*, 1213–1228.

Smith, M., Hunter, R., Stellenboom, N., **Kusza, D. A.**, Parker, M. I., Hammouda, A. N. H., Jackson, G., and Kaschula, C. H. (2016) The cytotoxicity of garlic-related disulphides and thiosulfonates in WHCO1 oesophageal cancer cells is dependent on S-thiolation and not production of ROS. *Biochim. Biophys. Acta - Gen. Subj. 1860*, 1439–1449.

Conferences

4-8 December 2016, Oral presentation, "**Frank Warren Conference 2016**", Rhodes University, Makhanda (Grahamstown), Eastern Cape, South Africa.

7-8 August 2017, Oral presentation, "**Annual Science Postgrad Symposium**", University of Cape Town, Cape Town, Western Cape, South Africa.

6th April 2018, Oral presentation, "**SACI/RSC Young Chemists' Symposium**", University of Cape Town, Cape Town, Western Cape, South Africa.

3-5 July 2018, Oral presentation, "**CANSA Research in Action Conference**", University of Pretoria, Pretoria, Gauteng, South Africa.

14-16 September 2018, Poster presentation, "**3rd International Conference on Nutraceuticals and Chronic Diseases - Role of nutraceuticals in chronic diseases**", Swami Rama Himalayan University, Jolly Grant, Dehradun, India.

28th August 2019, Oral presentation, "**PhD Seminar, Department of Chemistry**", University of Cape Town, Cape Town, Western Cape, South Africa.

Acknowledgements

This thesis is dedicated to my late grandfather, Hans-Jürgen Kusza.

Ruhe in Frieden

First and foremost, my gratitude goes out to my family, namely my brother Ashley, my mother Yvonne and my father Andreas. Thank you for your enduring support, encouragement and love.

To my doctoral supervisors, thank you both for shaping the scientist that I am now. I am proud to be the progeny of your academic lineage.

Dear Catherine, I thank you for your guidance throughout my MSc and PhD studies. Our work together has greatly expanded my scientific repertoire beyond that of an organic chemist and encouraged me to confidently navigate the space of interdisciplinary research. We know it wasn't always easy and many hurdles were encountered along the way, but your enthusiasm was contagious and invigorated me to push ahead. Your attention to detail and the diligence by which you conduct research, has moulded my approach to scientific inquiry. Beyond the lab, I greatly appreciated the numerous discussions at cafeterias and the trip to the conference in India was certainly a highlight of my degree.

Dear Roger, I thank you for your mentorship. Already in my undergraduate years, your lecturing style and passion for organic chemistry were compelling for me to further pursue the field. It was a great privilege to be able to join your research lab as postgraduate student. Your philosophy tough me to both respect and love organic synthesis. In this regard, two of your statements (noted in my lab meeting notebook) resonated deeply with me:

1) "Synthesis is an all or nothing thing. Nail it!"
2) "It takes three things to get you through your PhD: Passion, Faith and Self-realisation"

Organic synthetic chemistry is no easy task and I know that I am still far from proficient at it, but you engrained into me that with the right mindset and dedication, mother nature will reveal her beauty at her most fundamental (molecular) level.

Further academics that deserve acknowledgement are:
Dr. Georgia Schäfer, who unofficially supervised a great deal of my research at the Institute for Infectious Disease and Molecular Medicine. I appreciate you taking me under your wing and showing me the ins and outs of molecular biology. *Vielen Dank!*
Prof. Arieh Katz, for availing his laboratory space to me.
Dr. Maré Vlok, Dr. Stoyan Stoychev (ReSyn Biosciences), Dr. Tariq Ganief, Dr. Muneerah Smith and Dr. Shaun Garnett, for their assistance with my proteomics project.

I need to also thank the past and current students in the Hunter research lab, and the UCT Department of Chemistry, with whom I have shared my plight and with several of which I have formed long-lasting friendships. With special mention: Wade Petersen, Ana Andreijvic, Fabrizio L'abbate, Shankari Nair, Rudy Cozett, Myles Smith, Allan Huysamen, Olaolu Fadeyi, Muhammad Iqbal, Doa'a Ali, Fanuel Mebrathu, Jasmin Ferreira, John Woodland, Zaheer Timol, Marwaan Rylands, Stephen De Doncker, Ana de Sousa and, last but not least, Dr. Sophie Rees-Jones.

Then outside of campus, I thank my friends who were there even when times were tough: Brett and Jazmyne Yarlett, Eldon and Tracy de Waal, Nicholas Bowler, Richard Gregorowski, Sebastian Scholle, Matt Maybery and Matt Esof.

Finally, to my better half, Rolanda Londt: Thank you for standing by me over this long arduous journey, for your unquestioning support and for accepting me as me. I love you!

Table of Contents

List of Figures

List of Tables

List of Schemes

Abbreviations

^{13}C-NMR	Carbon-13 nuclear magnetic resonance
^{1}H-NMR	Hydrogen-1 nuclear magnetic resonance
ABP	Activity-based probe
ABPP	Activity-based protein profiling
ACCN	1,1-Azodi(hexahydrobenzonitrile)
AGE	Aged garlic extract
AP-MS	Affinity-purification mass spectrometry
ATR	Attenuated total reflectance
BnOH	Benzyl alcohol
Boc	*Tert*-butyloxycarbonyl protecting group
BSA	Bovine Serum Albumin
BSL2	Biosafety Level 2
BtOH	Hydroxybenzotriazole
C18	Octadecyl carbon chain
CD_3OD	Deuterated methanol
$CDCl_3$	Deuterated chloroform
CH_3CN	Acetonitrile
CuAAC	Copper(I) catalysed alkyne-azide cycloaddition
Cys	Cysteine
DADS	Diallyl disulfide
DAS	Diallyl sulfide
DATS	Diallyl trisulfide
DATTS	Diallyl tetrasulfide
DCC	*N,N*'-Dicyclohexylcarbodiimide
DCM	Dichloromethane
DIPEA	*N,N* Diisopropylethylamine
DMAP	4-Dimethylaminopyridine
DMEM	Dulbecco's modified eagle's medium
DMF	*N,N*-Dimethylformamide
DMSO	Dimethyl sulfoxide
DTT	Dithiothreitol

EDTA	Ethylenediaminetetraacetic acid
EGF	Epidermal growth factor
ER	Endoplasmic reticulum
ESI	Electrospray ionisation
EtOAc	Ethyl acetate
FA	Formic acid
FBS	Foetal bovine serum
FDR	False detection rate
FMO	Frontier molecular orbital
GE	Garlic extract
GSH	Glutathione
GSSG	Glutathione disulfide
Hb	Haemoglobin
HiPPR	High protein and peptide recovery
HOMO	Highest occupied molecular orbital
HPLC	High-performance liquid chromatography
HRMS	High-resolution mass spectrometry
HRP	Horseradish peroxidase
HSQC	Heteronuclear single quantum coherence spectroscopy
IAA	Iodoacetamide
IC_{50}	Half maximal inhibitory concentration
IGEPAL® CA-630	Octylphenoxy poly(ethyleneoxy)ethanol
LFQ	Label-free quantitation
LG	Leaving group
LUMO	Lowest unoccupied molecular orbital
m/z	Mass to charge ratio
MeOH	Methanol
MetHb	Methaemoglobin
MS	Mass spectrometry
MTT	3-(4,5-Dimethylthiazol-2-yl)-2,5-diphenyltetrazolium bromide
OSC	Organosulfur compound
PBS	Phosphate-buffered saline
PCM	Protein cysteine modification

Pet. Ether	Petroleum ether
PMBCl	4-Methoxybenzyl chloride
PMBSH	4-Methoxybenzyl mercaptan
PTM	Post-translation modification
RCF	Relative centrifugal field
R_f	Retention factor
RNS	Reactive nitrogen species
ROS	Reactive oxygen species
RSS	Reactive sulfur species
rt	Room temperature
SAC	*S*-allylcysteine
SAMC	*S*-allylmercaptocysteine
SAMG	*S*-allylmercaptoglutathione
SD	Standard deviation
SDS	Sodium dodecyl sulfate
SDS-PAGE	Sodium dodecyl sulfate–polyacrylamide gel electrophoresis
SPF	Specific-pathogen-free
SU	University of Stellenbosch
T	Treated
TBAI	Tetrabutylammonium iodide
tBuOH	*Tert*-butanol
TCEP	3,3′,3′′-Phosphanetriyltripropanoic acid
TFA	Triflouroacetic acid
THPTA	Tris(3-hydroxypropyltriazolylmethyl)amine
TLC	Thin layer chromatography
Tol	Toluene
Tris	2-Amino-2-(hydroxymethyl)propane-1,3-diol
Triton X-100	2-[4-(2,4,4-Trimethylpentan-2-yl)phenoxy]ethanol
Tween-20	Polyoxyethylene (20) sorbitan monolaurate
UCT	University of Cape Town
UT	Untreated
WB	Western blot

Literature Review

Chapter 1 : Chemopreventative and Antitumour Activity of Organosulfur Compounds from Garlic

1.1 Cancer

Cancer is a hyperproliferative disease in which abnormal cells undergo uncontrolled growth. Over the past century, cancer has become an immense societal and economic burden. In 2018, there were 18 million new reported cases of cancer worldwide with close to 10 million cancer-related deaths.[1] Globally, cancer incidence is rising, and the WHO's international agency for research on cancer (IARC) predicts 29 million new cases per year by 2040, which is more than a 60% increase.[2] These current trends forecast that one in three individuals are likely to develop cancer within their lifetime.[3] While the growing number of cancer cases correlates, in part, to the rise in global population with a longer life expectancy, much evidence points towards industrialisation and modern lifestyle as a major contributing factor. A 21st century lifestyle is often associated with poor dietary habits, sedentary life and exposure to environmental pollutants which have been identified as key contributors to carcinogenesis. With increasing modernisation of African societies, the incidence of non-communicable diseases such as cancer is also on the rise. For Southern Africa, statistics predict a 67% rise in yearly cancer incidence by 2040.[4] Currently, the lifetime risk for South African men to develop cancer lies is 1 in 7, and 1 in 8 for women, with the average, age standardised mortality rate of ~70%, which is below the global average.[5,6] Late diagnosis, limited access to treatment and high medical costs have been attributed to this high mortality rate. The challenges of improving early detection together with the toxicity of current therapies have made the search for preventative measures and alternative treatments a priority.

Malignancies in cancer are characterised by various alterations on a molecular and cellular level, driven by DNA mutations. These mutations may be hereditary or acquired during one's lifetime through intrinsic and extrinsic factors. While hereditary traits are unavoidable, they are modestly implicated in the development of cancer and contribute to less than 10% of the lifetime risk (see **Figure 1.1**).[7] Intrinsically acquired mutations arise spontaneously during DNA replication as a result of nucleotides undergoing

hydrolysis, modification and tautomerism or becoming crosslinked.[8,9] An organism is able to curb these malignancy-causing mutations in most cases by means of DNA repair and immune function.[10]

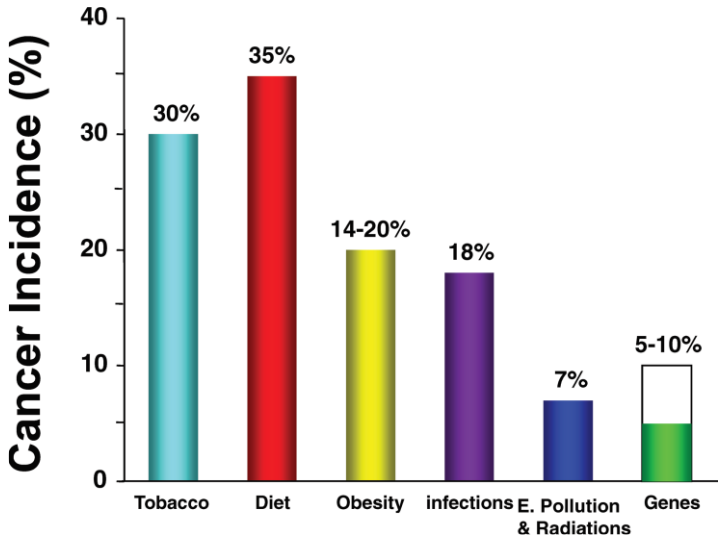

Figure 1.1: Risk factors contributing to cancer incidence rates.
Taken from Aggarwal *et al*.[11]

Extrinsic DNA damage and mutations arise through exposure to mutagens such as chemical carcinogens or ionising radiation. High and frequent exposure to these cancer-causing agents can easily overwhelm the body's ability to control the effects of DNA damage (**Figure 1.1**). Habitual risk factors such as smoking and obesity are related to lifestyle choices, which is why medical authorities advocate a cancer-conscious lifestyle as a primary cancer-prevention measure, which in turn has directed a considerable amount of research towards understanding routes of exposure to mutagens that induce cancers. The WHO has compiled this combined effort as an extensive list of monographs on mutagenic agents (carcinogens) and their underlying mechanisms.[12,13] Surprisingly, the endeavour to understand chemically induced cancers, has also led to the discovery of compounds, so called antimutagens, that are able to counteract mutations as they arise.[14] The search for novel antimutagens represents a rapidly expanding field of cancer research.

1.2 Nutraceuticals from Plant Sources as Anticancer Agents

The word nutraceutical is a portmanteau comprising of nutrition and pharmaceutical, defined as "a food (or part of a food) that has medical or health benefits". Increasing evidence supports that the dietary intake of plant-based, nutraceutical foods have

beneficial medical properties and may aid in the prevention and treatment of disease.[15] In this regard, many plants show promising anticancer properties.[11] The source of these anticancer effects is partly attributed to small molecules, referred to as secondary metabolites, that interfere with a number of cellular events associated with carcinogenesis and cancer progression. These compounds tend to be safe to use and non-toxic, easily accessible on a daily basis, often through the diet, and affordable, making many plant-based nutraceuticals an attractive strategy for cancer prevention and treatment.[16]

1.3 Garlic as a Nutraceutical

The curiosity of modern medical research towards the nutraceutical properties of garlic was initially sparked by its age-old reputation as a "cure-all" folk-remedy, renowned in many cultures as a herb that boosts immunity, protects from illness and enhances performance.[17,18] By the turn of the 20th century, scientists had identified garlic as a potent, easily accessible antimicrobial agent, with few side-effects and less prone to pathogen-resistance than contemporary synthetic drugs.[19] In addition to its curative properties, a wealth of evidence on the plant's capacity to maintain cardiovascular health and to prevent disorders, such as hypertension, thrombosis and arthrosclerosis cardiac injury, supports the prophylactic intake of garlic in health promotion and protection from disease.[20] Its ability to prevent and treat many life-style related disorders has made garlic one of the most studied medicinal plants today. The tumour-inhibiting properties of garlic extracts were first described in 1958 by Weisberger and Pensky.[21] Since then, there has been extensive research efforts to understand these cancer-fighting properties.

1.4 Epidemiological Studies on the Cancer-Preventative Properties of Dietary Garlic

Populations with diets rich in vegetables and spices have noticeably higher life expectancies and decreased incidences of cancer. Several smaller observational studies in countries of the Mediterranean, as well as South and East Asia have associated this lowered cancer risk with their high consumption of *Allium* vegetables, especially garlic. These observations have been followed-up with case-control and cohort studies, and extensively reviewed and scrutinised by meta-analyses. The overall findings on this topic are summarised in **Table 1.1**.

Type of Study	Year	Findings	Ref.
Meta-analysis	2000	High intake of garlic may be associated with a protective effect against stomach and colorectal cancers.	22
Review	2001	Evidence from available studies suggests a preventive effect of garlic consumption in stomach and colorectal cancers.	23
Cohort study	2005	Protective effect of onion and garlic (*Allium* vegetables) was suggested for cancer of the intestinal type.	24
Review	2007	Meta-analysis of 7 studies confirms the inverse association, with a 30% reduction in relative risk in colorectal cancer.	25
Review	2007	Several epidemiological studies link a lowered risk of stomach, oesophageal and colorectal cancer to a high dietary garlic consumption.	26
Meta-analysis	2011	Consumption of high levels of *Allium* vegetables reduced the risk for gastric cancer risk.	27
Meta-analysis	2014	No evidence that higher intake of *Allium* vegetables reduced the risk for colorectal cancer.	28
Review	2015	Epidemiologic studies indicate some associations of *Allium* vegetable consumption with decreased risk of cancer, particularly cancers of the gastrointestinal tract.	29
Review	2015	Frequent consumption of *Allium* vegetables was associated with reduced risk of several cancers.	30
Cohort study	2018	The findings from this large prospective study do not support the hypothesis that high garlic intake reduces risk of gastric cancer.	31
Case-control study	2018	High consumption of certain *Allium* vegetables, in particular garlic and leek, may reduce the risk of breast cancer.	32

Table 1.1: Epidemiological literature on dietary garlic intake and cancer incidence rates.

Most case-control and cohort studies report that garlic consumption reduces the incidence of several cancers including those of the lung, oesophagus, prostate, breast, and the digestive tract. Following on with case-control and cohort studies, however, the

heterogeneity in effect estimates (choice and sample categories) that the small sample sizes and a lack of controls for overall dietary patterns and other exposures lead to the conclusion that the results generally lack statistically significant associations.[22,23] Subsequent systematic reviews and meta-analyses on cancer risk and garlic consumption, therefore, only support negative associations in the cases relating to stomach and colon. Publications that have reviewed the available epidemiological data have suggested that further biases such as possible alternative hypotheses (e.g., confounded by total vegetable and other *Allium* consumption), as well as differences in dose estimates and exposure misclassification, warrant the need for more definitive research and improved nutritional epidemiologic analyses on the topic.[28,31,33,34] It is proposed that randomised and double-blind control trials in humans is needed to overcome the reliance on these summative effects. In addition, further details regarding the preparation, efficacy, dose and toxicity of active constituents in garlic is needed for clinical recommendations.

1.5 Phytochemistry of Garlic and its Organosulfur Compounds

A wealth of minerals, vitamins, and antioxidants make garlic a nutritious food, whose characteristic strong flavour and pungent smell also makes it a desirable spice. The olfactory and gustatory character of garlic, and other *Alliums*, is attributed to a unique collection of small organosulfur compounds (OSCs) which are also responsible for garlic's many health benefits, including its observed anticancer activity.[26,35,36] The exploration of its sulfur-chemistry has been integral to the understanding the biological properties of garlic.

The first contemporary investigation into the chemistry of garlic was conducted by Theodor Wertheim in 1844 who attributed the strong smell of the steam distilled oil of garlic to a hydrocarbon he discovered in the mixture. This was named allyl, after "*Allium"*, and the odiferous volatiles were thus called "Allylschwefel" (German: allylsulfur) compounds.[37] In 1892, Friedrich W. Semmler, who also worked on steam-distillates of garlic, isolated 2g (per kg of garlic) of a pure compound which he identified as diallyl disulfide (DADS) which was accompanied by smaller amounts of diallyl trisulfide (DATS).[38] Later, in 1944, Chester J. Cavallito identified allyl 2-propenethiosulfinate, the *S*-oxide of DADS, in room-temperature ethanolic extracts of garlic, which he named allicin.[39] Allicin exhibits a more pungent odour than its chemical relatives, DADS and DATS, and is

celebrated for its strong antibacterial properties.[40] Another related OSC, *S*-allyl-L-cysteine sulfoxide (alliin) was first isolated from low temperature (below 0 °C) ethanolic extracts of garlic by Arthur Stoll and Ewald Seebeck in 1948, and revealed a final clue to the biosynthetic origin of the garlic OSCs.[41] The pioneering findings of Block, summarised in **Scheme 1.1**, exemplify how the method and conditions of the extraction can vastly impact the OSC profile obtained in the final product.

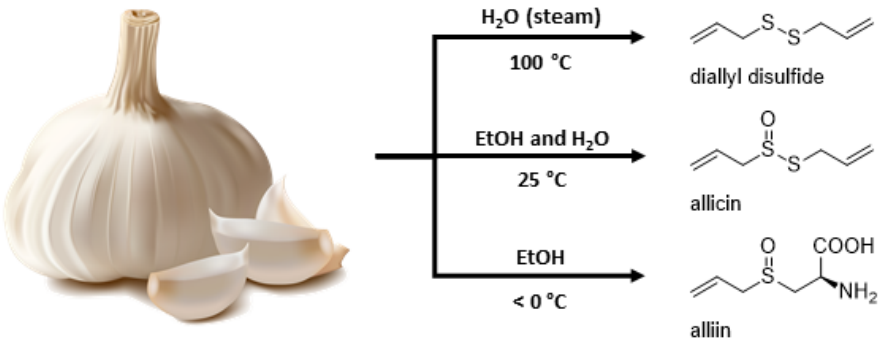

Scheme 1.1: Variations in extraction methods produce different OSCs.
Adapted from Block *et al.*[37]

The choice of extraction solvent, temperature and time play a crucial role, as OSCs readily undergo a number of chemical transformations.[42] For example, the high temperature of a steam distillation will result in the loss of allicin and alliin due to their volatility and degradation but favour the formation of thermodynamically stable products, such as DADS.[43] The milder extraction conditions of low temperature with a nonpolar solvent, enables the isolation of principal OSCs such as allicin and alliin, which paved the way for understanding the biosynthetic pathway of garlic OCSs, as shown in **Scheme 1.2**.[44]

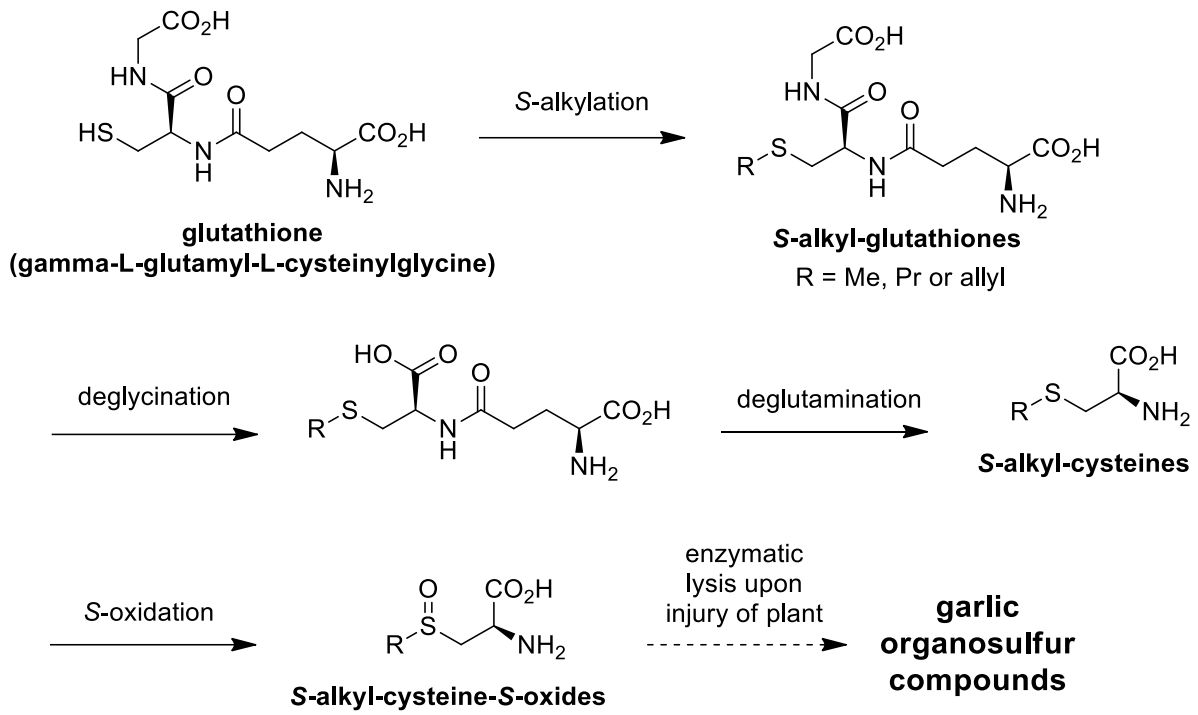

Scheme 1.2: Biosynthetic origin of garlic organosulfur compounds.

In Nature, OSC secondary metabolites evolved in the garlic plant as a deterrent against herbivores and pests. Tissue injury triggers the rapid generation of thiosulfinates from a feedstock of *S*-alkyl-cysteines as an allelochemical response.[45] **Scheme 1.2** shows the four-step biosynthetic transformation of glutathione towards *S*-alkyl-cysteine-*S*-oxides. Glutathione is first *S*-alkylated at the cysteine sulfur to form *S*-alkyl glutathione, which is subsequently deglycinated then cleaved at the γ-peptide bond to release glutamate to form *S*-alkylcysteines. The oxidation of the sulfide to the sulfoxide yields *S*-alkylcysteine-*S*-oxides.[40] While the majority of garlic OSCs (around 85%) contain a recurring *S*-allyl motif and have their biosynthetic origin in *S*-allyl-L-cysteine sulfoxide (alliin), *S*-methyl and *S*-propyl OSCs, from *S*-methyl or *S*-propyl-L-cysteine sulfoxide respectively, can also be identified in small amounts in garlic preparations.[46]

Alliin is stored within the cytosolic vacuoles of the plant, which is compartmentalised away from its enzymatic counterpart, alliinase. Upon tissue damage, alliin is brought into contact with alliinase, resulting in an enzymatic-controlled lysis via a concerted, intramolecular elimination to release allyl sulfenic acid (2-propenesulfenic acid) and dehydroalanine (2-aminoprop-2-enoic acid), which hydrolyses to ammonia and pyruvate

(**Scheme 1.3**).[40] Subsequently, the condensation of two molecules of allyl sulfenic acid produces allicin.

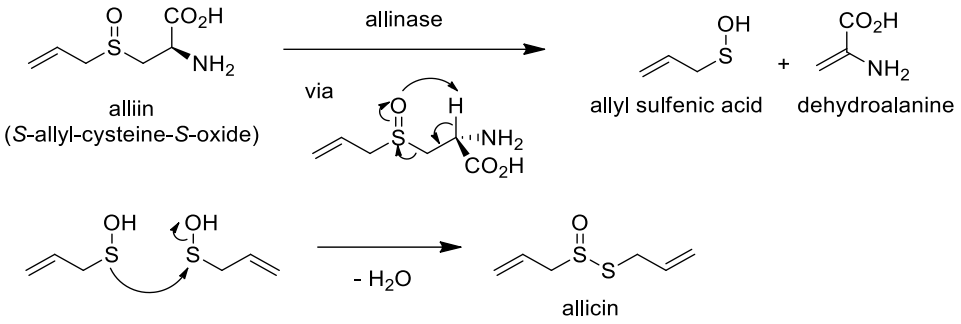

Scheme 1.3: Enzymatic transformation of alliin to allicin by alliinase.

The primary plant chemical-defence response to tissue damage results in a spike in the concentration of allicin, which is designed to "fight the attacker". The bioactivity stems from the chemical reactivity of the thiosulfinate (TS; e.g. allicin), which also contributes to its transient nature and rapid disappearance through decomposition. The degradation products constitute a second wave of more thermostable but similarly bioactive OSCs, which are the active principles responsible for the medicinal benefits of aged or heated garlic preparations.[47,48]

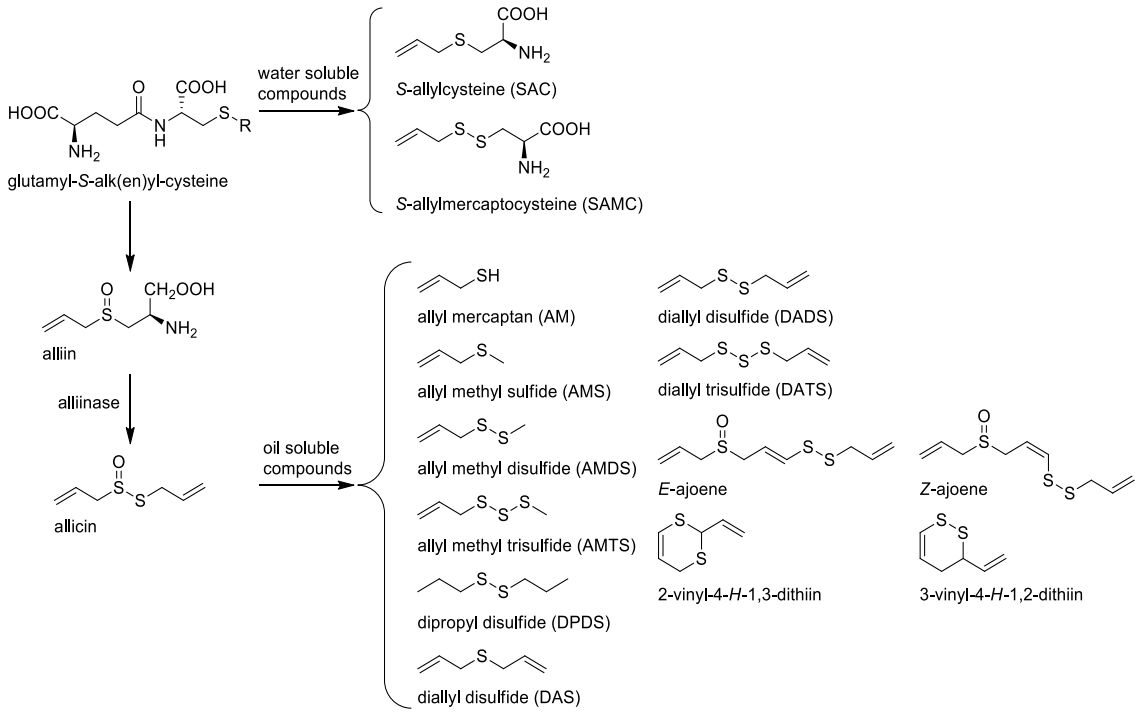

Scheme 1.4: A collection of the water- and oil-soluble OSCs formed during the processing of garlic.
Adapted from Haina Wang *et al.*[49]

In 1990, Lawson *et al.* quantitated the organosulfur content of various garlic preparations and reported that the degradation products of allicin could be grouped according to their solubility: i.e. water- or fat-soluble (see **Scheme 1.4**).[43] He also noted that their formation and detection was influenced by solvent, temperature, pH, time and processing method. The water-soluble OSCs, which consist primarily of cysteine adducts, are mainly *S*-allylcysteine (SAC), *S*-allylmercaptocysteine (SAMC) and *S*-allylmercaptoglutathione (SAMG) as well as their methyl and propyl counterparts. The oil-soluble metabolites of allicin include the diallyl polysulfanes (diallyl sulfide (DAS), diallyl disulfide (DADS), diallyl trisulfide (DATS), diallyl tetrasulfide (DATTS) and higher polysulfanes.), dithiins, ajoenes and ajothiolanes.[50] While water-soluble OSCs are primarily cysteinyl adducts that are formed by alkylation or *S*-alkylation of the cysteine thiol sulfur, the formation of lipophilic garlic OSCs from allicin involves a more complex set of chemical transformations that were first elucidated by Block and co-workers in the 1980s.[37,50,51] The degradation of allicin to form some of the major lipophilic allyl sulfur compounds is shown in **Scheme 1.5** and involves three distinct reaction pathways.

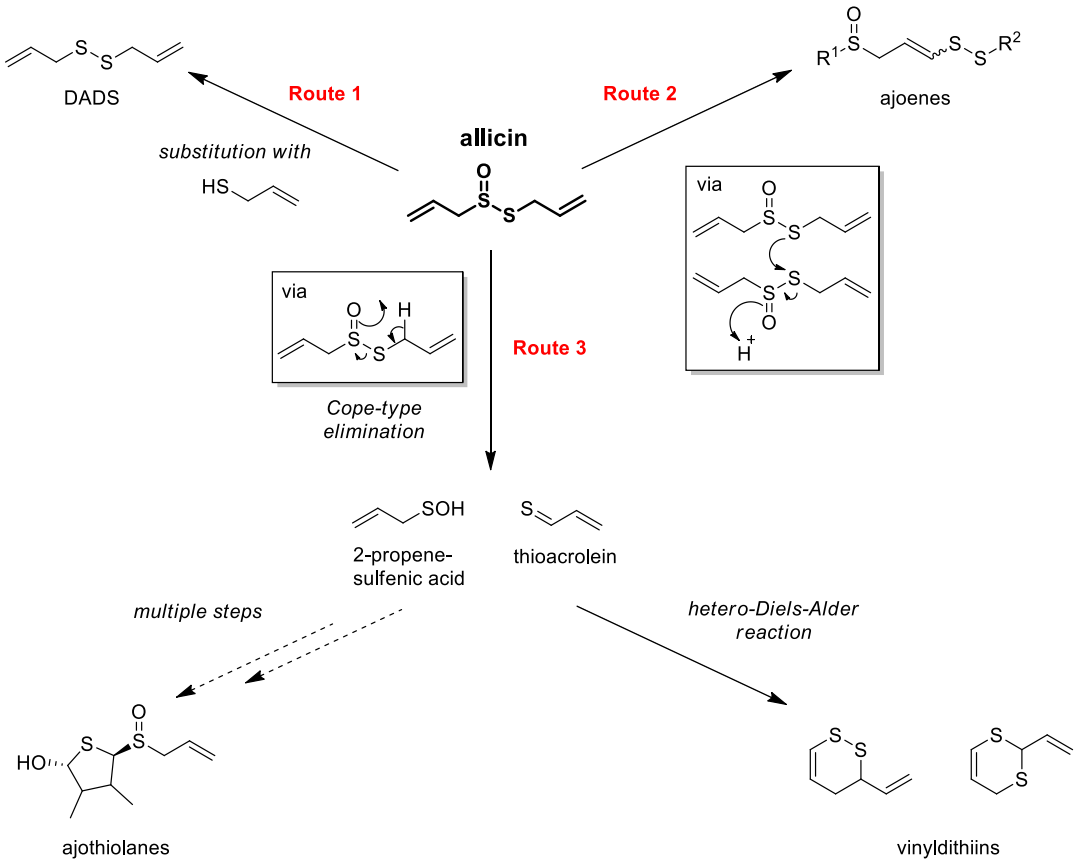

Scheme 1.5: Degradation pathways of allicin to form oil-soluble second-generation OSCs.

Each route can produce varying amounts of second-generation OSCs and is directed by the reaction environment (temperature, solvent, pH etc.) during allicin transformation. **Route 1** yields diallyl disulfide involving a substitution at the sulfur of the thiosulfinate moiety by allyl mercaptan. Higher polysulfanes are adducts from further substitutions with perthiol sulfinates. **Route 2** involves self-condensation of two allicin molecules via thioallylation to give a sulfonium ion, which undergoes elimination and subsequent Michael addition of 2-propenesulfenic acid to form ajoene (*vide infra*). **Route 3** involves a Cope-type elimination (depicted as concerted) to give 2-propenesulfenic acid and thioacrolein. Two molecules of thioacrolein can then undergo a Diels-Alder cycloaddition to give the vinyldithiins, while it was recently proposed that a multiple step pathway, involving the condensation of two molecules of 2-propenesulfenic acid follow by a [3,3]-shift and [2+3]-cycloaddition, produces the ajothiolanes.[50]

The exploration of these biosynthetic pathways of garlic OSCs required the careful isolation and identification of, often transient, intermediate compounds from complex biological mixtures. Although advances in scientific instrumentation and analysis have assisted in generating a detailed picture of the sulfur chemistry of garlic, the recent discovery of a new class of OSCs, the ajothiolanes by Block *et al*. in 2018,[50] as well as the growing reports of novel physiological effects,[52,53] have highlighted that the understanding of the clove's biology is far from complete.

1.6 Molecular Mechanism and Cellular Interactions of Garlic OSCs

Even though the intracellular molecular mechanism of garlic OSCs is still under debate, it is commonly agreed that the bioactivity of garlic is centred around its sulfur chemistry. OSCs undergo a wide range of redox reactions, as sulfur can take on several stable oxidation states (II^- to VI^+). This not only accommodates the formation of multicoordinate covalent bonds to biochemically important elements (H, C, N, O, P), including itself (-SS-), but also allows for complexation to Zn, Cu, Fe, elements that are central to the structure and function of metalloproteins.[54]

The chemical properties of sulfur allow for the generation of numerous second-generation OSCs from allicin (or alliin), as seen in **Scheme 1.6**, in which the redox reaction pathways of sulfur produce a range of chemotypes with unique chemical properties.

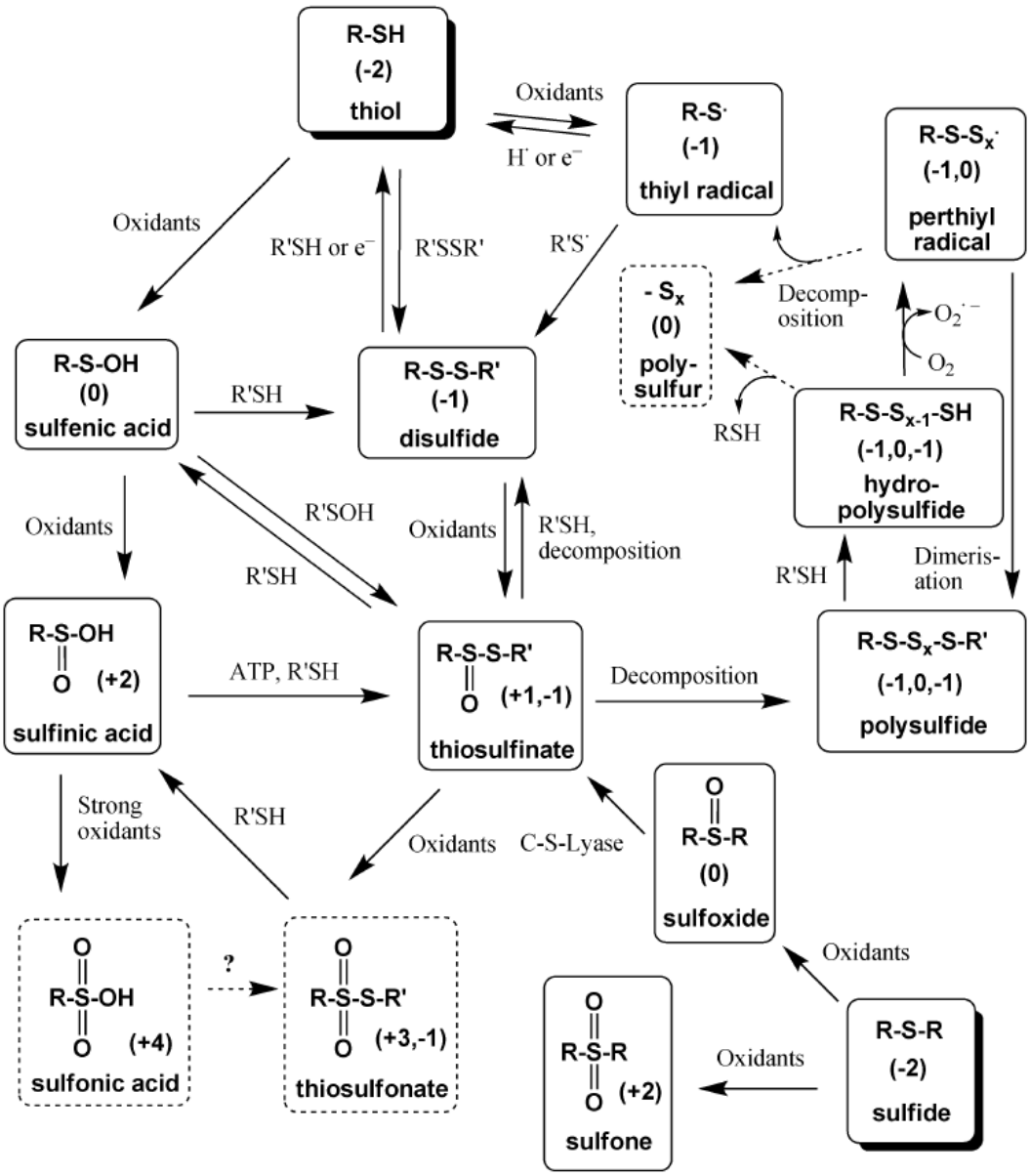

Scheme 1.6: The formation and transformation pathways of the sulfur redox network for known OSCs in garlic.
Taken from Jacob *et al.*[55]

These biochemical transformations are influenced by factors such as the solvent, pH, relative concentration of the OSCs and the presence of other redox partners. While the sulfur-containing functional groups of the OSC are produced by oxidation and/or nucleophilic substitution reactions, the individual steps may include several one and two-electron transfer reactions, including thiol/disulfide exchanges, redox/metal catalysis, oxygen and/or hydride transfers.[55]

In early publications by Weisberger *et al.* and Wills *et al.*,[21,56] it was suggested that OSCs target reactive sulfur moieties within cells, interacting with these centres and driving biological responses. Although the OSC (trans)formation network is complex, there is a

concensus that thiol moieties of catalytic enzymes and other biomolecules are the most likely site of direct interactions. While cysteine is one of the least abundant amino acids, it occupies a unique functional role in cellular chemistry. Evolutionarily, its flexible reactivity has resulted in the conservation of the thiol in catalytic sites of cellular enzymes, where up to 80% of all transcribed cysteine residues are reported to occupy functional roles.[54] As a result, thiol enzymes can be found in six of the seven enzyme classes, including oxireductases, transferases, hydrolases, isomerases, translocases and ligases. Their catalytic sites are characterised by single- or double-redox active cysteine residues that act as electron donors for a wide array of substrates.[57] These redox-active cysteine thiols are generally sensitive to modifications through environmental events such as xenobiotic insults, shifts in pH, and the redox status of the cell. In turn, these modifications trigger functional and structural changes that affect cell sensing and signalling pathways as well as catalytic activities of enzymes. Commonly encountered modifications of cellular cysteine include *S*-sulfenylation (-SOH), *S*-sulfinylation (-SO_2H), *S*-sulfonylation (-SO_3H), *S*-nitrosylation (-SNO), *S*-sulfhydration (-SSH), *S*-glutathionylation (-SSG) and disulfide bond formation (-SS-), as illustrated by **Scheme 1.7**.[58]

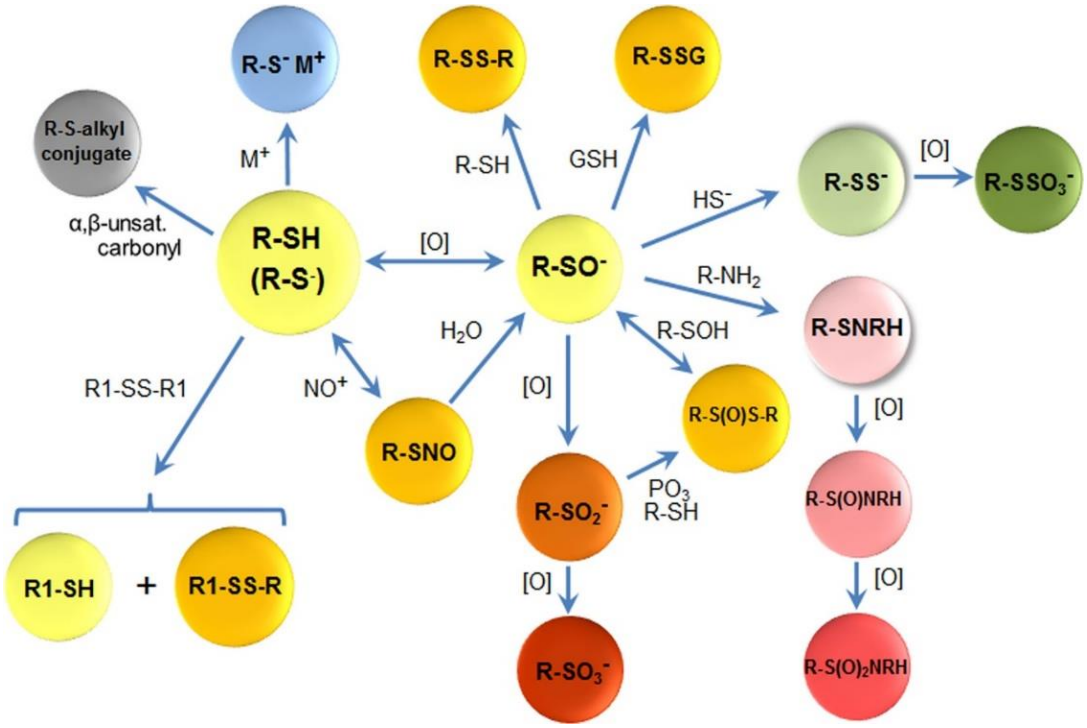

Scheme 1.7: Functional modification of cellular cysteine residues.
Taken from Go *et al*.[54]

The large number of interactions between garlic-derived OSCs and their respective cellular targets are largely unexplored, yet recent mechanistic studies on chemotypes and their biological activities have allowed the identification of several "first-line" molecular events with cellular sulfur sites. The upcoming section aims to provide an overview of the sulfur chemistry that is central to the anticancer effects of OSCs.

1.7 Sulfur and Oxidative Stress

Within the cell, sulfur chemistry forms part of a redox network that links molecular events on a chemical level with structual and functional changes on a biological one.[59,60] Several proteins performing vital biological functions contain redox-accessible cysteine residues with low pK_a values, which become targets for reversible and irreversible oxidative modifications during ongoing metabolic processes or via the oxidative stress of xenobiotics.[61] Under basal conditions, the cellular oxidant levels are maintained by an endogenous antioxidant system. This system is comprised of both enzymatic and non-enzymatic redox regulators that maintain an overall reducing environment, that also ensures that cellular thiols are maintained in their reduced state.[62] Reactive oxygen species (ROS), reactive sulfur species (RSS) or reactive nitrogen species (RNS), are metabolic byproducts of electron transfers between oxidants and/or molecular oxygen. Owing to their high reactivity, they are the most common cellular oxidative stressors and the primary drivers of thiol oxidation. Although thiol oxidations are essential to normal cell signalling and function, elevated levels of oxidants (e.g ROS/RSS/RNS) may cause the indiscriminate and irreversible conversion of thiols to higher oxidation states. This may cause alterations in protein structure and function leading to disruptions in redox signalling and control, as well as damage to biomolecules, referred to as oxidative stress (**Figure 1.2**). Redox homeostasis is controlled by cellular antioxidant pathways that prevent thiol overoxidation, reverse cysteine modifications and scavenge reactive species. The related antioxidant enzymes have demonstrated a central role in the regulation of a number of biological functions including signal transduction, metabolism and cell proliferation.[54,60]

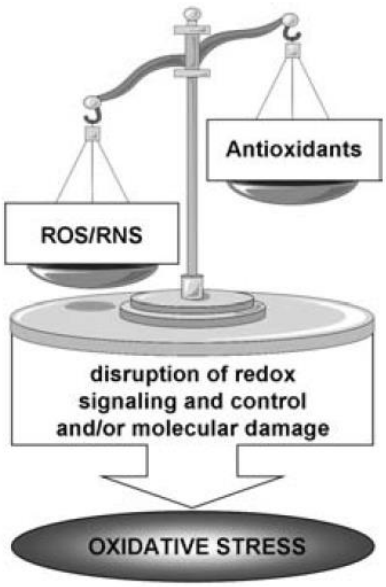

Figure 1.2: Oxidative stress can be described as the redox imbalance between oxidants and antioxidants in favour of the oxidants.
Taken from Dalle-Donne *et al*.[63]

Oxidative stress may lead to an impairment of cellular metabolism and viability, which has been associated with the initiation and progression of many degenerative pathologies, including cancer.[64,65] Cancer initiation is often triggered by an oxidative stress event leading to cellular transformation. Cancer cells are characterised by an uncontrolled increase in metabolic and proliferation rates, which is pivotal to their aggressive spread, but is also associated with an elevation of intracellular ROS to damaging levels. Their survival, therefore, involves the oncogenic activation of existing antioxidant pathways to protect them from oxidative damage.[66]

1.8 Oxidative Modifications of the Sulfur Atom in Protein Thiols

During oxidative stress, the shift in the redox state of the cell is most observable in the oxidative modifications of protein thiol groups. The antioxidant system presents a competing pathway to shield these vunerable protein thiols from oxidative damage. Thiol groups are oxidised by two distinct pathways, which involve either one-electron or two-electron oxidation (**Scheme 1.8**). Thiols with enhanced reactivity towards oxidation present themselves as easily ionisable at physiological pH and are generally solvent-accessible and located on the surface of the protein.

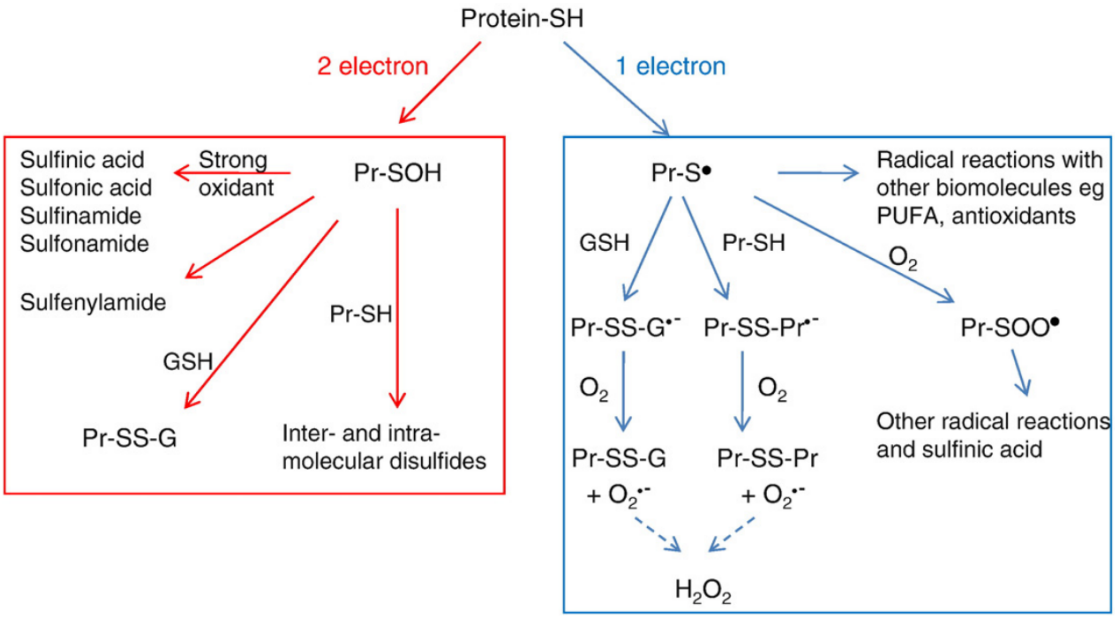

Scheme 1.8: One- and two-electron pathways leading to oxidation of protein thiol groups.
Taken from Winterbourn.[67]

The two-electron oxidation of thiols produces a sulfenic acid intermediate (RSOH) that undergoes several secondary reactions. The electrophilic nature of the sulfenic acid sulfur allows for its condensation with thiol groups to give mixed disulfides. A similar reaction with an amine gives a sulfenamide. Strong oxidants may irreversibly oxidise the sulfenic acid and sulfenamide into sulfinic or sulfonic acid and sulfinamide or sulfonamide, repectively.

The single-electron oxidation of a protein thiol is caused by radicals or transition metal ions to give a thiyl radical intermediate. Under aerobic conditions, the thiyl radicals may favourably react with cellular thiolates to give disulfide anion radicals. The reaction of these sulfur radicals with oxygen produces superoxide species, which are drivers of oxidative stress. The reversible and excessive reactivity of these products requires their rapid removal to curb cellular damage. Thiyl radicals are effectively scavenged through direct interactions with antioxidants.[60,67] The antioxidant system maintains the redox homeostasis of protein thiols by quenching reactive intermediates (e.g. thiyl radicals or sulfenic acids), reducing the oxidised cysteine thiols and reversibly protecting (or "capping") these redox-sensitive thiols. The two main mechanisms through which this occurs involves radical and thiol-disulfide exchange reactions.

1.9 Glutathione

The tripeptide glutathione (GSH) is the primary non-enzyme antioxidant in eukaryotic cells, as well as the most abundant cellular thiol. GSH represents the cell's primary storage of cysteine, as it is known to rapidly autooxidise. The GSH-dependent antioxidant system is mostly localised in the cytosol, the endoplasmic reticulum and the mitochondria, where GSH reaches millimolar concentrations.[68] Here, a pool of reduced GSH acts as a redox buffer, acting as a suitable cysteine decoy towards toxic products of oxygen, electrophilic molecules, and xenobiotics. It also provides a reducing potential to a system of enzymes that perform antioxidant functions. Glutathione can scavenge ROS, either directly, or by acting as a substrate for glutathione peroxidases (GPxs) and glutathione *S*-transferases (GSTs), which detoxicify oxygen radicals (e.g. H_2O_2, lipid hydroperoxides) and electrophilic compounds.[63] For this purpose, a high ratio (>99:1) of the redox couple between GSH and its oxidised GSSG disulfide form is maintained in the mitochondria and cytosol by the enzyme glutathione reductase (GR) which uses the NADPH/$NADP^+$ redox couple as an electron source for the reduction of GSSG to GSH (**Scheme 1.9**).

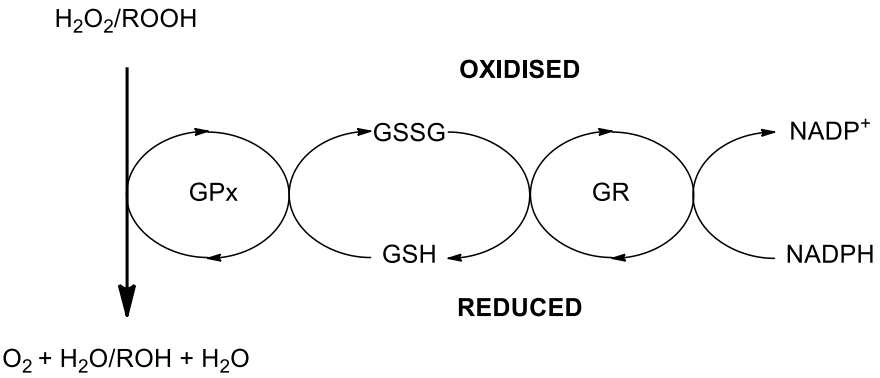

Scheme 1.9: The GSH-dependent redox cycle for the intracellular elimination of ROS

During increased oxidative load, the oxidation of GSH by GPxs leads to the production of GSSG, which increases the formation of mixed disulfides with cellular proteins. Protein *S*-glutathionylation is a term used to describe the reversible conjugation of glutathione to protein thiols and has an important cellular function. This process protects cysteine residues from irreversible oxidation but also serves as a means of GSH storage, as well as playing a role in redox regulation and signalling. Spontaneous or enzyme-catalysed glutathionylation can occur either through thiol-disulfide exchange (as mentioned above)

or through the reaction of GSH with oxidant-activated thiol moieties as shown in **Scheme 1.10**.

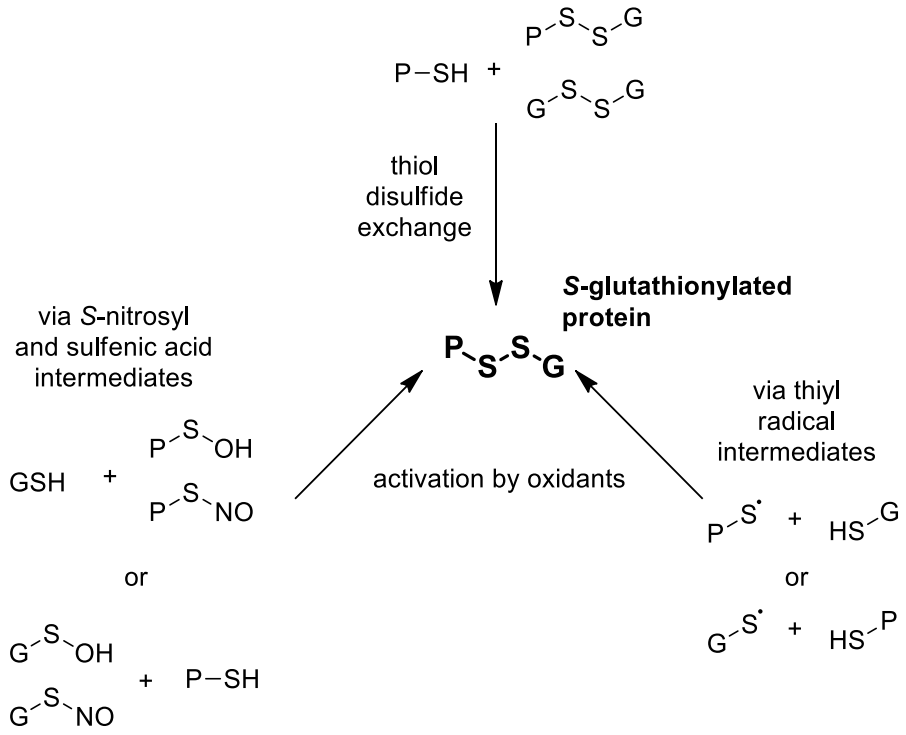

Scheme 1.10: *S*-glutathionylation pathways for cellular protein thiols.
P-SH = protein

While *S*-glutathionylation is a global cellular event coinciding with increased oxidative stress, it can also occur selectively upon ROS generation as part of signalling events to aid in detoxification.[60] Although not directly linked to the GSH-dependent antioxidant system, the glutathione *S*-transferases (GSTs) family constitutes the enzymes that most frequently perform *S*-glutathionylation reactions within cells. GSTs confer redox protection by catalytically producing GSH-adducts with reactive biomolecules, radicals and xenobiotics, which promotes their excretion into the extracellular space.[69] During oxidative/nitrosative stress, GSTs cap redox sensitive thiol proteins with GSH to protect them from overoxidation.[70] The reversal of *S*-glutathionylation of proteins is achieved by the oxidoreductase enzyme, glutaredoxin (Grx), which catalyses the reduction of protein-GSH adducts, as well as other protein disulfides, using GSH as an electron source (**Scheme 1.11**).

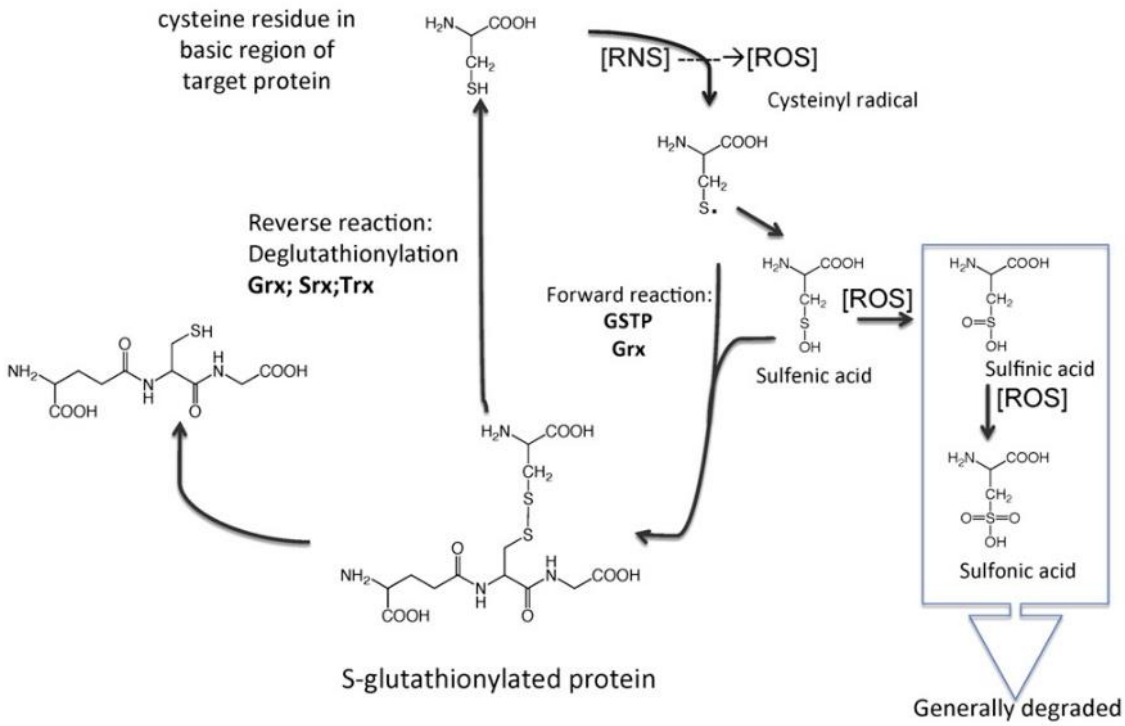

Scheme 1.11: Schematic representation of the enzymatic S-glutathionylation cycle. Taken from Tew *et al,*[70] where **Grx** is glutaredoxin, **Srx** is sulfiredoxin, **Trx** is thioredoxin, **GTSP** is glutathione *S*-transferase π.

Increasing evidence suggests that altered, often enhanced, *S*-glutathionylation and GST activity is a common phenotypic trait in cells undergoing carcinogenic transformation.[70] Since cancer cells have higher proliferation rates, they also have increased levels of metabolic byproducts, as well as altered cellular signalling, particularly attributed to upregulation of kinase and phosphorylase pathways.[71–74] Research has shown that GSH is able to *S*-glutathionylate several important redox-sensitive protein thiols, with an implication in the functioning of cytoskeletal, cell signalling, membrane channel and heat shock proteins as well as protein folding and metabolic enzymes.[54,60,70] The close association between malignant diseases and GSH-protein interactions have been proposed as promising drug targets for anticancer therapeutics.[7576]

1.10 Thiol-Modifying Properties of Garlic OSCs

Garlic OSC's can interact with cellular thiol systems by similar mechanisms to those of glutathione and enzymes of the GSH-antioxidant system.[77,78] The thiol-modifying ability of OSC chemotypes bearing electrophilic sulfur atoms, including thiosulfinates, polysulfanes (for $S_n \geq 2$) and vinyl disulfides, have been extensively reported.[78–83] Akin to

S-glutathionylation, the exchange reaction proceeds at physiological pH and/or oxidising conditions via the two-electron pathway, as shown previously in **Scheme 1.8**. Here, the thiol residue is ionised to the thiolate, which reacts with the electrophilic sulfur of the garlic OSC to produce "pseudo posttranslational modifications" (e.g. R-SS-allyl) within treated cells. The study of these pathways, however, is complex, as these oxidative modifications are often transient and in competition with other redox systems (e.g. antioxidant enzymes). As the structural motifs of allicin, ajoene and diallyl polysulfanes are biosynthetically related, they are all able to modify cysteine through thioallyl transfer during an exchange reaction, called *S*-thioallylation (**Scheme 1.12**). This thiol disulfide exchange reaction with OSCs is pH-dependent as evidenced by a direct correlation between the rate and the concentration of available thiolate ions (RS^-).[84,85]

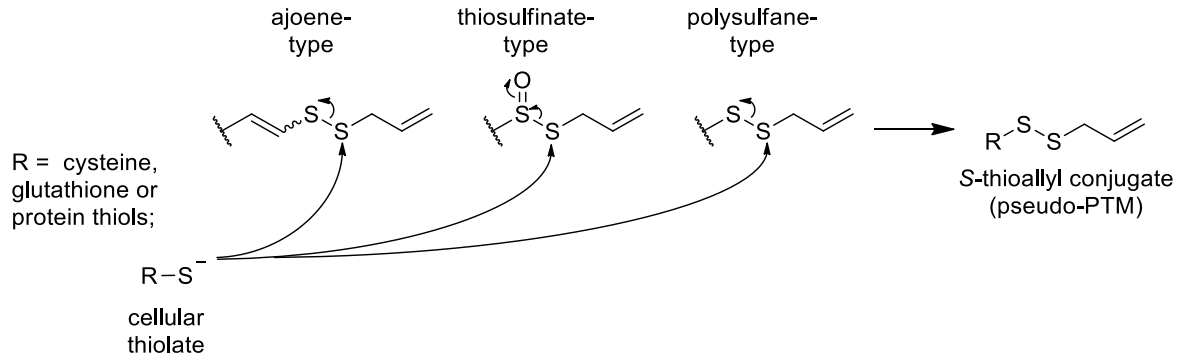

Scheme 1.12: Thiol-disulfide exchange reactions between OSC chemotypes and cellular thiols to produce *S*-allylated, mixed disulfide conjugates.

Redox-sensitive proteins have been identified as critical targets of exchange processes with garlic OSCs.[78] The *S*-thioallylation of cysteine residues by allicin has gained substaintial attention as the primary bioactive principle of garlic. A study by Rabinkov *et al.* has attributed the bioactivity of allicin and other thiosulfonates to its ability to form conjugates with GSH or cysteine, in which the resulting reaction products have shown the same thiol-modifying properties and antioxidant properties as allicin.[84] One equivalent of allicin can produce two equivalents of *S*-thioallyl conjugates by reacting with two equivalents of cellular cysteine according to the mechanism illustrated in **Scheme 1.13**.

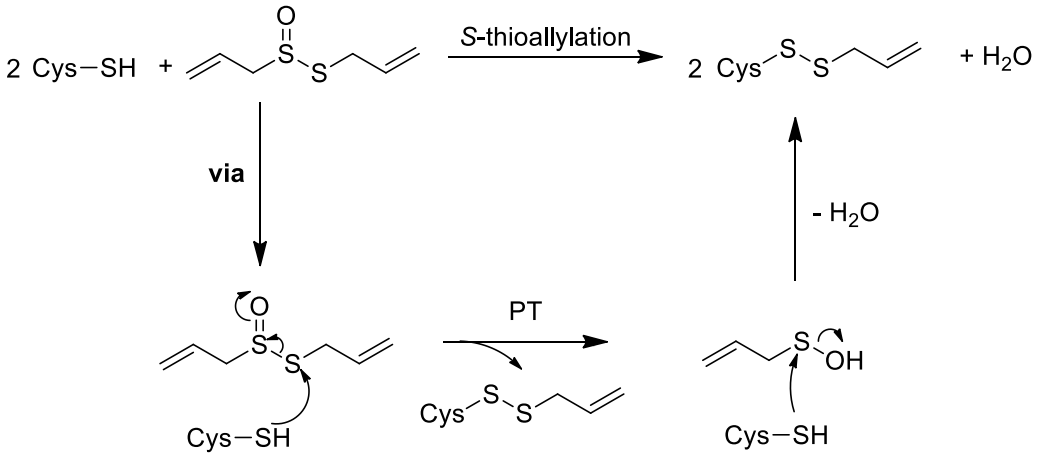

Scheme 1.13: *S*-thioallylation reaction of allicin with cysteine to produce *S*-thioallylated conjugates.

At physiologial pH, the reaction between a cysteine thiol and allicin takes place rapidly (allicin and GSH, $k = 3.0\ M^{-1}\ s^{-1}$) to give *S*-allylmercaptocysteine and allylsulfenic acid. The sulfenic acid produced can react with another equivalent of cysteine to give another equivalent of *S*-allylmercaptocysteine and H_2O.[79] This reaction is proposed to be key to the biological activity of allicin and its related OSC family members.[84]

A recent study by Gruhlke *et al*., investigated the thiol-modifiying properties of allicin on the proteome of Jurkat T lymphocyte cells.[86] Analysis of shotgun LC-MS/MS data revealed that 332 proteins were modified by *S*-thioallylation, in which the addition of a thioallyl group onto cysteine was tracked by a mass shift of 72 Da. The proteins were classified into functional categories that included: cytoskeletal proteins, chaperones, glycolytic enzymes and translation factors as the primary targets of *S*-thioallylation, as shown in **Figure 1.3**.

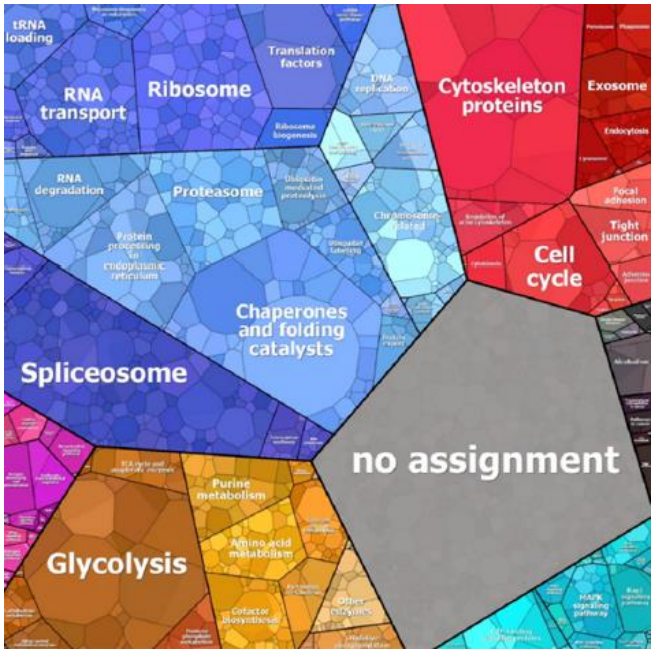

Figure 1.3: Treemap showing the classificiation of the allicin-modified proteins into functional categories according to KEGG ontology annotations.
Taken from Gruhlke *et al*.[86]

The authors demonstrated that allicin disrupts the actin cytoskeleton, decreases enolase activity and modulates the immune system by enhancing Zn^{2+} release which supports its *S*-thioalylation of some of the targets.[86]

The chemistry that allows for thiol-disulfide exchanges to occur with redox-sensitive protein thiols is mirrored by the ajoene and dialkyl/dialkenyl polysulfane chemotypes. This suggests that these chemotypes may target similar proteins in treated cells to produce *S*-thioallylated conjugates, and furthermore, may show an overlap of the biological and anticancer effects of allicin.

1.11 Garlic OSCs Produce ROS

Garlic OSC's have been shown to produce ROS, which may also play a role in the bioactivity of garlic.[87–89] An increased concentration of ROS causes oxidative stress, which in turn, can induce cell death in physiological and pathological conditions.[90] The shifting of the redox homeostasis inside a cancer cell by directly increasing the intracellular levels of ROS is commonly utilised as a therapeutic strategy against cancer. The increase in ROS caused by ionising radiation or chemotherapy drugs, such as doxorubicin, camptothecin or cisplatin, is aimed at saturating the antioxidant capacity, which when combined with the damaging effect on cellular components, leads to the activiation of apoptosis

pathways.[91,92] Interaction with antioxidant systems by modifying cellular cysteine residues through OSC thiolysis exchange reactions, may affect the cell's ability to withstand oxidative insults and indirectly raise levels of ROS.[78] However, there are also direct pathways through which OSCs are able to generate ROS. These proceed via the aforementioned single electron, thiol oxidation mechanisms (**Scheme 1.8**), involving radical oxidants as well as activation at transition metal centres.[67]

Munday *et al.* reported that polysulfane chemotypes (S≥2, i.e. DADS, DATS, DATTS etc.) are able to produce ROS (in the form of hydrogen peroxide (H_2O_2), superoxide ($O_2^{\bullet-}$) and hydroxyl radicals ($HO^{\bullet}$)) through non-enzymatic chemical pathways involving GSH and single-electron transfer reactions under physiological conditions.[93] Under these conditions, thiols and perthiols easily ionise and equilibrate to thiolate and perthiolate anions.[94] In the presence of certain transition metals (such as Fe^{3+}) and molecular oxygen, these ionised species generate hydrogen peroxide and thiyl or perthiyl radicals, respectively (**Equation 1** and **2** in **Table 1.2**). The (per)thiyl radicals either regenerate polysulfides (**Eq. 3**) or oxidise available (per)thiolates to produce disulfide radical anions (**Eq. 4**) that react with molecular oxygen to give superoxide radical anions (**Eq. 5**). The reaction of hydrogen peroxide with Fe^{2+} (Fenton reaction) generates the highly reactive hydroxyl radical (**Eq. 6**).[93]

Eq.	Reaction
1	$2RSH + O_2 \xrightarrow{Fe^{2+}/Fe^{3+}} 2RS^{\bullet} + H_2O_2$
2	$2RSSH + O_2 \xrightarrow{Fe^{2+}/Fe^{3+}} 2RSS^{\bullet} + H_2O_2$
3	$2RS^{\bullet} \rightarrow RSSR$ **or** $2RSS^{\bullet} \rightarrow RSSSSR$ **or** $RS^{\bullet} + RSS^{\bullet} \rightarrow RSSSR$
4	$RS^{\bullet} + RS^{-} \rightarrow RSSR^{\bullet-}$
5	$RSSR^{\bullet-} + O_2 \rightarrow RSSR + O_2^{\bullet-}$
6	$H_2O_2 + Fe^{2+} \rightarrow HO^{\bullet} + HO^{-} + Fe^{3+}$
7	$RSSH + RSH \rightarrow H_2S +$ RSSR

Table 1.2: Reactions of the garlic polysulfane chemotype leading to the cellular production of ROS.

The cytotoxicity of polysulfanes towards cancer cells has been attributed to their ability to generate ROS,[87,88] where one publication describes the order of ROS-forming ability for these chemotypes as follows: DATTS>DATS>DADS>DAS.[93] Compared to thiols, a perthiol has a lower pK_a and greater reducing power, resulting in a more ionised species and a rapid reaction with cellular oxidants (e.g. O_2) to generate ROS. This may explain why DATTS is more cytotoxic than DATS, as its GSH-mediated cleavage produces two equivalents of perthiol instead of one equivalent for DATS. Accordingly, DADS is less potent than DATS, possibly because its GSH-mediated cleavage only yields thiols.[95]

1.12 Higher Polysulfanes Produce H_2S

With a growing interest in the therapeutic potential of DATS and higher polysulfanes (S≥3), recent investigations into their anticancer activity have revealed their ability to act as H2S donors.[96] Although still under debate, it has been hypothesised that the mechanism of action involves the sulfhydration of intracellular thiol groups (to form persulfide adducts) with the release of H_2S (**Table 1.2**, **Eq. 7**). H_2S has been identified as a novel cellular gasotransmitter and its release from exogenous sources, such as polysulfides, has been shown to inhibit cancer progression in vitro.[97,98] Interestingly, a recent paper by Olson *et al*. has highlighted the chemical similarily of ROS with reactive sulfur species (RSS) generated through thiol modifications by H_2S, both showing competive involvement in numerous signalling mechansims.[99] In light of the potent anticancer properties of garlic-related trisulfides, our group at UCT/SU has recently developed a synthetic methodology towards synthesising asymmetric organotrisulfides for biological evaluation and exploration into their mechanism of action.[100]

1.13 Anticancer Effects of Garlic and its Constituents

Carcinogenesis in humans is a multistep process that involves alterations of regulatory pathways to drive the progressive transformation of a normal cell into a malignant tumour. Cancer development may be divided into three stages, namely: initiation, promotion, and progression (**Figure 1.4**).

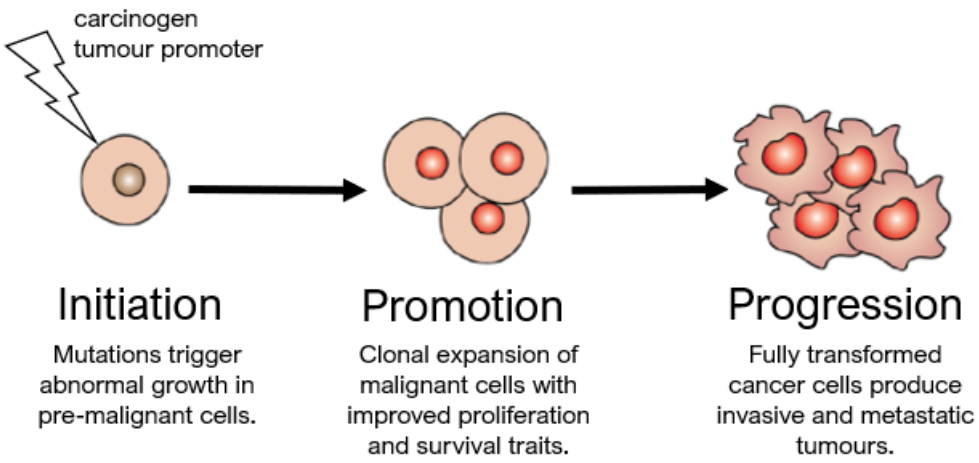

Figure 1.4: The three stages of cancer development.

During the initiation stage, carcinogens and/or tumour promoters cause genetic alterations that lead to the abnormal growth of pre-malignant cells. In the subsequent stage, the assimilation of genetic instability produces additional mutations that transform normal cells into malignant neoplasms. Natural selection favours cell populations that are able to outgrow and dominate the surrounding tissues with traits such as independently-sustained, proliferative signalling, evasion of growth suppressors and replicative immortality.[101] A cell is considered cancerous once it has developed ten underlying cellular adaptations (**Figure 1.5**) which Hanahan *et al*. describe as the "hallmarks of cancer".[102,103] These traits do not need to emerge in a specific order and can be activated through independent pathways; however, their combined effect marks the final stage of carcinogenesis. Angiogenesis and tissue invasion allow the malignant growth to gain full control of its microenvironment, after which metastasis permits the spread of secondary tumours throughout the body in a more advanced stage.

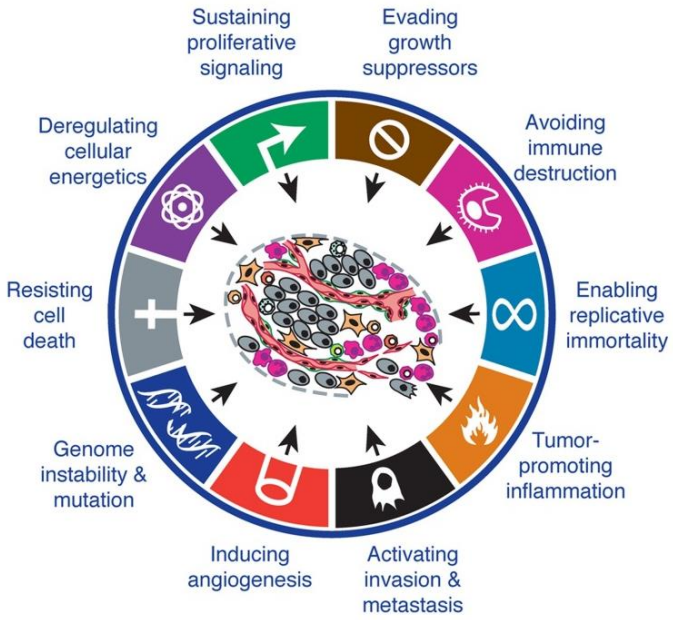

Figure 1.5: The hallmarks of cancer.
Taken from by Hanahan *et al*.[102]

It is well documented that garlic-derived OSCs trigger cellular responses that disrupt a wide range of cancer hallmarks.[26,95,96,104] The anticancer activity of OSCs may be ascribed to their ability to upregulate antioxidant and drug-metabolism enzymes, induce cell cycle arrest, modulate inflammatory responses, promote apoptotic pathways, and inhibit tissue invasion.

1.14 The Upregulation of Antioxidants and Drug-Metabolism Enzyme

The chemopreventative activity of OSCs is attributed to their ability to scavenge radicals, inhibit metabolic carcinogen activation, and promote xenobiotic detoxicifation.[105] OSCs reduce free radical concentrations (ROS/RNS) by activating antioxidant pathways as described previously in **Section 1.5.3**.[44,106] The modulation of carcinogen metabolism pathways by OSCs had been attributed to the downregulation of phase I enzymes (e.g. cytochrome p450-dependent enzymes) that are responsible for the activation of pro-carcinogens, while simultaneously upregulating phase II enzyme (e.g. GPx, GST, catalase and superoxide dismutase (SOD)), which protect the cell against oxidative stress and inflammation.[83,93,107–111]

1.15 The Induction of Cell-Cycle Arrest

Under normal physiological conditions, cell-division is controlled by signalling checkpoints, which constitute a series of control mechanisms that monitor and regulate the progress of the cell cycle. Since, uncontrolled cell growth is a defining characteristic of malignant cells, the initiation of cell-cycle arrest along signalling checkpoints provides an attractive target for anticancer therapeutics. Cell-cycle analysis of cancer cells treated with garlic OSCs, namely allicin, DAS, DADS DATS, SAMC and ajoene, are reported to cause an accumulation of cell populations in the G_2/M phase.[95,112–114] Experimental evidence supports that OSCs trigger cycle arrest via two known signalling events. The first involves the blocking of cancer cells at the G_2/M checkpoint, which is essential for the surveillance of DNA damage, by decreasing cyclin B1 along the ATR/Chk1/Cdc25c/cyclinB1 signalling axis.[95,112] The second involves the inhibition of the mitotic spindle formation that is responsible for chromosome separation during the M-Phase, by oxidatively modifying β-tubulin (microtubule) subunits at cysteine residues (βCys-12 and βCys-354).[82,115,116]

1.16 Modulation of Inflammatory Responses

The pathology of cancer is known to capitalise and manipulate the dysregulation of the host's inflammatory responses for sustained growth. It is well known that the emergence of cancer is associated with chronic inflammation, which creates a favourable environment for tumour development. Once established, the survival of cancer cells requires the evasion of the immune system by upregulating anti-inflammatory and immunosuppressive responses. It is generally believed that garlic may exert chemopreventative and therapeutic activity by modulating the secretion of cytokine and chemokines that counter tumourogenesis.[117]

As part of their chemopreventative repertoire, OSCs have been shown to reduce chronic inflammation by decreasing the expression of pro-inflammatory cytokines, which has been linked to their ability to inhibit tumorigenesis.[118–121] On the other hand, in established tumours, garlic derived-OSCs influence the host immune responses to facilitate immune destruction of cancerous cells. Numerous *in vitro* and *in vivo* studies have shown that OSCs enhance the proliferation and activation of immune cells including natural killer (NK), CD8+ T cells, NK T-cells and macrophages, as well as induce their infiltration into tumour masses.[122] These effects have been attributed to the ability of OSCs to stimulate the release of pro-inflammatory mediating cytokines that include IFN-

γ, TNF-α, and IL-2 and IL-6. Furthermore, it has been shown that garlic OSCs promote the production of natural antibodies that target the cancer cells.[122–124]

Two independent reviews by Kaschula and Arreola have highlighted that garlic and its constituents exert paradoxical stimulatory and inhibitory effects.[125,126] It has been hypothesised that its non-specific, immunomodulatory bioactivity counteracts a dysfunctional immune system by selectively up- or downregulating pathways, as illustrated in **Figure 1.6**.

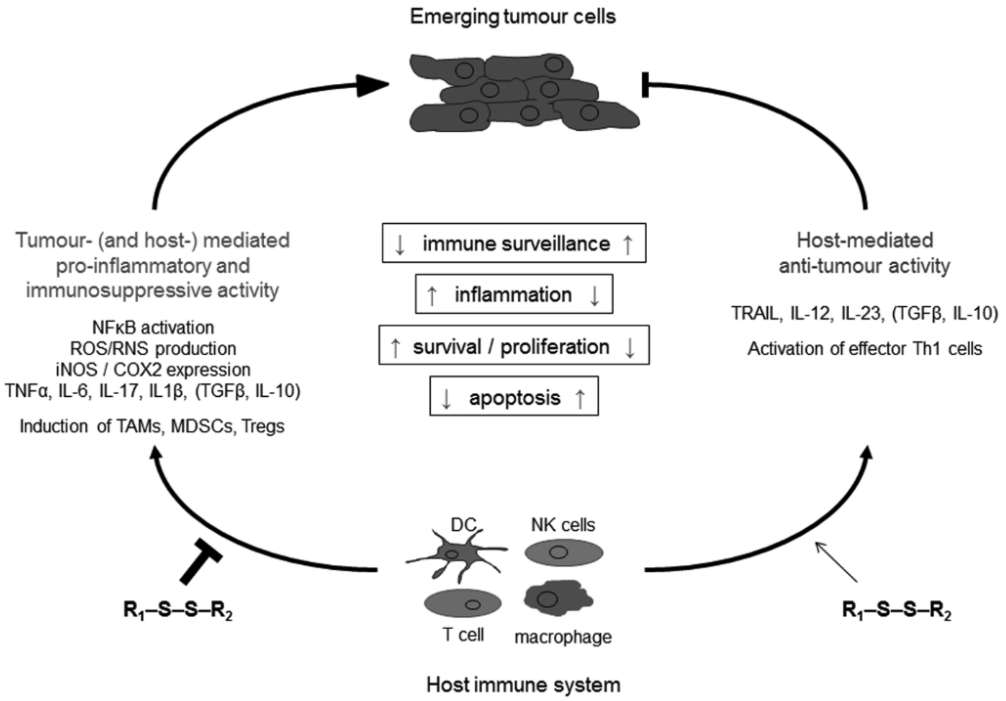

Figure 1.6: Immunogenic pathways of garlic OSCs.
Taken from Kaschula *et al*.[125]

In light of this, further mechanistic studies are required to better understand the immunomodulating effects of garlic OSCs at the various stages of tumorigenesis.

1.17 Induction of Apoptotic Pathways

Apoptosis, also known as programmed cell-death, is a tightly regulated cellular event that involves coordinated DNA fragmentation and the degradation of cytoskeletal and nuclear proteins, which leads to the collapse of the cell without eliciting an inflammatory response. It is initiated by two distinct signalling pathways, namely the intrinsic or extrinsic pathway, along the caspase cascade, which are shown in **Figure 1.7**.

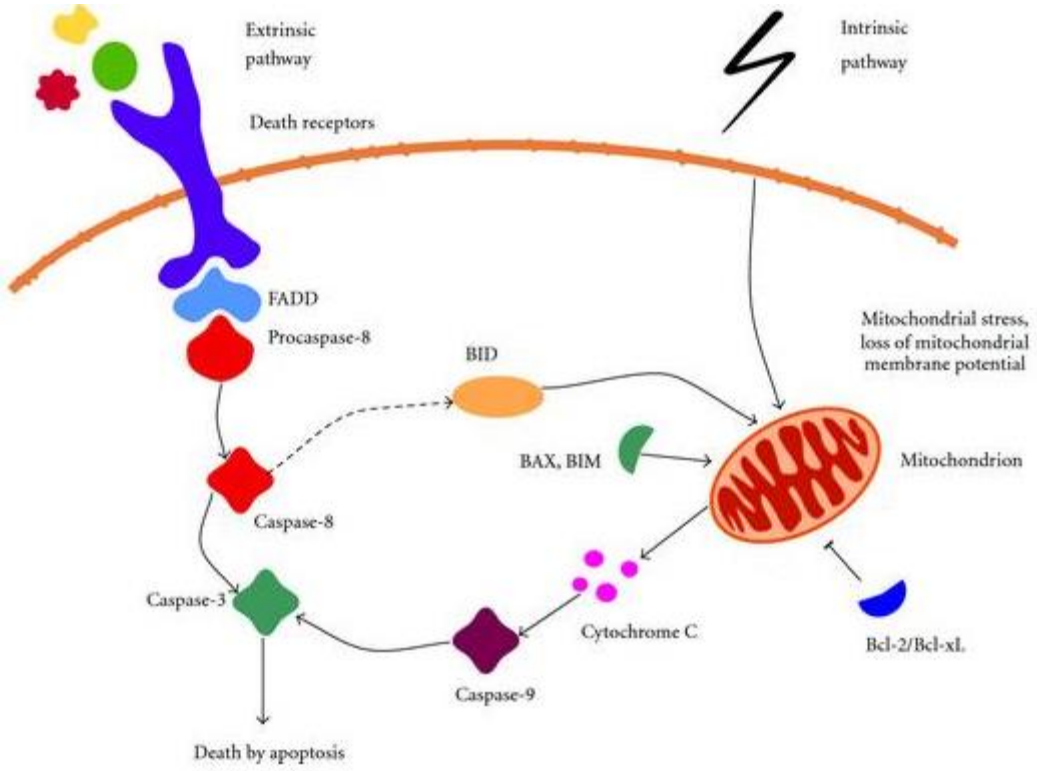

Figure 1.7: The two initiation pathways leading to apoptosis.
Taken from Filén *et al*.[127]

The extrinsic pathway relies on the activation of cell-surface death receptors by extracellular ligands, which subsequently activate caspase-8. The intrinsic pathway, also known as the mitochondrial pathway, is activated in response to intracellular stimuli such as DNA damage, cell-cycle abnormalities and oxidative stress. The subsequent upregulation of pro-apoptotic (e.g. Bim, Bak and Bax) and the downregulation of pro-survival (e.g. Bcl-2 and Bcl-xL) members of the Bcl-2 protein family induce the permeabilization of the outer mitochondrial membrane, which causes a release of cytochrome c, resulting in the activation of caspase-9. The activation of initiator caspases (e.g. caspase-8 and/or caspase 9) then activate the executioner caspase, caspase-3, to initiate a proteolytic chain reaction that degrades cellular components.[128]

The bioactivity of garlic OSCs has been described in a wide range of cancer cell-lines and is believed to involve mitochondria-mediated apoptosis.[83,96,104] Although the exact mechanisms still remain unclear, there is a consensus that individual garlic OSCs may share analogous effects on certain apoptotic pathways. These include the promotion of pro-apoptotic signalling in mitogen-activated-kinase (MAPK) pathways, including JNK, p38 and ERK1/2, as well as the inhibition of the survival Akt pathway, as shown in **Figure 1.8**.[87,129]

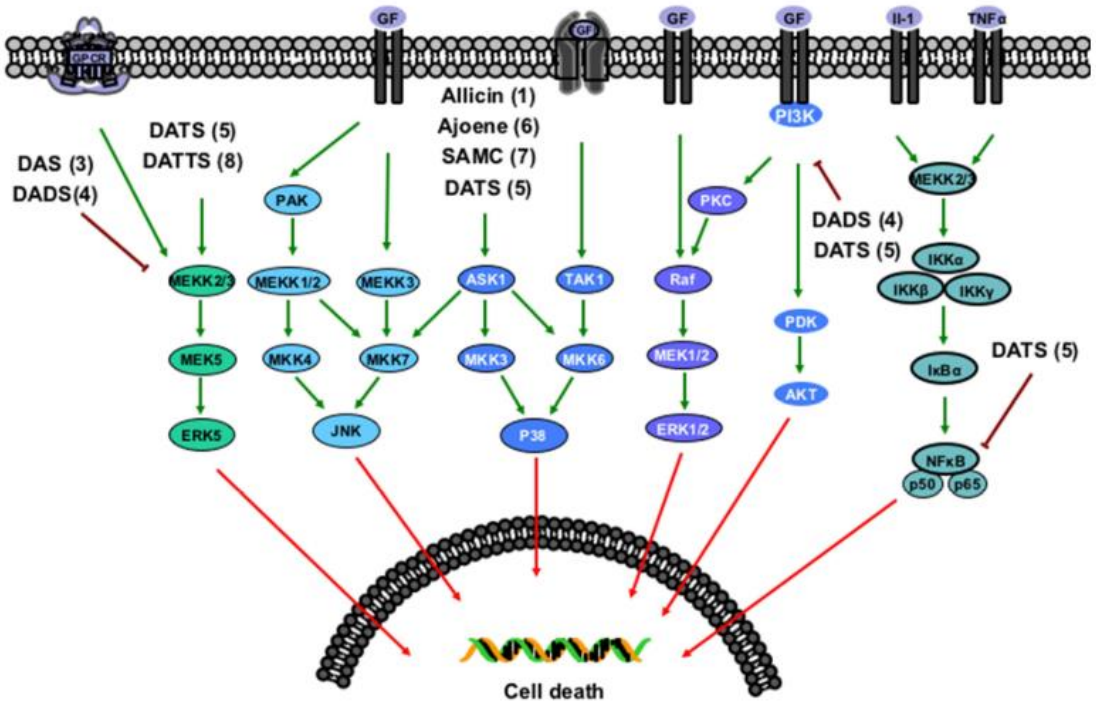

Figure 1.8: Upstream kinase pathways involved in the pro-apoptotic effect of OSCs.
Taken from Yagdi *et al*.[96]

Several studies have shown that OSCs upregulate the expression of p53, a cellular sensor for DNA damage, which lies downstream in the kinase signalling pathways. p53 is one of the primary upstream effectors that regulates the expression of the Bcl-2 family, which coincides with experimental observations that OSCs most commonly increase pro-apoptotic Bax and decrease antiapoptotic Bcl-2.[89,96,130–132]

The direct targeting of redox-sensitive signalling proteins at their thiol residues by OSCs within the cell leads to an increase in intracellular ROS, DNA damage, ER stress, and G_2/M arrest which are in turn responsible for the expression of the stress-induced apoptotic pathways.[81,83,86,104,133]

1.18 Metastasis

In advanced stages of cancer, malignant tumours alter their microenvironments to invade adjacent tissues, achieve vascularisation, enhance nutrient supply, and metastasise throughout the body via the circulatory system .[102,103]

The garlic OSCs, allicin, ajoene, SAMC, DADS, and DATS, have been shown to inhibit the migration and invasion of cancer cells by suppressing histone deacetylase activity and disrupting cell migration through the interaction with cytoskeletal proteins.[134–142] More

specifically, in our lab, we have found that ajoene binds to vimentin, which affects its ability to form functional filaments that may be related to the observed antimetastatic activity of ajoene.[137]

1.19 Cancer Intervention Strategies using Garlic OSCs

Garlic OSCs have successfully been investigated in clinical studies for non-communicable diseases, such as cardiovascular disease and diabetes, where they are shown to be effective and safe.[44,143,144] Despite this, and the numerous studies supporting the *in vitro* and *in vivo* anticancer activities of garlic and its OSC constituents, there is little published clinical evidence showing their therapeutic potential in cancer. Cancer is a complex pathology, and garlic, possessing many bioactive compounds, lacks the luxury of having a standardised preparation, which, in turn, makes the recommendation of a therapeutic dose of its active ingredients challenging. Emerging insights into the anticancer properties of garlic OSCs have highlighted potential intervention strategies that involve their use as chemopreventative, chemosensitizing and multi-target therapy agents.[26,145,146]

Chemoprevention has been the most consistently recognized anticancer property of garlic, the latter recommended as a food supplement for cancer patients. Epidemiological studies have attributed a high garlic intake with a decreased risk of several cancers, and this is attributed to an improvement in bodily antioxidant status, the modulation of oxidative stress and immune function. Some reports on garlic OSCs have drawn attention to their ability to counteract chemoresistance. Considering the molecular complexities of cancer, the development of chemoresistance is common when mono-chemotherapy is adopted as the first line of treatment.[147] Garlic compounds, specifically allicin, ajoene and SAMC, have demonstrated chemosensitizing effects by synergistically enhancing the therapeutic responses of commonly used cytotoxic drugs, including tamoxifen, cytarabine, fludarabine and rapamycin.[148–150] Moreover, DATS and ajoene have shown to reverse multidrug resistance by directly interacting with multi-drug resistance proteins (MRPs) and P-glycoproteins.[151,152]

Insights into the unique sulfur chemistry of garlic OSCs have attributed the anticancer potential of OSCs to its ability to target multiple cysteine residues inside cancer cells. These constitute the redox-mediated regulatory framework that control many cellular

functions, including antioxidant, enzyme function, cytoskeletal structures, and protein folding, to name a few.[86,104,153] In cancer, this manifests as OSCs simultaneously targeting multiple, if not all, of the hallmarks of cancer (**Figure 1.9**).[96,146]

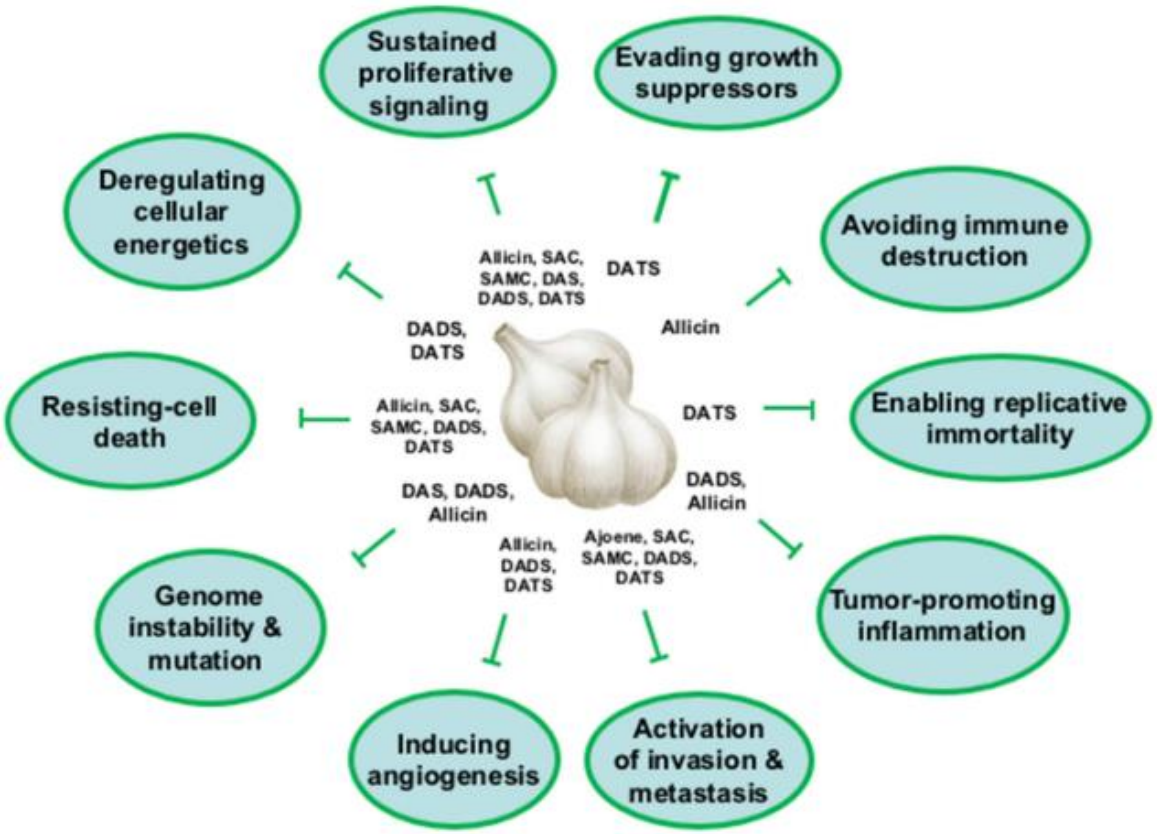

Figure 1.9: Overview of anticancer potential of OSCs targeting cancer hallmarks.
Taken from Yagdi *et al*.[96]

Since multi-targeted therapy has shown to provide a necessary avenue for combating a multi-faceted disease like cancer, garlic OSCs may provide interesting therapeutic solutions.[154] In this regard, a further understanding of the sulfur chemistry of OSCs, and investigations into cancer-related cysteine targets, may also contribute to the discovery of novel anticancer drug targets and intervention strategies.

Chapter 2 : The Chemistry of Ajoene

2.1 Ajoene

Ajoene is a second-generation OSC that arises from the thermal rearrangement of allicin and is encountered in high concentrations when macerated garlic is cooked or aged as in the preparing of food.[155,156] Numerous studies on ajoene have ascribed a variety of beneficial health effects to garlic such as anti-inflammatory,[118] antioxidant,[109] antithrombotic,[157] antimalarial,[158] antiobesity,[159–161] antibacterial,[162,163] antifungal[164–166] as well as anticancer activity.[153,167,168] Our research has been aimed at exploring the potential of ajoene as a chemopreventative and chemotherapeutic agent against cancer cell growth and metastasis.[145,148,167,169–171] The following chapter reviews the chemistry of ajoene with emphasis on: i) the discovery of ajoene and its biosynthesis, ii) the total synthesis of ajoene and its analogues, and iii) the biological chemistry of ajoene with emphasis on the thiol-disulfide exchange reaction and a structure-activity relationship analysis of its pharmacophore.

2.2 Exploration of the Biosynthesis of Ajoene

Ajoene, (*E*,*Z*)-1-allyl-2-(3-(allylsulfinyl)prop-1-en-1-yl)disulfane (**Figure 2.1**), was first reported in 1983 by Apitz-Castro from the CSIC in Caracas, Venezuela, during investigations into the antithrombotic activity of garlic extracts.[172]

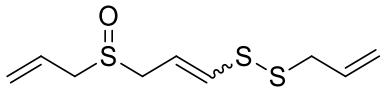

Figure 2.1: Chemical structure of (*E*,*Z*)-ajoene.

In collaboration with Professor Eric Block of Albany University in the US, the structure of ajoene was elucidated and reported in two papers published in 1984 and 1986, in which the name "ajoene" was coined after the Spanish word for garlic "*ajo*" (pronounced "*aho*") together with the suffix "*-ene*" for alkene.[51,157] Ajoene occurs naturally as a mixture of *E*/*Z*-stereoisomers that contain a unique sulfoxide vinyl disulfide motif rarely found in other natural products. These two papers postulated a possible biosynthetic mechanism to ajoene, involving the combination of two allicin molecules,[51] as shown in **Scheme 2.1**.

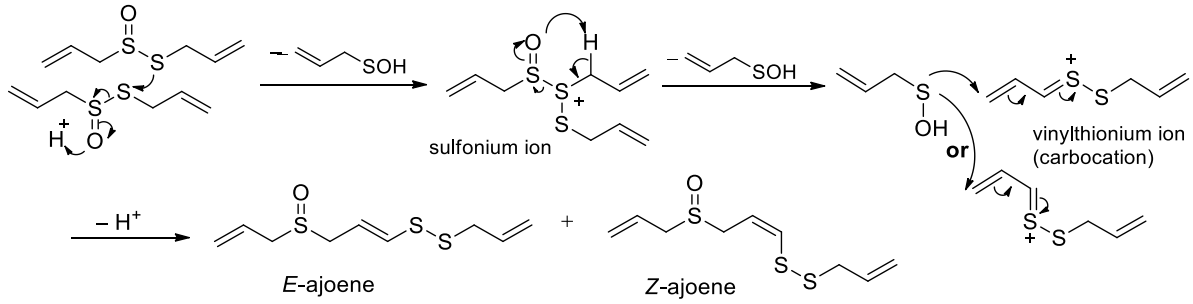

Scheme 2.1: Proposed ajoene biosynthesis by Block *et al*.

In the first step, *S*-thioallylation of allicin produces a sulfonium ion with the elimination of 2-propenesulfenic acid. The sulfonium ion then undergoes β-elimination to give a thiocarbocation (a vinylthionium ion), which undergoes a γ-addition (Michael-type) with 2-propenesulfenic acid at the terminus of the vinylthionium moiety to give ajoene as an *E*/Z-mixture of stereoisomers. After some synthesis trials that employed an unsuccessful sulfoxide thio-Claisen rearrangement approach, Block *et al.* achieved the first "total" synthesis of ajoene using biomimicry. He postulated that all garlic allyl-OSCs originate from allicin via variations of the rearrangement pathway depicted in **Scheme 2.1**, and thus achieved the synthesis by heating allicin in aqueous acetone,[157] as illustrated in **Scheme 2.2**.

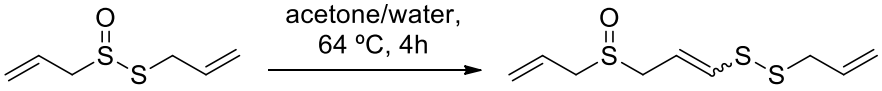

Scheme 2.2: Block's synthesis of (*E*,*Z*)-ajoene.

One of these thermal rearrangement products was ajoene, which was obtained in 34% yield after column chromatography in an *E*:*Z* ratio of 4:1.[157] Interestingly, when ajoene is isolated from fresh preparations of oil-macerated garlic, it yields predominantly the *Z*-isomer as the kinetically favoured product.[43] In 2008, Nanzin *et al*. showed that ajoene is more stable to UV-light than temperature and that on prolonged (9-month) storage, the *E*:*Z* ratio of ajoene shifted to 5:1 in favour of the thermodynamically stable but less biologically active *E*-isomer.[155] The isomerisation is formally a 1,3-hydride shift in which the release of 1,3-allylic strain drives the equilibrium. However, as a thermal sigmatropic, concerted process, [1,3]-hydride shifts are antarafacial and geometrically unfeasible. Hence, under basic conditions, the rearrangement is likely to be heterolytic in view of the

sulfoxide's ability to stabilise an adjacent α-carbanion. A summary of each mechanism is given in **Scheme 2.3**.

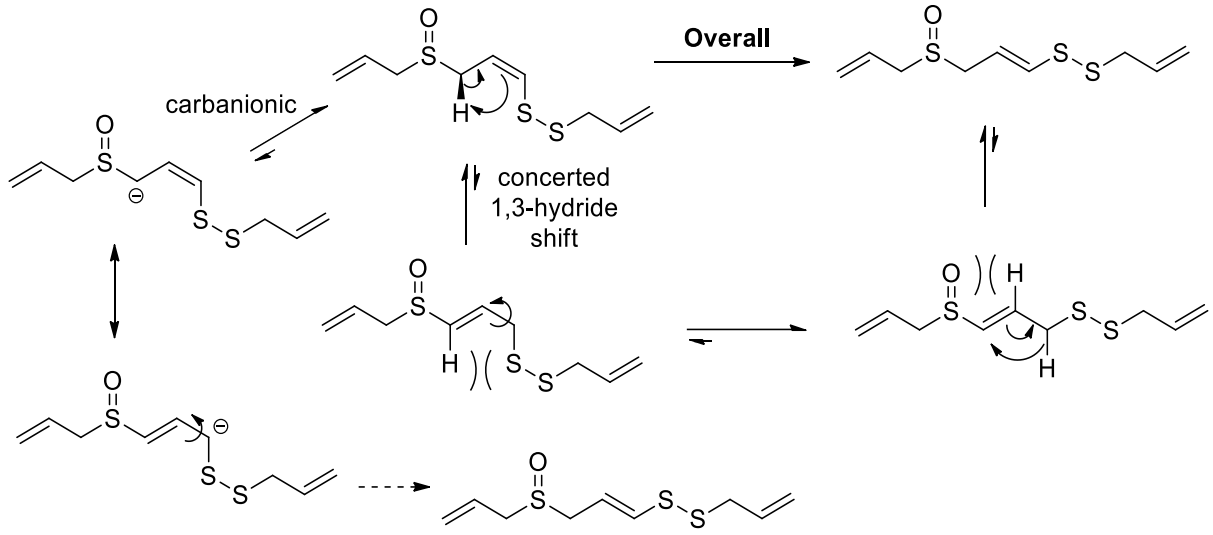

Scheme 2.3: Thermal isomerisation of *Z*-ajoene to *E*-ajoene.

This seminal work by Block *et al.* gave access to synthetic ajoene, which enabled further research into the molecule's promising biological properties. Although subsequent multiple patents, attempting to improve the efficiency of this one-pot conversion of allicin were filed, before 2008 a method of generating substituted ajoenes for SAR studies was not available.[173]

2.3 The UCT Ajoene Derivative Synthesis

With an interest in studying the antiproliferative properties of ajoene analogues in cancer cells, in 2008 our laboratory at UCT published a concise 4-step synthesis that allowed access to end-group modified analogues in an overall 30% yield (**Scheme 2.4**).[170] The first step of the method involves the *S*-propargylation of an appropriately R^1-substituted thiol in which the R^1-group ends up on the sulfoxide end (left-hand side) in the final ajoene molecule. In the case of a commercially available R^1-substituted thiol, standard propargylation conditions (KOH, propargyl bromide, MeOH) affords thioether **A**. Alternatively, it is possible to access the thiol by first preparing an isothiouronium salt by refluxing a suitable R^1-substituted alkyl halide and thiourea in acetonitrile. The filtered and washed salt is then hydrolysed to generate the thiol, which is propargylated *in situ* to form the desired R^1-substituted thioether **A**. Yields in this step are high (> 90%).

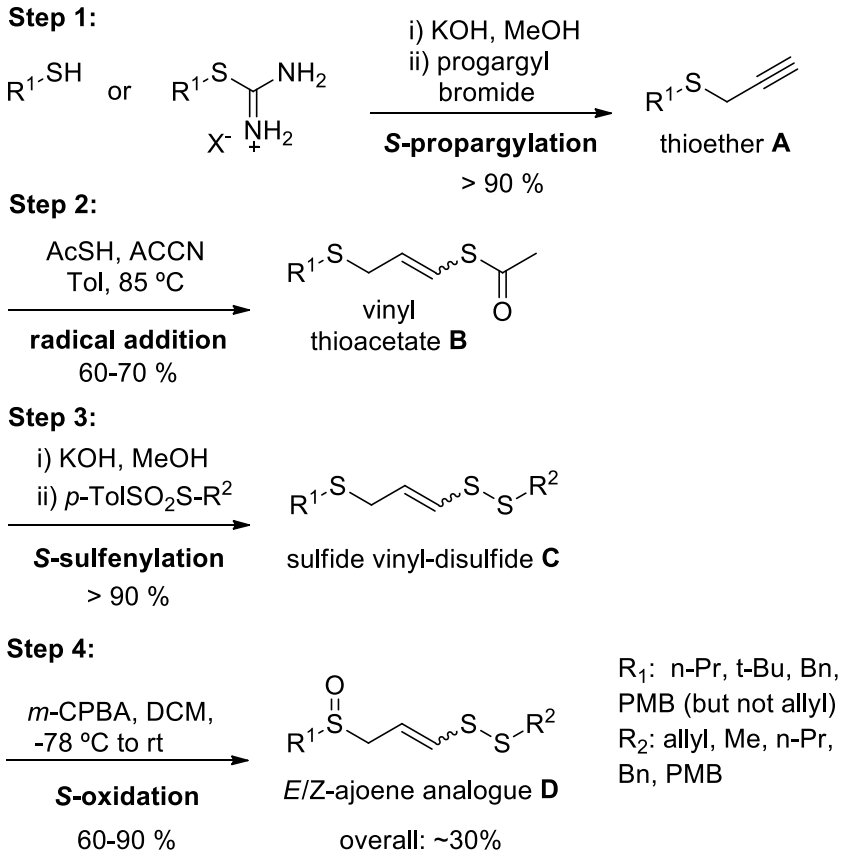

Scheme 2.4: UCT synthesis for doubly end-substituted ajoene analogues.

In the second step, thioacetic acid regioselectively adds to the thioether **A** via radical addition to the triple bond terminus under thermal conditions. This generates the protected vinyl thioacetate **B** relevant to the target. ACCN (1,1′-azobis(cyclohexanecarbonitrile)) is used as the radical initiator for the reaction. Its labile 1,1'-azobis core undergoes thermal radical cleavage at 85 °C to give an active α-cyano radical.[174] The full mechanism for the radical addition step is shown in **Scheme 2.5**.

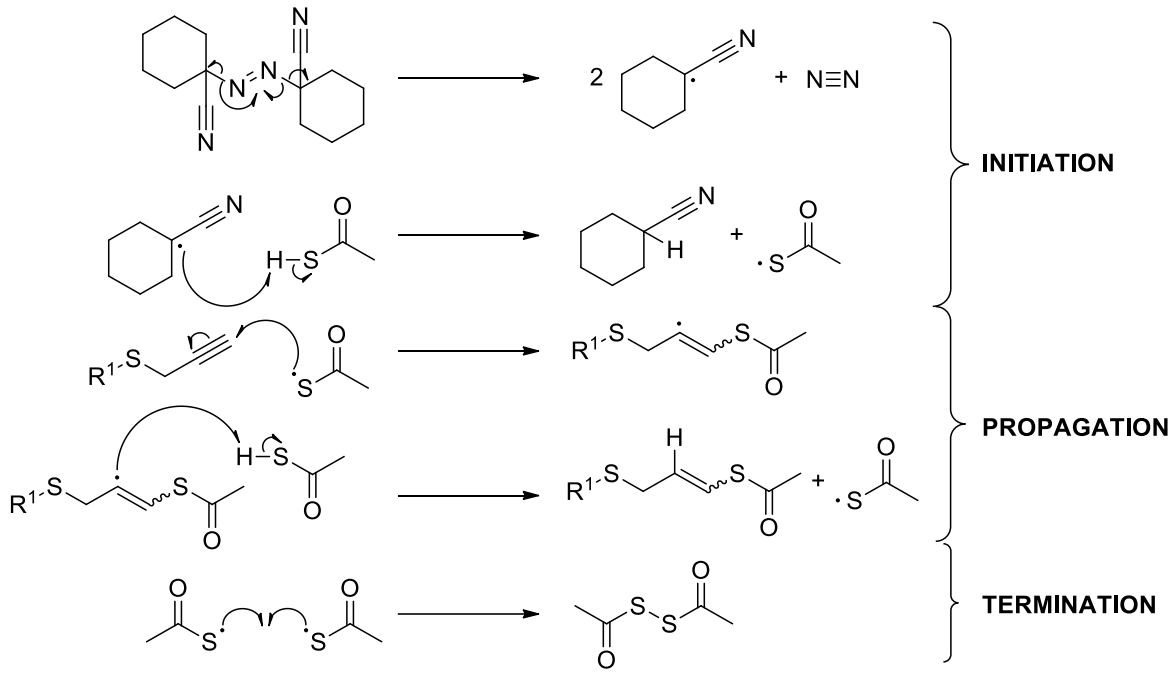

Scheme 2.5: Radical addition of thioacetic acid onto the propargylic thioether A.

In the initiation step, the α-cyano radical abstracts a proton from thioacetic acid. For the propagation steps, the resultant thiyl radical then regioselectively adds to the alkyne terminus of the propargylic thioether **A** to form a vinyl thioacetate β-radical. This radical then abstracts a proton from thioacetic acid to afford the desired stereoisomeric vinyl thioacetate **B** as a mixture of *E*:*Z* isomers in a ratio of approximately 1:2. This step propagates the chain reaction, since it regenerates another thiyl radical. Reduction of the *Z*-thioacetate radical intermediate is sterically less demanding than that of the *E*- and thus the *Z*-isomer is formed faster than the *E*-isomer (kinetic control). Coincidentally, the *Z*-isomer represents the more desirable product in view of its superior bioactivity.[170] Undesirable termination involves dimerization of two thiyl radicals to form a disulfide diacetate by-product. Yields for this step of the sequence vary depending on the substrate but are generally around 60-70% in a 1:2 (*E*:*Z*) ratio. The preparation of the natural product ajoene itself is not possible via this route owing to a suspected intramolecular cyclisation (5-*exo*-trig or 6-*endo*-trig) of the radical onto the allyl-substituent (R^1 = allyl) during the radical addition step.

The vinyl disulfide formation in Step 3 introduces an -SR^2 substituent into the right-hand side (disulfide end) of the ajoene molecule in the form of the vinyl disulfide. From a practical perspective, thioacetate ester **B** is first hydrolysed with KOH to generate an enethiolate anion. Thereafter, the enethiolate is sulfenylated at its soft sulfur end with the

R^2-substituted *p*-toluenethiosulfonate (sulfenylating agent) to afford vinyl disulfide **C**. The product ratio of *E:Z* (1:2) does not change significantly towards favouring the *E*-isomer when the temperature is kept low (less than 0 °C). However, at higher temperature, isomerization can occur, presumably via a bond rotation about the C_α-C_β axis (shown via the carbanion but this could also involve neutral tautomers as enethiol and thioaldehyde) to enrich the thermodynamically more stable *E*-isomeric form, as shown in **Scheme 2.6**.

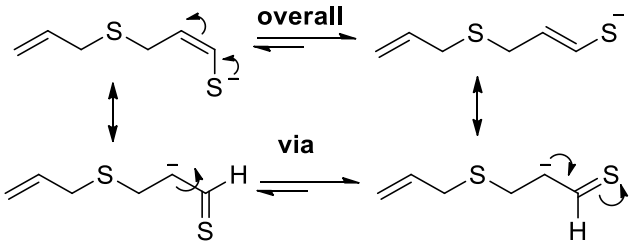

Scheme 2.6: Stereoinversion mechanism for ajoene enethiolate.

Yields for the overall transformation to afford the vinyl disulfide **C** were usually fairly acceptable in the region of >75%. The final step in the ajoene analogue synthesis involves a low temperature chemoselective oxidation. Reaction of the sulfide vinyl disulfide **C** with a molar equivalent of *m*-CPBA at low temperature (-78 °C), results in only the sulfide sulfur, the most nucleophilic of the three, being (mono)oxidised to afford the sulfoxide **D**. The sulfoxide **D** is produced as a racemate in which its *E:Z* ratio (quantified by NMR) is retained from the previous compound within experimental (column chromatography) consideration. Yields for this step were normally around 75%, making for a 30 – 40% overall yield for the sequence.

The UCT method has been used by Prof R. Jeon at the Sookmyung Women's University, in South Korea, to produce ajoene analogues as active ingredients in preparations and pharmaceutical compositions to prevent and/or treat various cancer types. After the expiry of our 2010 patent on the synthesis of substituted ajoene derivatives, the Sookmyung Women's University Industry Academic Cooperation Foundation filed their own application of the method in July 2016 (accepted Jan 2018).[175,176] This falls in line with the investigations by Hwang *et al.* into the activities of SPA3015 ((*E*)-1-phenyl-7-phenyl-2,3,7- trithiahepta-4-ene 7-oxide, shown in **Figure 2.2** in multidrug-resistant cancer.[152]

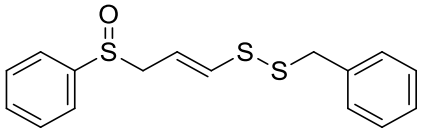

Figure 2.2: Hwang's pharmaceutical lead, SPA3015.

2.4 Further Development of Ajoene Total Synthesis

In 2012, Givskov and Jakobsen *et al.* working at the Costerton Biofilm Centre at the University of Copenhagen on the antibacterial effect of garlic, discovered that ajoene inhibits small regulatory RNAs (sRNA) in *Pseudomonas*. *aeruginosa* as well as in *Staphylococcus aureus* that control gene expression (e.g. for virulence factors) controlled by quorum sensing.[163] Their patent, filed in the same year, was subsequently obtained by the UK Biotech Company, Neem Biotech Ltd., whose lead compound, NX-AS-401, aims to treat patients with cystic fibrosis and is going into clinical trials.[177,178] In 2018, Wirth *et al.*, funded by Neem Biotech Ltd., published the first total synthesis of ajoene, which is shown in **Scheme 2.7**.[179]

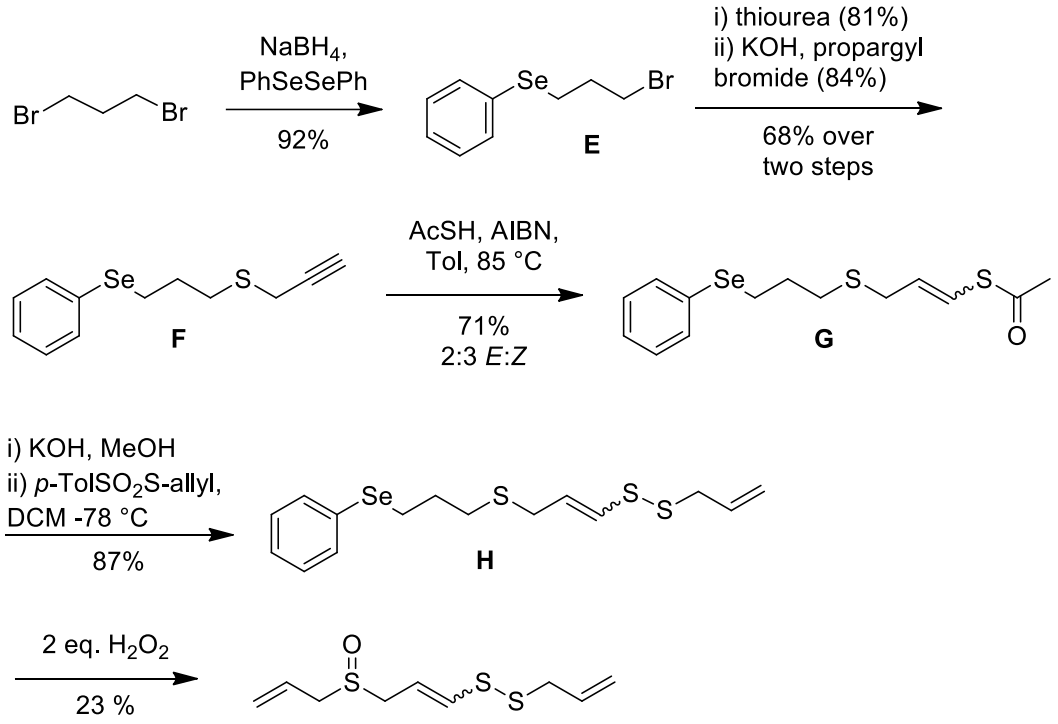

Scheme 2.7: Total synthesis of ajoene.
Adapted from Wirth *et al.*[179]

This route builds onto our previously published synthetic route, which fell short of being to synthesise the natural product itself. This was overcome by employing a masked form

of the left-hand allyl group to avoid the radical cyclisation mentioned previously. Selenoxide elimination chemistry at the end then installed the allyl group. Thus, the first step of this sequence begins with the instalment of the selenide. Here 1,3-dibromopropane was treated with an *in situ* generated phenylselenide anion, generated from diphenyl diselenide, to give the bromide **E**. Compound **E** is then thiopropargylated, followed by the regioselective radical addition of thioacetic acid to terminus of **F** to give the thioacetate **G** (viz. **Scheme 2.5**). This is hydrolysed *in situ* and sulfenylated using allyl toluenethiosulfonate to give the vinyl disulfide **H** as per our 2008 synthesis.[170] In the final step of this synthesis, the selenide sulfide vinyl disulfide **H** is treated with 2 equivalents of H_2O_2 to form ajoene as a 2:1 mixture of *E*/Z-stereoisomers in 23% yield. Although this step only produces a low yield, it is elegant in that both the sulfide and selenide moiety are both oxidised in a single step to generate the left-hand allyl group through elimination, and sulfur oxidation to the desired sulfoxide.

To address the drawbacks of using selenium chemistry, which had resulted in poor scalability and low yields of this method, Wirth *et al.* published a revised 6-step total synthesis of ajoene in 2020, which is shown in **Scheme 2.8**.[180]

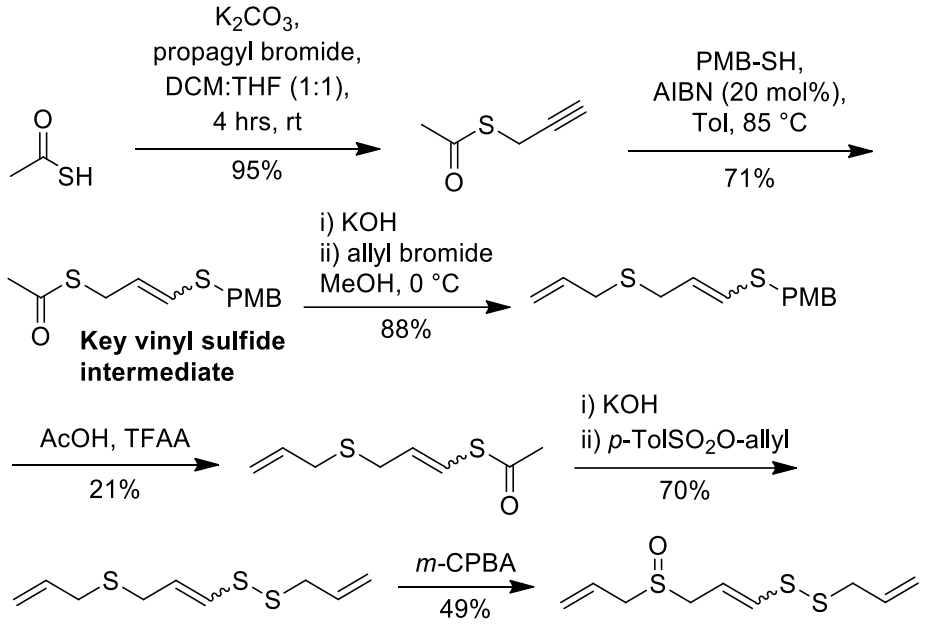

Scheme 2.8: Revised synthesis of ajoene.
Adapted from Wirth *et al.*[180]

Again, the chemistry essentially follows the same sequence as that of our 2008 paper,[170] but with the crucial difference of using two protecting groups to generate the key

protected vinyl sulfide intermediate as shown. Compared to our 2008 synthesis, PMBSH is used in the radical addition step to generate an acetylthio-vinyl sulfide (labelled as the "key vinyl sulfide intermediate" in **Scheme 2.8**) rather than an allylthio-vinyl thioacetate. Thereafter, the thioacetate can be selectively deprotected and allylated to install the ajoene left-hand side without using selenium chemistry, while the *S*-PMB can be deprotected under acidic acylation conditions to generate a novel allylated vinyl thioacetate. The weak step is the PMB deprotection of 21%, which significantly reduces the overall yield of the synthesis. The synthesis was followed up by Wirth in ajoene derivative medicinal chemistry studies against *P. aeruginosa*. in conjunction with combatting cystic fibrosis.[181]

2.5 The Mechanism of Action of Ajoene

Numerous studies have reported that the antitumorigenic effects of ajoene are attributed to its ability to induce cell-cycle arrest and apoptosis in cancer cells.[83,145,148] However, ajoene has also been shown to inhibits metastasis,[137,168,182] angiogenesis,[145] cell proliferation[80,183,184] and cell adhesion,[137,185]. Furthermore, ajoene has been shown to have a level of selectivity for cancer over normal cells,[167,186] while being relatively non-toxic *in vivo.*[187] Although the underlying chemical biology is still unclear, it has been postulated that ROS generation[89,115,188] and/or *S*-thioallylation reactions with a biological thiol may be important.[81,153,189] Although several publications ascribe the cytotoxicity of ajoene to the intracellular generation of ROS, a deeper inspection of the chemistry of its vinyl disulfide pharmacophore has suggested that its ability to form mixed disulfides with target proteins is more likely to be the primary molecular event in which ROS generation may constitute a secondary/downstream event to thiolysis exchange.[81]

2.5.1 Ajoene Targets Cellular Cysteine Residues

Several studies have shown that garlic OSCs containing a thiosulfinate or polysulfide (S ≥ 2) functional group, can undergo thiol-disulfide exchanges with cysteine to produce mixed disulfides with the expulsion of allyl mercaptan as the leaving group.[45,56] To date, several cysteine residues of redox-sensitive proteins have been shown to be susceptible to *S*-thiolation by garlic OSCs.

In one study, Gruhkle *et al.* found that allicin modifies proteins through *S*-thioallylation in the proteome of immortalised human T-Cell leukaemia (Jurkat) cells.[86] Their study

revealed that allicin treatment caused widespread oxidative modification of targets of essential cellular function, many of which are known targets for cancer therapy. The induced apoptotic effects of allicin were attributed to the modification of cysteine residues on structural proteins such as tubulin and actin, heat shock chaperones HSP90 and HSPA4, glycolytic enzymes GAPDH and PKM, as well as the protein translation factor EEF2. In another study on DATS, Hosono *et al.* demonstrated that it supresses the proliferation and induces apoptosis in human colon cancer cells (HCT-15 and DLD-1) by *S*-thioallylating Cys-12β and Cys-354β in β-tubulin.[82]

The *S*-thioallylation properties of ajoene were first reported by Scharfenberg *et al.* in 1991, who demonstrated that ajoene is capable of reacting with the thiol group of cellular glutathione in cultured cancer cells.[186] The detection of *S*-thioallylated glutathione and cysteine conjugates in the lysates of the treated cells suggested that disruption in cellular thiol homeostasis had occurred, and that *S*-thiolation may be responsible for the observed cytotoxic effect, which were twice as pronounced in cancer cells versus normal cells.[190] In another paper by Gallwitz *et al.* in 1999, ajoene was shown to directly inhibit the activity of glutathione reductase (GR) through the formation of a mixed disulfide with the active site cysteine (Cys-58).[189] GR is a central regulator of oxidative stress. Our group has recently found that ajoene modifies the structural protein vimentin through *S*-thioallylation at Cys-328 leading to antimetastatic effects.[137] These combined insights into the thiol-modifying behaviour of ajoene suggested that ajoene may similarly affect other cellular proteins to modulate their structure and function by mimicking the mechanistic principle of GSSG as an electrophile.[191–193]

One of our group's recent investigations on ajoene aimed to explore its mechanism of action in MDA-MB-231 breast cancer cells by synthesising a fluorescently-tagged ajoene analogue called dansyl ajoene (DP).[153]

Following a regioselective thiol-disulfide exchange with a protein thiol (this regioselectivity aspect will be extrapolated on later), the fluorescent dansyl label of DP was expected to be transferred to its intracellular protein targets, as shown in **Figure 2.3**.

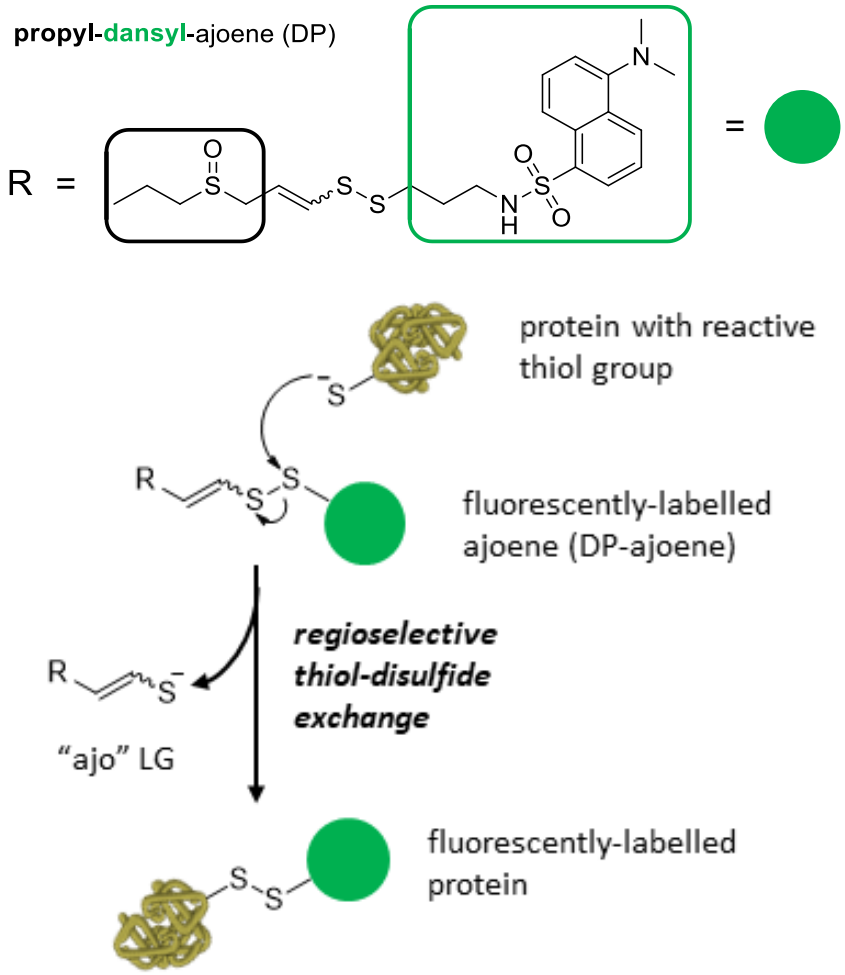

Figure 2.3: The fluorescent-labelling of proteins with DP in MDA-MB-231 cancer cells.

In such a way, by fluorescently labelling ajoene, we were able to track its movement and localisation in MDA-MB-231 cancer cells using confocal laser microscopy. In this study, it was shown for the first time, that ajoene localises to the endoplasmic reticulum (ER) in MDA-MB-231 breast cancer cells.[153] A western blot experiment on untreated and DP-treated MDA-MB-231 cell lysates, probed if proteins had been labelled with the dansyl fluorophore using an antibody specific to the dansyl label. The proteins were separated by SDS-PAGE under both non-reducing and reducing conditions as treatment of the cell lysate with a reducing agent was expected to cleave the dansyl label from the protein. The resulting western blot visualised using an anti-dansyl primary antibody and a chemiluminescent secondary antibody, is shown in **Figure 2.4**.

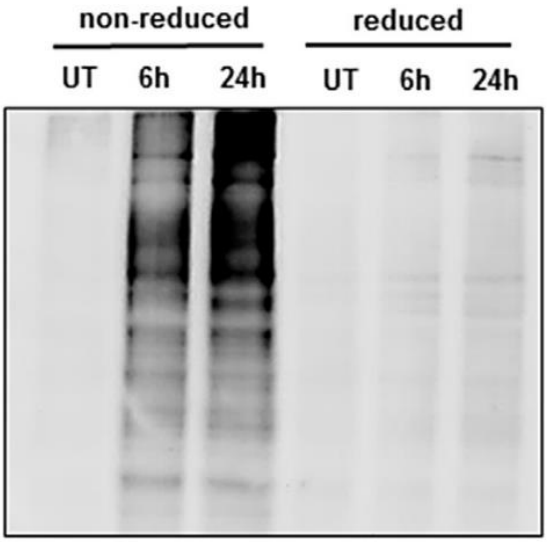

Figure 2.4: Western blot of lysate from MDA-MB-231 cells treated with DP for 6h and 24h.
UT = untreated. Taken directly from Kaschula *et al.*[153]

Surprisingly, multiple dansylated proteins were observed in the lysate of treated MDA-MB-231 cells, and the intensity of the labelling increased with time indicating a time-dependent effect after 6 and 24 hours. The lane marked "UT" is the untreated lysate representing the negative control. The addition of a disulfide reducing agent (DTT) to the lysate prior to the western blot analysis resulted in a loss of the anti-dansyl signal (**Figure 2.5**), supported our hypothesis that the dansyl tag was attached to the target proteins via a disulfide linkage.

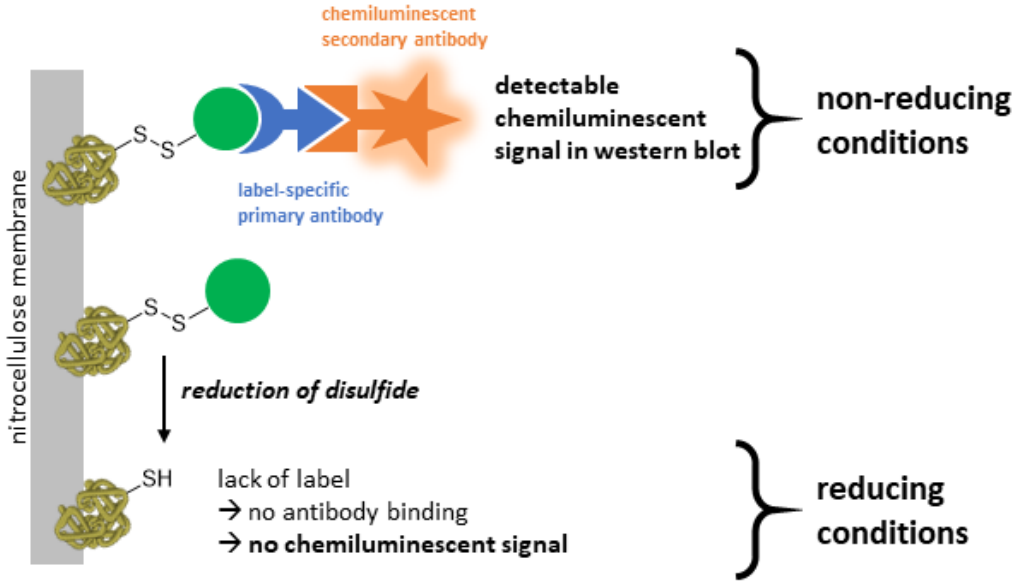

Figure 2.5: Detection of the DP protein targets in MDA-MB-231 cancer cells.

This study demonstrated that many *S*-thiolation reactions occur in breast cancer cells between ajoene and protein thiol. The covalent modification of a number of proteins via thiolysis exchange is likely the driver behind its anticancer activity.

Thiol-disulfide exchange reactions are continuously occurring in biological systems, where they play a central role in protein folding, in maintaining the metabolic redox state of a cell, and in modulating the activity of several regulatory enzymes in fundamental intra- and intercellular signalling pathways.[54,60,194] A closer look at the chemistry of the thiolysis exchange between ajoene and its cellular targets is required to understand its mechanism of action in cancer cells.

2.5.2 Ajoene and the Chemistry of the S-thiolysis Exchange

Thiolysis exchange reactions, also known as thiol-disulfide exchanges, are pH-dependent bimolecular nucleophilic substitution reactions. Here, the single, rate-determining step involves the attack of a thiolate nucleophile onto the disulfide, with the formation of a linear, anionic trisulfide transition state, followed by the expulsion of a thiolate leaving group and the formation of the disulfide product, as shown in **Scheme 2.9**.

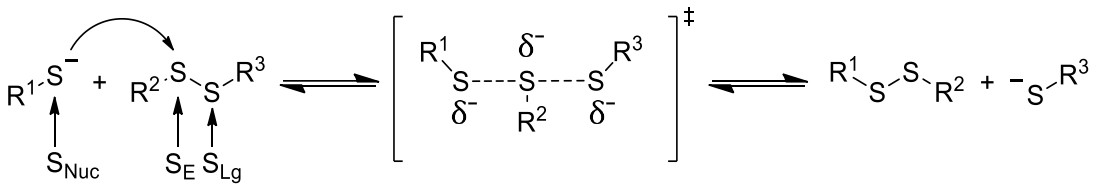

Scheme 2.9: *S*-thiolysis exchange.

To be able to explain the reactivity of ajoene and its selectivity towards cellular thiol targets, the kinetic and thermodynamic parameters that govern thiolysis exchange reactions needs to be considered. These relate to the chemical influence of the three participating sulfur atoms: namely, the incoming nucleophilic sulfur (S_{Nuc}), the electrophilic central sulfur (S_E) and the expelled leaving group sulfur (S_{Lg}).

2.5.2.1 Factors Affecting Thiol Reactivity

Before addressing the mechanistic details of the thiolysis exchange, some important features pertaining to the formation of the thiolate (S_{Nuc}) and its nucleophilicity will be

discussed. With its larger sulfur atom, a thiol RSH with R as an alkyl group, as with cysteine, is a weak acid. However, it is more acidic (pK_a 9-10; pK_a(Cys) = 8.6) than an alcohol ROH (pK_a 16-18). This is counter-intuitive based on electronegativities (O > S) and may be attributed to the much weaker SH bond compared to that of OH on account of the larger size of sulfur and its third row character (S overlap with H is poorer). The larger size of sulfur also helps to accommodate the negative charge through dispersion. Consequently, in aqueous medium the thiolate is more readily formed, as the pK_a of a thiol is lower than that of water (pK_a 15.7). The Brønsted-Lowry proton-transfer reaction, with water acting as the base, is shown in **Equation A**.

Equation A: $$RSH + H_2O \rightleftharpoons RS^- + H_3O^+$$

Once ionised, the thiolate (RS^-) anion provides an excellent, soft nucleophile, which is far more nucleophilic than alkoxide in view of the thiolate's higher-energy HOMO. Nucleophilicity is crucial for understanding thiolysis rates in biological disulfide exchanges. In kinetic (i.e. rate) terms, the deprotonation of the thiol to its thiolate enhances the nucleophilicity of the sulfur atom by approximately 10^6-fold at a given pH. This large difference in nucleophilicity between the thiol and thiolate, highlights that the thiolate will dominate over the thiol in thiolysis over an extremely large ratio of the two.[85,195]

Thus, in a biological medium, pH is extremely important because it governs the degree of thiol dissociation. According to the Henderson-Hasselbalch equation for the reaction in **Equation A**, the thiolate concentration (as the conjugate base RS^-) increases logarithmically with decreasing pK_a for any thiol acid (RSH) at a particular pH as shown in **Equation B**, which is presented in the classical form on the left followed by a more user-friendly one on the right.[194]

Equation B: $$pH = pK_a + \log\frac{[SR^-]}{[RSH]} \qquad \text{or} \qquad 10^{(pKa-pH)} = \frac{RSH}{RS^-}$$

Looking at the two parameters of pH and pK_a, while the former in biological systems is controlled at around 7.4, the pK_a of a cysteine thiol (Cys-SH) in a protein, as a thiol of interest in this study, can vary from about 7.4 to 9.1 in non-catalytic cysteines.[196]

However, the pK_a of catalytic cysteine thiols can be as low as 2.9 due to stabilising effects within the local microenvironment. To put things into perspective, at pH 7, a thiol with a pK_a of 10 will be 0.1% dissociated in its thiolate form, whereas decreasing its pK_a to 9, increases the thiolate concentration 10-fold to 1%. Importantly, when the pH = pK_a (i.e. about 7), the concentrations of thiolate and thiol are equivalent.

Assuming a biological pH of 7, as the Cys pK_a reduces below 7, the thiolate concentration starts to significantly outweigh that of the thiol, which implies a significant increase in nucleophilicity of the system, with a significant increase in the rate of thiolysis exchange. However, there is a caveat, and that is that the nucleophilicity of the thiolate does not stay constant with decreasing pK_a. As the pK_a lowers, the strength of Cys-SH as a Brønsted acid increases, which means that its conjugate base stability increases too. In turn, this translates to a lower nucleophilicity of the thiolate anion. In orbital energy terms, lowering the pK_a lowers the thiolate (as conjugate base) HOMO energy, which for the thiolysis places the thiolate HOMO energy further away from that of the soft disulfide LUMO. According to FMO theory relating to HOMO/LUMO orbital energy changes in the transition state affecting the reaction rate, this HOMO/LUMO energy difference appears as a denominator term in the Klopman-Salem equation, and its increase through separation results ultimately in a lower stabilisation of the transition state, meaning a higher activation energy and hence lower overall rate of thiolysis. Put together means that as the pK_a lowers, thiolate concentration increases while its nucleophilicity decreases, making for a non-straightforward relationship between pK_a and the rate of thiolysis exchange. Whiteside *et al.* were the first to demonstrate that alkyl and aryl thiolate nucleophilicities (as measured by the rate of nucleophilic attack on an electrophilic disulfide) follow a linear Brønsted relationship with pK_a as represented by **Equation C**.[195,197]

Equation C:

$$\log k = \beta_{\mathrm{Nuc}} \mathrm{p}K_{\mathrm{a}}^{\mathrm{RSH}} + \mathrm{C}$$

Where k is the rate constant for the nucleophilic attack of the thiolate, β_{Nuc} is a nucleophilicity constant (Brønsted coefficient) and C is a constant applicable to reactions of a disulfide with a series of thiolates under specified conditions. The Brønsted coefficient β_{Nuc} reflects the sensitivity of the reaction to the pK_a in which it establishes the change in atomic charge as the reaction proceeds from the ground state to the transition

state.[198] Using this equation, an empirical determination of values of the Brønsted coefficient (slope) and C (y-axis intercept) of a given disulfide system thus allows the future estimation of *k* for any thiol group based on its pK_a value. The results of extensive experimentation by Whitesides *et al.* and Hupe *et al.* on the rate of substitutions between disulfide substrates (GSSG and Ellman's reagent) and alkyl and aryl thiol groups showed that β_{Nuc} has an average value of 0.5 for disulfide exchange reactions at the physiological pH of 7.[199–201] This translates to the rate constant for the reaction of a thiolate anion, on average, decreasing by factor of 3.2 for each unit decrease in its pK_a value.[202]

With decreasing pK_a, the Whiteside **Equation C** therefore predicts a linear drop in the rate constant *k* for thiolysis exchange reactions. However, this is counterbalanced by an increasing concentration that follows a logarithmic relationship as given by the Henderson-Hasselbalch equation (**Equation B**), which has the reverse effect of increasing the rate. Putting these opposing effects together, the following combined equation is obtained:

Equation D:

$$\log k_{app}^{pH} = pK_a^{RSH}(\beta_{Nuc} - 1) + C - \log([H^+] + K_a^{RSH})$$

Where k_{app} is the rate of substitution at constant pH, the pK_a^{RSH} is for the thiol, β_{Nuc} is the Bronsted coefficient, $[H^+]$ ($=10^{-pH}$) is the proton concentration and K_a ($=10^{-pKa}$) is the acid dissociation constant of the thiolate. Using **Equation D** with empirical values for the thiol-disulfide exchange on GSSG at pH 7 (β_{Nuc} = 0.5, C = -1.29), Whitesides *et al.* extrapolated the rates for various Cys pK_as (ranging from 4 - 10) and constructed a plot of the reaction rate versus pK_a which, interestingly, gave the bell-shaped curve shown in **Figure 2.6**.

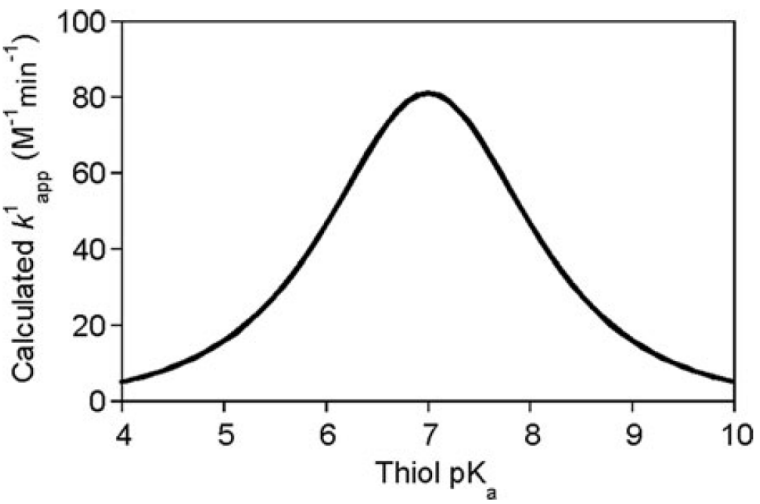

Figure 2.6: Calculated rate constant for the thiol-GSSG exchange reaction at pH 7 as a function of thiol pK_a
Taken from Whitesides *et al*.[85]

The increase in rate from pK_a 10 to 7 reflects a logarithmic increase in concentration outweighing an equivalent decrease in nucleophilicity. This then reverses below pH 7, meaning that the maximum rate of this reaction is when the thiol pK_a approximates the biological pH of ~7. Hence, it emerges that the most nucleophilic thiols in biology are those with a pK_a close to 7.[203]

Hence, as the pK_a of a biological protein thiol is expected to have a strong bearing on the rate of thiolysis exchange, this parameter is an attractive one for indicating selectivity towards individual disulfide substrates in multicomponent and dynamic cellular environments. In the case of many catalytic and redox-reactive biological thiols in proteins, however, the pK_a values and nucleophilicity may show deviations from the reactivity predicted by the aforementioned relationship. This is because biological thiol groups are invariably embedded inside the three-dimensional structure of a protein, where their reactivity can additionally be influenced by steric interactions, electric fields, solvent exclusion, and specific hydrogen bond networks that arise from adjacent amino acids and secondary structures.[198,201]

For ajoene, this translates to individual cysteine thiolate reactivity (relating to pK_a) playing an important role in selectivity, but that other factors are also important to consider for understanding which protein thiols present themselves as suitable *S*-thiolation targets. These factors include the pH of the reaction environment (affecting thiol ionisation), ajoene's ability to access the binding site of the thiol protein (based on

steric and stereo-electronic factors) and, of course, the concentration of ajoene and the protein thiol itself.

2.5.2.2 Factors Affecting Substrate Reactivity

Attention now turns towards the second and third parameters (disulfide electrophilicity and leaving group stability) of **Section 2.4.2**, which together reduce to determine the regioselectivity of the disulfide exchange and describe the overall reactivity contribution of the substrate.[204]

In an unsymmetrical disulfide, the question of regioselectivity presents itself, which, apart from any steric and/or stereo-electronic factors, is primarily determined by stabilisation of the anionic leaving group. The stability of such a thiolate (as the leaving group), in turn, is primarily affected by adjacent electron-withdrawing or electrostatic influences, which link back to the pK_a of the thiol, i.e. the lower pK_a of the two sulfur atoms (as a thiol) in the disulfide provides the better leaving group. This rationale can aptly be applied to the vinyl disulfide functionality of ajoene, in which the double bond provides extra resonance stabilisation, making the regioselectivity unambiguous. **Figure 2.7** summarises these ideas.

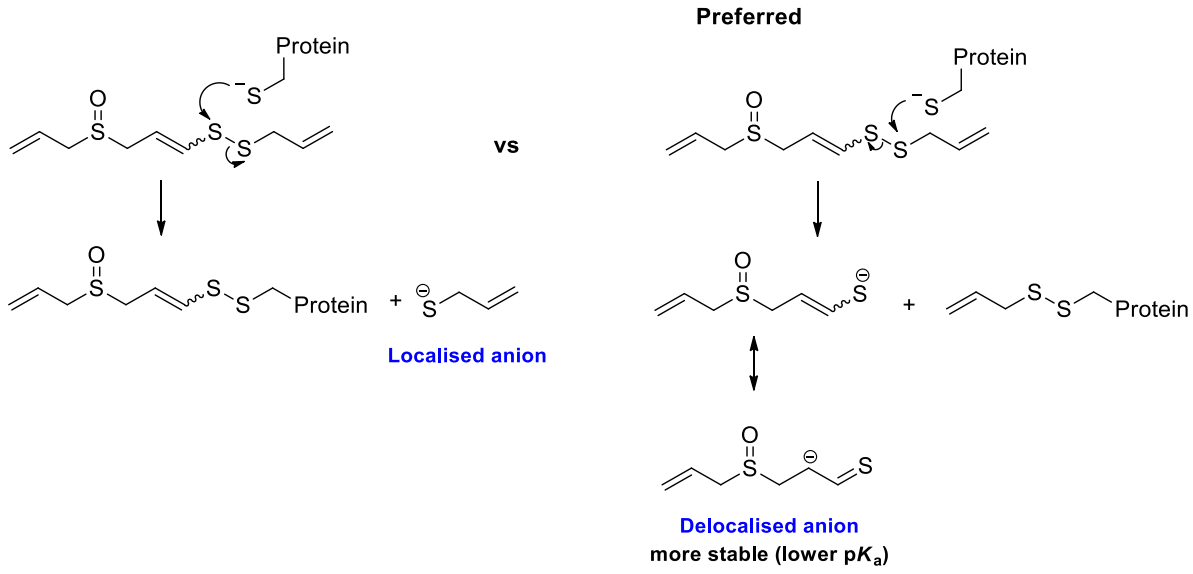

Figure 2.7: The regioselectivity of the ajoene disulfide exchange.

Previous studies in our laboratory have confirmed that *S*-thiolation of *N*-Boc-cysteine by ajoene is regioselective (**Scheme 2.10**),[183] with nucleophilic attack occurring exclusively

at the allyl-*S* (red arrow) and not the vinyl-*S* of the ajoene disulfide during thiolysis exchange.

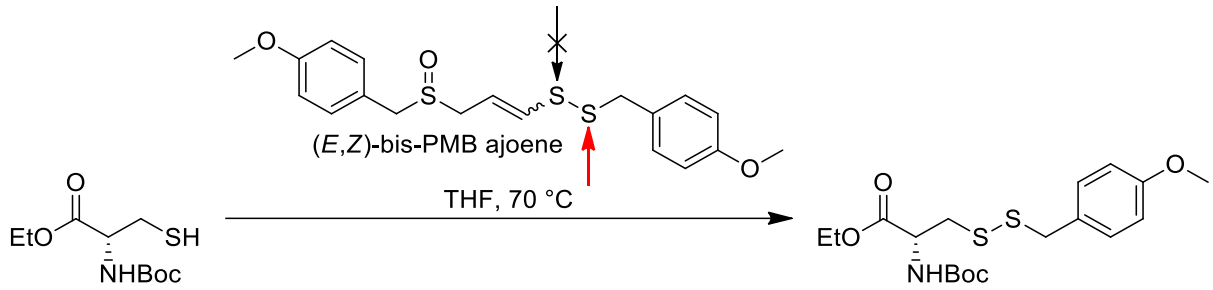

Scheme 2.10: Reaction of *N*-Boc cysteine Et ester with (E,Z)-bis-PMB ajoene.

Apart from dictating the regioselectivity of the nucleophilic attack, the superior leaving ability of the enethiolate/"ajo" group increases the electrophilicity of the allyl sulfur, and hence the rate of exchange, as depicted in the resonance interpretation shown in **Figure 2.8**.

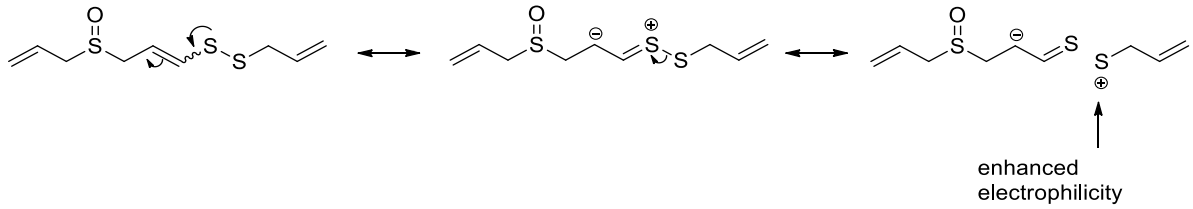

Figure 2.8: Resonance depiction of *S*-allyl S_c electrophilicity enhancement.

The superior leaving group ability of the enethiolate also plays an important role in the reactivity of ajoene, making it a privileged disulfide substrate for thiolysis exchange reactions. Expanding on the kinetic model that links thiolysis rate to the pK_a of the incoming thiol (equations **C** and **D** earlier), studies by Szajewski and Whitesides established that the reaction rate *k*, of a thiolysis exchange follows a Brønsted relation with respect to the pK_a's of the three participating sulfur atoms, namely the nucleophilic/incoming, central and leaving sulfur, as expressed by the following equation:

Equation E:
$$\log k^{\mathrm{RSSR}} = 6.3 + \beta_{\mathrm{Nuc}} \mathrm{p}K_{\mathrm{a}}^{\mathrm{Nuc}} + \beta_{\mathrm{C}} \mathrm{p}K_{\mathrm{a}}^{\mathrm{C}} + \beta_{\mathrm{Lg}} \mathrm{p}K_{\mathrm{a}}^{\mathrm{Lg}}$$

Where *k* is the second-order rate constant (M^{-1} min^{-1}) for the reaction of a thiolate anion of pK_a^{Nuc} with a disulfide with a leaving group of pK_a^{Lg} and central thiol of pK_a^{C}. Their

analysis of rate and equilibrium data resulted in approximate values for the Brønsted coefficients β_{Nuc}, β_{C} and β_{Lg} for thiol-disulfide exchange reactions to be 0.59, 0.40 and -0.59, respectively. From these values it can be seen that the attacking and leaving thiols will have a larger influence on the rate compared to the central thiol when their pK_as are similar, which is in line with the postulate that the negative charges in the anionic trisulfide transition state, although delocalised, will be most abundant on the two distal sulfur atoms (S_{Nuc} and S_{Lg}).[85,205]

Interestingly, the negative value for β_{Lg} describes an opposite effect on the rate compared to that of the attacking thiol (β_{Nuc}) which can be explained as follows: While the lowering of the pK_a of the attacking sulfur comes at a price of decreased nucleophilicity/reactivity (smaller product of $\beta_{Nu}pK_a^{Nuc}$), the lowering of pK_a^{Lg} (smaller negative product $\beta_{Lg}pK_a^{Lg}$ = lower rate reduction) results both in an increased stability of the leaving thiolate as well as the transition state complex (S_{Nuc}-S_C-S_{Lg}),[199] depicted in the energy profile of the thiol-disulfide exchange in **Figure 2.9**.

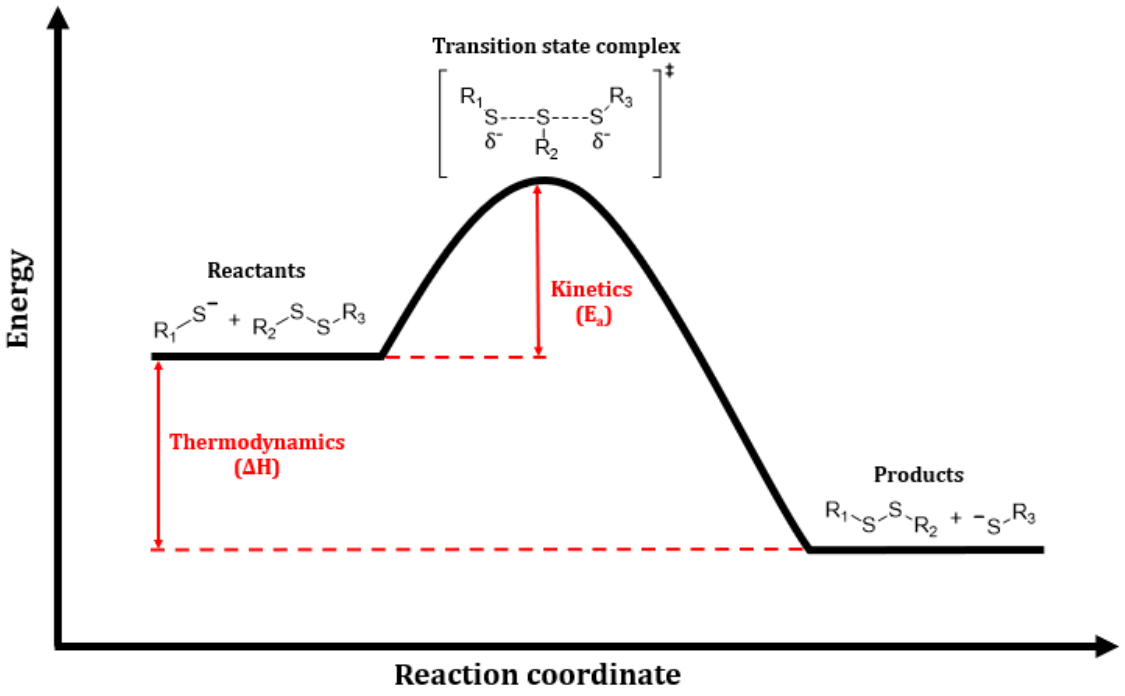

Figure 2.9: Schematic energy profile of the thiolysis exchange reaction as a function of the reaction coordinate.

For ajoene, the increased stability of its enethiolate leaving group (lowered pK_a^{Lg}) affects both reaction kinetics and thermodynamics favourably. Hence, the thiolysis rate

increases as a result of a lowering of activation energy of the initial thiolate addition due to transfer of the charge of the localised thiolate (S_{Nuc}) to a more stable (resonance-stabilised) trisulfide (S_{Nuc}-S_c-S_{Lg}) transition state, while a larger ΔH through the expulsion of a lower energy product (more stable leaving group) drives the reaction forward.

Simple disulfide exchange reactions are reversible and the position of equilibrium (ΔG) is primarily determined by ΔH, since ΔS is effectively negligible. In turn, ΔH is determined by the relative stabilities of the incoming and leaving thiolate, which links to their pK_a values and defines the overall feasibility of the reaction. When applying this concept to the vinyl disulfide functionality of ajoene, the increased stabilisation of the thiolate leaving group makes for a ΔH = negative, which, in turn, makes the reaction favourable in free energy terms and effectively irreversible.

These ideas fit with our recently published study on the relationship between the *in vitro* cytotoxicity (as an IC_{50} on WHCO1 oesophageal cancer cells) of garlic-related disulfides and thiosulfinates with respect to the stability of their leaving group (pK_a).[81] The results indicated that the increase in cytotoxicity (in terms of a lowering of IC_{50}) could be correlated with a lowering of the pK_a of the leaving group. **Figure 2.10** shows the plot of pK_a versus Log IC_{50} for this library of disulfides.

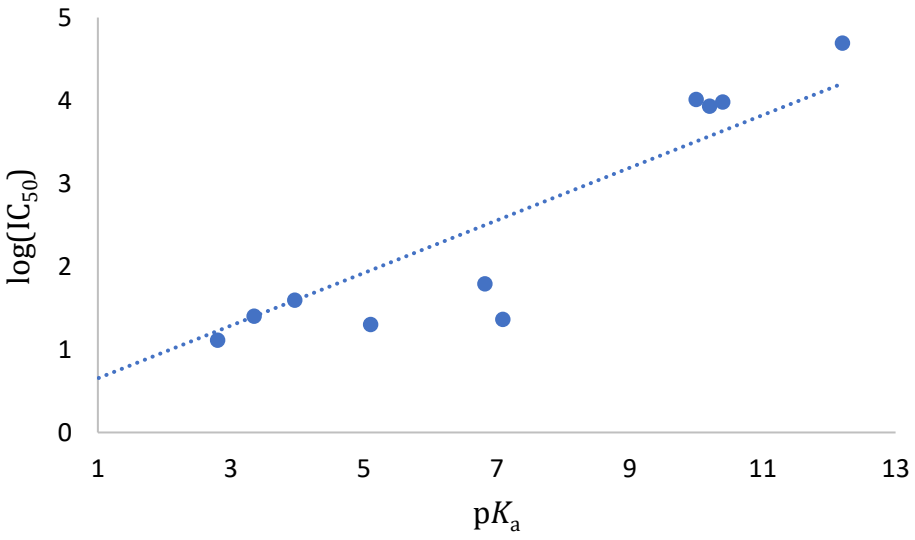

Figure 2.10: Plot of pK_a against log(IC_{50}(WHCO1)) for garlic-related disulfides and thiosulfinates
R^2 = 0.78, Fcrit (7,1) α = 0.001.[81]

These findings reveal that poor leaving groups (pK_a > 8) set up an equilibrium in the thiolysis exchange, making for a modest IC_{50}. Conversely, with superior leaving groups,

the exchange becomes essentially irreversible, providing IC_{50} values similar to that of ajoene (< 25 μM) involving irreversible *S*-thiolation exchanges.

Within a cellular environment, where thiol-disulfide exchanges can proceed via diverse pathways and give a variety of different products and intermediate species,[206] the irreversibility (effectively) of the ajoene reaction takes on a huge significance in terms of the degree of *S*-thiolation of key protein thiols, leading to cancer cell cytotoxicity.[153] Moreover, any reversibility of the *S*-thiolation will also be hampered, as the enethiolate is expected to be reactive, tautomerizing to its thioaldehyde post-protonation, with the aliphatic thioaldehyde likely to react further via oligomerisation in the nucleophilic medium, **Scheme 2.11**.[207]

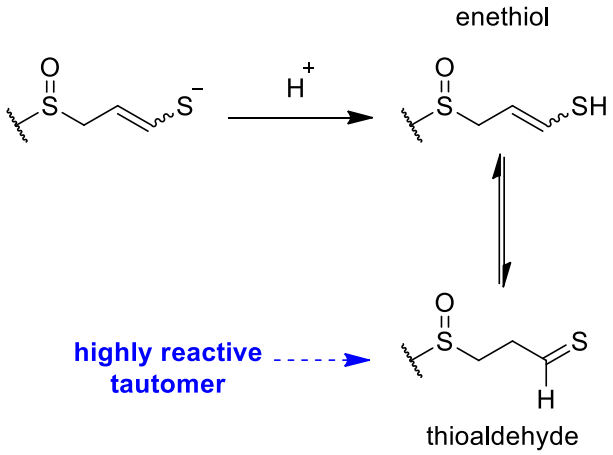

Scheme 2.11: Enethiol-thione/thioaldehyde tautomerization of the protonated ajoene leaving group.

Being essentially irreversible, any selectivity of ajoene towards a plethora of biological thiols *in vitro* will be determined by kinetic considerations. Apart from the roles of three sulfur species in the transition state (**Scheme 2.9**), the S_N2-like reaction mechanism can be influenced by other molecular features involving solvation, steric, electronic and binding interactions.[85]

2.5.2.3 Structure Activity Relationships for the Anticancer Properties of Ajoene

A further question arising about the behaviour of ajoene in thiolysis exchange concerns the results from SAR studies. Following the development of our four-step synthetic route towards accessing end-group substituted ajoene analogues,[170,183] our group set out to establish an ajoene SAR focusing on the end-allyl groups (R^1 and R^2), the sulfoxide, the

double bond and the disulfide, and their influence on bioactivity against cancer cells, as illustrated in **Figure 2.11**.

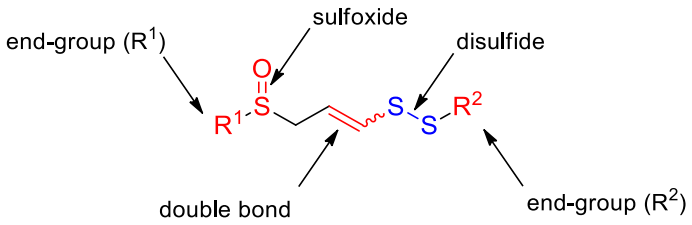

Figure 2.11: Functionalities central to the structure-activity hypothesis of ajoene.

Varying the end groups (R^1/R^2) retained bioactivity and in some cases showed a significant improvement compared to ajoene. **Table 2.1** lists IC_{50} values for a cross section of ajoene derivatives in our first library against cultured WHCO1 cancer cells,[183] in which analogues containing bulky end-groups, such as *tert*-butyl, benzyl and *p*-methoxybenzyl (PMB), were tested as a mixture of *E*/*Z*-isomers that resisted separation by chromatography.

Entry	Compound	Structure	IC_{50} ± SD (μM)[183]
1	Ajoene	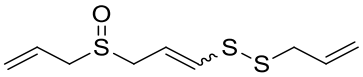	*E*: 39.0 ± 7.8 *Z*: 25.0 ± 2.8
2	Propyl/methyl ajoene	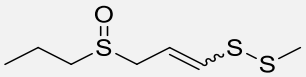	*E*: 28.0 ± 7.2 *Z*: 26.0 ± 7.5
3	bis-Propyl ajoene	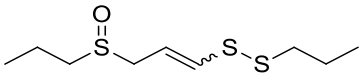	*E*: 24.0 ± 2.8 *Z*: 18.0 ± 4.1
4	*tert*-Butyl/allyl ajoene	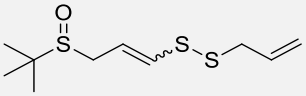	*E*/*Z*: 23.0 ± 6.7
5	Benzyl/allyl ajoene	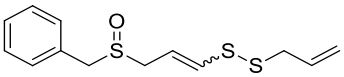	*E*/*Z*: 8.9 ± 1.2
6	PMB/ally ajoene	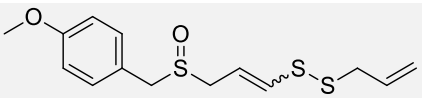	*E*/*Z*: 7.4 ± 0.7
7	PMB/benzyl ajoene	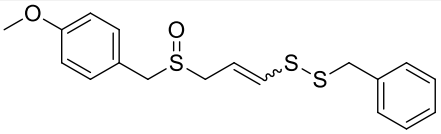	*E*/*Z*: 3.1 ± 1.1
8	bis-PMB ajoene	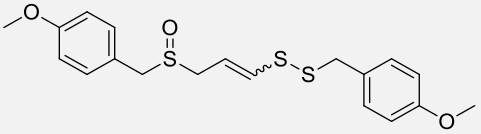	*E*/*Z*: 2.1 ± 0.4

Table 2.1: *In vitro* antiproliferative activity of ajoene analogues varying the R^1 and R^2 groups against WHCO1 cancer cells.

The retention of antiproliferative activity throughout the series confirmed that the ajoene pharmacophore does not reside in any specific end-group. Moreover, since varying the R^1/R^2 groups was not considered likely to greatly affect the pK_a of the enethiol (enethiolate) leaving group, the significant enhancement going from allyl to *p*-methoxybenzyl (entries **1** and **8**) was attributed to an increase in lipophilicity, affecting the rate at which the substrate reaches the protein-bound target thiols. Singh *et. al.* have reported that disulfide exchange reactions slightly favour aprotic over protic environments, as the hydrogen-bonding and ion-dipole effects of water stabilise the more densely charged thiolate ion (reactant) to a greater extent, rendering it less reactive.[197] This means that the rate of thiolate-disulfide exchange should increase as the medium dielectric constant decreases as in a hydrophobic/lipophilic environment. Even though the cellular milieu is considered to be aqueous (i.e. a rate-lowering environment), the catalytic sites of enzymes are commonly buried within hydrophobic regions of the protein structure.[208] The increased lipophilicity conferred by end-group substitutions therefore enhances its rate of binding into these lipophilic protein active sites; as well as improving the rate of passage through cellular membranes. Certainly increasing the potency from roughly 30 μM (**entry 1**) to 2 μM (**entry 8**; our lead, called bis-PMB ajoene) was extremely pleasing.[80]

With the development of a suitable pharmacological lead as bis-PMB ajoene, the focus of our structure-activity analysis of ajoene was directed in the second library towards identifying the roles of the sulfoxide, double bond and the disulfide functionality. For this purpose, we synthesised five structural analogues of bis-PMB ajoene (**Table 2.2**). Three of the five either lacked the sulfoxide (**entry 2**), the double bond (**entry 3**) or both (sulfoxide and double bond; **entry 4**), while the other two were sulfide analogues with the S-S functionality replaced by a single sulfur, which contained (**entry 5**) or lacked (**entry 6**) the sulfoxide. All compounds were tested for antiproliferative activity against WHCO1 up to a maximum concentration of 200 μM, and the results are shown in **Table 2.2** below.

Entry	Compound	Structure	IC_{50} ± SD (μM)[183]
1	bis-PMB ajoene	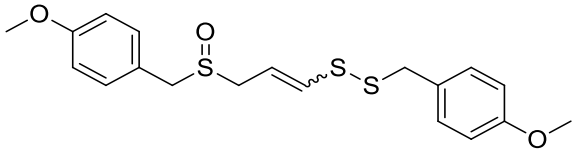	*E*/*Z*: 2.1 ± 0.4
2	bis-PMB *S*-desoxy-ajoene	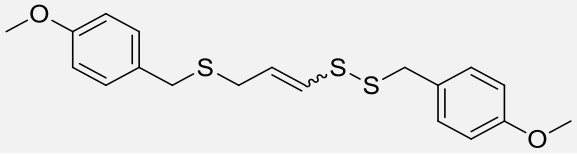	*E*/*Z*: 0.7 ± 0.3
3	bis-PMB dihydroajoene	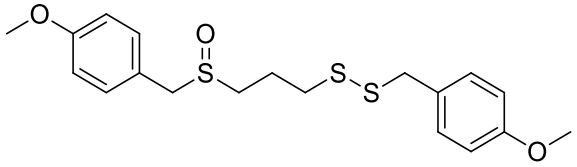	16 ± 3.7
4	bis-PMB *S*-desoxy-dihydroajoene	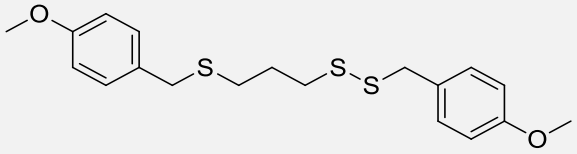	> 200
5	bis-PMB desthio-ajoene	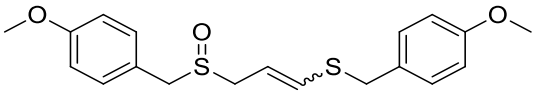	*E*: > 200 *Z*: > 200
6	bis-PMB *S*-desoxy-desthio-ajoene	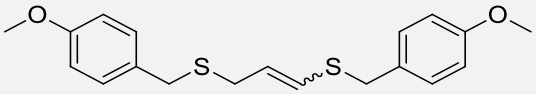	*E*/*Z*: > 200

Table 2.2: Structure-activity analysis of the bis-PMB ajoene core against WHCO1 cell proliferation by MTT assay.

In interpreting the results, the first important conclusion was that the ajoene pharmacophore resides in its disulfide (compare **entries 1** and **2** with **5** and **6**). This pleasingly corroborated our hypothesis around the disulfide and thiolysis exchange driving the bioactivity.[183] It is also supported by reports of DAS and SAC being inactive at inhibiting the growth of colon, lung and skin cancer cells,[130,209,210] as these sulfides similarly cannot undergo disulfide exchange.

A second notable observation were the outcomes in **entries 2** and **3** in which, respectively, the sulfoxide was removed retaining the double bond (IC_{50} = 0.7 μM) followed by the double bond retaining the sulfoxide (IC_{50} = 16 μM) respectively. These results indicate the relative roles played by the double bond and the sulfoxide in stabilising the thiolate leaving group (with a lowering of pK_a) - the double bond via resonance and the sulfoxide via an inductive effect. This indicates that the double bond is far superior to the sulfoxide in stabilising the leaving group charge as one would expect from a resonance argument. The unexpected lowering of the IC_{50} of **entry 2** (lacking the

sulfoxide) into the nanomolar region points once again towards the importance of lipophilicity in promoting entry into the cell. Here, a hydrophobic effect may well be operating (binding into a cysteine site with expulsion of water molecules resulting in ΔS = +ve, favouring the free energy). Removal of both functional groups as in **entry 4**, as expected, pushed the IC_{50} beyond 200 μM and effectively into the inactive range, in accordance with our ideas on thiolate stabilisation and the thiolysis equilibrium ΔG. A final comment is appropriate for **entry 3** with a respectable IC_{50} (16 μM), retaining the sulfoxide but lacking the double bond, as it creates a new disulfide design motif, which we have called dihydroajoene. Although, no regioselectivity studies were carried out on this disulfide (no vinyl component), theory predicts that the thiolysis exchange will also be regioselective, as depicted in **Scheme 2.12**. In pathway **a**, the exchange of anions has no increase in stabilisation, while pathway **b** can result in a lowering of energy via an inductive effect involving the sulfoxide. This would push the reaction equilibrium over to some extent along the lines previously discussed. The extent to which an H-bonding stabilisation effect might play a role in stabilising the anion also remains to be seen (**Scheme 2.12**). The dihydroajoene motif might well be worth examining further in future studies in the group.

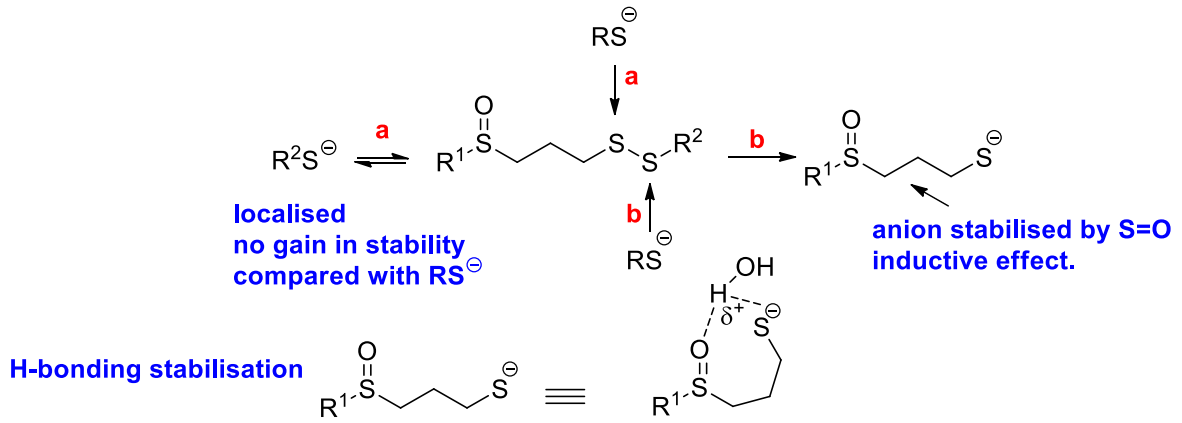

Scheme 2.12: Proposed electronic effects operating on the leaving group stability in dihydroajoenes.

A more subtle reactivity trend conferred by the vinyl functionality relates to the absolute stereochemistry about the double bond in which the *Z*-isomer (where separable) revealed a 1.5-fold increase in cytotoxicity activity over its *E*-isomer. We hypothesise that two possible factors might account for the greater (negative) ΔG of the *Z*-isomer being: i) a greater release of steric strain (due to the removal of the *S*-allyl group) in the thiolysis

in the case of the *Z*-isomer compared to that in the *E*-, and ii) the possibility, as just mentioned, that the *Z*-isomer enethiolate can benefit from H-bonding through water and the sulfoxide; a facet that the *E*-isomer cannot enjoy. Although the energy of the *E*-enethiolate might be expected to be lower than that of its *Z*-counterpart in accordance with enthalpy considerations ($Enthalpy_E < Enthalpy_Z$), the ΔG Gibbs free-energy change for the *Z*-isomer thiolysis must be greater (negative), resulting in a more favourable equilibrium. This will be due to the two aforementioned factors. **Figure 2.12** depicts this possibility.

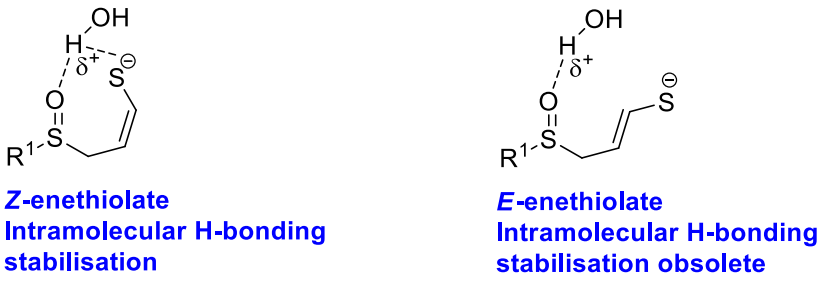

Figure 2.12: H-bonding stabilisation accounting for the greater ΔG of the *Z*-enethiolate

Finally, the activity enhancement for the *S*-desoxy bis-PMB analogue (**entry 2**) compared to its parent bis-PMB (**entry 1**) is worth mentioning. It was seen that the presence of a sulfide moiety (instead of the sulfoxide) produced an approximately 2-fold increase in antiproliferative activity. Here, the removal of the sulfoxide causes an overall increase in lipophilicity of the molecule. We observed a similar trend for bis-PMB compared to its parent, where an increase in lipophilicity of the end groups correlated with a lowering of its IC_{50} value (see **Table 2.1**). Apparently, this lipophilicity factor is able to override the loss of enethiolate stabilisation going from sulfoxide to sulfide.

2.6 SAR Hypothesis

The previous sections discussed the chemistry of the disulfide exchange and our SAR study of ajoene. The understanding of ajoene cytotoxicity primarily centres around the thermodynamic effect of its powerful leaving group. However, several kinetic influences, namely solvation, steric, electronic and binding interactions, also play an important role in lowering the activation energy (E_a) of the reaction with its biological thiolate targets.

Figure 2.12 presents the resulting SAR hypothesis for the thiolysis-mediated anticancer effects of ajoene.

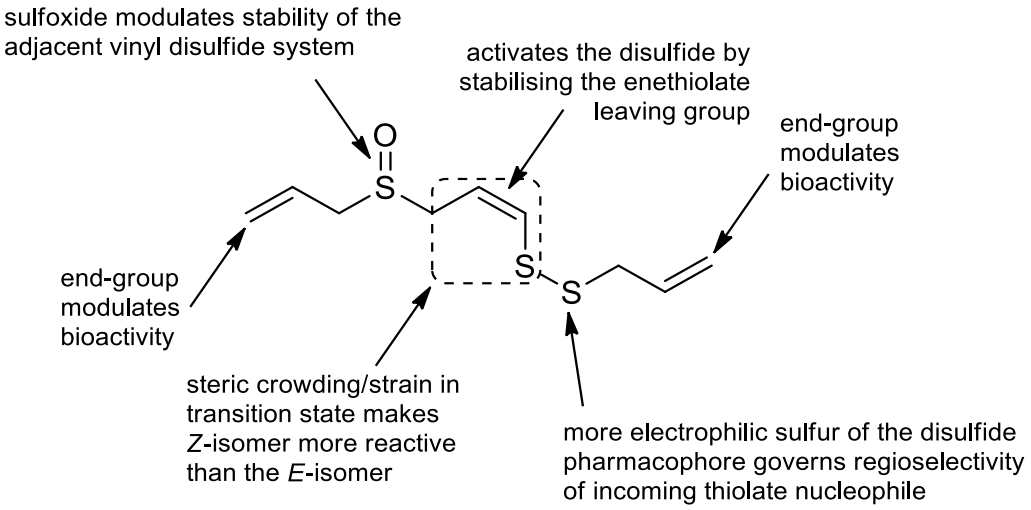

Figure 2.13: Proposed structure-activity hypothesis for *Z*-ajoene as a disulfide substrate in thiolysis exchange reactions.

In summary, this chapter introduced the synthetic routes to ajoene and its analogues, showed that ajoene is able to *S*-thiolate protein targets in MDA-MB-231 breast cancer cells through a *S*-thiolysis exchange, as well as the development of an SAR model for ajoene which described that: i) the origin of cytotoxicity (pharmacophore) of ajoene resides in the disulfide, ii) the R^1 and R^2 substituents are not essential to this bioactivity, but their modification with an increase in lipophilicity increases antiproliferative activity *in vitro*; iii) the sulfoxide, which is also not essential to bioactivity, likely enhances the stability of the transition state through an inductive effect on the vinyl disulfide; iv) the double bond offers resonance stabilisation to the vinyl sulfide anion, which drives the position of equilibrium in the forward reaction. Importantly, it also ensures a regioselective exchange. It was proposed that the reactivity of the enethiolate of the "ajo"-LG, makes this exchange essentially irreversible. Together, these mechanistic insights together with the development of a synthetic route to ajoene analogues laid the foundation for exploring the cytotoxicity of ajoene using chemical biology techniques as the principal objective of this thesis.

Results and Discussion

Chapter 3 : Drug Metabolism and Pharmacokinetic Studies on Ajoene

3.1 Background

Chapter 1 described the different chemotypes that are found in garlic and concluded that the OSC profile is highly dependent on the type of processing of the cloves. This is because a chemical interconversion of compounds occurs that is dependent on reaction conditions (pH, temperature, solvent, time etc). Thus, variability in the method of preparation in turn leads to variability in the compound distribution and the medicinal properties of the preparation. In addition, individual OSCs exhibit distinct pharmacokinetic profiles which are exemplified by parameters, such as bioavailability and bioaccessibility. Bioavailability describes the rate and extent of absorption, i.e. whether a compound is available at the site of action. Bioaccessibility on the other hand, is defined as the fraction of a compound that is released from its matrix into the gastrointestinal (GI) tract. This parameter describes whether the compound is available for absorption into the blood stream.[211]

To date, several studies have investigated the pharmacology of garlic preparations and their OSC constituents from ingested garlic.[83,95,112,212,213] The OSC metabolites of allicin, *S*-allyl cysteine, diallyl disulfide (DADS) and diallyl trisulfide (DATS), have been well studied within the physiological environments of the gastric system, liver, breath and blood. There is, however, little available information on ajoene, possibly because the other compounds are commercially available, whereas ajoene needs to be synthesised. In this project, we set out to expand the understanding of the pharmacology of ajoene and its synthetic analogues.

3.2 Bioavailability and Metabolism of Garlic OSCs

A whole garlic bulb has a sulfur content of 0.35% (w/w), stored predominantly as γ-glutamylcysteine and *S*-alk(en)ylcysteine sulfoxides, which are odourless and with no reported anticancer activity.[214] However, once the plant tissue is damaged, these derivatives of cysteine undergo biochemical transformation to allicin and the second-

generation garlic OSCs described in **Chapter 1** exhibiting a plethora of medicinal properties.[215] **Figure 3.1** gives an overview of these transformed products.

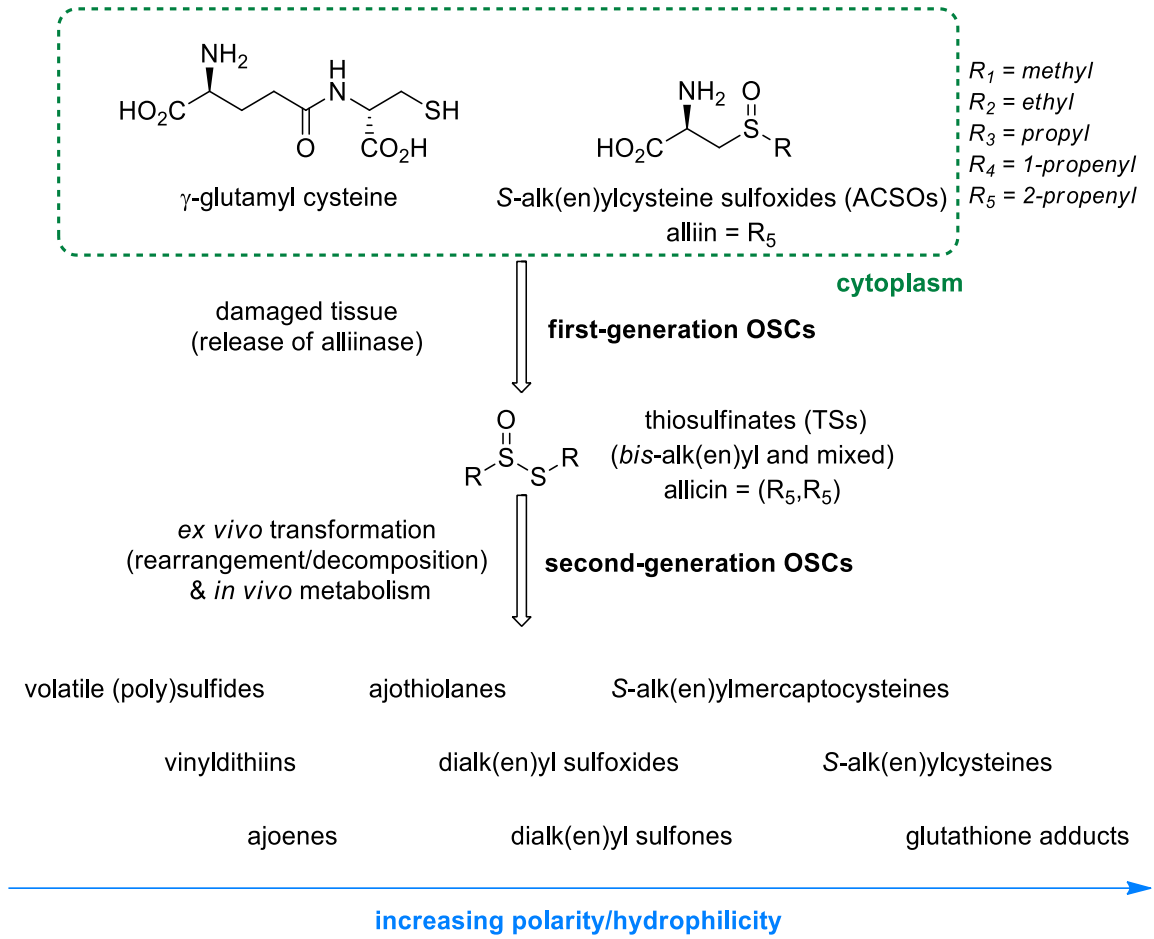

Figure 3.1: Overview of the OSCs found in garlic.

3.2.1 The Pharmacokinetics of Allicin

The first group of transformation products (first-generation OSCs) are the thiosulfinates, with allicin being the most studied as it is present in common garlic (*Allium Sativum*), accounting for 70% w/w of total thiosulfinates.[216] Allicin is described as the principal active component with regard to the beneficial effects of garlic preparations and supplements.[217,218] Although allicin has a concentration of 4-5 mg/g in freshly crushed garlic, and up to 200 mg in the garlic supplement Allimax®,[219] its chemical instability and thermolability lead to its rapid transformation during culinary processing, and to its rapid metabolism once consumed. The resulting products, aka. second-generation OSCs, differentiate themselves from allicin by virtue of their chemical stability, biological effects

and metabolic behaviour. **Figure 3.2** shows the chemical structures of the most studied second-generation OSCs from allicin.

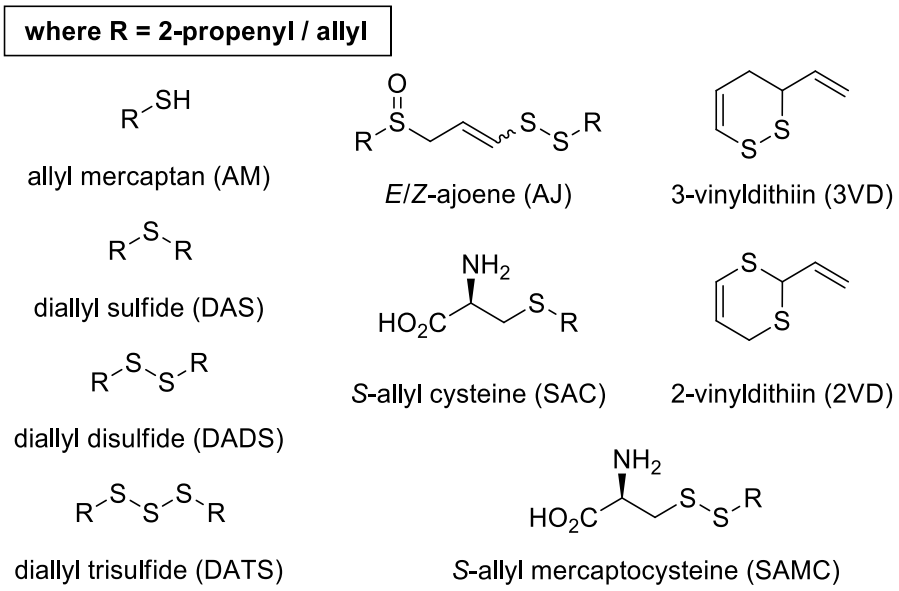

Figure 3.2: Commonly encountered and studied transformation products of allicin.

Most dietary preparations and extracts of garlic use one or a combination of the following processes: chopping or crushing, cooking (bake, grill, fry), distilling, pickling, fermenting, storing and aging. These processes influence the ability of allicin to transform into its secondary metabolites. A recent study by Camargo *et al.*, that compared the OSC content of raw and cooked garlic, found that allicin is only detectable in raw garlic. Indeed, cooked preparations are devoid of allicin but contain its transformation products DAS, DADS, DATS, ajoene and the vinyl dithiins.[211] Interestingly, the medium in which allicin is processed has the greatest influence over the classes of second-generation OSCs that are formed. Methods that enrich the oil-soluble OSC's include heating in vegetable oil, oil-maceration/ether-extraction and steam distillation. The aging or fermentation of a garlic extract results in mostly water-soluble OSCs (primarily the *S*-alk(en)ylcysteines and *S*-alk(en)ylmercaptocysteines).[105,155] These OSCs are produced from the reaction of allicin with cysteine, where the latter is generated from the breakdown of proteins during aging. *In vivo*, the allicin from freshly prepared garlic interacts with its physiological environment. In this regard, the nature of the physiological matrix affects its rate of metabolism and the profile of second-generation OSCs that are produced. The most notorious metabolic effect associated with the ingestion of raw garlic is garlic breath, which is experimentally detectable within seconds. Interestingly, this distinctive garlic

breath does not originate from the digestive tract (mouth, oesophagus) but from the lungs, where it is not caused by allicin itself, but by a variety of small, volatile OSCs such as AM, DADS, DAS, allyl methyl sulfide (AMS), allyl methyl disulfide (AMDS).[220,221] Not only does this indicate allicin's rapid metabolism, but also its high bioavailability. It takes only a few seconds for allicin to pass through the digestive tract and to be transformed into its volatile metabolites, which travel through the blood into the lungs.

The ingestion of garlic is the most common route of administration (ROA), but it is also the most complicated to study pharmacologically, as the ingested compounds pass through several distinct physiological environments where they undergo several metabolic transformations. The oral ROA involves delivery through the stomach to the liver via the hepatic portal vein where most OSCs undergo first pass metabolic transformations (first pass effect).[211,222,223] While polar OSCs are excreted in the urine,[224] the non-polar and volatile OSCs are mostly secreted in the sweat and breath.[225,226]

The pharmacokinetics of allicin has been extensively studied via most ROAs and physiological matrices. Although the low pH of gastric fluid deactivates alliinase, thereby inhibiting allicin formation in the stomach, allicin itself is relatively stable in the hydrophilic intestinal tract and at gastric pH.[227] In one study, it was found that up to 80% of allicin remained following a one-day incubation in simulated gastric fluid at 37 °C (shown in **Figure 3.3**). Of this, only 10% was transformed into the polysulfides, ajoene and vinyl dithiins.[228,229]

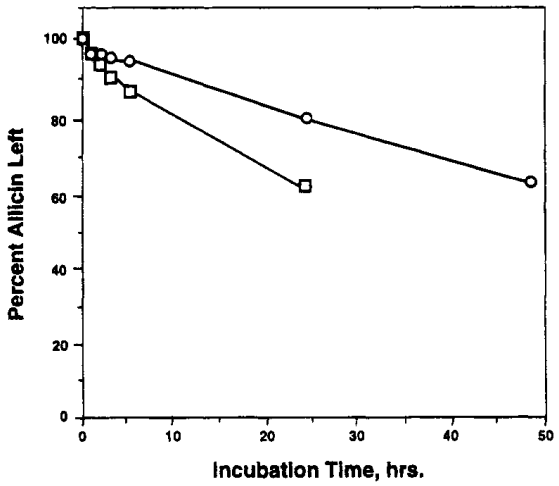

Figure 3.3: Stability experiments on allicin in simulated gastric and intestinal fluid.
○ = gastric fluid (pH 1.2) and □ = intestinal fluid (pH 7.5), measured at 37 °C. Percentages determined by HPLC peak area.[228]

Being lipophilic, allicin has good phospholipid permeability, although it exhibits poor stability in non-polar environments.[227,230] Several lines of evidence suggest that although allicin is bioaccessible, it is not bioavailable beyond the gastrointestinal tract.[231] For example, when entering the liver, allicin shows a remarkable first pass where it is rapidly metabolised into secondary OSCs (shown in **Scheme 3.1**).[223]

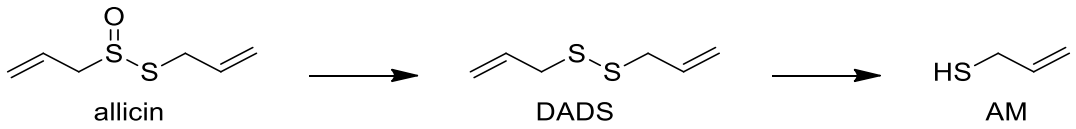

Scheme 3.1: The metabolism of allicin in the liver.

In a separate experiment on isolated rat livers,[223] allicin concentrations were found to significantly decrease following single passage through this organ. Infusions of allicin up to 400 μg/mL showed no detected allicin after the first liver passage. The administration of 1100 μg/mL of allicin resulted in some allicin detection however this concentration also caused considerable damage to the hepatocytes. The resulting perfusion medium showed DADS and AM to be the major metabolites. DADS is the metabolic precursor of AM, as it is also the compound formed following perfusion with DADS alone.

Allicin has a similar short-lived existence when entering the cardiovascular system. When incubated with whole blood at 37 °C, allicin was found to have a half-life of less than two minutes, indicating that it is rapidly metabolised in blood, as shown in **Figure 3.4**.

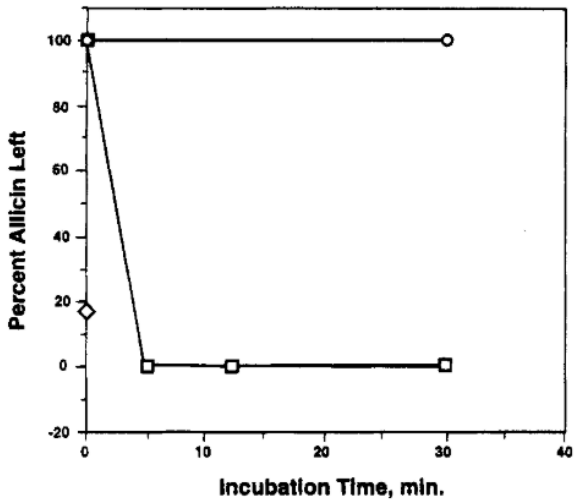

Figure 3.4: Stability of allicin in blood samples.
Control (○); blood (□) and denatured blood (◇). Percentages determined by HPLC peak area.[228]

The authors also showed that when allicin was incubated separately with either the plasma or red blood cells (RBC) fractions (**Figure 3.5**), it was selectively metabolised in the latter.

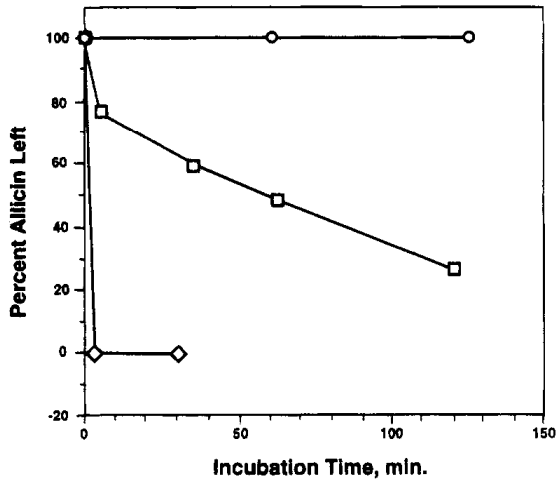

Figure 3.5: Stability experiments on allicin in plasma and RBC fractions.
Control (○), plasma fraction, and (□) RBC fraction (◇). Percentages determined by HPLC peak area.[228]

The HPLC quantification showed that allicin has a greater stability in plasma than in RBCs, suggesting that it may be reacting with erythrocytes. It was also found that allicin was less stable in denatured blood than in whole blood (shown in **Figure 3.4**),[228] indicating that erythrocyte contents and their proteolysis products may be important in its metabolic transformation.

The detection of *S*-allyl mercaptocysteine (SAMC) and *S*-allyl glutathione (GSSA) metabolites in this experiment suggest that allicin acts as a soft sulfenylating agent toward cysteine and GSH in RBC's via a thiolysis exchange mechanism,[232] indicating that this may be the indicated intraerythrocytic target as shown in **Scheme 3.2**.

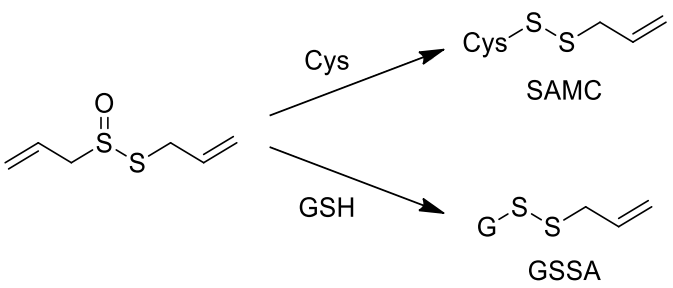

Scheme 3.2: Potential thiolysis exchange reaction of allicin in the RBC fraction of blood.

To investigate this further, the authors incubated allicin with cysteine and GSH at physiological pH and temperature. HPLC analysis of the reaction products confirmed that the reaction was complete within two minutes and that all the allicin had been converted into SAMC and GSSA thereby demonstrating the feasibility of the reaction (**Scheme 3.2**). This reaction likely represents the central mechanism by which allicin is metabolised in the RBC fraction of blood.[79,230,233] Indeed the majority of free thiols in blood are stored inside erythrocytes as GSH.[234] The blood plasma, on the other hand, has a lower relative concentration of free thiol, which rather exist in their oxidised form: cystine, GSSG or disulfide bridges in proteins.[235]

In summary, while the gastric or intestinal pH partially stabilises allicin, its rapid metabolic transformation in the hepatic and cardiovascular system implies that its bioavailability beyond these tissues is limited, and that the metabolites of allicin may be responsible for much of its bioactivity.[79,95,236]

3.2.2 Pathways Involved in the Metabolism of OSCs from Garlic

The second-generation OSCs formed from allicin exhibit important biological activities; however, they are not the endpoint and undergo further metabolic transformation themselves. OSC metabolism aims to add polar functionalities to enhance hydrophilicity and promote excretion. Interestingly, this modification also enhances the bioactivity of the metabolites compared to their precursors.[211] A review by Gao *et al.* identified four primary metabolism pathways of OCSs, namely: a) reduction and methylation, b) oxidation, c) "cysteine/GSH" conjugation (disulfide formation), and d) *N*-acetyl conjugation, as illustrated in **Figure 3.7**.

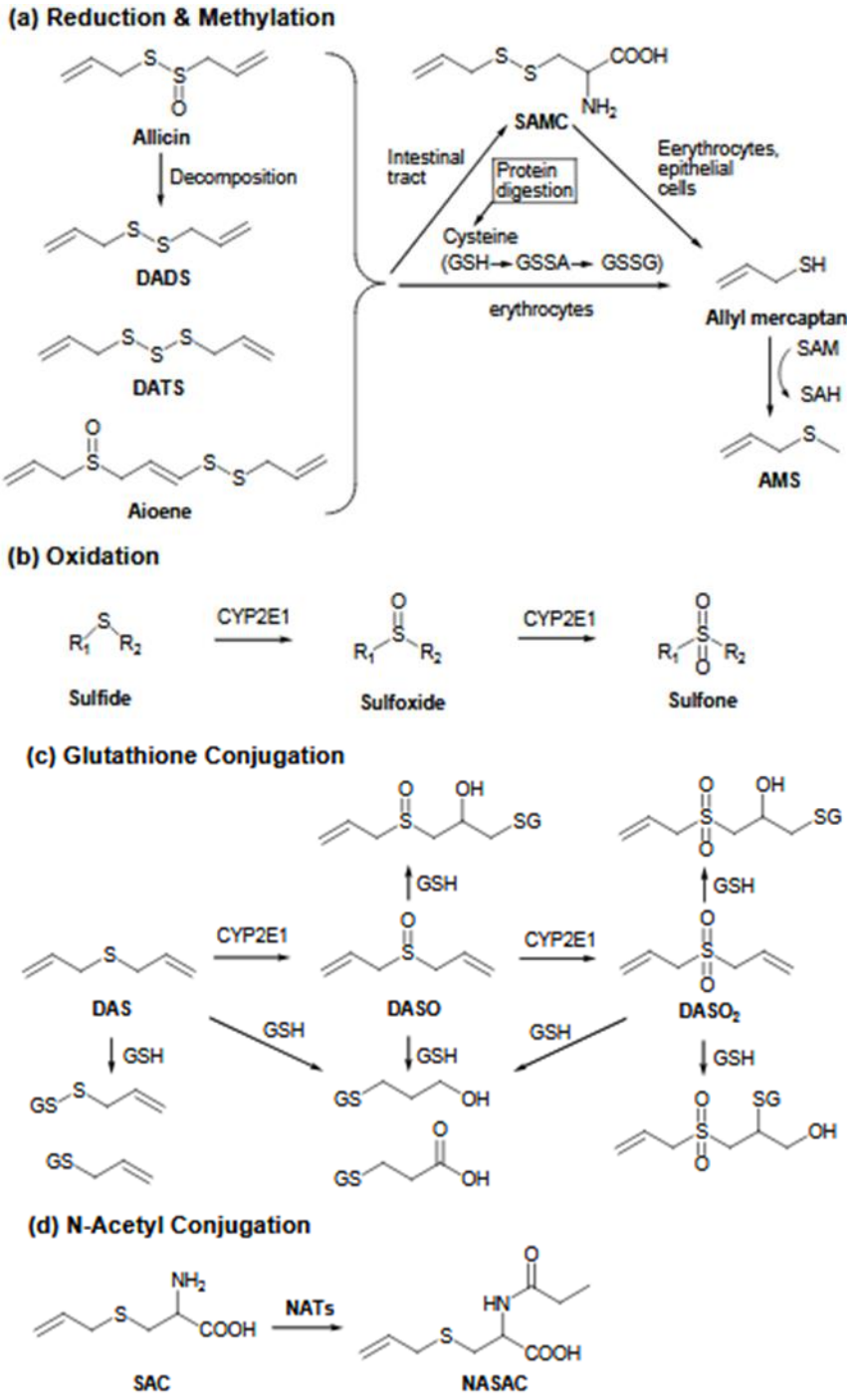

Figure 3.6: Overview of metabolic pathways affecting the biochemical transformation of OSCs.
Taken directly from Gao *et al.*[236]

For example, Nagae *et al.* demonstrated that SAC, an allicin metabolite with high systemic bioavailability and bioaccessibility, is conjugated to acetyltransferases in the liver and kidney where it is excreted as *N*-acetyl-*S*-allylcysteine (see NASAC in **Route (d)** in **Figure 3.6**).[222] The oxidation of sulfides (e.g. DAS) in the liver (**Route (b)**) produces dialk(en)yl

sulfoxides and dialk(en)yl sulfones. These are long-circulating metabolites that produce potent chemopreventive effects by inhibiting phase I and II metabolising enzymes (e.g. CYP2E1). This effect was originally attributed to DAS but has now also been attributed to its metabolites.[237]

The metabolic pathways of particular interest in this project involves the oxidation of thiol residues by garlic OSCs (**Routes (a)** and **(c)**) to form disulfide conjugates. As described in **Chapters 1** and **2**, the formation of disulfide conjugates proceeds via a thiol-disulfide, for polysulfanes (DADS, DATS, ajoene etc.), or a thiosulfinate exchange for allicin, involving cysteine and cysteine residues on peptides (GSH) and proteins. Although this metabolic process destroys the parent OSC, the resulting *S*-alk(en)ylation of cysteine may lie at the origin of garlic's biological activity and is a focal point of this thesis.

All OSCs with polysulfide (S≥2) and thiosulfinate moieties are susceptible to this type of metabolic transformation. The reactivity of the S-S bond in the aforementioned chemotypes, may be a metric by which their systemic pharmacology can be measured. For example, the exchange reaction for allicin with blood can be linked to the high chemical lability of the thiosulfinate leading to its rapid disappearance in this matrix. In a recent study by Palazzolo *et al.*,[211] the bioaccessibility and blood stability of second-generation OSC's was investigated following an *in vitro* gastric digest. The experiment involved the incubation of garlic in simulated gastric fluid for 2 hours at 37 °C, followed by HPLC analysis. Bioaccessibility (%) was calculated as the ratio of OSCs in the supernatant compared to the initial OSCs in the cooked garlic, as shown in **Table 3.1**.

OSCs	ajoene	2VD	DADS	DATS
% Bioaccessibility	52	57	66	87

Table 3.1: OSC bioaccessibility for garlic OSCs in simulated gastric fluid.

Since all the second-generation OSCs were found to be detectable following the incubation period, the results show that similar to allicin, digestion is not a limiting step for bioaccessibility. Because OSCs can remain in the intestinal tract for prolonged periods of time, the authors indicated that they may act as *in situ* antioxidants, where they can protect the gastrointestinal tract from oxidative damage and delay the development of inflammation (gastritis and ulcerative colitis) and cancers (for example of the colon and

rectum).[48,238] Indeed, allicin, DADS and DATS were found to successfully suppress colitis associated cancer (CAC) in a AOM/DSS murine model when administered orally.[239–241]

A separate blood stability experiment by Palazzolo *et al.* involved spiking whole rat blood with 100 µg/mL of the second-generation OSC's DAS, DADS, DATS, ajoene and 2VD followed by incubation at 37 °C.[211] **Figure 3.7** shows the percentage remaining at timepoints up to 240 min.

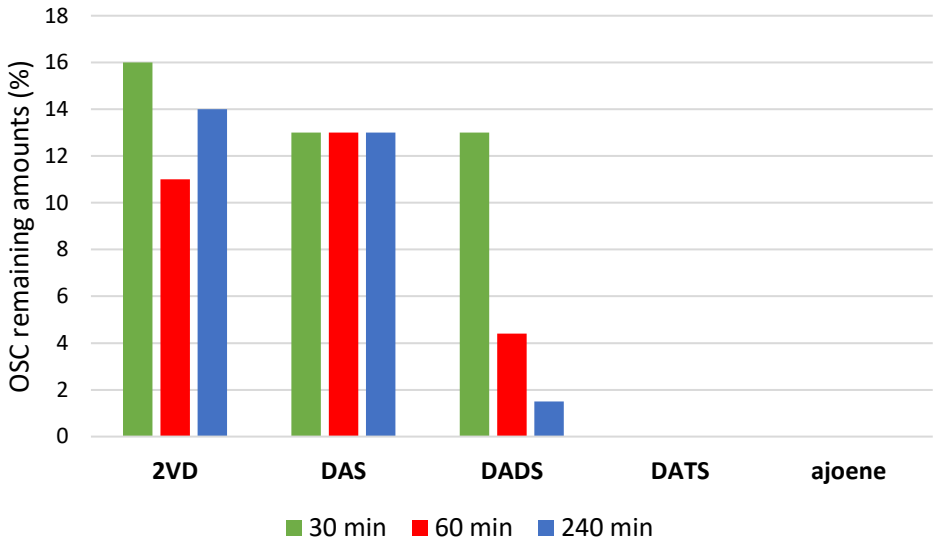

Figure 3.6: Percentage of OSCs remaining in blood following incubation at 37 °C.
Adapted from Palazzolo *et al.*[211]

After 30 min, ajoene and DATS were not detectable, which is consistent with previous studies.[231,242] However, for 2VD, DAS and DADS, around 20% of spiked amounts remained. This observation supports a relationship between the relative rates of reaction of the OSC with a biological thiol in the blood which probably underpins their ability to reach the site of pharmacological action via the circulatory system. Indeed, 2VD and DAS, each lacking a disulfide functional group, are the most blood stable of all the OSC's tested. On the other hand, the vinyl disulfide of ajoene and the trisulfide of DATS (akin to the thiosulfinate of allicin), are chemically primed to undergo thiolysis exchange, which likely explains their rapid transformation in blood. In agreement, the symmetrical disulfide, DADS, is less reactive towards thiolysis, which may explain its intermediate half-life in blood. A similar observation was made for the *in vitro* stability of DADS and DATS in rat blood, where it was found that 99.5% of the initial DATS was already degraded after 3

minutes, while DADS had only degraded by 74.9% in the same time interval suggesting that it is more bioavailable.[242]

This literature summary brings together findings that allicin and the second-generation OSCs are stable in the gastrointestinal system but are metabolically unstable in the liver and blood. Investigations of related metabolic process have shown that sulfides are readily oxidised by hepatic enzymes for excretion, whereas polysulfide-containing OSCs react more readily with biological thiols (in blood and the liver) to from mixed disulfides.[79,84,243] Since the similarities in the sulfur chemistry of subsets of garlic OSCs cause them to engage analogously inside of the body, the study of their chemistry is pivotal to understanding how they are metabolically transformed. Furthermore, the chemistry may explain how these compounds engage with cellular pathways and how these engagements may be harnessed for therapeutic effects. For us, it became evident that an understanding of the mechanistic background to the physiological interaction of garlic and its organosulfur constituents is central to consolidate the broad pharmacological effects against cancer, particularly *in vivo*.

3.3 In vitro Anticancer Studies with Garlic OSCs

Numerous animal models and clinical trials on garlic OSCs demonstrate their therapeutic potential against cardiovascular disease, diabetes, liver injury, bacterial, viral and protozoal infections and cancer (reviewed in [112,244,245]). In cancer, garlic OSCs are promising candidates as they display a broad range of anticancer effects. While it is long known that dietary consumption of garlic offers protection against cancer, more recent investigations have shown that certain OSCs target multiple pathways in cancer and are able to selectively kill cancer cells while exhibiting a low level of toxicity.[146]

One patent reports that no notable side effects were observed in a 70 kg person treated intravenously with 5 mL of pure garlic extract.[246] Scaled down doses in mice have also showed no apparent morbidity or mortality.[146,247] Regarding the toxicity, it should be noted that some patients and animals do show hypersensitivity to ingestion,[126] with rodents being particularly sensitive to gut irritations and disruptions of the microflora therein following oral allicin administered.[248,249] In a recent murine cancer model by Li *et al.,*[247] it was shown that the intraperitoneal administration of raw garlic extract (RGE) was able to cure animals from the highly aggressive malignancies of sarcoma 180 and

EL4-induced lethal ascites (not yet curable by conventional therapies), while oral administration via gavage failed to produce an effect. Furthermore, it was shown that half of the anticancer activity could be inactivated by heating the RGE at 100 °C for 10 min suggesting that predominantly allicin and not its second-generation products are responsible for this activity. Interestingly, these findings imply that much of the anticancer activity of RGE may be lost as it passes from the GI tract into the hepatic and circulatory system and that the extract needs to be directly applied to the cancer cells (i.e. intraperitoneal injection to the ascites). Given that there are many active compounds in garlic with varying chemical activity, contradictory experimental findings may arise from differences in the methods of preparation or administration. In the above mentioned study, it was argued that intraperitoneal or intravenous injection may bypass metabolism in the intestinal tract and liver, thereby making these ROA more efficient in delivering agents to cancer lesions.[250]

In spite of the blood instability and metabolism affecting OSCs, there are a number of studies that show specific compounds (i.e. allicin, DADS, DATS, SAC and ajoene) are able to inhibit tumour growth (and in some cases metastasis) in murine animal models for cancer when delivered by various routes including intraperitoneal, intravenous as well as oral. A selection of these studies is presented in **Table 3.2**. The ROA, dose, cancer model and outcomes are listed in respective columns.

OSC	ROA & dose	Cancer model	Outcome	Study
allicin	**Oral** (in feed), 12 mg/kg daily	AOM/DSS Colitis-associated cancer (CAC)	Treated mice showed a significant decrease in number and size of tumours after 95 days	**Li & Ni 2018**[239]
DADS	**Intraperitoneal** or **oral** (gavage), 1 mg/kg (in saline or corn oil) thrice weekly	HCT-15 human colon cancer	Intraperitoneal treatment caused a 63% reduction in mean tumour volume, whereas oral treatment reduced mean tumour volumes by 29% after 21 days	**Sundaram 1996**[209]
	Intraperitoneal, 50 mg/kg (in saline), every second day	MCF-7 and MDA-MB-231 breast cancer xenograft	Treatment significantly inhibited the growth of breast cancer tumour xenografts after 28 days	**Xiong 2018**[251]
	Intraperitoneal, 20 or 40 mg/kg (in PBS), every third day	ECA-109 human oesophageal carcinoma	Treatment with 20 and 40 mg/kg of DADS decreased the mean tumour volumes by 27 and 39%, respectively, after 22 days	**Yin 2014**[252]
DATS	**Intravenous**, 6 mg/kg (in 90% saline, 5% ethanol, 5% cremophore EL), every third day	HCT-15 human colon cancer	A reduction of the tumour size by 70% was observed after 18 days	**Hosono 2005**[82]
	Intraperitoneal, 20–40 mg/kg (in β-cycloamylose and saline), daily	BGC-823 human gastric cancer xenograft	Treatment significantly and dose-dependently reduced tumour volume and tumour weight after 32 days	**Jiang 2017**[253]
	Oral (gavage), 10 or 50mg/kg (in olive oil), daily	HT-29 human colon adenocarcinoma xenograft	Treatment (10 and 50 mg/kg) reduced tumour volume and significantly decreased the tumour weight after 28 days	**Lai 2015**[254]
	Oral (gavage), 50 mg/kg (in PBS), thrice weekly	PC-3 human prostate cancer	The average tumour volume in treated mice was lowered by 55% after 20 days	**Xiao 2006**[255]
SAC	**Oral** (gavage), 5 and 40 mg/kg (in distilled H_2O) daily	CAL-27 human oral cancer xenograft	Treatment caused a 30 and 74% inhibition in tumour growth in the 5 and 40 mg/kg groups, respectively, after 28 days.	**Pai 2012**[256]
ajoene	I**ntraperitoneal**, 2 -8 mg/kg (in 0.1% DMSO in PBS) daily	S-180 sarcoma and H-22 hepatocarcinoma xenograft	After 12 days, inhibition rates were 10 and 32% for S180 implanted mice which received 4 and 8 mg, respectively. The rates in H22 transplanted mice reached 34% and 42% which received 2 and 4 mg/kg, respectively.	**Li & Ciu 2002**[167]
	Intraperitoneal, 25 mg/kg (in Intralipid®) every second day	B16/BL6 melanoma model	The growth of tumours was notably inhibited with tumour size being reduced by between 70 and 90% after 28 days.	**Taylor & Noriega 2006**[168]
	Intraperitoneal, 25 mg/kg (in Intralipid®) daily	A549 lung adenocarcinoma xenograft	Treatment reduced the volume and growth rate of xenograft tumours after 28 days.	**Wang & Sun 2016**[89]

Table 3.2: Summary of *in vivo* studies using pure garlic OSC's to inhibit tumour growth in murine models for cancer.

There are three reported tumour xenograft studies using ajoene which all use intraperitoneal injection as the ROA. In all cases, ajoene was reported to significantly inhibit the rate of tumour growth, and to reduce the final tumour weight compared to the control groups, see **Figure 3.8**. For the regimens where mice were treated with ajoene doses of 25 mg/kg for 28 days, Taylor *et al.* and Wang *et al.* both reported the reduction of tumour size in the range of 80%. Furthermore, the treatment with ajoene at these doses showed no apparent side-effects.

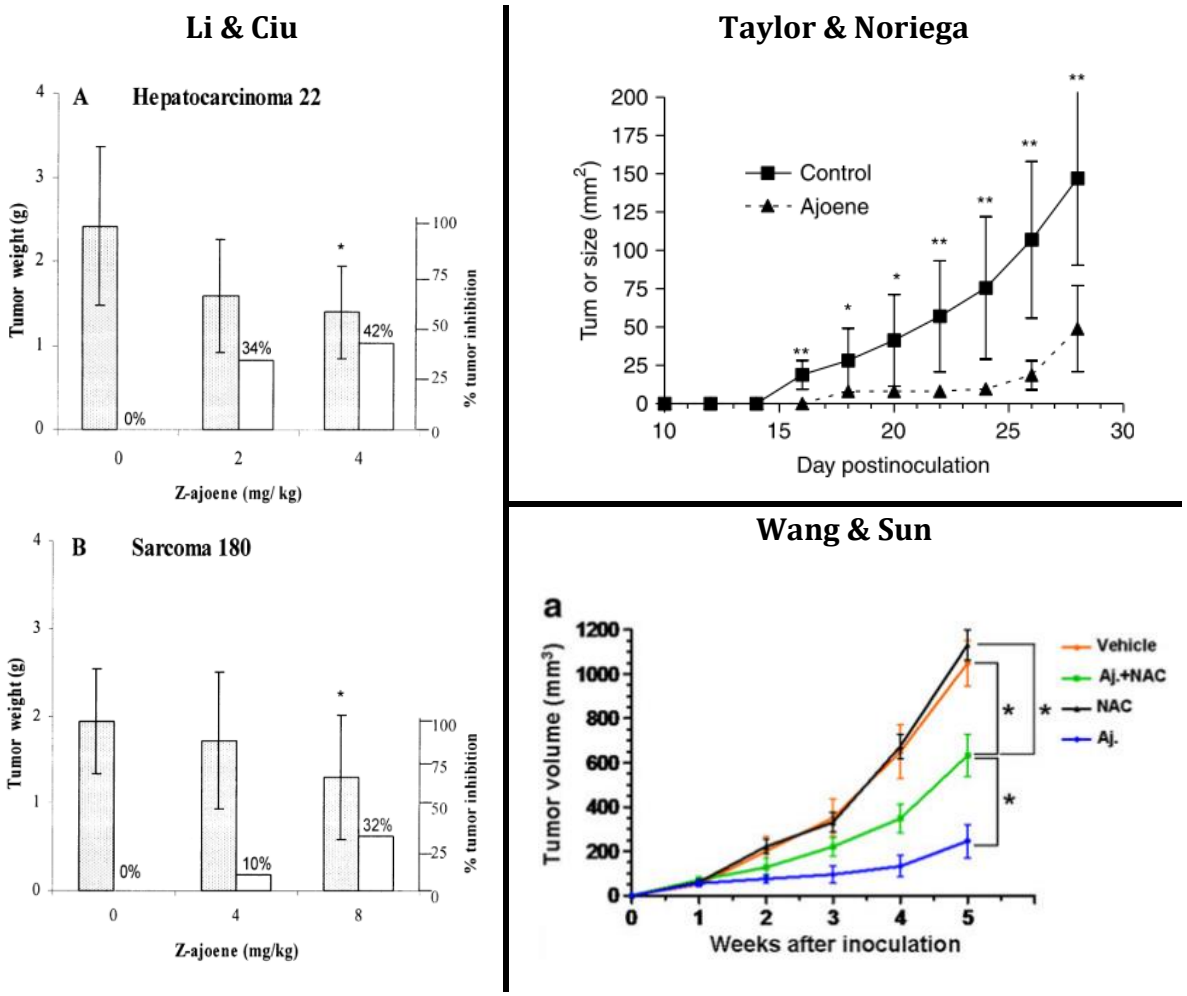

Figure 3.7: Intraperitoneal administration of ajoene reduces the final weight and growth rate of xenograft tumours in mice.
The graphs were taken directly from the studies by Li *et al.*,[167] Taylor *et al*[168] and Wang *et al.*[89]

While there is a wealth of *in vivo* studies on the garlic OSCs allicin, DATS and DADS; there are only a few studies on ajoene. Ajoene is an understudied and attractive anticancer candidate as it displays excellent *in vitro* cytotoxicity against cancer cell lines, and it is reported to be active against mouse models for cancer. It is also an interesting chemotype

having the unique vinyl disulfide sulfoxide functional group, making it chemically primed for thiolysis exchange. We therefore aimed to investigate structure-activity relationships into the bioavailability and *in vivo* anticancer activity of ajoene. As garlic is ingested orally (through the diet or as a supplement), we investigated its effect on tumour growth in a mouse xenograft model delivered via the oral route.

3.4 *In Vitro* Experiments on Orally Administered Ajoene

Previous *in vitro* cytotoxicity testing and SAR studies of ajoene in our lab have found it to be active against the WHCO1 human oesophageal cancer line (**Table 3.3**).[80,183] The cytotoxic IC_{50} values were determined by an MTT assay, which is a colorimetric assay that quantitates viable cells by detecting mitochondrial reductase activity after treatment. The assay monitors the conversion of yellow MTT reagent (3-(4,5-dimethylthiazol-2-yl)-2,5-diphenyltetrazolium bromide) into purple formazan crystals.[257] The cells were treated in 96-well plates with varying concentrations of ajoene or its analogue for 48 hours. Thereafter MTT reagent was added and the plate was incubated for a further four hours after which the reaction was stopped by the addition of a denaturing solubilizing reagent (0.01 M HCl, 10% SDS). As a negative control, the compounds were incubated with MTT in the absence of cells. The resulting colour change (yellow to purple) was colorimetrically quantified using a multiwall scanning spectrophotometer from which a dose-response curve was generated. The IC_{50} is a quantitative measure of the concentration of drug found to inhibit the growth of 50% of the cells.

OSC	IC_{50} (μM)	SD
E-ajoene[80]	39.2	± 7.8
Z-ajoene[80]	25.2	± 2.8
E/*Z*-bis-PMB[80]	2.1	± 0.4
DATS[a]	6.3	± 4.4

Table 3.3: Antiproliferative activity of ajoene and DATS against WHCO1 cells from a UCT study
[a] = unpublished result

Previous studies in our lab had shown that WHCO1 tumours are able to grow in nude mice, and therefore this model was chosen for the study.

In order to conduct animal experiments, an accreditation (authorisation number: AL17/16489) was obtained by the South African Veterinary Council (SAVC). The process included undertaking an introductory course in laboratory animal science (the ethics, care and use of animals for scientific purposes), and a competency training course covering animal welfare, handling and experimental procedures (gavage, injections and euthanasia), both held at the Research Animal Facility at the University of Cape Town (UCT).

3.4.1 Outline of the WHCO1 Xenograft Experiment

The experimental protocol was approved by the UCT Faculty of Health Sciences Animal Ethics Committee (Project number 018/003). The review by the committee ensures that all animal procedures are performed in accordance with UCT policies as well as South African legislation and standards for the ethical medical research on animals (Act 71 of 1962, Act 19 of 1982 and SNS 10386:2008). An outline of the experimental timeline of the approved protocol is depicted in **Figure 3.9**.

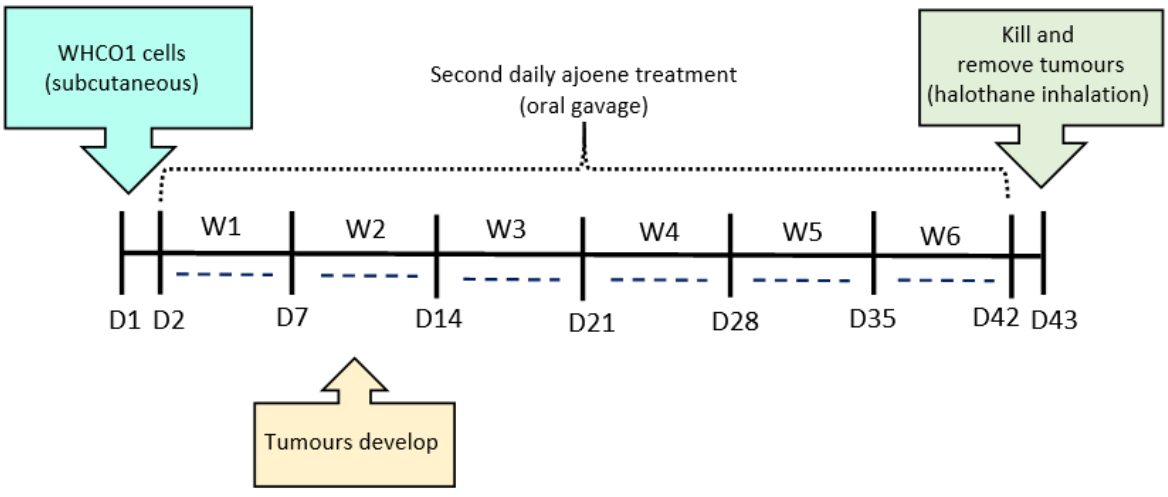

Figure 3.8: Overview of the experimental design.

In this study, the aim was to quantify the inhibitory effects of ajoene by comparing the rate of tumour growth between a treated and untreated group of mice. The experiment involved the inoculation of WHCO1 cancer cells by subcutaneous injection into the right

flank. Nude mice are used as they are genetically engineered to not mount an immune response, which allows the xenografting of human tissues (= interspecies tumour model). Over six weeks, the treated group received an oral gavage of ajoene while the control group received the vehicle alone, thrice weekly. The mice were monitored daily and weighed every second day to assess the animal wellbeing. Once tumours are palpable, the volume is measured every third day using a digital calliper and calculated using the modified formula for an ellipsoid, where volume = ½ (length × width^2).[258] These measurements are approximations as the tumours are not necessarily ellipsoid. In addition, if the tumour is largely subcutaneous, its volume measurement is assumed with error.[259] After the treatment, all animals were killed by 5% halothane inhalation in air and death was confirmed by cervical dislocation. A post-mortem was performed on each mouse and all tumours are excised and weighed.

3.4.2 Pilot Studies on Tumour Growth and Dose Determinations

Before commencing with the full experiment, we conducted two independent pilot studies to demonstrate that: 1) WHCO1 cells could be successfully xenografted to the nude mouse strain (UCT21) with satisfactory growth, and 2) the selected dosage (25 or 50 mg/kg of body weight) of ajoene was tolerated by the animals.

In the first pilot study, six female mice each received a subcutaneous injection of 2.5x10^6 WHCO1 cells in sterile PBS into the right flank and the animal weights and tumour volumes were monitored every second and third day, respectively (**Figure 3.10 A** and **B**). At the end of the experiment, the mice were euthanised, and the tumours were excised and weighed (**Figure 3.10 C**).

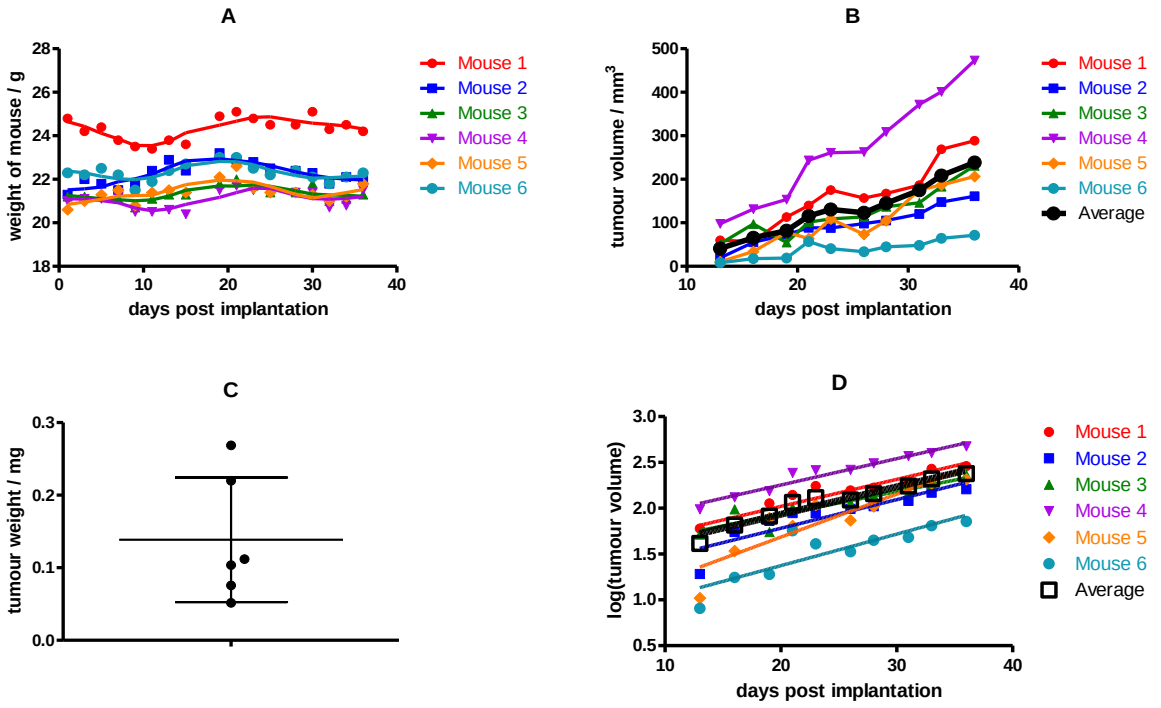

Figure 3.9: Data from the first pilot study verifying WHCO1 tumour growth over 36 days. Graphs of: **A**: animal weight vs time; **B**: tumour volume vs time; **C**: weight of excised tumours at the experimental end point; **D**: log(tumour volume) vs time.

All animals appeared normal and gained weight throughout the experiment (**Figure 3.10 A**). All mice had developed palpable tumours within 10 days of inoculation, with sustained growth until the endpoint. There was a high degree of variability (averaged observed variance = 46.9%) in the measured tumour volumes (**Figure 3.10 B**), as some mice grew small tumours while others grew larger ones. The tumour weights measured at the end of the experiment (**Figure 3.10 C**) reflected the high degree of variability in the tumour size (62.06%), of 0.1385 ± 0.086 g. To correct for the large inherent differences in the tumour sizes, the exponential tumour growth curve was linearised by logarithmization (**Figure 3.10 D**). Using this analysis, we were able to compare differences in the tumour growth rates (slope) across animals which pleasingly, showed no significant difference ($p = 0.1067$). Corrected for inter-variability between tumour sizes, the log of the average growth rates of 0.030 ± 0.003 showed a lower degree of variability (14.1 %). We realised that the high variability (~50%) in the baseline tumour size would complicate the detection of differences between group averages, however if the data is converted to growth rate then it may be compared regardless of the actual tumour size. Following a consultation with a biological statistician, we were advised to

increase the group sizes to 10 mice to account for the high biological variability, and to observe a significant 2-fold difference in tumour size when p = 0.05 with a power of 0.8. In conclusion, the pilot study showed that human WHCO1 cancer cells grow in UCT21 nude mice supporting their suitability for our study. Owing to the large apparent intergroup variation in tumour size, growth rate may be a better comparison than average size of the exponentially growing tumours.

The second pilot study involved determining an appropriate oral dose of *Z*-ajoene. Several publications have documented the effects of garlic OSCs on tumour xenograft growth (see **Table 3.2**) where doses up to 100 mg/kg were delivered by oral gavage. We treated two groups of three mice with 25 mg/kg or 50 mg/kg of *Z*-ajoene in Intralipid® thrice weekly over two weeks (total of 6 doses). The 25 mg/kg dose was selected based on the previous *in vivo* studies on ajoene,[89,168] and included the 50 mg/kg dose to account for any potency loss associated with the lower bioavailability of this ROA, as compared to the intraperitoneal injection. The weights, appearance and general wellbeing of the animals were monitored over the course of the experiment. **Figure 3.11** shows the animal weight measurement over the two-week experiment.

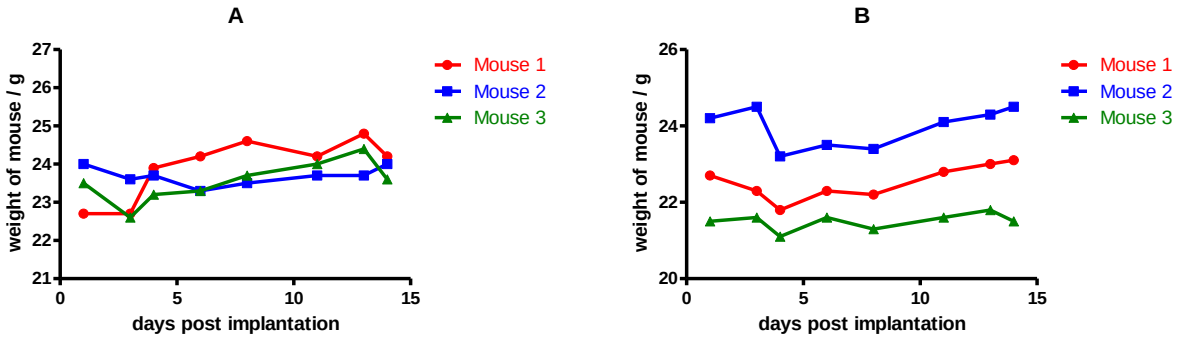

Figure 3.10: Animal weights of nude mice orally administered with ajoene thrice weekly over 14 days.
A = 25 mg/kg and **B** = 50 mg/kg *Z*-ajoene in Intralipid®

After the first dose, it was observed that five of the six animals lost weight. Over the next two weeks, however, the animals proceeded to gained weight. A follow-up autopsy of the animals at the end of the experiment revealed that the oesophagus, lungs, spleen and liver looked normal, but although the mice had food in their stomach, the small intestine was

empty up until the saecum. As the mice appeared healthy and gained weight overall, we concluded that both of the administered ajoene doses were tolerated.

3.4.3 Orally Administration of Ajoene in a Murine WHCO1 Tumour Xenograft Model

Following completion of the pilot studies, we proceeded to test if ajoene had any effect on tumour growth in the WHCO1 tumour xenograft model. DATS was included as a positive control,[254,255] and the vehicle only was included as a negative control. We opted to treat the mice at the higher ajoene dose (50 mg/kg) which was tolerated in the pilot study. **Figure 3.12** outlines the procedural details of the experiment performed.

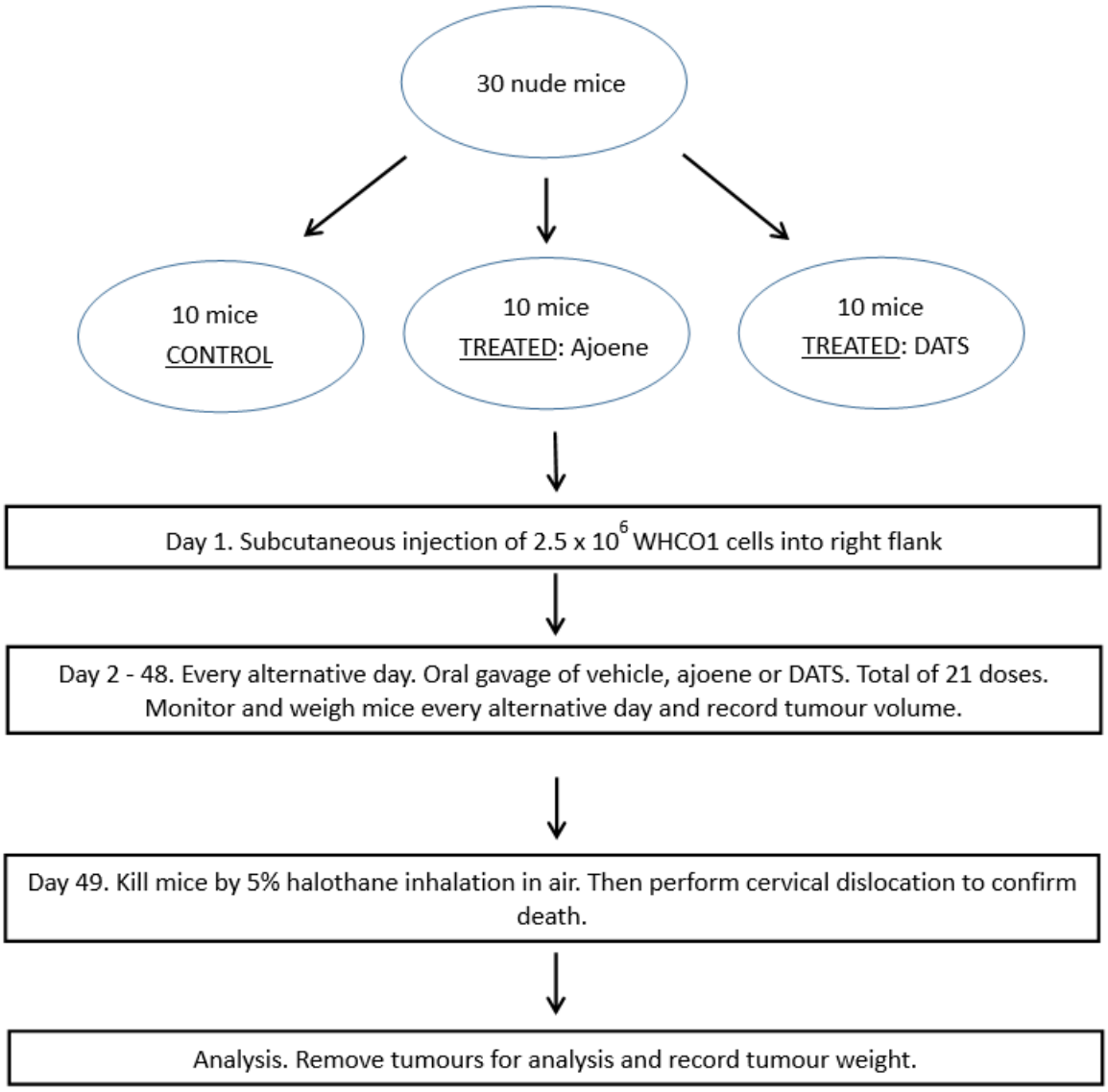

Figure 3.11: Procedural details of the murine xenograft study.

On day 1, each mouse received a subcutaneous injection in the right flank of tumour cells. Over the course of 7 weeks (day 2 – 48), the treated mice received an oral gavage of 100 µL ajoene (50mg/kg) or DATS (50 mg/kg) and the control mice received the vehicle alone (Intralipid®). The mice were monitored daily and weighed every second day. From day 10 when the tumours became palpable, their volumes were measured. On day 49, all animals are euthanised, an autopsy was performed, and the tumours were removed and weighed.

Figure 3.13 shows the mean animal weights (**A**) and the averaged tumour volumes (**B**) as well as the weights of the tumours (**D**) collected by biopsy at the end of the experiment.

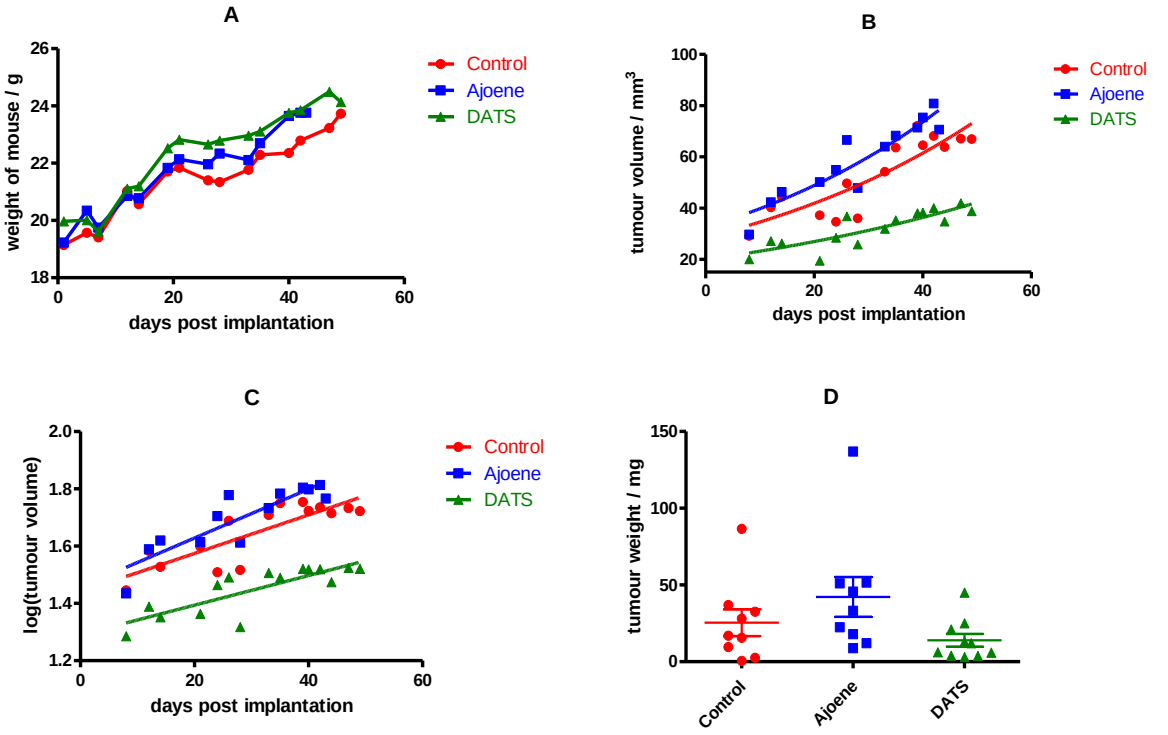

Figure 3.12: Effect of ajoene and DATS on WHCO1 tumour growth in a nude mouse xenograft model.
Graphs of: **A**: Average mouse weight vs time; **B**: Average tumour volume vs time; **C**: log(average tumour volume) vs time; **D**: Individual weights of tumour biopsies excised for control (day 49), ajoene (day 43) and DATS (day 49).

All mice gained weight throughout the experiment (**Figure 3.13 A**), and all, except one, developed measurable tumours within 10 days. The mouse that did not grow a tumour was in the control group and was omitted from the statistical analysis. In week 5, we observed that some of the mice in the ajoene-treated group were becoming agitated after receiving the gavage. After consultation with the resident animal technician, the

behaviour was attributed to discomfort caused by the ajoene. However, the animals returned to normal behaviour the following day and gained weight throughout the experiment, so the treatment was continued. At week six, however, two of the mice in the ajoene-treated group died following the gavage. A supervised autopsy revealed that the mice had a severe reddening and swelling of the stomach and duodenum. The ajoene experimental group was therefore terminated early on day 43 by euthanasia and the final tumours were removed and weighed. The control and DATS groups appeared healthy, so the experiment was continued a bit longer until day 49.

As before, the large inherent variations between tumour sizes within a group complicated the interpretation of data. For this reason, the average tumour volume for the entire group was fitted to an exponential growth curve $y = y_0\, e^{(kx)}$, where y_0 = volume at day 1 and k = rate constant, (**Figure 3.13 B**) and a student's *t*-test was performed. From the growth equations, DATS ($y = 19.94e^{(0.01499x)}$) was found to have 43% lower tumour volume compared to the control group ($y = 28.53e^{(0.01918x)}$) at the end of the experiment and this was statistically significant ($p < 0.0001$). This result agreed with a previous literature report where DATS was shown to have significant inhibitory effects on tumour growth when administered orally at 50 mg/kg in murine xenograft model for PC-3 human prostate cancer.[255] From our results, DATS appears to also inhibit tumour growth in oesophageal WHCO1 cancer cells. Disappointingly, from the growth curve of ajoene ($y = 32.39e^{(0.02051x)}$) and the control ($y = 28.53e^{(0.01918x)}$) it was deduced that the treatment did not inhibit tumour growth and that there was no statistically significant difference ($p = 0.2743$).

Table 3.4 lists the summary of the student's *t*-test results for the tumour volumes for the control, ajoene and DATS groups.

tumour volume	*t*-score	df	*p*-value	MD	± SEM	Significant?
control vs ajoene	1.117	26	0.2743	-6.304	5.644	No
control vs DATS	4.855	28	<0.0001	20.61	4.244	Yes****
ajoene vs DATS	6.159	26	<0.0001	26.91	4.369	Yes****

Table 3.4: Results of student's *t*-test group statistics
Unpaired *t*-test (equal variance), where df = degrees of freedom, MD = mean difference, SEM = standard error of the mean, *$p < 0.05$; **** $p < 0.0001$; two-tailed.

To further quantify the effect of ajoene and DATS on the rates of tumour growth, the tumour volume data was logarithmised and a linear regression analysis (**Figure 3.13 C**) as well as a student's *t*-test were performed.

log(tumour volume)	*t*-score	df	*p*-value	MD	± SEM	Significant?
control - ajoene	1.108	26	0.2780	-0.045	0.0410	No
control - DATS	5.887	28	<0.0001	0.202	0.0343	Yes****
ajoene - DATS	6.6	26	<0.0001	0.247	0.0374	Yes****

Table 3.5: Summary of *p*-values for the group comparison of tumour growth rates.
Unpaired *t*-test (equal variance), where df = degrees of freedom, MD = mean difference, SEM = standard error of the mean, *$p < 0.05$; **** $p < 0.0001$; two-tailed.

The analysis showed that the difference in mean tumour growth of the DATS-treated group was statistically different ($p < 0.0001$) to the control group. Again, the difference in the mean rate of tumour growth between the ajoene-treated and control groups was not statistically significant.

Upon inspecting the tumour weights (**Figure 3.13 D**), it became apparent that each test group had one value with an abnormal distance from the mean. To test if these three values may be excluded as outliers, two statistical outlier identification methods were applied. We applied the standard deviation method (assuming a Gaussian distribution of the data), where an outlier may be omitted if it falls outside of the range spanning the mean ± 2 x standard deviations. Then for the interquartile range (IQR) method (assuming a non-Gaussian distribution), the exclusion of an outlier is valid when it falls outside of the range that is defined as the mean ± 1.5 x IQR. The two test conditions were true for each of the indicated values and they were omitted from the data sets, as indicated in **Figure 3.15**.

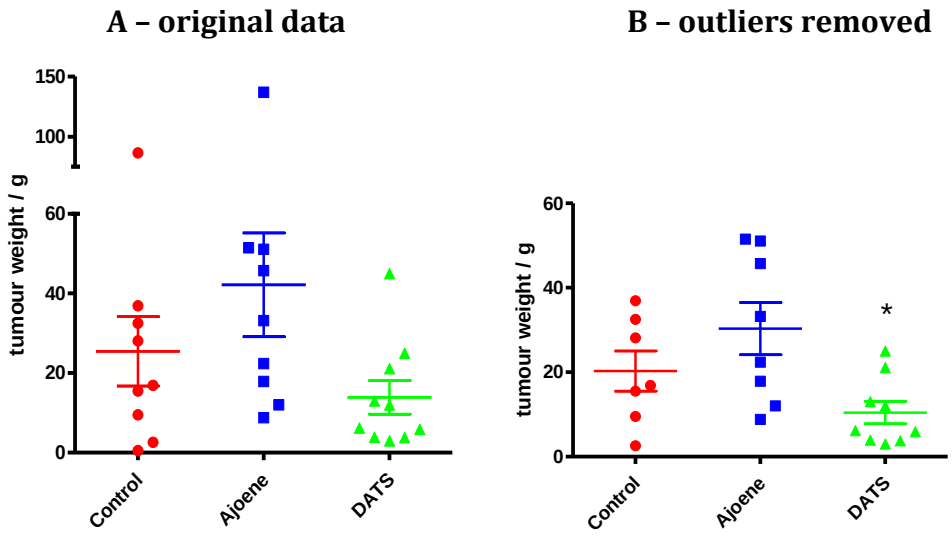

Figure 3.13: Tumour weight data before and after removing outliers from the data.
A = original data, **B** = outliers removed from data

Subsequently, the tumour weight data was re-analysed, where the results are listed in **Table 3.6**.

	original data		outliers removed	
	***p*-value**	**Significant?**	***p*-value**	**Significant?**
control - ajoene	0.3023	No	0.4007	No
control - DATS	0.2345	No	0.0204	Yes*
ajoene - DATS	0.0450	Yes*	0.0077	Yes**

Table 3.6: Summary of *p*-values for the group comparison of the tumour weight data before and after the exclusion of outliers.

Although the scatter plot of the original data in **Figure 3.14 A** showed that the mean of the tumour weight of the DATS-treated group was lower than the control, the presence of the outliers made the results statistically insignificant (p = 0.2345). The removal of the outliers (**Figure 3.14 B**) not only drastically decreased the average variance of the data by 54% (from ±52.39 mg to ±24.22 mg), but also showed a statistically significant 55% reduction of the mean tumour weight (p = 0.0204) for the DATS-treated group. The analysis of the tumour weight for ajoene, corroborated what was seen in the tumour volume data; namely that there was no significant difference. The data on the weight of

the excised tumours was deemed to be the most convincing, as it lacked the inaccuracies associated with calliper measurements.

Overall, it was pleasing that our positive control (DATS) produced a significant inhibitory response in tumour growth. For ajoene, our results indicate that orally administered ajoene, at the high dose of 50 mg/kg, is not able to significantly inhibit WHCO1 tumour growth in a nude mouse xenograft model. Although ajoene has been reported to be active when administered intraperitoneally at doses up to only 25 mg/kg daily for 4 weeks,[89,168] we found that a dose of 50 mg/kg administered by gavage is also non-toxic for up to 4 weeks however for an extended period of 6 weeks, toxicity was observed. One explanation for its failure to inhibit tumour growth may relate to the higher dose. It is known that the overdosing of a drug overwhelms normal physiological functions to cause undesirable effects. In our case, the dose of ajoene might have caused a pathologic level of toxicity.

In summary, ajoene was not found to decrease tumour volume under the experimental conditions of our experiment. Considering that this experiment was only done once, we recommend a follow-up animal study at a lowered ajoene dose. It may also be useful to repeat the experiment using an intraperitoneal route of delivery instead of oral. Based on the large standard deviations in the experiment, it may be advisable to use a larger group of mice to obtain better statistical significance. As there is literature to suggest that ajoene is not stable in blood, we suspected that a *S*-thiolysis exchange reaction with blood components might lower its bioavailability. Thus, we decided to take a closer look at the ajoene structure-activity relationships that govern its cancer cell cytotoxicity as well as blood stability and bioavailability.

3.5 A Structure-Activity Study into the Cytotoxicity and Blood Stability of the Ajoene Pharmacophore

With the above in mind, we designed a small library of ajoene analogues to probe the structure-activity effects of the vinyl disulfide sulfoxide core in relation to blood stability. Following our finding that replacement of the two allyl end groups of ajoene for PMB showed favourable enhancement of antiproliferative activity, we used the bis-PMB ajoene template as the basis for this study. The end groups were chosen as PMB, and

modifications were made in both the vinyl/disulfide sulfoxide core and the methoxy group to probe SAR effects as indicated in **Figure 3.15**.

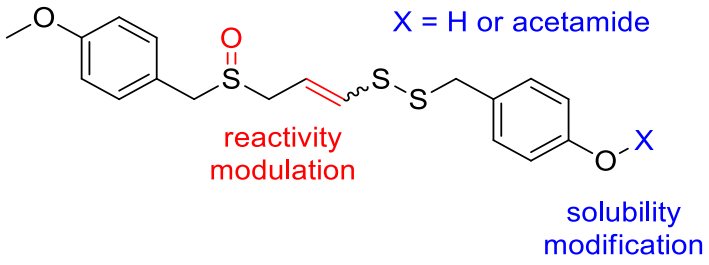

Figure 3.14: Ajoene modification with respect to polarity and reactivity modulation.

3.5.1 Solubility

To enhance the aqueous solubility of bis-PMB, a polar group was introduced at the *para*-position of PMB with improved hydrogen-bonding capability. Large changes were avoided for fear of introducing other activity issues. To this end, the methoxy methyl group (X in **Figure 3.15**) was replaced by H (OH overall), or an amidomethylene moiety (CH_2CONH_2) as two more polar groups. We expected the phenol and amidomethylene groups to enhance blood solubility, while retaining the desired lipophilic character due to the presence of the other PMB group.

3.5.2 Reactivity

Lowering the inherent reactivity towards thiolysis exchange was seen to require removing the double bond to create a dihydroajoene series. This was expected to lower the reactivity of the disulfide as an *S*-thiolating agent in the disulfide exchange in view of a reduced stabilisation of the straight thiolate versus the enethiolate/ajo leaving group. This hypothesis is supported by the literature in terms of DADS being stable in blood, whereas ajoene is not.[211] In this regard, the sulfoxide functionality was considered to provide an inductive stabilisation of the thiolate leaving group, so the redox level at sulfur as sulfide or sulfoxide was also included as part of the study.

3.5.3 Synthesis Overview

The library selected comprised an exhaustive combination of all structural variations aimed to probe the SAR of ajoene with respect to blood stability and cancer cell

cytotoxicity. The eight derivatives (**6 – 9, 11 – 14**) selected as synthetic targets are shown in **Table 3.7**.

parent compounds	
E/*Z*-ajoene	*E*/*Z*-bis-PMB ajoene
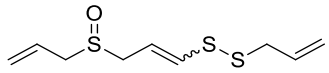	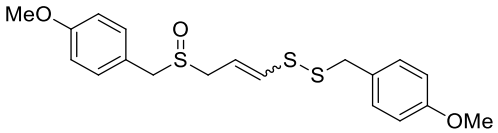
phenol series	**amide series**
phenol-desoxy-PMB-dihydroajoene **11**	amide-desoxy-PMB-dihydroajoene **13**
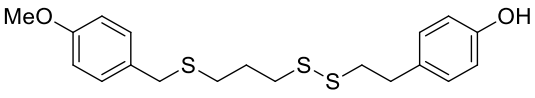	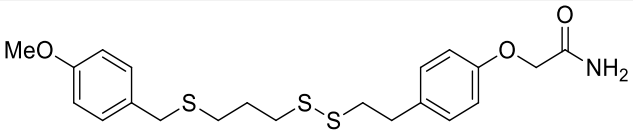
phenol-PMB- dihydroajoene **12**	amide-PMB-dihydroajoene **14**
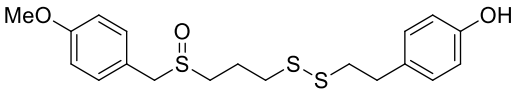	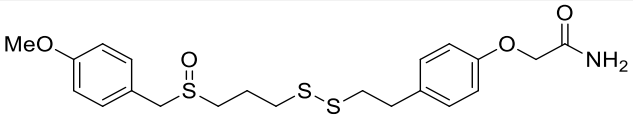
E/*Z*-phenol-desoxy-PMB-ajoene **6**	*E*/*Z*-amide-desoxy PMB-ajoene **8**
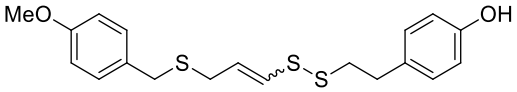	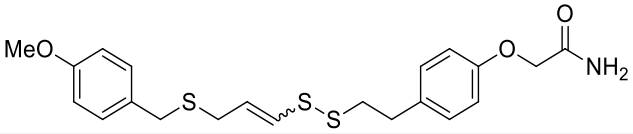
E/*Z*-phenol-PMB-ajoene **7**	*E*/*Z*-amide-PMB-ajoene **9**
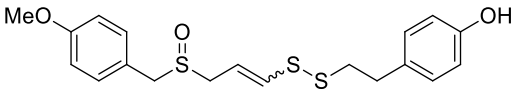	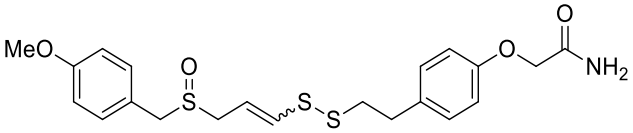

Table 3.7: The SAR analogue library of ajoene.

The ajoene analogues were synthesised using the UCT synthesis previously described (**Chapter 2 – Section 2.3**), which required the solubility tag being placed on the sulfenylating agent. By comparison, the dihydroajoene series was prepared using selective functionalisation of 1,3-propanedithiol. The synthesis of compounds in the two series is described below.

3.5.4 Synthesis of the Ajoene Series

The retrosynthetic strategy for preparing the "water-soluble" ajoenes is shown in **Scheme 3.3**, which led to identifying fragments **2** and **5** as key intermediates, followed by modification involving alkylation of the phenol hydroxyl group.

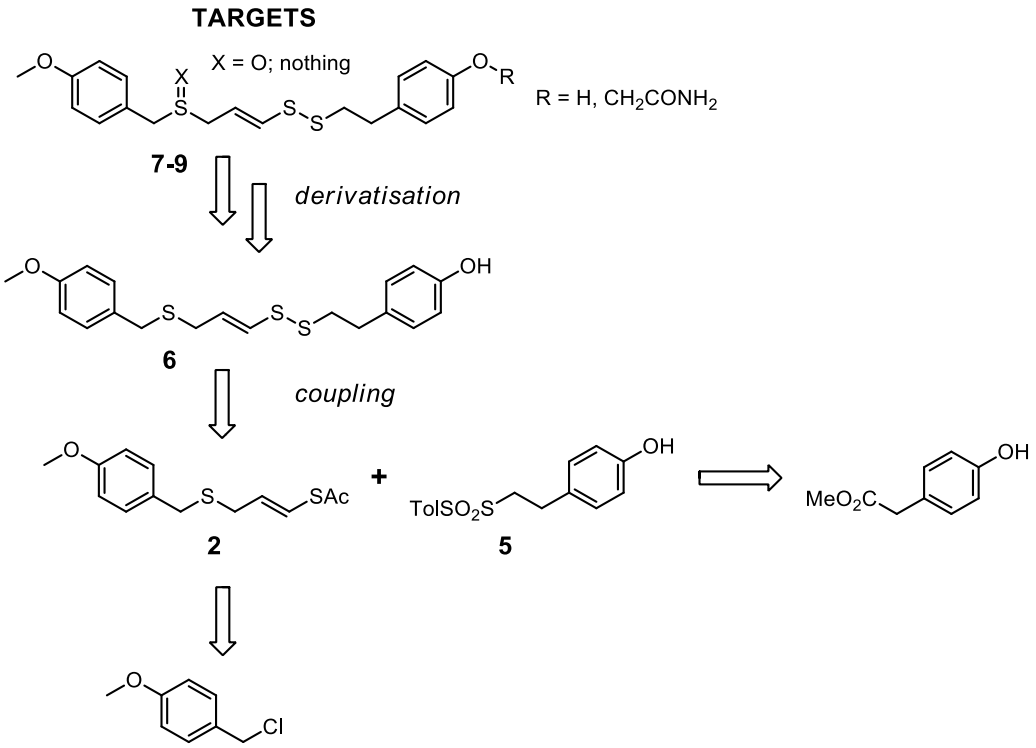

Scheme 3.3:Retrosynthesis of ajoene analogues with polarity modification.

3.5.4.1 Synthesis of Coupling Fragments 2 and 5

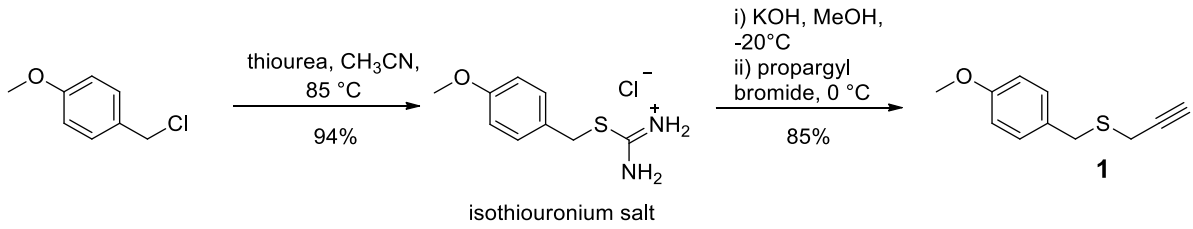

Scheme 3.4: Synthesis of propargylic thioether, 1.

The first step towards the synthesis of coupling partner **2** involved the formation of the isothiouronium salt as shown in **Scheme 3.4** via refluxing PMBCl with thiourea (1.2 eq) in acetonitrile for fourteen hours. Following cooling of the solution, the product precipitated, and was filtered then washed. Without any further purification, the salt was taken up in methanol and hydrolysed with KOH (2 eq, for 2 hours at -20 °C) to generate the thiol *in situ*, which was subsequently alkylated using an excess of propargyl bromide (1.5 eq) at 0 °C to form the desired thioether **1** within 30 minutes. Silica gel column chromatography afforded **1** as a clear-yellow oil in an overall 85% yield, going from the isothiouronium salt.

The ^{1}H-NMR spectrum of **1** showed propargylic methylene and terminal alkyne proton resonances as a doublet at 3.80 ppm (2H) and a triplet (1H) at 2.28 ppm, respectively. Also, the eleven carbon atoms of **1** could be observed in the ^{13}C-NMR spectrum as nine resonances due to symmetry in the benzene ring. The diagnostic quaternary alkyne carbon (**C-8**) signal appeared at 80.1 ppm.

The regioselective radical addition step proceeded as normal by dissolving **1** in toluene and heating the solution to 85 °C before adding the radical initiator ACCN (0.1 eq) followed by thioacetic acid dropwise. The mixture was then refluxed for three hours. TLC analysis showed the formation of a more polar spot that was isolated via silica gel column chromatography to afford the odiferous vinyl thioacetate oil, **2**, as a 1:2 mixture of *E/Z*-isomers in 48% yield.

The IR spectrum of **2** showed a C=O stretch at 1700 cm^{-1} for the thioacetate group. Importantly, disappearance of the propargylic system in the ^{1}H-NMR spectrum with the appearance of two vinylic resonances with *cis* (9.6 Hz) and *trans* (15.6 Hz) vicinal couplings indicated that regioselective addition of the thioacetyl group had taken place to the alkyne terminus (**Figure 3.16**). The complete assignment of eleven resonances for each isomer in the ^{13}C-NMR spectrum could be achieved with the help of HSQC. Notably, the carbonyl carbon (**C-10**) resonated far downfield at 191.4 ppm (*Z*) and 193.1 ppm (*E*), while the vinyl carbon signals were observable at 130.3 (*Z*), 128.7 (*E*) for the α-vinyl carbon **C-9**, and 119.7 (*E*), 119.5 (*Z)* for the β-vinyl carbon **C-8**. In total, twenty-two carbon resonances could be observed for the two isomers.

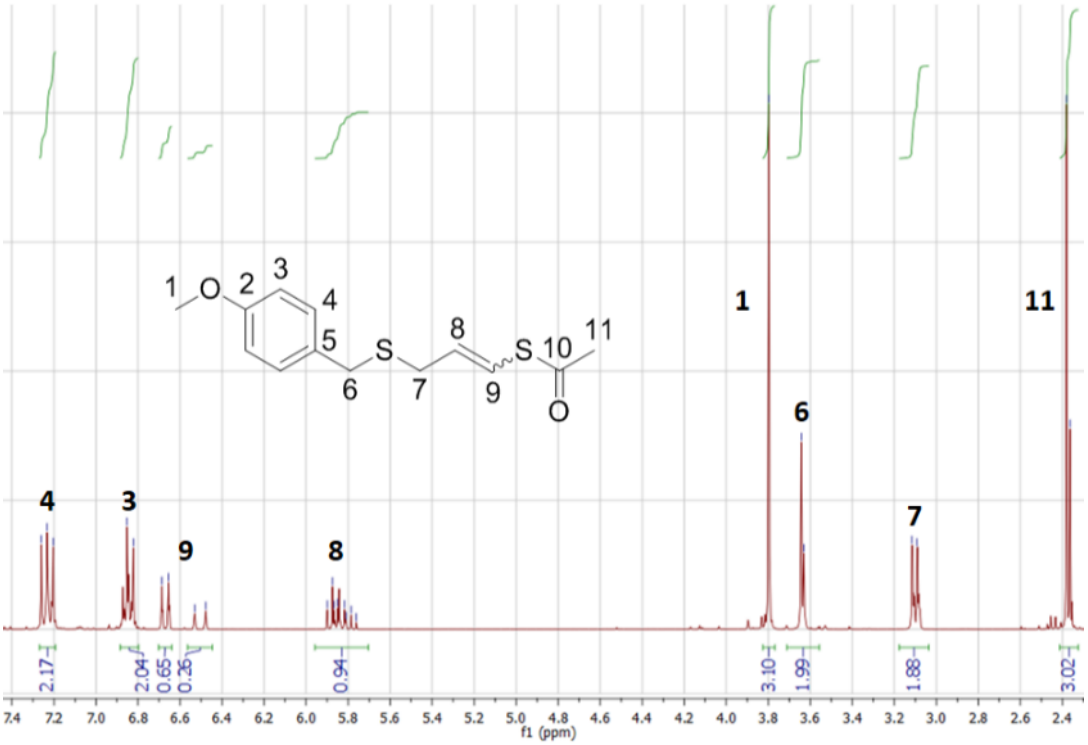

Figure 3.15: ^{1}H-NMR spectrum of PMB-vinyl thioacetate, 2.

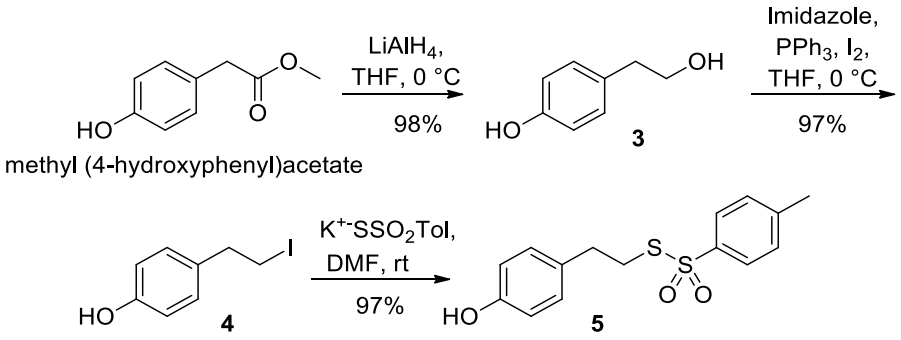

Scheme 3.5: Synthesis of hydroxyphenethyl thiotosylate, 5.

Synthesis of the coupling partner, **5**, involved applying standard functional group conversion reactions (**Scheme 3.5**), starting with the $LiAlH_4$ (2.2 eq) reduction of commercially available methyl (4-hydroxyphenyl) acetate. This was achieved in dry THF at 0 °C, and the reaction was complete after two hours as monitored via TLC, with the formation of a single UV-active spot of higher polarity. The reaction was quenched under acidic conditions to liberate the product from the aluminium alkoxide salts. A subsequent work-up and purification via flash chromatography yielded **3** as a colourless solid in 98% yield that could be recrystallised from EtOAc/hexane. Its resulting melting point range of 91-93 °C corresponded sufficiently well with the literature value of 90 °C.[260]

Formation of the primary alcohol was confirmed by the ^{1}H-NMR spectrum of **3** which revealed the disappearance of the methoxycarbonylmethylene functionality (as two singlets). This was replaced by two triplets for the two vicinal methylene groups. Similarly, the ^{13}C-NMR spectrum confirmed the presence of all six expected resonances in a 4:2 aromatic:aliphatic split.

The next step involved an Appel reaction to convert the primary hydroxyl group of **3** into its iodide **4**. This was achieved using triphenylphosphine and iodine, with imidazole as a base to neutralise the HI produced. The mechanism of the reaction is shown in **Scheme 3.6** and involves an S_N2 reaction in the final step.

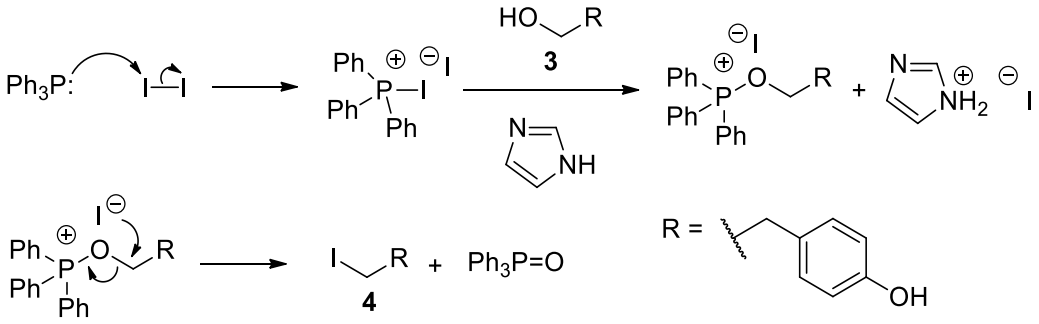

Scheme 3.6:Mechanism of the Appel transformation of 3 to iodide, 4.

The reaction was fast, as indicated by TLC, and was worked up after two hours at room temperature in THF. Purification via silica column chromatography successfully removed the triphenylphosphine oxide by-product to obtain **4** as a yellow crystalline solid in 97% yield.

The ^{1}H-NMR spectrum of **4** showed the disappearance of the alcohol hydroxyl peak of **3** together with an upfield shift of the methylene group bearing the heteroatom. In the ^{13}C-NMR spectrum, the highly shielded signal at 6.4 ppm represented a characteristic iodoalkyl carbon.

The sulfenylating agent **5** was obtained by the S_N2 reaction of **4** with an excess of potassium thiotosylate (2 eq) in DMF at room temperature overnight. Diluting the resulting reaction mixture with EtOAc and subjecting it to copious washings with H_2O successfully removed the DMF and any inorganic by-products. Silica gel column chromatography afforded **5** as a clear, yellow oil in 97% yield. We were glad to see that the phenolic hydroxyl group could be taken through the sequence without the need for protection.

Its ^{13}C-NMR spectrum (run in $CDCl_3$) displayed eleven resonances that were assigned to the fifteen carbon atoms in the molecule. The addition of a tosyl group showed an extra set of double doublets (**H-8/-9**) at 7.82 and 7.34 ppm and a methyl singlet (**H-11**) at 2.45 ppm in the ^{1}H-NMR spectrum run in $CDCl_3$ (**Figure 3.17**). The IR spectrum showed the retention of the phenolic group by virtue of an O-H stretch at 3436 cm^{-1}.

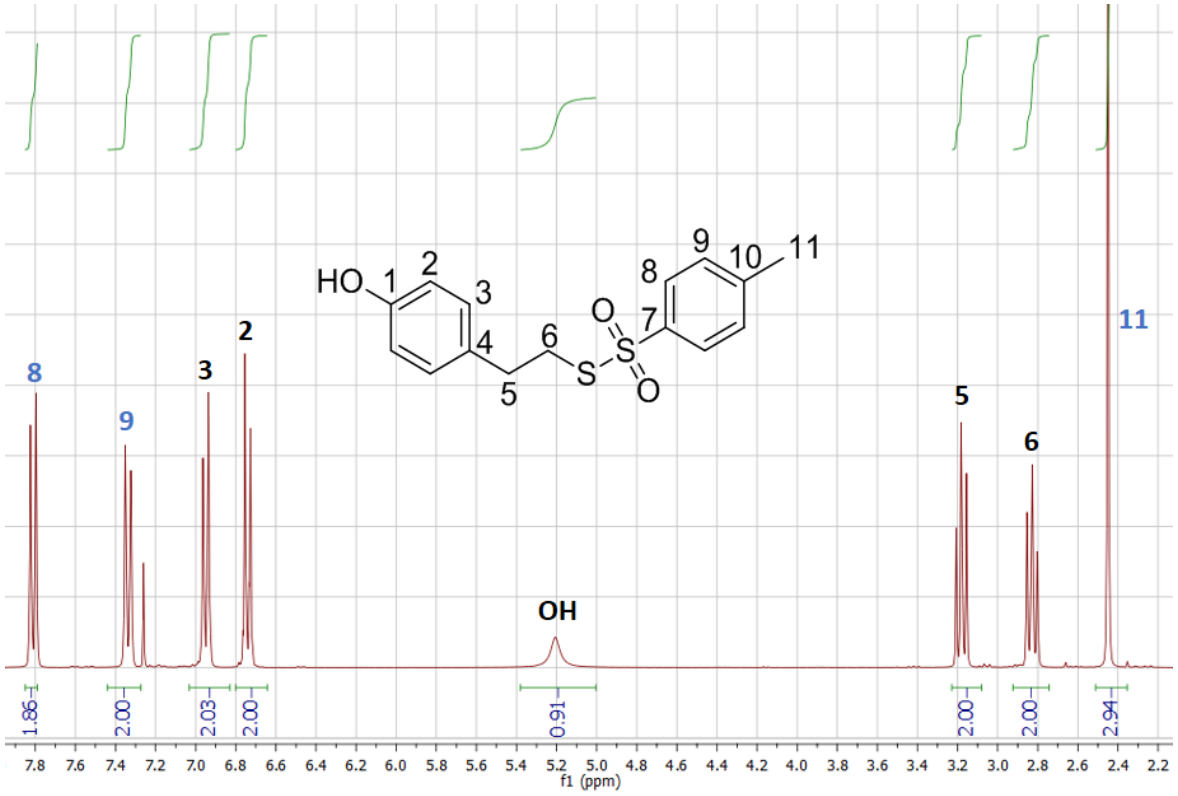

Figure 3.16: ^{1}H-NMR spectrum of sulfenylating agent, 5.

3.5.4.2 Coupling of 2 and 5 to Disulfide 6

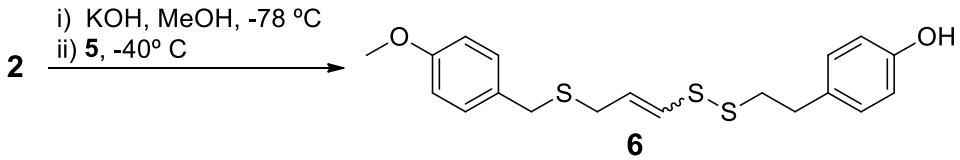

Scheme 3.7:Fragment coupling by sulfenylation.

The coupling of **2** and **5** was achieved using the UCT synthesis which involved treating **2** with potassium hydroxide (MeOH, -78 °C) to generate an enethiolate followed by sulfenylation with **5** at the soft end of the enethiolate. Isolation via an extractive work-up

and purification by silica column chromatography gave **6** (**Figure 3.18**) in 72% yield and as a 3:5 mixture of *E*/*Z* isomers according to the ^{1}H-NMR spectrum.

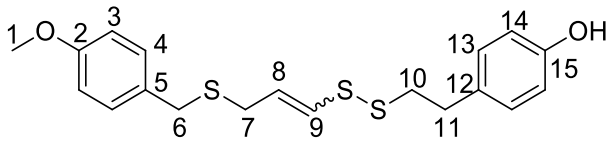

Figure 3.17:Phenol-ajoene, 6.

Support for the formation of **6** was given by the appearance of both coupling fragments in the ^{1}H-NMR spectrum of **6**, with the exception of the thioacetyl methyl singlet (the IR also lacking the carbonyl stretch) as well as thiotosylate signals. *Cis* and *trans* isomers were detected by virtue of the appearance of two distinct geometric sets of doublets of triplets at 6.24 and 6.09 ppm for the H_α proton (**H-9**) of the *Z*- and *E*-isomers respectively. The triplet arose due to an allylic coupling with the allylic methylene hydrogens (**H-7**), while a vicinal coupling with **H-8** of 9.3 Hz could be assigned to the *Z*-isomer at 6.24 ppm and a 14.6 Hz coupling for the *E*-isomer at 6.09 ppm. Similarly, the H_β (**H-8**) hydrogen appeared as two sets of doublet of triplets at 5.88 and 5.70 ppm, with the same *cis* and *trans* couplings with **H-9** but a larger vicinal coupling of 7.3 Hz with **H-7**, as shown in **Figure 3.19**.

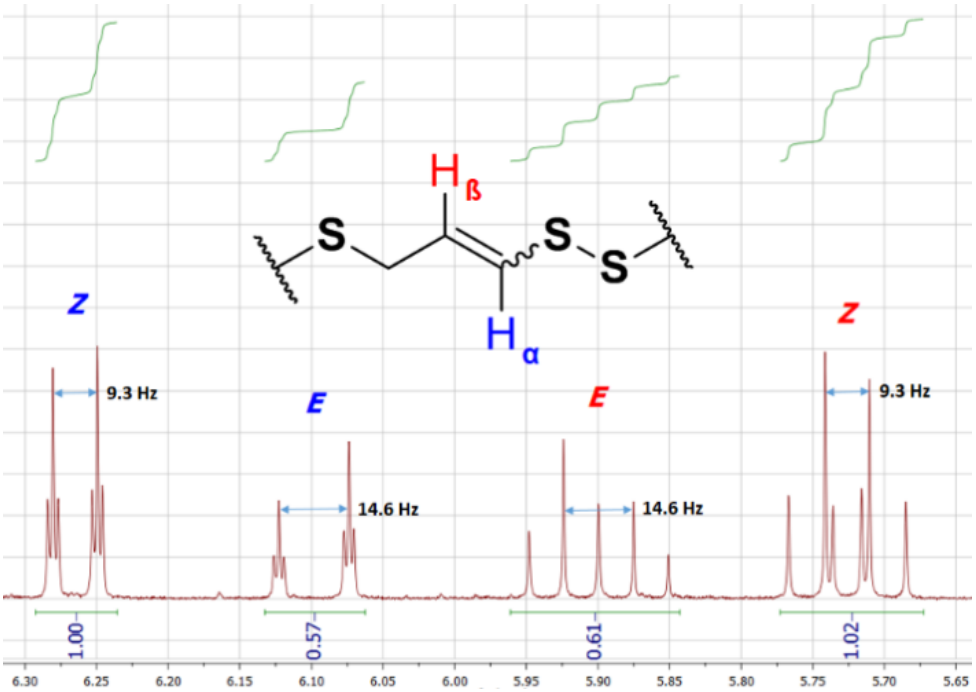

Figure 3.18: Expansion of ^{1}H NMR vinylic signals of 6.

The ^{13}C-NMR spectrum of **6** showed resonances for all 19 carbon atoms for each isomer, in which some carbons away from the stereogenic axis resonated at the same chemical shift. Two downfield signals at 158.8 and 154.3 ppm could be assigned to the deshielded quaternary aromatic carbons, **C-2** and **C-15** respectively. The remaining two quaternary centres, **C-5** and **C-12**, were identified at 132.2 and 130.7 ppm. Although **H-10** and **H-11** were indistinguishable in the ^{1}H-NMR spectrum, HSQC analysis of the ^{13}C-NMR spectrum revealed **C-10** as having distinct *E*- and *Z*- signals (39.9 and 40.6 ppm), while the benzylic **C-11** appeared as a single resonance at 34.8 ppm for both isomers, as seen in **Figure 3.20**.

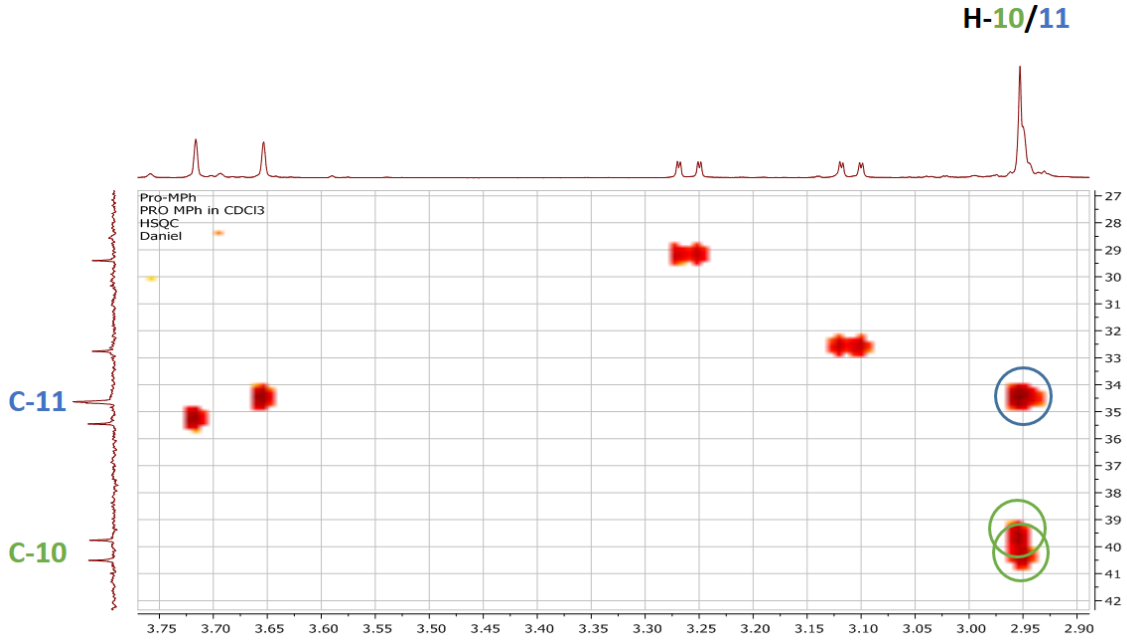

Figure 3.19: Expansion of HSQC for C-10/-11 of 6.

3.5.4.3 Final Derivatisations

The various options for final derivatisations to access targets in **Table 3.7** are shown in **Scheme 3.8**.

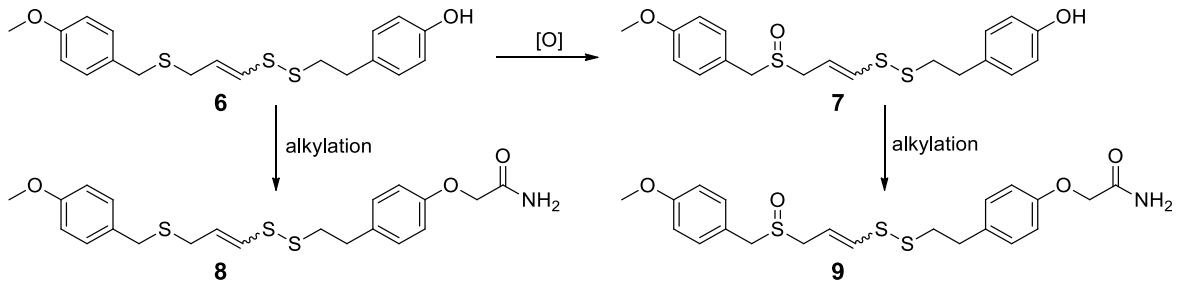

Scheme 3.8: Derivatisation sequence, depicting oxidation and alkylation steps.

Hence, chemoselective oxidation, as usual, of the more nucleophilic sulfur of **6** with *m*-CPBA in DCM at -78 °C afforded the ajoene-phenol derivative **7**. Following a basic work-up to remove the benzoic acid by-product as well as excess *m*-CPBA, isolation by chromatography produced **7** as a 1:2 mixture of *E*/*Z*-isomers in 60% yield.

Formation of the sulfoxide as opposed to the sulfone was indicated by the presence of diastereotopic **H-7** hydrogens due to the adjacent chiral sulfoxide, with a large geminal coupling of about 13 Hz. The details and spectrum are presented in **Figures 3.20** and **3.21** respectively.

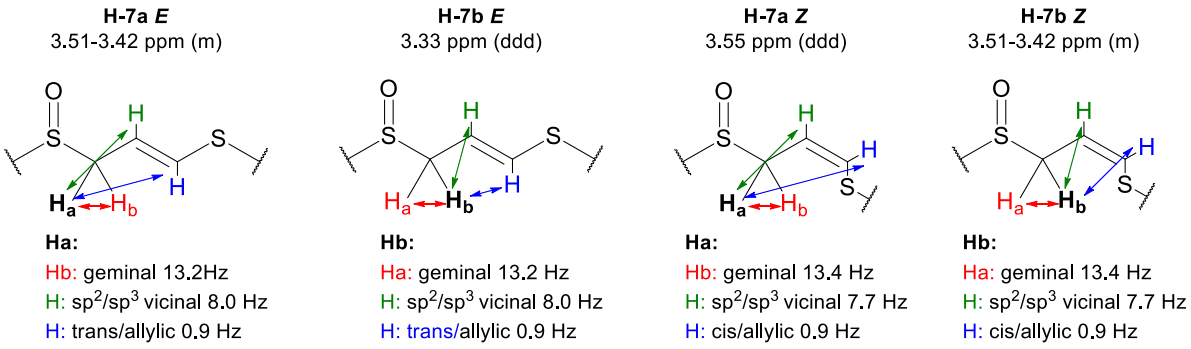

Figure 3.20: H-7 coupling patterns for 7.
J-values of multiplets are estimated

Taking overlapping signals and geometric isomerism into account, all 38 carbon atoms (19 per isomer) could be identified through the aid of ^{13}C-NMR and HSQC analysis. The ^{13}C-NMR spectrum revealed the strong deshielding effect of the sulfoxide on adjacent carbon atoms, **C-6** and **C-7**. The *E*- and *Z*-isomers of **C-6** in **7** resonated higher at 56.4 and 57.0 ppm, compared to at 34.8 and 35.6 ppm in **6**. Similarly, the two isomeric signals for **C-7** had shifted from 32.9 and 29.5 ppm (in **6**) to 52.9 and 49.6 ppm, for *E* and *Z* respectively in **7**.

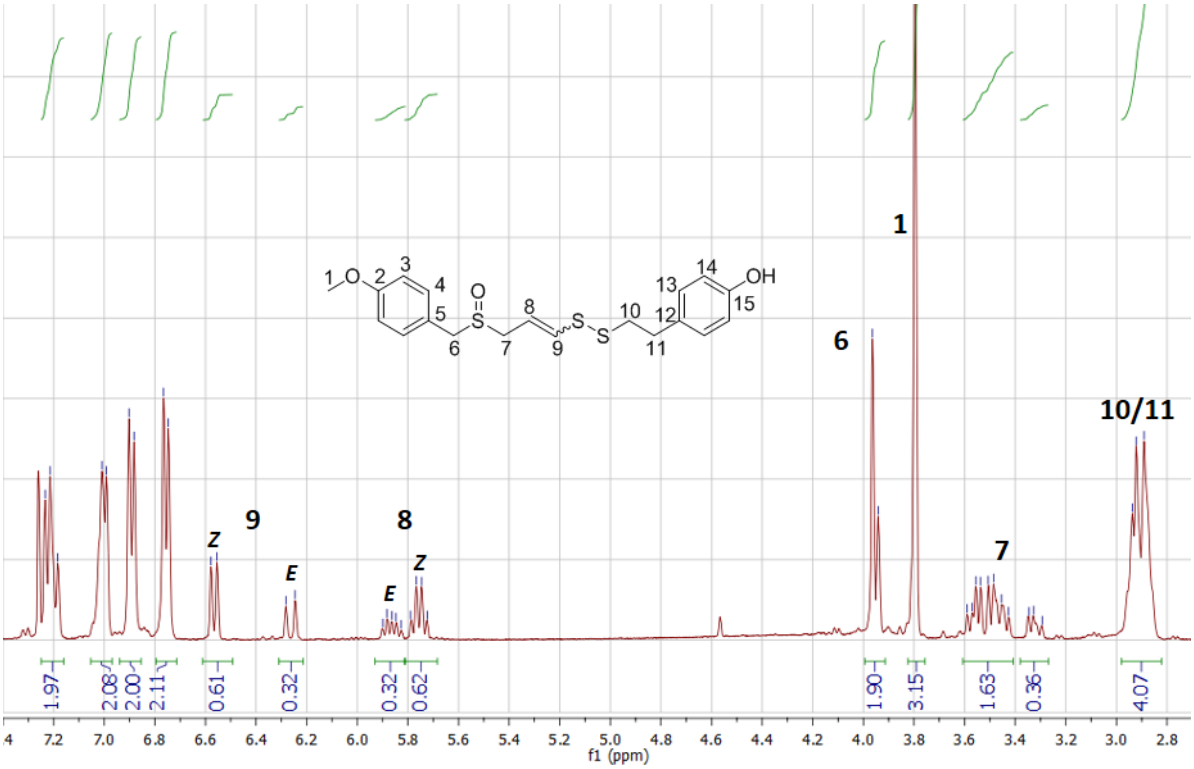

Figure 3.21: ^{1}H-NMR spectrum of phenol-ajoene, 7.

As shown in **Scheme 3.8**, alkylation to the amide was required at the two different oxidation levels. This could be achieved by using potassium carbonate (2 eq) as base with 2-chloroacetamide (2 eq) and TBAI (0.1 eq) in acetonitrile for twelve hours at 40 °C. The TBAI was used to generate iodoacetamide *in situ*. **Scheme 3.9** summarises the S_N2 reaction involved. For ajoene-amide **9**, it was found best to alkylate last, post sulfide oxidation.

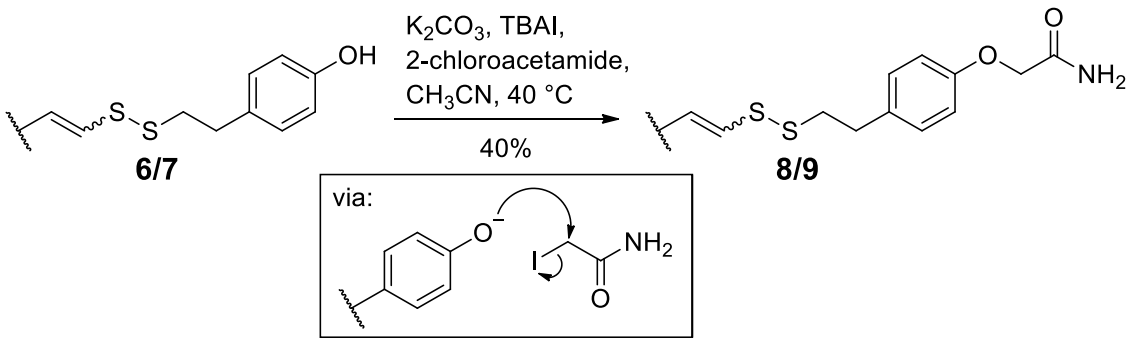

Scheme 3.9: Phenol alkylation.

Application of this methodology afforded the sulfide-amide **8** as a 3:4 mixture of *E*/*Z*-isomers in 40% yield, and the sulfoxide-amide, **9**, in 48% and an *E*:*Z*-ratio of 3:2.

Interestingly, inversion of the ratio from 1:2 in **7** to 3:2 in **9** implies that the reaction in some way enriches in the *E*-isomer, presumably via deprotonation of one of the acidic α-sulfoxide protons, followed by double bond isomerisation to the more stable *trans*-isomer with reprotonation. However, a selective reactivity of the *E*-isomer over the *Z*-isomer cannot be discounted.

The ^{1}H-NMR spectra of **8** and **9** were analogous to those of **6** and **7**, with diagnostic *E/Z* splitting observed for the vinylic protons (order of chemical shift = *Z-E-E-Z*), the presence of two sets of aromatic signals (dd x 2) and the five methylene proton signals accounting for the methoxy, benzylic (x2) and α-sulfide (x2) (sulfoxide for **7** and **9**) positions. However, an extra methylene singlet at around 4.5 ppm in both spectra (**8/9**) for each isomer could be observed for the newly introduced amidomethylene moiety (**Figure 3.23**). Moreover, a pair of N-H resonances at ~6.6 and 6.0 ppm (*E*- and *Z*- coincidental here) could be observed for the non-equivalent amide hydrogens. Two N-H stretching bands in the IR spectrum at around 3200 and 3400 cm^{-1} as well as an amide carbonyl stretch at 1700 cm^{-1} confirmed the presence of the primary amide. The ^{13}C-NMR spectrum provided further evidence as it showed two additional acetamide carbon signals for **C-16** and **C-17** at 67.5/67.4 ppm (CH_2) and 171.2/171.1 ppm (carbonyl) for **8/9** respectively. The HRMS data for **8** gave a molecular ion $[M+H]^+$ at 436.1068 $[M+H]^+$, for which $C_{21}H_{26}NO_3S_3$ requires 436.1080, thus further corroborating that successful amide modification of these analogues had been achieved.

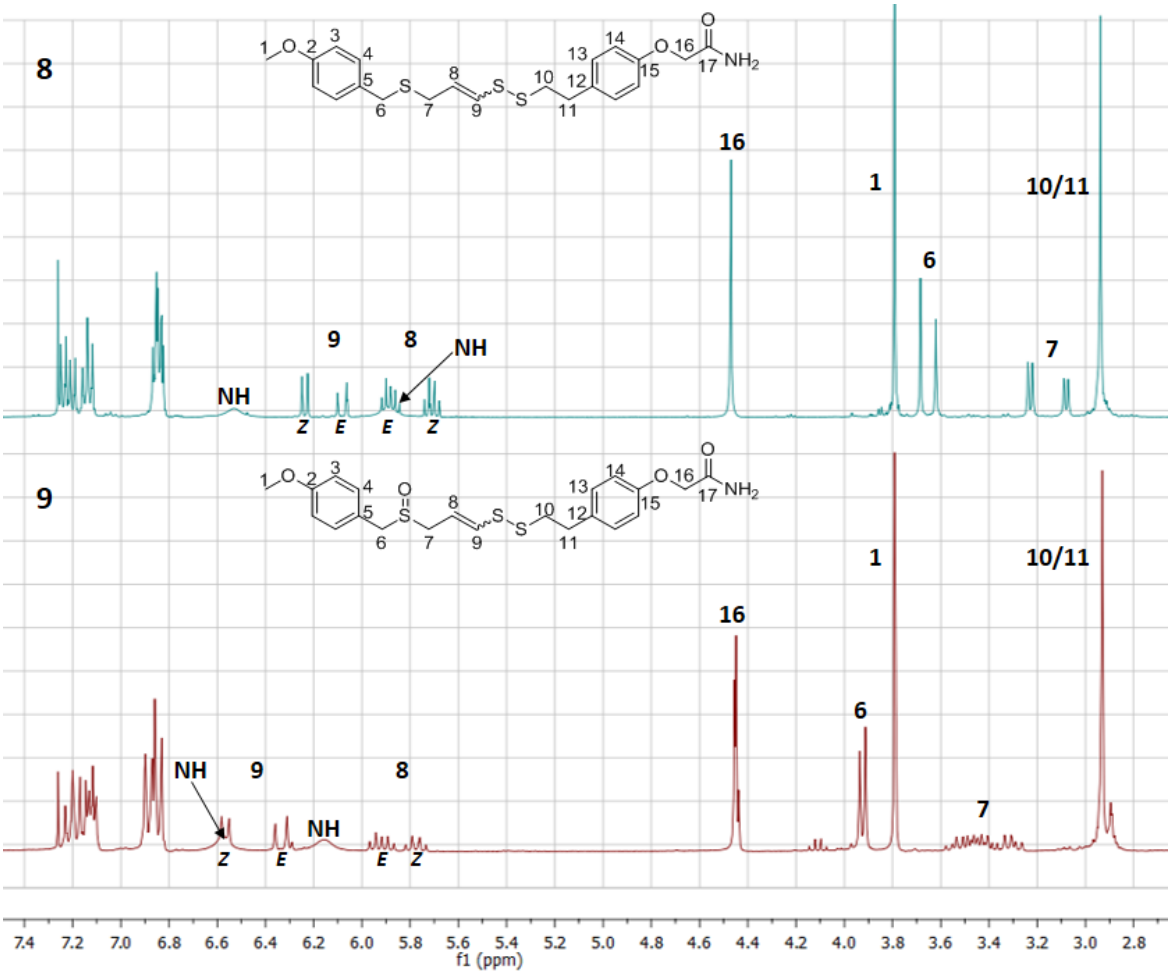

Figure 3.22: ^{1}H-NMR spectrum of amide-ajoene analogues, 8 and 9.

With the bis-PMB ajoene analogues in hand, attention was turned towards accessing the analogous compounds in the dihydroajoene series, which is described in next section.

3.5.5 Synthesis of the Dihydroajeone Series

The synthesis envisioned (**Scheme 3.10**) proceeding via the mono-alkylation of 1,3-propanedithiol by exerting careful stoichiometric control to avoid formation of the dialkylated product. Thereafter, the remaining thiol would be sulfenylated with **5** to obtain **11**. Subsequent chemoselective oxidation of the more nucleophilic sulfur of **11** was expected to afford the sulfoxide disulfide, **12**. Finally, alkylation of **11** and **12** would afford the targets **13** and **14**.

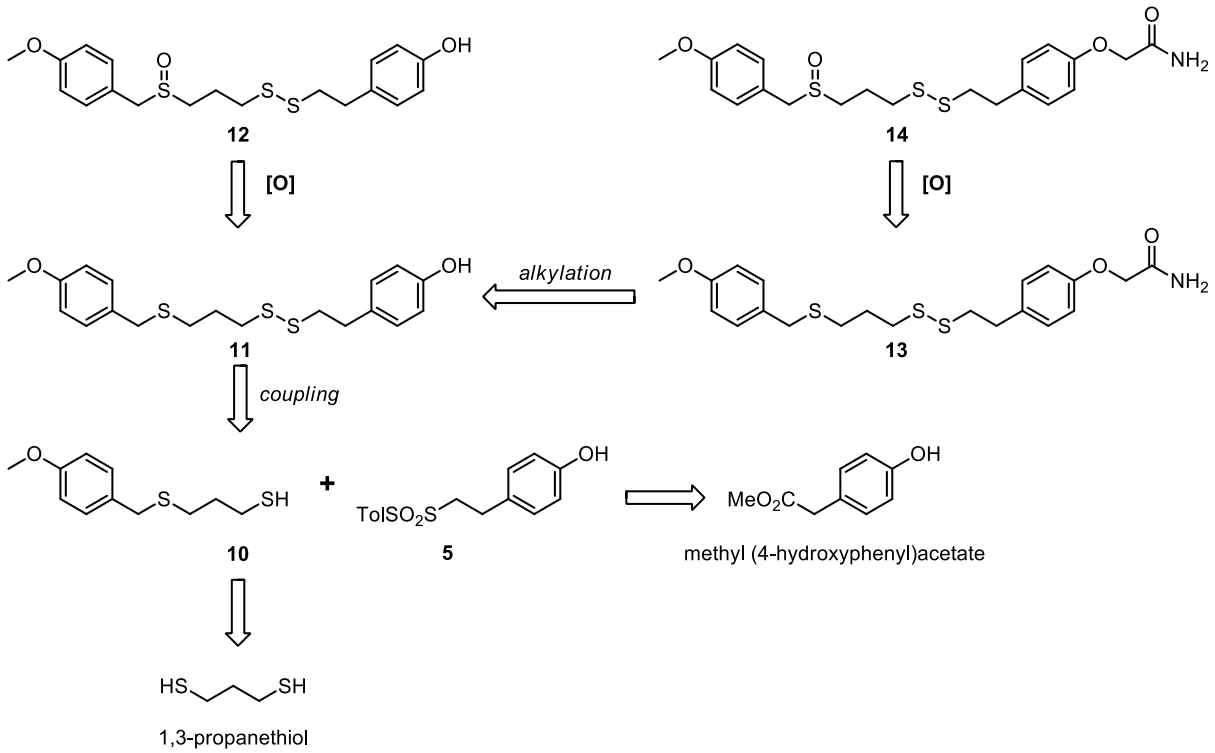

Scheme 3.10: Retrosynthesis of dihydroajoene analogues containing polarity modification.

3.5.5.1 Synthesis of 11 and 12

Scheme 3.11 below summarises the two substitution and oxidation steps.

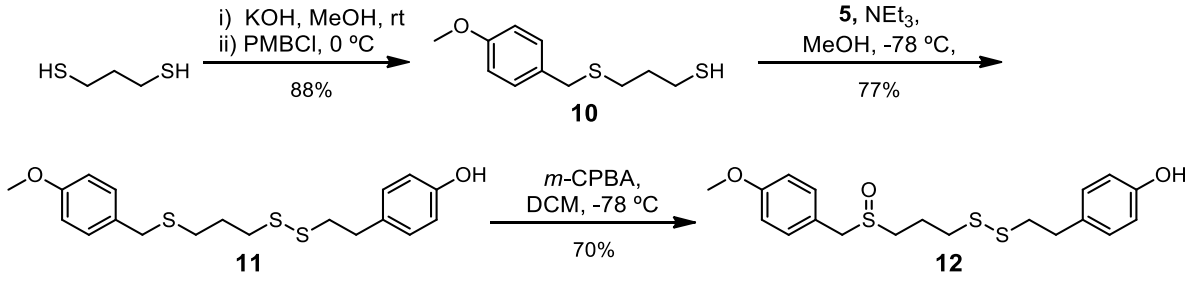

Scheme 3.11: Synthesis of PMB-*S*-propanethiol, 10.

Optimal conditions for the first step involved mixing an excess of 1,3-propanedithiol (1.2 eq) with potassium hydroxide (1.4 eq) in anhydrous methanol at 0 °C and then adding PMBCl (1 eq) dropwise. After two hours, TLC analysis showed that PMBCl had been completely consumed, and the reaction was neutralised with 1M HCl. Purification via silica gel column chromatography afforded the desired mono-alkylated thiol **10** in 88% yield.

Two pairs of aromatic doublets at 7.23 and 6.85 ppm together with two methylene triplets at 2.52 and 1.84 ppm from the propanedithiol partner with an integration ratio of 2:2:2:2 in the ^{1}H-NMR spectrum of **10** indicated a successful mono-alkylation. In addition, a triplet for a single thiol hydrogen was observed at 1.33 ppm.

The second thioalkylation proceeded by sulfenylating **10** with **5** in MeOH at -78 °C using triethylamine (1.5 eq) as reagent (for the expelled sulfinic acid) and base catalyst. Warming the mixture to room temperature over one hour followed by an acidic work-up and purification gave the sulfide disulfide, **11**, as a colourless waxy solid in 77% yield.

A successful coupling could be discerned by the appearance of signals for the sulfenylating agent in the ^{1}H-NMR spectrum of **11**, in which a correct relative integration for the two reactant fragments (**10** and **11**) was evident. The IR spectrum of **11** showed the appearance of a S-S stretching band at 550 cm^{-1}, while the phenolic hydroxyl showed a strong O-H stretching band at 3433 cm^{-1}. All 15 carbon resonances could be accounted for in the ^{13}C-NMR spectrum. Lowfield signals resonating at 158.8 and 154.3 ppm, respectively, represented the quaternary aromatic signals adjacent to the methoxy and hydroxyl groups, respectively.

Analogous to the ajoene synthesis, the last step in this sequence involved a regioselective oxidation of **11** of the benzylic sulfide sulfur with *m*-CPBA (1.5 eq) in DCM at -78 °C. The reaction proceeded over one hour and gave the sulfoxide, **12**, in 70% yield after work-up and chromatography.

Figure 3.24 confirms previous observations regarding the effect of the chiral sulfoxide on the prochiral hydrogens, **H-6** of **12**, which were observed as a diastereotopic pair of AB doublets at 3.99 and 3.95 ppm, shifted downfield from 3.67 ppm in **11**. The other diastereotopic hydrogens, **H-7**, as a multiplet at 2.77-2.58 ppm, were found mixed with **H-9**, which in **11** were separated as two distinct signals at 2.51 and 2.73 ppm. This could be accounted for by the deshielding inductive effect of the sulfoxide. Similarly, all 15 carbon signals were accounted for in the ^{13}C-NMR spectrum in which notably both the α-carbons to the sulfoxide experienced strong deshielding shifts caused by the electron-withdrawing sulfoxide, **C-6** from 35.8 ppm (in **11**) to 57.7 ppm in **12**, as well as **C-7** from 29.9 ppm to 49.0 ppm. Finally, the HRMS data supported formation of **12**, with the molecular parent ion $[M+H]^{+}$ found at 397.0966, $C_{19}H_{25}O_3S_3$ requires 397.0960. Generally, the NMR spectra in this dihydroajoene series were much easier to assign than in the ajoene series because of the absence of *E/Z*-geometrical isomers.

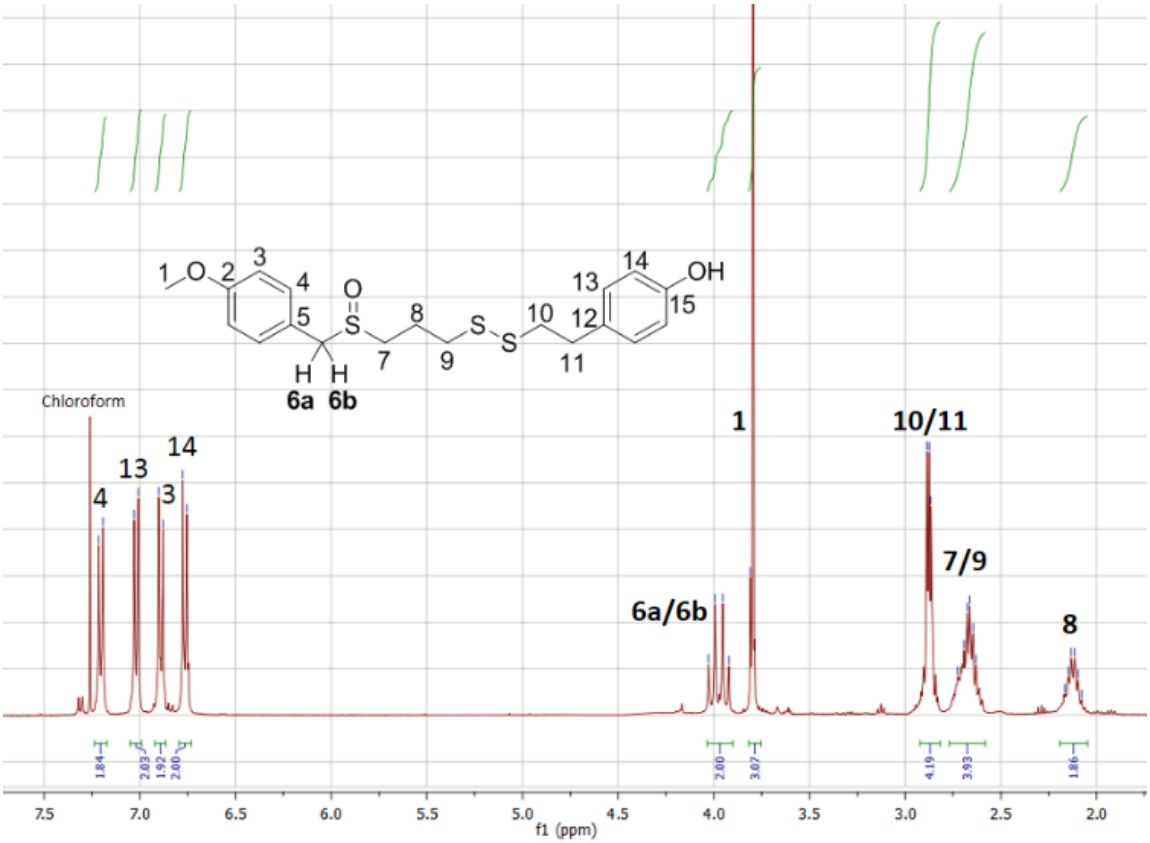

Figure 3.23: ^{1}H-NMR spectrum of phenol-dihydroajoene, 12.

3.5.5.2 Synthesis of 13 and 14

The last two compounds of the dihydroajoene series were accessed linearly via their phenol parent, **11**, through first alkylation followed by oxidation to **14**, **Scheme 3.12**.

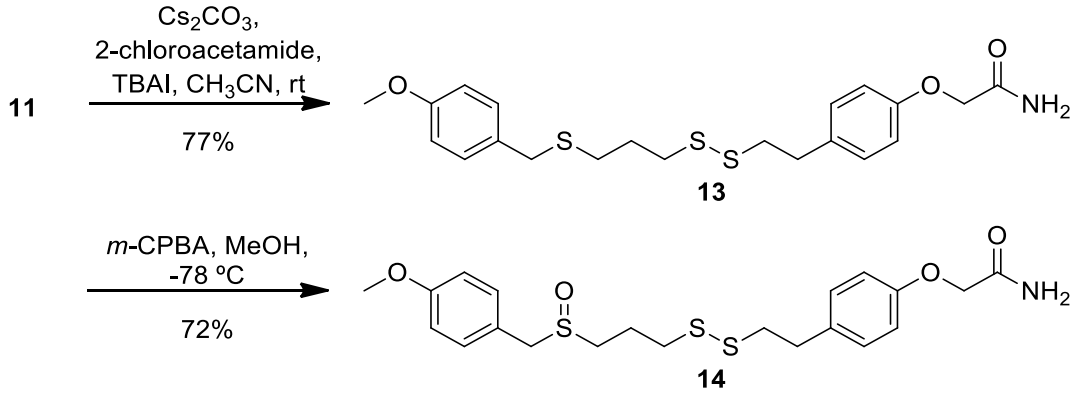

Scheme 3.12: Synthesis of amide-dihydroajoenes, 13 and 14.

The first attempts at alkylation of the phenol OH with chloroacetamide using our previous method for forming **8** and **9** with K_2CO_3 and TBAI at 40 °C resulted in the decomposition

of **11** with none of **13** being detected. Although the lowering of the reaction temperature to rt resulted in some conversion to **13**, the reaction was sluggish (> 24 hours) which caused a significant loss of starting material *in situ*. We worked around this by replacing K_2CO_3 with Cs_2CO_3. Therefore, to generate **13**, sulfide **11**, caesium carbonate (1.5 eq), 2-chloroacetamide (1.5 eq) and TBAI (0.1 eq) were reacted in acetonitrile at room temperature for eighteen hours. Pleasingly, compared to the alkylation of the ajoene analogues **8** and **9**, the dihydroajoene compound, **13**, was obtained in a much higher yield of 77%, also as a more polar spot on TLC.

A singlet at 4.48 ppm in its ^{1}H-NMR spectrum for the newly introduced amidomethylene group together with two broad non-equivalent (due to amide resonance) amide hydrogen singlets at 6.53 and 5.71 ppm indicated a successful alkylation. The ^{13}C-NMR spectrum of **13** showed further evidence of the new functionality in the form of a strongly deshielded carbonyl carbon at 171.1 ppm as well as a much less deshielded methylene carbon neighbour resonating at 67.5 ppm. The infrared spectrum showed characteristic amide N-H stretches and a carbonyl C=O stretch at 3160/3380 cm^{-1} and 1666 cm^{-1}, respectively.

The amide sulfoxide, **14**, was obtained via a regioselective oxidation with *m*-CPBA in 72% yield, as previously described for **12**.

A diagnostic diastereotopic pair of AB doublets at 3.96 and 3.93 ppm in the ^{1}H-NMR spectrum for **H-6** proved that oxidation had taken place at the sulfide sulfur only, **Figure 3.25**. Seventeen distinct carbon resonances were detected and accounted for. Lastly, the successful synthesis of **14** was confirmed via its HRMS data, in which its parent ion $[M+H]^+$ was found at 454.1187; where $C_{21}H_{28}NO_4S_3$ requires 454.1186.

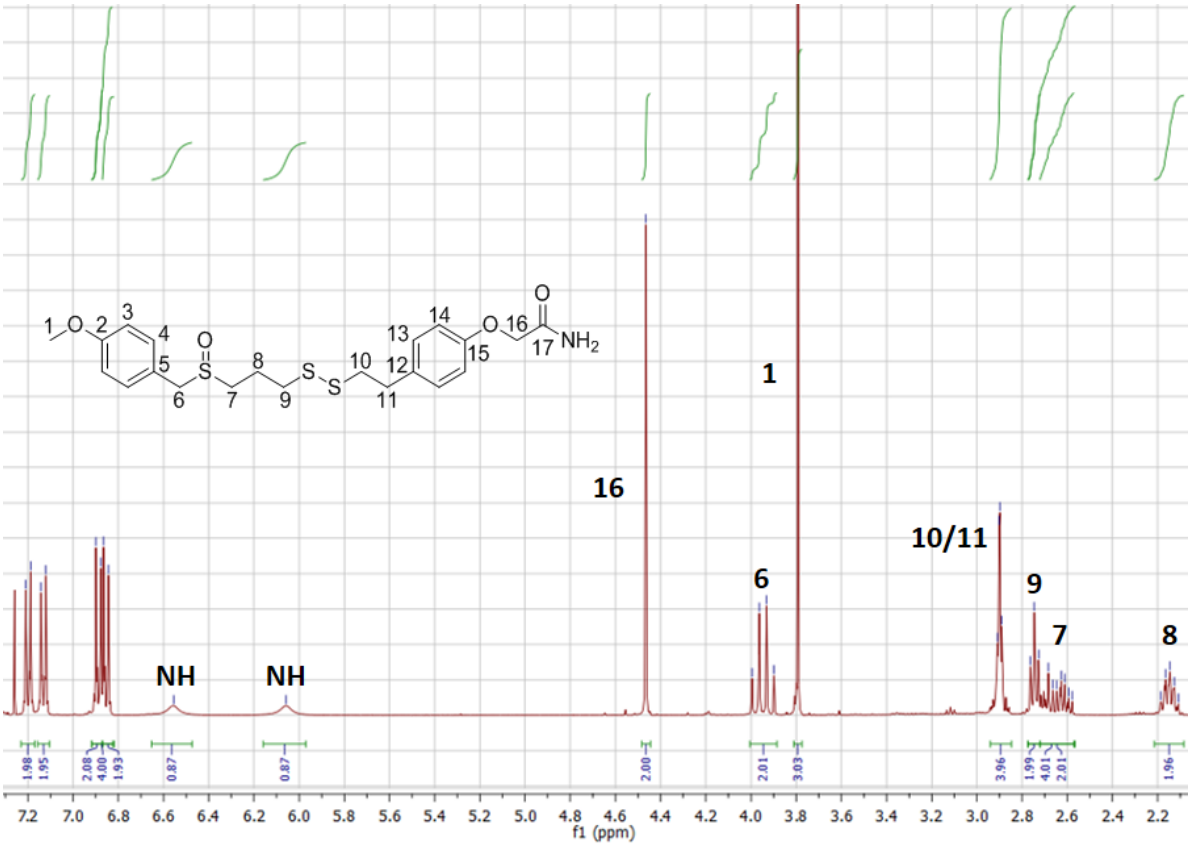

Figure 3.24: ^{1}H-NMR spectrum of amide-dihydroajoene, 14.

3.5.6 Biological Evaluation of Bis-PMB Analogues

With the successful synthesis of the eight new ajoene analogues, we set out to test these analogues for cytotoxicity against WHCO1 cells and to perform an *in vitro* LC/MS experiment to evaluate their stability in mouse blood. The IC_{50} values for the analogues are summarised in **Table 3.8** as an average and standard deviation of at least 3 independent determinations.

Compound	WHCO1 IC_{50} (μM)
Ajoene 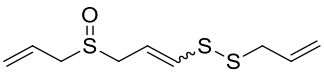	***E*:** 39.0 ± 7.8 [80] ***Z*:** 25.0 ± 2.8 [80]
bis-PMB ajoene 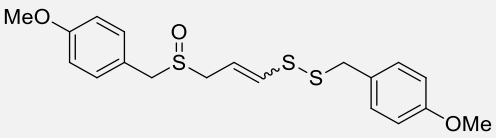	2.1 ± 0.4 [183]
phenol series	
11 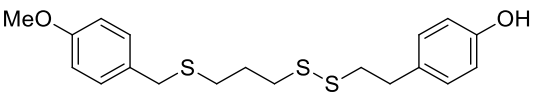	14.3 ± 3.1
12 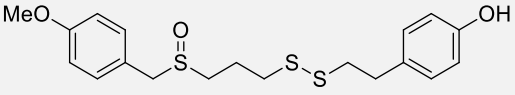	4.9 ± 0.6
6 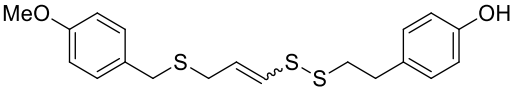	0.48 ± 0.28
7 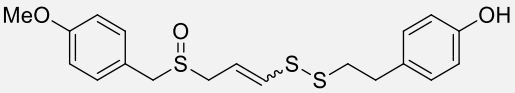	2.65 ± 0.50
amide series	
13 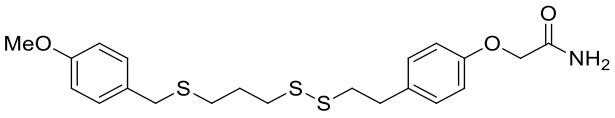	23.2 ± 0.9
14 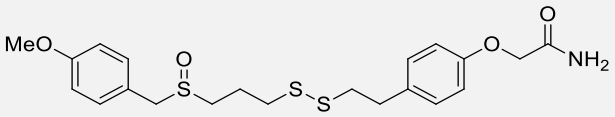	13.6 ± 0.7
8 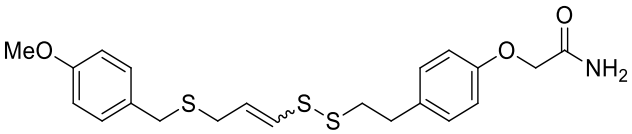	8.6 ± 4.2
9 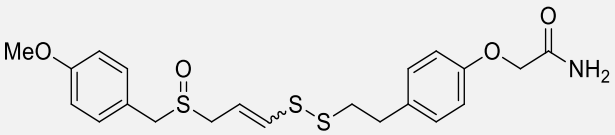	7.4 ± 1.7

Table 3.8: Cytotoxicity IC_{50} of ajoene analogues in WHCO1 cells.

In previous work (see **Chapter 2**), the ajoene disulfide was identified as the pharmacophore responsible for cytotoxicity against WHCO1 cells. Its vinyl group was shown to enhance ajoene's activity by labilising the disulfide towards thiolysis exchange, as its removal in bis-PMB dihydroajoene demonstrated an 8-fold reduction in activity.[183] The removal of the sulfoxide, in the presence of the vinyl group, was found to enhance activity threefold. However, the ajoene analogue lacking both the double bond and the sulfoxide (desoxydihydroajoene) was inactive (IC_{50} > 200 μM), implying some synergism between the sulfoxide and vinyl disulfide functionality.

In this study, we found that our library of desoxyajoene/ajoene analogues (**6, 8** and **7, 9** as phenols and amides respectively) all had comparable activity to the parent, bis-PMB, with the compounds falling into the strongly active range (IC_{50} = 0.5 – 8.6 μM). Similarly, though slightly less active than the former, the desoxydihydroajoene/dihydroajoene phenols and amides, both lacking the double bond of the vinyl sulfide, were still more active (14.3 and 23.2 μM for desoxydihydroajoenes **11** and **13**; 4.9 and 13.6 μM for dihydroajoenes **12** and **14**) than ajoene in WHCO1 cancer cells (IC_{50} = 39.2 μM (*E*) and 25.2 μM (*Z*)),[80] but slightly less so than the same series containing the double bond.

In our newly synthesised series, the desoxyajoene phenol, analogue **6**, lacking the sulfoxide, was found to be the most active, with an IC_{50} in the nanomolar range of 0.48 μM, in agreement with our previous findings for the bis-PMB series, and more active than the equivalent ajoene compound **7** (IC_{50} = 2.7 μM).[183] In the amide case, however, this trend marginally reversed (IC_{50} of desoxyajoene **8** as 8.6 μM going to ajoene derivative **9** at 7.4 μM). Although the phenol **11** and amide **13** desoxydihydroajoenes were the least active in their respective series, they were still strongly active overall, with IC_{50}'s in the range of 15 - 25 μM. Overall, the phenol-substituted analogues were 2 to 3-fold more active than their amide counterparts and of similar activity to the bis-PMB series (methoxy derivatives).[183]

The removal of the double bond resulted in a 2-fold decrease in activity, when comparing the ajoene with its dihydroajoene (saturated vinyl disulfide) partner in both the phenol and amide series (**7** versus **12** and **9** versus **14**) although this was found to be more pronounced in the previous bis-PMB series (8-fold decrease). In support of a thiolysis exchange mechanism, the double bond stabilises the enethiolate anion leaving group

through resonance delocalisation, which effectively drives the disulfide exchange as discussed earlier.[81] The loss of the double bond in the dihydroajoene series, lacking disulfide activation, may therefore explain the reduced cytotoxicity. When, however, comparing desoxydihydroajoenes **11** and **13** (these are thio-functionalised disulfides) to an analogous dialkyl disulfide such as dipropyl disulfide, it can be seen that the desoxydihydroajoenes are still extremely active (14.3 and 23.2 μM, respectively, versus 50,000 μM).[81] This 10^5-fold increase in activity implies a very important role for the overall molecular structure involving the sulfide/sulfoxide and aromatic end-groups.

Regarding the role of the sulfoxide oxygen in the dihydro series (**11** - **14**), its removal in **11** and **13** caused a decrease in activity (3-fold phenol and 2-fold amide). This is in agreement with our group's previous finding in which the sulfoxide restored the activity of the methoxy dihydroajoene in the PMB series.[183] The role of the sulfoxide moiety appears to be more subtle, though, where it may produce a long range inductive withdrawing effect through the molecule's sigma framework to make the sulfur distal to the sulfoxide more electrophilic. The increased electrophilicity of the sulfur in the disulfide would be expected to promote thiolysis and thus effectively lower the IC_{50}. However, it must be stressed that the sulfoxide overall probably plays a comparatively minor role, as the presence of the disulfide alone (in the desoxydihydroajoenes **11** and **13**) yields analogues which are still strongly active. Interestingly, lack of a sulfoxide in the desoxyajoene series has shown to yield a more active compound (phenol **6** and the bis-PMB analogue from previously published data[183]). The findings that the amide series was overall less active than the phenol and methoxy analogues may lend some support to our previous observations that lipophilicity may contribute favourably towards the activity of ajoenes in cancer cells.

In summary, the sulfoxide does not appear to play much of a role in enhancing the cytotoxicity of the vinyl disulfide series (and in some cases it is favourable to not have it at all), although it does increase the activity of the desoxydihydroajoenes. This presumably occurs through an increase in the electrophilicity of the disulfide due to inductive electron-withdrawal via the σ-framework (as a compensation for not having the double bond to stabilise the thiolate charge generated on thiolysis), which in turn enhances the leaving ability of the thiolate. It has been previously proposed that the

sulfoxide may promote hydrogen bonding to adjacent amino acid residues in the cysteine peptide microenvironment.[189] Nevertheless, this argument does not appear to apply here for the ajoene series in cancer cells. Importantly, however, and in line with our previous findings on ajoene and its analogues, this study supports the disulfide being the pharmacophore, in which the double bond plays an activating role by stabilising the leaving group anion in thiolysis.

To better understand the structure-stability relationships of ajoene in blood we tested the library for stability in mouse blood. This was done *in vitro*, by incubating the analogues in fresh mouse blood at 37 °C for up to 120 min upon which the reaction was quenched with acetonitrile. The percentage of the compound remaining was quantitated using the peak area from an LC/MS chromatogram. **Figure 3.26** shows the *in vitro* stability data of the 8 analogues.

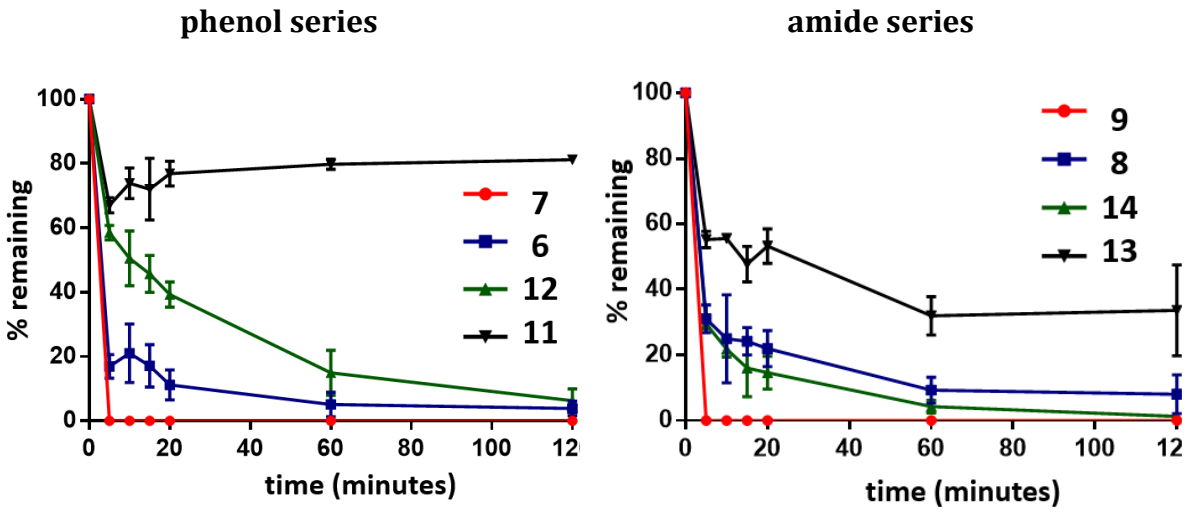

Figure 3.25: Blood stability of ajoene analogues in whole mouse blood.
Experiments performed in triplicate and data points expressed as an average with standard deviation.

Table 3.9 list the half-lives of both phenol and amide ajoenes, obtained by fitting the % compound remaining versus time to a non-linear one phase decay model. The endpoint concentration of some analogues did not reached zero as their curves had flattened out, equating to 80%, of **11**, and 40%, of **13**, remaining in the blood after 120 minutes.

bis-PMB			
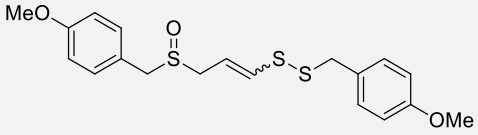			
1.5 minutes			
phenol series			
6	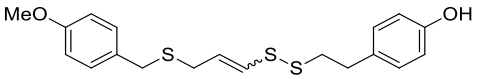	**11**	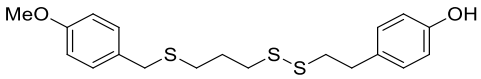
1.4 minutes		**> 120 minutes**	
7	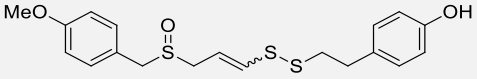	**12**	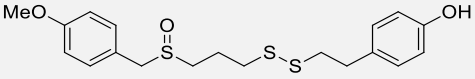
< 1 minutes		**10.6 minutes**	
amide series			
8	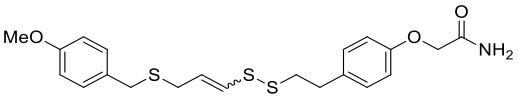	**13**	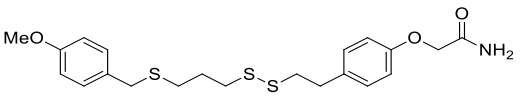
2.3 minutes		**11.1 minutes**	
9	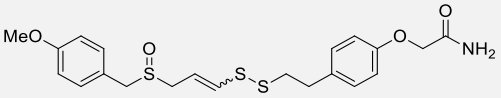	**14**	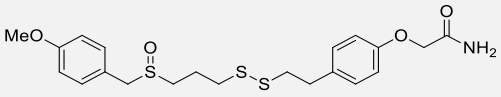
< 1 minutes		**2.8 minutes**	

Table 3.9: *In vitro* half-lives of bis-PMB and its analogues in mouse blood.

All analogues containing a vinyl disulfide group (**6, 7, 8** and **9**) were found to have a shorter half-life in blood than their dihydroajoene counterparts (**11**, **12**, **13** and **14**, respectively). This was most noticeable for desoxyajoene **6** and desoxydihydroajoene **11** in the phenol series, where the presence of a vinyl group in **6** showed a dramatically lower half-life (1.4 minutes) than its dihydroajoene counterpart **11** (>120 minutes). It was also found that the bis-PMB analogues containing a sulfoxide group (**7**, **9**, **12** and **14**) had a shorter half-life in blood than their desoxy counterparts (**6**, **8**, **11** and **13**). The shortening of half-lives was most pronounced in the dihydroajoene series, where the presence of the sulfoxide lowered the half-life by 75% and by more than 90% for the amide (**13** vs **14**) and phenol series (**11** vs **12**), respectively.

These observations are an indication that the blood half-life may also mirror the reactivity of the disulfide bond, rendering the compound more reactive towards thiolysis exchange reactions within the blood matrix. As observed previously for cytotoxicity, the

vinyl group appears to have a greater effect on the reactivity of the disulfide than the sulfoxide, due to strong resonance stabilisation of the leaving group versus a weaker and more subtle inductive effect of the sulfoxide. Although some synergism appears to exist between these two effects, one must compare analogues **7** and **9** containing both the vinyl and sulfoxide groups with extremely low half-lives (< 1 minute). These influences on the reactivity of the disulfide pharmacophore may provide an explanation as to why ajoene (**Section 3.2.2**) and bis-PMB (1.5 minutes) are unstable in blood. Conversely, the absence of the LG stabilisation by the vinyl and sulfoxide group in the desoxydihydroajoenes (**11** and **13**) may impart a significantly longer half-life by placing them at the other end of the reactivity scale.

Overall, for the phenol and amide series of compounds, the former produced an overall greater blood stability than the latter. This suggests that polar end groups (amide>hydroxyl>methoxy) do not favour blood instability, which was contrary to the findings on cytotoxicity where more lipophilic compounds showed enhanced activity. When comparing the results of the structure-activity and structure-stability relationships of ajoene, it becomes apparent that the reactivity of the pharmacophore affects both the stability and cytotoxicity, viz.: the more activated the disulfide, the higher its cytotoxicity (low IC_{50}) and the lower its blood stability (short half-life). To illustrate this mirroring trend, **Figure 3.27** shows a dual y-axis plot of IC_{50} values versus the percentage remaining in the blood after 20 minutes.

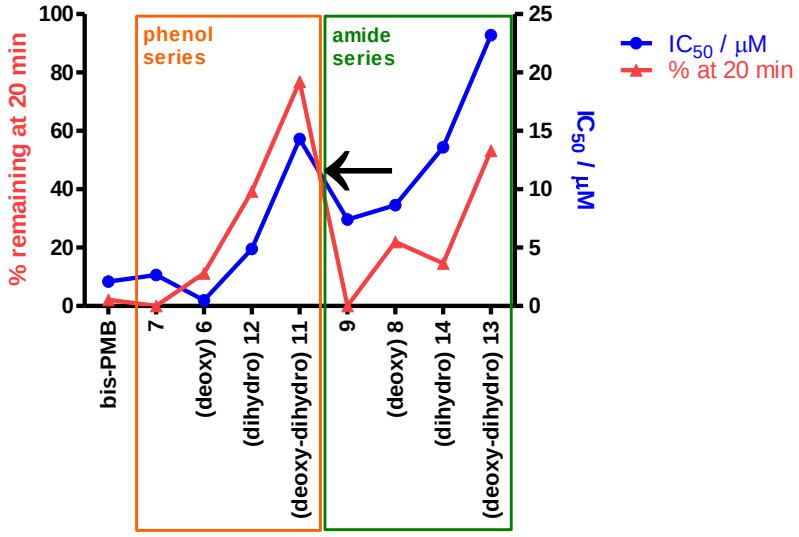

Figure 3.26:The mirroring trend of cytotoxicity and blood stability of ajoene analogues in the amide and phenol series.

A successive removal of the disulfide-activating vinyl and/or sulfoxide group from the pharmacophore (ajoene → desoxyajoene → dihydroajoene → desoxydihydroajoene) results in the analogues becoming less cytotoxic and more stable in blood. These trends support the disulfide reactivity playing a major role in the blood stability of ajoene which is driven by thiolysis exchanges with biological thiols present in the blood as the likely cause for its disappearance.

Interestingly there is a striking difference when comparing the relationship of cytotoxicity and blood stability in the amide and phenol series. The black arrow in **Figure 3.27** indicates an inversion point between the blue cytotoxicity line and the red blood stability line from phenol to the amide series. Regarding the cytotoxicity, it appears that the more lipophilic phenol analogues have lower IC_{50} values compared to their amide counterparts. Previously, us and others have found that lipophilicity favours cytotoxicity in ajoene and indeed this appears to also follow the trend for the lipophilic phenol ajoenes in this SAR study.[261,262] Conversely, it appears that blood instability favours more hydrophilic ajoenes. These opposing reactivity preferences may speak to the different thiolysis targets of ajoene in blood and cancer cells. Reasons for this may relate to the absence of a nucleus and ER inside erythrocytes as well as the high concentration of water soluble free thiols (i.e. GSH) in blood.[235] Indeed, we have found that ajoene targets the ER in cancer cells in which high concentrations of membrane (i.e. lipophilic) proteins are found.[153]

In the process of our SAR studies on ajoene, we have uncovered analogues that appear to be stable in blood while retaining good cancer cell cytotoxicity. The dihydroajoenes may be particularly attractive pre-clinical candidates with low IC_{50} values (14.3 ± 3.1 μM for **11** and 23.2 ± 0.9 μM for **13**) and improved blood stability. We uncovered an inverse trend between blood stability and cytotoxicity which in turn correlates to the SAR efficiency to undergo thiolysis exchange. Interestingly, lipophilicity appears to favour cancer cell cytotoxicity; whereas hydrophilicity seems to favour the blood instability, implying that thiolysis exchange is the underlying mechanism but that different thiolysis exchange targets may be involved in these different environments.

3.6 Metabolism of Ajoene in Blood: Thiolysis Exchange with a Thiol in Blood?

Studies on allicin have shown that it acts as a potent redox toxin in living cells and blood where it is able to deplete cellular low molecular weight thiols such as GSH by forming *S*-allyl disulfide conjugates.[84,263,264] Although the *S*-thioallylation of allicin can be likened to a thiol-disulfide exchange, the polarised bond between the *O*-atom and the *S*-atom of its thiosulfinate moiety makes it more reactive than a disulfide (and therefore a stronger oxidant). This enhanced electrophilic nature is likely responsible for allicin's incredibly short half-life in the liver and blood as these environments maintain a high concentration of free GSH of 2-5 mM in blood and up to 10 mM in hepatocytes.[68,265]. Comparatively, our studies and those of others show that ajoene is unstable in blood, which follow the same SAR trends that govern thiolysis exchange. Thus thiol-bearing components in the blood are responsible for its rapid disappearance.[211,228] Ajoene in turn may be more selective to thiol-disulfide exchange reactions due to its lowered reactivity compared to allicin. Support for this is given in a study by Yun *et al.* (**Figure 3.28**),[266] who showed that an oral dose of 20 µM ajoene did not lower GSH levels in the serum of mice. This suggests that although, highly abundant, GSH may not constitute the main thiol residue susceptible to thiolysis exchange reactions with ajoene.

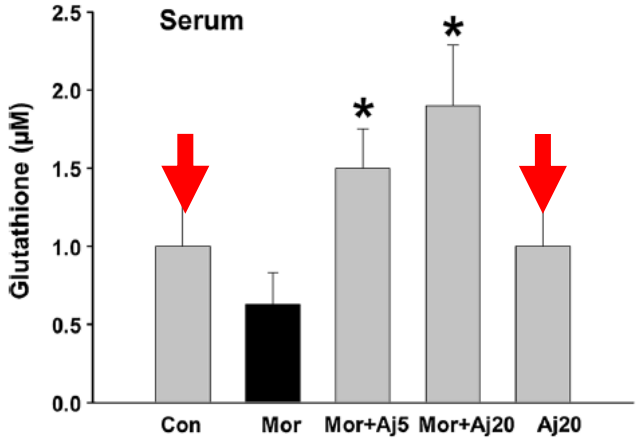

Figure 3.27: Ajoene does not significantly decrease GSH levels in serum.
Con = Control, Mor = morphine-treated, Mor + Ajo5/20 = combination of morphine with 5 or 20 µM ajoene, Ajo20 = 20 µM ajoene-treated.[266]

Two other major thiol sources in blood are serum albumin (representing >50% of total plasma proteins)[267] and haemoglobin (7.5 - 11.2 mM).[268,269] We conducted an *in vitro* experiment on separate plasma and RBC fractions, as well as whole blood (WB) from

mice. The blood fractions were incubated with bis-PMB and aliquots were taken at several timepoints over two hours and quantified using LC/MS as described before.

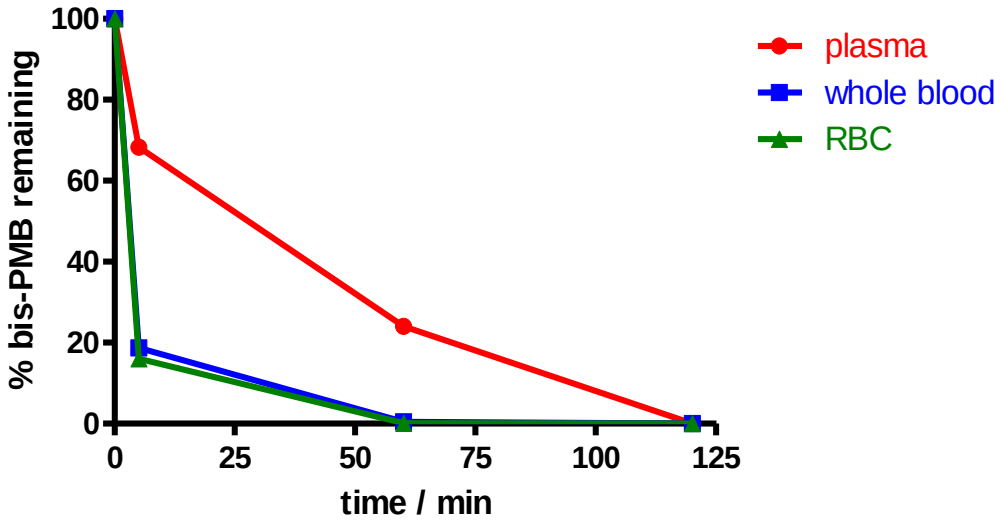

Figure 3.28: LC/MS quantification of *in vitro* bis-PMB concentration in whole blood, plasma and RBC fractions remaining over 120 min.

The quantification showed that bis-PMB was unstable in WB and RBCs (> 20% remaining after 5 minutes) but was comparatively more stable in plasma (~25% remaining after 60 minutes), similar to what was found for allicin in **Figure 3.4** and **3.5**. This indicated that the instability of bis-PMB in the RBC fraction and whole blood may be attributed to an intraerythrocytic target.

Interestingly, we observed that the ajoene-treated RBC-containing samples had turned darker in colour. This matched with a previous observation on allicin-treated blood by Freeman and Kodera,[228] where the darkening of blood was attributed to the oxidation of ferrous to ferric heme iron due to the a decrease in haemoglobin absorbances at 541 and 577 nm, with a concurrent increase in the 630 nm absorbance for methaemoglobin (see red arrows in the visible spectrum, **Figure 3.30**).

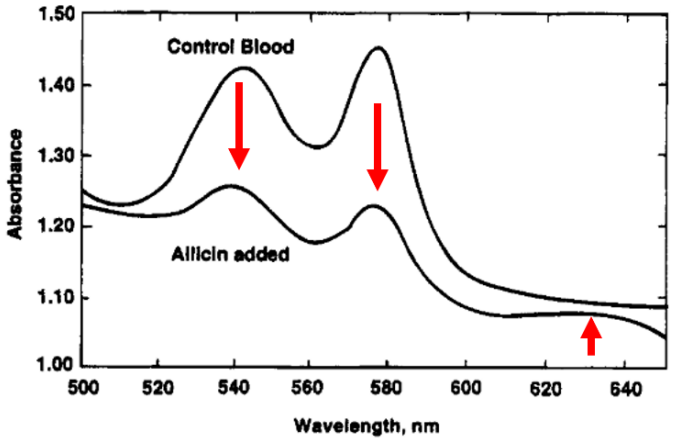

Figure 3.29: Visible spectral shifts of allicin-treated mouse blood.[228]

To investigate if bis-PMB had oxidised the heme iron in Hb, we conducted UV-Vis measurements on blood samples that were incubated with varying concentrations of bis-PMB, ranging from 0 - 200 μM, as shown in **Figure 3.31**.

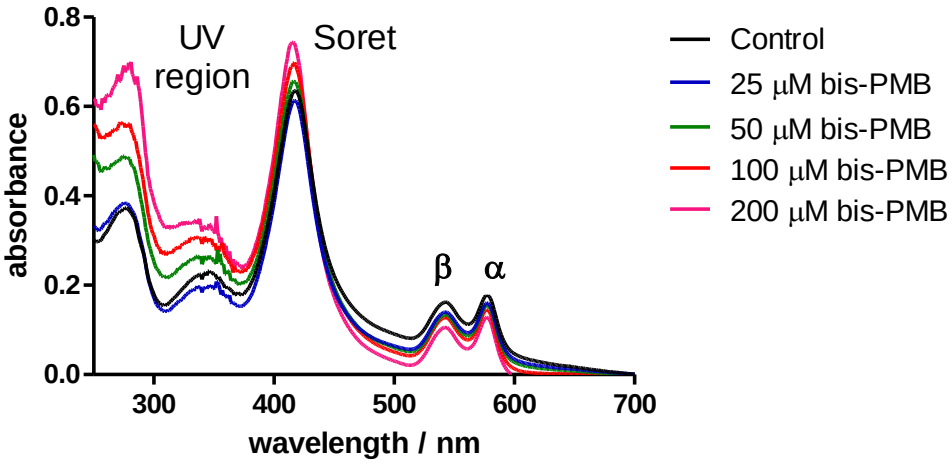

Figure 3.30: UV-Vis spectrum of murine whole blood samples incubated with bis-PMB.

The treatment of the blood with bis-PMB showed a dose-dependent flattening of two absorption bands at 540 and 575 nm and an increase in the absorption band at around 410 nm, and a sharp increase of absorption in the long- and medium-wave UV region (280 - 400 nm) of the spectrum.

The electronic absorption spectra of heme-containing proteins, such as Hb, are characterized by a strong band located at around 400 - 440 nm, called the Soret band (or B band) and up to four weaker Q bands between 480 and 600 nm range.[270] The spectra of untreated fresh blood (black line in **Figure 3.30**), rich in ferrous (Fe^{+2}), oxygenated

haemoglobin (oxyHb), is dominated by a Soret band at 415 nm and two Q bands at 542 nm (β band) and 578 nm (α band) (**Figure 3.31 A**).

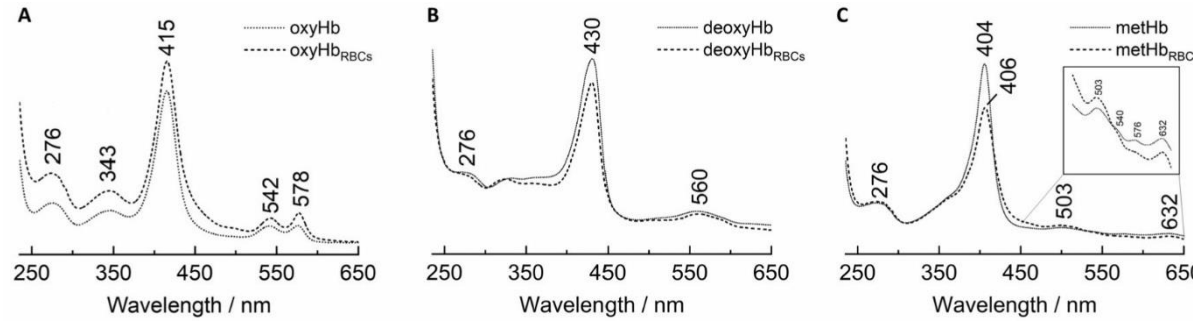

Figure 3.31: UV–Vis absorption spectra of isolated and RBC-enclosed haemoglobin species.
A = oxyHb, **B** = deoxyHb, **C** = and MetHb; solid line = isolated Hb, dotted line = RBC-enclosed Hb. Taken from Dybas *et al*.[270]

Our spectra (**Figure 3.30**) showed a decrease of the Q band (540 and 575 nm), but there was no increase in the characteristic absorption band of MetHb at 630 nm. This suggests that the treatment with bis-PMB had not caused the oxidation of the heme iron. This is contrary to what was found for allicin where the darkening of blood was attributed with formation of MetHb, as a characteristic increase of the 632 nm Q band (illustrated in **Figure 3.31 C**) was measured.[228,271,272]

Nevertheless, the darkening of the blood sample as well as the isosbestic points produced indicates a reaction and the conversion of one species to another. The changes in intensity of the Hb Soret and Q bands indicates that Hb is involved. It is known that cysteine residues (βCys-93 and βCys-112) on intraerythrocytic haemoglobin, which are susceptible to glutathionylation and oxidation, are also susceptible to *S*-thioallylation.[73,269] The oxidation of these residues in Hb can alter the redox state of the haem iron centre leading to changes in oxygen binding of the haem group.[230,273–276] Since oxygenation affects the colour of the blood (e.g. deoxygenated blood is darker),[277] the *S*-thiolation one of the these cysteine residues on the Hb protein by bis-PMB may provide a possible explanation for the observed blood discolouration. To further investigate whether the ajoene pharmacophore reacts with Hb, we set out to conduct a proteomics study in search of any cysteines modified by ajoene.

3.6.1 Proteomic Study of Ajoene-Hb Interactions

The workflow as outlined in **Figure 3.32** was followed. In the first step (Step **i** in **Figure 3.32**), two samples of purified human Hb were prepared by incubation without (control) or with 100 µM *Z*-ajoene.

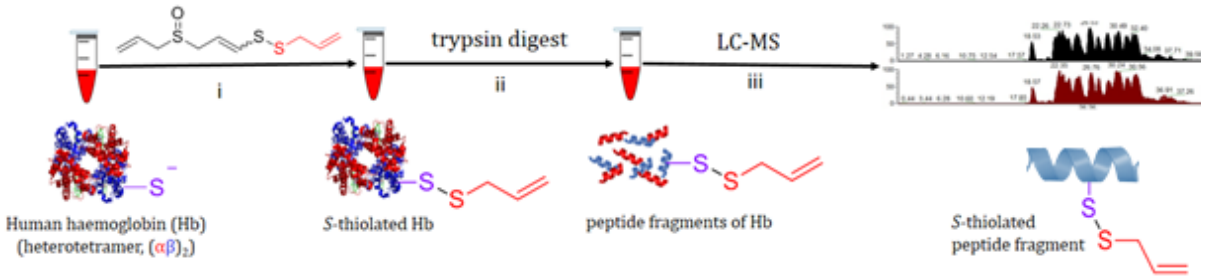

Figure 3.32: Workflow of sample preparation for proteomic analysis.

The samples were subsequently digested using the protease, trypsin, which site-specifically hydrolyses protein amide bonds at the carboxylic ends of lysine (**K**) and arginine (except if followed by proline) to afford tryptic peptide fragments (Step **ii** in **Figure 3.32**). In the final step (**iii**), the samples were analysed using an LC-ESI-MS system at the Centre for Proteomics and Genomics Research (CPGR), Cape Town, South Africa. From visual inspection of the spectra, it became evident that two isotope clusters with the mass to charge ratios (m/z) at 1421 and 711, seen in the untreated sample, were absent in the treated sample and had been replaced with two new clusters that appeared at 1494 and 747. With the help of the Expasy peptide prediction software, we inspected a sequence library of tryptic fragments of Hb and discovered that the $[M+H]^+$ ion (m/z = 1421.6729) and the $[M+2H]^{2+}$ ion (m/z = 711.3401) of the peptide GTFATLSELHCDK coincided with signals that were absent in the ajoene-treated sample, as indicated in red in **Figure 3.33**.

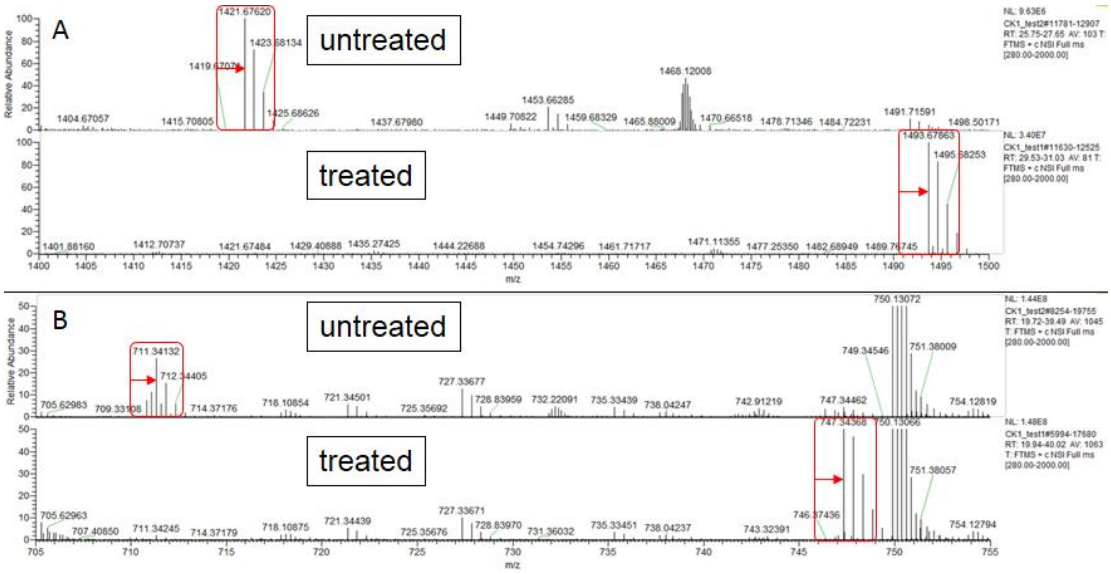

Figure 3.33: Mass spectra of untreated and *Z*-ajoene-treated Hb samples. A showing the $[M+H]^+$ and B showing the $[M+2H]^{2+}$.

This peptide fragment was identified to be GTFATLSELHCDK, containing a cysteine residue. This cysteine residue, also known as βCys-93, is a redox-reactive cysteine residue (*vide infra*).[80,84] As this peak is mass shifted, it appears that βCys-93 is an *S*-thiolation target of ajoene which requires a mass increase of prop-2-ene-1 thiolate, aka. *S*-allyl group (= 73.01 Da). For the calculation of the mass of the *S*-thioallylated peptide fragment, we had to consider that the peptide fragment (-SH) also loses a proton when the disulfide bond is formed. We proceeded to determine the mass differences between the peptides identified in the treated and untreated samples by performing the following calculations using the *m/z* of the $[M+H]^+$ and $[M+2H]^{2+}$ ion pairs:

For $[M+H]^+$: $Mass[adduct] = Mass[fragment(-SH) - H^+] + Mass[difference]$

$Mass[difference] = Mass[adduct] - Mass[fragment(-SH) - H^+]$

$Mass[difference] = 1493.67863 - (1421.67620 - 1.0078)$

$Mass[difference] = Mass[adduct] - Mass[fragement(-S^-)]$

$Mass[difference] = 1493.67863 - 1420.6684 = \mathbf{73.01023}$

For $[M+2H]^{+2}$: $Mass[adduct] = Mass[fragment(-SH) - H^+] + Mass[difference]$

$where\ Mass[X] = (peak \times 2) - 2H$

$\therefore Mass[adduct] = (747.34462 \times 2) - 2 \times 1.0078 = 1492.67364$

$\therefore Mass[fragment(-S^-)] = ((711.34132 \times 2) - 2 \times 1.0078) - 1.0078 = 1419.65924$

$\therefore Mass[difference] = Mass[adduct] - Mass[fragement(-S^-)]$

$Mass[difference] = 1492.67364 - 1419.65924 = \mathbf{73.01440}$

The results of the calculated mass differences and the *m*/*z* ratios of the observed peptide ions are summarised in **Table 3.10**.

	Fragment (GTFATLSELH**C**DK)	**Adduct** (GTFATLSELH**C**DK-*SS*-allyl)	**Calculated difference** (-*S*-allyl)
$[M+H]^+$ (**A**)	1421.67620	1493.67863	73.01023
$[M+2H]^{2+}$ (**B**)	711.34132	747.34462	73.01440

Table 3.10: Mass difference detected on *S*-allylated peptide fragment.

It was pleasing to see that the mass difference between the treated and untreated fragments for the $[M+H]^+$ and $[M+2H]^{2+}$ ion corresponded to 73.01023 and 73.01440 Da, respectively. In both cases, these values agreed with the theoretical mass of the *S*-allyl group (73.01175 Da) to two decimal points accuracy demonstrating that *Z*-ajoene modifies Hb at βCys-93.

In all vertebrates, the oxygen-carrying metalloprotein, haemoglobin (Hb), consists of a pair of subunits (α + β) which each contain a prosthetic non-protein heme group, shown in **Figure 3.34**.

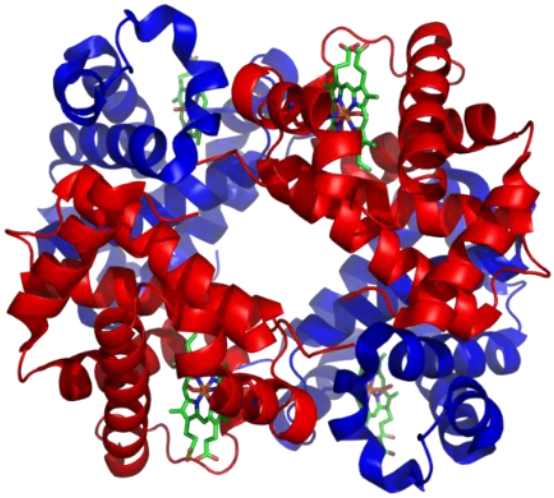

Figure 3.34: Structure of human haemoglobin.
The α and β subunits are shown in red and blue, respectively, and the iron-containing heme groups in green.

βCys-93 is located in a solvent accessible region of Hb and is susceptible to *S*-glutathionylation which causes structural changes in the heme pocket and alters its oxygen-binding properties.[278–281]

A seminal paper by Bonaventura *et al.* on the metabolism of OSCs in blood demonstrated that interactions of garlic extracts (GE) with RBCs caused a similar modification of intraerythrocytic haemoglobin cysteinyl residues.[269] Their mass spectrometry analysis of GE-treated human RBCs revealed a mass addition for the *S*-allyl group in the β-chain at βCys-93. The same observation was made for purified human Hb treated with DADS.[269] Interestingly, the analysis showed that each subunit could only be *S*-thioallylated once, suggesting that modification at one cysteine precludes or blocks the other (in the same β-chain) from being modified. These reports support our finding that *Z*-ajoene modifies Hb at βCys-93 through the transfer of an *S*-allyl group, thereby providing a possible explanation for the instability of ajoene in whole blood (see **Figure 3.35**).

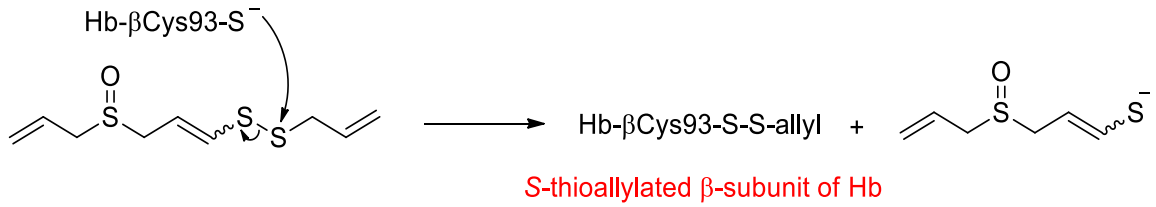

Figure 3.35: Proposed metabolic fate of ajoene in blood.

3.6.2 S-thioallylation of βCys-93 in Hb and Erythrocyte Toxicity

The βCys-93 residue in Hb plays a central role in oxygen-linked conformational changes.[279] **Figure 3.36** illustrates that βCys-93 is positioned in a solvent accessible region close to the heme-iron centre of the subunit which makes it particularly susceptible to modification by ROS or other thiophilic species.[278,281–283]

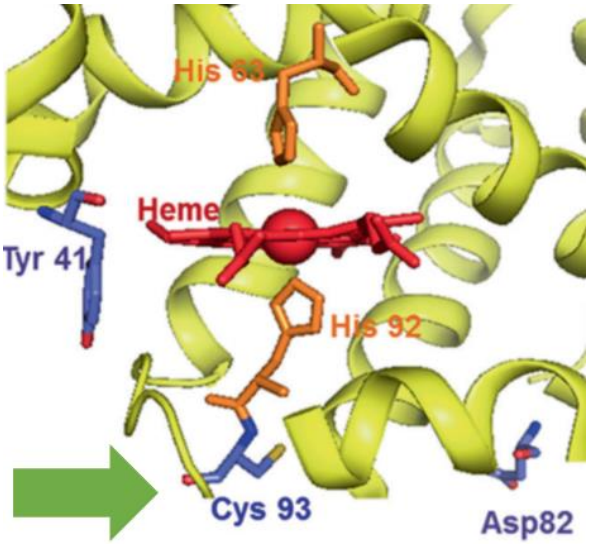

Figure 3.36: Location of the βCys-93 residue in the β-subunit of Hb.
The heme group is in red, the green arrow shows βCys-93; Taken directly from Alayash *et al.*[279]

Since Hb is involved in the highly oxidative process of carrying oxygen, erythrocytes contain elevated levels of antioxidants (e.g. GSH) to protect both Hb and the RBC membrane from oxidative stress. One of the protective measures is the capping of its reactive cysteines, like βCys-93, by glutathione to form mixed disulfides with GSH (Hb-SSG). Although the *S*-glutathionylation of Hb is a protective and reversible modification, it leads to a temporary structural change that increases the protein's binding affinity to oxygen and prevents its release into the tissue, termed the alkaline Bohr effect.[278,284] However, in prolonged states of oxidative stress this causes a more permanent impairment of the physiological function of Hb.[285,286] More specifically, it has been shown that irreversible oxidation of βCys-93 leads to an alteration in the folding of the protein which induces a loss of heme leading and a breakdown of the RBCs.[279] Over time, this leads to a pathological condition, termed haemolytic anaemia, which coincides with the formation of these denatured RBCs (Heinz bodies) and their accumulation in the spleen, thereby enlarging it.

In the context of the toxicity we observed in mice with the prolonged treatment (5 weeks) of the high doses of ajoene, a literature search revealed a connection between the ingestion garlic and its constituents and the occurrence of haemolytic anaemia in several mammals, including rodents, which may lead to the poisoning of the animals (*Allium spp.* Toxicosis).[287–289] It is reported that toxic effects are caused by plant-derived OSCs and that their primary toxicological mechanism relates to interactions with intraerythrocytic

proteins which, in turn, causes oxidative haemolysis.[93,290,291] Different garlic compounds exhibit varying toxicity,[292] for example, it was shown that the sulfide SAC is 30-fold less toxic in mice than allicin and DADS, a thiosulfinate and disulfide respectively.[248] The literature also indicates that there is a significant difference in toxicity between raw garlic and AGE in rodents. In two separate studies, the oral administration of raw garlic juice to rats caused anaemia, weight loss, stomach injury and death within 3 weeks,[293,294] whereas even a prolonged treatment with AGE did not induce any of these toxicities.[294,295] These findings coincide with the reactivity profiles of the OSC sulfur chemotypes as discussed in **Section 3.2.2**.

Long storage of AGE results in the loss of thiophilic OSCs, such as allicin and DADS, to the more stable antioxidants, such as SAC. Conversely, other garlic preparations, including crushed and cooked garlic, are known to still contain several OSCs that have thiol modifying chemotypes which are toxic to mammalian erythrocytes.[93,269]

Although numerous studies have tested thiophilic garlic OSCs in rodents, including ajoene, allicin and DATS, *in vivo* there are only limited reports that mention their toxic effects on RBCs. One study by Lai *et al*. mentions that the treatment of HT-29 xenograft mice with 50 mg/kg DATS had lower Hb concentration in the tumour sections.[254] Here, the decrease in Hb was not attributed to the haemolytic effects of DATS but was identified as a marker for the antiangiogenic effects of DATS, in spite of prior studies by different authors reporting that DATS significantly decreased RBC count and Hb levels ($p < 0.05$) at these concentrations.[296]

In comparison to human, there appears to be a marked difference in the thiol-metabolising ability of thiol reactants in rodent erythrocytes, which may explain why rodents are susceptible to the toxic effects of garlic. There are three identified key features that affect their biochemical detoxification mechanisms, i) rodent erythrocytes contain thiol groups that are specialised to rapidly metabolise thiol reactants and electrophiles.[297]; ii) rodents have a different isoform of the detoxification enzyme theta-class glutathione transferase T1-1 (GST T1-1), which shows has a higher affinity to electrophilic substrates than human isoforms.[298] [299]; and iii) the βCys-93 residue on rodent Hb is an important effector in the antioxidant network of rodents.[276]

Thus, the ability of rodents to metabolise garlic OSCs efficiently and rapidly inside their erythrocytes may be disadvantageous to them, since several OSCs transformation

products also possess thiol-modifying properties of which some are more toxic than the original substance. Ajoene, for example, not only modifies erythrocytic cysteine residues (e.g. βCys-93), which may alter their redox function, but also releases a vinyl thiolate (or thial) LG. Although the pharmacological and toxicological effects of the "ajo" LG are still unknown, the high reactivity of its thials moiety suggest that an accumulation of the LG will be problematic to erythrocytes. A prolonged exposure or a high concentration of ajoene, may therefore damage erythrocytes.

In summary, we report the following *in vivo* observations: i) ajoene was not found to inhibit WHCO1 tumour xenograft growth in nude mice when treated for 5 weeks by oral gavage (50 mg/kg thrice/week); ii) orally administered ajoene at a dose of 50mg/kg produces toxic effects after prolonged treatment (5 weeks); iii) the ajoene pharmacophore has a short half-life in mouse blood of under 2 min which was attributed to fast thiolysis exchange and the presence of the vinyl disulfide/sulfoxide functional group; iv) ajoene causes the darkening of mouse blood *in vitro*; v) ajoene and its analogues may deregulate the haemostatic balance through thiol modification of βCys-93 in Hb.); and vi) the targeting of βCys-93 (an effector for Hb toxicity) may contribute to erythrocyte toxicity of garlic in mice.

3.7 Conclusion

In comparison to the numerous reports on the mouse tumour inhibitory activity of several of the major garlic OSCs, there are three *in vivo* literature reports on ajoene. As garlic and its constituents are primarily ingested in the diet, our aim was to test the chemotherapeutic effects of orally administered ajoene in a murine xenograft model for cancer.

It was found that treatment of a relatively high dose of ajoene (50mg/kg) for 5 weeks did not significantly affect tumour growth. What did emerge, however, was that the prolonged treatment caused adverse effects. A follow-up *in vitro* experiment on ajoene-treated mouse blood revealed a reactivity between ajoene and erythrocytes, where a *S*-thioallylation of intraerythrocytic protein targets was hypothesised. Based on our knowledge of the thiol-modifying properties of the ajoene, it became apparent that the modulation of the reactivity of its disulfide pharmacophore may improve its pharmacokinetic profile.

A structure-activity study was performed on ajoene using the bis-PMB analogue as a template to produce a small library of modified analogues in which the vinyl disulfide/sulfoxide groups were varied. Polar modifications were also introduced to improve blood solubility. The previously developed UCT ajoene synthesis allowed access to the vinyl disulfide series (**6-9**), in which the key *S*-thiolation step between the vinyl thioacetate **2** and the phenolic sulfenylating agent **5** integrated the pharmacophore and the handle for polar modifications into the molecule. Synthesis of the dihydroajoene series (**10-14**) also utilised the modified sulfenylating agent and was accomplished via the dialkylation of 1,3-propanedithiol. The amide derivatives of both series were accessible through alkylation at the phenol moiety.

The testing of these analogues for their *in vitro* stability in fresh mouse blood as well as their cytotoxicity against WHCO1 cells demonstrated an inverse relationship between cytotoxicity and blood stability, where it is proposed that these two parameters are directly correlated to ajoene's susceptibility towards thiolysis exchange (better leaving group), which agrees with our group's previous findings on garlic-related disulfides. The double bond of the vinyl disulfide group was the most active in cancer cells and the least stable in blood possibly related to the greatly increased stability of the resulting leaving group (enethiolate) in thiolysis exchange. The dihydroajoenes lacking the double bond showed greatly enhanced *in vitro* blood stability. The presence of the sulfoxide group enhanced the activity of the dihydroajoenes but decreased activity in the vinyl disulfides which implies a long-range inductive electron-withdrawing effect on the disulfide through the σ-framework of the molecule. The phenol and methoxy functionalities had similar effects on cytotoxicity, whereas the incorporation of an amide caused the compounds to be less active against cancer cells but less stable in blood.

An important observation from this study is that although an inverse relationship between cancer cell cytotoxicity and blood stability is observed, it is weighted. Thus, the dihydroajoenes were found to be slightly less cytotoxic than their vinyl disulfide counterparts; however, they still had impressively active IC_{50}'s around 20 μM. The improvement in blood stability is, however, notable having increased to more than 40% remaining at 120 minutes. The dihydroajoenes present themselves as good leads for future therapeutic development.

A further investigation into the interactions between ajoene and erythrocytes by UV-Vis spectroscopy and proteomics demonstrated that it regioselectively *S*-thioallylated the cysteine residue, βCys-93, of Hb. As modifications of βCys-93 modulate the oxygen-carrying capacity and redox homeostasis of erythrocytes, this finding provides a possible explanation for the blood instability and the reported hemotoxic side-effects of garlic.

The metabolism of ajoene in blood, and its cytotoxicity in cancer cells appears to be related to its ability to act as an efficient *S*-thioalkylating agent. These insights prompted us to develop a strategy to target and identify the protein targets of ajoene in cancer cells, which is the subject of the next chapter.

Chapter 4 : Synthesis and Biological Evaluation of Biotinylated Ajoenes

4.1 Background

While our results on the *in vivo* anticancer activity of ajoene described in the preceding chapter were somewhat disappointing, ajoene certainly displays good cytotoxicity against a range of different cancer cell lines. Significantly, there are three literature reports on its *in vivo* efficacy of ajoene in mouse models for cancer, which suggest that fine-tuned experimental conditions, such as the mode of delivery and the cancer-type, may be important. With a particular interest in understanding the cytotoxic mechanism of action of ajoene in cancer cells, we set out identify its cellular protein targets.

Our initial focus was drawn towards the unique vinyl disulfide functionality of ajoene, which was shown through SAR studies to be the pharmacophore.[183] This was pivotal in shaping our hypothesis that thiol-disulfide exchange between ajoene and cellular targets provide the basis for its biological activity.[182] Further mechanistic studies revealed that such exchange reactions were regioselective in transferring the ajoene *S*-allyl group onto thiol(ate) cysteine residues to produce *S*-allyl-Cys adducts.[183,300] This regioselectivity was due to the superior leaving ability of the enethiolate in the exchange due to resonance stabilisation of the leaving group anion. These insights on ajoene's ability to modify thiol groups on protein targets in a regioselective and covalent manner culminated in the replacement of the ajoene transferable *S*-allyl group with a chemical reporter (aka. label or tag). What followed was the design and synthesis of an activity-based probe (ABP) with a transferable fluorescent tag that allowed the tracking of ajoene in cancer cells by confocal laser microscopy (see **Scheme 4.1**).[153]

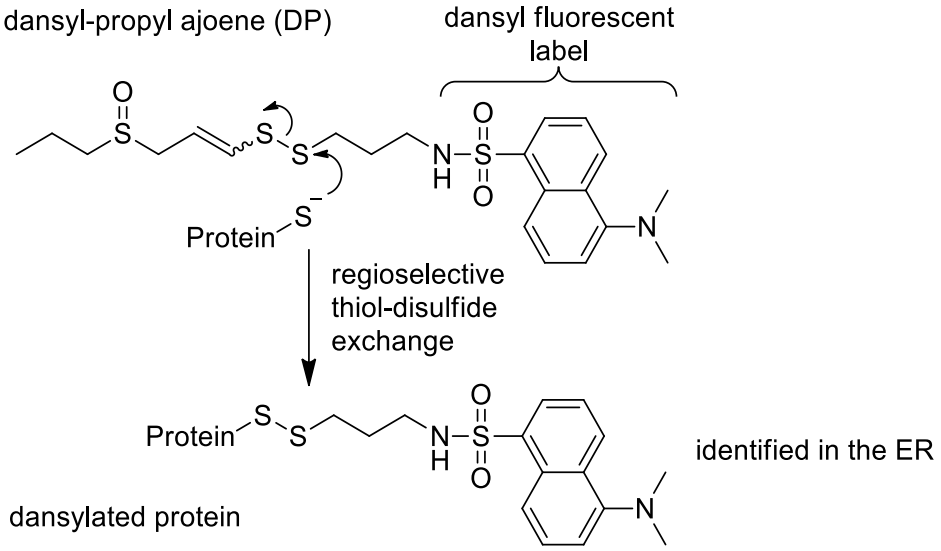

Scheme 4.1: Regioselective S-thiolation reaction between dansylated ajoene and a protein thiolate.

The endoplasmic reticulum (ER) was uncovered as the site of dansyl localisation, and western blot analysis of the cancer cell lysate, when probed with an anti-dansyl antibody, revealed that ajoene has numerous proteins targets (**Chapter 2/Section 2.5.1**). The aim of this project is to isolate and identify these protein targets through the design and synthesis of an ajoene probe using a chemical proteomic approach.

4.2 Activity-Based Proteomics in Target Identification

Activity-based proteomics, or activity-based protein profiling (ABPP), is a chemoproteomic technology that combines an activity-based probe (ABP) and mass spectrometry (MS) to elucidate the protein targets of small bioactive molecules.[301] Broadly speaking, the ABP is a chemically modified version of the bioactive molecule of interest and, generally, consists of three parts (**Figure 4.1**): i) a reactive group that retains the same activity as its parent molecule and can form a covalent bond to its pharmacological targets; ii) a reporter group/tag for target enrichment and detection; iii) a linker, sometimes cleavable, that connects the reactive group and the reporter tag but is also long enough to avoid steric hindrance between the two as well as at the site of action.[302]

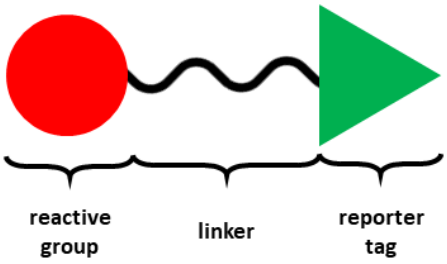

Figure 4.1:General molecular structure of an ABP for ABPP experiments.

In a typical ABPP experiment for target identification (**Scheme 4.2**), the ABP is incubated with cells or tissues to allow its covalent binding to protein targets. The subsequent enrichment of the targeted proteins is achieved involving the reporter tag. In the last step, the isolated protein is identified by MS analysis.[303]

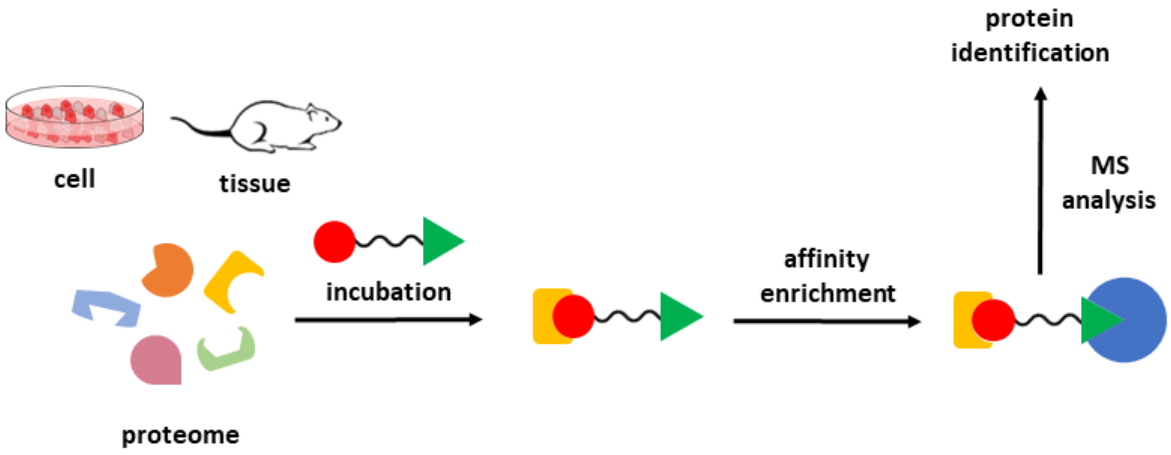

Scheme 4.2:Overview of ABPP workflow for protein target identification.

In contrast to detecting target proteins with a fluorescent tag (as with DP-ajoene), the enrichment and isolation of tagged proteins requires an affinity tag on the ABP.

4.2.1 The choice of Biotin as an Affinity Reporter Tag for ABPs

Biotin is a naturally occurring small molecule, aka. vitamin H (B_7). It is chemically robust, binding with high specificity and affinity to (strept-)avidin.[304,305] The strength of the avidin-biotin conjugate complex (K_d of $\sim 10^{-15}$ M), as well as its resistance to a wide range of pH, temperatures, organic solvents, and denaturants makes it popular for affinity applications. Synthetically, the carboxylic acid moiety at the end of the valeric acid side

chain of biotin enables its synthetic attachment to molecules of interest in a process called biotinylation, as shown in **Figure 4.2**.

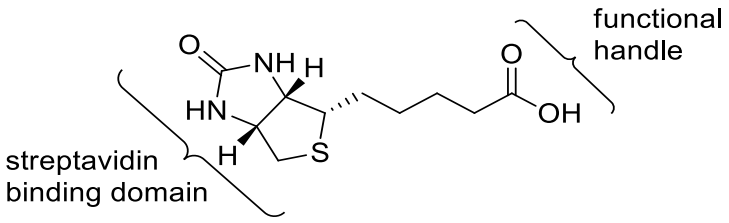

Figure 4.2: Biotin as an affinity reporter tag.

The biotinylated molecules can be efficiently isolated from complex samples using commercially available avidin-functionalised surfaces (e.g. resins) and avidin-coated nanoscale objects (e.g. magnetic beads).[306] Overall, these features make biotin a powerful tool for ABPP-based applications which prompted us to use it as the affinity tag in our ABP to capture the protein targets of ajoene.

4.3 General Aspects of the Design and Synthesis of a Biotinylated Ajoene Probe

The overall design of the probe comprised the vinyl disulfide reactive group, a biotin reporter tag and a connective linker as shown in **Figure 4.3**. Also illustrated is the anticipated site of substitution in the regioselective thiolysis exchange on the vinyl disulfide, a crucial design feature that dictated placement of the biotin tag. We decided to retain the sulfoxide group based on our SAR findings (in **Chapter 2** & **3**) which revealed a favourable contribution to the anticancer activity of the vinyl disulfide pharmacophore.

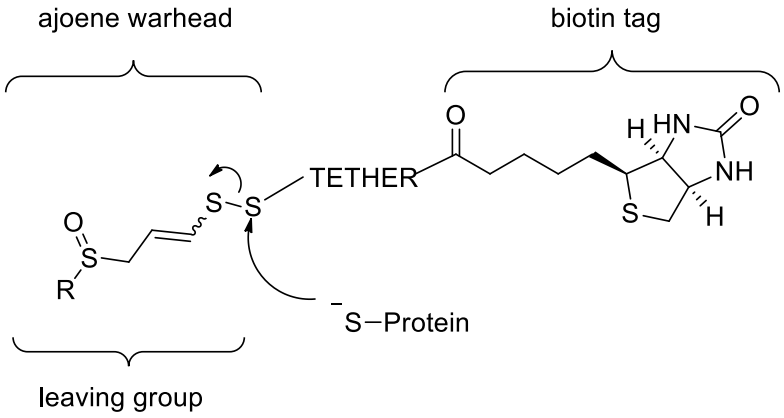

Figure 4.3: Biotin-ajoene probe design.

As with our fluorescent probe, the ajoene pharmacophore would serve as an electrophilic molecular "bait" for cellular nucleophilic thiols to ensure biotinylation of the ajoene protein targets. The R-group on the sulfoxide end could be varied as *n*-propyl (modelled on the ajoene allyl group) or *p*-methoxybenzyl, which emerged as the most active end group in the SAR study (modelled on bis-PMB ajoene). In sight of the solubility challenges that were encountered with ajoene analogues such as bis-PMB in **Chapter 3**, the introduction of the polar/water-soluble biotin group onto ajoene was hoped to improve the overall solubility of the probe in cell culture media.

The envisaged steps of our ABPP workflow are shown in **Scheme 4.3**.

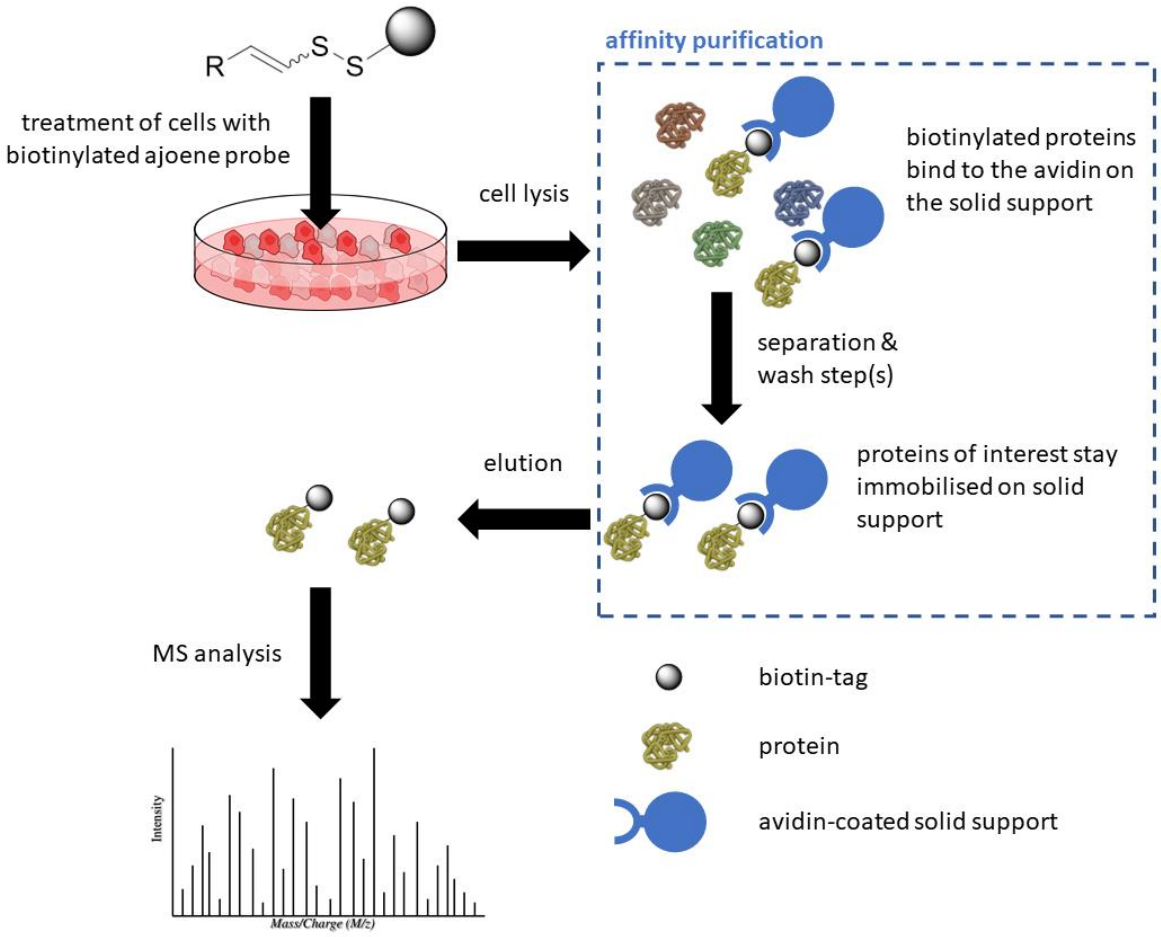

Scheme 4.3: Proposed affinity-purification of biotinylated proteins from cancer cell lysate.

Following incubation of the cells with ABP, the streptavidin magnetic beads capture the biotinylated proteins from the lysate of cells. During the enrichment step, the protein-bead conjugate is immobilised by magnetisation, while non-specifically bound proteins

are separated from the beads through several washes with buffers containing detergents and/or organic solvents. Thereafter, the proteins may be eluted from the beads by reducing the disulfide bond between the biotin tag and the cysteine residue of the target and/or by directly releasing the peptides from the protein-ligand complex by an on-bead digest.[307,308] The recovery of the enriched proteins is followed by a tryptic digest, to yield peptide fragments, and a sample clean-up step to remove contaminants to avoid later interferences during data acquisition in the final MS-analysis.

4.4 Development of Biotinylated Ajoenes

Several prototype biotin-ajoenes were synthesised varying the R and tether groups before arriving at the best version for effective biotinylation. **Table 4.1** below shows the four versions which are each discussed.

Entry	Name	Structure
1	Biotin-ajoene v1 C. Pike	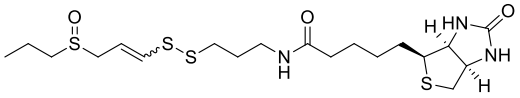
2	Biotin-ajoene v2 **26** D. Kusza	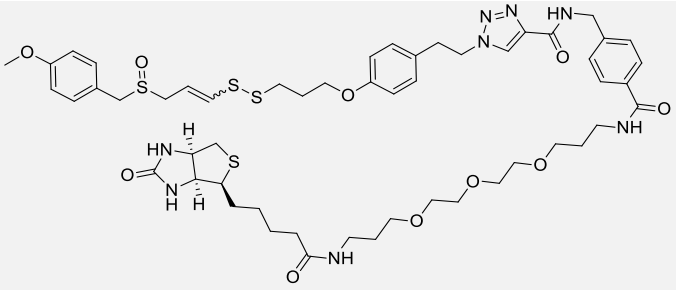
3	Biotin-ajoene v3 **33** D. Kusza	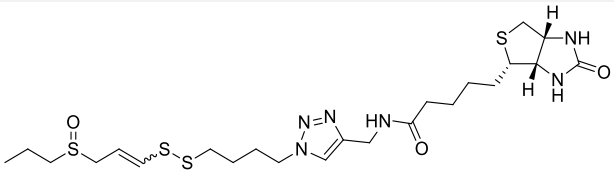
4	Biotin-ajoene v4 **40** D. Kusza	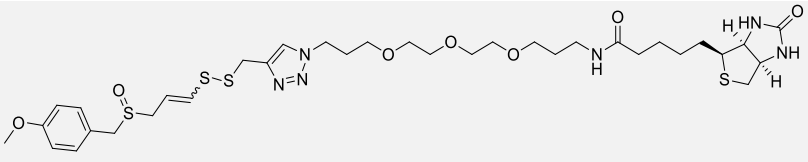

Table 4.1: Structures of biotinylated ajoene probes.

Our first synthetic strategy made use of our previous work on the synthesis of ajoene, wherein the biotin tag was envisaged to be introduced in the sulfenylation step (in red), as shown in **Scheme 4.4**.

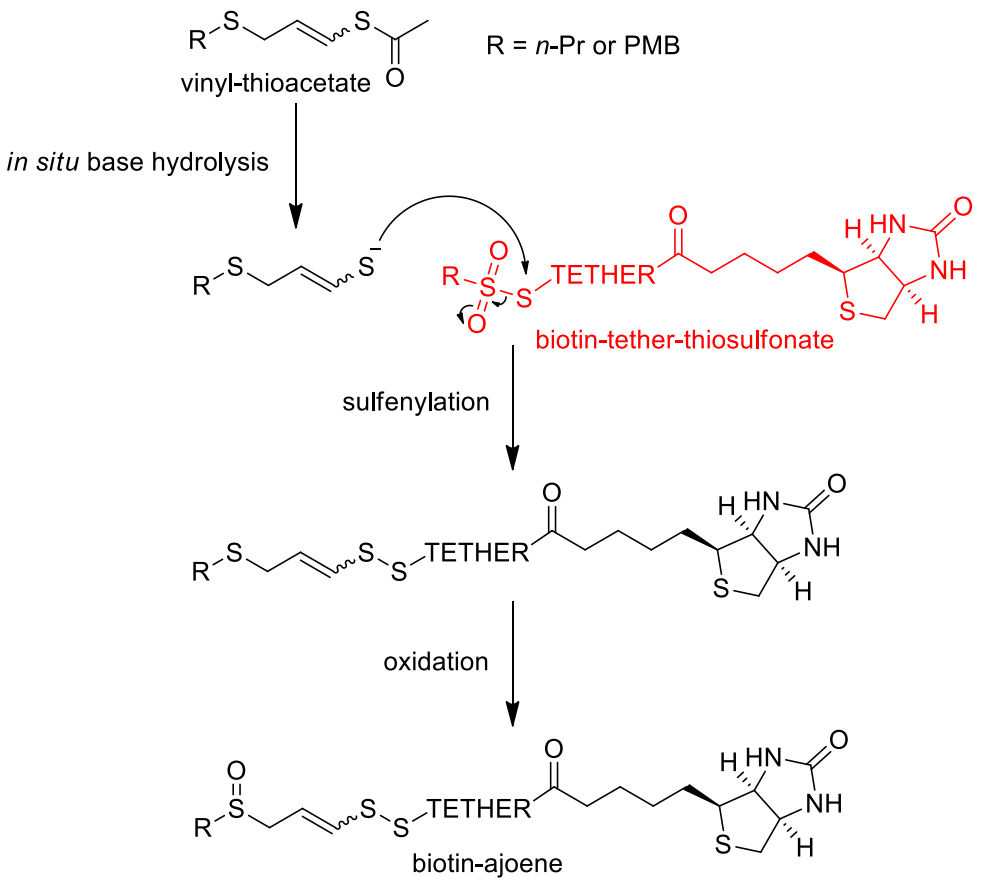

Scheme 4.4: Proposed synthetic route to biotin-ajoene.

Access to the vinyl thioacetate followed that of our established synthetic route. Then, to attach the biotin moiety, the vinyl thioacetate would be deprotected with KOH in MeOH and sulfenylated with a biotin-tether-thiosulfonate (red in **Scheme 4.4**). Thereafter, oxidation was hoped would furnish the target sulfoxide-vinyl disulfide tethered to biotin (called biotin-ajoene) chemoselectively over oxidation of the more hindered biotin sulfide.

4.4.1 Biotin-Ajoene V1

According to this synthetic rational, the synthesis of the first biotinylated ajoene probe (biotin-ajoene v1) was undertaken by Ms C. Pike in an Honours project at UCT in 2013 before this PhD (see **Entry 1**, **Table 4.1**).[309] Commercially available biotin was used as the starting material to introduce a tether for incorporating a thiosulfonate at the terminus to produce a biotin-tagged sulfenylating agent (**Scheme 4.5**).

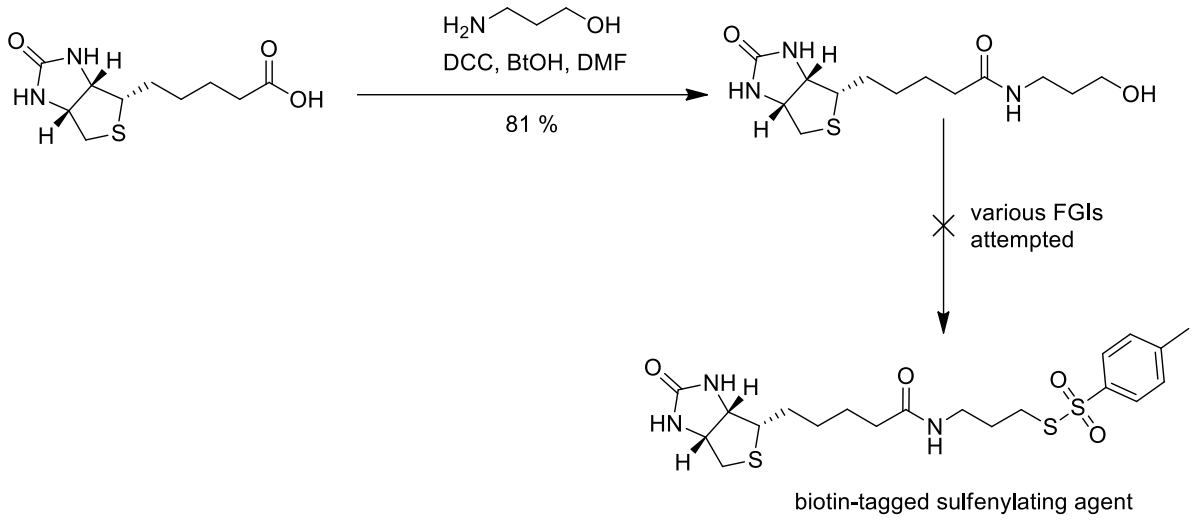

Scheme 4.5: Synthesis of a biotin-tether sulfenylating agent for biotin-ajoene v1.

More specifically, the proposed synthetic route involved coupling a bifunctional aminopropanol tether to the biotin free acid using a DCC-promoted coupling, and then converting the free hydroxyl group into its thiotosylate to generate the sulfenylating agent for the vinyl disulfide formation step**.** Unfortunately, following a successful DCC coupling between biotin and 3-aminopropanol, the synthesis broke down at the introduction of the thiosylate. It was speculated that the electrophilic thiotosylate may have been reacting with the nucleophilic tetrahydrothiophene sulfur of biotin.

4.4.2 Biotin-Ajoene V2

Valuable insights gained from synthetic endeavours of our first prototype pointed the way forward for designing an improved probe version 2, **26**, which was carried out in my MSc studies from 2014 to 2016.[310] These included utilising a convergent approach involving "Click"-coupling to join the two fragments, rather than a linear one, which rendered the synthesis more manageable and avoided potential complications arising from substitution between the nucleophilic biotin sulfur and the electrophilic thiosulfonate group. The convergent sequence is depicted in **Scheme 4.6**.

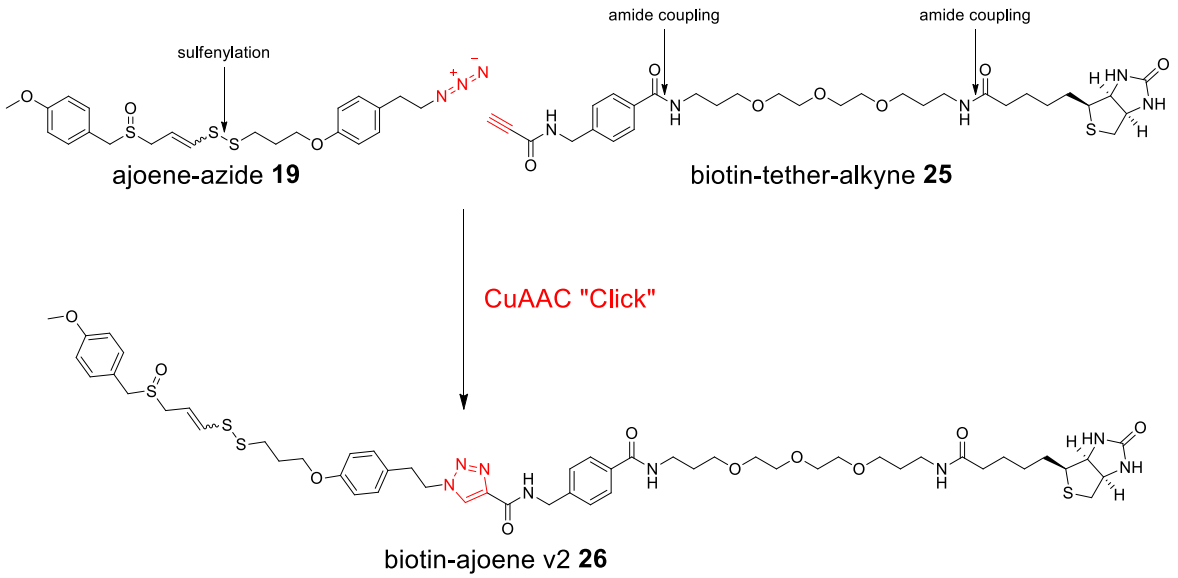

Scheme 4.6: Synthetic strategy towards biotin-ajoene v2 26 using a convergent "Click"-approach.

Thus, two "Click"-fragments as ajoene-azide **19** and biotin-tether-alkyne **25** were envisaged as being generated from a combination of amide couplings and substitution chemistry. The biotin-tether-alkyne **25** partner was designed based on the work of Jezowska *et al*,[311] using an aromatic amino acid piece to extend the standard diamine linker in which the extra length was perceived as assisting entry of biotin into the streptavidin binding pocket. The choice of a polyethylene-glycol (PEG) tether was standard and suited to further increase the solubility of the molecule in water.[304,312] The synthesis of **25** involved attaching end synthons **21** and **24**, stepwise, at each end of the tether. **Scheme 4.7** depicts the intended synthesis of these tether end synthons.

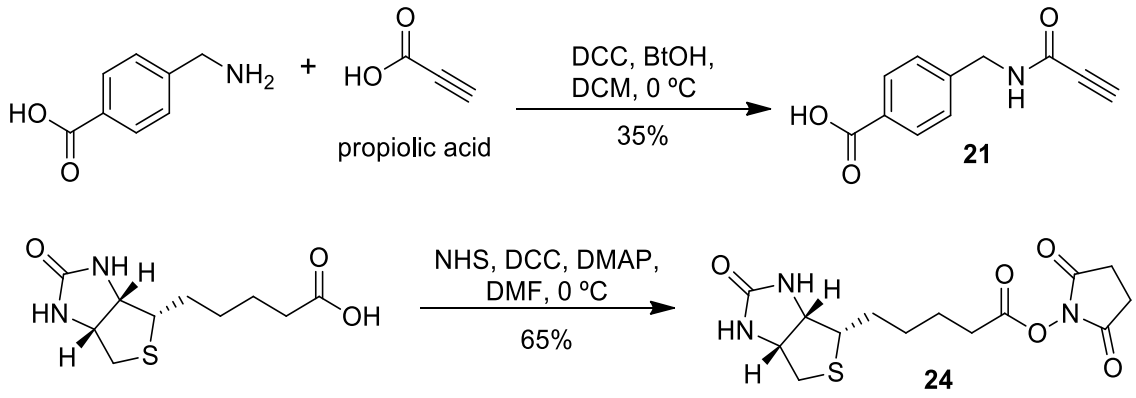

Scheme 4.7: Synthesis of the tether connecting synthons for biotin-tether-alkyne, 25.

Fragment **21** was synthesised using a standard DCC/BtOH (DCC chosen because of its low cost) procedure in poor yield (35%), owing to an issue with chemoselectivity between the two carboxylic acids. The failure of a direct DCC coupling of biotin acid to the amino group of the tether led us to consider using biotin-*N*-hydroxysuccinimide ester **24** as the electrophilic partner in the amide coupling,[313] which was obtained via the Steglich esterification of biotin with *N*-hydroxysuccinimide (NHS) in a moderate yield of 65%, as shown in **Scheme 4.7**.

With **21** and **24** fragments ready for coupling, the two ends of the diamine tether were differentiated by first mono-*N*-Boc protection in only 46% yield due to some formation of a di-Boc-protected derivative that could be easily separated via column chromatography. Thereafter, a smooth series of sequential couplings were achieved in high yield (>80% each), first with fragment **21** and then with **24** once the Boc group had been removed from **22** using TFA. In such a way, the biotin-tether-alkyne **25** partner in the "Click"-coupling was accessed, see **Scheme 4.8**.

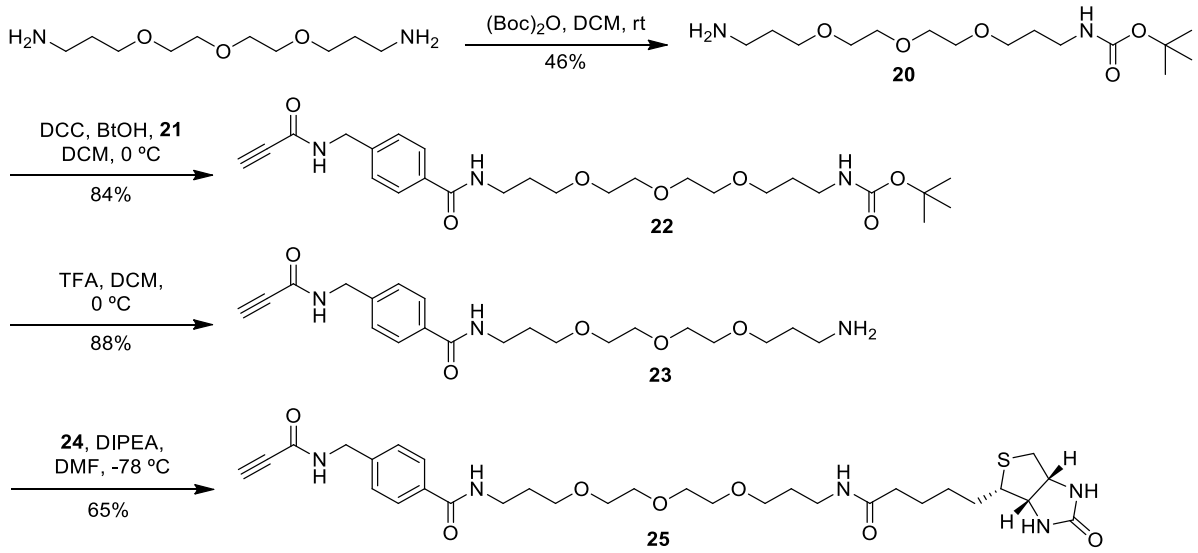

Scheme 4.8: Assembly of the biotin-tether-alkyne partner, 25.

All intermediate products **20** - **24**, and the biotin-tether-alkyne **25** were satisfactorily characterised by IR, ^{1}H-NMR, ^{13}C-NMR and HRMS spectroscopic and analytical techniques. The assigned ^{1}H-NMR spectrum of the pivotal biotin-tether-alkyne **25** together with its HRMS are shown in **Figures 4.4** and **4.5**.

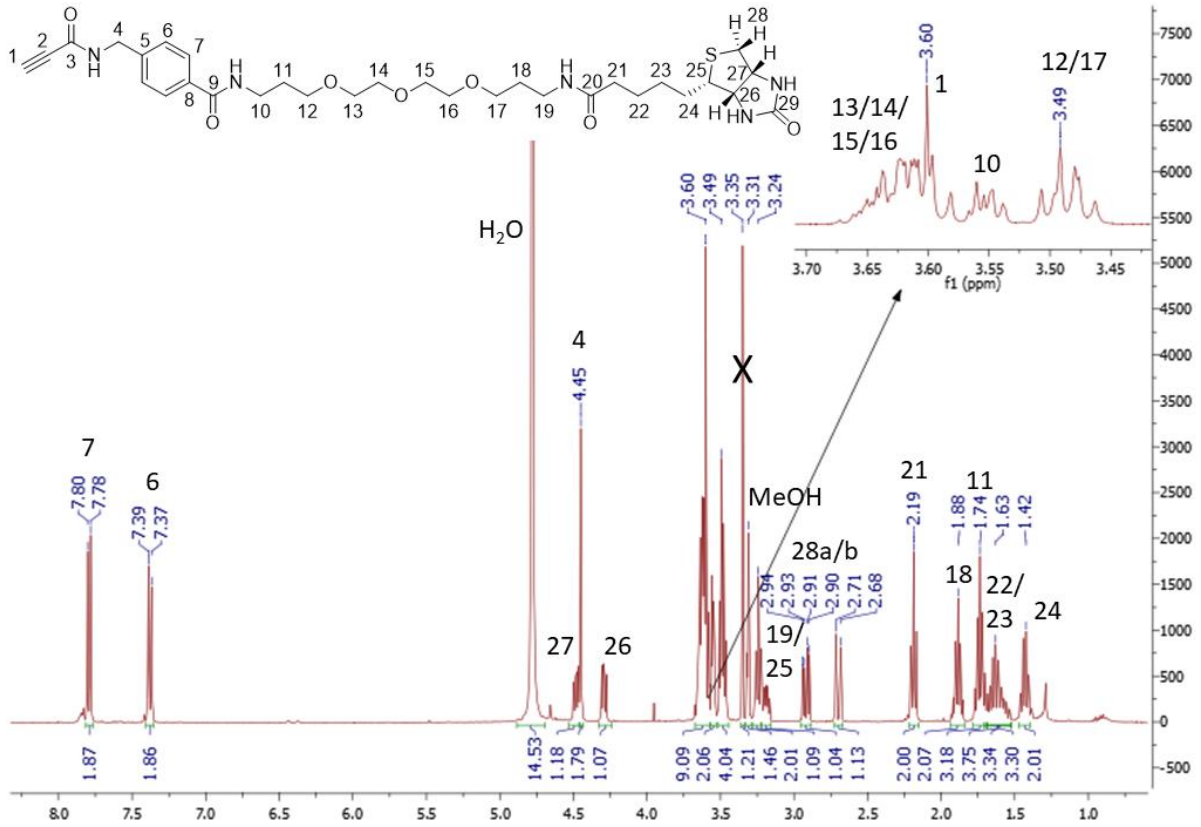

Figure 4.4: ^{1}H-NMR spectrum of biotin-tether-alkyne, 25.

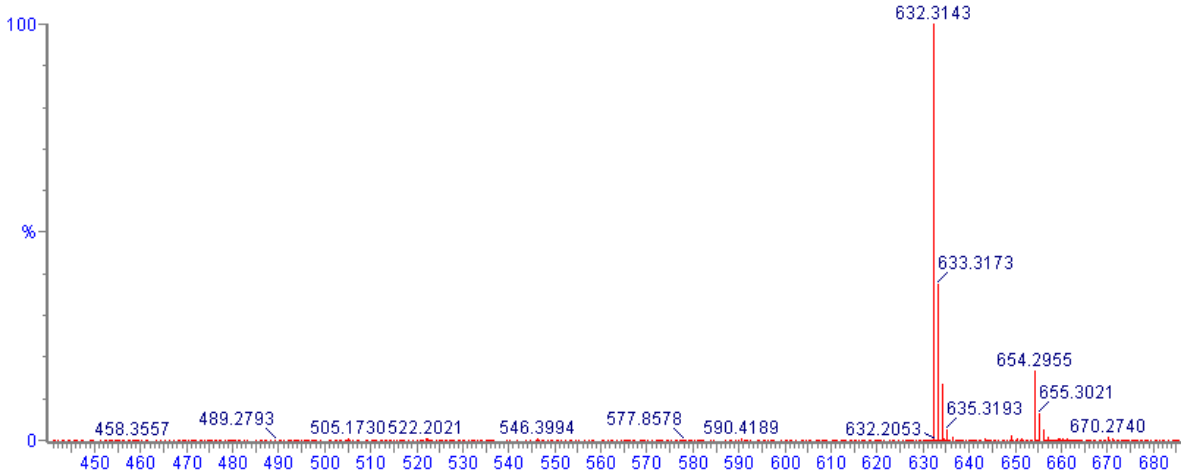

Figure 4.5: HRMS spectrum of biotin-tether-alkyne, 25.

The presence of a biotin moiety was confirmed by virtue of the distinct *cis* ring junction hydrogens (H-26 and H-27) with their respective couplings to each other as well as to H-25 and to the diastereotopic proton pair of H-28. The valeric acid chain hydrogens (H-21 to H-24) were also clearly visible in the highfield region as were the downfield AB aromatic pair. Finally, the diagnostic alkyne (H-1) singlet was seen at 3.60 ppm. Strong additional evidence in support of formation of the biotin-tether-alkyne partner **25** was

given by its HRMS (TOF ES+) spectrum (**Figure 4.5**), which revealed a molecular ion $[M+H]^+$ at 632.3143, with $C_{31}H_{46}N_5O_7S$ requiring 632.3113.

Regarding synthesis of the other "Click"-partner, the ajoene-azide **19**, the azide functionality was placed on the non-vinyl sulfur side of the ajoene moiety. This required synthesis of an azido-sulfenylating agent **17**, as shown in **Scheme 4.9**.

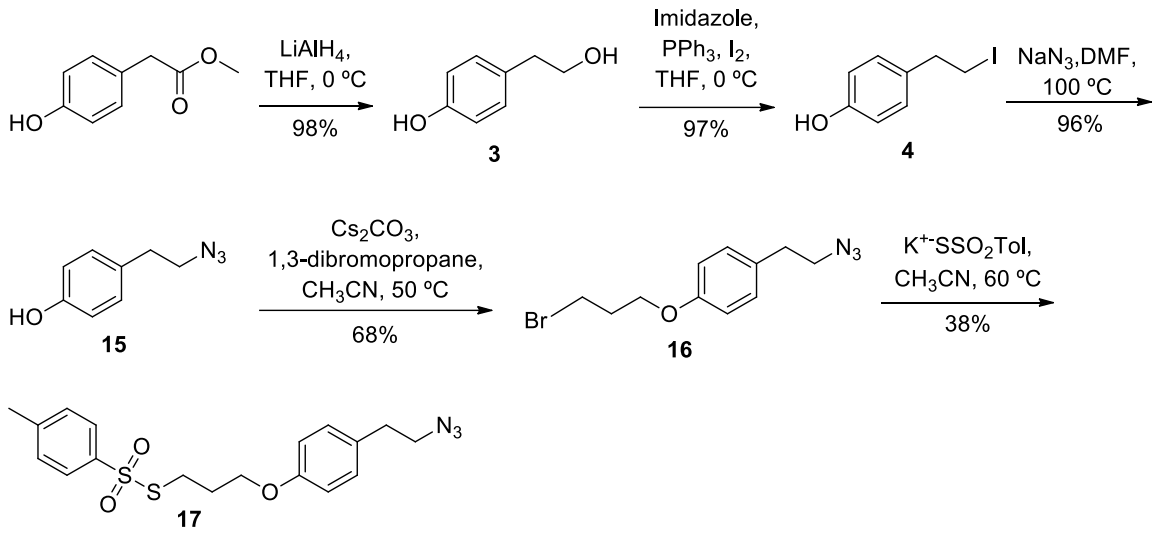

Scheme 4.9: Synthesis of the azide sulfenylating agent, 17.

Thus, starting from commercially available methyl (4-hydroxyphenyl)acetate, the required functional group interconversion sequence proceeded with a LAH reduction of the ester to its primary alcohol **3**, followed by an Appel reaction to afford the iodide **4**, which underwent subsequent S_N2 substitution with NaN_3 to give the desired azide **15** in 91% yield over the three steps. Mono-substitution of 1,3-dibromopropane with the phenoxide of **15** in a Williamson ether synthesis using Cs_2CO_3 as base then gave **16** in 68% yield. In the final step, S_N2 substitution of the terminal bromide with potassium thiotosylate gave the azido toluenethiosulfonate **17**, although disappointingly only in a low 38% yield. Nevertheless, the materials were all cheap and readily available so the synthesis could be scaled up to produce sufficient quantities of **17**.

An assigned ^{1}H-NMR spectrum for **17** is shown in **Figure 4.6**, revealing four sets of deshielded AA'BB' double doublets for the two aromatic protons as expected, in which the more downfield pair were assigned to the toluenesulfonyl ring in view of electron-withdrawal. The six highfield proton resonances at 2.12 (H-2'), 2.44 (H-5"), 2.83 (H-5), 3.18 (H-3'), 3.46 (H-6) and 3.95 ppm (H-1') accounted for the aliphatic proton signals of

the central tether methylene groups, as well as the azidoethyl and methyl substituents. Finally, HRMS spectral data corroborated the structure by showing an $[M+H]^+$ at 392.1103, for which $C_{18}H_{22}O_3N_3S_2$ requires 392.1108. IR spectroscopy, importantly, also revealed an azide stretch at 2094 cm^{-1} (data not shown).

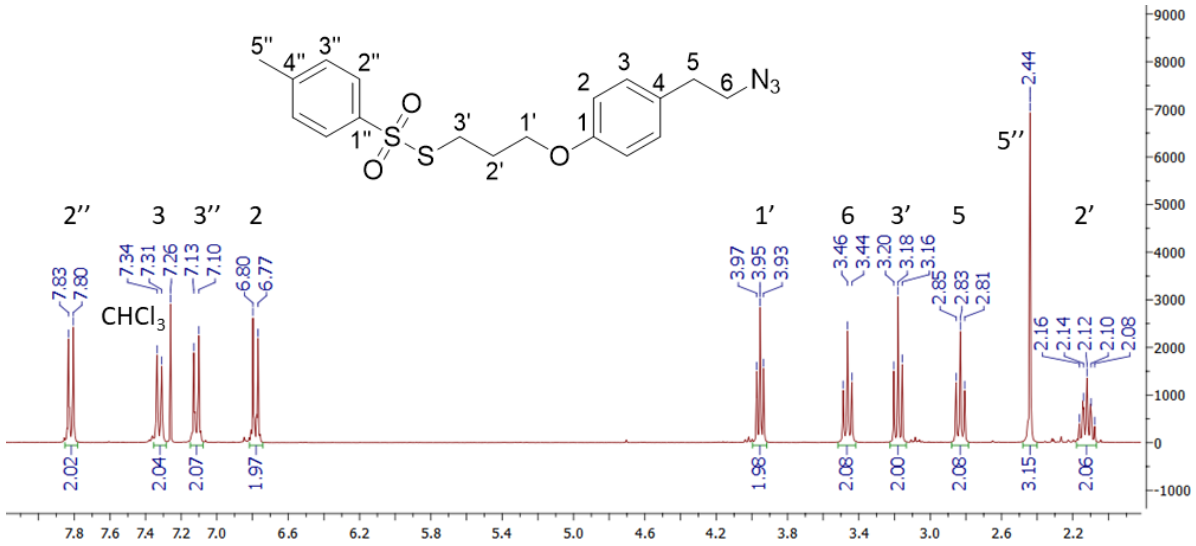

Figure 4.6:^{1}H-NMR spectrum of the azide thiotosylate sulfenylating agent, 17.

The coupling of the azide thiotosylate **17** to the vinyl thioacetate **2** proceeded in high yield (85%) according to the previously established conditions (**Scheme 4.10**). This was followed by chemoselective mono-oxidation of the sulfide **18** to afford the sulfoxide **19** in moderate yield (62%), the product isolated as an inseparable mixture of geometrical isomers with the *Z*-isomer slightly predominating. The R group was chosen as PMB in view of our success with this group in the SAR study.

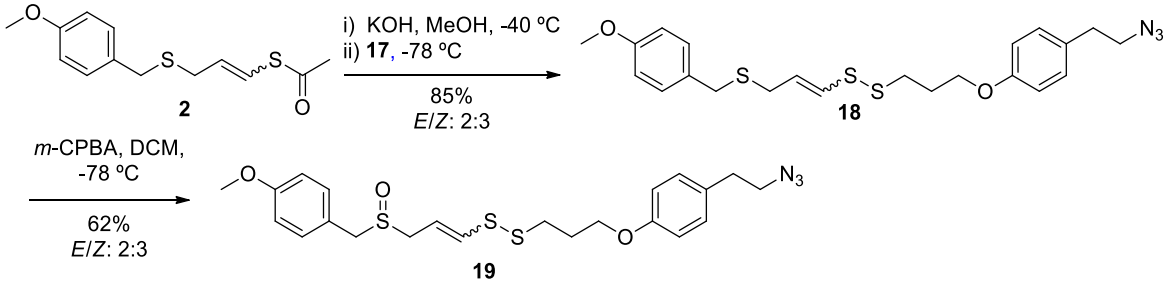

Scheme 4.10: Synthesis of the ajoene-azide fragment, 19.

The ^{1}H-NMR spectrum of **19** (**Figure 4.7**) revealed the typical *Z-E-E-Z* motif for the vinyl signals of the two geometrical isomers characteristic of ajoene (H-8 and H-9). Two sets of AA'BB' aromatic double doublets accounted for the two 1,4-disubstituted aromatic rings.

The diastereotopic splitting of the H-6 and H-7 methylene hydrogens into one pair of collapsed doublets for H-6, and two pairs of double doublets (coupling also with H-8) for H-7, one for each isomer, supported a successful sulfide oxidation to give the sulfoxide. Finally, HRMS data (**Figure 4.8**) revealed a molecular ion $[M+H]^+$ at 462.1344, for which $C_{22}H_{28}N_3O_2S_3$ requires 462.1349, providing conclusive evidence for the formation of the azide coupling partner **19**.

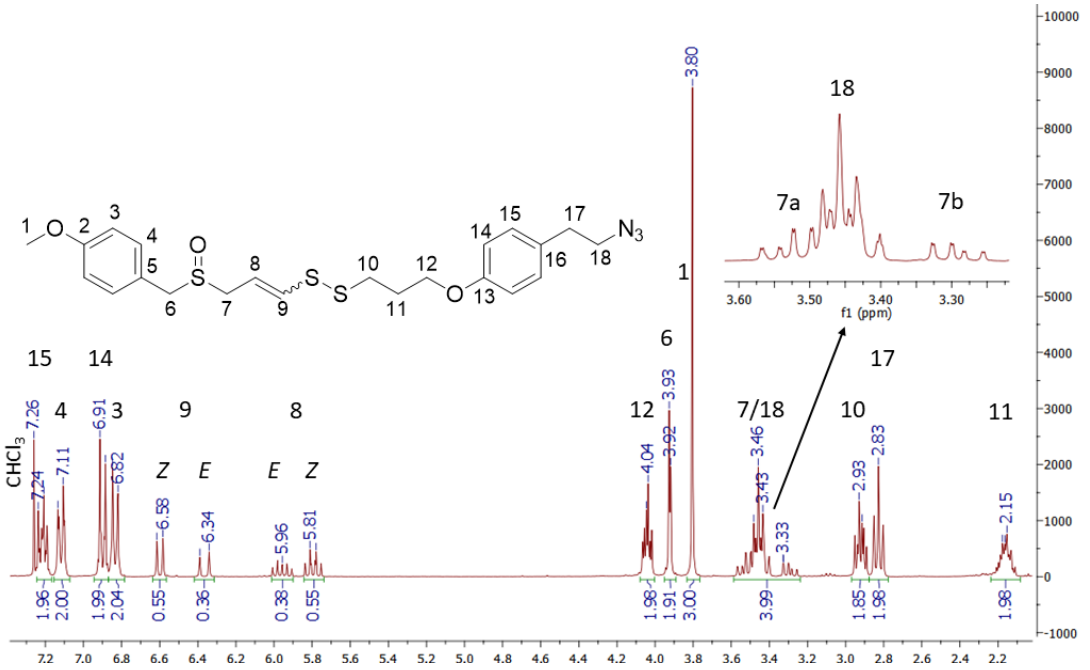

Figure 4.7: ^{1}H-NMR spectrum of azide-ajoene, 19.

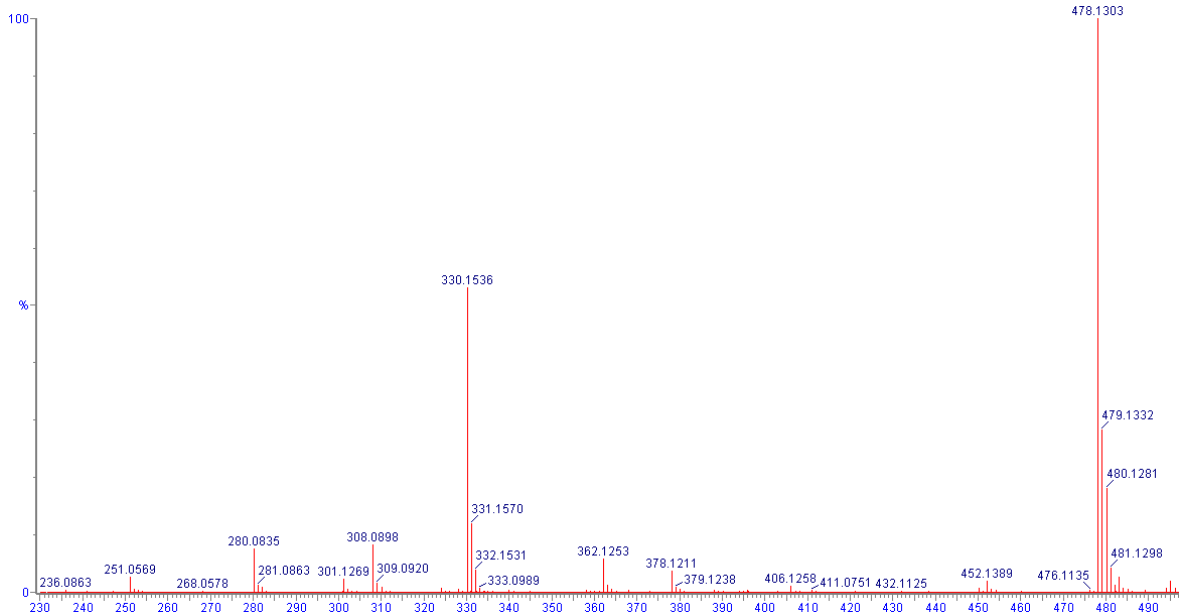

Figure 4.8: HRMS spectrum of azide-ajoene, 19.

The use of benign "Click"-technology, involving Sharpless' copper(I)-catalysed alkyne-azide cycloaddition (CuAAC) reaction, in the final step (**Scheme 4.11**) enabled the coupling of the two partners (**19** and **25**) under mild reaction conditions using one equivalent of each.[314–316]

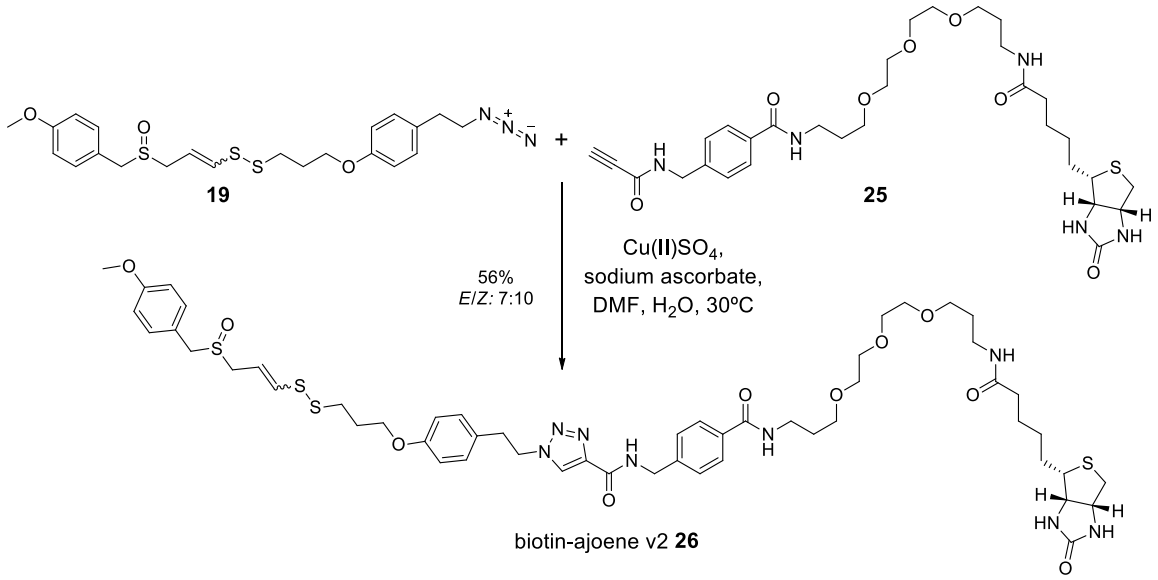

Scheme 4.11: Synthesis of biotin-ajoene v2, 26.

The two substrates (**19** and **25**) were found to dissolve best in DMF which was selected as the solvent. The copper catalyst was added as an aqueous solution and the reaction was run at 30 °C in which the consumption of the equimolar "Click"-partners was monitored by TLC. It was observed that several side products were being formed after about 18 hours without more of the starting material being consumed, which could not be improved by varying the reactant stoichiometry, catalyst loading, and/or reaction time/temperature. It was found that increased reaction temperatures (+40 °C) and reaction times of >24 hours generally resulted in product degradation and the formation of side products, so we accepted a moderate yield of 56% under the original conditions (1:1, 30 °C, 18 h).

The coupled product **26** showed a high degree of instability in d_6-DMSO. The isolation of a product from a 1:9 MeOH:DCM silica column chromatography system motivated us to run the ^{1}H-NMR spectrum in 1:9 MeOD:$CDCl_3$, which gave a satisfactory spectrum, shown in **Figure 4.9**.

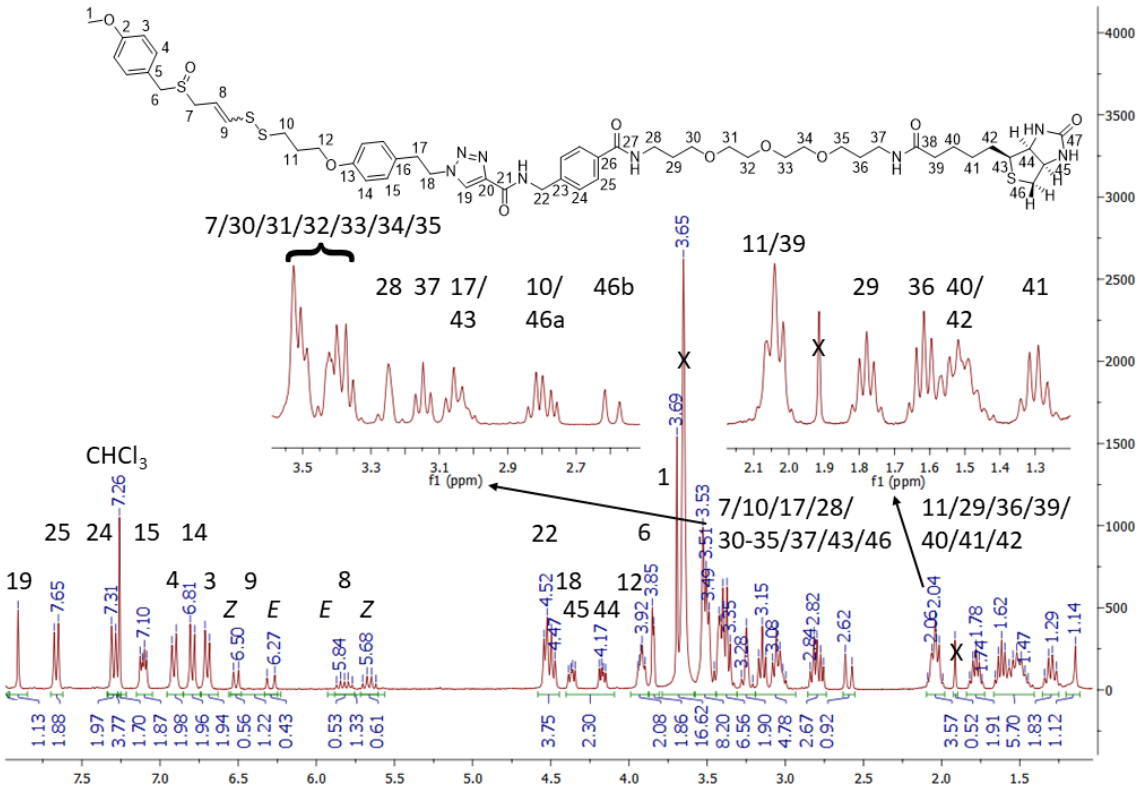

Figure 4.9: ^{1}H-NMR spectrum of biotin-ajoene v2, 26.

Resonances for each coupling partner could be observed in the spectrum. Downfield, the diagnostic triazole (H-19) singlet appeared at 7.91 ppm suggesting that a successful coupling reaction had occurred. This was further supported by the appearance of six aromatic doublets for the three 1,4-disubstituted aromatic rings (H-3/4, H14/15 and H24/25) in a correct integration ratio of 2:2:2:2:2:2. The ajoene vinyl signals (H-8/9) presented themselves as a characteristic *Z-E-E-Z* motif in the region of 5.66 - 6.51 ppm which supported the retention of the pharmacophore. The signals at 4.37 and 4.17 ppm for the two vicinal ring junction protons of biotin (H-44/45) could also be observed. The HRMS data in **Figure 4.10** corroborated the synthesis of biotin-ajoene v2 **26** by showing the molecular mass peak $[M+H]^+$ at 1109.4358, where $C_{53}H_{73}N_8O_{10}S_4$ requires 1109.4338, and showing the sodium adduct $[M+Na]^+$ at 1131.4161, where $C_{53}H_{72}N_8NaO_{10}S_4$ requires 1131.4152.

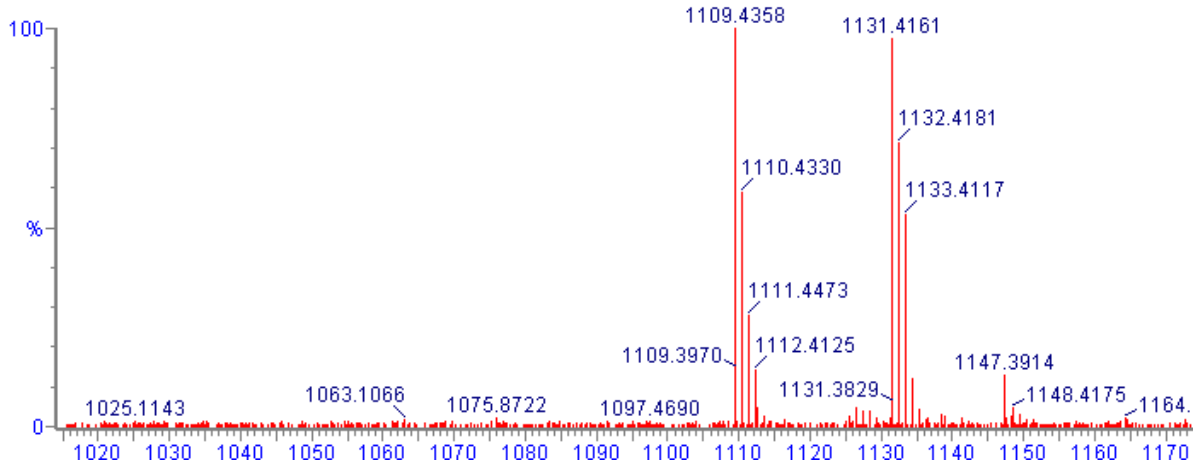

Figure 4.10: HRMS spectrum of biotin-ajoene v2, 26.

Sadly, particularly after such a substantial synthesis effort, biotin-ajoene v2 **26** was found to be unstable in DMSO. Probe solubility and stability in DMSO is necessary for its biocompatible delivery to cells. This unfortunate finding thus prevented us from continuing with any further cell culture experiments. **Figure 4.11** shows a magnified image of treated WHCO1 cancer cells where aggregates of precipitated (and possibly degraded) probe are visible on the bottom of the cell culture plate.

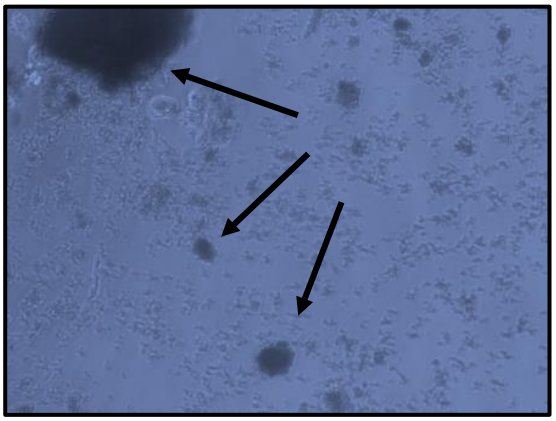

Figure 4.11: Magnified image of treated WHCO1 cells showing precipitated biotin-ajoene following DMSO delivery.
Image taken at 100x magnification.

Instead of using the fully assembled probe, an alternative approach involves first treating the cells with the ajoene-azide fragment **19**, to allow transfer of the azide group to the target protein via thiolysis exchange. Following the lysis of the cells and the collection of azidated proteins, biotinylation of the targets is then achieved through an *in vitro* "Click"-conjugation with the biotin-tether-alkyne fragment **25**, as illustrated in **Scheme 4.12**.

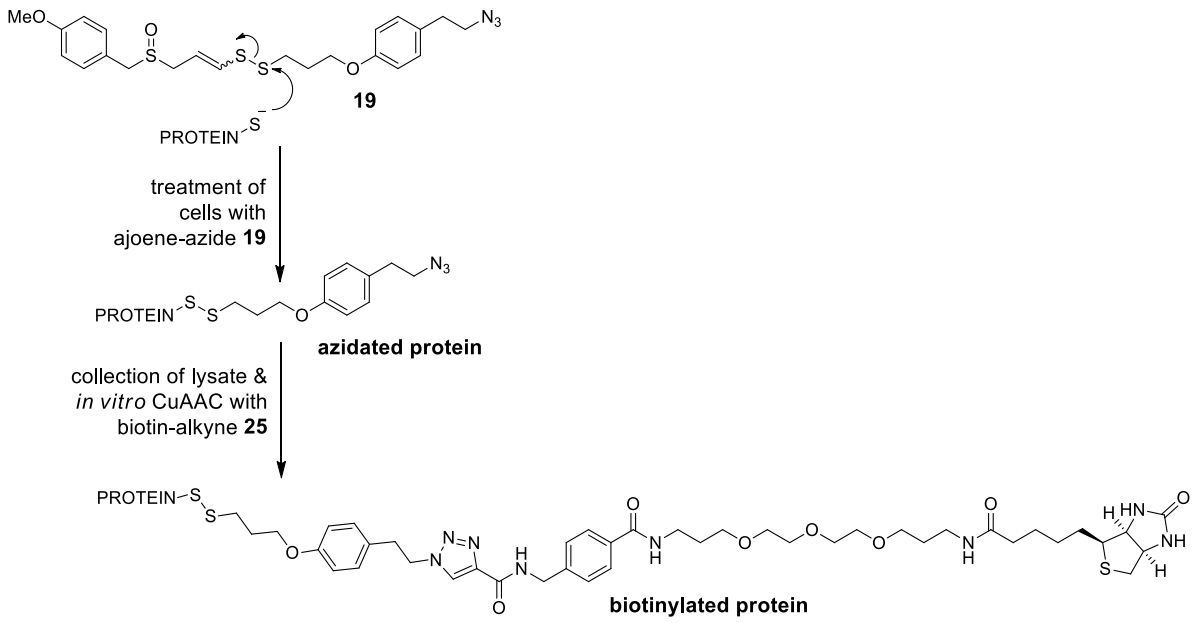

Scheme 4.12 : *In vitro* "Click"-biotinylation of proteins.

We first ascertained whether the individual fragments, **19** and **25**, displayed antiproliferative activity in cancer cells by testing them in an MTT-assay against MDA-MB-231 cancer cells. The ajoene analogue **19** could not be separated into *E*- and *Z*-isomers and was thus tested as an *E*/*Z*-mixture. Pleasingly, azide-ajoene **19** was found to be strongly active with an IC_{50} of 15.0 μM, which was in the same range as its parent of 13.7 μM (*Z*- ajoene) and 18.6 μM (*E*-ajoene).[80] By comparison, and as expected, the biotin-tether-alkyne **25**, lacking the ajoene pharmacophore, was inactive with no cell death observed up to the maximum tested concentration of 200 μM. We performed a western blot experiment to probe the feasibility of *in vitro* biotinylation of proteins by this method. Lysates were prepared from MDA-MB-231 cells that had either been treated with ajoene-azide **19** at the IC_{50} concentration for 24 hours (treated), or with the vehicle alone (0.1% DMSO) for 24 hours (untreated).

The cells were lysed on ice using a lysis buffer containing the non-denaturing detergent, IGEPAL CA-360 and protease inhibitors to prevent proteolysis of the released proteins. The resulting lysate was concentrated by centrifugation, the supernatant was collected and the total protein concentration was determined using the colorimetric bicinchoninic acid (BCA) assay.

This assay relies on two reactions: firstly, the Cu^{2+} ions in the BCA stock solution are reduced by peptide bonds of the protein to form Cu^{1+} which is proportional to the amount of protein in the assayed solution. Secondly, the bicinchoninic acid chelates to the Cu^{1+}

ions to form a purple-coloured complex that absorbs light at a wavelength of 562 nm that can be measured using an absorption reading on a spectrophotometer.[317] The protein concentration was determined using a standard curve of bovine serum albumin (BSA) of known concentrations (0-2 mg/mL). For the "Click"-conjugation, equal amounts of the lysate protein were treated with different combinations of biotin alkyne **25** (100 µM) and "Click"-catalyst (100 µM $CuSO_4$/NaAsc) followed by a one hour, 37 °C incubation. **Scheme 4.13** summarises the workflow used to prepare the western blots.

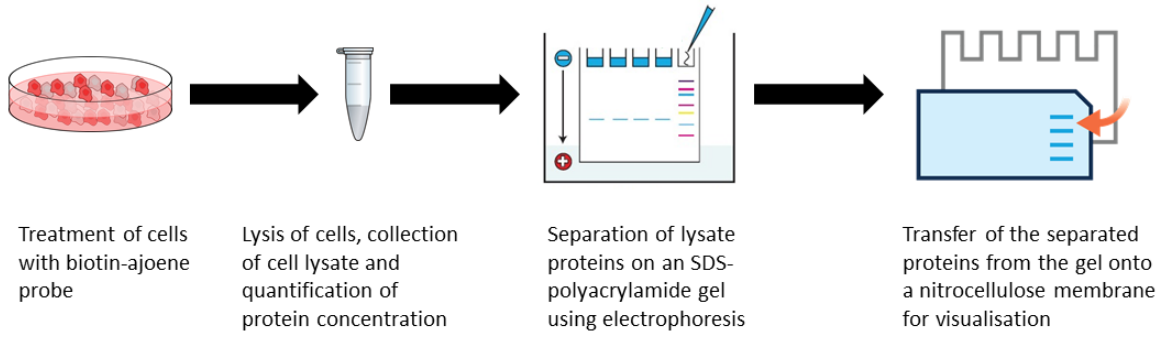

Scheme 4.13: Workflow for the preparation of a nitrocellulose membrane for western blotting.

To allow for visualisation of the individual protein bands, the six samples were separated by SDS-PAGE. This electrophoresis technique allows for the charge-based separation of proteins according to their molecular weight inside of a polyacrylamide gel. The detergent sodium dodecyl sulfate (SDS) denatures the proteins, which eliminates the influence of tertiary structures and simplifying the proteins into long peptide chains. Therefore, the greater the length of the chain, the greater the overall negative charge which in turn moves more slowly through the gel in an applied electric field. Generally, this technique employs reducing denaturants (e.g. DTT) to cleave any disulfide bonds to allow for complete denaturing of the protein, however since our biotin label was attached through a disulfide linkage, we omitted this step and the gel was run under non-reducing conditions. A marker for molecular weights was used as a reference. Thereafter, the separated protein bands were transferred onto a nitrocellulose membrane for visualisation. This step involves running an electrical current from the gel onto the membrane to migrate the proteins out of the gel and onto the membrane.

Prior to the application of the antibody, the membrane was blocked to avoid any non-specific binding. After some unsuccessful visualisation attempts using the streptavidin antibody, we realised that the 3% de-fatted dried milk powder, which we had initially

used in the blocking reagent, contained endogenous biotin. The presence of biotin in the blocking reagent may have resulted in the antibody binding with background non-specifically to the membrane. Therefore, the milk powder was replaced with 3% bovine serum album (BSA) in the blocking buffer, and thereafter the antibody binding became more selective. After blocking, the membrane was incubated overnight with a streptavidin(anti-biotin)-horseradish peroxidase (HRP) antibody, allowing visualisation by chemiluminescence. Horseradish peroxidase finds various applications in biochemistry as it selectively catalyses the oxidation of various substrates by hydrogen peroxide.[318] In our application, the HRP conjugate oxidises a chemiluminescent substrate (LumiGLO Reserve® Chemiluminescent Substrate Kit, SeraCare) that is added to the membrane, as illustrated in **Figure 4.12**.

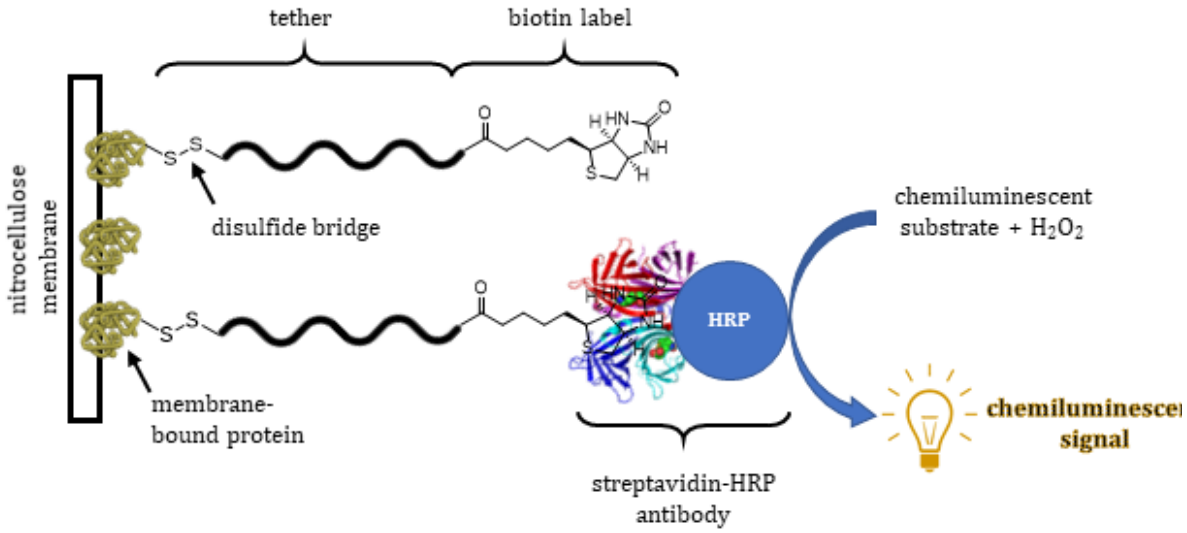

Figure 4.12: Visualisation of biotinylated proteins on the western blot using a streptavidin-HRP antibody that produces a chemiluminescent signal.

The ensuing reaction produces a chemiluminescent signal in the region of the membrane where the antibody has bound to its target, in our case, a biotinylated protein. The signal is detected and captured using an imager with a built-in camera. Lastly, the quantification of the fold-change difference between each lane was achieved by applying a total protein normalization across the signals of interest (chemiluminescent bands).[319] The experimental blot is shown in **Figure 4.13**.

Lane	1	2	3	4	5	6
ajoene azide **19**	-	-	-	+	+	+
biotin alkyne **25**	-	+	+	-	+	+
$CuSO_4$/NaAsc	-	-	+	-	-	+
fold-change	-	1	13	-	1	11

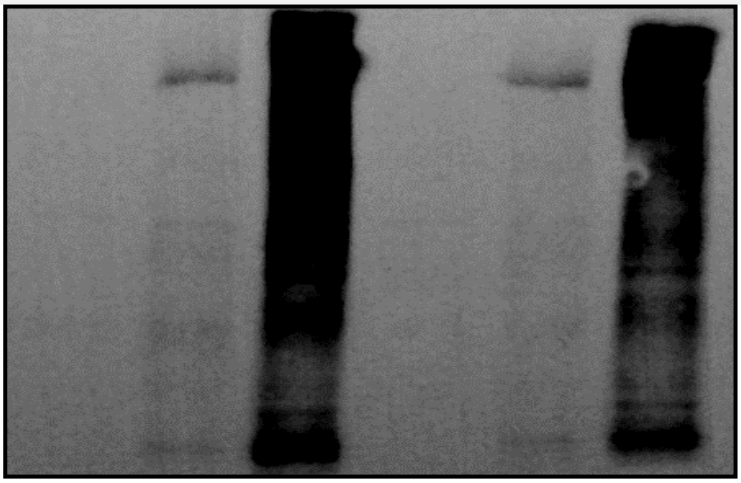

Figure 4.13:Western blot of the *in vitro* biotinylation of treated MDA-MB-231 cells.

As expected, **lanes 1** and **4** showed no signal owing to the lack of biotinylation reagent. The large number of chemiluminescent protein bands in both the untreated (**lane 3**) and treated (**lane 6**) samples implicated that many proteins had been biotinylated as detected by the anti-biotin antibody. This result was expected for **lane 6** but not for **lane 3** where the ajoene pharmacophore was missing. We rationalised that a Michael addition between cellular cysteine thiol groups and the triple bond of the propynone moiety of **25** had occurred, generating biotinylated proteins via an alternative route to the one intended, namely thiolysis exchange with vinyl disulfide. Similarly, we attributed the faint signals in **lanes 2** and **5** also to the Michael addition of protein thiols to the alkyne to generate a protein-*S*-tether-biotin species picked up on the membrane, with the bands being fainter due to the lack of the catalyst. It was also speculated that the slight decrease in band intensities for the treated lysates (**lane 5** and **6**), when compared to the untreated lysates (**lane 2** and **3**), may relate to a decrease of available cysteine sites for the Michael addition of the alkyne, as these sites are already *S*-thiolated by ajoene. The greater intensity of bands in **lane 3/6** compared to **lane 2/5** (no copper) suggests catalysis is involved in the Michael addition by copper(I). The proposed Michael addition is represented in **Scheme 4.14**.[320]

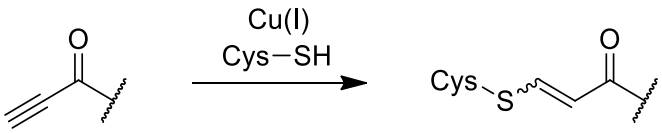

Scheme 4.14: Proposed off-target reactivity of biotin-alkyne fragment during *in vitro* "Click"-reactions.

Subsequent optimisation attempts, which included changing incubation times and reagent concentrations, turned out to be futile. In view of the instability of the assembled probe **26** in the delivery vehicle DMSO, its insolubility in cell culture media and overall lack of bioactivity, as well as the lack of selectivity of the biotin-tether-alkyne **25** for ajoene azidated proteins in the *in vitro* approach, resulted in a redesign of the probe.

4.4.3 Biotin-Ajoene V3

The underlying reasons for the instability of **26** in DMSO and its insolubility in water were indeed far from clear. Furthermore, the *in vitro* biotin-ajoene "Click"-reaction of the individual fragments (**19** and **25**) was not yielding the expected conjugation results, as biotinylation was also occurring from a thiol-yne "Click"-reaction. For version three **33**, it was decided to start by simplifying the probe in terms of functionality. This was achieved by reducing it structurally back into the core elements of the ajoene pharmacophore, the tether, the biotin moiety and the "Click"-functional handles, while retaining a convergent click-based coupling strategy which was giving success as the synthetic route. **Figure 4.14** and **4.15** show the design changes (removed elements shown in red) from version 2 **25** to version 3 **32**. We were aware of the shorter length of the new version (v3), which might not be optimal for the steptavidin pocket, but decided to stick with the new plan.

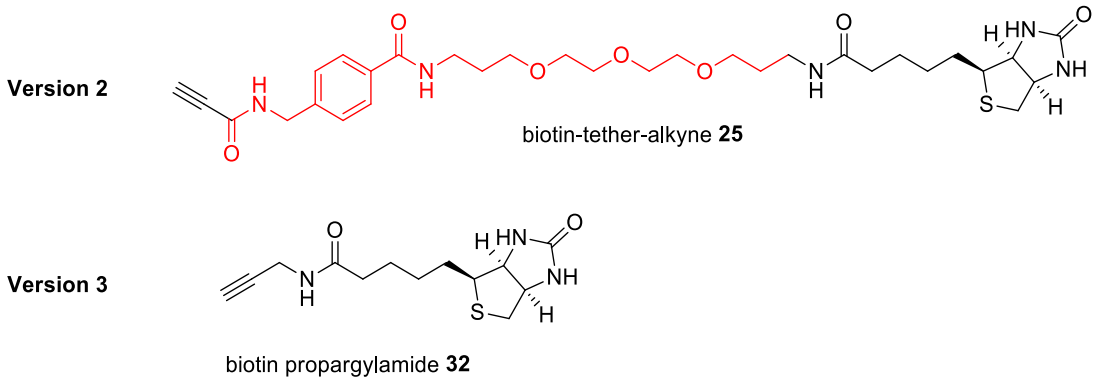

Figure 4.14: Changes of the biotin-tether-alkyne going from version 2 to version 3.

We suspected that the α-carbonyl group to the alkyne moiety of the biotin-alkyne **25** was activating the alkyne towards a Michael addition with protein thiols within the lysate, especially when in the presence of the "Click"-catalyst. This effectively reduced the selectivity for the ajoene azide reaction partner. For this reason, we decided to try a non-activated *N*-propargyl group as our "Click"-alkyne partner. In line with our approach to reduce the complexity of the probe, we also stripped away the PEG tether and the *p*-aminomethylbenzoic acid-linking structure (marked together in red in **Figure 4.14**), generating a much simpler coupling fragment as biotin-propargylamide, also a known molecule in the chemical biology literature.[321] Similarly, for ajoene-azide, we replaced the PMB group of **19** with a simpler *n*-propyl group on the sulfoxide end of the ajoene in **31** (**Figure 4.15**) so as to simplify the molecule to resemble ajoene as much as possible.

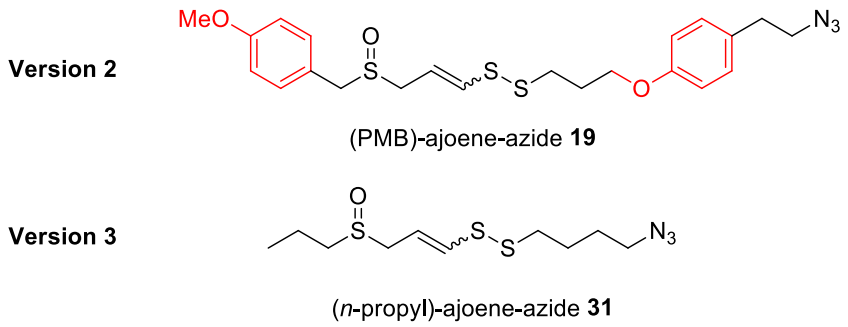

Figure 4.15: Changes of the ajoene-azide going from version 2 to version 3.

The replacement of the phenoxy tether in **19** with a simpler *n*-butyl chain for **31** also provided a shorter tether and reduced the overall number of synthetic steps for accessing the required azido-thiotosylate **17**.

As with the previous "Click"-approach, we again gave ourselves the option to either perform an *in vitro* biotinylation, or to couple **31** and **32** to give biotin-ajoene version 3 **33**, as illustrated in **Scheme 4.15**.

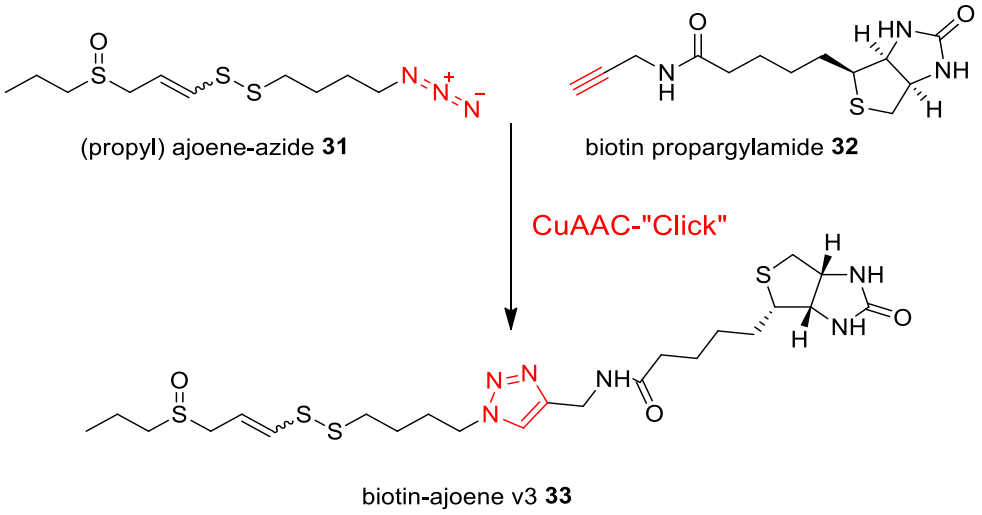

Scheme 4.15: Biotin-ajoene v3, 33, and its "Click"-fragments, 31 and 32.

The ajoene-azide target partner **31** required an azidobutyl thiotosylate **27**, serving as the sulfenylating agent in line with our previous strategy. **Scheme 4.16** below shows its synthesis via a one-pot sequential double substitution of 1,4-dibromobutane, first with azide and then with thiosulfonate. Column chromatography allowed separation of any bis-substituted by-products.

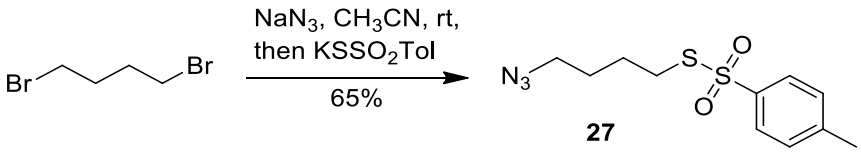

Scheme 4.16: Synthesis of the azide sulfenylating agent, 27.

The ^{1}H-NMR spectrum of the azidobutyl thiotosylate **27** is shown in **Figure 4.16**. The presence of the thiotosylate group was supported by the appearance of the AA'BB' doublet of doublets of the 1,4-disubstituted aromatic ring protons (H-2'/3') as well as the singlet for the methyl protons (H-1'). The signals of the methylene groups in the butyl chain were given by the two overlapping multiplets at 1.84 ppm (H-2/3), while two triplets at 3.33 (H-1) and 3.02 (H-4) denoted the butyl terminal methylenes, in which the more downfield shift (H-1) was assigned to the azidomethylene protons (azide being more electron-withdrawing than thiotosylate).

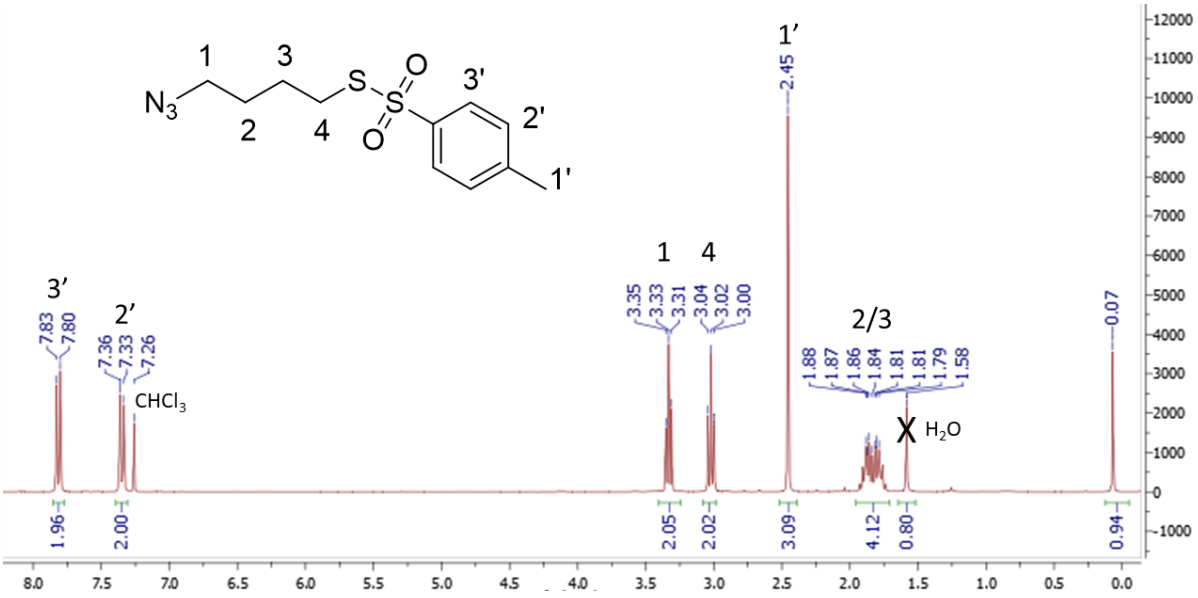

Figure 4.16: ^{1}H-NMR of azide-butyl-thiotosylate, 27.

According to our established methodology we then furnished the azide-ajoene **31** as shown in **Scheme 4.17**.[153]

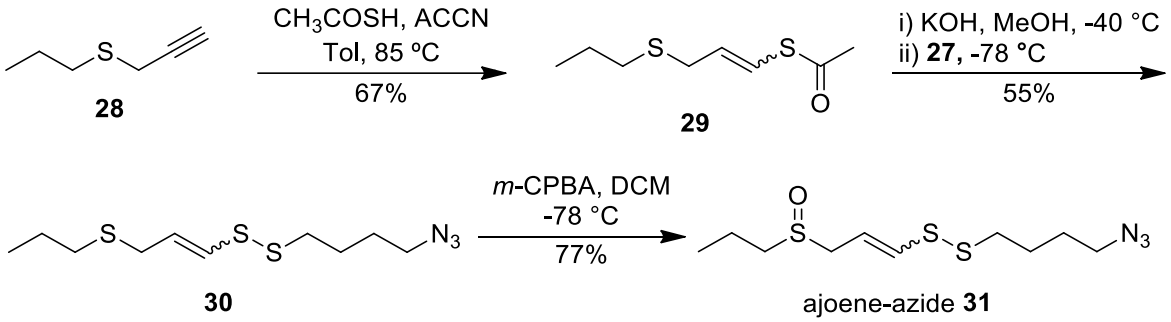

Scheme 4.17: Synthesis of ajoene-azide, 31.

The sulfenylation of the propyl vinyl thioacetate **29** with the thiotosylate **27** gave the disulfide **30**. In this step, we observed a low yield and several side-products, which was attributed to the possibility of reduction of the azide by the enethiolate ion, a process that Henthorn *et al*. has compared to the Staudinger reaction.[322] The oxidation of **30** gave the sulfoxide **31** as an *E:Z* mixture of 5:6 in an overall moderate yield of 42% over two steps. Its ^{1}H-NMR spectrum is shown in **Figure 4.17**.

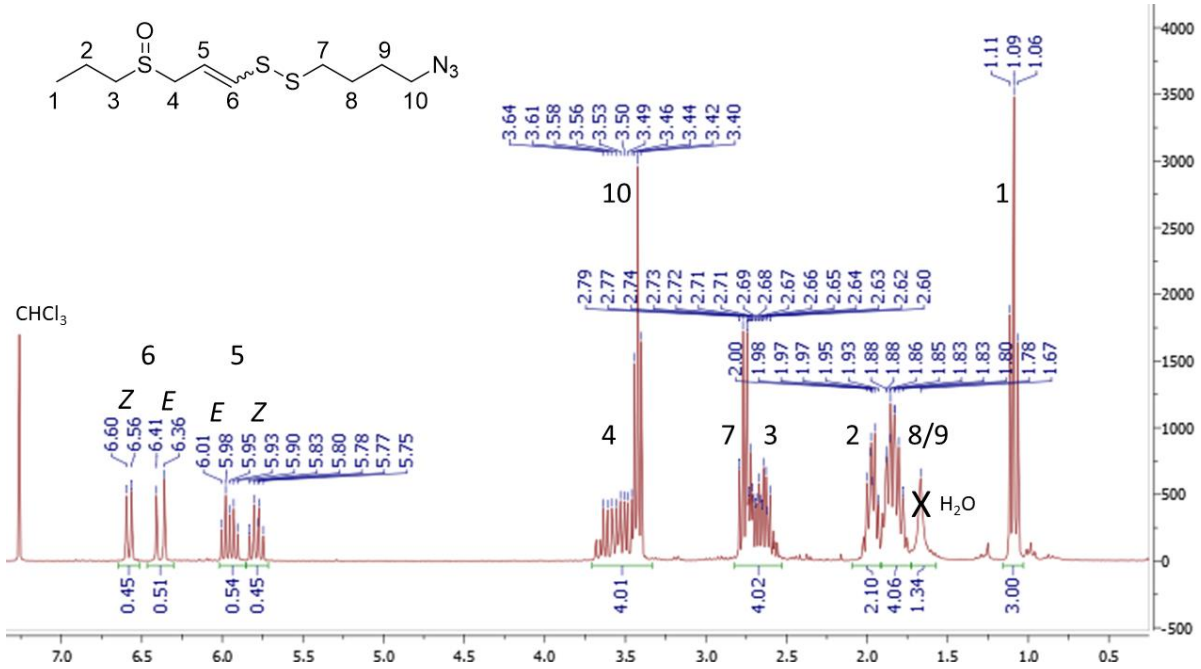

Figure 4.17: ^{1}H-NMR of ajoene-azide, 31.

The diastereotopic splitting of the α-protons to the newly synthesised sulfoxide were seen by the multiplets at 3.56 ppm (H-3) and 2.68 ppm (H-4), now more complex than before (with PMB) in view of additional couplings. The protons of the vinyl moiety (H-5 and H-6) produced signals in the typical *Z-E-E-Z* motif as before. The methylene proton adjacent to the azide group (H-10) remained at the same chemical shift (3.44 ppm) as that in **27**, whereas H-7 appeared upfield due to the replacement of the thiotosylate by the less electron-withdrawing disulfide.

For the other partner, biotin propargylamide **32**, propargylamine was coupled to the NHS ester of biotin in 80% isolated yield as shown in **Scheme 4.18**.

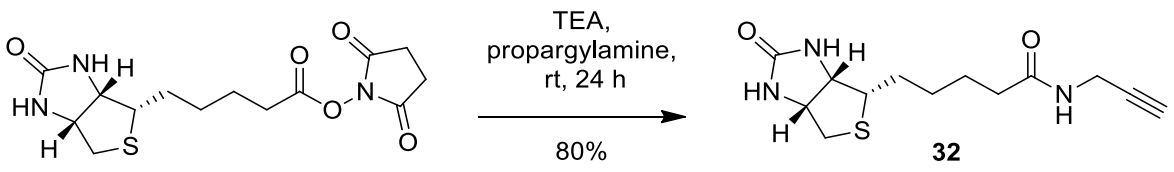

Scheme 4.18: Synthesis of biotin-alkyne, 32.

The method by Villemin *et al.* was followed and the spectroscopic data matched those reported by them in the literature for biotin propargylamide **32**.[321]

Finally, the CuAAC-coupling of fragments **31** and **32** was carried out as before using a 1:1 stoichiometric ratio of reactants at 30 °C, as shown in **Scheme 4.19**.

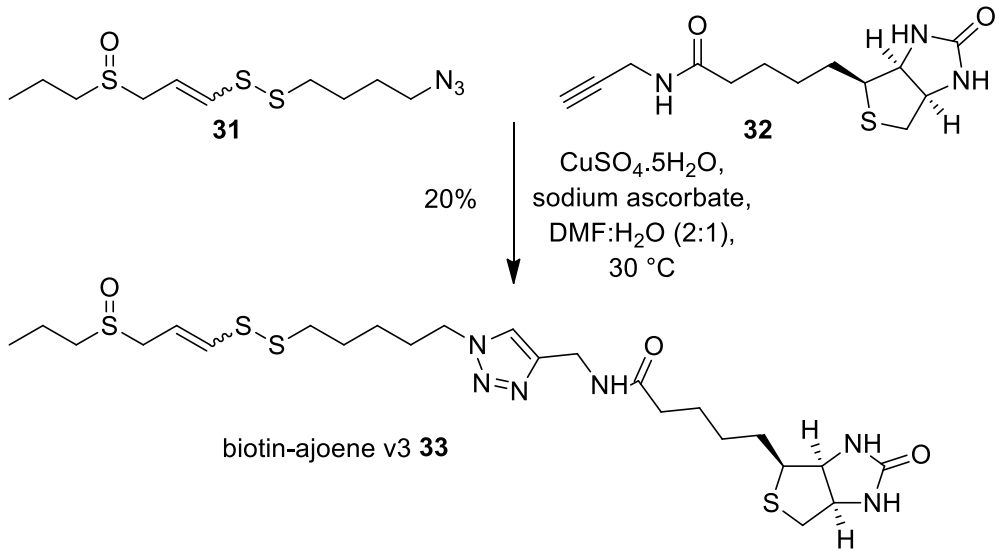

Scheme 4.19: "Click"-coupling to afford biotin-ajoene v3, 33.

As with probe version two, **26**, by TLC, the reaction produced substantial side-products at the 18-hour mark and was halted even though full conversion had not been achieved. The reaction was quenched and the product isolated via silica column chromatography using 1:9 MeOH:DCM as the eluent to give **33** as single spot on the TLC plate, with an approximate yield of 20% by TLC. Unfortunately, once again, we observed rapid degradation of the biotin-ajoene probe **33** in DMSO as NMR solvent. The degradation became apparent as a colour change of the NMR sample, where the decomposition appeared to be faster than for **26**. Although characteristic resonances of **33**, specifically the triazole H, could be discerned within the crude ^{1}H-NMR spectrum (not shown), a subsequent TLC analysis of the NMR sample showed multiple spots on the plate, which substantiated the degradation of **33**. This made characterisation of the product impossible. Although we could have continued the characterisation by using a mixed NMR solvent system (mimicking the chromatography solvent), the inability to dissolve the compound in DMSO for the downstream treatment of cells, led us to abandon further investigations of the assembled probe **33**. We therefore proceeded to explore the *in vitro* option of our strategy with the alkyne group now deactivated towards nucleophilic addition.

Ajoene azide **31** did show antiproliferative activity in the MTT assay, but with a 3-fold reduction in IC_{50} compared to that of the PMB equivalent in probe 2 **26**, of 45 μM. A

similar 3-fold reduction in activity had also been observed in our original SAR study going from *n*-propyl to PMB in ajoene.[183] As previously, we then treated MDA-MB-231 cancer cells with ajoene-azide **31** followed by *in vitro* biotinylation of the lysate using biotin-alkyne **32** under "Click"-conditions. The visualisation of the resulting western blot unfortunately showed no chemiluminescent signals for any of the sample lanes, indicating that no biotinylation had taken place. **Figure 4.18** shows a comparative western blot in which MDA-MB-231 cells had either been treated with the ajoene azide fragment of probe version 2 (**19** for **26**) or probe version 3 (**31** for **33**), at their respective IC_{50} values, and the resulting lysate was then incubated with 100 μM of its complementary biotin-alkyne (**32** for **33** and **25** for **26**) under catalytic (1 mM $CuSO_4$ and sodium ascorbate, **lanes 3** and **6**) or non-catalytic (**lanes 2** and **5**) conditions.

Probe	Version 2 (26)			Version 3 (33)		
Azide/Alkyne	**19 / 25**			**31 / 32**		
Lane	**1**	**2**	**3**	**4**	**5**	**6**
ajoene-azide	-	+	+	-	+	+
biotin-alkyne	-	+	+	-	+	+
$CuSO_4$/ NaAsc	-	-	+	-	-	+
fold-change	0	1	5	0	0	0

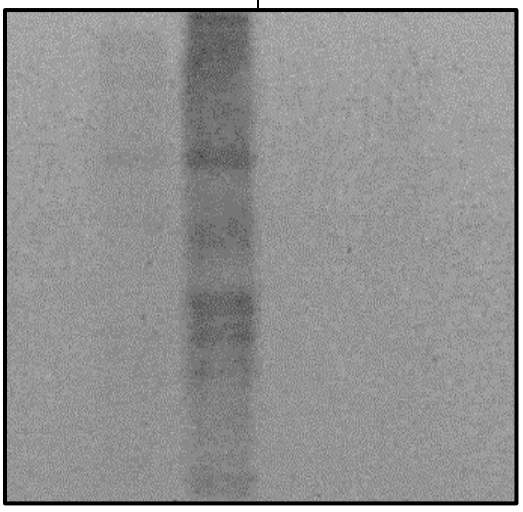

Figure 4.18: Comparative western blot of the *in vitro* "Click"-reaction for the fragments of probe version 2 and version 3 on treated MDA-MB-231 cancer cells lysates.

Lanes 2-3 showed a similar biotinylation profile to the previous experiment showing the result of non-specific Cu-mediated thiol-yne binding interactions of probe version 2. As

expected, the untreated lysates in **lane 1** and **4** showed no signal, but unfortunately, neither did **lanes 5**-**6**, which account for the cells that had been treated with the "Click"-fragments of probe version 3 (**31** and **32**). However, it was encouraging to see that the biotin-alkyne **32** (version 3) did not produce non-specific binding interactions, however the lack of chemiluminescent signals in **lanes 5** and **6** indicated that the *in vitro* "Click"-assembly of the probe in cell lysate had not worked.

Although there could have been many reasons for the lack of "Click"-reaction on the cell lysate, the reaction was taking place on a complex cellular mixture and two possible explanations were considered: Firstly, the now shortened tether between the pharmacophore and biotin tag could have hampered access of **32** into the elongated streptavidin binding pocket. Secondly, the incubation of cell lysate with the "Click"-catalyst was conducted for a much shorter period of one hour at 37 °C compared to the CuAAC coupling in the chemistry lab setting of 18 hours at 30 °C, as prolonged heating of lysates at this temperature would promote protein degradation. The short reaction time in this experiment may have led to a low yield of labelling.[323]

Considering all the lessons learned, we proposed three changes to our design for a fourth-generation probe. When comparing the instability of our PMB-version 2, **26,** with that of the *n*-propyl version 3, **33**, a more rapid degradation of the latter suggested the need to reinstall the PMB group. We also took into consideration, as alluded to previously, that *n*-propyl-ajoene analogues showed weaker antiproliferative activity than their respective PMB analogues.[170] Additionally, it is known that diagnostic and therapeutic molecules containing PEG polymers exhibit various advantages such as increased water-solubility, reduction in non-specific interactions with proteins and reduced *in situ* degradation by metabolic enzymes.[324–326] These improvements in pharmacological properties of PEG linkages supported the reintroduction of this moiety in **33**. Lastly, it was wondered whether the Cu-mediated thiol-yne coupling between the biotin-alkyne and cellular thiols during *in vitro* biotinylation might be mitigated by reversing the "Click"-partners, namely by furnishing an ajoene-alkyne and biotin-azide, as shown in **Figure 4.19**.

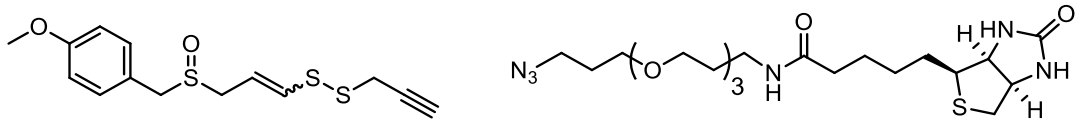

(PMB)-ajoene-alkyne **36** biotin-(PEG)-azide **39**

Figure 4.19: Inversion of alkyne and azide "Click"-partners.

In the event, we were gratified to find that all these modifications paid off as shown below in the synthesis of probe version 4.

4.4.4 Biotin-Ajoene V4

Before embarking on the synthesis of probe version 4, **40**, a literature search was carried out, which identified biotin-PEG-azide **39** (**Figure 4.19**) as a known and stable compound that had been used for "Click"-conjugations by Chambers *et al.*,[327] which gave us some confidence that this route might be successful. A retrosynthetic analysis of the two fragments (**36** and **39**) is shown in **Scheme 4.20**.

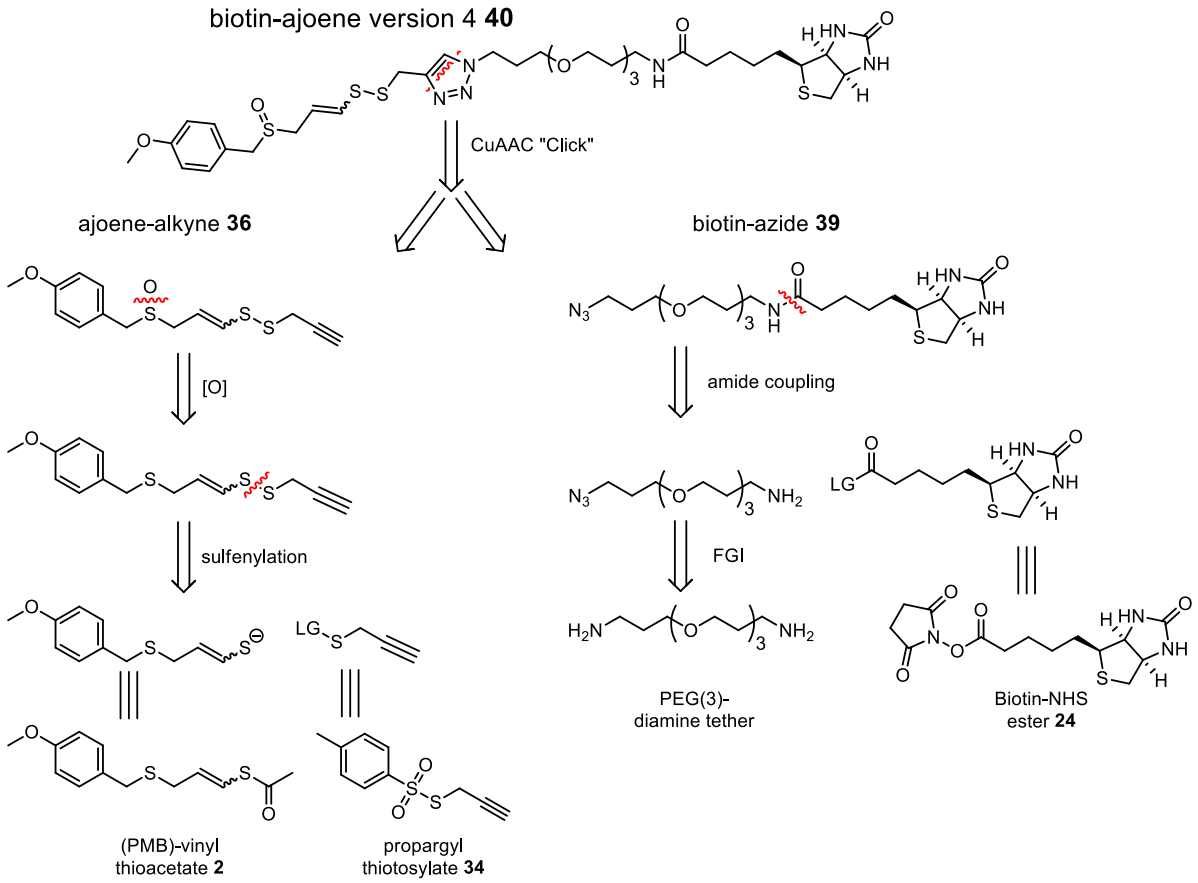

Scheme 4.20: Retrosynthesis of "Click"-fragments of biotin-ajoene v4, 40.

The synthesis of the two fragments, **36** and **39**, was expected to be quite straightforward. The ajoene-alkyne fragment (**36**) was envisioned to arise from the chemoselective oxidation of the sulfide-vinyl disulfide formed from the sulfenylation of the well-established vinyl thioacetate **2** (three steps from PMBCl) intermediate, with a suitable sulfenylating agent. The sulfenylating agent in question, propargyl thiotosylate **34**, could easily be accessed from the reaction between propargyl bromide and potassium thiotosylate. For the biotin-azide fragment (**39**), an amide-coupling between biotin-NHS ester **24** and a mono-functionalised azide-PEG-amine tether was proposed.

The tether itself was envisioned to arise from an *N*-Boc-mono-protection of a diamine, subsequent FGI of the free amine to the azide, followed by an *N*-Boc-deprotection to avail the amine for coupling in the last step. The forward synthesis was performed as described below.

4.4.4.1 Synthesis of Fragment 36

Synthesis of the propargyl sulfenylating reagent **34**, as depicted in **Scheme 4.21**, was achieved via reaction of potassium thiotosylate and propargyl bromide in DMF for 4 hours at room temperature. Upon completion, the reaction mixture was diluted with diethyl ether and the DMF was removed by several water washings. Purification by column chromatography afforded the propargyl thiotosylate **34** as a colourless crystalline solid in 85% yield.

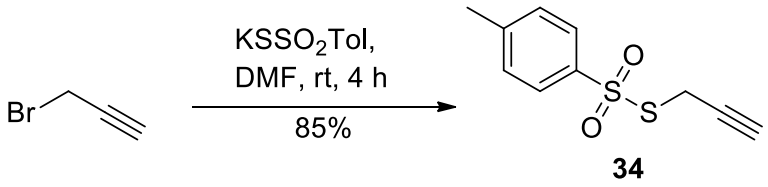

34

Scheme 4.21: Synthesis of the propargyl thiotosylate, 34.

The formation of the sulfenylating agent **34** was corroborated by melting point analysis, which was in the same range as the literature (43-44 °C; lit[328] 45-46 °C). An assigned ^{1}H-NMR spectrum is displayed in **Figure 4.20**, showing all the expected resonances. The structure was also corroborated by HRMS data, which revealed a molecular mass peak $[M+Na]^{+}$ at 249.0012, in which $C_{10}H_{10}NaO_2S_2$ requires 249.0020.

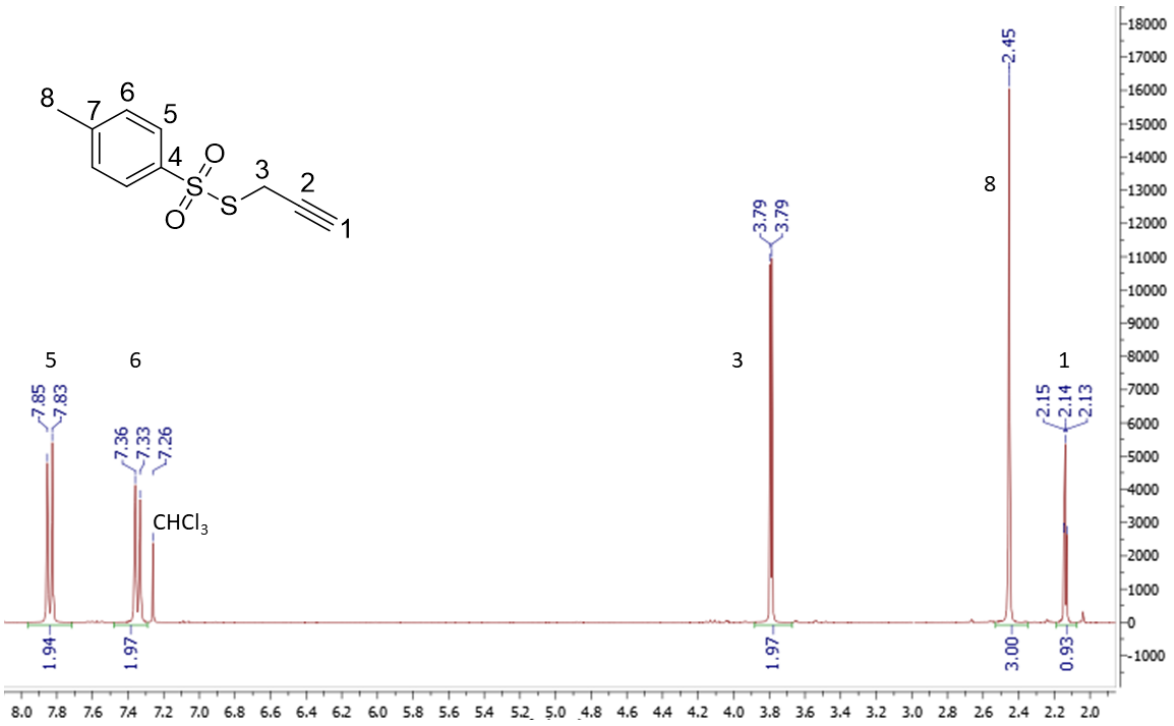

Figure 4.20: ^{1}H-NMR spectrum of propargyl thiotosylate, 34.

The propargyl thiotosylate **34** was subsequently reacted with the PMB-vinyl thioacetate **2** to furnish the probe's vinyl disulfide pharmacophore **35** in 65% yield according to our previous method, as shown in **Scheme 4.22**.

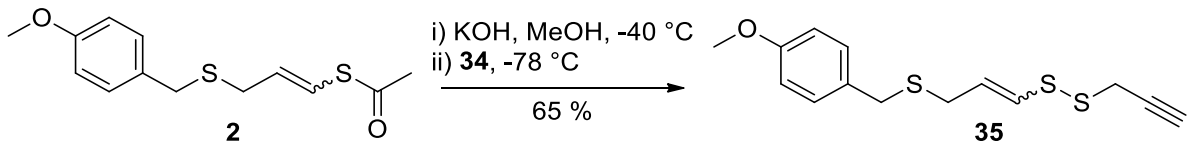

Scheme 4.22: Synthesis of the vinyl disulfide, 35.

Low temperature (-40 °C) *in situ* hydrolysis of the thioacetate **2** with KOH over 30 minutes was followed by *S*-alkylation with the propargyl thiotosylate **34** at -78 °C. Subsequent silica column chromatography produced the vinyl disulfide **35** in 58% yield as a 1:2 mixture of *E*/*Z*-isomers. As with the previously synthesised ajoene analogues bearing aromatic end-groups, the *E*/Z-isomers were inseparable, for which the ^{1}H-NMR spectrum (**Figure 4.21**) clearly identified individual vinylic proton resonances as two sets of doublet signals at 6.19 ppm (H-4) and 5.93 ppm (H-5) for the *E*-isomer, and 6.37 ppm (H-4) and 5.74 ppm (H-5) for the *Z*-isomer (as a *Z*/*E*/*E*/*Z* foursome from lowfield to highfield). The successful incorporation of the alkyne functional group was shown by the

characteristic propargyl triplet and doublet at 2.30 ppm (H-1) and 3.47 ppm (H-3), respectively. Further evidence for this was given by the alkyne C-H stretch at 3286 cm^{-1} in the IR spectrum. The formation of the vinyl disulfide **35** was also corroborated by ^{13}C-NMR spectroscopy, in which 12 carbon resonances were produced for each diastereomer in the ^{13}C NMR spectrum, noting the symmetry in the phenyl ring (**C-9/10**).

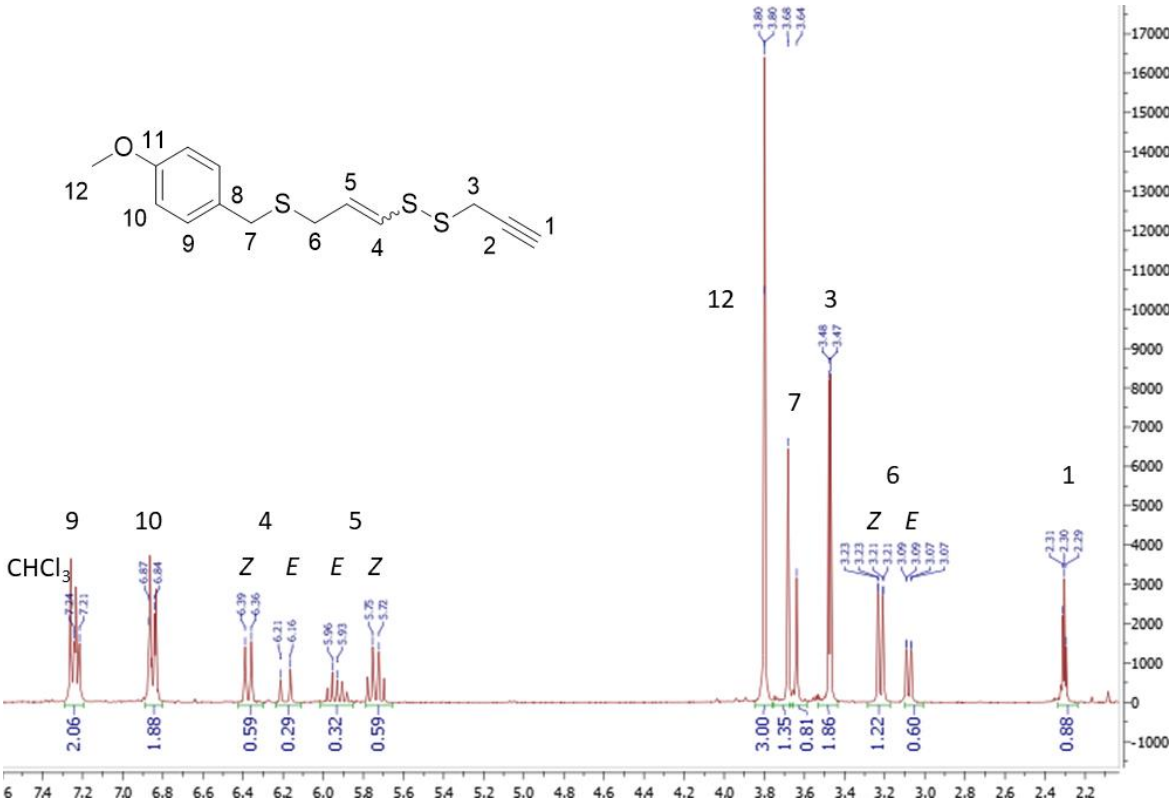

Figure 4.21: ^{1}H-NMR spectrum of vinyl disulfide, 35.

The chemoselective oxidation of the sulfide **35** to the sulfoxide **36** is shown in **Scheme 4.23**. As previously, the reaction of the sulfide **35** with *m*-CPBA in DCM at -78 °C over 2 hours, with subsequent purification by column chromatography, yielded the sulfoxide **36** in 61% as *E*/*Z*-isomers in a ratio of 3:5. Its assigned ^{1}H-NMR and HRMS spectra are shown in **Figure 4.22** and **4.23**, respectively.

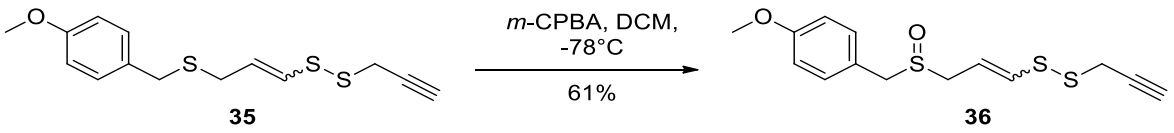

Scheme 4.23: Synthesis of ajoene-alkyne, 36.

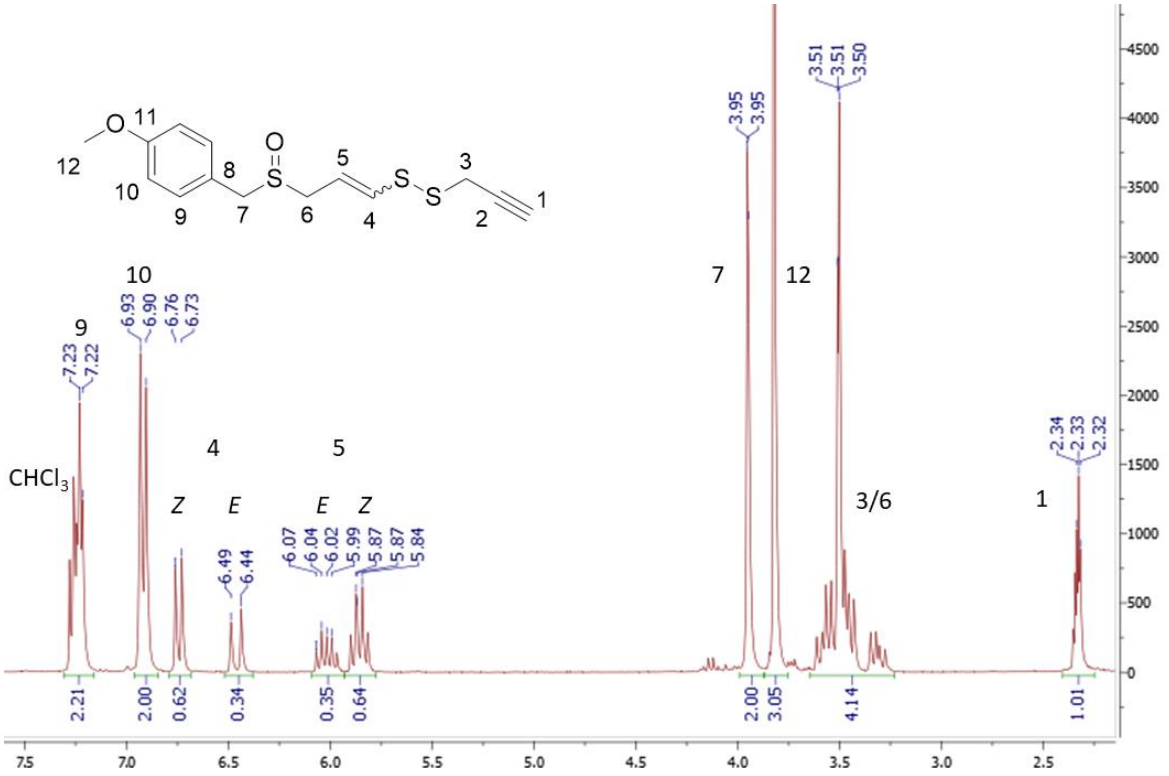

Figure 4.22: ^{1}H-NMR spectrum of ajoene-alkyne, 36.

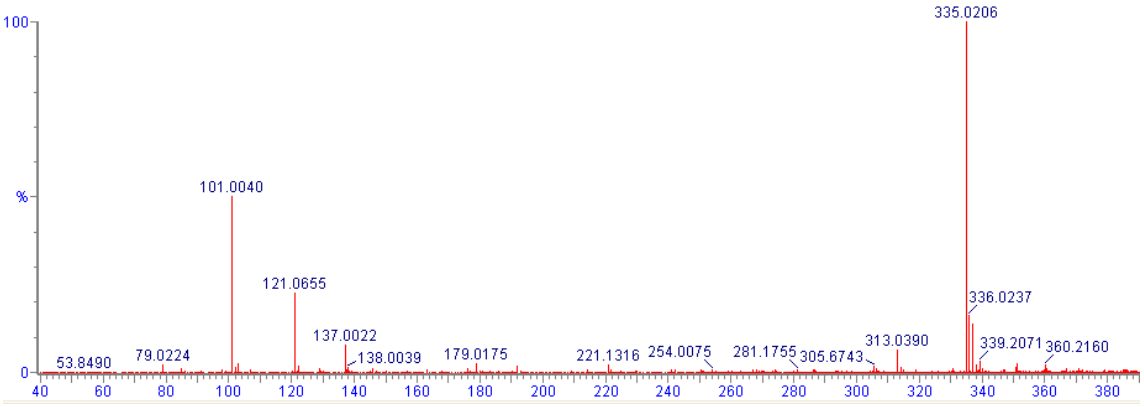

Figure 4.23: HRMS spectrum of ajoene-alkyne, 36.

In the ^{1}H-NMR spectrum, the downfield shift of H-4 is significant for sulfoxide oxidation. Site selectivity was confirmed by virtue of the diastereotopic splitting and downfield shift of the two methylene protons (H-6 and H-7) alpha to the sulfoxide. The allylic proton H-6 showed the two multiplets between 3.27 - 3.60 ppm for the *E*- and *Z*- diastereomers while the benzylic proton H-7 was observable as a singlet (a collapsed AB pair) at 3.95 ppm. Furthermore, the IR spectrum showed an absorption at 1030 cm^{-1} accounting for the sulfoxide stretch. The HRMS finally confirmed the formation of ajoene-alkyne **36**, by showing a peak at 335.0206 accounting for the $[M + Na]^{+}$ ion of $C_{14}H_{17}NaO_2S_3$, which requires a *m/z* ratio of 335.0210.

4.4.4.2 Synthesis of Fragment 39

The route towards the biotin-tether-azide coupling partner **39** utilised a similar protection/deprotection strategy to that of our previous biotin-tether-alkyne **25** synthesis. The use of a novel diazo-transfer reagent, imidazole-1-sulfonyl azide,[329] allowed the conversion of the unprotected primary amine of the protected PEG diamine **20** into the required azide chemical handle, which was followed by its deprotection (at the other end) and subsequent amide-coupling to the previously synthesised biotin NHS-ester **24**, as depicted in **Scheme 4.24**.

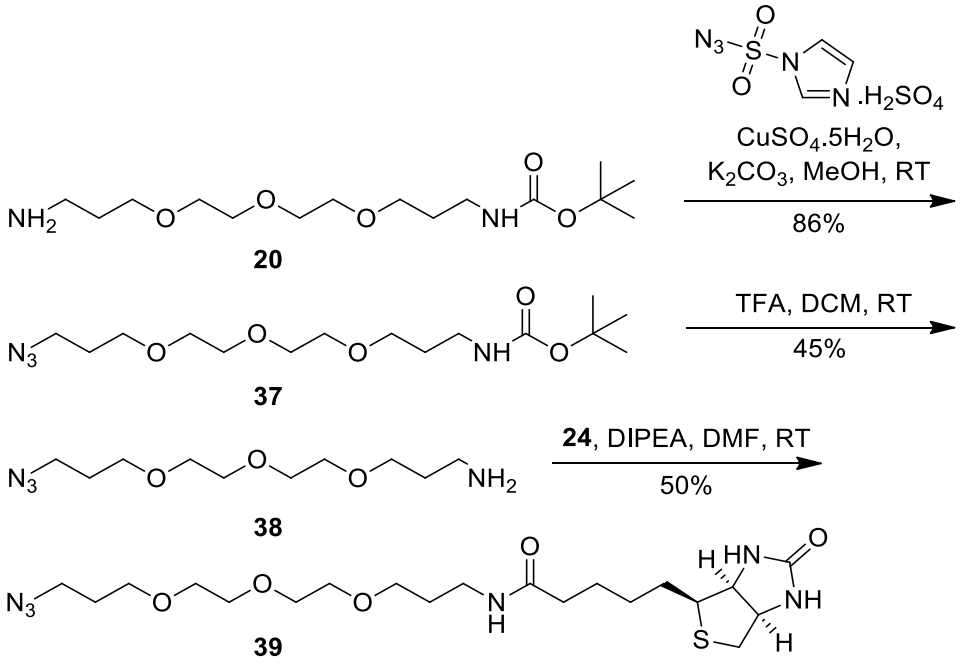

Scheme 4.24: Synthesis of biotin-tether-azide, 39.

The safety risks of handling diazo transfer reagents were mitigated by using the shelf-stable hydrogen sulfate salt of imidazole-1-sulfonyl azide, which was synthesised according to the method by Gardiner *et al*. using NaN_3, sulfuryl chloride and imidazole.[329] The amino group of the *N*-Boc protected PEG tether **20** was reacted in a methanolic solution of the above diazo transfer reagent, $CuSO_4$ and K_2CO_3 at room temperature over 3 hours to produce the azide **37** in 86% yield.

The success of the conversion was corroborated by the appearance of a N≡N stretch at 2097 cm^{-1} in the IR spectrum and by the $[M + H]^+$ mass ion of 347.2284 in its HRMS spectrum, in which $C_{15}H_{31}N_4O_5$ was calculated as 347.2294.

The TFA deprotection of the *N*-Boc protected amine terminus of **37** in DCM at room temperature produced azide-PEG-amine **38** in poor yield (45%), which was attributed to loss of the water-soluble product in the basic (aq. $NaHCO_3$) extraction step designed to neutralise acidic by-products (once the excess DCM and TFA had been removed under low vacuum). When omitting the basic extraction step, however, the purification of the product by silica column chromatography was unsuccessful.

The ^{1}H-NMR spectra of both the protected and deprotected azide-PEG intermediates as **37** and **38** respectively, are depicted in **Figure 4.24**.

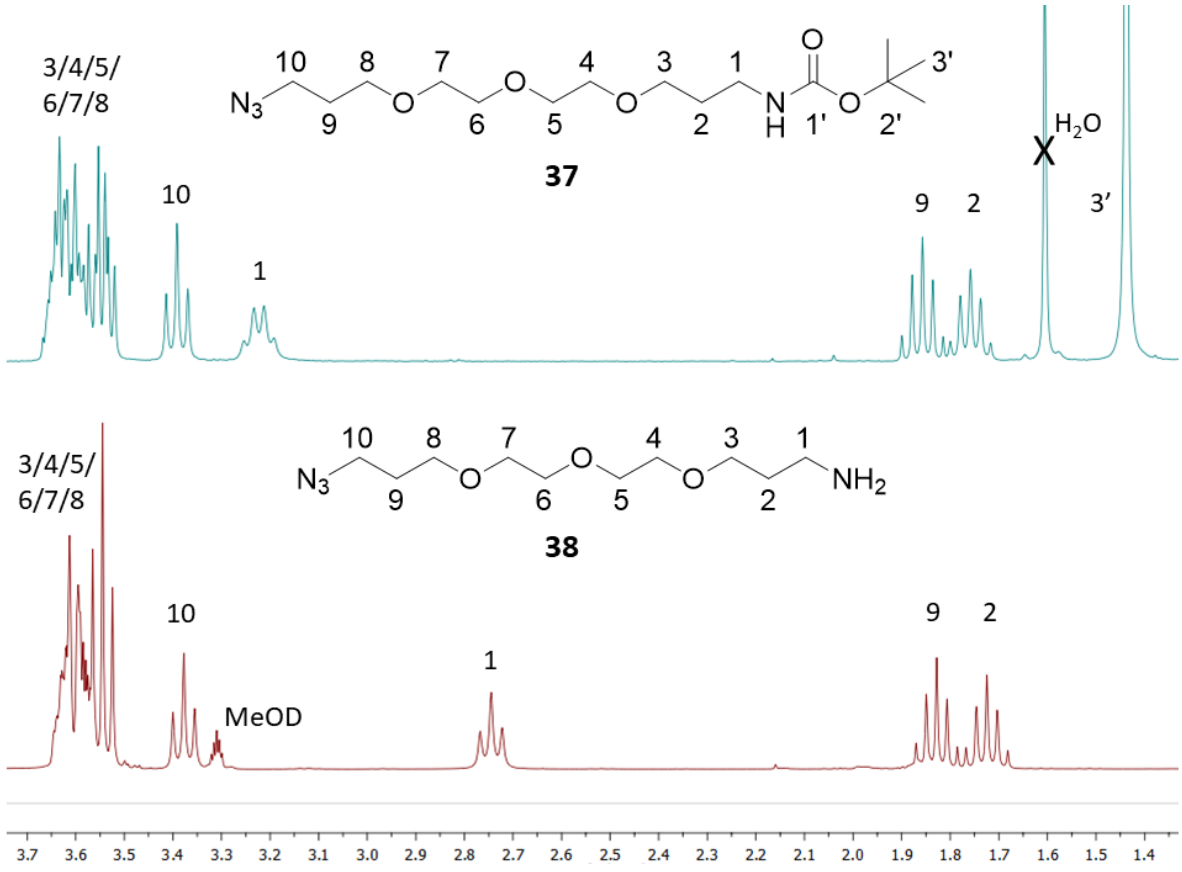

Figure 4.24: Stacked ^{1}H-NMR spectra of azide-PEG-*N*-Boc 37 and azide-PEG-amine, 38.

Although the samples were run in different NMR solvents ($CDCl_3$ for **37** and MeOD for **38**), the signals for the central PEG chain ranging from H-2 to H-10 showed satisfactory correlation between spectra. The successful deprotection could be observed by the loss of the *tert*-butyl (H-3') signals previously at 1.44 ppm in the spectra of **37**. Finally, the α-methylene proton (H-1) of amide **38**, as anticipated, were downfield to those of amine **37** (3.22 ppm vs 2.74 ppm).

In the final coupling step, the amine linker **38** and the biotin succinimide ester **24** were dissolved in equimolar amounts in DMF. DIPEA (1.1 eq) was then added, and the solution stirred at room temperature for 2 hours. Silica column chromatography afforded the biotin-azide **39** as a colourless wax in 50% yield.

The characteristic N≡N stretch at 2092 cm^{-1} in the IR spectrum confirmed the retention of the azide group. The biotin ureido carbonyl groups and the newly formed amide carbonyl group gave C=O stretching absorption frequencies at 1695 cm^{-1} and 1640 cm^{-1} respectively. The ^{1}H-NMR spectrum, shown in **Figure 4.25**, corroborates the addition of the biotin group onto the linker by showing the diastereotopically split H-19a/b α-thiomethylene pair at 2.82 and 2.58 ppm as well as the two protons H-17 and H-18 of the *cis*-ring junction bridge at 4.31 and 4.11 ppm, respectively. The formation of the amide caused a downfield shift in H-10. All 20 carbon resonances of **39** could be identified in the ^{13}C-NMR spectrum. The $[M + Na]^+$ mass ion of 495.2363 in the HRMS spectrum, shown in **Figure 4.26**, agreed well with the 495.2366 required for $C_{20}H_{37}N_6NaO_5S$.

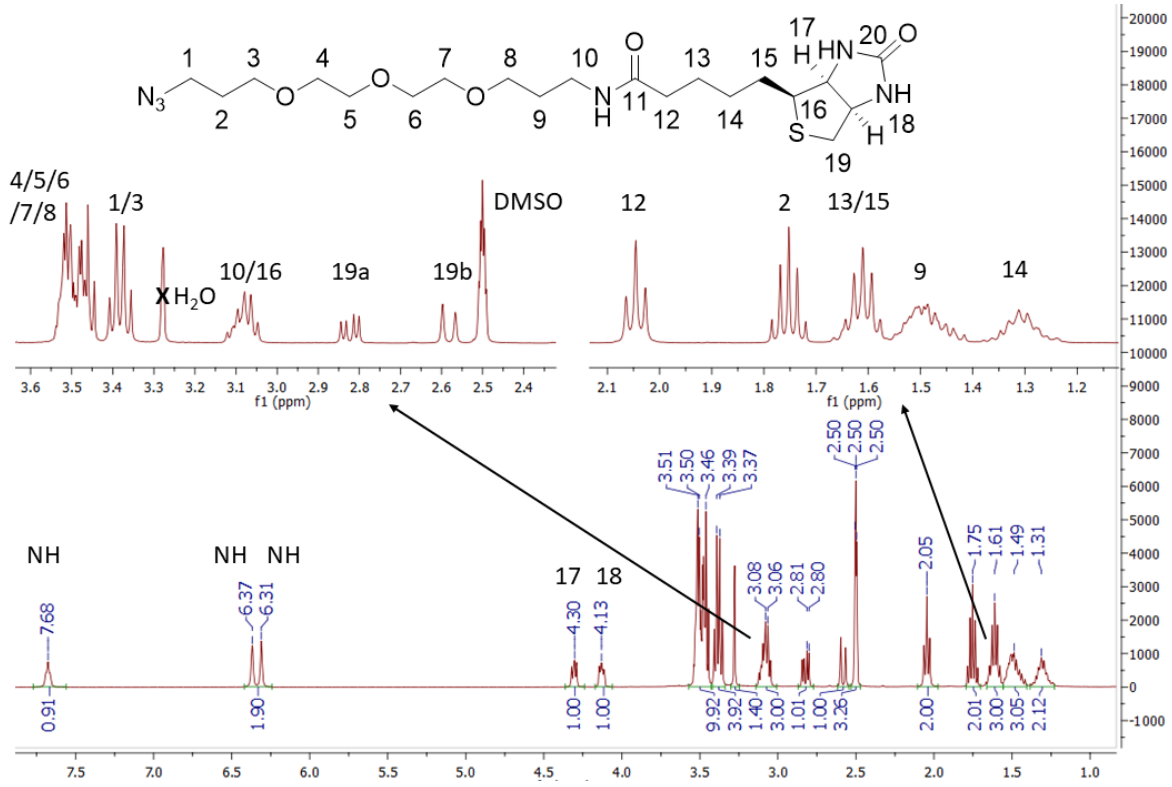

Figure 4.25: ^{1}H-NMR spectrum of biotin-tether-azide, 39.

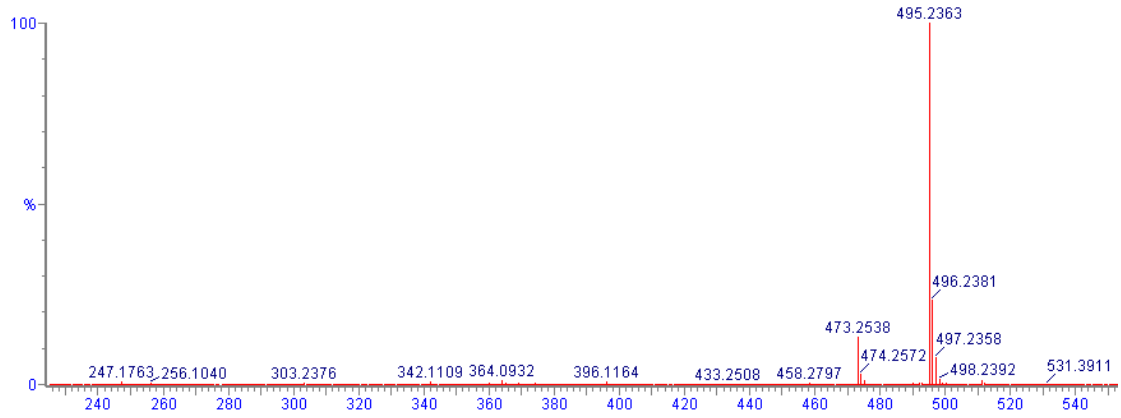

Figure 4.26: HRMS spectrum of biotin-tether-azide, 39.

4.4.4.3 CuAAC-coupling of Fragments 36 and 39

The coupling of the two partners, **36** and **39**, was achieved under mild conditions using a CuAAC-"Click"-reaction, as shown in **Scheme 4.25**.

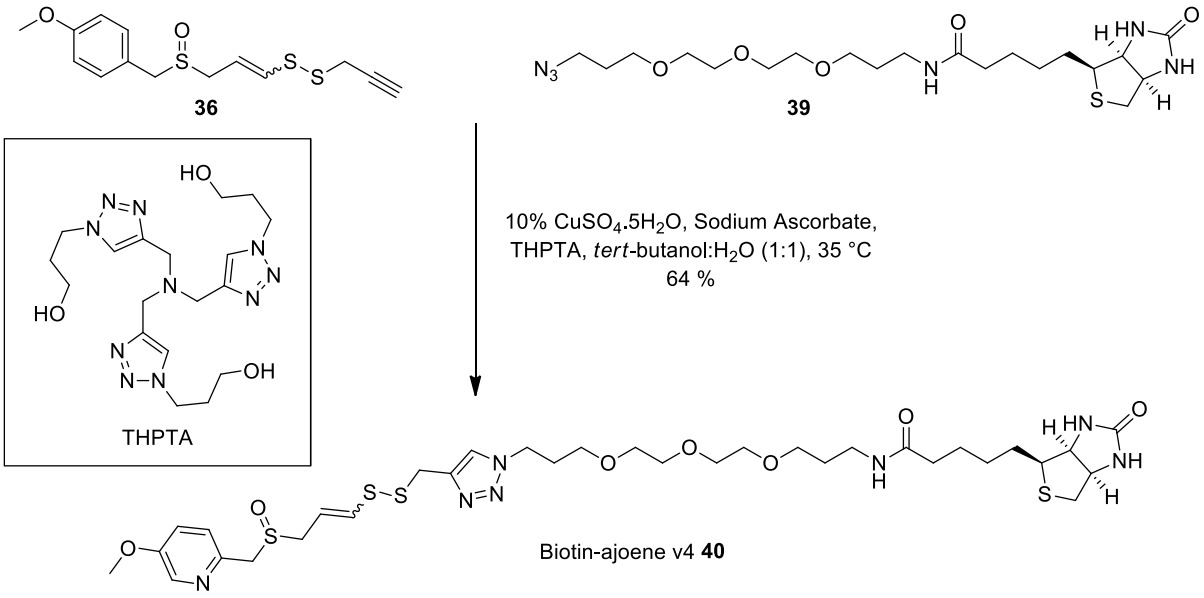

Scheme 4.25: Synthesis of biotin-ajoene v4, 40.

Our previous probes had only shown conversion in moderate yields using the standard CuAAC conditions i.e. when reacting the two coupling partners at equimolar quantities with 0.01 equivalents of $CuSO_4$ and 0.02 equivalents of sodium ascorbate for up to 24 hours. This suggested that this probe version was more stable in solution. However, for our initial runs for the probe construct **40**, a yield of no more than 20% was achieved, even when catalyst loading, reagent stoichiometry and reaction conditions were varied. We suspected that the copper catalyst was being poisoned (by sulfur by-products or

oxidation Cu(I) to Cu(II)) and therefore explored the use of a commercially available tris-triazole-ligand called THPTA (see **Scheme 4.25** for structure), as this ligand is known to stabilise the catalytically active Cu(I) species, increasing the CuAAC reaction rate.[330] The copper catalyst was added as an aqueous solution of pre-chelated $CuSO_4$.THPTA (0.05 eq) to a solution of the biotin-azide **39** (1 eq) and ajoene-alkyne **36** (1 eq) in *tert*-butanol:water (1.3:1) under argon. The addition of sodium ascorbate (0.2 eq) for reducing Cu (II) into the catalytically active Cu(I) species was then added and the mixture was heated to 37 °C. TLC was used for monitoring purposes, and after 36 hours, the reaction was worked-up and the products purified by silica column chromatography to afford the colourless biotin-ajoene v4 **40** as a 3:5 mixture of *E*/*Z*-isomers, in a much improved yield of 64%. Pleasingly, and to much relief, this probe was stable in DMSO and therefore could be fully characterised by ^{1}H-NMR, ^{13}C-NMR, and IR spectroscopies, as well as HPLC and HRMS. The ^{1}H-NMR spectrum, the HPLC trace and HRMS spectrum of the biotin-ajoene v4 probe **40** are depicted in **Figure 4.27**, **4.28** and **4.29**, respectively.

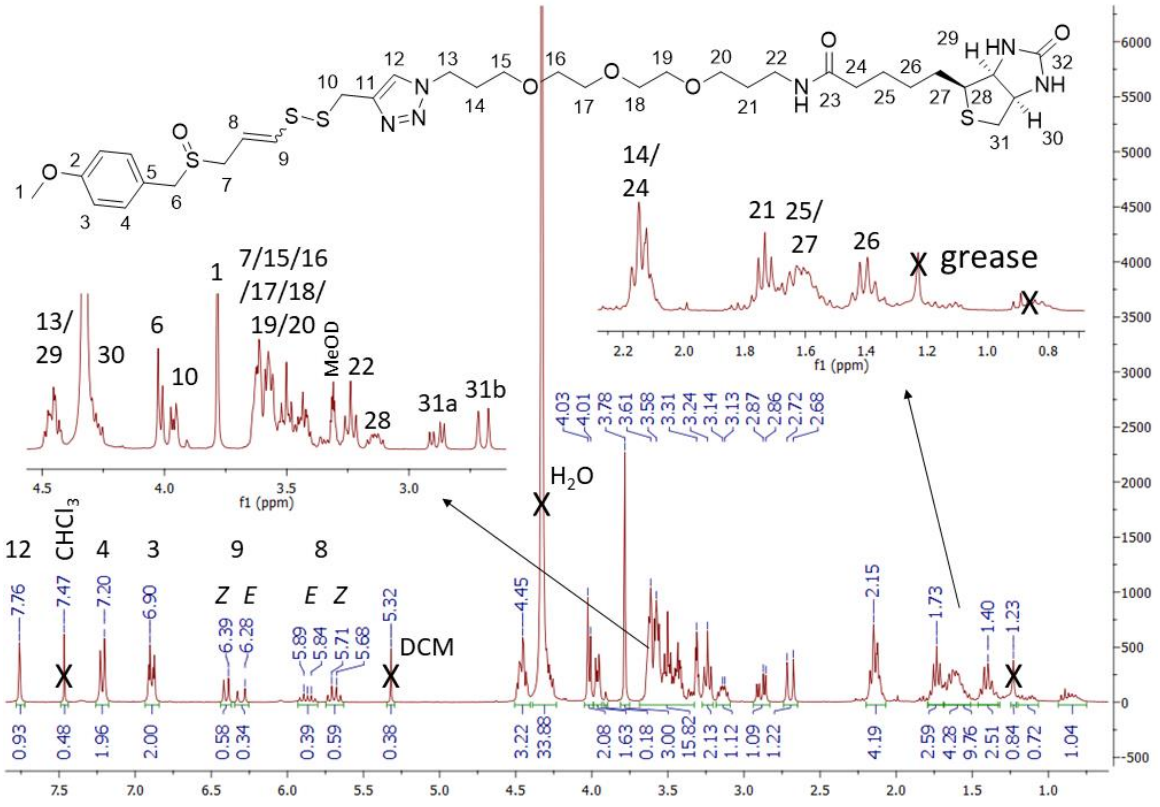

Figure 4.27: ^{1}H-NMR spectrum of biotin-ajoene v4, 40.

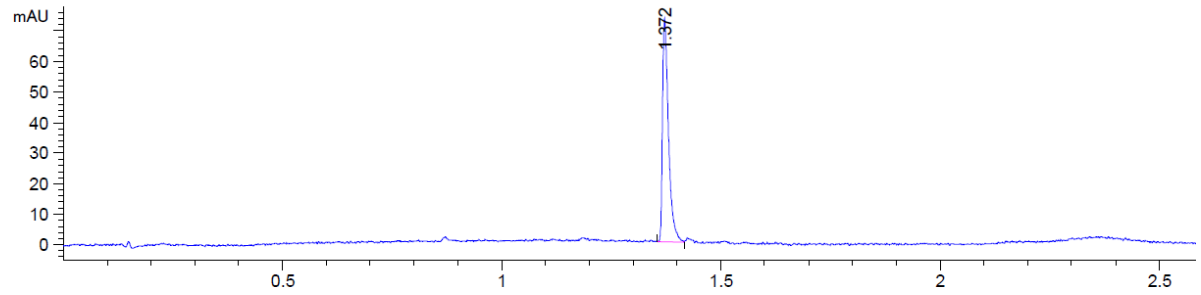

Figure 4.28: HPLC trace of biotin-ajoene v4, 40.

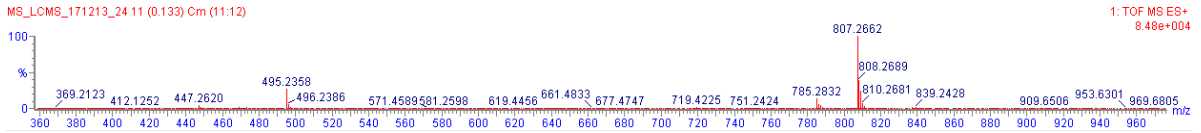

Figure 4.29: HRMS spectrum of biotin-ajoene v4, 40.

The diagnostic signals for the successful formation of the triazole ring were given by the singlet at 7.76 ppm for the vinylic proton H-12 in the ^{1}H-NMR spectrum and the 1642 cm^{-1} and 1462 cm^{-1} absorbance frequencies for the C=C and N=N stretch in the IR spectrum, respectively. Signals in the ^{1}H-NMR spectrum that confirmed the coupling of both intact fragments included: the doublet of doublets at 7.22 and 6.90 ppm of H-4 and H-3 on the phenyl ring; the resonances of the vinylic protons of the ajoene pharmacophore represented by H-8 and H-9 showing the characteristic *Z-E-E-Z* motif between 6.40 and 5.69 ppm; the diastereotopic methylene protons H-31a and H-31b at 2.89 and 2.70 ppm respectively; and the multiplet at 3.31 ppm of the stereogenic centre H-28. Similarly, the ^{13}C-NMR spectrum revealed all 32 carbon resonances, allowing for doubling up of resonances near to the double bond due to the presence of *E/Z*-isomers. (NB: the two *ortho* C-3 and C-4 carbons are equivalent due to symmetry in the 1,4 disubstituted ring). Lastly, the HRMS data showed the molecular mass peak $[M + Na]^{+}$ at 807.2662, for which $C_{34}H_{52}N_6NaO_7S_4$ required 807.2678, thus strongly corroborating the formation of **40**. Prior to its use in a biological setting, the purity of **40** was confirmed to be above 95% by virtue of its HPLC trace.

4.5 Biological Evaluation of Biotin-Ajoene v4

Upon completing the probe synthesis and characterisation of the DMSO-stable probe v4 **40**, the biological utility was tested in three phases: i) Antiproliferative and apoptotic activity of the probe in cancer cells and an assessment of its toxicity in normal cells; ii)

The testing of the probe's ability to successfully transfer the biotin label to proteins via a disulfide linkage; iii) Confirmation that ajoene and biotin-ajoene **40** share the same protein targets in cancer cells. Each of these will be described in sequence.

4.5.1 Antiproliferative and Apoptotic Activity

The biotin-ajoene probe version 4, **40**, was tested for cytotoxic activity against two cancer and one normal cell-line using the MTT cell proliferation assay. The *E*/*Z*-isomers of the probe could not be separated by silica column chromatography and were thus tested as an *E*/*Z*- mixture. The extent of cytotoxicity was quantified as an IC_{50} value, defined as the concentration of drug found to inhibit 50% of cell proliferation after an incubation period. The IC_{50} value for biotin-ajoene **40** was determined over 24 hours in alignment with the time course chosen for subsequent experiments, shown in **Table 4.2**. For comparison the IC_{50} of bis-PMB ajoene and *E*- and *Z*-ajoene is also shown[80], all tested over 48 hours Compounds were tested against MDA-MB-231 (human breast tumour epithelial), WHCO1 (human oesophageal epithelial) and MCF-12A (normal human breast epithelial) cells.

Cell Lines		MDA-MB-231		WHCO1		MCF-12A	
Compound		IC_{50} (μM)	SD[a]	IC_{50} (μM)	SD[a]	IC_{50} (μM)	SD[a]
E/*Z*-	biotin-ajoene **40**	34.6	± 6.7	30.4	± 6.6	98.2	± 24.0
E/*Z*-	bis-PMB ajoene[80]	1.4	± 0.9	2.1	± 0.4	3.7	± 1.5
Z-	ajoene[80]	13.7	± 2.0	25.2	± 2.8	nd	nd
E-		18.6	± 5.5	39.2	± 7.8	nd	nd

Table 4.2: Comparison of the *in vitro* antiproliferative activity of biotin-ajoene 40, bis-PMB ajoene and *E*- and Z-ajoene on cancer and normal cells lines
IC_{50} values reported as an average ± SD; [a] = based on a minimum of three independent determinations; nd = not determined.

The biotin-ajoene probe **40** was found to retain activity against both cancer cell lines, with a 2-fold reduction against MDA-MB-231 cells and retention of activity against WHCOSD1 cells when compared to the parent, ajoene. It was also pleasing to see that the probe was approximately 3-fold more selective for cancer cells over normal cells (MDA-MB-231 vs MCF12A). A similar trend in selectivity was previously observed for bis-PMB ajoene on the same cell lines.[80] To determine if the biotin tag itself had any cytotoxicity, the biotin-azide fragment **39** was also tested on the cell lines and found to have no

cytotoxicity up to 200 μM. As expected, the ajoene-alkyne fragment **36** was found to be cytotoxic, with an IC_{50} value of 26 μM against MDA-MB-231 cells.

To further investigate the cytotoxic effects of **40**, the morphological changes of cultured MDA-MB-231 and MCF-12A cells treated with **40** at the IC_{50} concentration (MDA-MB-231 cells, 40 μM) were observed under a light microscope. Representative images of these cells are shown in **Figure 4.30**.

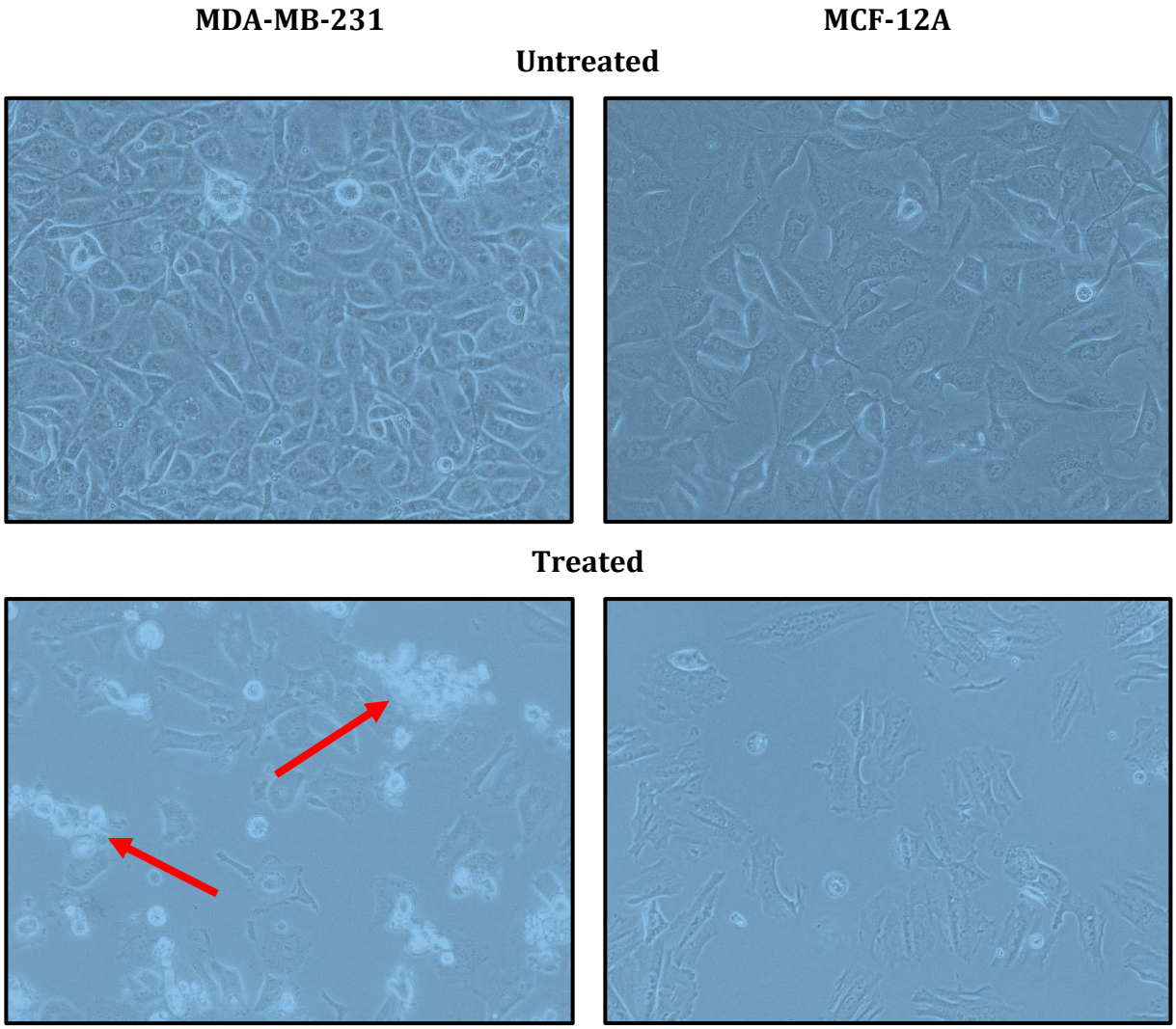

Figure 4.30: Microscopy images of probe-treated and untreated MDA-MB-231 and MCF12A cells.
Top panel: Treated with DMSO only; bottom panel: Treated with 40 μM biotin-ajoene **40**; Cells were incubated for 24 h and pictures are at 400× magnification.

In both cell lines treated with biotin-ajoene **40**, a visible reduction in proliferation was observed with the cells appearing stressed and shrunken. Apoptotic bodies showing membrane blebbing was however only observed in the MDA-MB-231 cells (red arrows in

Figure 4.30). These morphological observations agree with the cytotoxicity data which indicated that normal MCF12A cells are more resistant to the effects of biotin-ajoene **40** than MDA-MB-231 cells.

4.5.2 Detection of Biotinylated Proteins

Having determined the cytotoxic IC_{50} value for biotin-ajoene probe version 4 **40** on MDA-MB-231 cells, we proceeded to assess its ability to transfer the biotin label to the ajoene protein targets in these cells. Based on the expected regioselectivity of thiolysis exchange, we anticipated transfer of the label from the non-vinyl sulfur of the ajoene disulfide with the expulsion of the "PMB-ajo" leaving group, as shown in **Scheme 4.26**.

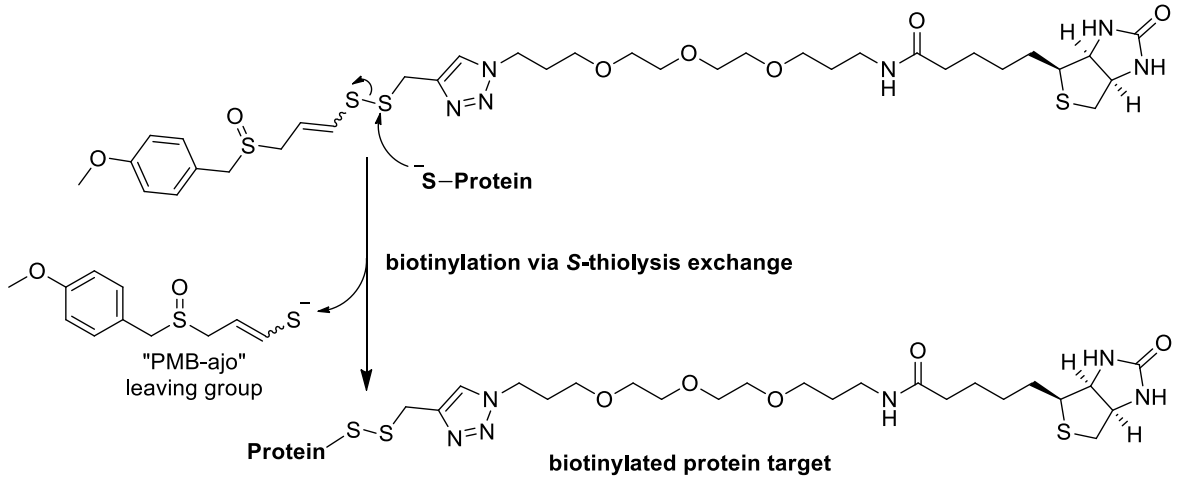

Scheme 4.26: Proposed biotinylation of protein thiols by thiolysis exchange.

The experiment was performed by western blot of the protein lysates which was probed using an anti-biotin antibody. The disulfide bridge that connects the triazole-PEG tether-biotin construct to the protein proved to be a useful molecular feature to test if the biotin label was covalently bound to a protein and not an off target, non-covalent association. Covalent attachment via a disulfide linkage was tested by treating the lysate with the disulfide reducing agent DTT prior to SDS-PAGE. This is expected to result in the loss of the label from the protein due to the cleavage of the connecting disulfide bond, as illustrated in **Figure 4.31**.

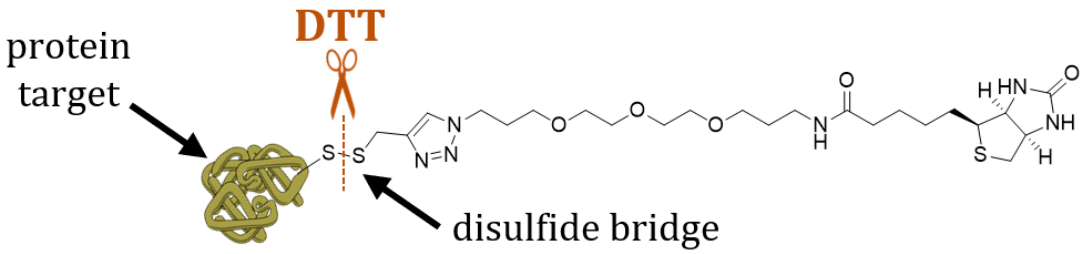

Figure 4.31: DTT-mediated cleavage of biotin label from the protein target.

Figure 4.32 shows a representative western blot of MDA-MB-231 and MCF-12A lysates treated with the IC_{50} concentration of biotin-ajoene **40** (40 μM) for 24 hours, compared to lysates of untreated cells (DMSO control). We treated both cell lines at the same IC_{50} concentration (40 μM, MDA-MB-231) to ascertain extend of labelling in the normal cell line (MCF-12A) at the given ajoene dose. An aliquot of the treated lysate was also pre-incubated with DTT (50 mM) prior to SDS-PAGE. Each well of the acrylamide gel was loaded with an equal quantity of protein (15 μg), and a protein ladder was used as a reference in **lane 1**. Total protein loading was quantitated using a colloidal silver stain (also shown in **Figure 4.32**).[331]

		MDA-MB-231			MCF-12A		
Lane	**1**	**2**	**3**	**4**	**5**	**6**	**7**
40	protein ladder	-	+	+	-	+	+
DTT		-	-	+	-	-	+
fold-change		1.0	18.7	1.5	1.0	46.7	5.5

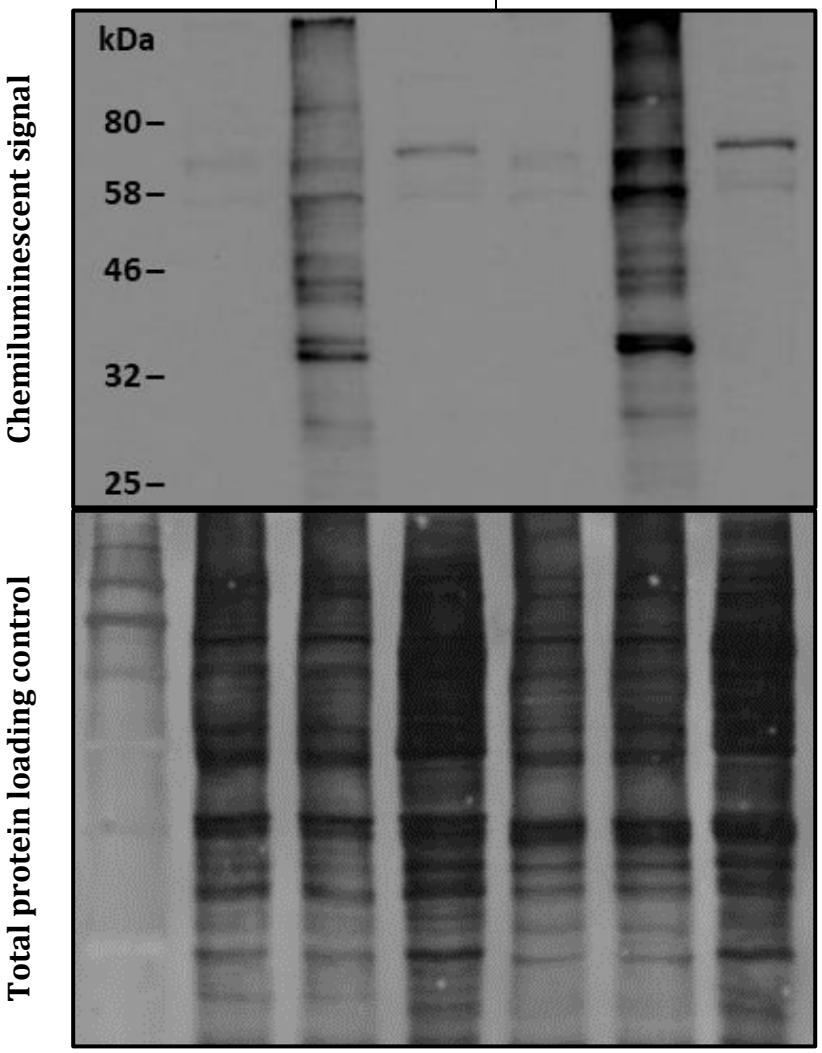

Figure 4.32: Western blot comparing the biotinylation of proteins by biotin-ajoene v4 40 in lysate from MDA-MB-231 and MCF-12A cells.
Chemiluminescent signal produced by the anti-biotin antibody (top) and silver stain visualisation of total protein loading (bottom). Result of a single experiment, which was performed independently three times.

As lanes (**2-7**) were loaded with lysate, taken as the total protein (TP) loading control. As expected, **lanes 2** and **5**, which did not receive biotin-ajoene **40**, showed no chemiluminescent signal. The lanes with the treated lysate, **3** and **6**, showed chemiluminescent signals from multiple bands, implying that there are many protein targets of biotin-ajoene **40** in both cell lines. After normalisation of chemiluminescent

signal for protein loading, it is evident that approximately 2-fold more proteins were labelled in the MCF12A than in the MDA-MB-231 cells which was observed in 3 independent experiments (fold-change: 2.21 ± 0.26, n = 3). This result was not expected. The lanes (**4** and **7**) treated with DTT, showed the disappearance of the chemiluminescent signal as expected for a disulfide attachment. Interestingly the protein loading control was visibly higher in both bands which is expected as running a western blot under non-reducing conditions is not optimal as the proteins remain folded with their disulfide bridges intact. In the reduced **lanes 4** and **7**, we observed a clear protein band between 58 and 80 kDa. This band was also observed in the lanes (**1** and **4**) containing untreated lysate, indicative of the antibody interacting with biotin-ajoene independent binding partners. It is reported that biotin-avidin systems for antibody detection will commonly capture endogenous proteins containing a biotin prosthetic group as spurious bands in western blots.[332] In this regard, the most commonly cited artefacts are the biotin carboxylases, which are metabolic enzymes that contain a covalently attached biotin domain in their the active site.[333] The prominent bands around 58-80 kDa in the blot may therefore represent β-methylcrotonoyl-CoA carboxylase (72 kDa) and/or propionyl-CoA-carboxylase (74 kDa).[334]

The probe design and synthesis appeared to be successful and working as designed. It appears that the ajoene pharmacophore is successfully targeting proteins in cultured MDA-MB-231 breast cancer and normal MCF12A cells and that these proteins become biotinylated. The lack of chemiluminescent signal in the treated lysate following DTT treatment supports the attachment of the biotin label to a cysteine residue on the protein via a cleavable disulfide linker, formed through a thiol-disulfide exchange reaction between ajoene and the protein.

The binding of a ligand to a protein is expected to be dose-dependent. To investigate whether the binding of biotin-ajoene to the proteins in MDA-MB-231 cells was dose-dependent, we performed a concentration-dependent labelling experiment. The lysate from individual dishes of cultured MDA-MB-231 cells with varying concentrations of biotin-ajoene v4, **40**, were prepared. The cells were treated in 2-fold dilutions spanning the ranges of 1/8-fold IC_{50} to 2-fold IC_{50} (which equated to 5 – 80 μM) over 24 hours. The lysates were collected as described before and biotinylated proteins were analysed by western blot, as shown in **Figure 4.33**.

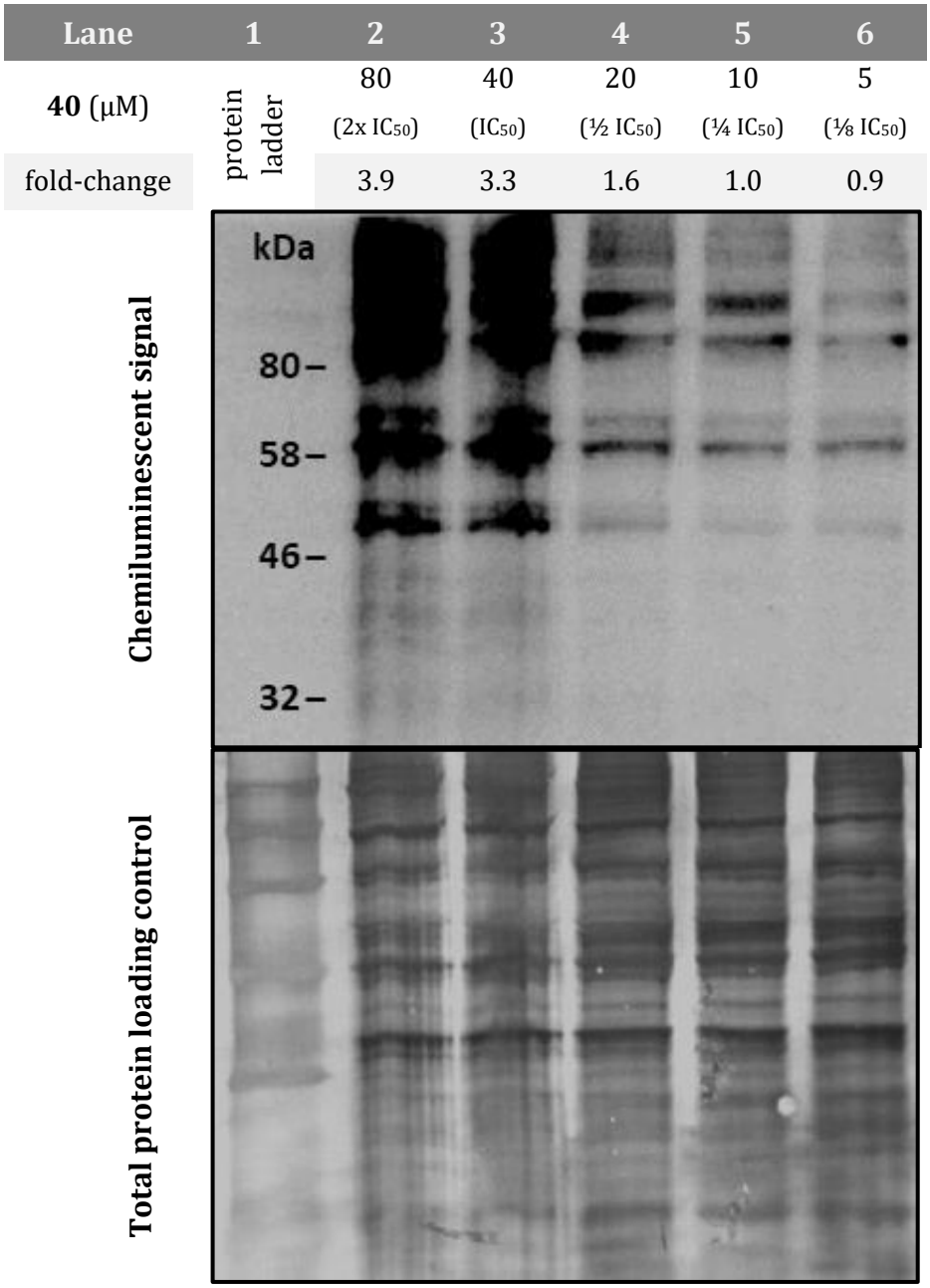

Figure 4.33: Dose-response labelling of proteins by biotin-ajoene 40 from 5 - 80 μM in MDA-MB-231 cells.
Chemiluminescent signal produced by the anti-biotin antibody (top) and silver stain visualisation of total protein content (bottom). Normalised for protein loading and with respect to lane 5.

The equal loading of lysate proteins onto the gel was confirmed by a silver stain with similar band distributions and intensities from **lanes 2** to **6**. In the western blot, the steady decrease in band intensity displayed a dose-dependent labelling of proteins in MDA-MB-321 cells. Some bands only became labelled at the higher concentration whereas others were already labelled at the lower concentration, indicating that the

probe **40** may be more selective for certain targets over others. It was interesting to see that some proteins are sensitive to biotinylation (*S*-thiolysis exchange reactions) even at the very low and non-cytotoxic concentration of 5 μM (1/8 of IC_{50}).

The same experiment was also performed on MCF-12A cells in the same concentration range of biotin-ajoene v4 **40**. The resulting western blot is depicted in **Figure 4.34**.

Lane	1	2	3	4	5	6
40 (μM)	protein ladder	80	40	20	10	5
fold-change		4.0	3.0	2.0	1.0	0.2

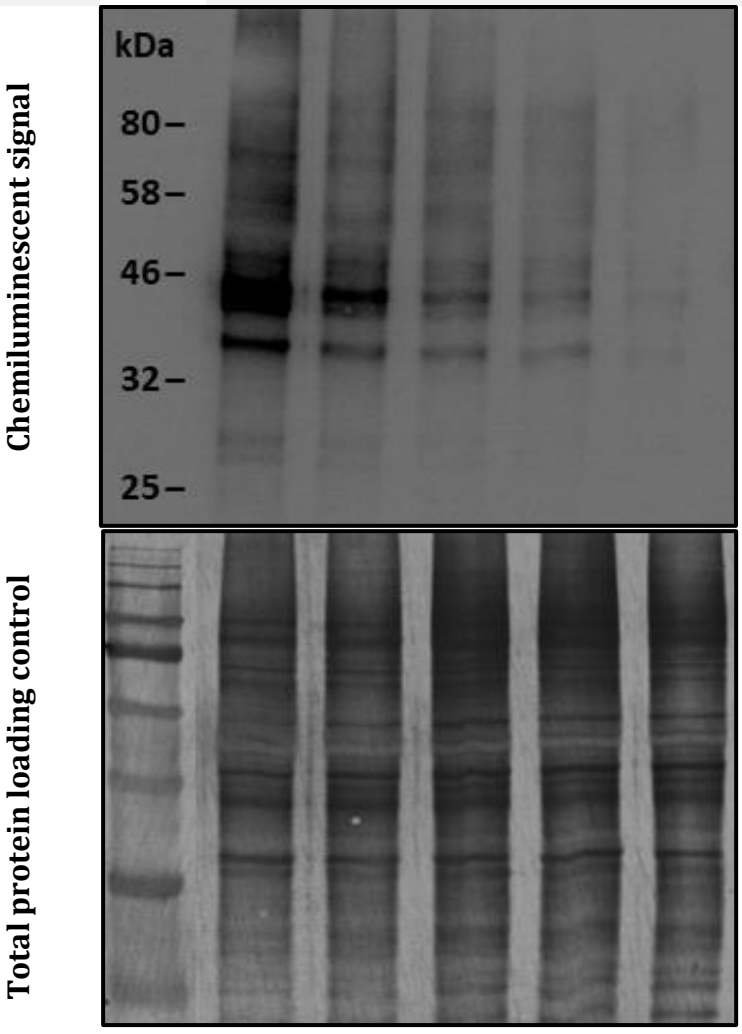

Figure 4.34: Dose-response labelling of proteins by biotin-ajoene 40 from 5 - 80 μM in MCF-12A cells.
Chemiluminescent signal produced by the anti-biotin antibody (top), silver stain showing total protein loading (bottom). Normalised with respect to protein loading and with respect to lane 5.

The loading controls indicated that all lysate-containing lanes (**2** to **6**) contained similar amounts of proteins. Again, an increase in chemiluminescent signal was observed from **lanes 2** to **6** confirming the dose-response binding of biotin-ajoene **40** to its protein targets. Similar to MDA-MB-231 cells, an approximately 4-fold increase in signal was observed from 10 to 80 μM.

These investigations showed that biotin-ajoene **40** was able to efficiently biotinylate protein targets in both MDA-MB-231 and MCF-12A cells. It was found that the biotinylation was reversed under disulfide reducing conditions, confirming the attachment of the biotin tag to a cysteine residue of the protein, in accordance with the mechanistic design of the probe. In addition, the protein targets in both cell lines were biotinylated in a dose-dependent manner and follow a binding saturation curve, see **Figure 4.35.**

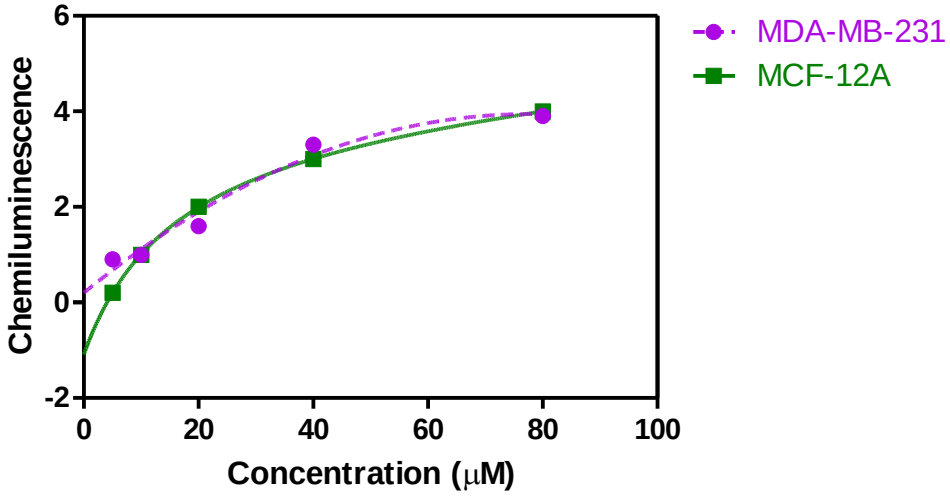

Figure 4.35: Relative protein biotinylation by biotin-ajoene 40 in MDA-MB-231 and MCF-12A cells over a concentration range of 0 – 80 μM.

It was found that biotin-ajoene **40** caused an overall 4-fold increase in protein biotinylation over the concentration range of 0 – 80 μM. A comparison of the slopes indicated that biotinylation activity was the same in the MDA-MB-231 and MCF-12A cells, which supported that the mechanism which controls the biotinylation was the same in both cell lines. Taken together with the difference in cytotoxic effects observed in the cell lines, however, this finding indicated that global protein biotinylation does not lead to cell cytotoxicity. This suggested that the *S*-thiolation of specific, cancer-related targets or pathways may be responsible for the cytotoxic activity observed for our probe in MDA-

MB-231 cells. It may also be that cancer cells are simply more susceptible to the effects of biotinylation.

Biotin-ajoene was developed as a model compound to study the mechanism of action of ajoene. Although biotin-ajoene was labelling protein targets in cells, it was important to show that biotin-ajoene and ajoene share common protein targets, i.e. that any biotin-ajoene targets are also the targets of ajoene. This was tested using a competition assay.

4.5.3 Competition Assay Between Ajoene and Biotin-Ajoene

To assess if biotin-ajoene **40** shares the same protein targets as ajoene, we performed a competition assay. MDA-MB-231 cells were pre-treated with *Z*-ajoene for two hours at varying concentrations (20, 40 and 60 μM), followed by treatment with 40 μM (IC_{50} concentration) biotin-ajoene **40** for an additional six hours. Our rational was that if biotin-ajoene **40** and ajoene *S*-thiolate the same targets, the pre-treatment of the lysate with ajoene would hinder proteins from becoming biotinylated by probe **40**. Pre-treatment with ajoene would be expected to decrease the number of biotin-tagged proteins, observable by a loss of chemiluminescent signal. Cells that had been treated with ajoene or biotin-ajoene alone acted as negative and positive controls, respectively.

The experimental western blot is shown in **Figure 4.35** on the next page.

As expected, biotin-ajoene **40** treatment of cells resulted in many proteins becoming biotinylated (**lane 2**), while the lysate of the cells treated with with *Z*-ajoene alone showed no biotinylation (**lane 3**). Increasing the concentration of *Z*-ajoene (**lanes 4** to **6**) caused a dose-dependent reduction in the number of biotinylated proteins. This suggests that *Z*-ajoene and biotin-ajoene **40** compete for the same sites and therefore share the same protein targets in MDA-MB-231 cells. It also implies that biotin-ajoene can confidently be used as a model compound to study the cancer targets of ajoene.

Lane	1	2	3	4	5	6
Z-ajoene (μM)	protein ladder	-	60	20	40	60
40 (μM)		40	-	40	40	40
fold-change		6.8	1.0	5.3	2.9	1.4

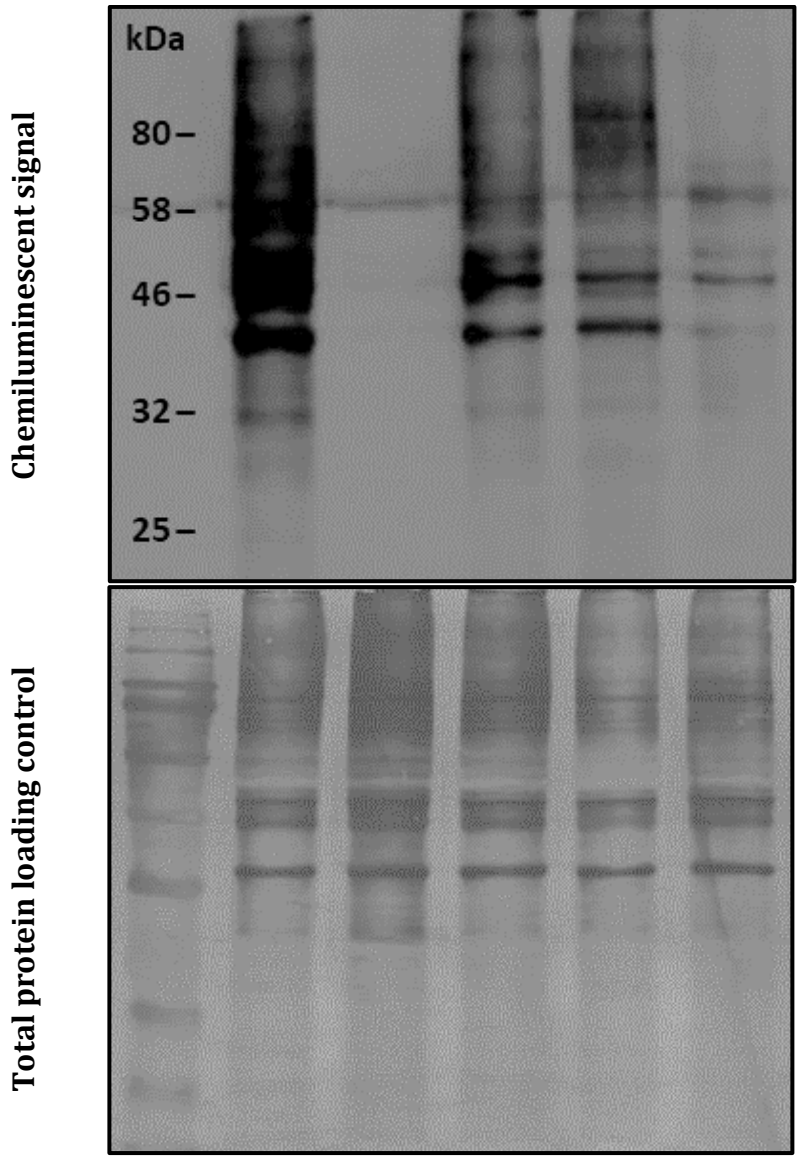

Figure 4.36: Competition assay between ajoene and biotin-ajoene 40 in MDA-MB-231 cells.

4.6 Conclusion

Previous work on the activity-based labelling of several protein targets in cancer cells with a fluorescently tagged ajoene has led to the design of an ABP designed to identify these targets using an ABPP approach. Based on our understanding of the mechanism of action of ajoene, the probe in question was designed to selectively transfer a biotin affinity tag to cellular proteins via a thiolysis exchange reaction. The envisaged ABP

scaffold incorporated an ajoene vinyl disulfide (re)active group tethered to a biotin affinity tag. Before arriving at a functional version of our biotin-ajoene probe, **40**, the following insights on suitable design features were made: i) To overcome challenges with possible cross-reactivities between the reactive group and the biotin tag, we employed a convergent synthesis of the probe using a CuAAC-"Click"-chemistry. That way, the functionalities could be coupled as "Click"-fragments under mild reaction conditions in the last step; ii) It was found that the alkyne "Click"-functionality on the ajoene fragment and the azide on the biotin fragment was paramount, as the other way round had resulted in non-specific biotinylation of cysteine residues (likely due to its thiol-yne addition to the biotin-alkyne fragment); iii) The linking of the pharmacophore and the reporter using a more polar and flexible PEG3 tether was preferable over an alkyl derivative; iv) The placement of a PMB group at the vinyl disulfide terminus of the probe appears to contribute to the stability of the overall construct.

To ensure the suitability of probe **40** for target enrichment and identification using ABPP, *in vitro* biochemical assays were performed to confirm that: i) the probe retained the bioactivity of its parent molecule; ii) the probe shared the same protein targets as ajoene; iii) the probe could effectively biotinylate protein targets to allow for downstream affinity purification.

First, the cytotoxicity of biotin-ajoene **40** was tested against a normal (MCF-12A) and two cancer (MDA-MB-231 and WHCO1) cell lines using the MTT cell proliferation assay. Compared to ajoene, biotin-ajoene **40** was found to have similar activity in WHCO1 cells, while showing a slightly reduced activity in MDA-MB-231 cells. When comparing the breast cancer cell line (MDA-MB-231) to its normal counterpart (MCF-12A), it was shown that biotin-ajoene **40** was 3-fold more selective towards the cancer cells, which had also been previously seen for other ajoene analogues, such as bis-PMB ajoene. A competition assay showed that the pre-treatment of cancer cells with ajoene reduced the ability of the probe to biotinylate proteins, demonstrating that biotin-ajoene **40** shares the same protein targets as ajoene.

The transfer of the biotin label to the ajoene protein targets was shown to occur in a dose-dependent manner to produce the same relative labelling in both cell lines, confirming

that the same mechanism of action was controlling the biotinylation (i.e. *S*-thiolation of protein thiols). Although the relative biotinylation activity in both cell lines was comparable, it was surprising to see that the probe biotinylated twice as many proteins in the MCF12A (normal) cells compared to the MDA-MB-231 (cancer) cells. While similarities in labelled protein bands between the two cell lines could be observed, there were also some distinct differences in the bands. This, and the greater cytotoxicity of the probe in cancer cells than normal, suggested that ajoene may be targeting cancer-specific vulnerabilities to produce its cytotoxic effects. We envisaged that the identification of the direct targets of ajoene with our probe (in **Chapter 5**) would reveal more information on the interactions that may be responsible for its selective cytotoxicity towards cancer cells. Lastly, the presence of a disulfide bond between the biotin tag and the cysteine residues of the protein target was demonstrated by its cleavage with DTT which takes place via a thiol-disulfide exchange. Furthermore, the presence of disulfide, as cleavable linker, may allow for a selective release of the biotinylated protein from the avidin beads during the enrichment step of the ABPP protocol.

Overall, these insights provided confidence to proceed with proteomics experiments to identify the protein targets of ajoene in cancer cells, which will be covered in **Chapter 5**.

Chapter 5 : Identification of Protein Targets of Ajoene in Cancer Cells

5.2 Background

Epidemiological, animal and cell culture studies support ajoene as a chemopreventative and therapeutic agent active against all the stages of cancer. Ajoene's anticancer properties may arise from a number of biological activities, **Figure 5.1**, that produce anti-inflammatory, antioxidant, antimetastatic, antiproliferative, antiangiogenic and proapoptotic effects.[80,83,137,145,148,167,168,182–186]

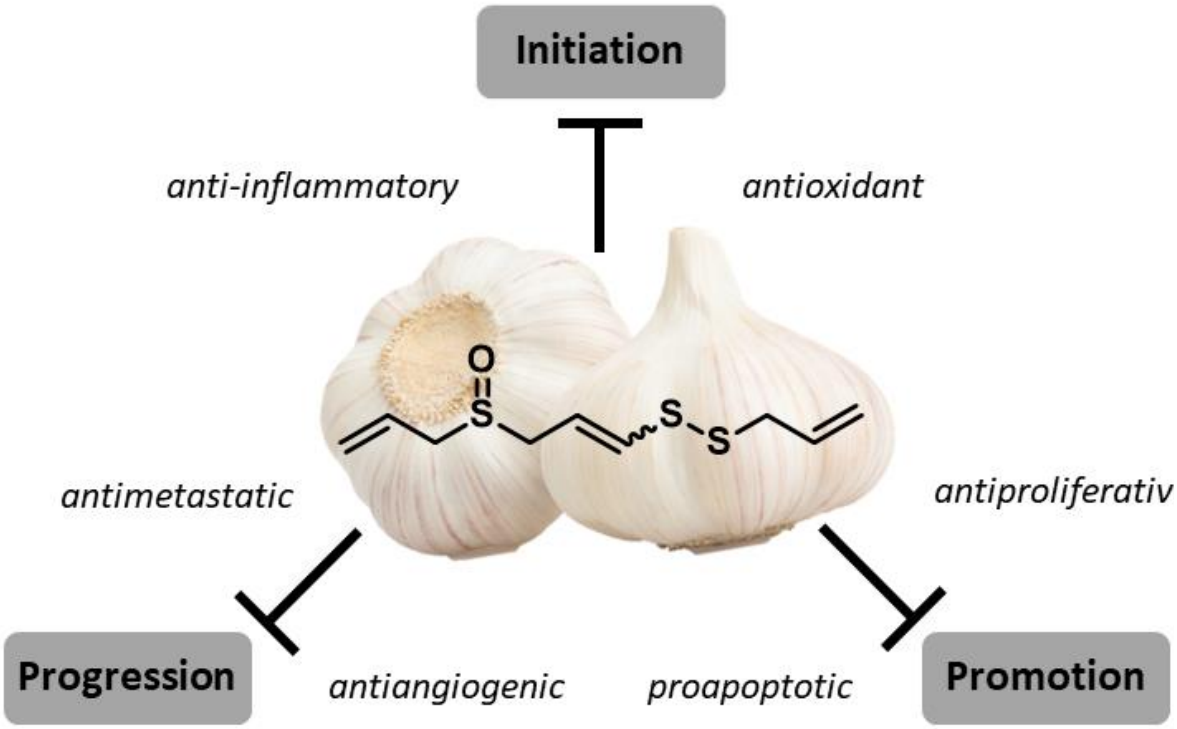

Figure 5.1:Biological activities that contribute to the broad-spectrum anticancer activity of ajoene.

Table 5.1 gives an overview of publications that have identified how ajoene modulates specific biological pathways and processes of relevance to its anticancer activity.

Anticancer effect	Mode of action	Proposed cellular events	Study
Anti-proliferative	Interference with protein prenylation	Covalent modification of the cysteine SH group of a peptide substrate for protein PGGTase-I.	Ferri 2003[335]
	G_2/M phase and increase in total amount of cytosolic proteasome	Inhibition of 20S proteasome	Xu 2004[336]
	Modulation of the Hh/Gli signalling pathway	Down-regulated expressions of Gli-target proteins and FoxM1-target proteins	Lee 2019[184]
	Modulation of CK1α activity and the Wnt/β-catenin signalling pathway.	Down-regulation of intracellular β-catenin levels, and its representative target protein levels (c-Myc and cyclin D1)	Li 2020[171]
Proapoptotic	Inhibition of NF-κB function	Physical interaction with the p65 subunit and PPARG at the nucleus	Kim 2016[152]
	Intrinsic mitochondrial-dependent pathway	Activation of caspase-3, cleavage of antiapoptotic protein Bcl-2.	Dirsch 2002[337]
	Mitogen-activated kinase (MAPK) pathways	Induction of c-Jun NH_2-terminal kinase (JNK), p38, extracellular signal regulated kinases (ERK) ½ and survival kinase Akt	Antlsperger 2003[338] Jung 2014[339] Wang2016[89]
	ER Stress and Unfolded protein response (UPR)	Activation of the UPR through CHOP/GADD153	Kaschula 2016[153] Kaschula 2017[340]
Anti-metastatic	Disassembly of the microtubule network	Targeting of microtubule cytoskeleton	Li 2002[167]
	Inhibition of invasion and migration	Covalent modification of vimentin by *S*-thiolation of Cys-328	Kaschula 2019[137]
	Reduction of tumour endothelial cell-adhesion	Caspase-3 activation and altered expression of α4β1 integrin	Ledezma 2004[185] Taylor 2006[168]
Anti-inflammatory	Suppression of inflammatory responses by inhibition of SMADs/forkhead box (FoxO) signalling pathways	Decrease of myokines secretion, Janus kinase/signal transducer and activator of transcription 3 (JAK/STAT3).	Kim 2019[341]
	Interference with the COX2 pathway	Inhibition of the COX2 enzyme	Dirsch 2001[342]
	Inhibition the inflammatory response in RAW264.7 macrophages	Covalent modification through *S*-thiolation of STAT3 and COX2	Kaschula 2020[343]

Table 5.1: Reported pathways involved in the anticancer activity of ajoene.

Ajoene has been found to interact with the cytoskeletal proteins vimentin and catenin, as well as the microtubule network leading to inhibition of cell proliferation and metastases. Ajoene has also been shown to upregulate apoptotic signalling via the MAPK/ERK and

JAK-STAT pathways.[89,338,339,341] Its primary target appears to be protein folding and protein metabolism in the ER, which leads to ER stress and activation of the unfolded-protein response (UPR).[153,340] Ajoene has also been shown to exhibit anti-inflammatory effects by directly inhibiting the activity of COX2 and STAT3.[342,343]

Although some of these anticancer pathways have been studied, most of the cellular targets remain unknown. Indeed, several lines of evidence suggest that ajoene may modulate these pathways through a distinct interaction with the proteome.[153,189,335] Mechanistic investigations into garlic OSCs, including ajoene, have revealed that thiolysis exchange with a cysteine thiol leads to the covalent modification of certain proteins.[21,56,78,84,263] The extensive biochemistry of cysteine sulfur, as well as the many functional roles that cysteine residues occupy in the proteome,[54,58,344,345] make the biology of the interactions between garlic OSCs and protein thiols a complex topic, as summarised in a review by Go *et al.* (**Figure 5.2**).[54]

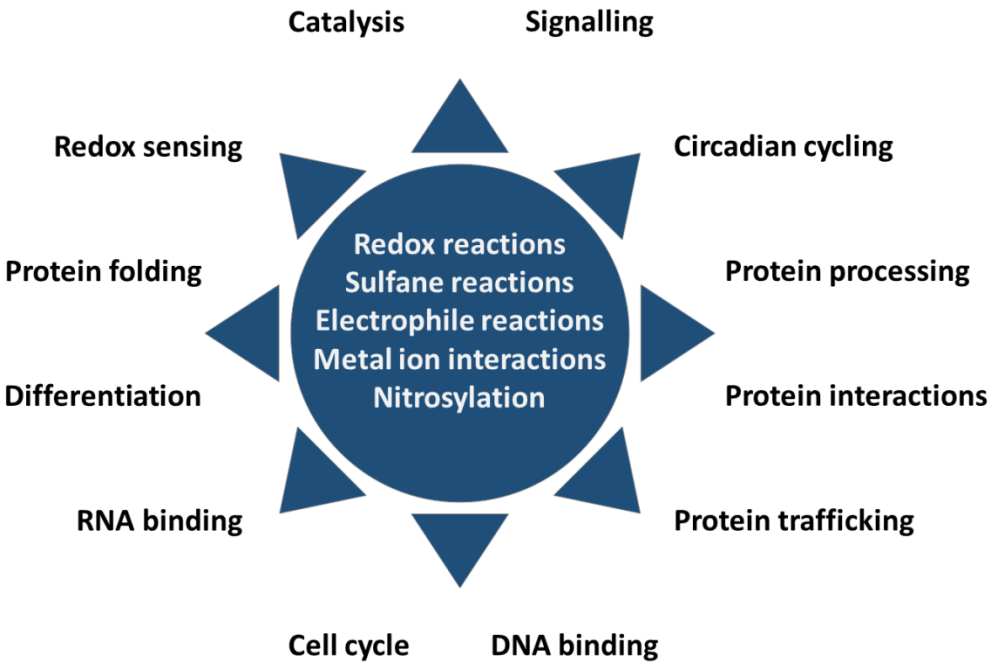

Figure 5.2 : Functional roles of cysteine within the cysteine proteome.
Adapted from Go *et al.*[54]

The inherent nucleophilicity and polarisability (pK_a) of a cysteine thiol, allows for its participation in a broad range of chemical reactions (**Chapter 1**).[346] Cysteine is exploited within the catalytic domains of many enzymes, such as: i) mitochondrial proteins; ii)

cytosolic glycolytic proteins and those related to energy metabolism; iii) signalling proteins-particularly kinases and phosphatases; and proteins involved in iv) protein folding and editing; v) ion channel/calcium homeostasis; and vi) redox balance.[72,347–350] Cysteine also assumes regulatory functions in signal transduction pathways, cellular sensing, redox homeostasis and protein function. Protein regulation is achieved through the interactions of cysteine with reactive oxygen (ROS), nitrogen (RNS) and sulfur (RSS) species which produce several reversible and irreversible post-translational modifications (PTMs). The reversible PTMs include *S*-sulfenylation, *S*-sulfhydration, *S*-acetylation, *S*-nitrosylation, and *S*-glutathionylation, which regulate a number of redox sensing and signalling cascades.[57,351,352] In this way, cysteine can act as a powerful molecular switch, akin to protein phosphorylation-dephosphorylation signalling cycles.[353]

A study by *Gould et al.* established that individual PTMs target specific cysteines, even when they occur on the same protein.[352] This, and the finding that PTMs mostly occur in non-catalytic regions, indicate that subsets of cysteines form biologically unique networks that possess different capacities for redox regulation and signalling. Although the biological significance of these PTM networks, in both healthy and disease states, has been increasingly recognised, their integration into the proteome still remains largely unknown.[354–356] Nonetheless, advances in the field of redox proteomics over recent years, has allowed for the detection of thousands of redox reactive cysteines in cells and tissues.[357–362] For further reading on the application of activity-based proteomics for reactive cysteine profiling, I can recommend a fantastic review published by Backus.[363] It is interesting to note that, compared to other amino acids, the vast majority of functional cysteines are conserved along the evolutionary tree,[54] which highlights how thiol redox-reactivity and regulation are central to the cellular mechanisms of life.

In this context, it is apparent that garlic OSCs, are faced with a wide landscape of potential targets within the cysteinome. To date there have been four proteome-wide studies investigating the cellular targets of OSCs in three species of bacteria, and one human cancer cell line. The findings of these studies are summarised in **Table 5.2** below.

OSC	Cell	# identified *S*-thioallylated protein targets and their functions	Findings	Ref
Allicin	*E. coli*	**73** High abundance proteins mostly involved in the primary metabolism and oxidative stress defence.	*S*-thioallylation events: - decrease free thiol concentration, - inactivate metabolic enzymes, - cause protein aggregation, - trigger oxidative and unfolding stress response pathways.	364
Allicin	*S. Aureus*	**57** Translation factors, metabolic and redox enzymes as well as redox-sensitive regulators.	*S*-thioallylation elicits a strong thiol-specific oxidative and sulfur stress response and protein damage.	365
Allicin & DATTS	*B. subtilis*	**108** **(79 for allicin; 66 for DATTS; 44 in common)** Enzymes involved in the biosynthesis of surfactin, amino acids and nucleotides, translation factors, antioxidant enzymes and redox sensitive growth regulators.	Allicin and DATTS *S*-thioallylate some common redox-sensitive proteins which elicits a strong oxidative, disulfide and sulfur stress response as well as protein and DNA damage.	263
Allicin	Jurkat (human T-lymphocyte)	**322** Cytoskeletal proteins, chaperones, glycolytic enzymes and translation factors.	Widespread *S*-thioallylation of proteins essential to cellular functions, many of which are targets for cancer therapy.	86

Table 5.2: Overview of proteomic studies on the *S*-thioallylation targets of garlic OSCs, allicin and DATTS.

Although these proteomic studies focus on allicin and DATTS, there may be cross-over with the targets of other OSCs based on their common mechanism of *S*-thioallylation of the cysteine proteome. This hypothesis is supported by the finding that DATTS and allicin share 44 *S*-thioallylation targets within the proteome of *B. subtilis*.[263] Many of the identified targets fall within the category of "redox-reactive" and "solvent-accessible", corroborating the kinetic arguments presented on the chemistry of thiolysis exchange in **Chapter 2**. A large proportion of the targets from allicin-treated Jurkat cells are also

highly abundant proteins with involvement in metabolic processes, transcriptional regulation, cytoskeletal function and protein thiol homeostasis.[86] Other researchers have suggested that the *S*-thioallylation of specific proteins, by garlic OCSs, leads to disruption of structural networks,[82,137] altered biogenesis of proteins,[104,153] and the inactivation of metabolic enzymes.[86] These activities have been validated for a few proteins such as glutathione reductase, the cysteine protease papain, the inflammatory regulators COX-2 and STAT3, metabolic enzymes, including alcohol dehydrogenases, enolase, isocitrate lyase and glyceraldehyde-3-phosphate dehydrogenase (GAPDH), and structural proteins such as vimentin and β-tubulin.[86,137,189,263,343,364,366]

Cancer cells are particularly vulnerable to the inactivation of metabolic enzymes and impairment of their antioxidant pathways, since they require reprogramming of these cellular features for enhanced cell growth and survival.[367] Their increased demand for energy and their higher basal metabolic rates results in an overproduction of metabolic by-products, including ROS,[368] leading to increased oxidative stress, often to dangerous levels. For this reason, cancer cells also require the oncogenic activation of existing antioxidant pathways as a protective measure, which is a distinguishing feature over normal cells.[369] Since the garlic OSCs allicin and DATTS in the above studies have been shown to *S*-thiolate proteins associated with metabolic and antioxidant pathways, amongst others, they may be directly targeting these vulnerabilities in cancer.

5.3 Currently Known Targets of Ajoene

Although only a few of the protein targets of ajoene are known, the reactivity of its pharmacophore towards thiolysis exchange indicates that ajoene may also produce large-scale protein *S*-thioallylation, akin to allicin and DATTS.

The first evidence for this was presented by Gallwitz *et al*. in 1999, who showed that ajoene forms a mixed disulfide with Cys-58 in the active site of glutathione reductase (GR). This modification was also found to inhibit the enzyme.[189] GR plays a central role in redox homeostasis, where it acts as a gatekeeper for the oxidative stress response.[370] More recently, our group identified the filament protein, vimentin (VIM), as a *S*-thioallylation target of ajoene,[137] which was found to take place at Cys-328. This modification was shown to inhibit the invasive and migratory potential of MDA-MB-231 cells. In another study by our group, it was found that *Z*-ajoene *S*-thioallylates cysteine residues of two important regulators of inflammation namely, STAT3 (Cys-108, Cys-367

and Cys-687) and COX2 (Cys-9 and Cys-299), in RAW264.7 macrophages.[343] Although ajoene only caused a partial inactivation and inhibition of these proteins, the study demonstrated a causality between protein *S*-thiolation and its ability to modulate the immune response.

This notion that several of the anticancer activities of ajoene are associated with protein *S*-thioallylation prompted our group to conduct a proteome-wide study of ajoene's protein targets in cancer cells using a chemical biology approach. In our first chemical biology study,[153] we synthesised the two fluorescently labelled ajoene analogues shown in **Figure 5.3**.

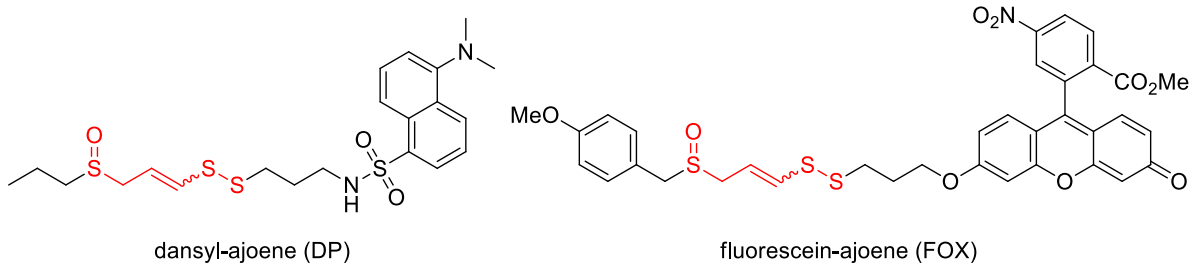

Figure 5.3: Chemical structures of fluorescently labelled ajoene analogues, dansyl-(DP) and fluorescein-ajoene (FOX).
The sulfoxide/vinyl disulfide pharmacophore of ajoene is shown in red.

These ajoene analogues allowed for the activity-based fluorescent tagging of their cellular targets and for tracking inside of cancer cells using live confocal laser scanning microscopy (CLSM). Both analogues were found to localise within the endoplasmic reticulum (ER) of MDA-MB-231 breast cancer cells. The localisation in the ER was further corroborated by generating an MDA-MB-231 cell line expressing yellow fluorescent protein (YFP) in the ER.

This was the first time that ajoene was shown to target the ER in cancer cells. The fluorescent label was found to be attached to proteins localised in the ER and closer inspection revealed possible protein aggregates as clumps of misfolded protein aggregates, illustrated in **Figure 5.4**. This indicated that ajoene might be interfering with the folding of proteins through disulfide bond formation, which is an ER-driven process.

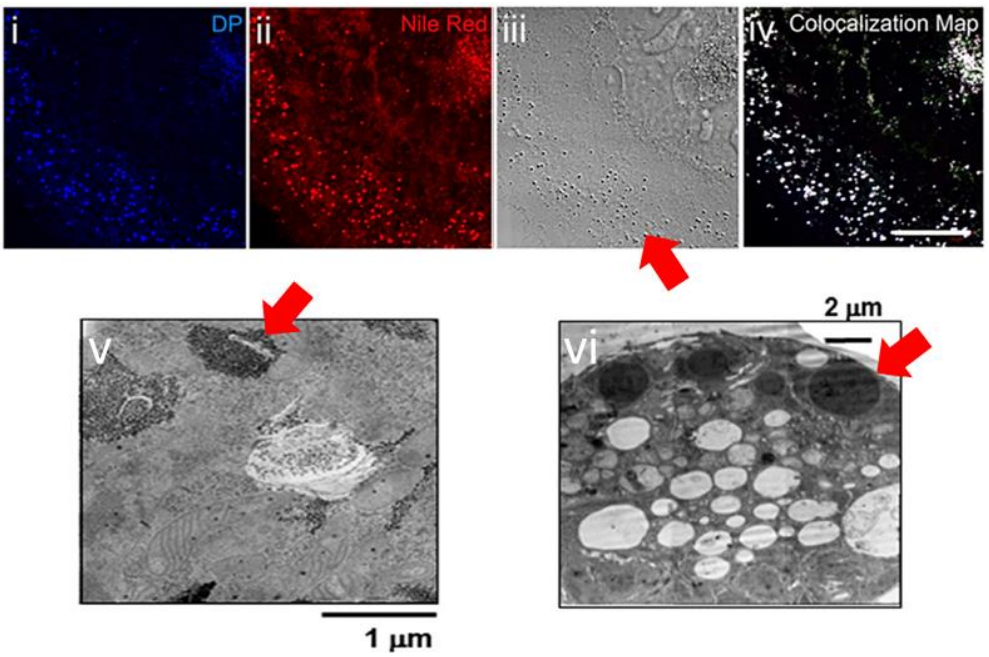

Figure 5.4: CLS and transition electron micrographs of MDA-MB-231 cells treated with ajoene or dansyl ajoene.
Treated with 25 mM for 3 h and stained with Nile Red. The red arrows indicate protein aggregate inclusions caused by ajoene.[153] (i) DP, (ii) Nile Red, (iii) phase contrast, (iv) colocalization map, (v) treated with 10 mM bis-PMB for 1 h, (vi) and 24 h.

Following translation on the ribosome, newly synthesised polypeptide chains enter into the ER, where they are folded into their native state by a number of molecular chaperones (foldases, holdases, isomerases and oxireductases).[371] The biogenesis of approximately one third of the proteins in the eukaryotic proteome involves the formation of intramolecular disulfide bonds, which positions the peptide chains in the correctly folded tertiary structure.[372] The ER supports the formation of disulfide bonds by maintaining an oxidative environment.[373] This is achieved by a significant shift in the GSH ratio towards its oxidised disulfide forms (GSSG and GSS-Protein) leading to 50% of the GSH in the ER being bound to proteins via *S*-glutathionylation.[374] Not only does the *S*-glutathionylation of free cysteine resiudes protect thiols from irreversible oxidation, it also plays a critical role in guiding disulfide synthesis, which is catalysed by protein disulfide isomerases (PDIs). Since many aspects of the folding process are tightly regulated by thiol chemistry, we speculated that ajoene may be interfering with unfolded cysteine residues of peptide chains and/or the folding enzyme machinery involved. Because ajoene is a more efficient thiolating agent than GSSG, the *S*-thioallylation of cysteine residues likely competes with *S*-glutathionylation.

Ajoene may rapidly enter the cancer cell by passive diffusion, where it crosses the cytoplasm to enter the oxidative environment of the ER. Inside the ER, ajoene may readily react with free cysteine residues of unfolded proteins through *S*-thioallylation. These unnatural modifications on cysteine may hamper folding and cause an accumulation of misfolded proteins as illustrated in **Figure 5.5**. Misfolded proteins have exposed hydrophobic side chains which make them prone to aggregation, as observed in our fluorescence study.

Under normal metabolic conditions, approximately 30% of newly synthesised proteins are misfolded,[375] which the ER is able to counteract with an assortment of refolding chaperones, or by removing misfolded proteins through endoplasmic-reticulum-associated protein degradation (ERAD). When the cell senses an accumulation of unfolded or misfolded proteins, it triggers an adaptive response, called the unfolded protein response (UPR). The early UPR aims to reinstate protein homeostasis and supports cellular survival by attenuating the global translational of proteins, upregulating corrective chaperones (e.g. heat-shock proteins) and accelerating the ubiquitin-mediated degradation of proteins in the protosome.[376] However, once the protein-folding imbalance overwhelms the system to produce ER stress, the UPR triggers an apoptosis pathway leading to cell death.[104]

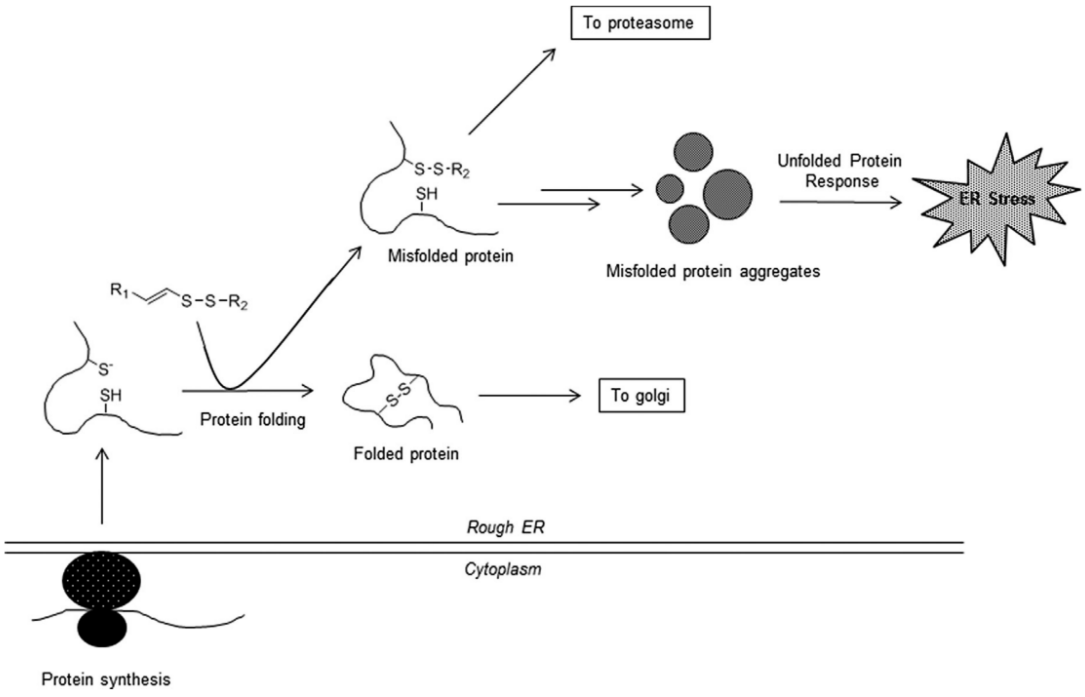

Figure 5.5: Hypothesis on the cytotoxic mechanism of action of ajoene in cancer cells. Taken from Kaschula *et al.*[153]

Our group was able to confirm UPR activation following treatment with the ajoene analogue bis-PMB in WHCO1 oesophageal cancer cells.[340] A DNA microarray experiment revealed that the treatment of WHCO1 cells with the ajoene analogue upregulated transcriptional pathways and processes involved in protein processing in the endoplasmic reticulum (ER) and the unfolded protein response. Bis-PMB was found to inhibit global protein synthesis, increased levels of ubiquitinated proteins and also induced alternate splicing of the critical transcription factor XBP-1, which is a driver of cell survival through the upregulation of chaperones in the early stages of the UPR.[377] An increased expression of the ER stress proteins GRP78 and CHOP/GADD153 was also observed. This data supports a mechanism whereby ajoene targets protein folding in the ER leading to ER stress and cell death. In addition to our findings on ajoene, there is a growing body of evidence that protein misfolding and the induction of ER stress may also be central to the cytotoxicity of other garlic OSCs in cancer cells.[86,104,153] Cancer cells, with their high level of secretory activity and metabolic requirements, are hypersensitive to the heightened accumulation of misfolded proteins, which is why their survival largely depends on the upregulation of UPR and ERAD pathways. The targeting of these pathways can potentially serve as an "Achilles heel" in cancer.[378,379]

Ajoene is proposed to *S*-thioallylate reactive cysteine residues on protein targets which constitutes the primary event leading its cancer cell cytotoxicity (**Figure 5.6**).

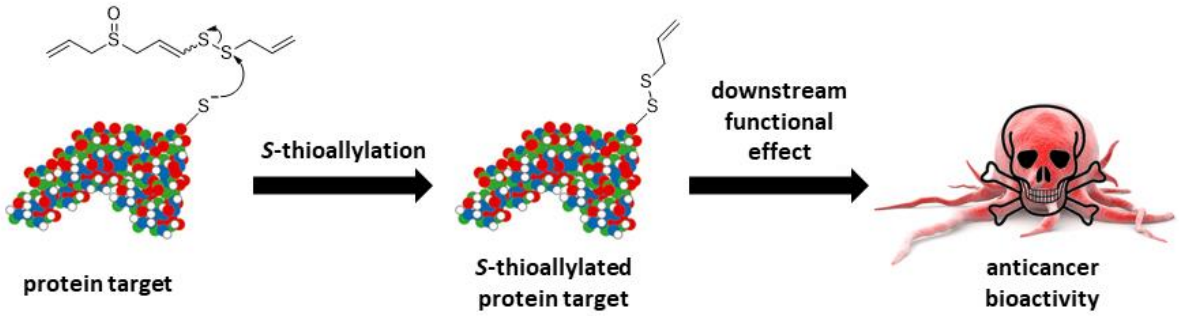

Figure 5.6: Proposed anticancer mechanism of action of ajoene.

In this project, we aimed to identify the protein targets of ajoene and to elucidate how proteome-wide *S*-thioallylation may drive its cytotoxicity in cancer cells. To this end, we adopted an affinity-based purification approach using a biotin-ajoene probe **40** (**Figure 5.7**), the synthesis of which was described in **Chapter 4**.

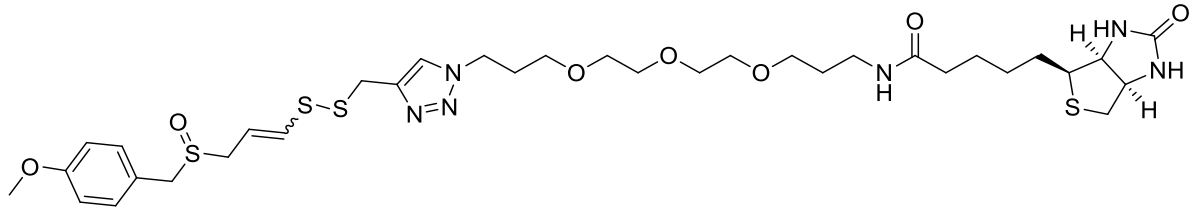

Figure 5.7: Chemical structure of biotin-ajoene, 40.

The probe was designed and tested to for its ability to transfer the biotin tag to the protein targets through an activity-based interaction on cysteine. This chapter will describe the affinity-based protein profiling (ABPP) method that was developed for the isolation and identification of ajoene's drug-interaction targets.

5.4 Mass Spectrometry as a Tool for Identifying Protein Targets

Mass-spectrometry, as MS-based proteomics, has become the analytical technique of choice for studying proteins in complex biological samples. The high sensitivity of modern MS instruments allows the extraction of detailed information from small quantities of material, which has greatly benefitted the field of cellular biology.

Mass spectrometers are used to measure the mass to charge (m/z) ratio of charged molecules in the gas phase, allowing for the determination of their molecular weight after charge-state resolution. Although large molecules such as proteins can be analysed as a whole, their identification more commonly involves enzymatic digestion to generate peptide fragments (**step i** in **Figure 5.8**). The proteolytic enzyme trypsin is most commonly used, as it cleaves proteins into peptides with an average size of 700-1500 Da, which is in the ideal range for MS.[380] It is also highly specific, cleaving the peptide chains on the carboxyl side of arginine and lysine, which allows for the prediction of peptide fragments from a known protein sequence. In modern mass-spectrometric experiments, the m/z ratio of a peptide is determined in two steps, called tandem MS. The first step involves an MS1 (MS) scan (**step ii**) where the m/z of the intact peptide and its relative abundance in the sample is determined. In the second step, individual peptides are selected and further fragmentation using an ion source or collision zone, after which an MS2 (MS/MS) scan is performed (**step iii**).

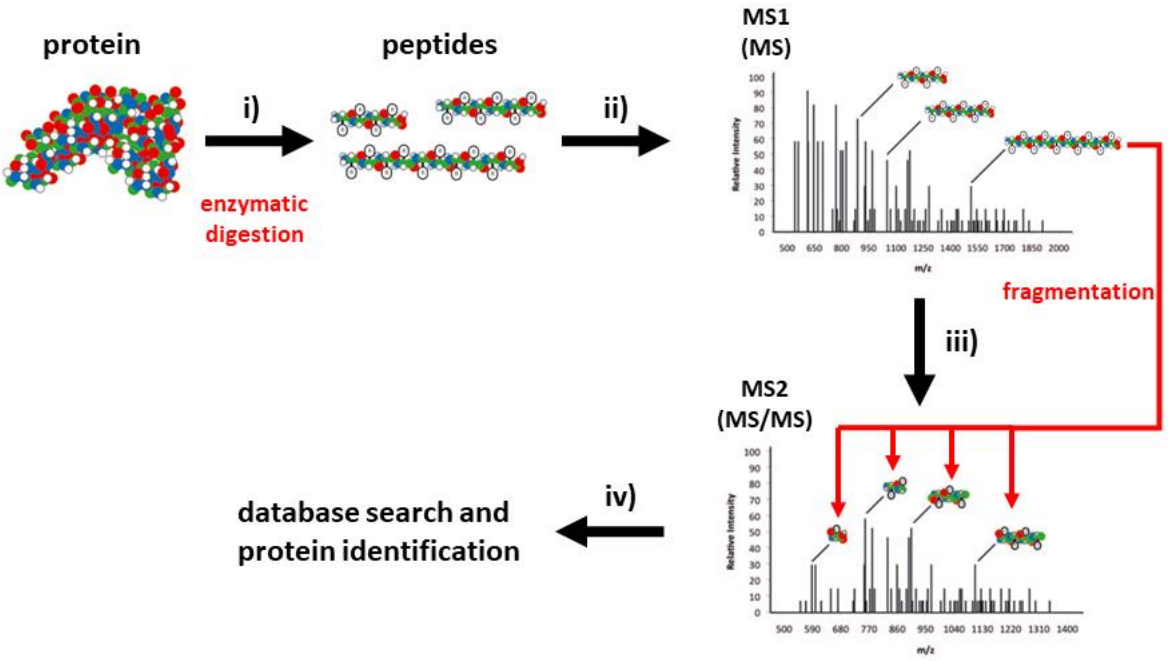

Figure 5.8:Overview of protein identification by tandem MS.

Since the digestion (**step i**) and fragmentation (**step ii**) give rise to cleavage products along the peptide bonds, it is possible to use the observed ion masses in spectra to reconstruct the original protein sequence. This is done using a proteomic software (**step iv**) which finds peptides in the MS2 spectrum and matches them to their parent peptides in the MS1 scan. The identified peptide is, in turn, compared to a database of *in silico* digested protein sequences to find a possible identification match. The software considers the number of peptides that match a sequence, to determine the overall sequence coverage, from which a statistical score for each protein is assigned. For the analysis of complex mixtures containing hundreds or thousands of proteins, an HPLC is coupled to the MS (LC-MS) to separate the peptide fragments on a reverse-phase column prior to elution into the mass-spectrometer.

5.4.1 Proteomic Studies on Garlic OSCs

Two recent proteomic studies on target interactions of garlic OSCs in cancer cells have demonstrated how this technology can be used.

The laboratory of Otterlei examined the changes in cellular signalling that ethanolic garlic extracts (called GE) produced in cancer cells, using a non-targeted multiple inhibitor bead (MIB)-assay.[104] The GE-treated lysates of NR67 murine breast cancer cells were passed over an affinity matrix of multiple kinase inhibitors coupled to Sepharose beads. This

interaction allowed for the enrichment, isolation and identification of kinases and NTP interacting proteins.[381,382] When comparing GE-treated and untreated lysates, significant changes in cellular signalling were identified involving over 1000 proteins. A KEGG (Kyoto Encyclopaedia of Genes and Genomes) analysis of these proteins showed that GE-induced changes were hierarchically observed in proteins involved in i) protein processing in the ER, ii) PI3K/AKT signalling, iii) MAPK signalling, iv) apoptosis, and v) Wnt signalling (**Table 5.3**).

Process name	Listed	Found	%	Up	Down
Proteins processing in ER	167	110	66	61	35
PI3/AKT signaling pathway	346	89	26	45	30
MAPK signaling pathway	252	77	40	45	19
Apoptosis	136	62	57	29	15
Wnt signaling pathway	146	39	37	21	10

Table 5.3: KEGG analysis of cellular pathways influenced by GE in NR76 cancer cells.
Taken from Otterlei *et al.*[104]

Quantitation of ER stress proteins involved in these pathways showed that a significant portion of them were upregulated. The authors concluded that the induction of ER stress was likely attributed to the *S*-thiolation of GSH and cysteine residues on proteins resulting in the alteration of the cellular redox state and protein folding capacity, similar to what we previously found for ajoene.[153,340]

In the other study, Gruhlke *et al.* used an activity-based proteomic approach to identify the *S*-thioallylation protein targets of allicin.[86] Covalent transfer of an *S*-allyl group to a cysteine residue through allicin *S*-thioallylation, resulted in a detectable mass shift of 72 Da (**Scheme 5.1**). Following the analysis of allicin-treated Jurkat (T-lymphocyte) cell lysates by shotgun Orbitrap LCMS/MS, a proteome search was performed for peptides containing this mass shift.

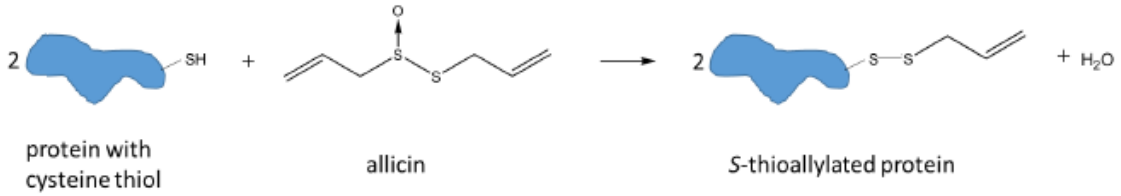

Scheme 5.1: *S*-thioallylation of a protein cysteine residue by allicin.
Taken from Gruhlke *et al.*[86]

The search yielded 332 proteins containing the *S*-thioallylated peptides. Subsequent KEGG analysis showed that *S*-thiolation had occurred most abundantly in the functional categories of the cytoskeleton, genetic information processing and cellular metabolism (**Figure 5.9**). To a lesser extent, proteins were found in the categories of cell cycle and junctions, vesicular transport, signal transduction and human diseases.

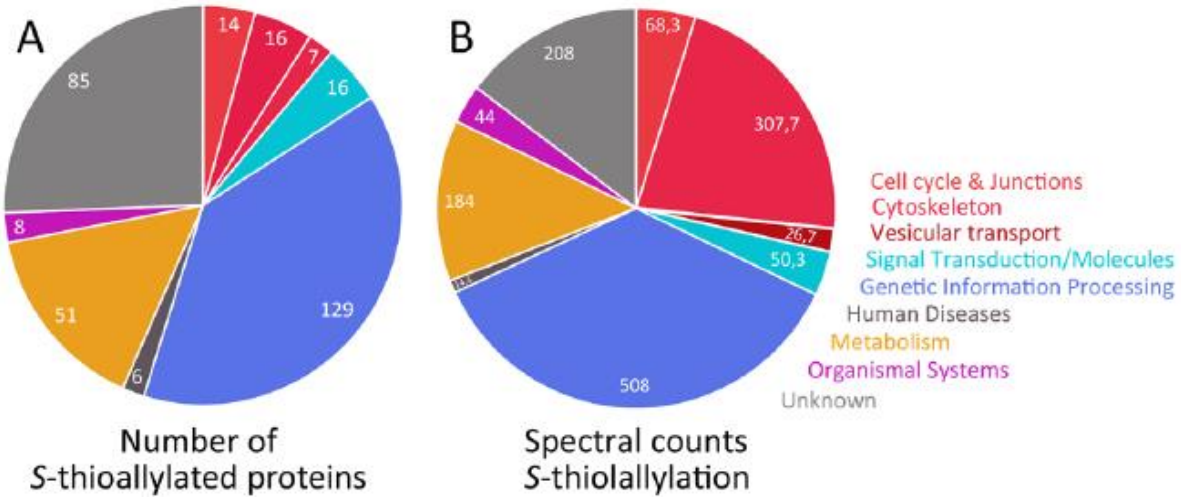

Figure 5.9: Total number and spectral counts of the 332 *S*-thioallylated proteins by allicin, isolated from human Jurkat cells.
Taken from Gruhlke *et al*.[86]

This study found that the most abundantly *S*-thiolated proteins were also abundant proteins in the proteome of Jurkat cells. These included the cytoskeletal proteins tubulin, actin, cofilin, filamin and plastin-2, the heat shock chaperones HSP90 and HSPA4, the glycolytic enzymes GAPDH, ALDOA and PKM, as well the protein translation factor EEF2.

In both publications, the use of MS-based proteomics allowed for the identification of hundreds of cancer protein targets of garlic OSCs. The scope and resolution of proteomics data is however highly dependent on the experimental design. The scope pertains to the choice of features or parameters that are investigated, whereas the resolution depends on the abundance of the proteins in the analysed sample.
A limitation in the study by Otterlei *et al*. was that it is not possible to distinguish if the effects of the garlic OSC's on the kinase proteome were a result of direct (activity-based) or indirect (downstream) events. This type of question is outside of the scope of the study since GE is a complex mixture of OSC chemotypes, and the interrogation of their unique

reactivity as well as their selectivity towards protein targets makes the search for direct target interactions too complicated.

In the study by Gruhlke *et al*., the detection of *S*-thioallylated peptides enabled the identification of allicin's targets. This study also allowed for quantification of the total number of modified cysteines. Since their investigation utilised a shotgun proteomics approach, the absence of an enrichment step may have resulted in a lower resolution picture. Ideally, shotgun proteomics facilitates the identification of the entire proteome with 100% protein sequence coverage. In reality, the large dynamic range and complexity of cellular proteomes results in oversampling of abundant proteins, while peptides from low abundance proteins are undersampled, or may remain undetected (as they fall under the instrument's detection cut-off due to their lower relative abundance).[383]

In this project, we realised that our exploration of ajoene's protein targets in cancer cells was a blended approach of the above two studies. Our chemical probe, **40**, with its ajoene pharmacophore, facilitates the direct tagging of its protein targets. Then, the presence of the biotin moiety allows for the enrichment and purification of the sample to reduce complexity and increase resolution. The affinity-based approach using the biotin-ajoene **40** probe was therefore envisioned to enhance both the resolution and the detectability of the protein targets of ajoene.

5.4.2 Affinity-Purification Mass Spectrometry

Affinity-purification followed by mass spectrometry (AP-MS) is a popular method that allows for the enrichment of proteins prior to MS analysis. AP allows for a reduction in sample complexity prior to proteomic analysis by taking advantage of specific binding properties between a protein and its ligand coupled to solid support, such as a magnetic bead or resin. As illustrated in **Figure 5.10**, the binding of proteins to an immobilised ligand may be achieved through the interaction of i) an epitope (antigen) with a specific antibody, called immuno-purification, ii) a chemical tag with its binding partner, (e.g. biotin-streptavidin technology), or iii) a protein's allosteric or active site with a substrate or effector molecule, (e.g. the MIB-assay used by Otterlei *et al.*).

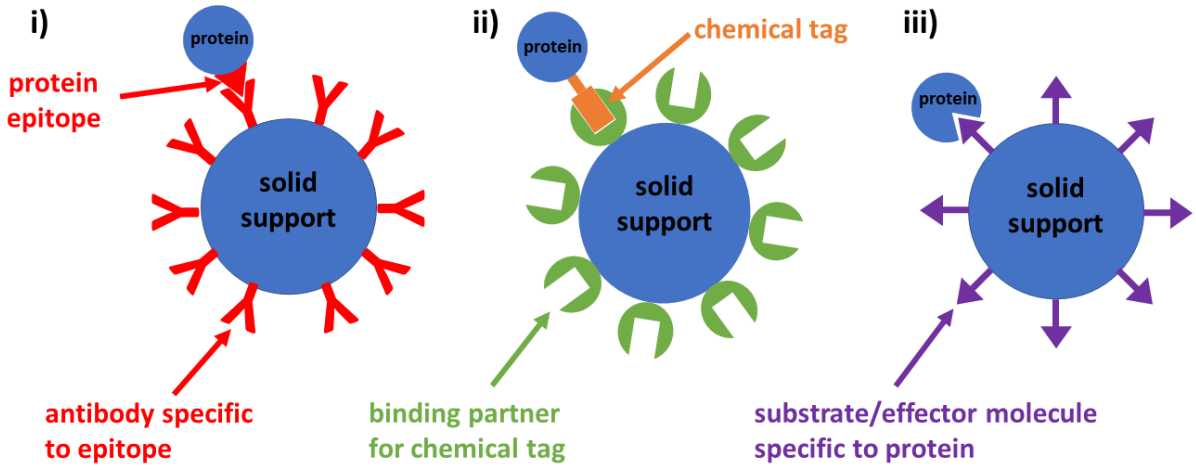

Figure 5.10: Classes of immobilised ligand systems for the affinity purification of proteins.

The enrichment of proteins using an AP approach is generally accomplished in three steps. First, a complex sample, such as cell lysate or serum, is incubated with the affinity support to allow proteins to bind to the immobilised ligand. Then, non-bound sample components, such as non-specific interactors and contaminant proteins, are removed using appropriate buffers that do not disrupt the protein-ligand binding. In the final step, the target is eluted from the immobilised ligand by changing the buffer components to disrupt the binding interaction, or by directly cleaving the peptides from the solid support using a tryptic enzyme (e.g. by on-bead digest).

Having developed a synthetic route to modified ajoene analogues, the choice of an AP-system involving a chemical tag was a reasonable choice for this project. The quality of affinity purification relies on the strength and selectivity of the interaction between the tag and ligand.[384] For this reason, biotin is a popular tag for AP-purification as the strong interaction between the biotin-avidin complex ($K_d \sim 10^{-14}$ M)[385] is unaffected by changes in pH and temperature, or the presence of organic and other denaturing agents. While this feature of the biotin-avidin system is compatible with the use of detergents, solvents and chaotropic agents, the strong binding interaction also complicates the elution of biotinylated proteins from the (strept-)avidin-coated solid supports. The direct release of biotinylated proteins therefore requires either the competitive displacement of the biotin tag from the avidin binding pocket using a buffer with a high concentration of free biotin, or the heat denaturation of the (strept-)avidin ligand to release the tag.[307,308] The harsh and denaturing conditions required are often incompatible with downstream processing of the sample for MS analysis. A gentler method of elution involving an on-

bead digest or a cleavable linker strategically placed between the affinity tag and the protein may be required.[386,387]

Since ajoene interacts with its protein targets through *S*-thiolation, the biotinylation of these targets represents the most direct path to elucidating these first-line interactions inside the cancer cell. Furthermore, the disulfide linkage between the biotin tag and the target protein revealed itself as a potential disconnection point to elute the targets from the solid support through reduction of the disulfide.

5.5 The Development of an AP-Method to Identify the Protein Targets of Ajoene

The development of a suitable workflow to isolate the biotinylated cysteine disulfide adducts using streptavidin coated magnetic beads, proved to be challenging. Several iterations of experimental conditions of the AP process were required to produce peptide samples that were suitable for MS analysis. During the process, we learned that the successful enrichment of our targets was dependent on a few critical steps: i) the effective removal of non-specific binding partners in the wash steps, ii) the specific elution method to recover target proteins from the beads, and iii) the removal of background contaminants (e.g. detergents) in the sample prior to the MS analysis.

In **Chapter 4**, we found that biotin-ajoene **40** biotinylated several proteins in MDA-MD-231 cells. The cell lysates for the proteomic study were prepared in the same manner as before (see **Section 4.5.2**), shown schematically in **Scheme 5.2**.

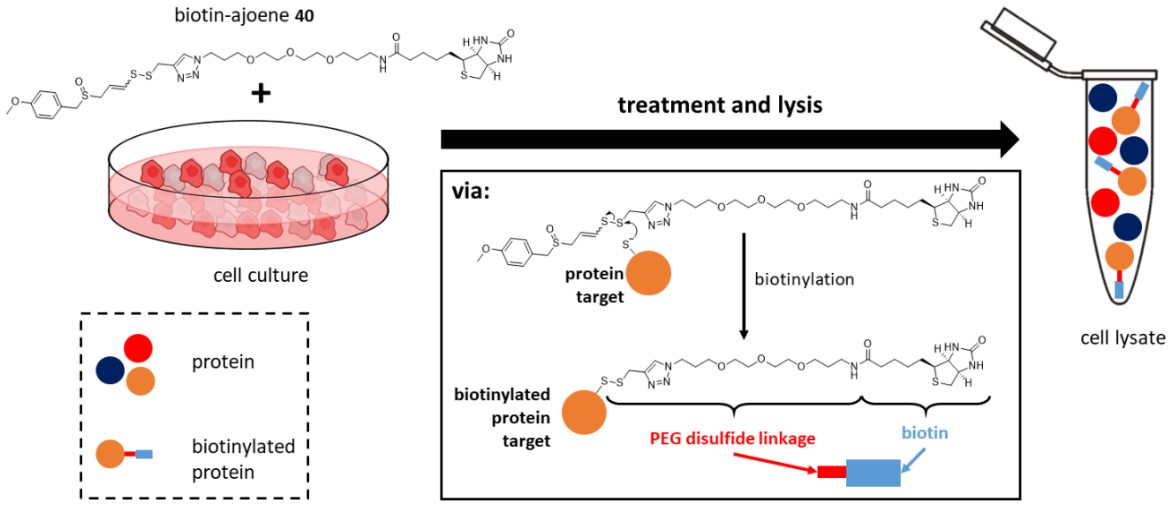

Scheme 5.2: Workflow of protein biotinylation in MDA-MB-231 cells by biotin-ajoene, 40.

After quantifying the protein content in the lysate (by BCA assay) and confirming the presence of biotinylated proteins (by immunoblot), the first step of AP involved assessing if our biotinylated proteins could be captured using streptavidin-coated magnetic particles. We employed a biotin-streptavidin magnetic bead pull-down assay published by our colleague Schäfer *et al.*,[388] which involved taking an aliquot at each step of the sample preparation (sample A, B, W and E in **Scheme 5.3**), separating by SDS-page and visualising the proteins by silver stain.

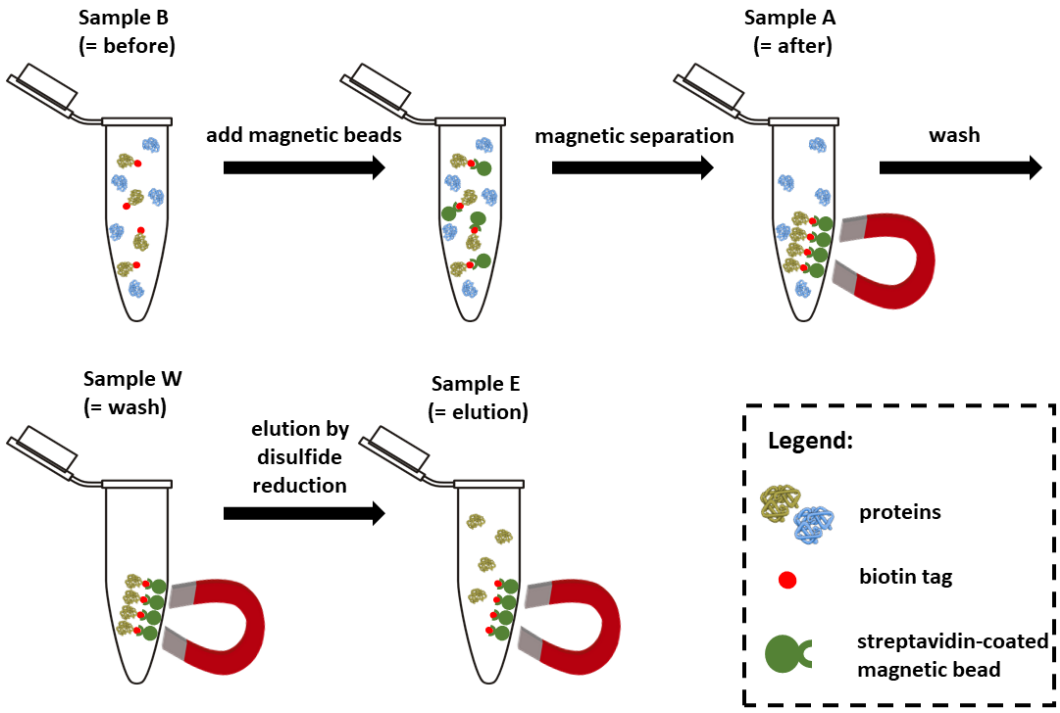

Scheme 5.3: Workflow of streptavidin-coated magnetic bead pull-down of biotinylated proteins.

A sample of treated cell lysate (B = before) containing 0.5 mg of protein was incubated with 1 mg streptavidin magnetic beads (Roche Diagnostics) to capture the biotinylated proteins (A = after). The immobilised protein-bead conjugates were then washed thrice (PBS containing 0.15 M NaCl, pH 7.5), and recovered by magnetic bead separation, while aliquots of the remaining supernatant were collected (W = wash). The proteins were eluted twice from the beads using the reducing agent TCEP (250 mM; E = elution). As a control, the same procedure was performed using the lysate of the untreated cells. The silver-stained polyacrylamide gel of the treated and untreated samples is shown in **Figure 5.11**.

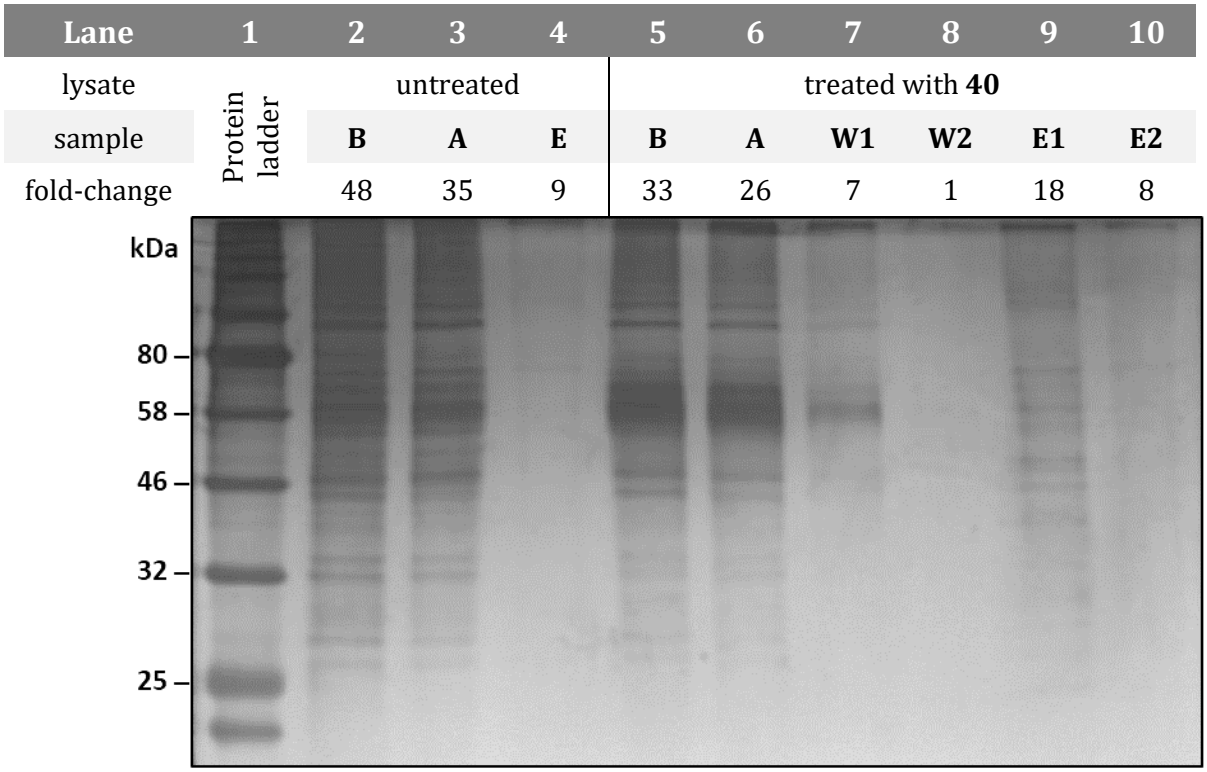

Figure 5.11: Silver-stained SDS-PAGE of magnetic bead pull-down assay run under non-reducing conditions.

The lanes marked as B (**Lane 2** and **5**) show the total protein content of the lysate before the addition of the magnetic beads for the untreated and treated lysate, respectively. The proteins remaining in the lysate following incubation with the beads (A) are shown in **lanes 3** and **6** for the untreated and treated sample, respectively. As expected, there is a drop in intensity of the protein bands from samples B to A (27% **lanes 2** vs **3** = UT; and 21% **lanes 5** vs **6**, T), indicating that a significant, and similar amount of protein, had bound to the streptavidin-coated magnetic beads in both samples. It was interesting that the beads removed an equal number of proteins in the untreated sample (**lane 3**), despite the lack of biotinylated proteins therein, indicating a large number of non-specific interactions between the beads and the proteins in the lysate. The buffer washes (**lanes 7** and **8**) of the treated sample contained proteins which faded through successive washes (W1 to W2), indicating that non-specifically bound proteins were removed from the beads with ensuing washes. In the final step, the proteins were removed from the beads by cleavage of their disulfide attachment using the reducing agent TCEP. It was pleasing to see that the first elution (sample E1 – **lane 9**) showed several distinct bands which,

faded upon a subsequent elution (sample E2 – **lane 10**). The proteins recovered in this step are presumed to be the biotinylation targets of ajoene. Although the bands in **lane 4** for elution of the untreated sample were very faint, we anticipated that these proteins would show up as false positives in the MS analysis due to the higher sensitivity of the instrument over silver stain.

The combined eluents (E1 and E2) of the untreated and treated samples were submitted for MS analysis at the Stellenbosch University (SU) proteomics unit. The resulting MS2 spectra of the runs are shown in **Figure 5.12**.

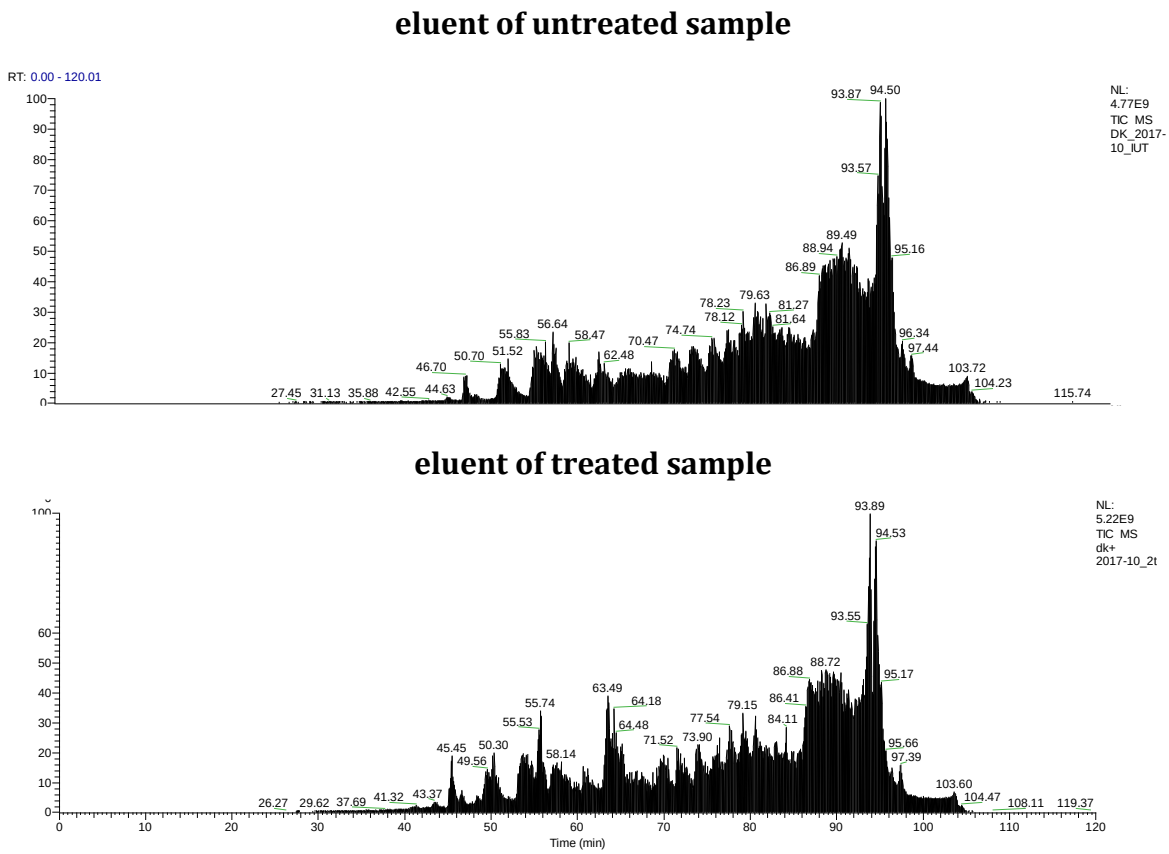

Figure 5.12: MS2 of affinity purified protein from untreated and treated MDA-MB-231 lysates.

The two MS2 spectra for treated and untreated samples displayed similar profiles of peptide fragmentation indicating that substantial proteins had been bound to the beads in both instances. The proteomic analysis of the spectra revealed that the total count of individual protein for both samples (UT + T) was 7296; however, only 68 of these proteins were unique to the treated sample. Hence, the large overlap in hits between the two samples, together with the large number of proteins identified in the eluent of the untreated sample, indicated that the beads were also capturing a large majority of

proteins that lacked a biotin tag. These are proteins that interacted non-specifically with the beads and remained stuck following our wash protocol. Sadly, the high number of hits in the untreated sample lowered our confidence in the 68 unique hits we obtained in the treated sample, as we were uncertain if the proteins were captured through the activity-based biotinylation by the probe (true positives), or if they were isolated because of non-specific interactions with the beads (false positives).

5.5.1 Progress Towards the Removal of False Positives

Following a discussion with the MS operator at SU, we received two suggestions for modifying our method to reduce the number of false positives. Firstly, it was suggested to try a different brand of streptavidin-coated beads, and secondly, we were instructed to perform more stringent bead wash-steps and elution.

5.5.1.1 Choice of Streptavidin-Coated Bead

Based on the first suggestion, we purchased another brand of streptavidin-coated magnetic beads made by a local South African supplier (ReSyn Biosciences). A comparative pull-down assay was performed to compare the two brands of beads (Roche versus MagReSyn®). We chose to also compare DTT and TCEP as a disulfide reducing agent. While TCEP is often used for proteomics experiments, DTT had previously been used to in our lab to cleave the biotin-label from its protein targets in immunoblot experiments (**Section 4.5.2**). The beads were incubated with lysate from untreated (UT) and probe **40** treated (T) MDA-MB-231 cells, washed thrice with the wash buffer, and then treated with DTT or TCEP to elute the proteins. The eluents were separated by SDS-PAGE and visualised by silver-stain (**Figure 5.13**).

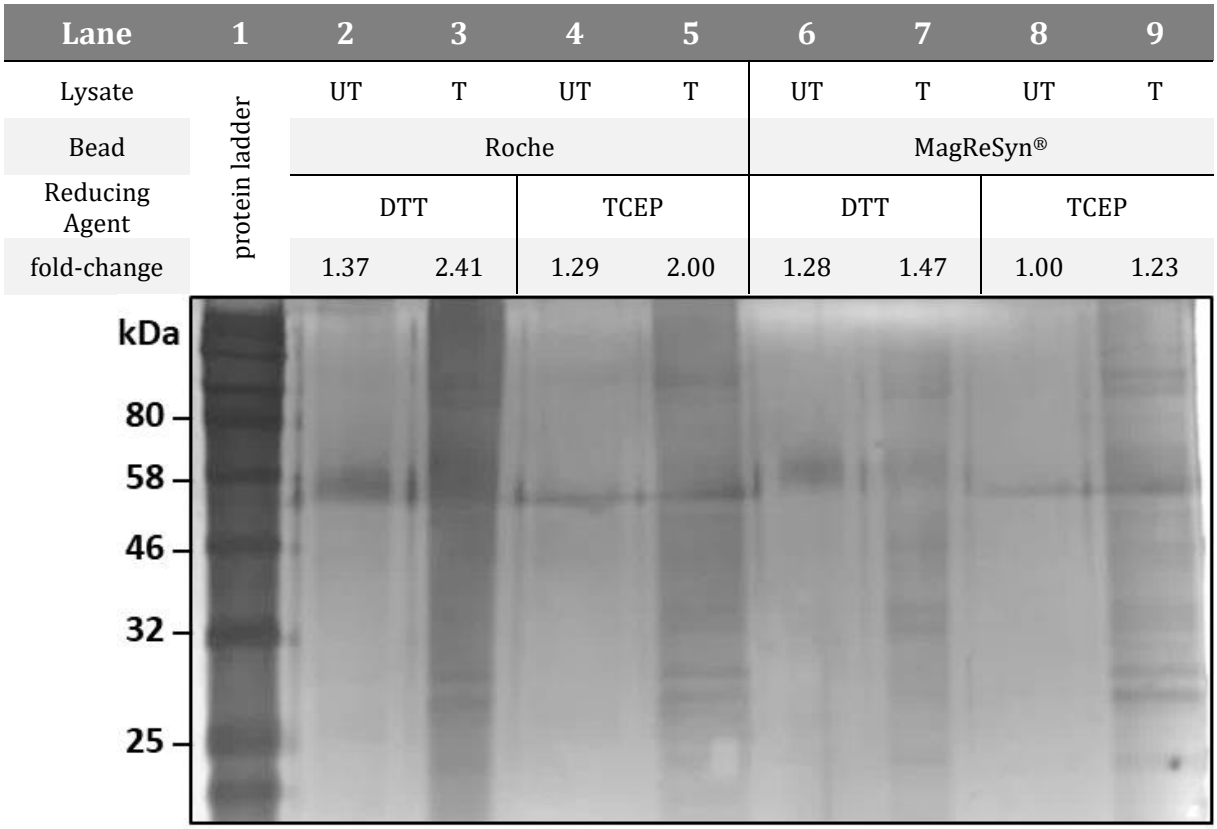

Figure 5.13: Comparison of streptavidin-coated beads and reducing agents.
Eluents obtained following a pull-down assay using biotin-ajoene probe 40 in MDA-MB-231 cells. The band intensity was normalised against the lowest value (lane 8) to allow a comparison across all samples.

As expected, the lanes (**3, 5, 7** & **9**) containing the eluent from treated lysates showed many more protein bands than those of the untreated lysate (**2, 4, 6** & **8**). This indicated that biotinylated proteins were being retained by both brands of beads. Although the protein band intensity of the Roche beads was ~40% higher than the MagReSyn® beads, the band intensity for the Roche beads was also ~15% higher in the lanes for the untreated lysates. This indicated that the Roche beads were retaining more non-specific proteins than the MagReSyn®. Therefore, we chose to continue our method development with the MagReSyn® beads, as it appeared that the Roche beads may be more prone to false positives.

When comparing DTT and TCEP (**Figure 5.14**) at the same concentration (30 μM), DTT showed a ~15% higher intensity of eluted protein bands, suggesting that DTT performed better at cleaving the disulfide bond to release the proteins from the beads. The smaller size and higher lipophilicity of DTT may promote better access to the disulfides thereby

leading to its better performance for our application. DTT was therefore selected over TCEP as an elution agent.

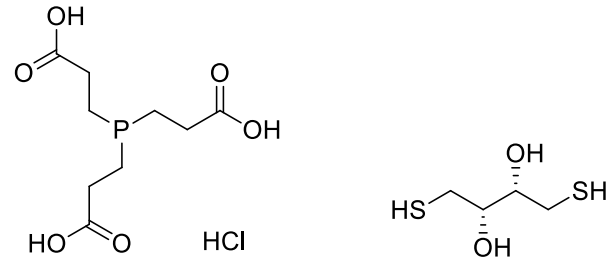

tris(2-carboxyethyl) phosphine hydrochloride (TCEP)

dithiothreitol (DTT)

Figure 5.14: Chemical structures of reducing agents TCEP and DTT.

5.5.1.2 Optimisation of Wash Steps and Preparation of Peptides

As part of our workflow, we were submitting the eluents from the magnetic beads to SU proteomics unit. Their workflow involved the separation of the samples using SDS-PAGE, followed by a reduction and alkylation of the cysteines, in-gel proteolytic digest of the proteins, extraction of the peptides from the gel matrix and a final peptide clean-up by desalting. It appeared the poor quality of our eluents, which contained too many contaminants, led to the collection weak spectral data. In view of this, we decided to perform the protein digestion and peptide clean-up ourselves. This equated to submitting purified peptides instead of eluted proteins, which expedited the analysis of samples and gave us more control over the experiment and the choice of reagents.

We identified that the removal of non-specifically bound proteins (false positives) from our beads was our central conundrum. To break the interactions to undesired/non-specifically bound protein without disrupting the biotin-streptavidin complex, the beads needed to be stringently washed using buffers that contained detergents and salts. Unfortunately, the use of certain detergents and salts comes with the complication that these reagents may be carried through into the MS and show up as contaminants that compromise the quality of the data and potentially clog up the LC columns. **Figure 5.15** shows an example of total ion chromatograms (TIC) of peptide samples that were found to contain a detergent contamination.

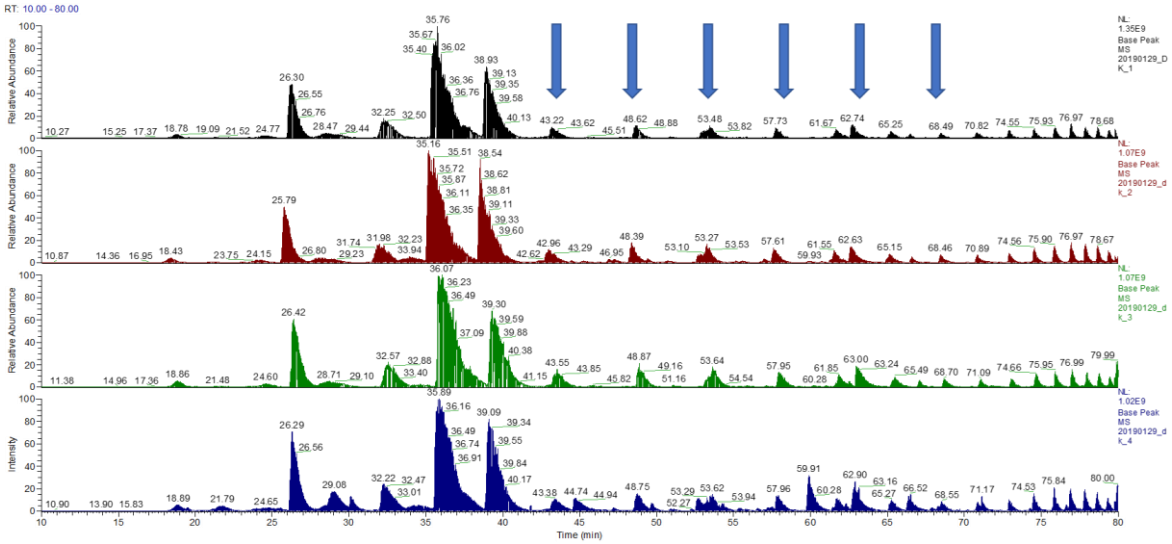

Figure 5.15: Total ion chromatograms of samples containing a detergent contamination. Blue arrows indicate the equally spaced peak profiles of the polymeric detergent contamination in the MS1 spectrum.

The equally spaced distribution and similarity of the peak profiles across all four samples is produced by the presence of a polymeric contaminant (indicated by the blue arrows in **Figure 5.15**). The contaminants were identified as residual non-ionic, non-denaturing detergents that had been used in the lysis buffer IGEPAL CA-630, and in the wash buffer Triton X-100 (**Figure 5.16**).

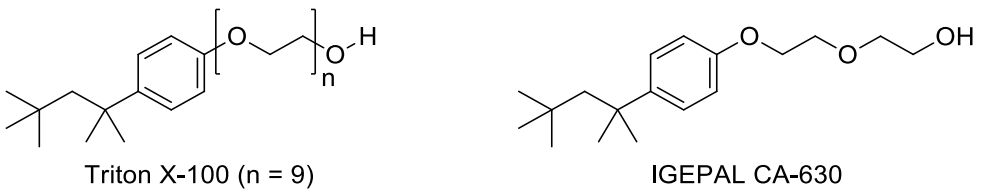

Figure 5.16: Detergent contaminants identified in the MS spectrum.

Since the AP process enriches all constituents of the samples prior to analysis, the presence of residual detergents in the sample overshadows the peptide peaks based on their lower relative abundance compared to a concentrated contaminant. Hence the spectra obtained were low quality and with little information on eluted peptides.

5.5.1.3 Removal of Detergent Contaminants

With regards to finding a balance between the necessity to use detergents for removing false positives, but with the avoidance of detergent contamination into the MS, invaluable assistance was provided by Dr. Muneerah Smith from the Blackburn group at UCT.

Muneerah had developed an AP-MS protocol during her doctoral work, and with her permission, several operational steps were included in our method to optimise the purification sequence.[389]

Firstly, it was recommended that the cell lysate should be diluted prior to the incubation with beads, as the lowered protein concentration would reduce the likelihood of beads interacting non-specifically. Secondly, we were advised to use the same buffer system for the lysis, washings and elution, as varying the buffer between steps may alter the binding between the proteins and beads. Since Tris lysis buffer was used, the wash and elution buffers were changed from PBS to Tris (50 mM). Thirdly, an increase in the number of bead washes (from three to five) and the use of a large volume of buffer (from 300 µL to 1 mL) containing a greatly reduced volume of detergent (from 1% to 0.1% Triton X-100) was suggested. The changes in the wash steps were aimed to remove more of the undesired proteins, whilst the lowered detergent concentration limits the carrying through of detergent into the MS sample. As a final precaution, the washes with the detergent buffer were followed by an additional five washes of detergent-free buffer to ensure any residual detergent was removed.

Our initial strategy for the elution of the proteins involved incubating the beads with DTT to cleave the disulfide bridge between the biotin label and the protein, then performing a tryptic digest on the eluent. It was noticed that, although the beads had captured many protein targets, our samples had a very low peptide yield. This indicated that the treatment with a reducing agent alone was insufficient to release all proteins from the beads, particularly because several disulfide bridges may be buried inside proteins or obstructed by the streptavidin. We were therefore advised to rather digest the proteins directly on the beads to minimise sample loss. The on-bead digest still involved the denaturation of the proteins with DTT, but instead of cleaving the disulfide bridge between the protein and the bead, the main function of the disulfide reduction was to unfold the peptide chains to provide better access to the trypsin.[390,391] Following incubation of the sample with trypsin, the peptide-containing supernatant could be removed from the magnetised beads. Although this technique may lead to the digestion of any residual non-specific binders, we had confidence that our stringent wash protocol would minimise this. Before the MS analysis, the peptides were run through a detergent

removal column (HiPPR® detergent removal resin – ThermoFischer) as a final assurance that the sample was indeed detergent-free.

These modifications to the method not only solved our detergent contamination issues, but also produced higher quality data sets with a greater number of protein hits. **Table 5.4** lists the total protein count as well as those unique to the untreated and treated samples before (**Run 1-3**) and after (**Run 4 & 5**) the method optimisation.

MS Run	Total	Untreated	Treated	Ratio Treated/Total
1	7256	n.d.	68	>0.01
2	26	15	17	0.65
3	53	22	42	0.79
4	1302	564	1294	0.99
5	7219	4086	6953	0.96

Table 5.4: Detected protein from the MS-analysis of AP purified samples.

It was encouraging to see that the optimisation of the binding and wash protocols as well as the on-bead digest had substantially improved the overall protein yield in runs **4** and **5**. It became apparent that the total protein yield for runs **2** and **3** was impeded by the contamination with detergent. Furthermore, the ratio of proteins unique to the treated sample, compared to the total proteins detected, had increased, indicating that the more stringent wash sequence had removed the non-specific binders and caused a better enrichment of the biotinylated targets. Nevertheless, we still needed to address the large overlap of hits common to both the untreated and treated samples as illustrated in **Figure 5.17**.

Figure 5.17: Venn diagrams showing the number of identified proteins enriched from untreated and probe-treated MDA-MB-231 cell lysates using streptavidin magnetic beads.

Despite the 46- and 12-fold increase in proteins unique to the treated samples (for runs **4** and **5** respectively), the analysis still showed that 42% and 53% of the total identified proteins were shared amongst both samples implying that, whilst substantial improvements had been made, too many non-specific binders were still being captured.

5.5.2 Optimised AP-MS Method for the Enrichment Ajoene Targets

Following the implementation of the workflow improvements, the AP-MS method used for the enrichment and purification of the biotin-ajoene **40** targets, is outlined in **Scheme 5.4**.

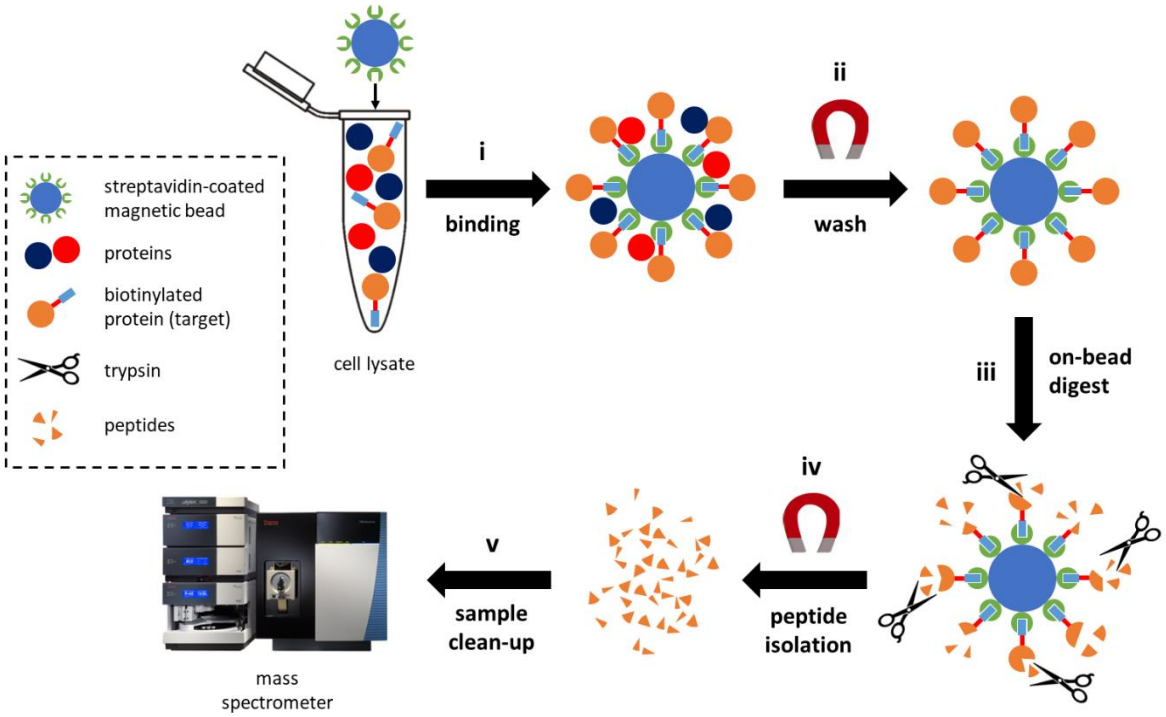

Scheme 5.4: AP-MS workflow for the identification of the protein targets of ajoene in MDA-MB-231 cancer cells.

Firstly, 500 µg of treated MDA-MB-231 lysate (40 µM biotin-ajoene **40** for 24 hours) was diluted with wash buffer 1 (WB1: 500 mM NaCl, 50 mM aq. Tris HCl, 0.1 % Triton X-100, pH 7.5) and added to 1 mg of streptavidin-coated magnetic beads (**Step i**). The mixture was left overnight on a shaker at 4 °C to allow for the capturing of the biotinylated proteins on the beads. The next day, the supernatant was removed, and the beads were washed thrice with WB1 to remove the remainder of any unbound lysate (**Step ii**). An additional wash with CH_3CN (60 % in H_2O) was then performed to disrupt the interactions between the bead and any non-specifically bound proteins; and the beads were then washed thrice with a detergent-free buffer (50 mM aq. Tris HCl, pH 7).

Elution of the biotinylated proteins from the beads (**Step iii**) was performed by incubation with the elution buffer (EB: 5 mM DTT in 50 mM aq. Tris HCl, pH 8) for 30 minutes at room temperature. The newly liberated cysteine thiol groups were then alkylated using iodoacetamide, to prevent their autooxidation.[392] The on-bead digest was performed overnight using MS-grade porcine-derived trypsin (0.5 µg/µL) at 37 °C. The next day, the supernatant was collected and the beads were washed once (50 mM aq. Tris HCl, pH 8). The supernatant and wash were pooled (**Step iv**) and incubated again with trypsin ensure that the proteins were fully digested. After two hours, the trypsin was inactivated by the addition of formic acid, to a final concentration of 2% (v/v).

The digested sample was further cleaned prior to MS analysis to remove any contaminants (**Step v**), such as detergents or salts introduced from the wash and elution buffers. This was done by passing the sample through a column of HiPPR detergent removal beads (Thermo Fischer), followed by a stage tip containing a bead of C18 resin for desalting. The peptides were then eluted into a glass vial insert and dried under a vacuum (the full protocol is reported in **Section 7.8**).

During the analysis of our previous proteomic datasets, it was noticed that the distribution of non-specifically bound proteins (false positives) was not uniform across the samples and that increasing the number of technical repeats could increase the statistical power to eliminate false hits. We therefore performed the above AP protocol on five technical replicates from each of the treated and untreated groups.

5.6 The Proteomic Analysis of Ajoene's Targets in MDA-MB-231 Cancer Cells

The collection and processing of the proteomic data was performed by the IDM Proteomics & Metabolomics Platform at UCT with the assistance of Dr. Tariq Ganief and Dr. Shaun Garnett.

5.6.1 LC-MS/MS

The sample analysis was performed on a Dionex Ultimate 3500 RSLC (Thermo Fisher Scientific) coupled to a Q Exactive mass spectrometer (Thermo Fisher Scientific) using a calibrated method (see **Section 7.8.5**). In short, the purified peptides were dissolved in 2% aq. CH_3CN spiked with 0.1% formic acid and loaded into the autosampler. The sample was injected onto a reverse-phase column to separate the individual peptides, followed by acquisition of the MS1, and the MS2 spectra on the Q Exactive mass spectrometer.

5.6.2 Mass Spectrometry Data Analysis

The resulting raw data that was generated by the mass-spectrometer was imported into MaxQuant (version 1.6.14.0) which is a quantitative proteomics software package for analysing large data sets, specifically high-resolution MS data.[393,394]

A database search on the canonical protein library for *homo sapiens* (Uniprot) was done using its integrated Andromeda search engine.[394] The Andromeda algorithm first performs an *in silico* tryptic digest on the individual proteins in the library to generate a dataset of their theoretical tryptic fragments. Since the experimental (*in vitro*) and theoretical (*in silico*) peptide fragments are produced by the same sequence cleavage pattern, the identified peptide masses in the analysed samples can be compared to peptide masses in the library.

Considering that trypsin is never completely efficient *in vitro*, the search parameters allowed for peptides from missed cleavages, i.e. peptide masses that contain an additional arginine or lysine (overall a total of two missed cleavages were allowed). Owing to mass ambiguities in peptides shorter than seven amino acids, these fragments were excluded from the search. The search also excluded individual peptides with a mass greater than 4600 Da, as these suffer from mass and sequencing inaccuracy (i.e. they have multiple charge states that impact peak intensity, resulting in a lower detection sensitivity).[395] The algorithm considers that some of the amino acids may be modified resulting in changes to the fragment mass. The oxidation of methionine and *N*-terminus acetylation are commonly encountered amino acid modifications and were included for consideration in the search as variable modifications. Since our sample preparation involved the *S*-alkylation of free thiols with iodoacetamide, the carbamidomethylation of cysteine was set as a fixed modification.

By applying these pre-set parameters, MaxQuant identified the peptides of the MS/MS data by comparing their precursor ion m/z, charge state and peak list to the target database containing the theoretically digested protein sequences. A summary of the MaxQuant output for the spectral processing is given in Table **5.5**.

		MS1 spectra collected	MS2 spectra collected	MS2 spectra submitted for analysis	MS2 matched to peptides	Unique peptides identified
Untreated	**1**	6488	13757	19832	1038	1040
	2	6133	14695	20932	1153	1161
	3	6748	12927	18983	591	583
	4	6033	14990	21337	1147	1135
	5	6862	12622	18431	573	583
Treated	**6**	4768	19162	23049	8599	8357
	7	4770	19178	23263	8402	8149
	8	4713	19394	23325	8950	8512
	9	4789	19042	23157	8009	7820
	10	4817	19103	23350	7194	7258
Total		**56121**	**164870**	**215659**	**45656**	**13115**

Table 5.5: Summary information for the raw files processed with MaxQuant.

The processing of 215659 MS2 spectra yielded the identification of 13115 unique peptides, which were only matched to a theoretical peptide when their precursor mass fell within the specified tolerance of 0.5 Da. Additionally, each match was assigned a probabilistic score (*q*-value/identification confidence), which is based on the matches between the theoretical fragment masses and the peaks in the MS spectrum.[396] The higher the number of peptides that match to the theoretical sequence of proteins, the lower the chance that this happened by chance (and the higher *q*-value of the protein). However, since the number of theoretical peptides in the database outweighs the number of peptides in the sample, it is likely that some matches occur by random chance. To determine the number of random matches in the sample, MaxQuant runs a second search against a decoy database, which is generated by reversing the sequences of the original protein database. All peptides matching to these sequences can be classified as an incorrect match (or false positive), because the *in silico* digest of a reversed sequence gives peptides that are not naturally occurring.[397] Since the target and decoy database will contain an equal number of peptides, the number of peptide matches in the decoy database gives an indication of how many random matches occurred when the sample peptides were initially screened against the target database. While this method does not

allow the identification and removal of individual false matches in the target database, it probes the quality of the data set and provides a measure of the percentage of random matches in the analysis. This metric, the so-called false discovery rate (FDR), is generated from the ratio between the number of matched hits in the decoy dataset and the total number of hits in the target database,[398] using the following equation:

$$\text{FDR} = \frac{\#\text{ hits in decoy database}}{\sum \text{hits in target and decoy database}}$$

In practice, MaxQuant was configured to omit peptide-spectrum matches with a q–value that was equal to a FDR threshold of 0.01, which meant that 99% of the list of peptides was not due to random chance and that we were willing to accept that 1% of the matches may be false positives.

From the matched peptides, a list of protein groups was generated. Proteins that shared all identified peptides were combined into a single protein group. Peptides that matched in multiple protein groups ("razor" peptides) were assigned to the protein group containing the most unique peptides. **Figure 5.18** shows the histogram of the number of proteins detected in the individual samples.

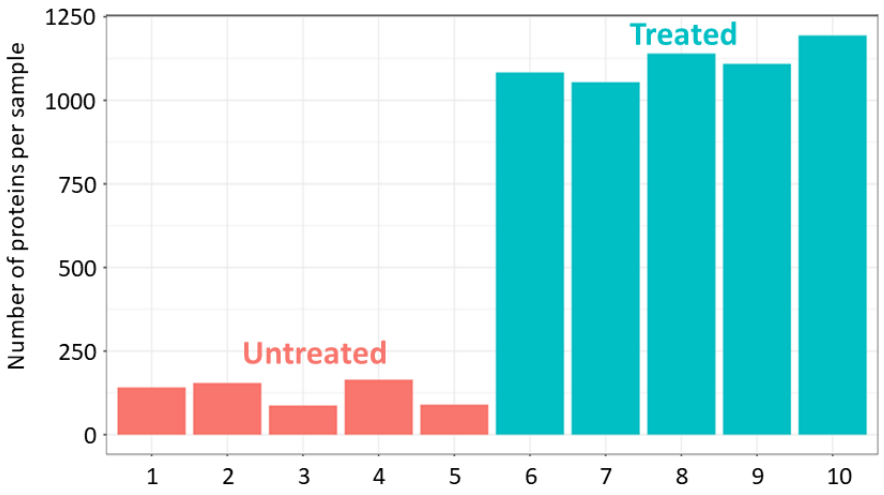

Figure 5.18: Total number of proteins per sample.
Red = untreated, blue = treated.

The data showed that the numbers of proteins detected were similar across the technical replicates, which indicated high data reproducibility. It could also be seen that the streptavidin beads isolated up to 9-fold more proteins from the biotin-ajoene **40** treated lysate. To determine the relative amounts of individual proteins per sample, the MaxLFQ

algorithm (LFQ = label-free quantitation) was applied.[399] This algorithm normalises the value individual protein intensity measurement against the mean of the total normalised intensities across the entire dataset to produce the LFQ intensity value. Since the normalisation also decreases the effects of outliers, it facilitated later statistical analyses which required information on the relative protein amounts between samples. A Venn diagram of the total number of identified proteins in the treated and untreated samples, as well as their overlapping hits as shown in **Figure 5.19** (excluding 26 proteins whose LFQ < 0 across all samples).

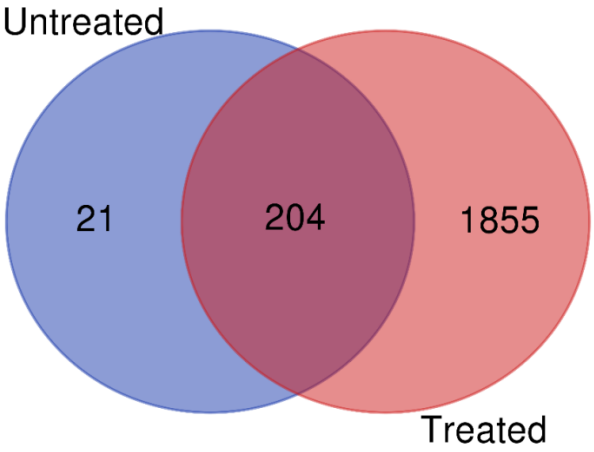

Figure 5.19: Number of proteins identified in the proteome of MDA-MB-231 breast cancer cells by AP-MS with MagReSyn® Streptavidin magnetic beads for biotin-ajoene, 40.
Data obtained from five technical replicates.

Although the ratio of hits in treated, to the total hits was slightly lowered compared to our previous runs [0.89 compared to 0.99 (run 4) and 0.96 (run 5) in **Table 5.4**], there were markedly fewer hits in the untreated, as well as a much smaller overlap of identified proteins between the two groups (10%). This showed a vast improvement in the quality of the data obtained.

5.6.3 Statistical Analysis

For the statistical analysis, the MaxQuant protein group file was imported into Perseus (version 1.6.15.0), a freely available package that provides statistical tools for interpreting protein quantification in proteomics data sets.[400,401]

First, the protein data of the ten samples was grouped according to condition (UT and T) and filtered to remove potential contaminants and reverse hits as well as proteins that

were only identified by site (i.e. those proteins identified only by a single peptide containing a modification (*vide supra*)). The site modification can introduce ambiguity in the search of the peptide mass within the library, which increases the probability of incorrect identification. The filtering of the data reduced the number of proteins from 2106, in the initial matrix, to 2004, in the filtered matrix.

Proteomics data typically shows a wide range of LFQ intensity values (0 to ~$2x10^9$) with a higher frequency of low abundant proteins, resulting in a large variance and non-normal distribution of the LFQ intensity data, shown in left panels of **Figure 5.20**. This distribution is normalised to smooth the data for subsequent parametric testing by log_2 transforming the LFQ intensities (shown in the right panels of **Figure 5.20**. This transformation also allows for a better visualisation of the differences between the groups.

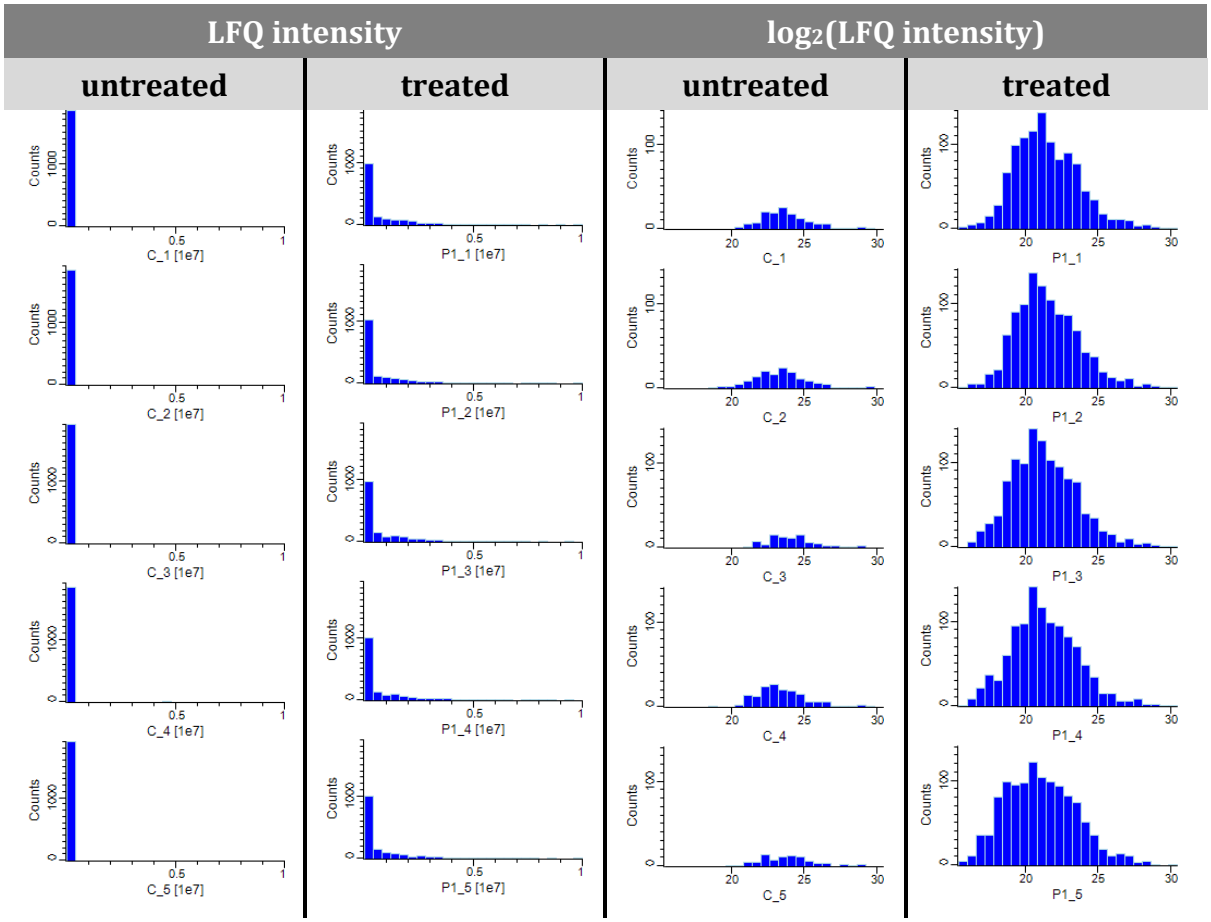

Figure 5.20: Histogram of protein LFQ intensities, before and after log_2 transformation.

Pleasingly, the histograms of the log_2(LFQ intensity values) showed that the data now followed a normal distribution, which allowed parametric testing of protein enrichment

between the two groups using a student *t*-test. The higher count of proteins in the treated (right column), versus untreated (left column) groups, again indicated that the beads had a higher specificity towards proteins treated with the biotin-ajoene **40**. Although MS-based proteomics has the advantage of detecting thousands of proteins from a single experiment, challenges arise from sample complexity as well as the variation in sampling from one run to another.

One challenge is the technical variability between samples, where the generated data from an individual run may contain misassigned proteins based on an overlap of a shared peptide with another protein, proteins of low abundance, as well as non-specific binders to the affinity matrix (false positives). Since the probability of consistently capturing these proteins is low, we filtered out proteins that did not appear in at least 4 out of 5 technical replicates in either group. A visual example of the filtering process on a set of arbitrary proteins **A**-**H** is given in **Figure 5.21**, where the bold "**X**"s indicate when the above condition was met, and the protein was therefore kept in the dataset.

Group	Untreated					Treated					
Replicate	1	2	3	4	5	1	2	3	4	5	
Protein A	X		X	X		**X**	**X**	**X**	**X**	**X**	Keep
Protein B		X	X			X	X	X			Remove
Protein C	X			X	X	X	X				Remove
Protein D						**X**	**X**	**X**	**X**	**X**	Keep
Protein E		**X**	**X**	**X**	**X**						Keep
Protein F						X	X		X		Remove
Protein G			X			**X**	**X**	**X**		**X**	Keep
Protein H											Remove

Figure 5.21: Filtering of proteins from data sets based on their valid representation. The protein is removed if it is not represented in ≥4/5 technical replicates.

Through this filtering process, we were able to reduce the data set by 57.5%, leaving 852 proteins that were deemed valid for further statistical analysis.

Another challenge is the presence of missing data points, which arise from a lack of quantification, in particular low intensity peptides that fall below the detection limit of the instrument. This typically skews the normal distribution of the $\log_2$(LFG intensity values) at its lower bound, which shifts the true median and alters the variance of the

sample. Since these missing values are primarily from proteins with low levels of expression, these missing values can be imputed. Although the filtering removed most proteins with a high proportion of missing values, several proteins with missing values remained in the data set, as illustrated by the gaps in the top table of **Figure 5.22**.

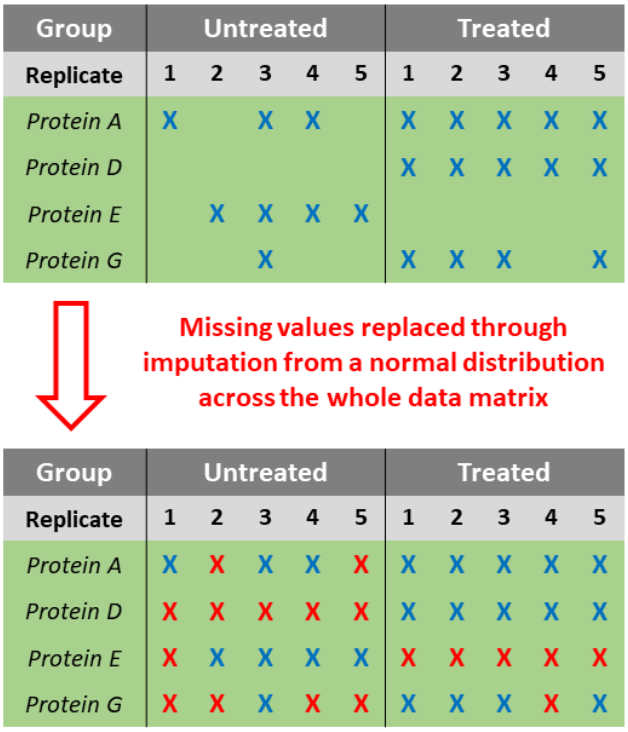

Figure 5.22: Replacement of missing values in the data set by imputation.
The red crosses represent imputed values.

These missing values were thus imputed using the built-in method of the Perseus software. This popular method draws the random numbers from a normal distribution with a mean that is downshifted from the sample mean and a standard deviation that is a fraction of the standard deviation of the sample distribution. We used the software's default imputation setting of a 1.8 standard deviation down shift and with a width of 0.3 for each sample. Due to its randomness, imputation does not create artefacts in *t*-tests or in intensity profile analyses.[402] The results of the imputation is illustrated in **Figure 5.23**.

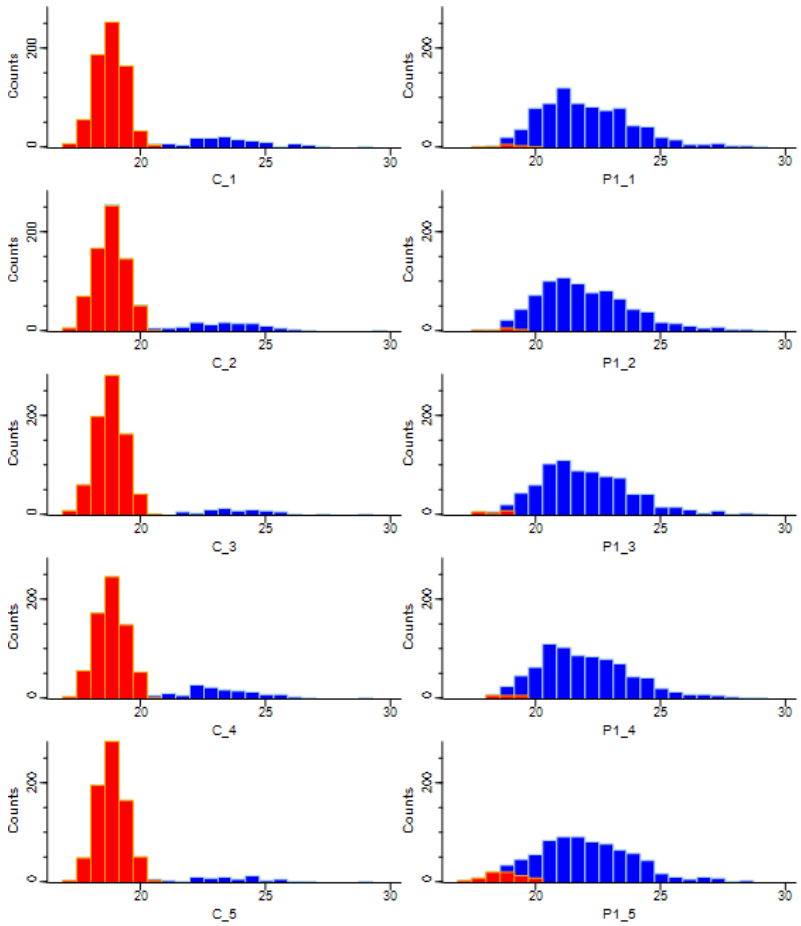

Figure 5.23: Imputation of missing values in the AP-MS data for biotin-ajoene 40.
The left column shows the untreated and the right column shows the treated samples. Original values and imputed values are shown in blue and red, respectively.

As seen above, the simulated low intensity values fit well to the profiles of the low abundant proteins in the treated sample, supporting the notion that the missing data was caused by their absence. Since the imputed values were taken from a normal distribution across the whole data set, the missing values took on an equally narrow spread at the lower end of the distribution. As expected, the number of missing values was greater in the untreated group (control) as the overall detection of peptides in this group was low.

To determine whether relative protein abundance was significantly different between the two groups, a two-sample *t*-test was performed on our curated and imputed datasets. A significance cut-off of 0.01 was applied using a permutation-based FDR (250 randomisation and no grouping preserved across randomisation) and the minimal fold-change difference between the $\log_2$(LFQ intensity values) of the treated and untreated group (S_0) was set to 3 ($2^3 = 8$). By applying two thresholds (FDR and S_0), only proteins with a *p*-value < 0.01 and a fold-change > 8 ($S_0 = 3$) were considered significant.

Figure 5.24 shows a volcano plot for convenient visualisation of the entire proteomic data set including replicates, together with the results of the *t*-test. The plot consists of statistical significance as -log *p* on the y axis, versus magnitude of change between the two tested groups, $\log_2$(T-UT), on the x axis. This plot enables a quick, visual identification of those proteins that display a large fold-change between treated and untreated groups, but which are also statistically significant.

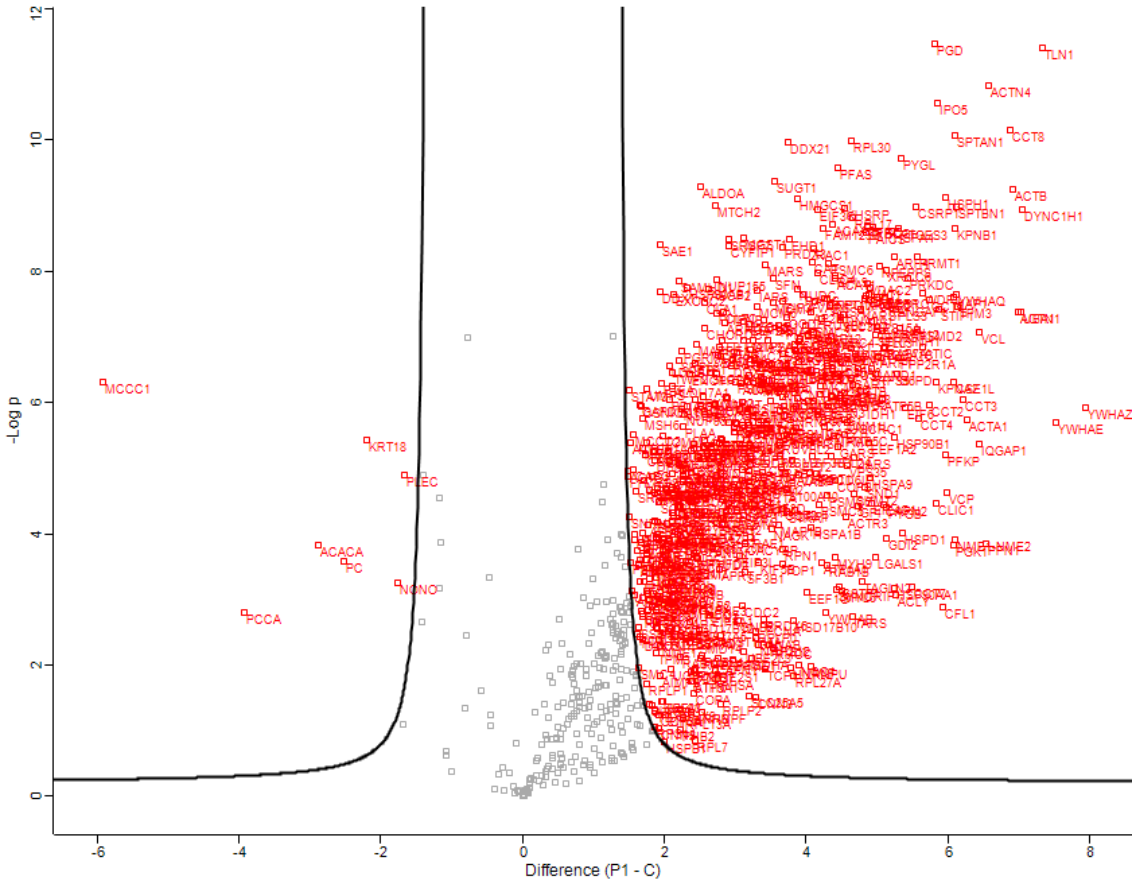

Figure 5.24: Volcano plot of the imputed proteomics data showing the statistically significant proteins enriched between treated and untreated groups.

The centre of the volcano plot represents the confidence level cut-off defined in the *t*-test. The curves unify the values for the minimum significance along the y-axis and minimum fold-change difference along the x-axis. The proteins coloured in red (640 in total), are statistically significant and above the minimum magnitude of (fold-)change. These proteins are selected with high confidence and represent the biotin-ajoene interactome. Our immediate attention fell on the 7 proteins on the left of the "volcano" column, as they represent the proteins enriched from the untreated sample only. These are proteins that

interact with the streptavidin magnetic beads in the absence of biotin-ajoene **40**, shown in **Table 5.6**.

Gene	Protein name	*p*-value	fold-change (UT/T)
PLEC	Plectin	1.30E-05	3.2
NONO	Non-POU domain-containing octamer-binding protein	5.63E-04	3.4
KRT18	Keratin, type I cytoskeletal 18	3.79E-06	4.6
PC	Pyruvate carboxylase, mitochondrial	2.59E-04	5.8
ACACA	Acetyl-CoA carboxylase 1; Biotin carboxylase	1.49E-04	7.4
PCCA	Propionyl-CoA carboxylase alpha chain, mitochondrial	1.60E-03	15.1
MCCC1	Methylcrotonoyl-CoA carboxylase subunit alpha, mitochondrial	4.79E-07	60.2

Table 5.6: Proteins enriched by streptavidin-coated magnetic beads from the untreated sample.

During our initial probe evaluation (**Figure 4.32** in **Chapter 4**), the lanes in our western blots that contained untreated cell lysate indicated that a small number of proteins were interacting with the anti-biotin (streptavidin) antibody. It was speculated that these were natural streptavidin binders containing an endogenous biotin prosthetic group. It was most rewarding to see that the 4 most enriched proteins (fold-change (UT/T) > 5), out of the 7, were identified as carboxylases, pyruvate carboxylase (PC), acetyl-CoA carboxylase 1 (ACACA), propionyl-CoA carboxylase (PCCA) and methylcrotonoyl-CoA carboxylase (MCCC1), which are known streptavidin binders.[403] Since the human proteome contains only 6 proteins with a biotin cofactor, and we were able to enrich for 4 of them, this finding validated the specificity of our AP method to enrich biotin-containing proteins. Although the three other proteins do not contain any known biotin moiety, and were less enriched than the carboxylases, the literature provided some evidence as to why they may have been retained by the beads. KRT18, is a type I cytokeratin which is highly abundant in human epithelial cells and is a notorious contaminant in proteomic data which is easily introduced during processing.[404] Plectin is giant multifunctional cytolinker protein and plays a crucial role in stabilizing and orchestrating intermediate filament networks in cells. Owing to its overexpression in several cancers, it is proposed as a biomarker, and in this context iron oxide nanoparticles are used for its detection.[405] This may indicate that PLEC might have bound directly to our MagReSyn® magnetic

beads, which are also made of iron oxide. Regarding, the DNA- and RNA binding protein, NONO aka. $p54^{nrb}$, something peculiar was noticed when searching the keywords "$p54^{nrb}$" and "streptavidin". Several papers identify this protein as a "surprising" target in their assays, but in all cases they used a streptavidin-reporter or streptavidin-coated resins/beads to identify the protein.[406–409]

The detection of the four endogenous biotin-containing proteins were a welcomed sight, and this provided much needed confidence that both the technical execution of the AP-MS method, as well as the stringent data analysis, had yielded valid biotinylation targets. These consist of 633 biotin-ajoene interactome targets which are listed in the **Table 7.1** in the **Appendix** (**Chapter 7**). This newly discovered probe interactome lays the foundation to the discussion in the upcoming section.

5.7 Interpretation of Protein Data

The first interrogation of the biotin-ajoene interactome involved identifying if the protein targets contained known reactive cysteine residues. To this end, we used a database of known protein cysteine modification (PCM) sites in the human proteome and searched for their occurrence in our list of enriched protein targets. The second objective was to examine if certain reactivity features were making cysteine thiols susceptible to interaction with the ajoene pharmacophore, and to ascertain their role in cancer biology and whether modification of these residues is known to modulate protein activity. Lastly, the third objective was to overlay the probe interactome onto cellular pathways to determine which interaction may be specifically associated with the cytotoxicity of ajoene.

5.7.1 Biotin-Ajoene Enriches Proteins with Redox-Active Cysteine Residues

Although the biological significance of protein cysteine modifications (PCMs) of catalytic as well as non-catalytic sites has been recognised in both healthy and diseased states, an understanding of the reactivity and function of cysteines in the human proteome is only partially understood.[54,355,410,411] Several recent studies have used high throughput activity-based proteomics techniques to map out cysteine residues susceptible to PCMs. Some studies have profiled these cysteines into a hierarchy of reactivity and ligandability.[412–417] Ligandability describes the ability of a protein target to bind small molecule *in vitro,*[412] and in the context of the upcoming discussion, ligandability describes

the ease at which a cysteine residue of a protein is oxidatively modified by an electrophilic group.

A research group led by Cheng and Lui has consolidated the findings of these proteomic discovery efforts into an integrative database, named iCysMod.[418] The database contains 31,483 manually curated proteins from 48 eukaryotes and provides detailed information on 85,747 experimentally identified cysteine sites, such as their location in the protein sequence, and the type of PCM event that can take place, such as *S*-nitrosylation (-SNO), *S*-glutathionylation (-SSG), disulfide formation (-SSR), *S*-sulfhydration (-SSH), *S*-sulfenylation (-SOH), *S*-sulfinylation (-SO_2H) and *S*-palmitoylation (-S-palm). We used the iCysMod dataset of the human proteome to look for overlap with our biotin-ajoene **40** interactome data set, as shown in **Figure 5.25**.

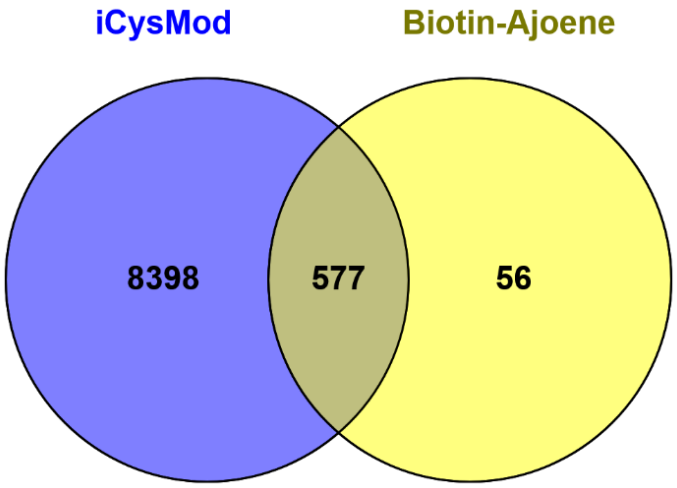

Figure 5.25: Overlap of biotin-ajoene probe-enriched proteins with known cysteine modification sites from iCysMod.

It was found that 91% of the discovered biotin-ajoene interactome (577 proteins) overlapped with known PCM sites. Thus, ajoene is targeting reactive cysteines in MDA-MB-231 breast cancer cells. With regards to the 56 non-overlapping proteins we envisaged that they may contain PCM sites which were not included in the iCysMod database (e.g. containing *S*-ubiquitination or *S*-glycosylation sites), or that they may have been captured through their interaction with the ajoene biotinylated targets through protein-protein interactions (e.g. being part of protein complex).[419]

The overlapping proteins in the iCysMod database were then categorised further into type of PCM event. **Figure 5.26** shows the relative frequency of a specific PCM event occurring across the 577 proteins.

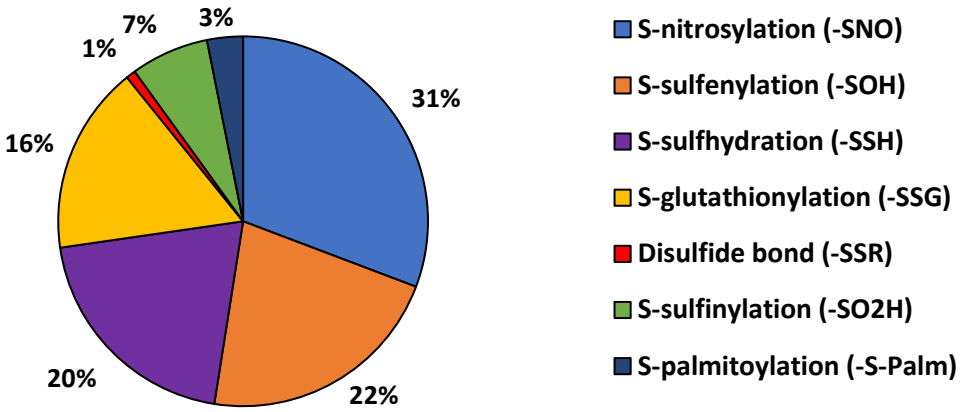

Figure 5.26: Distribution of known PCM events within the biotin-ajoene dataset.

The types of PCM events that were most associated with our protein targets were *S*-nitrosylation (-SNO) (31%), *S*-sulfenylation (-SOH) (22%), *S*-sulfhydration (-SSH) (20%) and *S*-glutathionylation(-SSG) (16%). These PCMs are strongly associated with redox sensing, signalling, and the functional regulation of proteins, which makes them ubiquitous within the human cysteine proteome.[420–422]

While our experimental data can identify the biotinylation targets of ajoene, it is not able to identify the specific cysteine residue involved. Where more than one cysteine is involved, it is likely that biotin-ajoene **40** *S*-thiolated these redox-active sites (also based on the 91% overlap between the ajoene interactome and the iCysMod database). To probe this further, we investigated whether there was an enrichment of proteins with these four redox-sites within the biotin-ajoene interactome. **Figure 5.27** compares the relative distribution of *S*-nitrosylation, *S*-sulfenylation, *S*-sulfhydration and *S*-glutathionylation sites across proteins in our dataset compared to that of the iCysMod dataset for the human cysteine proteome. The percentage value in the histogram represents the ratio of proteins containing the given PCM sites, to the total number of proteins in the dataset. Note that one protein may be susceptible to more than one PCM at a different site and that the same site may also be susceptible to more than one PCM event.

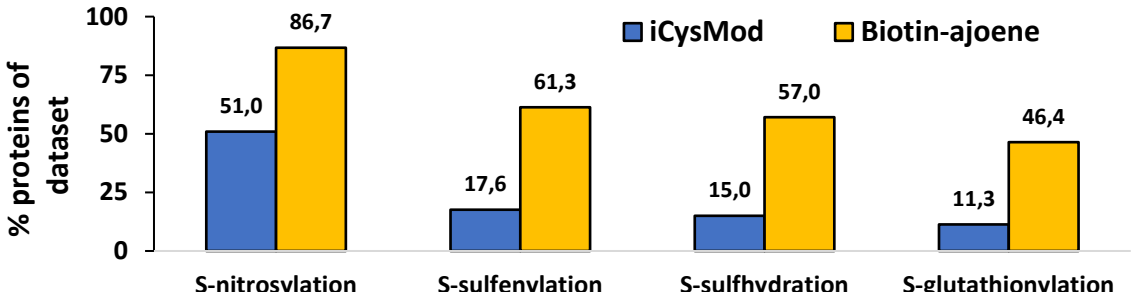

Figure 5.27: Comparison of the distribution of PCM sites across the probe-interactome and the iCysMod database for the human proteome.

It is remarkable that 51% of proteins in the iCysMod database contain at least one cysteine residue that is susceptible to *S*-nitrosylation. For the protein targets enriched by the probe, this figure is nearly twice as high (87%). For *S*-sulfenylation, *S*-sulfhydration and *S*-glutathionylation, it appears that our dataset has four times as many proteins containing at least one site for each of these PCM events than the iCysMod database. This finding suggested that these redox-regulatory PCM events equate well in electrophilicity terms to that of *S*-thiolation by ajoene. In **Chapter 2,** it was discussed that cysteine ligandability contributed the most to ajoene's selectivity for *S*-thiolysis exchanges on protein targets inside a physiological matrix, which was proposed as its central mechanism of action. As a result, ajoene's bioactivity is dictated primarily by two physicochemical features of its targets, namely the inherent reactivity of the protein thiol(s), defined by its pK_a and nucleophilicity,[413] and the thiol's amino acid microenvironment, which determines its solvent accessibility, surface exposure and charge state.[352,410] These two factors similarly apply to redox PCM events (i.e. -SOH, -SNO, -SSH or -SSG), wherein cysteine ligandability becomes synonymous with cysteine functionality in the redox-proteome.[352,413] Redox systems, mediating stress responses, antioxidant activity and redox homeostasis, are regulatory networks where PCM events act as signal transducers and their targets (PCM sites) which serve as allosteric "switches" on proteins. Thus, it is plausible that the *S*-thioallylation of redox-regulatory cysteine sites can modulate and/or disrupt the activity of redox systems. Owing to the ubiquitous nature and biological significance of redox-regulatory events in the proteome,[60] our finding that ajoene *S*-thiolysis shows selectivity towards redox-PCM sites is suggestive of an association with its anticancer effects downstream.

5.7.1.1 Biotin-Ajoene Targets: Enriched Proteins Versus Number of Known PCM Sites

It was envisaged that a protein would have a higher likelihood of being detected by the probe if it contains more than one ligandable cysteine residue.[423] To test this we used the iCysMod database to identify the number of PCM events associated with each protein in the biotin-ajoene interactome. This distribution is shown in **Figure 5.28**.

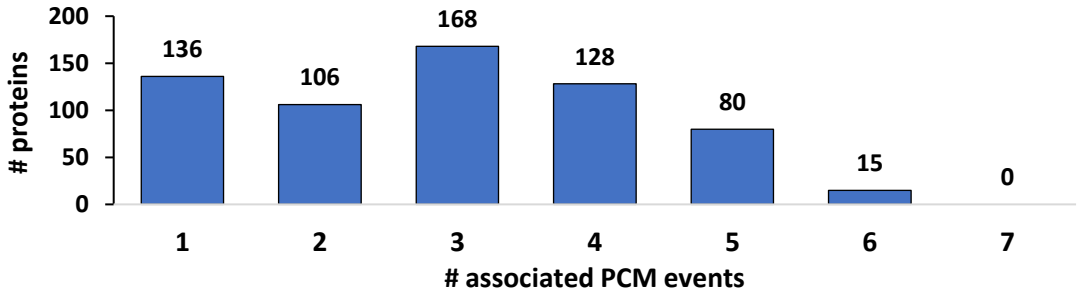

Figure 5.28: Frequency distribution of the number of PCM events associated with the protein targets of biotin-ajoene, 40.
Based on the number of PCM events reported by iCysMod database.[418]

It was found that more than 60% of the biotin-ajoene targets can be modified by 3 or more types of known PCMs. Interestingly, none of the targets were susceptible to all 7 PCMs reported by the iCysMod database. A manual inspection of the data showed that the co-occurrence of PCM events at several cysteine residues was common. In this regard, we took a closer look at the 15 protein targets susceptible to 6 PCM events. **Table 5.7** (below) lists these proteins and their number of modifiable cysteine residues (PCM sites).

Seven proteins (RPLP0, RPSA, RPL12, ATP1A2, PPIA, CAP1, TPI1) contained fewer cysteine residues (<6) than PCM events associated with it, indicating that these sites were highly ligandable and redox functional. Interestingly, there were also 7 proteins that had more cysteine sites (>6) than PCM events associated with them. The most pronounced example is Filamin-A, which is an abundant 280-kD protein that crosslinks actin filaments.[424] Filamin-A contains 24 cysteines located within 24 internal sequence repeat units, each of which are susceptible to up to 6 PCMs.

Protein	Name	Reported PCM events	Reported PCM sites	Protein class
RPLP0	60S acidic ribosomal protein P0	**6**	**2**	ribosomal protein
RPSA	40S ribosomal protein SA	**6**	**2**	ribosomal protein
RPL12	60S ribosomal protein L12	**6**	**3**	ribosomal protein
ATP1A2	Sodium/potassium-transporting ATPase subunit alpha-2	**6**	**4**	primary active transporter
PPIA	Peptidyl-prolyl cis-trans isomerase A	**6**	**4**	chaperone
CAP1	Adenylyl cyclase-associated protein 1	**6**	**5**	actin or actin-binding cytoskeletal protein
TPI1	Triosephosphate isomerase	**6**	**5**	isomerase
ACTG1	Actin, cytoplasmic 2	**6**	**6**	actin and actin related protein
EIF2S3	Eukaryotic translation initiation factor 2 subunit 3	**6**	**8**	translation initiation factor
TCP1	T-complex protein 1 subunit alpha	**6**	**8**	chaperonin
CSE1L	Exportin-2	**6**	**9**	transporter
VCP	Transitional endoplasmic reticulum ATPase	**6**	**10**	ATPase
UBA1	Ubiquitin-like modifier-activating enzyme 1	**6**	**12**	ubiquitin-protein ligase
EEF2	Elongation factor 2	**6**	**15**	translation elongation factor
FLNA	Filamin-A	**6**	**24**	actin-binding protein

Table 5.7: Targets from the biotin-ajoene interactome susceptible to 6 PCM events.

Even though our experimental data did not provide direct evidence as to which cysteine residues had been *S*-thiolated by biotin-ajoene **40**, proteins with multiple PCM sites and/or association with multiple PCM events appeared to be more susceptible to biotinylation, as shown by their enrichment and detection in the pulldown. Indeed, most proteins susceptible to 6 types of PCMs (67%), were shown to be highly significant and enriched in the volcano plot (**Figure 5.29**, top right corner where $p < 0.001$ and > 8-fold enrichment).

These findings indicated that biotin-ajoene **40** *S*-thiolated more than one site in most of the protein targets identified, which likely contributed to their enrichment and detection. This aligns with the proteomic study on allicin by Gruhlke *et al.*, where it was found that the most abundant *S*-thioallylated protein targets were also the most abundant thiol-containing proteins.[86]

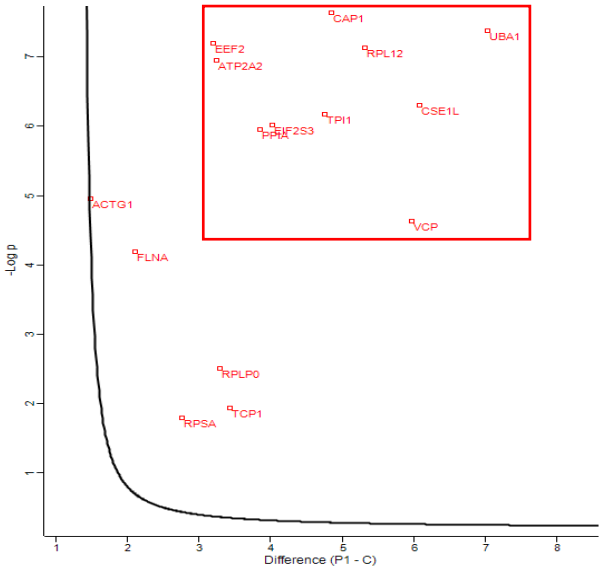

Figure 5.29: Scatterplot of enriched proteins susceptible to 6 PCM events according to the iCysMod database.

5.7.1.2 Biotin-Ajoene Targets: Enriched Proteins Versus Protein Abundance

FLNA and ACTG1 are highly abundant in the human proteome, yet they are less enriched than proteins with lower abundance such as CSE1L and UBA1. This prompted us to examine if protein abundance influenced the enrichment observed in the pull-down. The protein abundance of each protein was obtained as an average of eight human proteome datasets in the PAXdb protein abundance database.[425] The Log of their abundance values were plotted against their log(fold-change difference) to give the scatterplot in **Figure 5.30**. A Pearson correlation analysis was performed using GraphPad Prism 5 to measure any correlation between the two data sets.

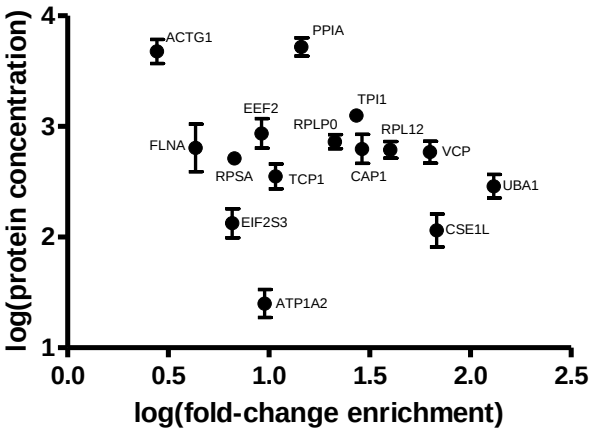

Figure 5.30: Logarithmic scatterplot of proteome abundance versus pulldown-enrichment for proteins in the biotin-ajoene interactome with 6 PCM sites.

The plot showed no relationship between natural protein abundance and its interaction with the probe, with a Pearson correlation coefficient of 0.2003, $p = 0.4742$. Although this does not prove causality, the finding suggests that it is not simply a matter of protein abundance but that biotin-ajoene **40** is specifically targeting proteins with redox-active cysteines (specifically those susceptible to *S*-nitrosylation, *S*-sulfenylation, *S*-sulfhydration and *S*-glutathionylation).

In support of this, a closer inspection of the three targets VCP, CSE1L and UBA1 was performed. These targets are all highly enriched by greater than 60-fold and indeed, they all contain cysteine residues that are highly susceptible to oxidative modifications, and these modifications are important in their biological function.

For example, the ATPase, VCP aka. p97, is a redox sensor involved in the ER stress response in eukaryotic cells.[426,427] VCP is inactivated through the accumulation of misfolded proteins, and oxidative modification of its Cys-522 with exogenous electrophiles is the event that triggers ER stress.[428]

CSE1L, aka. XPO2, is a microtubule-associated protein that is highly expressed in various cancers, where it plays multiple roles in cellular functions, including cell proliferation and migration associated with metastasis.[429–431] CSE1L is proposed as a target for metastatic breast cancer.[432] In a recent study on the thiol-reactive anticancer agent, gambogic acid, it was shown that it covalently modifies two cysteine residues of CSE1L (Cys-842 and Cys-939), leading to disruption of nuclear transportation and cancer cell death.[433]

The main function of ubiquitin (Ub) activating enzyme E1, UBA1, is to promote degradation of aberrant proteins via the 26S proteasome.[434] It was shown that oxidative modification at Cys-278 alters the structural conformation of UBA1, which leads to impaired ubiquitination activity.[435] It has been proposed that this oxidative stress-induced impairment of UBA1 activity, may trigger the accumulation of protein aggregates and the unfolded protein response,[436] which is a pathway that has been implicated in the anticancer activity of ajoene and related garlic OSC.[104,153,263,340]

It was promising to see that VCP, CSE1L and UBA1 are all redox-regulated proteins containing reactive cysteine residues, important in cancer biology.

In summary, the interrogation of the iCysMod database provided support that the biotin probe **40** enriched proteins with several known PCM sites, and that the featured PCM events were predominantly associated with the regulation of redox system involving the

redox signalling molecules GSH, RNS, ROS and RSS. Our findings suggest that the biotin-ajoene **40** targets are reactive cysteines with known redox functions, i.e. ajoene targets redox-regulatory networks, as has been previously observed for ajoene and related OSCs.[78,96,437] In the context of ajoene, the *S*-thioallylation of these sites may therefore constitute a competing, possibly irreversible, PCM event to *S*-nitrosylation, *S*-sulfhydration, *S*-sulfenylation and *S*-glutathionylation. In respect to target enrichments by biotin-ajoene **40**, we found that protein abundance is not a factor that defines which proteins are targeted by ajoene.

5.7.2 Ajoene Targets Cysteine Residues of Significance in Cancer

The functional diversity of cysteine thiols in proteins results in a spectrum of reactivities across the proteome. Apart from their obvious importance as catalytic centres, their redox-active and regulatory (**Figure 5.31**) activities have also been identified as biologically important.[410,413]

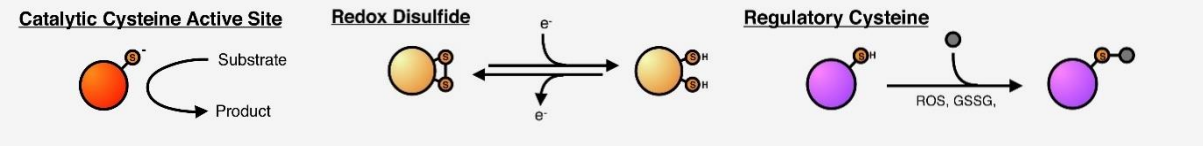

Figure 5.31: Functional classes of reactive cysteine residues.
Taken from Bak *et al.*[410]

The above reactivity profile suggests that the thiophilic ajoene pharmacophore can modulate protein activity allosterically, provided the thiols are sterically accessible and available for modification (i.e. ligandable). In this section, we aimed to determine whether the enriched protein targets of biotin-ajoene **40** included proteins with known allosteric cysteines of importance in cancer. Although the cysteine proteome is known to have an abundance of modifiable sites,[418] the proteome-wide annotation of these sites with respect to their reactivity, and their involvement in biological processes has proved to be challenging. This is due, in part, to the absence of canonical sequence motifs that define cysteine function, and the complexity of modelling interconnected redox systems.[421,438] In this regard, activity-based proteomics has provided an alternative approach to identifying allosteric cysteine, since it allows the identification of functional sites by profiling the reactivity and ligandability of the cysteine proteome using electrophilic ligands and chemical probes.[363,414] This growing body of evidence presented

itself as a fitting experimental reference for us to mine information on the allosteric cysteines within the biotin-ajoene **40** interactome.[417,439]

A literature search identified a study by Weerapana *et al*. in which the intrinsic reactivity of the cysteine proteome of human cancer cell-lines MCF7, MDA-MB-231 and Jurkat cells was profiled using a technique termed isotopic tandem orthogonal proteolysis–activity-based protein profiling (isoTOP-ABPP).[413,440] The technique allows for the mapping and reactivity quantification of nucleophilic cysteine sites on proteins by combining a well-designed multifunctional cysteine-reactive iodoacetamide-alkyne probe, that incorporates "Click"-chemistry, an AP tag, a cleavable linker and isotopically-differentiable labels, with a cunning MS analysis protocol (for more detail please consult the publications by Weerapana *et al.*).[413,414,441] The reactivity of a cysteine is quantified based on its propensity to be modified within a biological system (e.g. a cancer cell) following treatment either at a high or low concentration of the iodoacetamide probe. Analysis of the MS data (described in detail here[363]), generates a numerical R-value that describes the ratio of the ligandability of a cysteine residue at a high versus a low concentration of the probe. In the study of interest to us,[413] cancer cell lysates were treated with a 10-fold difference in probe concentrations to generate R-values that ranged from 1 to 10. Cysteine residues showing the largest difference in site labelling between the high and low concentrations, have R-value close to 10, indicating their low ligandability, while those with moderate ligandability show R-values between 3 and 5. An R-value close to 1 indicates equal labelling at both concentrations which is characteristic for cysteine sites with high ligandability (termed hyper-reactive sites by Weerapana *et al.*).[413]

Cysteine hyper-reactivity is strongly associated with catalytic active sites, but can also feature in 'non-catalytic' protein domains that undergo various forms of oxidative modification (e.g. redox-regulation).[413] Owing to their inherently high nucleophilicity, hyper-reactive cysteine residues generally have restricted exposure to the protein's surface, or are located within substrate-specific cavities of active sites, preventing unwanted oxidative insults.[144] Although functional cysteines may be inherently nucleophilic, it is important to note they may be inaccessible for steric reasons.

Since ligandability is a good predictor of cysteine functionality in proteins, the high ligandability of hyper-reactive sites made them attractive targets for further investigation.

A comparison of our biotin-ajoene **40** dataset to that of Weerapana appeared to be well suited, since: 1) both datasets were generated from the same breast cancer cell line MDA-MB-231; 2) both methods used thiophilic probes, suggesting an overlap of detected protein targets; and 3) reactivity quantification of protein-thiols in the Weerapana dataset could be used to identify functional targets in the ajoene interactome.

5.7.2.1 The S-thiolation of Proteins with Hyper-Reactive Cysteines Contributes to the Anticancer Effects of Ajoene

In the previous section we found that biotin-ajoene **40** enriched several protein targets with redox-reactive cysteines. We thus investigated if proteins with known hyper-reactive cysteines detected by Weerapana (i.e. R-value ≤ 3) were also targeted by biotin-ajoene **40**. The overlay of the biotin-ajoene **40** interactome (yellow) with the Weerapana dataset where R<3 (blue) is shown by the Venn diagram in **Figure 5.32**.

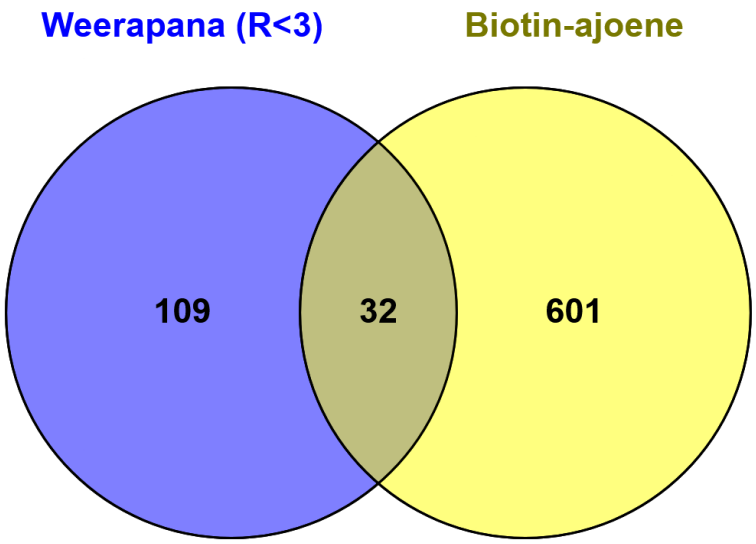

Figure 5.32: Overlap of the biotin-ajoene 40 interactome with proteins with hyper-reactive cysteine residues from the Weerapana dataset.

The overlap between the two data sets revealed that the biotin-ajoene **40** interactome contained only 32 proteins (5% of the ajoene interactome) with known hyper-reactive sites (listed in **Table 7.2** in the **Appendix**). Chemically speaking, the features that make a cysteine residue hyper-reactive also make it sensitive to *S*-thiolation by biotin-ajoene **40**, therefore it was surprising to find that only 5% of our proteins fell within this hyper-reactive data set. Some of the non-overlapping proteins may result from the fact that Weerapana's dataset is derived from a summation of three different cell lines, however

the MDA-MB-231 cells line is included. This very low overlap indicates little similarity between the proteins targeted by biotin-ajoene **40** and iodoacetamide which probably plays into differences in their chemoselectivity. The larger size of biotin-ajoene **40**, compared to the Weerapana probe, was identified as the main causal factor behind their differences in chemoselectivity. Since most hyper-reactive sites may be inaccessible for our probe for steric reason, they are therefore not readily targeted by biotin-ajoene **40** and hence only featured in 5% of our probe's interactome.

The inherent functionality of hyper-reactive cysteine residues suggested that the biological roles of the protein targets identified by the overlap of the two datasets required examination. Using the enrichment scores in our dataset, we set a cut-off at 20-fold enrichment to narrow the list down to 9 protein targets that fit the criteria of cysteine hyper-reactivity and show significant interactions with biotin-ajoene **40**. Their entries in the iCysMod database were examined to determine the presence of any additional PCM sites. **Table 5.8** lists these protein targets, with their enrichment score, R-value and the location of their hyper-reactive site as well as the number of additional, "non-hyper-reactive" PCM sites they contain.

Protein	Name	Protein class	Fold-enrichment	R-value	Other PCM sites
ACAT1	Acetyl-CoA acetyltransferase, mitochondrial	Acyltransferase	21.3	1.06 (Cys-126)	4
CAPN2	Calpain-2 catalytic subunit	Cysteine protease	34.1	1.50 (Cys-640)	9
EPRS	Bifunctional glutamate/proline-tRNA ligase	Aminoacyl-tRNA synthetase	33.6	2.52 (Cys-1301)	20
GSTP1*	Glutathione *S*-transferase P	Transferase	22.2	2.38 (Cys-48)	2
IDH1	Isocitrate dehydrogenase [NADP] cytoplasmic	Dehydrogenase	28.4	1.37 (Cys-269)	4
PFKP*	ATP-dependent 6-phosphofructokinase, platelet type	Carbohydrate kinase	62.6	2.18 (Cys-179)	6
PRMT1*	Protein arginine N-methyltransferase 1	Protein modifying enzyme	47.5	1.92 (Cys-119)	6
RPS5*	40S ribosomal protein S5	Ribosomal protein	31.7	1.63 (Cys-66)	2
TXN*	Thioredoxin	Oxidoreductase	29.5	1.05 (Cys-32/35)	3

Table 5.8: Highly enriched target proteins of biotin-ajoene 40 that contain hyper-reactive cysteine residues.
* = S-thioallylation targets of allicin.[86]

All 9 proteins were found to contain at least two additional PCM sites which corroborated the previously identified trend that a high number of PCM sites result in enrichment by biotin-ajoene **40**. Although our ABPP protocol could not demonstrate which cysteines were modified in the protein, it is likely that hyper-reactive cysteine, owing to their functional significance, are preferentially *S*-thiolated by biotin-ajoene **40** in the respective proteins. As seen in this example of the 40s ribosomal protein S5 (RPS5), which has 3 known PCM sites. Cys-66 is its hyper-reactive residue, which is also the most surface exposed and the only one susceptible to S-sulfenylation. Although the functional roles of cysteine sites on ribosomal proteins are not fully understood, it has recently been proposed that redox-mediated modifications of ribosomal subunits at their PCM sites may attenuate protein synthesis in response to oxidative stress.[442,443] Interestingly, RPS5 is also a *S*-thioallylation target for allicin.[86] Considering the redox-regulatory role of this site, it is possible that the *S*-thioallylation of Cys-66 represents a mechanism by which ajoene, and allicin, may modulate the function of RPS5.

Since the *S*-thiolation of hyper-reactive sites may be of similar functional relevance for the other 8 proteins of **Table 5.8**, we interrogated their biological significance in the context of cancer biology.

Acetyl-CoA acetyltransferase (ACAT1), which is highly expressed in oestrogen receptor negative basal-like breast cancer cells, is being investigated as anticancer therapeutic target, for its role in driving cancer proliferation.[444,445] Both calpain-2 catalytic subunit (CAPN2)[446] and thioredoxin (TXN)[447] have been identified as cysteine-modifiable targets for cancer therapeutic development. The bifunctional glutamate/proline-tRNA ligase (EPRS) is a redox-regulated mediator of the translation of vascular endothelial growth factor A (VEGFA), which is an angiogenic factor associated with the tumorigenesis in MDA-MB-231 cells.[448] Glutathione *S*-transferase P (GSTP1), has been identified as a driver of triple-negative breast cancer cell metabolism and pathogenicity,[449] and its inhibition by *S*-thioallylation contributes to the pro-apoptotic mechanism of several garlic OSCs.[450] Isocitrate dehydrogenase (IDH1) is a metabolic enzyme linked to cancer survival and drug resistance that can be inhibited through the covalent modification of its hyper-reactive Cys-269.[417] Furthermore, IDH1 is mutated in several cancers, where it gains neomorphic catalytic activity by acquiring additional cysteine residues, which are being investigated for novel therapeutic development.[451] PFKP is a rate-determining

enzyme in glycolysis and has been identified as a mediator of cancer cell metabolism, where its upregulation is a feature of malignant tumours.[452,453] And lastly, PRMT1 is an enzyme that is overexpressed in human breast cancer and elevated PRMT1 levels have been correlated to cancer malignancy.[454] It has been shown that the inhibition of PRMT1 significantly impedes the growth of cancer cells from patients with triple-negative breast cancer.[455] Interestingly, the 9 protein targets were found to be functionally significant in cancer biology. Literature provides support that *S*-thiolation of their hyper-reactive sites (e.g. TXN, IDH1 and GSTP1) can modulate the protein's activity, therefore, taken together, this finding suggests that these targets are contributors to the anticancer effects of ajoene and indicates the involvement of the *S*-thiolation of their hyperreactive sites.

5.7.2.2 Biotin-Ajoene S-Thiolates Ligandable Sites in Several Cancer-Associated Proteins

Since steric restrictions of hyperreactive sites make them less ligandable to our probe, we set out to identify more accessible, ligandable sites that are targeted by biotin-ajoene **40** and examine their relevance in cancer. We compared our dataset to the entire dataset of Weerapana, including the non-hyper-reactive sites, and the dataset of Gruhlke since both of these datasets were obtained from cancer cell proteomes and specifically report on ligandability of protein thiols by an electrophile, iodoacetamide-alkyne (Weerapana) and the related garlic OSC allicin (Gruhlke).[86,413] The Venn diagram in **Figure 5.33** illustrates that there was a notable overlap between the three datasets and that some of the proteins (88) were ligandable to all three of the cysteine-reactive electrophiles: iodoacetamide-alkyne, allicin and biotin-ajoene.

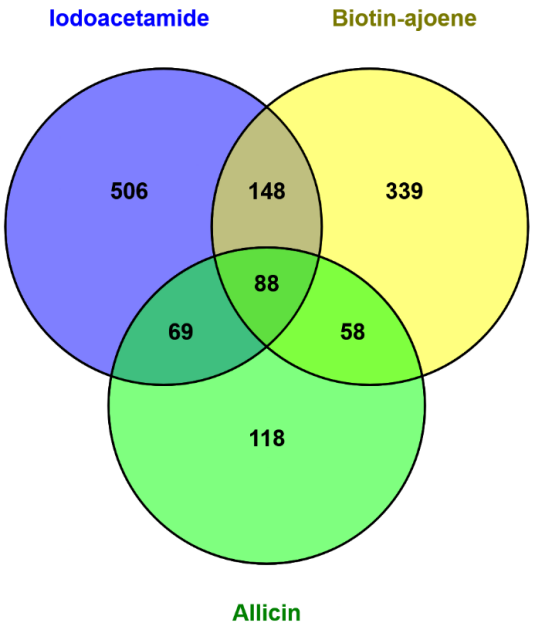

Figure 5.33: Comparison of datasets between the biotin-ajoene 40 interactome in MDA-MB-231, the allicin proteome in Jurkat cells and the iodoacetamide-reactive cysteine residues in combined MCF7, MDA-MB-231 and Jurkat cells.

Overall biotin-ajoene **40** shared 46% of its protein targets with the other two datasets, in which 23% and 37% of its targets were shared with the allicin and the iodoacetamide dataset, respectively. These overlaps, particularly the 13% (88 proteins) shared amongst all three datasets, indicated that a mechanistic commonality exists between the three small molecule electrophiles and that these proteins contain cysteine sites which are ligandable (i.e. reactive and accessible) by all three probes. The 88 common proteins between all three datasets were classified according to their protein classes to examine their functional roles. The pie-chart in **Fig 5.34** shows the distribution of protein classes for these 88 proteins, which are also listed in **Table 7.3** in the **Appendix.**

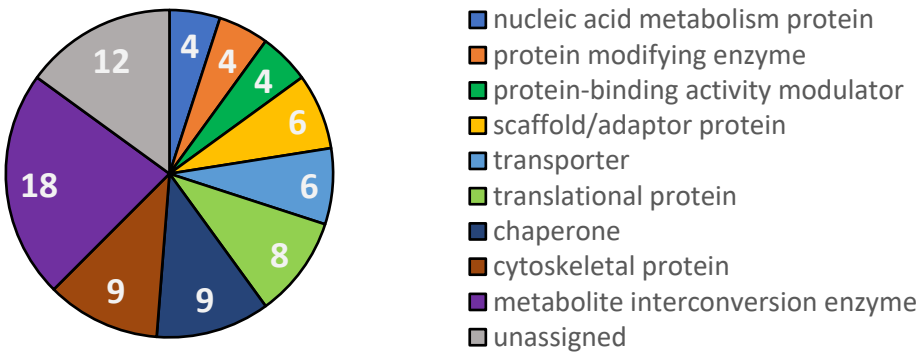

Figure 5.34: The 88 proteins identified in the overlapping data sets of Weerapana, Gruhlke and this study, classified according to protein class.

The largest clusters of protein classes were assigned to metabolite interconversion enzymes (22%), cytoskeletal proteins (10%), chaperones (10%) and translational proteins (9%). **Table 5.9** lists the protein targets associated with each of the four major clusters and includes their assigned protein function.

Protein Class	Related targets	Most represented protein function (#)
Metabolite interconversion enzymes	TKT, PFKP, HRPT1, GSTP1, PRDX1, PRDX3, ALDH18A1, IMPDH2, GAPDH, LDHA, PHGDH, TXN, HSD17B10, MIF, ALDOA, GMPS, TPI1, PPA1	Oxidoreductases (9), transferases (4) and lyases (2)
Cytoskeletal proteins	TUB1AC, NUDC, CCN2, CFL1, DSTN, CAPZB, WDR1, CAP1, SETP7,	Microtubule (2) and actin-binding proteins (6)
Chaperones	PPIA, FKBP4, PTGES3, NASP, HSP90AB1, TCP1, CCT4, CCT5, CCT8	Heat shock proteins (5) and isomerases (2)
Translational proteins	STRAP, EIF3C, EIF4G1, EIF3B, EEF2, EEF1A1, RPLP0, RPS5	Translation factors (6) and ribosomal proteins (2)

Table 5.9: Functional classification of protein clusters containing PCM sites with high ligandability.

These protein clusters are primarily associated with molecular functions such as cellular metabolism, protein biogenesis and microfilament-mediated processes. It was noteworthy that most of these proteins with high cysteine ligandability are linked to molecular functions critical for malignant transformation and progression. All of the identified proteins are known to have PCM sites which are susceptible to redox-modulation, as shown for glyceraldehyde 3-phosphate dehydrogenase (GAPDH),[456] fructose-bisphosphate aldolase A (ALDOA)[457] and transketolase (TKT).[458]

Strategies that target metabolic enzymes, particularly those involved in glycolysis are important in cancer where they have been shown to attenuate energy metabolism, leading to growth arrest and sensitisation to chemotherapeutic agents.[459,460] In addition, the inhibition of translational proteins and chaperones have been shown to attenuate cancer cell development,[461,462] as have agents that target microfilament-dependent processes that block the cell cycle progression and decrease the metastatic potential of cancers.[463,464] The involvement of ajoene in all of these functional classes is supported as being relevant to cancer.

5.7.2.3 Factors Affecting the Chemoselectivity of Cysteine-Reactive Electrophiles

While there was a 46% overlap of the ajoene interactome with that of Weerpana and Gruhlke, there were 54% of proteins that were unique to the ajoene interactome. These differences may be attributed to differences in the chemoselectivity of the electrophile probe used. Consideration of thermodynamic and kinetic factors, as well as differing experimental conditions may account for the target-selectivity. Biotin-ajoene **40**, allicin and iodoacetamide-alkyne all participate in a nucleophilic substitution reaction as a common mechanism of cysteine modification; however, closer inspection of their electrophilic group indicates a considerable difference in reactivities Since the ΔG for substitutions is primarily enthalpy-driven, the energetic differences in bond strength and the stability of charge transfer govern the chemoselectivities in reactivity terms. When comparing the bond enthalpies, the iodoacetamide comes out in front since *S*-alkylations (ΔH = -20 kJ/mol for C-I → C-S) are more exothermic than *S*-thiolations (no net change in ΔH). Additionally, the transfer of the negative charge from the cysteine thiolate onto the iodide LG of the iodoacetamide makes little energetic difference. For allicin, the sulfenate oxygen of its LG stabilises the negative charge of the thiolate during the transfer, which makes its *S*-thiolysis thermodynamically more favourable than the ajoene case (in which the charge delocalises only into a double bond). Taken together, this points towards the vinyl disulfide of biotin-ajoene **40** being the least reactive of the three electrophiles, with a reactivity order of: iodoacetamide > thiosulfinate > vinyl disulfide. Regarding the chemoselectivity argument, an increased reactivity makes a reactive group less selective overall, since it can interact with a wider range of biological cysteines. This may explain why the Weerapana dataset contains targets with a wide variety of cysteine reactivities and why iodoacetamide is the preferred reagent for the *S*-alkylation of reduced proteins samples for proteomic experiments (*vide supra*). Furthermore, the reactivity difference between vinyl disulfide and thiosulfinate provides an explanation as to why the depletion of physiological GSH is more strongly associated with allicin than with ajoene.[79]

The kinetic factor driving the chemoselectivity of cysteine-reactive electrophiles towards protein targets relates primarily to their accessibility towards cysteine residues. The accessibility of a target site depends on a favourable biophysical interaction between the probing molecule and the cysteine residue with respect to the latter's local microenvironment and distribution in the proteome.[346,417] Apart from the steric bulk of the electrophile, its access to a cysteine site is determined by its pharmacokinetic

parameters such as topological polar surface area (TPSA) and lipophilicity (e.g. partition coefficient, logP), which define membrane permeability and target binding affinity, respectively. With respect to its predicted logP, biotin-ajoene **40** is twice as lipophilic as allicin and iodoacetamide-alkyne (3.11 versus 1.61 and 1.88, respectively). This suggests that biotin-ajoene **40** favours interactions within hydrophobic subcellular regions, whereas allicin and iodoacetamide-alkyne would prefer hydrophilic or amphiphilic domains. Since cysteine residues are mostly found in hydrophobic regions of proteins,[262] the lipophilic nature of biotin-ajoene **40** may have conferred a chemoselectivity towards cysteine residues in relatively non-polar domains. This corroborates our SAR findings in **Chapter 2** and **Chapter 3**, in which the cancer-cell cytotoxicity, i.e. *S*-thiolysis activity, of an ajoene analogue correlated to its lipophilicity. The TPSA of biotin-ajoene **40** was found to be 4-fold, and 8-fold larger than allicin and iodoacetamide-alkyne, respectively (250 $Å^2$ versus 62 $Å^2$ and 29 $Å^2$, respectively). Taking into consideration that the upper limit of a suitable TPSA value for a pharmaceutical drug is 140 $Å^2$,[465] the TPSA value for biotin-ajoene **40** pointed towards it having a significantly lower membrane permeability than the other two compounds, which would effectively impair its entry into the cells, as well as intracellular organelles.[466] Taken together, it appears that biotin-ajoene's shape and size represents the main causal factor behind its chemoselectivity. It was acknowledged that its large size limited its membrane permeability and hindered its access to cysteines within sterically restricted domains, such as catalytic cysteine within active sites.[194] Since redox-regulatory functions are inherently tied to surface-exposed sites,[467,468] the lipophilicity of biotin-ajoene **40** and its steric limitations may explain the prevalence of proteins with redox-active cysteines in its interactome.

Whilst these thermodynamic and kinetic features highlighted differences in chemoselectivity, the experimental conditions also contributed to determining which proteins ultimate were labelled in the three datasets. **Table 5.10** summarises the experimental conditions that led to each dataset.

	Biotin-ajoene 40	Allicin	Iodoacetamide-alkyne
Cell line(s)	MDA-MB-231	Jurkat	MDA-MB-231, MCF7 and Jurkat (lysate)
Probe concentration (µM)	40	100	10 – 100
Treatment time	24 h	10 min	1 h
Protein targets identified	**633**	**333**	**811**

Table 5.10: Comparison of the cysteine labelling conditions between Biotin-ajoene 40, the Gruhlke and Weerapana datasets.

Apart from differences in cell lines, the most striking difference is that cysteine labelling in the Weerapana study was performed in lysate, whereas biotin-ajoene **40** and allicin were applied to whole cells. Cell lysates provide a probe with better access to the entire proteome, whereas intact cells require a probe to permeate the cell membrane and organelles to reach their protein targets. It is also to note that the intracellular environment is buffered and reducing whereas lysate is exposed to the oxidising atmosphere. According to the order of reactivity, one might have expected more overlap between iodoacetamide and allicin than between iodoacetamide and biotin-ajoene **40** (due to the greater reactivity difference); however, it is apparent that the treatment of lysate and intact cells may have contributed to this.

The probe concentrations and incubation times were similarly variable due to key differences in study objectives. Since we wanted to investigate the protein targets associated with ajoene's cytotoxic effects, the biotin-ajoene **40** probe was tested its IC_{50} for 24 hours. Weerapana *et al.* conducted a profiling of cysteine reactivities which required the testing of its probe in a range of concentrations. Lastly, the study on allicin by Gruhlke *et al.* used a high concentration likely to accommodate a shorter period of incubation and the known chemical instability of allicin. The total number of proteins identified in each dataset may reflect the reactivity differences between the probes when the incubation times are considered. Although all probes were incubated at a similar concentration, iodoacetamide labelled more protein targets in one hour than biotin-ajoene **40** in 24 hours. Allicin, which was also applied to whole cells, was able to label half as many targets than biotin-ajoene **40** in 10 minutes.

Several similarities can be drawn between the two garlic OSCs, ajoene and allicin, which both cause widespread *S*-thioallylation of redox-sensitive proteins and trigger strong oxidative, sulfur and heat stress responses.[86,153,263,340,364] Our findings for ajoene indicated that it is targeting proteins that are highly reactive towards sites prone to *S*-nitrosylation, *S*-sulfenylation, *S*-sulfhydration and *S*-glutathionylation, meaning that ajoene *S*-thioallylation favours proteins that are rich in PCM sites. Despite allicin and ajoene sharing a common thiolysis exchange mechanism (protein *S*-thioallylation) the differences in their protein targets highlights how the different chemistries of their pharmacophores gives rise to distinct anticancer modes of action and metabolic profiles (discussed in **Chapter 3**). Here, it is important to consider that some of the differences between the allicin and biotin-ajoene dataset might be attributed to the larger size of our probe compared to ajoene.

In this section, it was illustrated that biotin-ajoene **40** targets proteins that can be modulated by PCM events. By comparing its interactome to two other datasets reporting on cysteines ligandability within cancer proteomes, the overlaps revealed several proteins that are important in cancer biology. We also elucidated ajoene's chemoselectivity for redox-reactive cysteines. Although there were dissimilarities between the datasets, we identified many new protein targets that likely contribute to ajoene's anticancer activity. In the next section, the pathway analysis of the biotin-ajoene **40** interactome will be discussed.

5.7.3 Pathway Analysis of the Ajoene Interactome

To interpret the probe's interactome in the broader context of cellular functions, the list of its protein targets was mapped against the reference authorative pathways in KEGG and annotated with KEGG orthology (KO) identifiers (termed K number). The assigned K number provides information about the protein's function and location (termed pathway node) within an organism-specific version of pathways in the KEGG database.[469,470] The database itself categorises its pathways into three hierarchical levels (**Figure 5.35**) being: biological systems (KO Level 1), functional networks (KO Level 2) and biochemical pathways (KO Level 3). By assigning the KO indentifiers to the ajoene interactomewe were able to group them within the hierarchical level of the KEGG database to gain insights into the biological pathways involved.

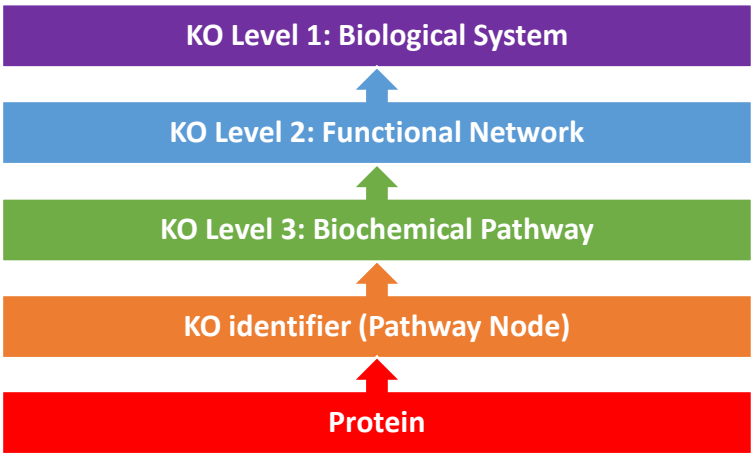

Figure 5.35: Hierarchical levels of the KEGG database.

The enrichment score (fold-change difference) of the proteins generated in Perseus was used to create proteome abundance treemaps with Proteomaps.[471] These are Voronoi diagrams which combine KO identifiers with the enrichment score. Each polygon represents the KO hierarchies, where all functionally related proteins are arranged in common regions that are marked by the same shade of colour, hence the polygon area is proportional to the enrichment score of the protein. **Figure 5.36** (below) shows the abundance treemaps of the biotin-ajoene **40** at the KO levels 1-3 as well as the protein level.

The KEGG analysis highlighted that protein enrichment had occurred most abundantly in the biological systems (KO Level 1) relating to genetic information processing, cellular processes and metabolism. The functional categories (KO Level 2) most represented were: 1) Translation and folding, sorting and degradation for genetic information processing; 2) Cell growth and death, cellular community, cytoskeleton and vesicular transport for cellular processes; and 3) Biosynthesis and central carbon metabolism. The KEGG analysis also showed how ajoene appears to target biochemical pathways that align with its reported anticancer modes of action; namely, its antiproliferative, proapoptotic and antimetastatic activities.

A) KO Level 1: **Biological systems**

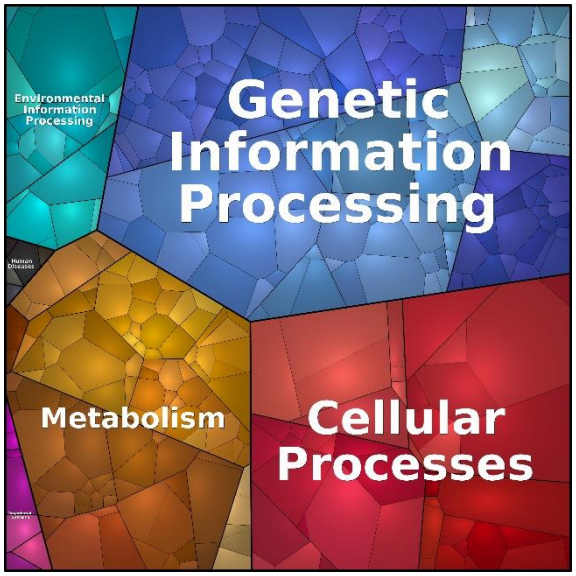

B) KO Level 2: **Functional networks**

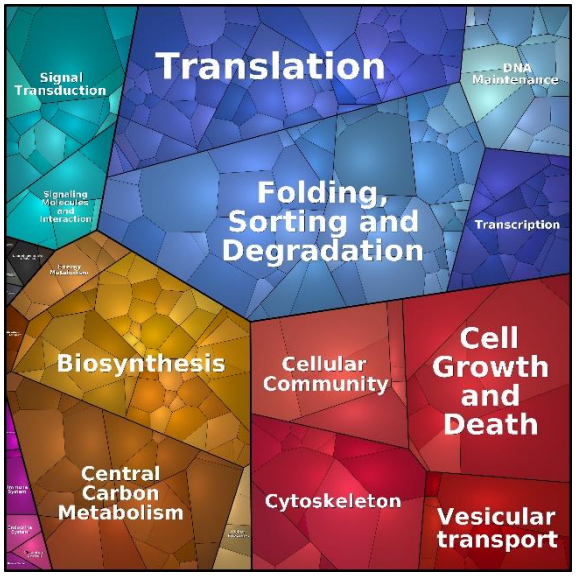

C) KO Level 3: **Biochemical pathways**

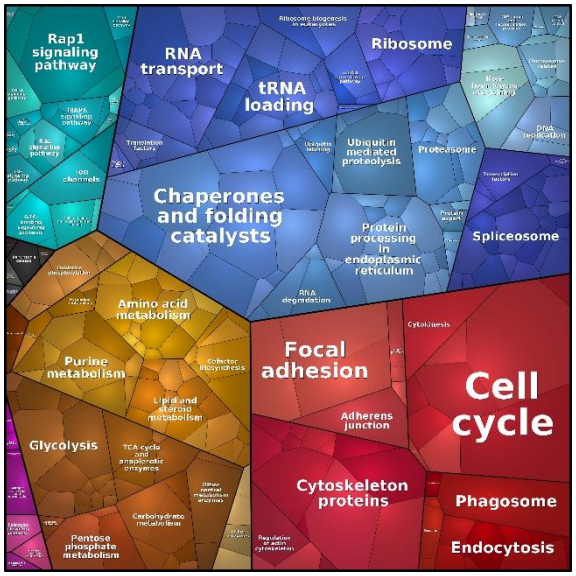

D) Protein level

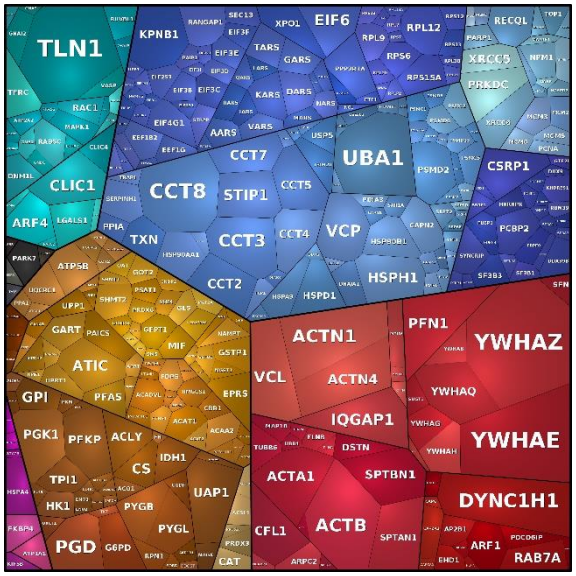

Figure 5.36: Abundance treemap diagrams of the biotin-ajoene 40 interactome in MDA-MB-231 cancer cells displaying the KO levels 1 - 3 and the protein level.
A,B,C: KO levels 1,2,3 resp.; D: Protein level.

5.7.3.1 Interactions with the Metabolic System

It was found in **section 7.3.1** and **7.3.2** that biotin-ajoene **40** *S*-thiolates redox-active cysteine residues in a number of metabolic enzymes, including PFKP, ALDOA, TKT, GAPDH, ACAT1, IDH1 and TPI1. The KEGG analysis revealed that approximately a quarter of all *S*-thiolation targets of biotin-ajoene **40** are metabolic enzymes, where the most enriched are associated with glycolysis, pentose phosphate metabolism, purine metabolism and cofactor biosynthesis (See **Figure 7.1** and **7.2** in the **Appendix**).

Glycolysis and pentose phosphate pathways: A total of 22 enzymes in glycolysis and pentose phosphate pathways were identified as *S*-thiolation targets of ajoene, of which PFKP, TPI1, Phosphoglycerate kinase 1 (PGK1), Glucose-6-phosphate isomerase (GPI), 6-phosphogluconate dehydrogenase (PGD) and Glucose-6-phosphate 1-dehydrogenase (G6PD) were each more than 20-fold enriched. Relative to normal cells, cancer cells upregulate glycolysis and pentose cycle activity (termed the Warburg effect[472]) as a means to increase energy production and anabolic growth, and to generate more reducing equivalents of NADPH for the protection against increased metabolic production of ROS.[473–475] The inhibition of enzymes in the glycolysis and the pentose cycle pathways can induce oxidative stress and cytotoxicity in cancer cells.[476–478] It has been reported that PCMs on glycolytic enzymes inhibit metabolic activity and block the entry of glucose equivalents into the pentose phosphate pathway.[479] It is reasonable that protein *S*-thioallylations in these pathways by ajoene may similarly produce ROS-mediated cytotoxicity in MDA-MB-231 cancer cells as reported in the literature.[115,480]

Sialic acid biosynthesis pathway: The role of UDP-N-acetylhexosamine pyrophosphorylase (UAP1) within sialic acid metabolism and its identification as a highly enriched *S*-thiolation target indicates another interesting pathway that may be relevant to ajoene's anticancer effects. This pathway controls the glycosylation of proteins with sialic acid, aka. sialylation, which is a cell surface PTM that mediates cell adhesion, immune recognition and signal transduction.[481] Upregulated sialic acid enzyme activity and the aberrant sialylation on the surfaces of several cancer types has been implicated with tumour growth, apoptotic escape, metastasis, and resistance to chemotherapy. The countering of the metastatic potential and drug resistance, particularly for untreatable cancer types, has stimulated research into targeting the sialic acid biosynthesis pathway.[482] With the discovery that UAP1 was able to achieve a reduction in proliferation, invasion, colony formation and migration capability of breast and bladder cancer cell lines, it was classified as a promising therapeutic target.[483,484] Apart from a 67-fold enrichment from probe-target interactions, UAP1 contains 4 modifiable cysteine residues in its sequence where one of them is located within its substrate binding site and appears to play a role in the non-covalent docking of its substrates.[485]

Purine metabolism: There were 3 highly enriched (>20 fold) targets of biotin-ajoene **40** associated with purine metabolism that participate in the inosine monophosphate biosynthesis pathway, namely: IMP cyclohydrolase (ATIC), phosphoribosylformyl-glycinamidine synthase (PFAS) and phosphoribosylamine-glycine ligase (GART). Purines and their derivatives are the scaffold substrates of nucleic acids, coenzymes, allosteric modulators and energy intermediates for cells. Cancer cells enhance enzymes for *de novo* purine biosynthesis as purine nucleotides are fundamental and necessary for tumour cell proliferation and survival, which makes the inhibition of this pathways an attractive strategy for cancer therapy.[486] The targeting of inosine biosynthesis is particularly suited, since inosine is a central intermediate within the purine biosynthetic and degradation pathway, and acts as a major modulator of translational efficiency and accuracy of mRNA and tRNA. Inosine is an absolute requirement for protein translation by tRNA. Studies have shown that the disruption of purine enzymes in cancer cells alters their cell cycle and enhances their sensitivity to chemotherapeutic agents. In this regard, the modification of the cysteine residue in the active site of ATIC, inhibits its activity and shifts the cell cycle into the G_2/M phase.[487,488] For GART and PFAS, it was found that both contain 15 cysteine residues. All three enzymes represent suitable *S*-thiolation targets which may contribute to the antiproliferative effects of ajoene.

Within the system of metabolism, several protein targets of ajoene have been identified as key regulators of glycolysis, the pentose phosphate pathway, the sialic acid biosynthesis pathway and purine metabolism. The relevance of these pathways to the survival and proliferation of cancer cells is suggestive of their involvement in the anticancer effects of ajoene.

5.7.3.2 Interactions with Cellular Processes

Cell cycle: Ajoene and its related garlic OSC's have been shown to inhibit cell proliferation by inducing cell cycle arrest at the G_2/M phase checkpoint.[26,83,167,336,489] It was found that biotin-ajoene **40** enriched two important regulators of this process, namely cyclin-dependent kinase 1 (CDK1) and 7, out of a total of 9, members of the 14-3-3 protein family (See **Figure 7.3** in the **Appendix**). CDK1 is activated by p53 in response to DNA damage and acts as a negative regulator of the cell cycle, triggering cell cycle arrest. Interestingly, CDK1 contains a single, ligandable cysteine residue (Cys-119) near its active site which

is being investigated as an allosteric site for CDK1 inhibition.[490] In this regard, it was demonstrated that the oxidative modification of Cys-119 decreases the association of CDK1 to Cyclin B, thus prolonging a G_2/M arrest.[491] The importance of CDK1 at the G_2/M cell cycle checkpoint as well as the ligandability and functionality of its Cys-119, support its involvement in the antiproliferative activity of ajoene.

The 14-3-3 protein family plays an important role in a wide range of cellular processes including signal transduction, apoptosis, cell cycle progression, and checkpoint activation within all eukaryotic cells. 14-3-3 proteins are also p53-mediated and negatively regulate the cell cycle to ensure that mitosis is not prematurely activated before the completion of DNA replication.[492] YWHAZ and YWHAE were the two most enriched protein targets in the biotin-ajoene **40** interactome, being 244-fold and 185-fold enriched respectively. YWHAZ contains 1 cysteine residue which is reportedly *S*-glutathionylated in response to metabolic stress, resulting in caspase-dependent degradation of YWHAZ.[493] According to the iCysMod database, YWHAE contains 1 cysteine, which is susceptible to *S*-nitrosylation and *S*-glutathionylation. YWHAZ and YWHAE are overexpressed in several cancers, including breast cancer,[494] and the increased expression of YWHAZ and YWHAQ in patients undergoing chemotherapy has been associated with a poor clinical outcome.[495–497] 14-3-3 protein interactions regulate several processes of relevance to cancer biology, including proliferation, apoptosis and mitogenic signalling.[498] Modulation of 14-3-3 protein activity can induce G_2/M cell cycle arrest and a global inhibition of 14-3-3 functions induces apoptosis, which makes them valuable targets for anticancer therapeutics. In A549 lung cancer cells, which highly express YWHAZ, the depletion of YWHAZ inhibits the anchorage-independent growth and triggers apoptosis via the mitochondrial pathway.[499] The 14-3-3 proteins, particularly the highly enriched YWHAZ, YWHAE and YWHAQ, are attractive anticancer targets.

Cytoskeleton: Our pulldown identified several cytoskeletal and cytoskeleton-binding protein targets, where the most enriched targets included talin-1 (TLN1, 162-fold), cytoplasmic dynein-1 (DYNC1H1, 132-fold), α-actinin-1 (ACTN1, 126-fold), cytoplasmic actin (ACTB, 120-fold), α-actinin-4 (ACTN4, 95-fold), profilin-1 (PFN1), vinculin (VCL, 86-fold), actin (ACTA1, 77-fold), α/β-chain of spectrin (SPTAN1 & SPTBN1, both 69-fold) and α/β-tubulin (TUBA and TUBB, 34-fold and 19-fold). To date, several of these cytoskeletal proteins have been described as *S*-thioallylation targets of garlic OSCs. The interaction of

ajoene and DATS with microtubule-associated proteins, including TUBA and TUBB, were shown to cause the disassembly of the microtubule network which has been attributed to their apoptotic and antimetastatic effects in cancer cells.[82,115,116,167] The proteomic studies on allicin's targets in Jurkat cells identified actin, tubulin, plastin, filamin and cofilin as being abundantly *S*-thioallylated,[86] supporting the finding that allicin causes impaired dynamics of the actin cytoskeleton and depolymerisation of the tubulin cytoskeleton.[40] Apart from targeting the microtubule network, ajoene has been shown to have effects on the cytoskeleton functions in cancer cells, leading to reduced cell adhesion,[171,185] as well as the inhibition of invasion and migration (i.e. the inhibition of epithelial-mesenchymal transition).[137] The functional analysis of the *S*-thiolated cytoskeletal targets of biotin-ajoene **40** revealed that 42 proteins were associated with the regulation of the actin cytoskeleton (see **Figure 7.4** in the **Appendix**).

The actin microfilaments in the cytoskeleton are essential for structural integrity of the plasma membrane and essential for the mobility and contraction of cells during cell division. Actin is susceptible to *S*-thiolation, since its five cysteine residues (Cys-374, Cys-272, Cys-285; Cys-217, Cys-257) are highly vulnerable to redox modifications. The most vulnerable is Cys-374, which undergoes many PCM's including *S*-glutathionylation, *S*-sulfenylation and *S*-nitrosylation. *S*-thiolation of Cys-374 is associated with monomer aggregation via disulfide bonds, decreased polymerization rates, increased critical concentrations, and weakening of actin filaments,[500] although modifications at the other cysteine residues are also linked to impaired function. Additionally, the *S*-thiolation of targets involved in focal adhesion and cytokinesis, i.e. actinin, talin, vinculin and profilin, supports a mechanism by which ajoene may alter the structural morphology and cytoplasmic signalling of cancer cells.[501] Mutations and abnormal expression of cytoskeletal and cytoskeletal-associated proteins play an important role in the ability of cancer cells to resist chemotherapy and metastasise.[502] Specifically, the role of actin and its interacting partners represent key signalling pathways and downstream effectors that, through the cytoskeleton, mediate tumour cell migration, invasion and metastasis.[503]

Cell adhesion: In a previous study, we found that ajoene *S*-thiolates intermediate filament protein, vimentin at Cys-328.[137] Although this study did not identify vimentin as a *S*-thiolation target of ajoene, we found Ras GTPase-activating-like protein (IQGAP1), Ras-

related C3 botulinum toxin substrate 1 (RAC1), Ras homolog gene family member A (RHOA) α-catenin (CTNNA1) and casein kinase 2 alpha 1 (CSNK2A1) as protein targets, which are involved in adherens junction formation. Due to its high enrichment (87-fold) and its known role as an oncoprotein, IQGAP1 is of particular interest since it binds directly to β-catenin and E-cadherin.[504,505] The binding of IQGAP1 to β-catenin increases its nuclear localization and promotes the expression of β-catenin's transcriptional targets, driving the disruption of cell-cell adhesion and allowing cancer cells to metastasise.[506] The overexpression of IQGAP1 in MDA-MB-231 cells has been identified as key driver for proliferation and migration,[507] suggesting that the antimetastatic activity of ajoene in MDA-MB-231 cells may be associated with its interaction with IQGAP1. Indeed, this is supported in a recent study by Li *et al.* in which *Z*-ajoene was found to inhibit the growth of colon cancer cells by modulating CSNK2A1 activity and the Wnt/β-catenin signalling pathway.[171]

Within the system of cellular processes, several protein targets of ajoene have been identified as key regulators of the cell cycle at the G_2/M checkpoint. Another important class of protein targets identified include cytoskeletal proteins important in cell adhesion, motility and tissue invasion in cancer.

5.7.3.3 Interaction with the Genetic Information Processing System

The most significant finding of the KEGG analysis was the enrichment of protein targets in the genetic information processing system. Biotin-ajoene appeared to target all major pathways of protein metabolism taking place in the ER, namely protein translation, folding, sorting (quality control) and degradation. **Figure 5.37** shows the KEGG pathway associated with the protein processing in ER, where the biotin-ajoene's **40** targets are highlighted in red.

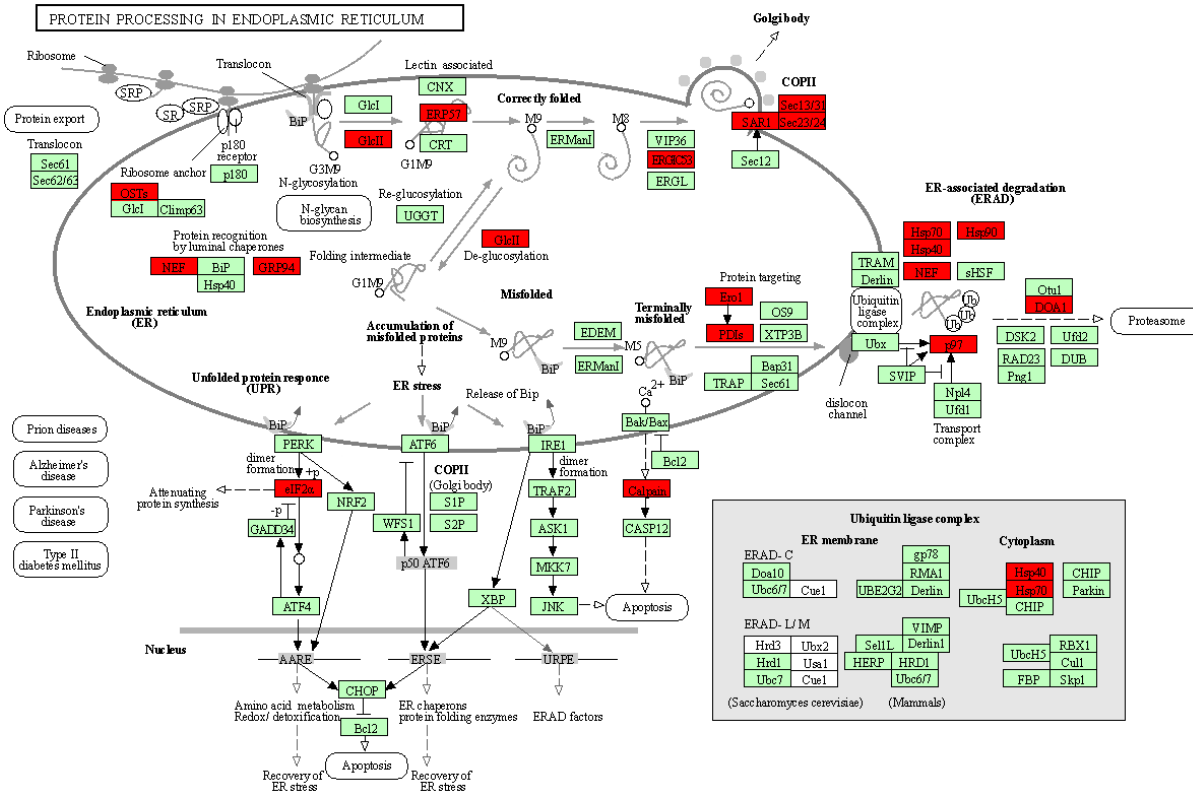

Figure 5.37: Targets of ajoene involved in the protein processing in the ER.
(highlighted in red)

The biotinylation of multiple ER-associated targets supported our previous findings on the ER-localization of our fluorescently-labelled ajoene analogue (DP) in MDA-MB-231 cells.[153] Ajoene was found to *S*-thiolate multiple proteins in the ER, and this was likely to interfere with protein folding, giving rise to misfolded protein aggregates (**Figure 5.4**). This is supported as the ajoene analogue bis-PMB was found to activate the Unfolded Protein Response (UPR) and resulting ER stress-mediated cytotoxicity (via the activation of CHOP/GADD153).[340] In this study, DNA microarray analysis of bis-PMB-treated WHCO1 cancer cells identified pathways involving protein processing in the endoplasmic reticulum (ER) and the unfolded protein response as being the most significantly enriched. Furthermore, it was shown that bis-PMB lead to increased levels of ubiquitinated proteins and inhibited global protein synthesis.

<u>Protein translation:</u> Ajoene appears to have a large effect on protein synthesis with more than 10% of its protein targets being involved in the translation process. Included are the 30 ribosomal subunits (both 40S and 60S – see **Figure 7.5** in the **Appendix**), 7 elongation factors, 19 initiation factors and 16 (of the 20) aminoacyl-tRNA synthases (aka. tRNA-

ligases). The most enriched targets were importin subunit beta-1 (KPNB1, 69-fold enriched, containing 8 PCM sites), eukaryotic translation initiation factor 6 (EIF6; 42-fold enriched; containing 5 PCM sites), 60S ribosomal protein L12 (RPL12; 40-fold enriched; containing 3 highly modifiable PCM sites) and serine/threonine-protein phosphatase 2A 65 kDa regulatory subunit A alpha isoform (PPP2R1A; 40-fold enriched; containing 9 PCM sites). On a side note, it was again observed that the presence of multiple (>>3) PCM sites and/or highly modifiable PCM sites in proteins favoured enrichment by biotin-ajoene **40**. Two interesting findings were made for KPNB1 and EIF6 with respect to cancer. KPNB1 is required for proteostasis maintenance and its inhibition was shown to induce apoptosis in glioblastoma cells through UPR-mediated deregulation of Bcl-2 family members.[508]. EIF6 is a factor necessary for 60S ribosome maturation which, due to its stimulating effect on glycolytic and fatty acid synthesis, is upregulated in several cancer types,[509] and its inhibition attenuates cancer cell growth.[510,511]

Overall, information on the functional roles of cysteine residues in the identified translation-associated proteins is still scarce since there has only recently been an increased interest in this topic of research. In **section 5.7.1**, it was demonstrated that >90% of the biotin-ajoene **40** interactome contained known PCM sites, suggesting that most of its translation-associated targets are susceptible to *S*-thiolation. A review of the protein targets not overlapping with the iCysMod database showed that 14, out of the 20 isolated, tRNA-ligases and 7 ribosomal subunits, out of the 29 isolated, did not contain known PCM sites, which indicated that their enrichment may have resulted from the isolation of an assembled ribosomal complex.

Protein synthesis is essential for cell growth and proliferation. In cancer, the rapid and continuous proliferation of cells requires 1) the reprogramming of global protein synthesis towards the selective translation of specific mRNAs that promote tumour cell survival, angiogenesis, transformation, invasion and metastasis; and 2) the deregulation of responses to hypoxia, oxidative and ER stress, since this normally leads to the attenuation of global protein synthesis.[442,512,513] As a result, cancer cells display increased ribosome biogenesis, alterations in initiation factor expression and tRNA optimisation, but also reduced quality control of translation.

Although the complexity of translation control in cancer cells makes it difficult to fully consolidate how the *S*-thiolation on translation-associated proteins by ajoene may produce anticancer effects, we suspected that three central mechanisms may be relevant.

Firstly, it is known that ribosomal proteins (e.g. RPS5) undergoes redox-mediated functional changes in response to oxidative stress,[443,514] thus the *S*-thiolation by ajoene may attenuate ribosomal activity, thereby halting or dysregulating protein synthesis. Secondly, the targeting of elongation and initiation factors may restore transcriptional activities that have been supressed by cancer cells, which include translational attenuation, via the PERK UPR pathway,[515] and proapoptotic responses, via the activation of CHOP.[516] Lastly, the oxidation of the Cys-182 of threonyl-tRNA synthetase (TARS) has been shown to induce protein mistranslation by the impairment of its editing capacity,[517] suggesting TARS and other tRNA-ligases as potential allosteric targets for ajoene *S*-thioallylation. The formation of mistranslated proteins puts additional strain on the folding and quality control mechanisms in the ER since mistranslated proteins are prone to misfolding and aggregation.

The modulation of translational processes has knock-on effects on later stages of the protein processing in the ER. Thus, the identification in this study, of the translation-associated proteins as targets of ajoene, is an important new finding that warrants further investigation.

Protein folding and quality control: Regarding ajoene's interaction with post-translation ER events, our proteomic data revealed that biotin-ajoene **40** had enriched several protein disulfide isomerases (P4HB, PDIA3, PDIA4 and PDIA6) as well as all subunits of the T-complex protein ring complex, TRiC (TCP1/CCT1, CCT2, CCT3, CCT4, CCT5, CCT6A, CCT7, CCT8), which are important molecular chaperones that assist with protein folding in the ER. Protein disulfide-isomerases (PDIs), are multifunctional redox enzymes involved with protein folding, quality control and homeostasis in the ER.[518] Due to their role in catalysing the formation and the rearrangement of native disulfide bond, PDIs are upregulated in several cancers to deal with the demands of a heightened protein biosynthesis.[519,520] The identification PDIs as *S*-thiolation targets of ajoene indicated a significant mechanism by which ajoene could affect protein folding in cancer cells. The targeting of the TRiC by ajoene is also particularly significant as this multiprotein complex assists in the folding of approximately 10% of the human proteome, including the large cytoskeletal proteins actin and tubulin as well as several cell cycle regulators.[521,522] Furthermore, CCT is known to prevent aggregation during stress by preventing protein misfolding. To mediate the folding process, the inner surface of the

barrel-like structure of TRiC contains cysteine thiol groups with low pK_a.[523] While it still unclear if ajoene targets the fully assembled complex, or the individual pre-assembled subunits, the *S*-thiolation of CCT cysteine residues may result in the disruption of the enzyme's folding capabilities. It has been shown that an altered expression of the TRiC complex is necessary for growth and survival of breast cancer, which provides a rationale for TRiC as a novel therapeutic target.[524,525] This strongly indicates that TRiC not only represents a plausible *S*-thioallylation target of ajoene, but that the *S*-thioallylation of TRiC may be associated with the formation of protein aggregates in the ER.

Further evidence for ajoene's effects on protein folding in the ER was given by the enrichment of many heat-shock proteins (HSPH1, HSPD1, HSP90AA1, HSP90B1, HSP4A, HSPA1A, TRAP1, HSP90AB1, HSPB1) and antioxidant enzymes maintaining the thiol homeostasis in the ER (ERO1L, GSTP1, GSTO1, PDRX1, PDRX2, PDRX3, PRDX6, MTGST1, TNX). The heat-shock proteins act as mediators of protein folding by assisting with the refolding, and directing the degradation of proteins that cannot refold through the proteasome pathway.[526,527]

Antioxidant enzymes in the ER control redox homeostasis as the reductive counterpart to the oxidative protein folding by detoxifying excess ROS and protecting the cysteine residues of proteins from oxidative insults.[528] During ER stress, both classes of enzymes are upregulated as part of the UPR to restore the capacity of the folding machinery and/or ER quality control (ERQC) mechanisms. The genomic instability, oncogene activation and increased protein secretion demands inherent to cancer cells pose challenges for protein processing in the ER, which results in the build-up of misfolded proteins in the ER to cause ER stress.[529] In this regard, cancer cells utilise UPR pathways in two distinct ways. On the one hand, UPR activation represents a survival strategy by which cancer cells can mitigate the damage caused by ER stress. On the other hand, several cancer types exploit the UPR pathways to promote angiogenesis, invasion, metastasis, and chemoresistance.[530,531] This dependence on the UPR highlights that the modulation of heat-shock proteins and antioxidant enzymes by ajoene will be detrimental to cancer cells. Since several activation mechanisms of the UPR are mediated by redox-active PCM sites,[532] they make suitable targets for ajoene *S*-thiolation.

Protein degradation (via the Proteasome): In addition to its interactions with the UPR, ajoene appears to target the endoplasmic-reticulum-associated protein degradation

(ERAD) pathway, which represents another branch of quality-control machineries in the cell. The ERAD pathway marks misfolded proteins of the endoplasmic reticulum for ubiquitination and subsequent degradation by a protein-degrading complex, called the 26S proteasome.[533] In **Section 5.7.1**, we identified that two key regulators of ERAD, VCP and UBA1, were likely to be inhibited by ajoene *S*-thiolation. This, and their high enrichment in our proteomics dataset, suggested that the attenuation of VCP and UBA1 activity may represent a mechanism by which ajoene induces ER stress in MDA-MB-231. Biotin-ajoene **40** had also enriched several subunits of the 20S core and 19S regulatory particles which assemble into the 26S proteasome (See **Figure 7.6** in the **Appendix**), which is responsible for the proteolysis of approximately 80% of cellular proteins. The 19S-20S dissociation/association correlates with cysteine oxidation/reduction, where it has been shown that acute oxidative stress caused by environmental insults or mitochondrial defects induces proteasome disassembly and impairment the ERAD pathway.[534] Since our data revealed the 19S and 20S subunits as *S*-thiolation targets, it was reasonable that the inhibition proteasome activity by ajoene is, in part, responsible for the accumulation of misfolded proteins in cancer cells. Indeed, the literature supports the inhibition of human 20S proteasome activity in human myeloid leukemia cells,[336] In cancer cells, the prolonged attenuation of proteasome activity rapidly induce stress responses that initiate apoptosis via the intrinsic pathway. The ability to selectively target cancer cells using this mechanism has set the stage for the development and clinical approval of several proteasome inhibitors as anticancer agents.[535]

The target-interactions of ajoene within the genetic information processing system strongly supports the induction of ER stress-mediated apoptosis as its primary anticancer mechanism. We propose that ajoene induces ER stress in MDA-MB-231 by simultaneously increasing misfolded proteins in the ER to overload the protein folding machinery, and by inhibiting UPR adaptive and pro-survival pathways to thwart restorative measures of the quality control machinery. This two-pronged mechanism of action is cytotoxic to cancer cells since it targets their reliance on the functional integrity of the ER and the ER stress-attenuating mechanisms of ERQC/ERAD.[536] Since normal cells are typically not subjected to ER stress events, their UPR pathways remain inactive and are not essential to their survival, which explains why ajoene's effects display selectivity towards cancer cells.

5.7.4 The Implications of Ajoene *S*-Thioallylation on the Hallmarks of Cancer

Taken together, our results revealed that biotin-ajoene **40** caused a widespread *S*-thiolation in the MDA-MB-231 proteome. It was found that the protein *S*-thiolation predominantly occurred within systems relating to the metabolism, cellular processes and genetic information processing. The KEGG analysis of the proteomics data indicated that ajoene was targeting functional and signalling pathways essential to the biology of cancer cells, classified under the hallmarks of cancer.[102,103] In addition, the enrichment scores of identified proteins in the probe interactome indicated that ajoene *S*-thiolation was selective towards many known anticancer targets. Although the data collected in this thesis does not show a functional relation to ajoene *S*-thiolallylation, there is a growing body of evidence, including the findings presented here, that ajoene mediates its anticancer effects through *S*-thiolation of its protein targets.

A distinguishing feature of carcinogenesis is the alteration of metabolic pathways which include the deregulation of cellular energetics to improve proliferative capabilities (even under hypoxic conditions) and the upregulation of anabolic pathways that satisfy the requirements associated with a high growth rate.[537–540] Our results suggest that ajoene targets key enzymes of the glycolysis and the pentose phosphate pathway, as well as several enzymes involved in the *de novo* biosynthesis of basic cellular building blocks, e.g. purines. Ajoene's interactions with purine biosynthesis, suggest that *S*-thiolation in the glycolysis and pentose phosphate pathways may be associated with antiproliferative and pro-apoptotic effects of ajoene.[86,365,541]

Cancer cells acquire the capability to independently sustain proliferative signalling and to evade growth suppressors. The effects of ajoene on these two cancer hallmarks may emerge from its interactions with the cell cycle clock, as ajoene *S*-thiolates regulators of the G_2/M cell cycle checkpoint, namely 14-3-3 proteins and CDK1. Taken together, ajoene's ability to induce G_2/M cell cycle arrest likely plays into its antiproliferative effects.[167,183] Ajoene's interaction with certain cytoskeletal targets was suggestive of another mechanism affecting the cell cycle transitions. Although tubulins are not directly associated with cell cycle regulation, they form the central component of the microtubule network involved in cell division. Ajoene may halt the cell cycle by targeting tubulins, since this interferes with the formation and stability of the microtubule network.[130,167,542]

Whilst actin microfilaments are also involved in cell division,[543] the main function of the actin cytoskeletal structures is to facilitate cell mobility and to confer mechanical stability. Like actin, intermediate filaments have intercellular functions relating to the maintenance of cell-shape, but they also serve as a structural component that anchors cellular organelles. On the exterior of the cell, intermediate filaments act as a "cellular scaffolding" that controls in cell adhesion and forms a protective layer against mechanical and chemical stress in epithelial cells. However, as cancer cells become more malignant, these cytoskeletal functions are hijacked for the activation of invasion and metastasis.[544] Akin to the antiproliferative effects associated with *S*-thiolation of tubulins, our analysis suggested that ajoene's antimetastatic effects may relate to the *S*-thiolation of protein targets in the micro- and intermediate filaments networks of cancer cells. Specifically, it was revealed that ajoene interacts strongly with actin as well as several protein targets of actin-associated pathways that regulate focal adhesion, adherens junctions and stress fibre formation. Our findings indicate that ajoene may destabilise the actin cytoskeletal network which could have knock-on antimetastatic effects. In support of this, the *S*-thioallylation of actin caused the disruption of the actin cytoskeleton in allicin-treated murine fibroblast.[86] In our own work, ajoene treatment of MDA-MB-231 cells causes cell shrinkage and membrane blebbing which is characteristic of actin depolymerisation (**Figure 4.30**). Secondly, that Biotin-ajoene **40** significantly enriched four members of the spectrin family (SPTAN1, SPTBN1, ACTN1 and ACTN4) which are important regulators of actin dynamics.[545–547] The differential expression of these protein targets in breast cancer highlighted their potential involvement in the antimetastatic effects of ajoene and warrants further investigation.

Cancer cells resist cell-death by employing multiple strategies to block apoptosis such as the amplification of the antiapoptotic signalling and/or the downregulation of the proapoptotic programs.[548] Apoptosis following treatment of cancer cells with ajoene and other OSCs has been well described and has been shown to proceed via the intrinsic mitochondrial-dependent caspase cascade.[89,337–339] Our findings suggest that ajoene *S*-thiolation of several protein targets in three key biological systems, including cellular processes, metabolism and genetic information processing, can modulate apoptotic signalling in MDA-MB-231 cancer cells. Ajoene's chemoselectivity for the *S*-thiolation of redox-regulatory cysteine sites and its protein targets in antioxidant pathways indicated its ability to alter the redox state, which is known to be compromised in cancer cells. It

has recently been proposed that wide-spread *S*-thioallylation of redox-sensitive protein leads to an increase in oxidative stress,[86,263] corroborating reports that ROS-induced activation of MAPK pathways contribute to the pro-apoptotic action of ajoene.[115,159] Our pathway analysis suggest that ajoene can increase mitochondrial ROS by attenuating enzymes within the glycolysis and pentose phosphate pathways, since they provide reducing power (NADPH) that fuels the protein-based antioxidant systems and recycles oxidized glutathione.[549] In this study, we have found that ajoene interacts with members of the 14-3-3 protein family, which are antiapoptotic regulators that are overexpressed in breast cancer cells, enabling them to evade apoptosis. All members of this family were enriched in the biotin-ajoene interactome and YWHAZ and YWHAQ were the most enriched protein in the entire dataset. Since the inhibition of these targets can dampen antiapoptotic signalling and promote cell death, we suggest further investigation into the effects of *S*-thiolation of the 14-3-3 proteins.[550,551] A significant advancement in the understanding of ajoene's cytotoxicity was our group's finding that ajoene targets protein folding in the ER of cancer cells and triggers apoptosis.[153,340] The proteomics data shows that the majority of ajoene *S*-thiolation occurred on protein targets associated with protein metabolism, including 1) protein translation (ribosomal proteins, initiation factors), 2) protein folding and quality control (chaperones), and 3) proteasome (ERAD pathway). The identification of these targets strongly supports a cytotoxic mechanism whereby ajoene induces ER stress and activates the UPR through the activation of CHOP/GADD153.

Ajoene is a cancer hallmark-targeting compound, since its mechanism of action is directed toward specific molecular targets that are involved with the capacity of cancer cells to survive under conditions of increased oxidative and proteotoxic stress. While the effects of *S*-thioallylation of cysteine residues on oxidative signalling events are still up for debate, its systemic interaction with the redox-regulated systems reflects its ability to exert broad-spectrum anticancer activity as shown by our findings illustrated in **Figure 5.38**.

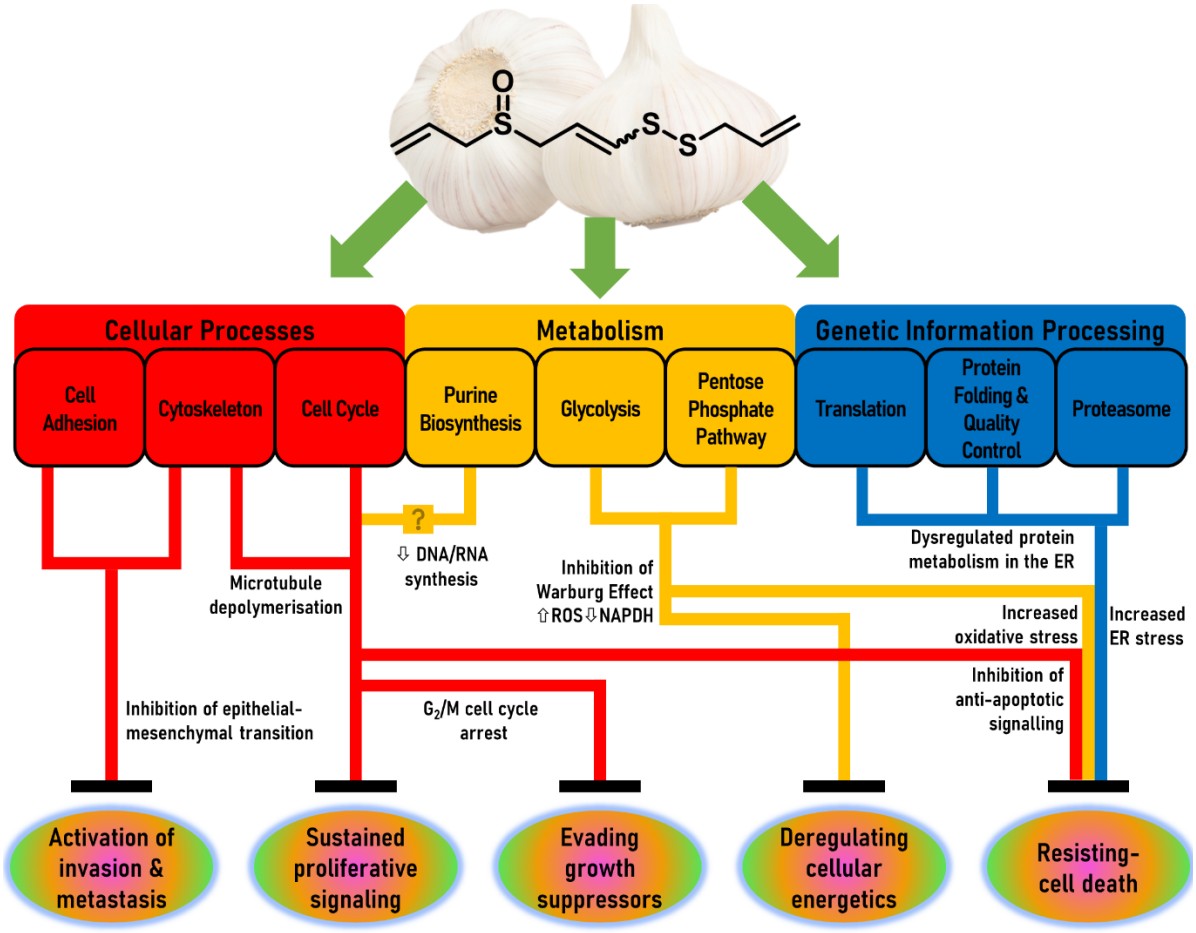

Figure 5.38: Ajoene *S*-thiolation targets several hallmarks of cancer.

5.7.5 Validation of GSTP1 as a Protein Target of Biotin-Ajoene

In order to validate if the protein targets of the biotin-ajoene **40** interactome are true targets of ajoene, a series of experiments using recombinant proteins is required. We performed this validation on Glutathione *S*-transferase P (GSTP1) which was found to be 22-fold enriched in the interactome. GSTP1 is an important regulator of protein *S*-glutathionylation and represents the closest endogenous PCM to *S*-thioallylation. Due to its role in the pathogenicity in triple-negative breast cancer, GSTP1 has been identified as therapeutic target since its inhibition impairs glycolytic metabolism and xenobiotic detoxification.[449] Lastly, the inhibition of GSTP1 by *S*-thioallylation has been attributed to the allicin's apoptotic effects in cancer cells.[450] A western blot experiment was performed by incubating 1 µg recombinant GSTP1 with 1 mM biotin-ajoene **40**, in the absence and presence of DTT (100mM). The biotin label was detected with streptavidin-HRP and the protein loading was confirmed by silver stain, as shown in **Figure 5.39**.

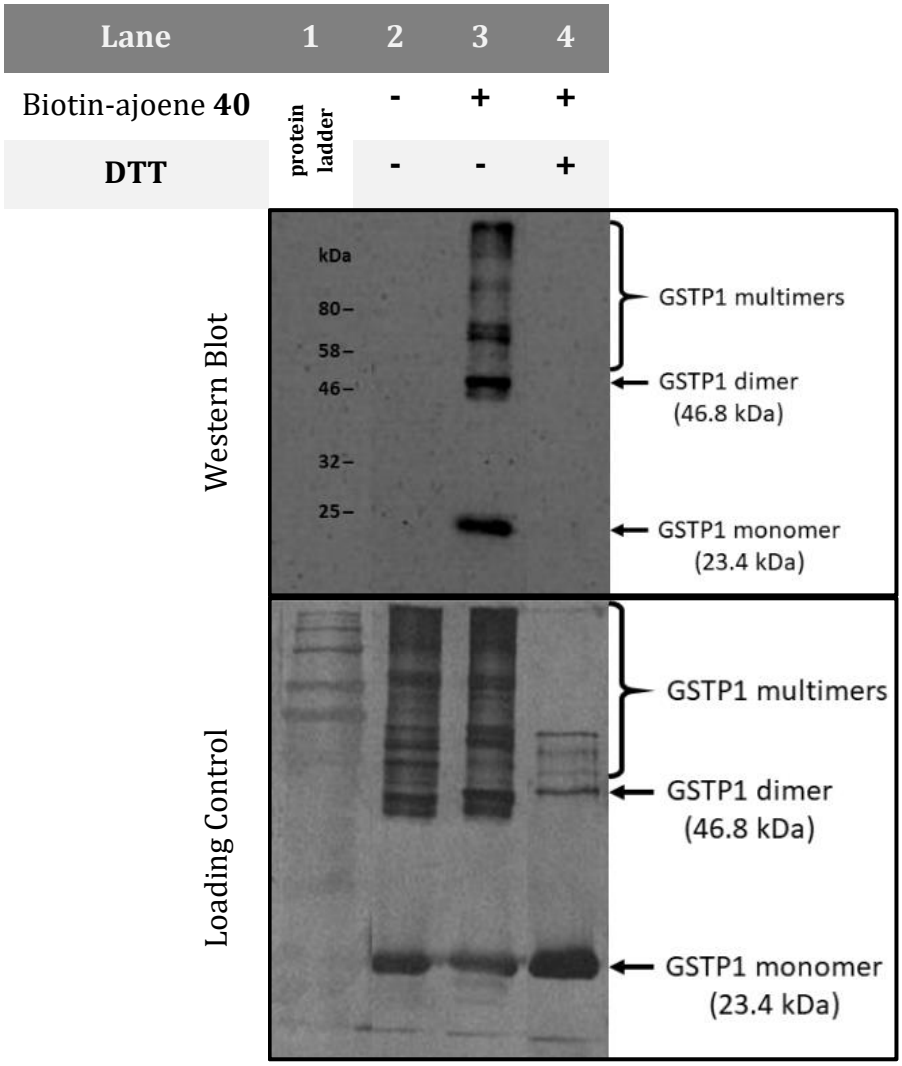

Figure 5.39: GSTP1 validation experiment.

The loading control showed that each sample lane had been loaded with protein. At this point it is to note that GSTP1 can exists in a monomeric, dimer and/or multimeric form.[552] Under non-reducing conditions (**lane 2** and **3**), the dimerisation and multimerisation of GSTP1 was particularly evident. Here the bands for the GSTP1 monomer and dimer were observed at 23.4 and 46.8 kDa, respectively, whereas the multimers appeared as several bands above that. Under reducing conditions, GSTP1 was mostly dissociated into its monomeric form, seen by the thickening of the band at 23.6 kDa in **lane 4**.

As expected, the untreated sample (**lane 2**) showed no signal, while the treated sample (**lane 3**) showed that biotinylation had occurred. The DTT treated sample (**lane 4**) showed no biotinylation. Together, this demonstrated that GSTP1 was biotinylated by biotin-ajoene **40** and that the biotin tag was connected to the protein by a disulfide bond.

These findings suggest that GSTP1 is true target of ajoene. This experiment could not, however, determine which cysteine residue(s) were *S*-thiolated. A targeted MS experiment on ajoene-treated GSTP1 would be required (akin to our MS experiment on Hb in **Chapter 3**).

To identify the specific *S*-thiolation sites of the 632 targets captured by biotin-ajoene **40**, a proteomics experiment similar to the study on allicin by Gruhkle *et al.* is suggested.[86] Since *S*-thioallylation is not a direct mimic of a specific cysteine PTM, its binding to cysteine residues may not necessarily phenocopy the function of the endogenous PTM. Which means that once a suitable *S*-thioallylated protein, and its modified cysteine sites, have been identified, the functional outcome of *S*-thioallylation would also have to be assessed using an enzyme activity/inhibition assay.

5.8 Conclusion

The identification of the ajoene *S*-thiolysis targets and analysis of this chapter demonstrate an association between the ajoene's targets and its anticancer mechanism of action. Following the synthesis of an activity-based biotin probe in **Chapter 4**, a proteomics approaches was developed to facilitate an affinity purification of *S*-thiolated proteins in the proteome of MDA-MB-231 breast cancer cells. A rigorous proteomic analysis of the MS data identified 633 proteins as targets of biotin-ajoene. Most of its protein targets were found to contain known modifiable PCM cysteine sites. The high prevalence of cysteine sites associated with PTMs involving ROS, RNS, RSS and GSH in the biotin-ajoene **40** interactome suggested ajoene's ability to interact with the redox proteome. Interestingly, it was discovered that proteins with a high number of redox-active cysteines and/or with highly ligandable sites were favourably enrichment by our probe. To elucidate the biological significance of our probe's targets, we compared our data with similar datasets of publications that examined the modification of cysteine residues in cancer cell proteomes, one reporting on cysteine reactivities and the other on *S*-thioallylation targets of allicin. The examination of the overlaps with these datasets highlighted targets of importance in the biology of cancer cells and their susceptibility to functional modulated by *S*-thiolation. These protein target represent promising leads for further studies on the therapeutic effects of *S*-thiolation. Although our competition assay showed congruence in protein labelling between the ajoene and biotin-ajoene **40**, it appeared the size of our probe presented a disadvantage in accessing cysteine residues

with low surface exposure. An enrichment-weighted KEGG pathways analysis of the biotin-ajoene **40** interactome elucidated significant interactions in the KEGG biological systems of metabolism, cellular processes and genetic information processing. We identified the main targets for *S*-thioallylations in MDA-MB-231 cells as cytoskeletal proteins, cell cycle regulators, glycolytic enzymes, biosynthetic enzymes, redox-sensors, antioxidant proteins, ribosomal proteins, proteosomal proteins, chaperones, heat-shock proteins and translation factors. Most notably, the discovery that the majority of *S*-thiolations target were associated with functions of the ER supported our group's previous findings that of ER stress-mediated apoptosis was critical to ajoene's cytotoxicity to cancer cells. Additionally, our findings also corroborated several other reported anticancer modes of action of ajoene and confirmed how *S*-thiolation produces modulatory effects responsible for it antiproliferative, antimetastatic and apoptotic effects in cancer cells, by targeting the hallmarks of cancer. More specifically, because several of these protein targets relate to pathways that distinguish cancer cells from normal cells (e.g. by facilitating higher metabolic rates and increased protein synthesis), the *S*-thiolation of these proteins can disrupt pathways relating to the proliferation and survival of cancer.

Not only is the discovery of these targets valuable to the understanding ajoene's cytotoxicity, but also its ability to selectively increased oxidative and proteotoxic stress in cancer cells provides an opportunity to further develop sulfur-based anticancer therapies.

Conclusion

Chapter 6 : Concluding Remarks

This chapter concludes the thesis. A summary of the main findings is presented in **Section 6.1**, while **Section 6.2** contains suggestions for future research.

6.1 Summary of Main Conclusions

Garlic is well-documented to contain several organosulfur compounds (OSCs) that show promising chemopreventative and therapeutic properties. Bioactivity arises from the OSCs acting as sulfenylating agents in a wide range of cellular processes, including redox homeostasis, metabolism, assembly of cytoskeletal networks and protein synthesis. Notably, protein *S*-thiolation has been identified as the process through which the garlic OSCs such as allicin, DADS, DATS and ajoene, produce cytotoxic effects in cancer cells. As a continuation of our group's investigations into the cytotoxic mechanism of action of the vinyl disulfide-sulfoxide ajoene, this thesis investigated the potential of ajoene as a chemopreventative and chemotherapeutic agent, with the specific aim of identifying its *S*-thioallylation targets in cancer cells.

Based on promising published *in vitro* studies on ajoene's potent and selective cytotoxicity towards cancer cell-lines, together with several reports on its *in vivo* activity, in **Chapter 3** we set out to test ajoene's anticancer activity in a WHCO1 cancer-xenograft model in nude mice. The results were disappointing, pointing towards a high blood instability of ajoene. Hence, this was followed up by carrying out an SAR study on the blood stability and cytotoxicity of the ajoene pharmacophore, which revealed that removal of the double bond of the vinyl disulfide afforded a disulfide that retained cytotoxicity but with a vastly improved blood half-life. From this study, we identified ajoene analogues with good cytotoxicity and an enhanced blood half-life for consideration as leads in future medicinal chemistry studies. From these studies, *S*-thiolation of the βCys-93 residue in haemoglobin was identified as a plausible explanation for ajoene's high blood instability and the likely reason for its inactivity in the WHCO1 cancer-xenograft nude mice *in vivo* study.

Regarding chemical biology aspects and ajoene targets, a previous project had developed a fluorescently tagged ajoene that allowed the tracking of ajoene in cancer cells by confocal laser microscopy based on a thiolysis exchange mechanism. This study demonstrated that ajoene predominantly localises in the ER and that it *S*-thiolates several protein targets in epithelial mammary gland adenocarcinoma (MDA-MB-231) cancer cells. From this work, a hypothesis emerged that ajoene's cytotoxicity was associated with its *S*-thiolation targets, which led to the research in this thesis on the isolation and identification of the said targets via an activity-based probe (ABP). **Chapter 4** detailed the design and synthesis of the ABP scaffold, incorporating an ajoene vinyl disulfide active group tethered to a biotin affinity tag for disulfide exchange with reactive cysteine residues resulting in the transfer of the biotin tag onto the target protein. Four iterations were necessary to develop a DMSO-compatible probe. Our final probe, biotin-ajoene **40**, was found to retain activity against cancer cells and was 3-fold less active against normal cells. An unexpected finding was that biotin-ajoene **40** labelled more proteins in normal than in cancer cells, prompting further studies. To confirm that protein biotinylation was mediated by *S*-thiolysis, we showed that the biotin tag was linked to the protein through a reversible disulfide bond. Lastly, a competition assay showed that biotin-ajoene **40** shared common targets with ajoene, making it a suitable model.

Chapter 5 described the development of affinity-purification mass spectrometry protocol for identifying ajoene's protein targets in MDA-MB-231 cell lines. Biotinylated proteins were isolated using streptavidin-coated magnetic beads. The beads were stringently washed and the peptides for mass spec analysis were obtained using an on-bead trypsin digest. Analysis of the proteomic data revealed that 91% of the proteins pulled out contained known redox-active cysteine sites indicating that ajoene targets proteins with reactive cysteines, where the highest specificity was observed for sites susceptible to *S*-glutathionylation, *S*-nitrosylation, *S*-sulfhydration and *S*-sulfenylation. In addition to targeting reactive cysteines, the enrichment was correlated to the number of reactive cysteines on a protein, i.e. those with multiple reactive cysteine sites showed higher enrichment by the probe. It is well known that cysteine ligandability drives many physiological processes which in turn was proposed to drive the observed cytotoxic effect of ajoene.

An enrichment-weighted KEGG pathway analysis showed that ajoene was targeting pathways critical for the growth and metastasis of cancer cells The most significant

interactions were observed within functional networks associated with 1) metabolic activity and cell-cycle regulation, 2) cytoskeletal systems controlling cell adhesion and migration, and 3) protein synthesis, including translation, folding, quality control and degradation. Our probe *S*-thiolated key protein targets associated with the hallmarks of cancer, which consolidated our lab's previous findings on ajoene's antiproliferative, antimetastatic and ER-mediated apoptotic effects as its mode of action against cancer cells. The selective cytotoxicity of ajoene towards cancer cells versus normal cells appears to emerge from its ability to target pathways that are essential for cancer cell initiation, proliferation and progression.

Overall, the results presented in this dissertation reaffirm ajoene as a natural dietary cancer preventative agent, and its analogues as valuable leads for chemotherapeutic drug development. The ability to engage subsets of the proteome via the *S*-thiolation of non-catalytic cysteine residues suggests that ajoene's sulfoxide vinyl disulfide pharmacophore can act as a warhead for promoting dysregulation in the redox systems of cancer cells.[410,421,553]

6.2 Outlook for Future Research

Owing to the multidisciplinary nature of this dissertation, future studies can engage in several avenues of scientific investigation, relating to the pharmacology, proteomics and chemistry of ajoene's anticancer properties.

Regarding the pharmacology, our murine experiments revealed ajoene to elicit off-target interactions within the blood as well as adverse effects following a prolonged intragastric administration. We developed dihydroajoene analogues displaying improved *in vitro* blood half-lives while achieving comparable cytotoxicity to ajoene. Future studies could, therefore, address their *in vivo* tumour growth inhibitory activity. Concerning the adverse effects, a chemoproteomic profiling of ajoene-treated blood and/or liver cells could address the toxicity and off-target effects that were observed.[554]

In the proteomics study, our experimental conditions determined the protein targets of biotin-ajoene **40** at cytotoxic (IC_{50}) concentration. While this elucidated several pathways associated with the cytotoxicity of ajoene overall, the first-line *S*-thiolation targets could be identified by treating the cells at a lower concentration of the probe (i.e. sub IC_{50}) and/or for a shorter amount of time (e.g. 1 hour instead of 24 hours). The proteomic analysis highlighted how steric effects may have limited the accessibility of biotin-ajoene

40 to access certain cysteine residues. In view of this, future experiments could revisit our *in vitro* "Click"-chemistry approach that was initially envisaged in **Chapter 4**. Propargyl-ajoene **36** provides a practical solution as a Clickable ABP[302] since it has a comparable size to the natural product. As shown in **Figure 6.1**, the experimental workflow would include: 1) treating cells with the ABP **36**, 2) cell lysis, 3) biotinylating *S*-propargylated protein targets via CuAAC (using biotin-azide **39** and the "Click"-catalyst complex, Cu(I)-THPTA), and 4) performing the AP-MS protocol as developed in **Chapter 5**.

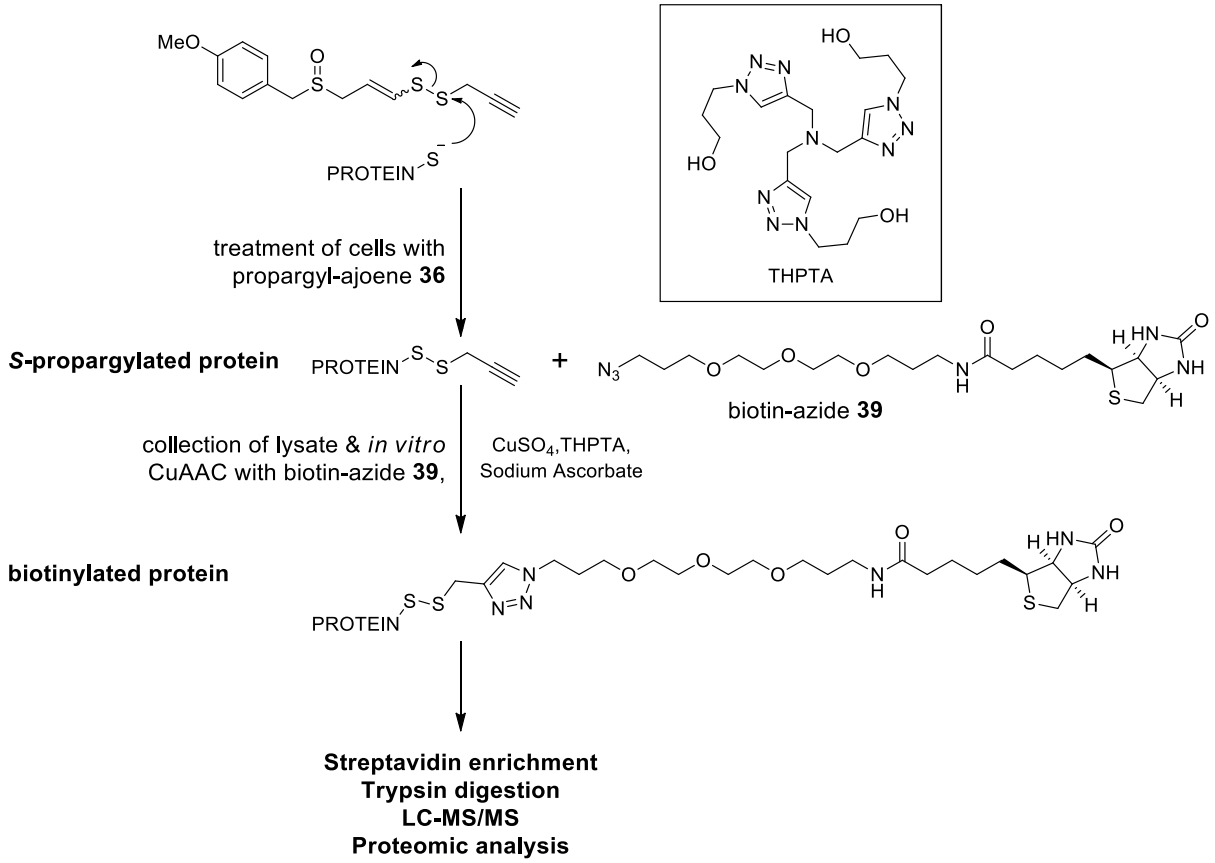

Figure 6.1: Workflow of "Click"-Chemistry Activity-Based Protein Profiling (CC-ABPP) of ajoene's *S*-thiolation targets in cancer cells.

The immunomodulatory and anti-inflammatory effects of ajoene were not examined in this thesis,[125] thus presenting an opportunity for future work. Since these effects are primarily mediated by gene expression, studies could examine the correlation between the transcriptome and proteome of ajoene's effects on cancer cells.[555–557]

Concerning the chemistry of ajoene *S*-thioallylation, the identification of cysteine sites on proteins and the fate of the enethiolate leaving group represent gaps in the literature. Ajoene's protein *S*-thioallylation sites could be investigated using the proteomics

protocol published by Gruhlke *et al.* for allicin.[86] Owing to its chemical instability, the biological effects of the enethiolate leaving group are still unknown and one equivalent of enethiolate is produced for every protein cysteine that is *S*-thiolated. The use of ajoene analogues with variations in their leaving group (see Raynbird *et al.*[181]) could provide a solution to address this gap.

Chapter 7 : Experimental Section

Synthetic Methods

All solvents were freshly distilled. Dichloromethane was distilled over phosphorus pentoxide under nitrogen. Tetrahydrofuran was distilled under nitrogen and dried over sodium wire benzophenone. Acetonitrile was distilled from calcium hydride under nitrogen. Other reagents were purified according to standard procedures. All reagents were purchased from Sigma-Aldrich (South Africa) or Merck (Darmstadt, Germany) and were used without further purification. Room temperature refers to ambient temperature. Low temperature reactions were carried out using liquid nitrogen in acetone (-78 °C)/acetonitrile (-40 °C)/benzyl alcohol (-20 °C) or a slurry of water and ice (0 °C).

Thin layer chromatography (TLC) was used to monitor reactions using aluminium backed Merck silica-gel 60 F_{254} plates. Compounds on TLC were visualised by a combination of ultra-violet light (V_{max} = 254nm), iodine vapour, by spraying with a 2.5% solution of anisaldehyde in a mixture of sulfuric acid and ethanol (1:10 v/v), ninhydrin (300 mg in 97 mL ethanol and 3 mL acetic acid) or $KMnO_4$ (1.5 g with 10g K_2CO_3 and 1.25 mL 10% NaOH in 200 mL H_2O) and then heating at 150°C. Column chromatography was performed using silica-gel 60 mesh (Merck 7734). All chromatography was carried out using petroleum ether (b.p. 40-60 °C), ethyl acetate, dichloromethane or methanol as eluents, or a combination of these.

NMR spectra were recorded on either a Varian Mercury 300 MHz (75.5 MHz for ^{13}C-NMR) or a Bruker 400 MHz (101 MHz for ^{13}C-NMR) instrument and were carried out in chloroform-*d*, acetone-d_6, DMSO-d_6, methanol-d_4 with the following references respectively in ppm: chloroform (δ = 7.26 in ^{1}H-NMR and δ = 77.00 in ^{13}C-NMR), dimethylsulfoxide (δ = 2.50 in ^{1}H-NMR and δ = 39.52 in ^{13}C-NMR) or methanol (δ = 3.31 in ^{1}H-NMR δ = 49.00 in ^{13}C-NMR).[558] All Chemical shifts (δ) are reported in ppm and *J* values are quoted in Hz. Melting points were measured on a Reichert-Jung Thermovar hot-stage microscope and are uncorrected. Infrared spectra were recorded on a Perkin Elmer Spectrum 100 FT-IR Spectrometer. High-resolution mass spectrometry was performed at the Central Analytical Facilities, School of Chemistry, University of Stellenbosch on a Waters Synapt G2 machine in ESI mode.

7.1 bis-PMB ajoene analogues

(4-Methoxybenzyl)(prop-2-yn-1-yl)sulfane, **(1)**[183]

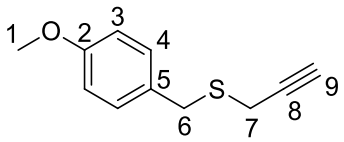

To a stirring solution of PMBCl (1.73 ml, 12.8 mmol, 1 eq) in acetonitrile (40 ml) under N_2 was added thiourea (1.17 g, 15.4 mmol, 1.2 eq) and the reaction heated to 85°C after which it was refluxed for 14 hours. The mixture was cooled in an ice bath and the resulting white precipitate was filtered, washed with ice-cooled acetonitrile (2 x 10 mL) and dried on the vacuum pump to afford the isothiouronium salt as a white solid (2.80 g, 94%).

ν_{max}/ cm^{-1} (ATR): 2974, 2950 (N-H stretch x 2); Mp (CH_3CN): 161-162 °C.

The isothiouronium salt (2.80 g, 12.03 mmol, eq) was added to a solution of KOH (1.35 g, 24.1 mmol, 2 eq), in anhydrous MeOH (24 mL) under N_2 at -20°C (benzyl alcohol/liquid nitrogen) and left stirring for two hours. Propargyl bromide (2 mL, 18.05 mmol, 1.5 eq) was then added and the reaction stirred at 0°C for 30 minutes upon which the reaction was quenched with saturated aqueous NH_4Cl (10 mL). The product was extracted with EtOAc (3 x 20 mL) and the combined fractions were washed with water (2 x 20 mL) and brine (1 x 15 mL). The solvent was removed under reduced pressure and the residue was purified via silica column chromatography (EtOAc:Hexane = 5:95) to afford propargyl sulfide **1** as a clear light-yellow oil (1.98 g, 85%).

R_f = 0.9 (EtOAc:Hexane, = 10:90); IR ν_{max}/ cm^{-1} (ATR): 3286 (alkyne C-H stretch); δ_H (300 MHz, $CDCl_3$) 7.26 (3H, d, *J* = 8.7 Hz, H-3), 6.86 (2H, d, *J* = 8.7 Hz, H-4), 3.83 (2H, s, H-6), 3.80 (3H, s, H-1), 3.07 (2H, d, *J* = 2.6 Hz, H-7), 2.28 (1H, t, *J* = 2.6 Hz, H-9); δ_C (101 MHz, $CDCl_3$) 158.9 (C-2), 130.2 (C-4), 129.5 (C-5), 114.1 (C-3), 80.1 (C-8), 71.3 (C-9), 55.4 (C-1), 34.8 (C-6), 18.4 (C-7).

(*E/Z*)-*S*-(3-((4-Methoxybenzyl)thio)prop-1-en-1-yl) ethanethioate, **(2)**[183]

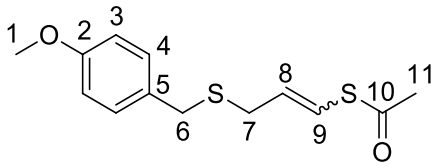

The propargyl sulfide **1** (1.40 g, 7.27 mmol, 1 eq) was suspended in toluene (35 mL) under N_2 and ACCN (0.18 g, 0.73 mmol, 0.1 eq) was added. The mixture was brought to reflux (85°C), at which point thioacetic acid (0.62 mL, 8.72 mmol, 1.2 eq) was added drop-wise. The reaction was held at 85°C and was allowed to progress for three hours. The reaction was brought down to room temperature and quenched with saturated aqueous sodium bicarbonate (5 mL). The toluene was removed under reduced pressure and the product was extracted with EtOAc (3 x 20 mL). The combined fractions were washed with water (2 x 15mL) and brine (1 x 10 mL), then dried over $MgSO_4$ and concentrated. The silica column chromatography (EtOAc:Hexane = 10:90) afforded thioacetate **2** as a 1:2 mixture of *E/Z*-isomers and as an odiferous clear colourless oil (0.98 g, 45%).

E/Z mixture: R_f = 0.7 (EtOAc:Hexane, = 20:80); IR ν_{max}/ cm^{-1} (ATR): 1700 (C=O);

E-isomer: δ_H (300 MHz,$CDCl_3$): 7.22 (2H, d, *J* = 8.7 Hz, H-4), 6.85 (2H, d, *J* = 8.7 Hz, H-3), 6.50 (1H, dt, *J* = 15.6, 1.2 Hz, H-9), 5.82 (1 H, m, H-8), 3.80 (3H, s, H-1), 3.63 (2H, s, H-6), 3.12 (3H, dd, *J* = 7.4, 1.2 Hz H-7), 2.39 (3H, s, H-11); δ_C (75 MHz, $CDCl_3$): 193.1 (C-10), 158.9 (C-2), 130.3 (C-8), 130.2 (C-4), 129.9 (C-5), 119.5 (C-9), 114.1 (C-3), 55.4 (C-1), 34.5 (C-6), 33.3 (C-7), 30.5 (C-11).
Z-isomer: δ_H (300 MHz, $CDCl_3$): 7.22 (2H, d, *J* = 8.6 Hz, H-4), 6.85 (2H, d, *J* = 8.6 Hz, H-3), 6.67 (1H, dt, *J* = 9.6 Hz, 1.1, H-9), 5.86 (1 H, m, H-8), 3.80 (3H, s, H-1), 3.64 (2H, s, H-6), 3.13 (2H, dd, *J* = 7.6, 1.1 Hz, H-7) 2.40 (3H, s, H-11); δ_C (75 MHz, $CDCl_3$): 191.4 (C-10), 158.9 (C-2), 130.0 (C-4), 129.9 (C-5), 128.7 (C-8), 119.7 (C-9), 114.1 (C-3), 55.4 (C-1), 35.3 (C-6), 31.0 (C-7), 30.8 (C-11).

4-(2-Hydroxyethyl)-phenol, **(3)**[260]

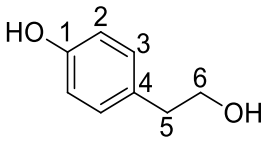

$LiAlH_4$ (2.00 g, 52.96 mmol, 2.2 eq) was added to THF (80 mL) at 0°C under N_2 and ethyl 2-(4-hydroxyphenyl)ethanoate (4.00 g, 24.07 mmol, 1 eq) in THF (20mL) added drop-wise. After two hours the reaction was quenched with 1M HCl (80 mL). Upon filtration through Celite the filtrate was extracted using EtOAc (3 x 100 mL), washed with saturated aqueous sodium bicarbonate (50mL) and then brine (50mL). The combined organic fractions were dried over $MgSO_4$ and concentrated under reduced pressure. Purification via column chromatography (EtOAc: Hexane) yielded alcohol **3** as a white crystalline solid (3.26g, 98%), which was crystallised from EtOAc/Hexane.

R_f = 0.35 (EtOAc: Hexane = 50:50); Mp (EtOAc/Hexane): 91-93 °C, lit[260] Mp: 90 °C; IR ν_{max}/ cm^{-1} (ATR): 3384 (O-H), 3130 (aromatic O-H); δ_H (300 MHz, d_6 acetone): 8.10 (1H, brs, OH), 7.05 (2H, d, *J* = 8.7 Hz, H-3), 6.73 (2H, d, *J* = 8.7 Hz, H-2), 3.67 (2H, t, *J* = 7.2 Hz, H-6), 2.94 (1H, brs, OH') 2.70 (2H, t, *J* = 7.2 Hz, H-5); δ_C (101 MHz, d_6-acetone): 156.3 (C-1), 130.8 (C-4), 130.5 (C-3), 115.7 (C-2), 64.1 (C-6), 39.2 (C-5).

4-(2-Iodoethyl)-phenol, **(4)**[559]

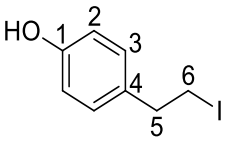

The alcohol **3** (3.26 g, 23.57 mmol, 1 eq) dissolved in THF (45 mL) at 0° C under N_2 and imidazole (3.21 g, 47.2 mmol, 2 eq), triphenylphosphine (12.40 g, 47.2 mmol, 2 eq) and iodine (12.00 g, 47.2 mmol, 2 eq) were sequentially added to the reaction vessel. The mixture was allowed to warm to room temperature and after two hours the reaction was quenched with aqueous saturated sodium thiosulfate (30 mL). The organic products were extracted into EtOAc (3 x 40 mL), which was then washed with HCl (1 M, 20 mL), aqueous saturated sodium bicarbonate (30 mL) and brine (20 mL). The solvent was dried ($MgSO_4$) and removed under reduced pressure. The residue was purified by column chromatography (EtOAc:Hexane) to afford iodide **4** as a yellow crystalline solid (5.66 g, 97%).

R_f = 0.7 (EtOAc:Hexane = 30:70); Mp (EtOAc/Hexane): 109-113°C, lit[559] Mp: 111-112°C; IR ν_{max}/ cm^{-1} (ATR): 3198 (aromatic O-H); δ_H (400 MHz, $CDCl_3$): 7.06 (2H, d, *J*= 8.6 Hz, H-3), 6.78 (2H, d, *J* = 8.6 Hz, H-2), 4.80 (1H, brs, OH), 3.31 (2H, t, *J* = 7.8 Hz, H-6), 3.10 (2H, t, *J* = 7.8 Hz, H-5); δ_C (101 MHz, $CDCl_3$) δ 154.5 (C1), 133.2 (C4), 129.7 (C-3), 115.6 (C-2), 39.6 (C-5), 6.4 (C-6).

S-4-Hydroxyphenethyl 4-methylbenzenesulfonothioate, **(5)**[560]

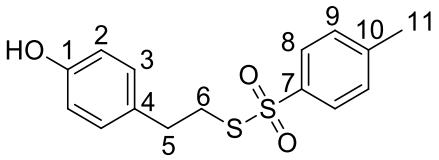

The Iodide **3** (1.20 g, 4.84 mmol, 1 eq) was dissolved in DMF (10 mL) under N_2 and potassium thiotosylate (2.19 g, 9.68 mmol, 2 eq) was added over 15 minutes. The reaction was allowed to proceed at room temperature overnight. The reaction mixture was diluted with EtOAc (15 mL) and water was added (10 mL). The product was extracted with EtOAc (3 x 15 mL). The combined organic fractions were washed copiously with water (4 x 15 mL) and brine (10 mL). The solvent was removed under reduced pressure and silica column chromatography (Hexane:EtOAc) afforded thiosulfonate **5** as a yellow clear oil (1.44 g, 97%).

R_f = 0.3 (EtOAc:Hexane, = 30:70); IR ν_{max}/ cm^{-1} (ATR): 3436 (phenolic O-H), 1136 (O=S=O), 521 (S-S); δ_H (300 Mhz,$CDCl_3$): 7.82 (2H, d, *J* = 8.3 Hz, H-8); 7.34 (2H, d, *J* = 8.3 Hz, H-9), 6.96 (2H, d, *J* = 8.7 Hz, H-3), 6.74 (2H, d, *J* = 8.7 Hz, H-2), 3.18 (2H, t, *J* = 7.5 Hz, H-5), 2.83 (2H, t, *J* = 7.7 Hz, H-6), 2.45 (3H, s, H-11); δ_C (101 MHz, $CDCl_3$): 154.7 (C-1), 145.0 (C-10), 142.2 (C-7), 130.9 (C-4), 130.0 (C-9), 129.9 (C-8), 127.2 (C-3), 115.7 (C-2), 37.6 (C-6), 34.4 (C-5), 21.8 (C-11).

(*E*/*Z*)-4-(2-((3-((4-Methoxybenzyl)thio)prop-1-en-1-yl)disulfanyl)ethyl)phenol, **(6)**[560]

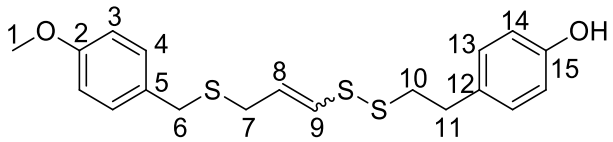

The vinyl thioacetate **2** (586 mg, 2.19 mmol, 1 eq) in anhydrous MeOH (1.95 mL, 1 M) was cooled to -40°C (Acetonitrile/liq. N_2) under N_2 and potassium hydroxide (129 mg, 2.30 mmol, 1.05 eq) in MeOH (2.05 mL, 1 M) was added. The reaction was stirred for 30

minutes upon which the reaction was cooled to -78 °C and thiotosylate **5** (743 mg, 2.41 mmol, 1.1 eq) in MeOH (2.43 mL, 1 M) was added. The reaction was allowed to proceed for three hours and was quenched at room temperature with saturated aqueous ammonium chloride (4 mL). The product was extracted with EtOAc (3 x 15 mL) and the combined organic fractions were washed with water (2 x 10 mL) followed by brine (1 x 10 mL). The solvent was removed under reduced pressure and the residue purified using silica column chromatography (EtOAc:Hexane = 15:85) to afford disulfide **6** as a clear colourless oil and as a 3:5 mixture of *E/Z* isomers (594 mg, 72%).

E/Z mixture: R_f = 0.35 (EtOAc:Hexane, = 20:80); IR ν_{max}/ cm^{-1} (ATR): 3382 (phenolic OH);

E-isomer: δ_H (300 MHz, $CDCl_3$): 7.21 (2H, d, *J* = 8.7 Hz, H-4), 7.07 (2H, d, *J* = 8.5 Hz, H-13), 6.84 (2H, d, *J* = 8.7 Hz, H-14), 6.76 (2H, d, *J* = 8.5 Hz, H-3), 6.07 (1H, dt, *J* = 14.6, 1.0 Hz, H-9), 5.88 (1H, dt, *J* = 14.6, 7.3 Hz, H-8), 3.80 (3H, s, H-1), 3.62 (2H, s, H-6), 3.08 (2H, dd, *J* = 7.1, 0.7 Hz, H-7), 2.92 (4H, s, H-10/-11); δ_C (101 MHz, $CDCl_3$): 158.8 (C-2), 154.3 (C-15), 130.7 (C-12), 132.2 or 132.1 (C-5), 130.2 (C-4), 130.0 (C-14), 128.2 (C-9), 128.0 (C-8), 115.6 (C-3), 114.2 (C-13), 55.5 (C-1), 39.9 (C-10), 34.8 (C-6), 34.8 (C-11), 32.9 (C-7).
Z-isomer: δ_H (300 MHz, $CDCl_3$): 7.24 (2H, d, *J* = 8.7 Hz, H-4), 7.05 (2H, d, *J* = 8.5 Hz, H-13), 6.90 (2H, d, *J* = 8.5 Hz, H-14), 6.75 (2H, d, *J* = 8.7 Hz, H-3), 6.24 (1H, dt, *J* = 9.3, 1.0 Hz, H-9), 5.70 (1H, dt, *J* = 9.3, 7.3 Hz, H-8), 3.80 (3H, s, H-1), 3.69 (2H, s, H-6), 3.23 (2H, dd, *J* = 7.6, 0.8 Hz, H-7), 2.92 (4H, s, H10/-11); δ_C (101 MHz, $CDCl_3$): 158.8 (C-2), 154.3 (C-15), 132.4 (C-9), 132.2 or 132.1 (C-5), 130.7 (C-12) 130.2 (C-4), 130.0 (C-14), 128.3 (C-8), 115.6 (C-3), 114.2 (C-13), 55.5 (C-1), 40.6 (C-10), 35.6 (C-6), 34.8 (C-11), 29.5 (C-7).

(*E/Z*)-4-(2-((3-((4-Methoxybenzyl)sulfinyl)prop-1-en-1-yl)disulfanyl)ethyl)phenol, **(7)**[560]

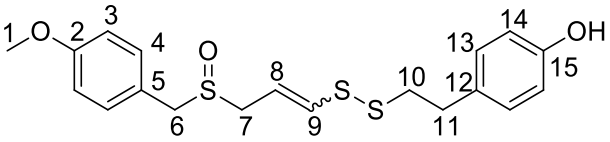

The sulfide **6** (250 mg, 0.66 mmol, 1 eq) was dissolved in DCM (10 mL) under N_2 and cooled to -78°C. *m*-CPBA (142 mg, 0.83 mmol, 1.25 eq) was added in portions and the reaction allowed to warm to room temperature over three hours before being quenched with saturated aqueous sodium bicarbonate (5 mL). The product was extracted with DCM (3 x 10 mL) and the combined fractions were washed with water (2 x 10mL) followed by

brine (5 mL). The solvent was removed under reduced pressure and the residue purified via silica column chromatography (EtOAc:Hexane = 80:20) to afford ajoene analogue **7** as a pale-yellow oil and as a 2:1 mixture of *Z/E* isomers, (155 mg, 60%).

E/Z mixture: R_f = 0.45 (EtOAc:Hexane, = 70:30); IR ν_{max}/ cm^{-1} (ATR): 3171 (phenolic OH); HRMS (ES): *m/z* found 393.0646 $[M-H]^+$, $C_{19}H_{21}O_3S_3$ requires 393.0658;

E-isomer: δ_H (400 MHz, $CDCl_3$): 7.23 (2H, d, *J* = 8.6 Hz, H-4), 7.03 (2H, d, *J* = 8.6 Hz, H-13), 6.90 (2H, d, *J* = 8.6 Hz, H-3), 6.77 (2H, d, *J* = 8.6 Hz, H-14), 6.24 (1H, d, *J* = 14.8 Hz, H-9), 5.86 (1H, dt, *J* = 14.7, 7.6 Hz, H-8), 3.91 (2H, m, H-6), 3.81 (3H, s, H-1), 3.51-3.42 (1H, m, H-7a), 3.33 (1H, ddd, *J* = 13.2, 8.0, 0.9 Hz, H-7b), 2.87-2.67 (4H, m, H-10/-11); δ_C (101 MHz, $CDCl_3$): 160.0 (C-2), 155.0 (C-15), 135.1 (C-9), 131.4 (C-4), 131.3 (C-12), 129.9 (C-13), 121.4 (C-5), 116.4 (C-8), 115.8 (C-14), 114.7 (C-3), 56.4 (C-6), 55.5 (C-1), 52.9 (C-7), 40.4 (C-10), 34.8 (C-11).
Z-isomer: δ_H (400 MHz, $CDCl_3$): 7.23 (2H, d, *J* = 8.6 Hz, H-4), 7.02 (2H, d, *J* = 8.6 Hz, H-13), 6.90 (2H, d, *J* = 8.6 Hz, H-3), 6.76 (2H, d, *J* = 8.6 Hz, H-14), 6.57 (1H, d, *J* = 9.4 Hz, H-9), 5.76 (1H, dt, *J* = 9.5, 7.9 Hz, H-8), 3.96 (2H, m, H-6), 3.80 (3H, s, H-1), 3.55 (1H, ddd, *J* = 13.4, 7.7, 0.9 Hz, H-7a), 3.51-3.42 (1H, m, H-7b), 2.87-2.67 (4H, m, H-10/-11); δ_C (101 MHz, $CDCl_3$): 160.0 (C-2), 155.0 (C-15), 139.0 (C-9), 131.4 (C-4), 131.2 (C-12), 129.9 (C-13), 121.5 (C-5), 118.1 (C-8), 115.8 (C-14), 114.7 (C-3), 57.0 (C-6), 55.5 (C-1), 49.6 (C-7), 40.9 (C-10), 34.8 (C-11).

(*E/Z*)-2-(4-(2-((3-((4-Methoxybenzyl)thio)prop-1-en-1-yl)disulfanyl)ethyl)phenoxy) acetamide **(8)**[560]

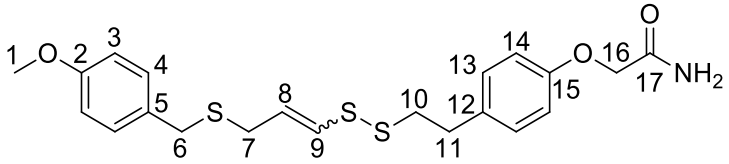

Phenol **6** (150 mg, 0.40 mmol, 1 eq) was suspended in acetonitrile (5 mL) under N_2 with potassium carbonate (111 mg, 0.80 mmol, 2 eq), 2-chloroacetamide (74 mg, 0.80 mmol, 2 eq) and *tert*-butylammonium iodide (15 mg, 0.04 mmol, 0.1 eq) and the mixture heated at 40°C. The reaction was allowed to proceed for 12 hours and was then quenched with saturated aqueous ammonium chloride (2 mL). The product was extracted into EtOAc (3 x 10 mL) and washed with water (2 x 5 mL) followed by brine (1 x 5 mL). The solvent was dried ($MgSO_4$), removed under reduced pressure and silica column chromatography

(MeOH:DCM = 2:98) afforded amide **8** as a clear light-yellow oil as a 3:4 mixture of *E/Z* isomers (70 mg, 40%).

E/Z mixture: R_f = 0.3 (MeOH:DCM = 5:95), IR ν_{max}/ cm^{-1} (APCI): 3438 (amide N-H), 1685 (amide C=O); HRMS (ES): *m/z* found 436.1068 $[M+H]^+$, $C_{21}H_{26}NO_3S_3$ requires 436.1080;

E-isomer: δ_H (400 MHz, $CDCl_3$): 7.24 (2H, d, *J* = 8.7 Hz, H-4), 7.15 (2H, d, *J* = 8.5 Hz, H-13), 6.89-6.82 (4H, m, H-3/-14), 6.54 (1H, brs, NH), 6.08 (1H, dt, *J* = 14.7, 1.0 Hz, H-9), 5.89 (1H, brs, NH), 5.88 (1H, dt, *J* = 14.6, 7.3 Hz, H-8), 4.47 (2H, s, H-16), 3.79 (3H, s, H-1), 3.62 (2H, s, H-6), 3.08 (2H, dd, *J* = 7.2, 0.7 Hz, H-7), 2.94 (4H, s, H-10/-11); δ_C (101 MHz, $CDCl_3$): 171.2 (C-17), 158.9 (C-2), 156.0 (C-15), 133.7 (C-5), 130.2 (C-4), 130.1 (C-13), 130.0 (C-12), 128.5 (C-8), 128.0 (C-9), 114.9 (C-14), 114.1 (C-3), 67.5 (C-16), 55.4 (C-1), 39.6 (C-10), 34.8 (C-6), 34.7 (C-11), 32.9 (C-7).
Z-isomer: δ_H (400 MHz, $CDCl_3$): 7.20 (2H, d, *J* = 8.7 Hz, H-4), 7.13 (2H, d, *J* = 8.5 Hz, H-13), 6.89-6.82 (4H, m, H-3/-14), 6.54 (1H, brs, NH), 6.24 (1H, dt, *J* = 9.3, 1.0 Hz, H-9), 5.89 (1H, brs, NH), 5.71 (1H, dt, *J* = 9.3, 7.7 Hz, H-8), 4.47 (2H, s, H-16), 3.79 (3H, s, H-1), 3.68 (2H, s, H-6), 3.28 (2H, dd, *J* = 7.7, 0.8 Hz, H-7), 2.94 (4H, s, H-10/-11); δ_C (101 MHz, $CDCl_3$): 171.2 (C-17), 158.9 (C-2), 156.0 (C-15), 133.7 (C-5), 132.2 (C-9), 130.2 (C-4), 130.1 (C-13), 130.0 (C-12), 128.2 (C-8), 114.9 (C-14), 114.1 (C-3), 67.5 (C-16), 55.4 (C-1), 40.4 (C-10), 35.6 (C-6), 34.7 (C-11), 29.5 (C-7).

(*E/Z*)-2-(4-(2-((3-((4-Methoxybenzyl)sulfinyl)prop-1-en-1-yl)disulfanyl)ethyl)phenoxy)acetamide, **(9)**[560]

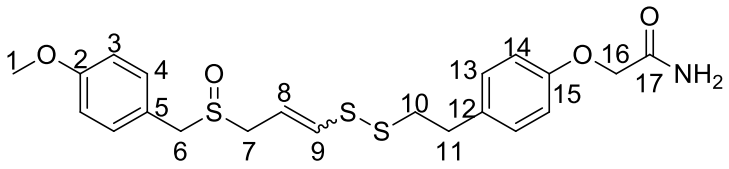

Sulfoxide **7** (107 mg, 0.27 mmol, 1 eq) was suspended in acetonitrile (2 mL) under N_2. Potassium carbonate (75 mg, 0.54 mmol, 2 eq) and 2-iodoacetamide (100 mg, 0.54 mmol, 2 eq) were added and the mixture was heated to 40°C. The reaction was left for 12 hours before being quenched with saturated aqueous ammonium chloride (5 mL). The product was extracted with EtOAc (3 x 5 mL) and washed with water (2 x 2 mL) followed by brine (2mL). The combined organic fractions were dried over $MgSO_4$ and concentrated under reduced pressure. The residue was purified via silica column chromatography

(MeOH:DCM = 5:95), which afforded ajoene analogue **9** as a clear colourless oil (58 mg, 48%) and as a 3:2 mixture of *E/Z* isomers.

E/Z mixture: R_f = 0.65 (MeOH:DCM = 5:95), IR ν_{max}/ cm^{-1} (APCI): 3418 (amide N-H), 1716 (amide C=O);

E-isomer: δ_H (600 MHz, $CDCl_3$): 7.19 (2H, d, *J* = 8.7 Hz, H-4), 7.13 (2H, d, *J* = 8.6 Hz, H-13), 6.89 (2H, d, *J* = 8.7 Hz, H-3), 6.85 (2H, d, *J* = 8.6 Hz, H-14), 6.56 (1H, brs, NH), 6.34 (1H, dt, *J* = 14.8, 0.9 Hz, H-9), 5.92 (1H, dt, *J* = 14.8, 7.5 Hz, H-8), 5.86 (1H, brs, NH), 4.46 (2H, s, H-16), 3.91 (2H, s, H-6), 3.80 (3H, s, H-1), 3.48-3.42 (1H, m, H-7a), 3.30 (1H, ddd, *J* = 13.2, 8.1, 0.9 Hz, H-7b), 2.94 (4H, s, H-10/-11); δ_C (151 MHz, $CDCl_3$): 171.1 (C-17), 159.9 (C-2), 156.1 (C-15), 134.4 (C-9), 133.5 (C-5), 131.3 (C-4), 130.1 (C-13), 121.7 (C-12), 117.2 (C-8), 114.9 (C-14), 114.7 (C-3), 67.4 (C-16), 56.5 (C-6), 55.5 (C-1), 52.9 (C-7), 39.7 (C-10), 34.6 (C-11).
Z-isomer: δ_H (600 MHz, $CDCl_3$): 7.22 (2H, d, *J* = 8.7 Hz, H-4), 7.13 (2H, d, *J* = 8.6 Hz, H-13), 6.89 (2H, d, *J* = 8.7 Hz, H-3), 6.85 (2H, d, *J* = 8.6 Hz, H-14), 6.57 (1H, dt, *J* = 9.4, 0.9 Hz, H-9), 6.56 (1H, brs, NH), 5.86 (1H, brs, NH), 5.78 (1H, dt, *J* = 9.4, 7.9 Hz, H-8), 4.46 (2H, s, H-16), 3.92 (2H, s, H-6), 3.80 (3H, s, H-1), 3.54 (1H, ddd, *J* = 13.4, 7.7, 1.0 Hz, H-7a), 3.48-3.42 (1H, m, H-7b), 2.94 (4H, s, H-10/-11); δ_C (151 MHz, $CDCl_3$): 171.1 (C-17), 160.0 (C-2), 156.1 (C-15), 138.5 (C-9), 133.4 (C-5), 131.4 (C-4), 130.1 (C-13), 121.6 (C-12), 118.7 (C-8), 114.9 (C-14), 114.6 (C-3), 67.4 (C-16), 57.0 (C-6), 55.5 (C-1), 49.7 (C-7), 40.5 (C-10), 34.6 (C-11).

7.2 bis-PMB dihydroajoene Analogues

3-((4-Methoxybenzyl)thio)propane-1-thiol, **(10)**[561]

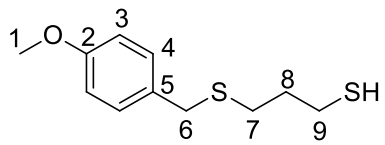

Propane-1,3-dithiol (0.93 mL, 9.2 mmol, 1.2 eq) was suspended in MeOH (30 mL) under N_2, and potassium hydroxide (0.73 g, 13 mmol, 1.4 eq) was added and the mixture left to stir at room temperature for 30 minutes. The reaction was then cooled to 0°C, PMBCl (1.2 g, 7.7 mmol, 1 eq) was added drop-wise and the reaction allowed to proceed for two hours. The reaction was quenched using aqueous HCl (20 mL, 1 M) and then neutralised

to pH 7 using saturated aqueous sodium bicarbonate. The product was extracted using EtOAc (3 x 30 mL). The combined fractions were washed with H_2O (2 x 30 mL) followed by brine (20 mL), dried over $MgSO_4$ and concentrated under reduced pressure. The resulting residue was purified via silica column chromatography (EtOAc:Hexane = 2:98) to afford thiol **10** as a clear, light-green oil (1.33 g, 88%).

R_f = 0.25 (EtOAc:Hexane = 2:98);); IR ν_{max}/ cm^{-1} (ATR): 2557 (S-H stretch), 1241, 1031 (C-O stretch, alkyl aryl ether); δ_H (300 MHz, $CDCl_3$): 7.23 (2H, d, *J* = 8.8 Hz, H-4), 6.85 (2H, d, *J* = 8.8 Hz, H-3), 3.80 (3H, s, H-1), 3.66 (2H, s, H-6), 2.52 (2H, t, *J* = 7.1 Hz, H-9), 1.84 (2H, t, *J* = 7.1 Hz, H-7), 1.33 (1H, t, *J* = 8.0 Hz, SH), 1.31 (2H, p, H-8).

4-(2-((3-((4-Methoxybenzyl)thio)propyl)disulfanyl)ethyl)phenol, **(11)**[561]

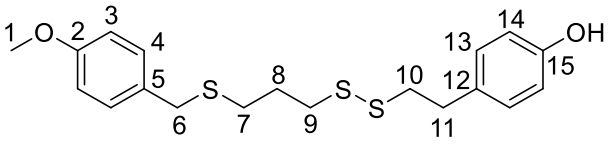

The thiol **10** (765 mg, 3.38 mmol, 1 eq) was taken up in MeOH (20 mL) under N_2 and cooled to -78°C. Triethylamine (0.68 mL, 4.9 mmol, 1.5 mmol) was added and after 20 minutes the thiotosylate **5** (1.44 g, 4.67 mmol, 1.4 eq) in MeOH (5 mL) was added. The mixture was allowed to warm to room temperature over one hour. The reaction was immediately quenched with saturated aqueous ammonium chloride (10 mL). The product was extracted with EtOAc (3 x 40 mL) and the combined fractions were washed with water (2 x 20 mL) followed by brine (10 mL). The organic solvent was dried with $MgSO_4$ and removed under reduced pressure. The resulting residue was purified via silica column chromatography (EtOAc:Hexane = 20:90) to afford disulfide **11** as a colourless waxy solid (992 mg, 77%).

R_f = 0.5 (EtOAc: Hexane = 20:80); Mp (EtOAc/Hexane): 84-86 °C; IR ν_{max}/ cm^{-1} (ATR): 3433 (phenolic OH), 550 (S-S); δ_H (400 Mhz, $CDCl_3$): 7.23 (2H ,d , *J* = 8.8 Hz, H-4), 7.06 (2H, d, *J* = 8.6 Hz, H-13), 6.85 (2H, d, *J* = 8.8 Hz, H-3), 6.76 (2H, d, *J* = 8.6 Hz, H-14), 3.80 (3H, s, H-1), 3.67 (2H, s, H-6), 2.89 (4H, brs, H10/-H11), 2.73 (2H, t, J = 7.1 Hz, H-9), 2.51 (2H, t, *J* = 7.1 Hz, H-7), 1.93 (2H, p, H-8); δ_C (101 MHz, $CDCl_3$): 158.8 (C-2), 154.3 (C-15), 132.3 (C-12), 130.5 (C-5), 130.0 (C-4), 129.9 (C-13), 115.5 (C-14), 114.1 (C-3), 55.4 (C-1), 40.7 (C-10), 37.6 (C-9), 35.8 (C-6), 34.9 (C-11), 29.9 (C-7), 28.6 (C-8); HRMS (ES): *m/z* found 379.0860 $[M-H]^+$, $C_{19}H_{23}O_2S_3$ requires 379.0866.

4-(2-((3-((4-Methoxybenzyl)sulfinyl)propyl)disulfanyl)ethyl)phenol, **(12)**

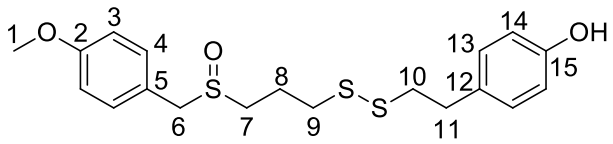

The sulfide **11** (200 mg, 0.53 mmol, 1 eq) was suspended in DCM (4 mL) under N_2 and cooled to -78°C. *m*-CPBA (178 mg, 0.8 mmol, 1.5 eq) was then added in portions and the reaction was allowed to warm up to room temperature over one hour. The reaction was quenched with saturated aqueous sodium bicarbonate (5 mL) and extracted with DCM (3 x 10 mL). The combined organic fractions were washed with water (2 x 10 mL) followed by brine (5 mL). The solvent was dried using $MgSO_4$ and the product was concentrated under reduced pressure. Purification via silica column chromatography (MeOH:DCM = 5:95) afforded sulfoxide **12** as a clear colourless oil (148 mg, 70%).

R_f = 0.25 (MeOH:DCM = 5:95); IR ν_{max}/ cm^{-1} (ATR): 3161 (S=O); δ_H (400 MHz, $CDCl_3$): 7.20 (2H, d, *J* = 8.6 Hz, H-4), 7.02 (2H, d, *J* = 8.4 Hz, H-13), 6.89 (2H, d, *J* = 8.6 Hz, H-3), 6.76 (2H, d, *J* = 8.4 Hz, H-14), 3.99 (1H, d, *J* = 13.0 Hz, H-6a), 3.95 (2H, d, *J* = 13.0 Hz, H-6b), 3.80 (3H, s, H-1), 2.92 – 2.82 (4 H, m, H-10/-11), 2.77-2.58 (4 H, m, H-7/-9), 2.19-2.07 (2H, m, H-8); δ_C (101 MHz, $CDCl_3$): 160.0 (C-2), 155.0 (C-15), 131.5 (C-5), 131.4 (C-4), 129.8 (C-13), 121.3 (C-12), 115.8 (C-3), 114.7 (C-14), 57.7 (C-6), 55.5 (C-1), 49.0 (C-7), 41.0 (C-11), 37.2 (C-9), 34.9 (C-10), 22.3 (C-8); HRMS (ES): *m/z* found 397.0966 $[M+H]^+$, $C_{19}H_{25}O_3S_3$ requires 397.0960.

2-(4-(2-((3-((4-Methoxybenzyl)thio)propyl)disulfanyl)ethyl)phenoxy)acetamide, **(13)**[561]

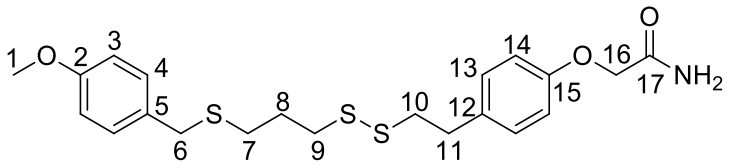

The sulfide **10** (222 mg, 0.58 mmol, 1 eq) was dissolved in acetonitrile (5 mL) under N_2. Cesium carbonate (286 mg, 0.88 mmol, 1.5 eq), *tert*-butylammonium iodide (22 mg, 0.58 mmol, 0.1 eq) and 2-chloroacetamide (81 mg, 0.87 mmol, 1.5 eq) were added and the reaction was left to stir at room temperature for 18 hours. The reaction was quenched with saturated aqueous ammonium chloride (5 mL) and the product extracted into DCM

(3 x 15 mL). The combined organic fractions were washed with water (2 x 10 mL) followed by brine (5 mL). The dried ($MgSO_4$) solvent was removed under reduced pressure. The resulting residue was purified via silica column chromatography (EtOAc:Hexane = 30:70) to afford sulfide **13** as a clear milky oil (195 mg, 77%).

R_f = 0.35 (EtOAc:Hexane = 20:80); IR ν_{max}/ cm^{-1} (ATR): 3380 (amide N-H) 3160 cm^{-1} (amide N-H) , 1659 cm^{-1} (amide C=O); δ_H (400 MHz, $CDCl_3$): 7.22 (2H, d, *J* = 8.8 Hz, H-4), 7.15 (2H, d, *J* = 8.8 Hz, H-13), 6.86 (2H, d, *J* = 8.5 Hz, H-3), 6.84 (2H, d, *J* = 8.5 Hz, H-14), 6.53 (1H, brs, NH), 5.71 (1H, brs, NH), 4.48 (2H, s, H-16), 3.79 (3H, s, H-1), 3.67 (2H, s, H-6), 2.97-2.85 (4H, m, H10/-11), 2.74 (2H, t, *J* = 7.0 Hz, H-9), 2.51 (2H, t, *J* = 7.1 Hz, H-7), 1.93 (2H, p, H-8); δ_C (101 MHz, $CDCl_3$): 171.1 (C-17), 158.8 (C-2), 156.0 (C-15), 134.0 (C-5), 130.4 (C-12), 130.1 (C-4), 130.0 (C-13), 114.9 (C-3), 114.1 (C-14), 67.5 (C-16), 55.4 (C-1), 40.4 (C-10), 37.7 (C-9), 35.8 (C-6), 34.8 (C-11), 29.9 (C-7), 28.6 (C-8); HRMS (ES): *m/z* found 460.1046 $[M+ Na]^+$, $C_{21}H_{27}NNaO_3S_3$ requires 460.1051.

2-(4-(2-((3-((4-Methoxybenzyl)sulfinyl)propyl)disulfanyl)ethyl)phenoxy)acetamide, **(14)**

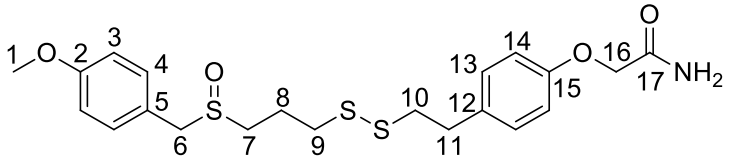

The sulfide **13** (104 mg, 0.24 mmol, 1 eq) was dissolved in DCM (3 mL) under N_2 and cooled to 78°C. *m*-CPBA (81 mg, 0.4 mmol, 1.5 eq) was added and the reaction allowed to warm to room temperature over two hours. The reaction was quenched with saturated aqueous sodium bicarbonate (4 mL) and the product extracted into DCM (3 x 10 mL). The combined organic fractions were washed with water (2 x 10 mL) and brine (5 mL). The solvent was dried with $MgSO_4$ and removed under reduced pressure. Silica column chromatography (MeOH:DCM = 5:95) afforded sulfoxide **14** as a clear light-yellow oil (78 mg, 72%).

R_f = 0.3 (MeOH:DCM = 5:95); IR ν_{max}/ cm^{-1} (ATR): 3413 (amide N-H), 3177 (S=O?) 1634 (amide C=O); δ_H (400 MHz, $CDCl_3$): 7.20 (2H, d, *J* = 8.7 Hz, H-4), 7.13 (2H, d, *J* = 8.7 Hz, H-13), 6.89 (2H, d, *J* = 8.7 Hz, H-3), 6.85 (2H, d, *J* = 8.7 Hz, H-14), 6.56 (1H, brs, NH), 6.06 (1H, brs, NH), 4.47 (2H, s, H-16), 3.96 (1H, t, *J* = 13.1 Hz, H-6a), 3.93 (1H, t, *J* = 13.1 Hz, H-6b),

3.79 (3H, s, H-1), 2.90 (4H, m, H-10/-11), 2.75 (2H, t, *J* = 6.9 Hz, H-9a), 2.74 (2H, t, *J* = 6.9 Hz, H-9b), 2.72-2.57 (2H, m, H-7) 2.22-2.08 (2H, m, H-8); δ_C (101 MHz, $CDCl_3$): 170.3 (C-17), 158.9 (C-2), 155.0 (C-15), 132.7 (C-5), 130.3 (C-4), 129.1 (C-13), 120.6 (C-12), 113.9 (C14), 113.6 (C-3), 66.5 (C-16), 56.8 (C-6), 54.4 (C-1), 47.9 (C-7), 39.4 (C-11), 36.3 (C-9), 33.7 (C-10), 21.2 (C-8); HRMS (ES): *m/z* found 454.1187 $[M+H]^+$, $C_{21}H_{28}NO_4S_3$ requires 454.1186.

7.3 Biotin-Ajoenes

4-(2-Azidoethyl)-phenol, **(15)**[562]

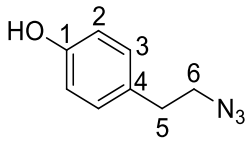

The Iodide **4** (560 mg, 2.26 mmol, 1eq) was suspended in DMF (3 mL) under N_2 and sodium azide (220 mg, 3.39 mmol, 1.5 eq) in DMF (1 mL) was added. The reaction was heated to 100°C and stirred for three hours. The reaction was cooled, diluted with 50 mL of diethyl ether, which was then washed copiously with H_2O (4 x 20 mL). The organic layer was dried over $MgSO_4$ and the solvent removed under reduced pressure. Column chromatography (EtOAc:Hexane) afforded azide **15** as a clear yellow oil (354 mg, 96%).

R_f = 0.3 (EtOAc:Hexane, = 10:90); IR ν_{max}/ cm^{-1} (ATR): 3342 (aromatic O-H), 2092 (N=N=N); δ_H (400 MHz, $CDCl_3$): 7.09 (2H, d, *J* = 8.5 Hz, H-3), 6.79 (2H, d, *J* = 8.5 Hz, H-2), 5.19 (1H, brs, OH), 3.46 (2H, t, *J* = 7.2 Hz, H-6), 2.83 (2H, t, *J* = 7.2 Hz, H-5); δ_C (75 MHz, $CDCl_3$): 154.5 (C-1), 130.3 (C-4), 130.1 (C-3), 115.7 (C-2), 52.8 (C-6), 34.6 (C-5).

1-(2-Azidoethyl)-4-(3-bromopropoxy)benzene, **(16)**

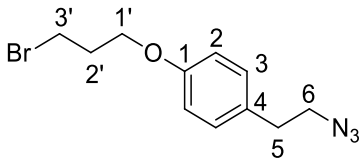

To a stirring solution of 1,3-dibromopropane (0.82 mL, 8.1 mmol, 3 eq) and Cs_2CO_3 (962 mg, 2.95 mmol, 1.1 eq) in acetonitrile (25 mL) was added the azide (**15**) (438 mg, 2.68 mmol, 1 eq) in acetonitrile (2 mL) slowly. The reaction was heated to 50°C and left stirring for six hours. It was then was quenched with saturated aqueous ammonium chloride (5 mL) and the product extracted with EtOAc (3 x 20 mL). The combined fractions were washed with brine (20 mL) and the solvent removed under reduced pressure. Column chromatography (EtOAc:Hexane) afforded bromide **16** as a clear colourless oil (518 mg, 68 %).

R_f = 0.78 (EtOAc:Hexane, = 30:70); IR ν_{max}/ cm^{-1} (ATR): 2092 (N=N=N), 1240 (aryl alkyl C-O-C); δ_H (400 MHz, $CDCl_3$): 7.14 (2H, d, *J* = 8.6 Hz, H-3), 6.87 (2H, d, *J* = 8.6 Hz, H-2), 4.09 (2H, t, *J* = 5.8 Hz, H-1'), 3.60 (2H, t, *J* = 6.5 Hz, H-3'), 3.47 (2H, t, *J* = 7.2 Hz, H-6), 2.84 (2H,

t, *J* = 7.2 Hz, H-5), 2.31 (2H, p, H-2'); δ_C (101 MHz, $CDCl_3$) 157.8 (C-1), 130.6 (C-4), 129.9 (C-3), 114.9 (C-2), 65.6 (C-1'), 52.8 (C-6), 34.7 (C-5), 32.9 (C-3'), 30.1 (C-2').

S-(3-(4-(2-Azidoethyl)phenoxy)propyl) 4-methylbenzenesulfonothioate, **(17)**

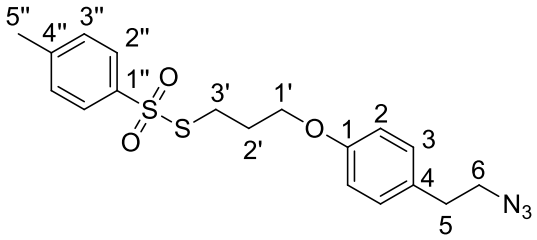

To a solution of potassium thiotosylate (639 mg, 2.83 mmol, 2 eq) in acetonitrile (10 mL) was added bromide **16** (400 mg, 1.41 mmol, 1 eq) in acetonitrile (5 mL) under N_2 and the reaction was heated to 60°C. The reaction was allowed to proceed over-night for 18 hours. The mixture was diluted with 25 mL EtOAc and washed with H_2O (3 x 20 mL). The organic layer was dried over $MgSO_4$ and the solvents removed under reduced pressure. Silica gel column chromatography (EtOAc:Hexane) afforded sulfonothioate ether **17** as a clear colourless oil (209 mg, 38%).

R_f = 0.3 (EtOAc:Hexane, = 20:80); IR ν_{max}/ cm^{-1} (ATR): 2090 (N=N=N); δ_H (300 MHz, $CDCl_3$): 7.82 (2H, d, *J* = 8.6 Hz, H-2''), 7.32 (2H, d, *J* = 8.4 Hz, H-3), 7.12 (2H, d, *J* = 8.6 Hz, H-3''), 6.78 (2H, d, *J* = 8.4 Hz, H-2), 3.95 (2H, t, *J* = 5.8 Hz, H-1'), 3.46 (2H, t, *J* = 7.1 Hz, H-6), 3.18 (2H, t, *J* = 7.2 Hz, H-3'), 2.83 (2H, *J* = 7.2 Hz, H-5), 2.44 (3H, s, H-5''), 2.12 (2H, p, H-2'); δ_C (101 MHz, $CDCl_3$): 157.6 (C-1), 144.9 (C-4''), 142.0 (C-1''), 130.6 (C-4), 130.0 (C-3''), 129.9 (C-3), 127.2 (C-2''), 114.8 (C-2), 65.7 (C-1'), 52.8 (C-6), 34.6 (C-5), 32.9 (C-3'), 28.9 (C-2'), 21.8 (C-5''); HRMS (ES): *m/z* found 392.1103 $[M+H]^+$, $C_{18}H_{22}O_3N_3S_2$ requires 392.1108.

(*E*/*Z*)-1-(3-(4-(2-Azidoethyl)phenoxy)propyl)-2-(3-((4-methoxybenzyl)thio)prop-1-en-1-yl)disulfane, **(18)**

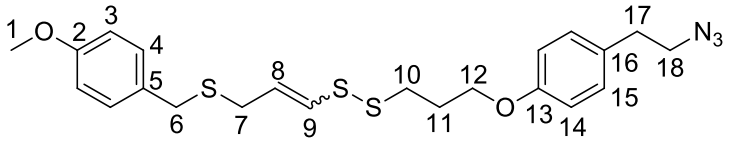

To stirred solution of thioacetate **2** (119 mg, 0.44 mmol, 1 eq) in MeOH (1 mL) at -40°C under N_2, was added potassium hydroxide (26 mg, 0.47 mmol, 1.05 eq) in MeOH (1.5 mL). The mixture was left for 20 minutes, upon which the temperature was lowered to -78°C

and the azidothiotosylate **17** (191 mg, 0.49 mmol, 1.1 eq) in MeOH (0.49 mL, 1 M) was added drop-wise. The reaction was allowed to proceed to room temperature over two hours before being quenched with saturated aqueous ammonium chloride (1 mL). The product was extracted into EtOAc (3 x 10 mL) and the combined fractions were sequentially washed (2 x 5 mL water, 5 mL brine), dried over $MgSO_4$ and concentrated under reduced pressure. Silica gel column chromatography afforded disulfide **18** as a 2:3 mixture of *E/Z*-isomers and as a clear colourless oil (172 mg, 85%).

E/Z mixture: R_f = 0.6 (EtOAc:Hexane, = 20:80); IR ν_{max}/ cm^{-1} (ATR): 2086 (N=N=N); HRMS (ES): *m/z* 462.1344 found $[M+H]^+$, $C_{22}H_{28}N_3O_2S_3$ requires 462.1349.

E-isomer: δ_H (300 MHz, $CDCl_3$): 7.22 (2H, d, *J* = 8.7 Hz, H-4), 7.12 (2H, d, *J* = 8.7 Hz, H-15), 6.85 (2H, d, *J* = 8.7, H-14), 6.84 (2H, d, *J* = 8.7 Hz, H-3), 6.09 (1H, dt, *J* = 14.7, 1.0 Hz, H-9), 5.89 (1H, dt, *J* = 14.6, 7.2 Hz, H-8), 4.07-4.02 (2H, m, H-12), 3.80 (3H, s, H-1), 3.63 (2H, s, H-6), 3.46 (2H, t, *J* = 7.2 Hz, H-18), 3.07 (2H, dd, *J* = 7.2, 1.0 Hz, H-7), 2.91 (2H, t, H-10), 2.83 (2H, t, *J* = 7.1 Hz, H-17), 2.22-2.12 (2H, m, H-11); δ_C (101 MHz, $CDCl_3$): 158.9 (C-2), 157.8 (C-13), 130.4 (C-5), 130.2 (C-15), 130.0 (C-16) 129.9 (C-4), 128.3 (C-8), 128.0 (C-9), 114.9 (C-14), 114.1 (C-3), 66.0 (C-12), 55.4 (C-1), 52.8 (C-18), 34.8 (C-6/-10), 34.6 (C-17), 32.9 (C-7), 29.0 (C-11).
Z-isomer: δ_H (300 MHz, $CDCl_3$): 7.22 (2H, d, *J* = 8.7 Hz, H-4)), 7.12 (2H, d, *J* = 8.7 Hz, H-15), 6.85 (2H, d, *J* = 8.7, H-14), 6.84 (2H, d, *J* = 8.7 Hz, H-3), 6.25 (1H, dt, *J* = 9.3, 1.0 Hz, H-9), 5.71 (1H, dt, *J* = 9.3, 7.6 Hz, H-8), 4.07-4.02 (2H, m, H-12), 3.80 (3H, s, H-1), 3.68 (2H, s, H-6), 3.46 (2H, t, *J* = 7.2 Hz, H-18), 3.21 (2H, dd, *J* = 7.6, 1.1 Hz, H-7), 2.91 (2H, t, H-10), 2.83 (2H, t, *J*= 7.2 Hz, H-17), 2.22-2.12 (2H, m, H-11); δ_C (101 MHz, $CDCl_3$): 158.9 (C-2), 157.8 (C-13), 132.1 (C-9), 130.4 (C-5), 130.2 (C-15), 130.0 (C-16), 129.9 (C-4), 128.6 (C-8), 114.9 (C-14), 114.1 (C-3), 66.0 (C-12), 55.4 (C-1), 52.8 (C-18), 35.6 (C-6/-10), 34.6 (C-17), 29.5 (C-7), 28.9 (C-11).

(*E/Z*)-1-(3-(4-(2-Azidoethyl)phenoxy)propyl)-2-(3-((4-methoxybenzyl)sulfinyl)prop-1-en-1-yl)disulfane, **(19)**

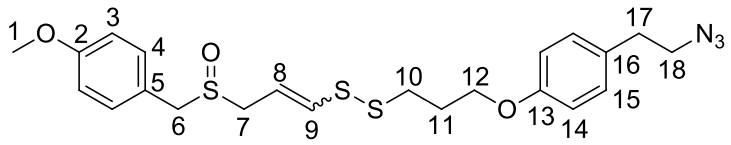

The sulfide **18** (50 mg, 0.11 mmol, 1 eq) was dissolved in DCM (0.5 mL) under N_2 and cooled to -78°C. *m*-CPBA (21 mg, 0.12 mmol, 1.1 eq) was added and the reaction was kept at -78°C, resulting in a more polar spot being observed on TLC (EtOAc:Hexane = 80:20). The reaction was allowed to warm to room temperature, and upon full consumption of the starting material by TLC the reaction was quenched with saturated aqueous sodium bicarbonate (2 mL). The product was extracted into DCM (3 x 3 mL) and the combined organic fractions were washed (2 x 2 mL water, 2 mL brine), dried over $MgSO_4$ and concentrated under reduced pressure. The purification via silica column chromatography afforded the azide-ajoene **19** as a 2:3 mixture of *E/Z*-isomers as a clear colourless oil (32 mg, 62%).

E/Z mixture: R_f = 0.4 (EtOAc:Hexane = 80:20); IR ν_{max}/ cm^{-1} (ATR): 2094 (N=N=N), 1031 (S=O); HRMS (ES): *m/z* found 478.1303 $[M+H]^+$, $C_{22}H_{28}N_3O_3S_3$ requires 478.1293;

E-isomer: δ_H(400 MHz, $CDCl_3$): 7.21 (2H, d, *J* = 8.7 Hz, H-15), 7.12 (2H, d, *J* = 8.7 Hz, H-4), 6.90 (2H, d, *J* = 8.7 Hz, H-14), 6.83 (2H, d, *J* = 8.7 Hz, H-3), 6.36 (1H, dt, *J* = 14.8, 1.0 Hz, H-9), 5.96 (1H, dt, 14.8, 7.4 Hz, H-8), 4.04 (2H, t, *J* = 5.9 Hz, H-12), 3.91 (2H, s, H-6), 3.80 (3H, s, H-1), 3.48-3.41 (1H, m, H-7a), 3.46 (2H, t, *J* = 7.3 Hz, H-18), 3.29 (1H, ddd, *J* = 13.2, 8.0, 1.1 Hz, H-7b), 2.91 (2H, t, *J* = 7.0 Hz, H-10), 2.83 (2H, t, *J* = 7.2 Hz, H-17), 2.16 (2H, m, H-11); δ_C (101 MHz, $CDCl_3$): 160.0 (C-2), 157.8 (C-13), 134.4 (C-9), 131.3 (C-15), 130.5 (C-16), 129.9 (C-4), 121.7 (C-5), 117.5 (C-8), 114.9 (C-3), 114.7 (C-14), 66.0 (C-12), 56.6 (C-6), 55.5 (C-1), 52.9 (C-7), 52.8 (C-18), 34.9 (C-10), 34.6 (C-17), 29.0 (C-11).
Z-isomer: δ_H(400 MHz, $CDCl_3$): 7.21 (2H, d, *J* = 8.7Hz, H-15), 7.12 (2H, d, *J* = 8.7 Hz, H-4), 6.90 (2H, d, *J* = 8.7 Hz, H-14), 6.83 (2H, d, *J* = 8.7 Hz, H-3), 6.60 (1H, dt, *J* = 9.4, 1.0 Hz, H-9), 5.80 (1H, dt, *J* = 9.4, 7.9 Hz, H-8), 4.05 (2H, t, *J* = 6.0 Hz, H-12), 3.92 (2H, s, H-6), 3.80 (3H, s, H-1), 3.53 (1H, ddd, *J* = 13.4, 7.6, 1.0 Hz, H-7a), 3.48-3.41 (1H, m, H-7b), 3.46 (2H, t, *J* = 7.3 Hz, H-18), 2.93 (2H, t, *J* = 7.1 Hz, H-10), 2.83 (2H, t, *J* = 7.2 Hz, H-17), 2.16 (2H, m, H-11); δ_C (101 MHz, $CDCl_3$): 160.0 (C-2), 157.8 (C-13), 138.3 (C-9), 131.4 (C-15), 130.5

(C-16), 129.9 (C-4), 121.8 (C-5), 118.9 (C-8), 114.9 (C-3), 114.7 (C-14), 65.9 (C-12), 57.1 (C-6), 55.5 (C-1), 52.8 (C-18), 49.7 (C-7), 35.7 (C-10), 34.6 (C-17), 28.9 (C-11).

tert-Butyl (3-(2-(2-(3-aminopropoxy)ethoxy)ethoxy)propyl)carbamate, **(20)**[563]

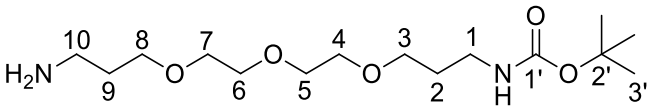

4,7,10-trioxatridecane-1,13-diamine (2.00 mL, 13.3 mmol, 1.5 eq) in DCM was reacted with di-*tert*-butyl dicarbonate (1.93 g, 8.86 mmol, 1 eq) at room temperature over two hours. The solvent was removed under reduced pressure and the resulting residue was purified via silica column chromatography (20% MeOH in DCM) to afford mono-Boc-protected diamine linker **20** as an amber oil (1.31 g, 46%).

R_f = 0.15 (MeOH:DCM = 20:80); IR ν_{max}/ cm^{-1} (ATR): 1694 (C=O); δ_H (400 MHz, $CDCl_3$): 5.21 (1H, brs, NH), 3.64-3.50 (12H, m, H-3/-4/-5/-6/-7/-8), 3.40 (2H, m, H-1), 3.19 (2H, t, *J* = 6.0 Hz, H-10), 2.76 (2H, s, NH_2), 1.80-1.71 (4H, m, H-2/-9), 1.41 (9H, s, H-3'); δ_C (101 MHz, $CDCl_3$): 156.2 (C-1'), 77.9 (C-2'), 70.7 (C-5/-6), 70.6 (C-7), 70.3 (C-4), 70.0 (C-8), 69.6 (C-3), 39.8 (C-10), 38.5 (C-1), 32.1 (C-9) 29.8 (C-2), 28.6 (C-3').

4-(Propiolamidomethyl)benzoic acid, **(21)**[564]

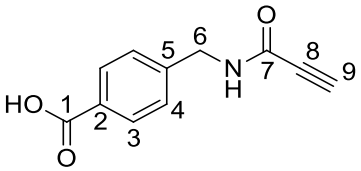

A solution of propiolic acid (0.49 mL, 7.9 mmol, 1.2 eq), 4-(aminomethyl)benzoic acid (1.00 g, 6.62 mmol, 1 eq) and hydroxybenzotriazole (202 mg, 1.32 mmol, 0.2 eq) in acetonitrile (40 mL) was cooled to 0°C under N_2, to which DCC (1.64 g, 7.94 mmol, 1.2 eq) was subsequently added. The reaction was kept at 0°C for one hour and then allowed to reach room temperature over one hour. The reaction mixture was filtered through Celite, and the solvent was removed under reduced pressure. The resulting oil was taken up in EtOAc (50 mL) and washed with H_2O (2 x 30 mL). Upon drying over $MgSO_4$ and removal of the solvent, silica gel column chromatography (MeOH:DCM = 10:90) afforded amide **21** as a colourless crystalline solid (476 mg, 35%).

R_f = 0.5 (MeOH:DCM = 10:90); Mp (MeOH:DCM): 190-193 °C; IR ν_{max}/ cm^{-1} (ATR): 3268 (carboxylic O-H), 2110 (alkyne C-H), 1684 (C=O)**;** δ_H (300 MHz, MeOD): 7.99 (2H, d, *J* = 8.1 Hz, H-3), 7.38 (2H, d, *J* = 8.1 Hz, H-4), 4.46 (2H, s, H-6), 3.60 (1H, s, H-9); δ_C (101 MHz, MeOD): 169.7 (C-1), 154.8 (C-7), 144.5 (C-2), 131.2 (C-5), 131.0 (C-3), 128.5 (C-4), 78.0 (C-8), 76.2 (C-9), 43.9 (C-6).

tert-Butyl (1-oxo-1-(4-(propiolamidomethyl)phenyl)-6,9,12-trioxa-2-azapentadecan-15-yl)carbamate, **(22)**

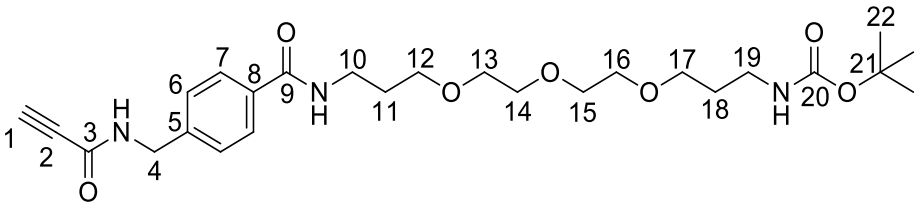

The acid **21** (250 mg, 1.46 mmol, 1 eq) and HOBt (246 mg, 1.61 mmol, 1.1 eq) were suspended in DCM (15 mL) at 0°C under N_2. DCC (392 mg, 1.84 mmol, 1.3 eq) and the amine **20** (592 mg, 1.85 mmol, 1.3 eq) in DCM (2 mL) were sequentially added, and the reaction was left to warm to room temperature. After four hours, the reaction was filtered through Celite and the solvent evaporated under reduced pressure. Silica gel column chromatography (MeOH:DCM = 10:90) afforded alkyne **22** as a clear-yellow oil. (620 mg, 84%).

R_f = 0.75 (MeOH:DCM = 10:90); IR ν_{max}/ cm^{-1} (ATR): 3340 (amide N-H), 2116 (alkyne C-H), 1696 (C=O)**;** δ_H (300 MHz, $CDCl_3$): 7.77 (2H, d, *J* = 8.2 Hz, H-7), 7.32 (2H, d, *J* = 8.2 Hz, H-6), 7.29 (1H, brs, NH), 6.87 (1H, brs, NH), 4.85 (1H, brs, NH), 4.51 (2H, d, *J* = 6.0 Hz, H-4), 3.68 – 3.56 (10H, m, H-13/-14/-15/-16/-17), 3.49 – 3.42 (4H, m, H-12/-19), 3.13 (2H, q, H-10), 2.82 (1H, s, H-1), 1.93-1.85 (2H, p, H-18), 1.69-1.63 (2H, p, H-11), 1.42 (9H, s, H-22); δ_C (101 MHz, $CDCl_3$): 167.0 (C-9), 156.3 (C-20), 152.4 (C-3), 140.7 (C_{quat}), 134.3 (C_{quat}), 127.9 (C-7), 127.6 (C-6), 79.3 (C-21) 77.4 (C-2), 73.9 (C-1), 71.0 (C-17), 70.6 (C-14), 70.6 (C-15), 70.5 (C-13), 70.2 (C-16), 69.5 (C-12),43.5 (C-4), 39.3 (C-19), 38.6 (C-10), 29.8 (C-18), 28.9 (C-11), 28.6 (C-22); HRMS (ES): *m/z* found 506.2866 $[M+H]^+$, $C_{26}H_{40}N_3O_7$ requires 506.2872.

N-(3-(2-(2-(3-aminopropoxy)ethoxy)ethoxy)propyl)-4-propiolamidomethyl)benzamide, **(23)**

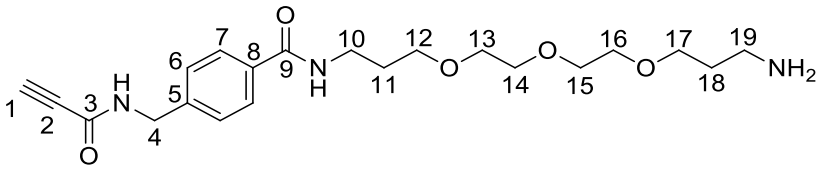

Carbamate **22** (437 mg, 0.86 mmol, 1 eq) was dissolved in DCM (6.4 mL) at 0°C under N_2, trifluoroacetic acid (0.66 mL, 8.6 mmol, 10 eq) was added and the mixture was allowed to warm to room temperature over three hours. The solvent and remaining acid reactant were then removed under reduced pressure. The resulting residue was purified via silica gel column chromatography (MeOH:DCM = 10:90) to afford the amine **23** as a clear-yellow oil (307 mg, 88%).

R_f = 0.65 (MeOH:DCM = 20:80); IR ν_{max}/ cm^{-1} (ATR): 3244 (N-H), 2106 (alkyne C-H), 1680 (C=O)**;** δ_H (300 MHz, d_6-DMSO): 9.30 (1H, brs, NH), 8.41 (1H, brs, NH), 7.79 (2H, d, *J* = 8.2 Hz, H-7), 7.31 (2H, d, *J* = 8.2 Hz, H-6), 4.33 (2H, d, *J* = 6.1 Hz, H-4), 3.54-3.43 (12H, m, H-12/-13/-14/-15/-16/-17), 3.17 (s, 1H, H-1), 3.30 (2H, q, *J* = 6.3 Hz, H-10), 2.86 (2H, m, H19), 1.82-1.71 (4H, m, H-11/-18); δ_C (101 MHz, d_6-DMSO): 165.9 (C-9), 151.7 (C-3), 141.5 (C_{quat}), 133.4 (C_{quat}), 127.2 (C-7), 127.0 (C-6), 78.1 (C-2), 76.1 (C-1), 69.7 (C-14), 69.6 (C-15), 69.5 (C-13), 69.4 (C-16), 68.3 (C-17), 67.3 (C-12), 42.0 (C-4), 36.8 (C-19), 36.6 (C-10), 29.3 (C-18), 27.1 (C-11); HRMS (ES): *m/z* found 406.2342 $[M+H]^+$, $C_{21}H_{32}N_3O_5$ requires 406.2347.

2,5-Dioxopyrrolidin-1-yl 5-((3a*R*,4*R*,6a*S*)-2-oxohexahydro-1*H*-thieno[3,4-*d*]imidazol-4-yl)pentanoate, **(24)**[313]

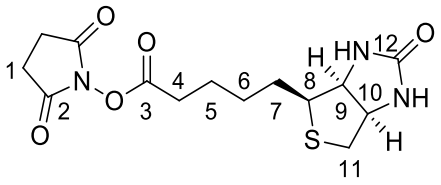

To a solution of biotin (500 mg, 2.05 mmol, 1eq), DMAP (37.0 mg, 0.31 mmol, 0.15 eq) and DCC (550 mg, 2.66 mmol, 1.3 eq) in DMF (10 mL) at 0 °C under N_2 was added N-hydroxysuccinimide (280 mg, 2.46 mmol, 1.2 eq). The reaction was allowed to warm to room temperature and stirred for 24 hours. The mixture was filtered through Celite and the bulk of the DMF removed by gentle heating in a steaming water bath under reduced

pressure on the rotoevaporator. Trituration with diethyl ether afforded a copious precipitate, which was filtered and washed with ice-cold diethyl ether (3 x 10 mL) to afford succinimide ester **24** (451 mg, 65%).

Mp (DMF:Diethyl Ether): 205-208 °C, lit[313] Mp: 206-207 °C; IR ν_{max}/ cm^{-1} (ATR): 3226 (N-H), 1747, 1728, 1700 (3 x C=O)**;** δ_H (300 MHz, DMSO): 6.39 (1H, s, NH), 6.34 (1H, s ,NH), 4.31 (1H, dd, *J* = 7.6, 5.2 Hz, H-9), 4.15 (1H, m, H-10), 3.11 (1H, m, H-8), 2.83 (1H, dd, *J* = 12.4, 5.1 Hz, H-11a), 2.81 (4H, brs, H-1), 2.66 (2H, t, *J* = 7.3 Hz, H-4), 2.58 (1H, d, *J* = 12.4 Hz, H-11b), 1.72-1.36 (6H, m, H-5/-6/-7).

<u>*N*-(15-Oxo-19-((3a*R*,4*R*,6a*S*)-2-oxohexahydro-1*H*-thieno[3,4-d]imidazol-4-yl)-4,7,10-trioxa-14-azanonadecyl)-4-(propiolamidomethyl)benzamide, **(25)**</u>[311]

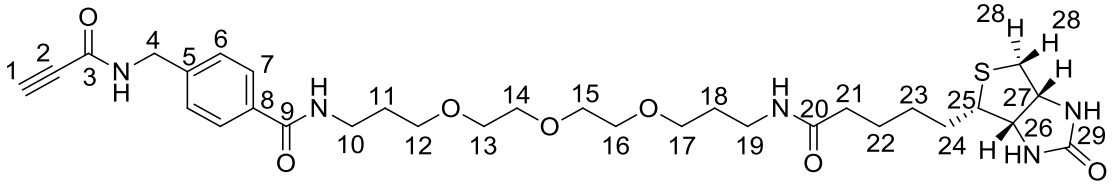

The amine **23** (449 mg, 0.86 mmol, 1.2 eq) and Ester **24** (246 mg, 0.72 mmol, 1 eq) were dissolved in DMF (2 mL) under N_2 and cooled to -78°C. DIPEA (0.25 mL, 1.4 mmol, 2eq) was added and the mixture was left to stir for two hours, while warming to room temperature. The bulk of the solvent was then removed under reduced pressure and the residue was lyophilised. Silica gel column chromatography (MeOH:DCM = 5:95) afforded biotin-alkyne **25** as a clear colourless wax (236 mg, 57%).

R_f = 0.60 (MeOH:DCM = 10:90); IR ν_{max}/ cm^{-1} (ATR): 3266 (amide N-H), 2106 (alkyne C-H), 1694 (C=O)**;** δ_H (400 MHz, MeOD): 7.81 (2H, d, *J* = 8.4 Hz, H-7), 7.40 (2H, d, *J* = 8.4 Hz, H-6), 4.50 (2H, ddd, *J* = 7.9, 4.9, 0.6 Hz, H-27), 4.47 (2H, s, H-4), 4.31 (1 H, dd, *J* = 7.9, 4.5 Hz, H-26), 3.68-3.62 (8H, m, H-13/-14/-15/-16), 3.57 (2H, t, *J* = 6.2 Hz, H-10), 3.51 (2H, t, H-17), 3.50 (2H, t, H-12), 3.37 (1H, s, H-1) 3.29-3.19 (3H, m, H-19/-25), 2.94 (1H, dd, *J* = 12.8, 5.0 Hz, H-28a), 2.72 (1H, d, *J* = 12.8 Hz, H-28b), 2.21 (2H, t, *J* = 7.4 Hz, H-21), 1.90 (2H, p, H-18), 1.76 (2H, p, H-11), 1.70-1.55 (4H, m, H-22/-23), 1.48-1.42 (2H, m, H-24); δ_C (101 MHz, MeOD): 175.9 (C-29), 169.7 (C-20), 166.0 (C-3), 154.7 (C-9), 143.0 (C_{quat}), 134.9 (C_{quat}), 128.7 (C-7), 128.6 (C-6), 78.1 (C-2), 76.2 (C-1), 71.5 (C-14 or 15), 71.5 (C-14 or 15), 71.3 (C-13), 71.2 (C-16), 70.4 (C-12), 70.0 (C-17), 63.4 (C-27), 61.6 (C-26), 57.0 (C-25), 43.9 (C-4), 41.0 (C-28), 38.8 (C-19), 37.8 (C-10), 36.9 (C-21), 30.4 (C-11 or 18), 30.4

(C-11 or 18), 29.8 (C-24), 29.5 (C-23), 26.9 (C-22); HRMS (ES): *m/z* found 632.3143 $[M+H]^+$, $C_{31}H_{46}N_5O_7S$ requires 632.3113.

(*E/Z*)-1-(4-(3-((3-((4-Methoxybenzyl)sulfinyl)prop-1-en-1-yl)disulfanyl)propoxy)phenethyl)-*N*-(4-((15-oxo-19-((3a*R*,4*R*,6a*S*)-2-oxohexahydro-1*H*-thieno[3,4-d]imidazol-4-yl)-4,7,10-trioxa-14-azanonadecyl)carbamoyl)benzyl)-1H-1,2,3-triazole-4-carboxamide, **(26)**

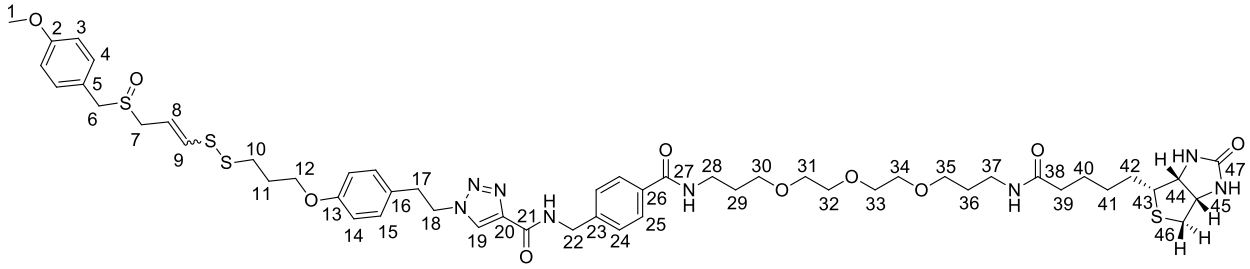

The reaction vessel was loaded with $CuSO_4.5H_2O$ (2.5 mg, 0.01 mmol, 0.1 eq) and sodium ascorbate (5.9 mg, 0.03 mmol, 0.3 eq) in H_2O (1 mL) under N_2. To the rapidly stirring solution the azide-ajoene **19** (52 mg, 0.11 mmol, 1 eq) in DMF (1 mL) and biotin-alkyne **25** (69 mg, 0.11 mmol, 1 eq) in DMF (1 mL) were added. The reaction was heated to 30°C and left to stir over-night for 18 hours. The solvents were removed via lyophilisation and the off-white solid residue was subjected to silica gel column chromatography (MeOH:DCM = 10:90) to afford biotin-ajoene **26** as 7:10 mixture of *E/Z*-isomers and as a white crystalline solid (68 mg, 56%).

E/Z mixture: R_f = 0.7 (MeOH:DCM = 0.2:0.8); IR ν_{max}/ cm^{-1} (ATR): 3310 (amide N-H), 1696/1649 (C=O); HRMS (ES): *m/z* found 1109.4332 $[M+H]^+$, $C_{53}H_{73}N_8O_{10}S_4$ requires 1109.4338;

E-isomer: δ_H (400 MHz, MeOD:$CDCl_3$ = 1:9): 7.91 (1H, s, H-19), 7.66 (2H, d, *J* = 8.4 Hz, H-25), 7.30 (2H, d, *J* = 8.4 Hz, H-24), 7.11 (2H, d, *J* = 8.7 Hz, H-15), 6.91 (2H, d, *J* = 8.7 Hz, H-4), 6.79 (2H, d, *J* = 8.7 Hz, H-14), 6.70 (2H, d, *J* = 8.7 Hz, H-3), 6.29 (1H, dt, *J* = 14.7, 1.0 Hz, H-9), 5.82 (1H, dt, *J* = 14.8, 7.8 Hz, H-8), 4.53 (2H, s, H-22), 4.50 (2H, t, *J* = 7.3 Hz, H-18), 4.37 (1H, ddd, *J* = 7.8, 5.0, 0.9 Hz, H-45), 4.17 (1H, dd, *J* = 7.8, 4.6 Hz, H-44), 3.93 (2H, m, H-12), 3.85 (2H, d, *J* = 4.1 Hz, H-6), 3.69 (3H, s, H-1), 3.56 – 3.35 (14H, m, H-7/-30/-31/-32/-33/-34/-35), 3.27-3.22 (2H, m, H-28), 3.15 (2H, t, *J* = 6.6 Hz, H-37), 3.08-3.01 (3H, m, H-17/-43), 2.84-2.76 (2H, m, H-10/-46a), 2.60 (1H, d, *J* = 12.8 Hz, H-46b), 2.09 – 2.00 (4H,

m, H-11/-39), 1.78 (2H, p, H-29), 1.62 (2H, p, H-36), 1.57 – 1.43 (4H, m, H-40/42), 1.29 (2H, p, H-41); δ_C (101 MHz, MeOD:$CDCl_3$ = 1:9): 173.8 (C_{quat}), 167.7 (C_{quat}), 164.0 (C_{quat}), 160.5 (C_{quat}), 159.9 (C_{quat}), 159.6 (C_{quat}), 157.9 (C_{quat}), 142.5 (C_{quat}), 141.5 (C_{quat}), 134.7 (C-9), 133.6 (C_{quat}), 131.2 (C-15), 129.6 (C-4), 128.7 (C_{quat}), 127.6 (C-25), 127.4 (C-24), 126.1 (C-19), 116.7 (C-8), 114.9 (C-3), 114.5 (C-14), 70.4 (C-32), 70.3 (C-33), 70.1 (C-28), 69.9 (C-31), 69.9 (C-34), 69.4 (C-37), 65.8 (C-12), 61.9 (C-45), 60.1 (C-44), 56.1 (C-6), 55.5 (C-43), 55.2 (C-1), 52.7 (C-7), 52.1 (C-18), 42.6 (C-22), 40.3 (C-46), 38.1 (C-30), 37.2 (C-35), 35.8 (C-39), 35.5 (C-17), 34.6 (C-10), 28.9 (C-36), 28.9 (C-29), 28.7 (C-11), 28.4(C-41), 28.1 (C-42), 25.4 (C-40).

Z-isomer: δ_H (400 MHz, MeOD:$CDCl_3$ = 1:9): 7.91 (1H, s, H-19), 7.66 (2H, d, *J* = 8.4 Hz, H-25), 7.30 (2H, d, *J* = 8.4 Hz, H-24), 7.11 (2H, d, *J* = 8.7 Hz, H-15), 6.91 (2H, d, *J* = 8.7 Hz, H-4), 6.79 (2H, d, *J* = 8.7 Hz, H-14), 6.70 (2H, d, *J* = 8.7 Hz, H-3), 6.51 (1H, dt, *J* = 9.5, 0.9 Hz, H-9), 5.66 (1H, dt, *J* = 14.8, 7.8 Hz, H-8), 4.53 (2H, s, H-22), 4.50 (2H, t, *J* = 7.3 Hz, H-18), 4.37 (1H, ddd, *J* = 7.8, 5.0, 0.9 Hz, H-45), 4.17 (1H, dd, *J* = 7.8, 4.6 Hz, H-44), 3.92 (2H, m, H-12), 3.85 (2H, d, *J* = 4.1 Hz, H-6), 3.69 (3H, s, H-1), 3.56 – 3.35 (14H, m, H-7/-30/-31/-32/-33/-34/-35), 3.27-3.22 (2H, m, H-28), 3.15 (2H, t, *J* = 6.6 Hz, H-37), 3.08-3.01 (3H, m, H-17/-43), 2.84-2.76 (2H, m, H-10/-46a), 2.60 (1H, d, *J* = 12.8 Hz, H-46b), 2.09 – 2.00 (4H, m, H-11/-39), 1.78 (2H, p, H-29), 1.62 (2H, p, H-36), 1.57 – 1.43 (4H, m, H-40/42), 1.29 (2H, p, H-41); δ_C (101 MHz, MeOD:$CDCl_3$ = 1:9): 173.8 (C_{quat}), 167.7 (C_{quat}), 164.0 (C_{quat}), 160.5 (C_{quat}), 159.9 (C_{quat}), 159.6 (C_{quat}), 157.9 (C_{quat}), 142.5 (C_{quat}), 141.5(C_{quat}), 138.6 (C-9), 133.6 (C_{quat}), 131.3 (C-15), 129.6 (C-4), 128.7 (C_{quat}), 127.6 (C-25), 127.4 (C-24), 126.1 (C-19), 118.2 (C-8), 114.9 (C-3), 114.5 (C-14), 70.4 (C-32), 70.3 (C-33), 70.1 (C-28), 69.9 (C-31), 69.9 (C-34), 69.4 (C-37), 65.7 (C-12), 61.9 (C-45), 60.1 (C-44), 56.6 (C-6), 55.5 (C-43), 55.2 (C-1), 52.1 (C-18), 49.4 (C-7), 42.6 (C-22), 40.3 (C-46), 38.1 (C-30), 37.2 (C-35), 35.8 (C-39), 35.5 (C-17), 35.5 (C-10), 28.9 (C-36), 28.9 (C-29), 28.6 (C-11), 28.4(C-41), 28.1 (C-42), 25.4 (C-40).

<u>*S*-(4-azidobutyl) 4-methylbenzenesulfonothioate, **(27)**</u>

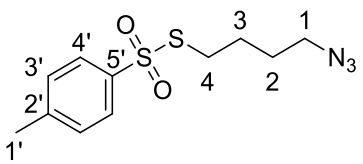

Sodium azide (136 mg, 2.09, 1 eq) was added to a stirring solution of 1,4-dibromobutane (0.25 mL, 2.09 mmol, 1 eq) in acetonitrile (15 mL) under argon. The reaction was left

stirring at room temperature. The conversion of the dibromide to the azide was monitored using a $KMnO_4$ and a triphenylphosphine (to get the amine via the Staudinger reaction)/Ninhydrin combination stain, to detect the dibromide and the azide respectively. Once the starting material was fully consumed (after approximately ten hours), potassium thiotosylate (474 mg, 2.09 mmol, 1 eq) was added and the mixture was left to stir over night at room temperature. The next day, the solvent was removed under reduced pressure, the resulting residue was then taken up in EtOAc and washed (3 x H_2O, 1 x sat. aq. NaCl) to remove the bromide salts. The mixture was dried over $MgSO_4$, concentrated under vacuum and purified using silica-gel column chromatography (EtOAc:Hexane = 10:90) to obtain **27** as a clear colourless oil (387 mg, 65%).

R_f = 0.5 (EtOAc:Hexane, = 10:90); δ_H (400 MHz, $CDCl_3$): 7.82 (2H, d, *J* = 8.3 Hz, H-3'), 7.35 (2H, d, *J* = 8.3 Hz, H-2'), 3.33 (2H, t, *J* = 6.3 Hz, H-1), 3.02 (2H, t, *J* = 6.9 Hz, H-4), 2.45 (3H, s, H-1'), 1.86 (2H, m, H-2), 1.81 (2H, m, H-3).

Prop-2-yn-1-yl(propyl)sulfane, **(28)**[153]

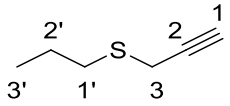

Potassium hydroxide (9.70 g, 174.6 mmol) was dissolved in degassed MeOH (30 mL) at 0 °C under N_2. 1-Propanethiol (10.0 g, 131.3 mmol) was added drop-wise, followed by propargyl bromide (16.4 mL, 147.1 mmol, 80% in toluene) and the reaction was allowed to warm to room temperature, after which TLC (hexane) showed the formation of a less polar UV-active spot to the progargyl bromide. The MeOH was removed under reduced pressure and the residue was extracted with diethyl ether (3 x 100 mL), then washed with H_2O (3 x15 mL). The ether extract was dried ($MgSO_4$) and concentrated under vacuum, then purified by distillation (80 °C, 20 mmHg) to give **28** as a yellow oil (12.21 g, 81%).

R_f = 0.8 (Hexane); IR ν_{max}/ cm^{-1} (ATR):3303 (C-H alkyne); δ_H (400 MHz, $CDCl_3$): 3.22 (2H, d, *J* = 2.6 Hz, H-3), 2.64 (2H, t, *J* = 7.4 Hz, H-1'), 2.21 (1H, t, *J* = 2.6 Hz, H-1), 1.63 (2H, m, H-2'), 0.98 (3H, t, *J* = 7.4 Hz, H-3'); δ_C (101 MHz, $CDCl_3$): 80.1 (C-2), 70.7 (C-1), 33.6 (C-1'), 22.2 (C-2'), 19.0 (C-3), 13.3 (C-3').

(*E*/*Z*)-*S*-(3-(propylthio)prop-1-en-1-yl) ethanethioate, **(29)**[153]

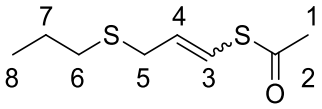

The sulfide **28** (2.63 g, 23.0 mmol) was added to dry toluene (20 mL) at room temperature and the solution heated to 80 °C. ACCN (480 mg, 2.0 mmol) was added, followed by drop-wise addition of thioacetic acid (3 mL, 42 mmol). The mixture was heated at 80 °C under N_2 for 2 hours, after which the solution was allowed to cool. Sat. aq. Na_2CO_3 (20 mL) was then added to quench any remaining thioacetic acid and the toluene was removed under vacuum. The residue was extracted with DCM (3 x 30 mL), which was washed with sat. aq. NaCl and dried over $MgSO_4$. The solvent was removed under reduced vacuum and the resulting residue purified by silica-gel column chromatography (EtOAc: Hex = 1:49) to give compound **29** in a 3:5 mixture of *E*/*Z*-stereoisomers and as a yellow oil (2.93 g, 67%).

E/*Z* mixture: R_f = 0.6 (EtOAc:Hex = 1:9); IR ν_{max}/ cm^{-1} (ATR): 1701 (C=O carbonyl), 634 (C-S); HRMS (ES): *m/z* found 190.0485 $[M+H]^+$, $C_8H_{14}OS_2$ requires190.0486;

E-isomer: δ_H (400 MHz, $CDCl_3$): 6.51 (1H, dt, *J* = 15.6, 1.2 Hz, H-3), 5.81 (1H, dt, *J* = 15.6, 7.6 Hz, H-4), 3.19 (2H, dd, *J* = 7.4, 1.2 Hz, H-5), 2.42 (2H, t, *J* = 7.5 Hz, H-6), 2.33 (3H, s, H-1), 1.58 (2H, m , H-7), 0.95 (3H, t, *J* = 7.1 Hz, H-8); δ_C (101 MHz, $CDCl_3$): 192.8 (C-2), 130.5 (C-4), 118.7 (C-3) 34.0 (C-5), 32.9 (C-6), 30.3 (C-1) 22.5 (C-7), 13.3 (C-8).
Z-isomer: δ_H (400 MHz, $CDCl_3$): 6.64 (1H, dt, *J* – 9.5, 1.1 Hz, H-3), 5.84 (1H, dt, *J* = 9.7, 7.4 Hz, H-4) 3.16 (2H, dd, *J* = 7.7, 1.0 Hz, H-5), 2.42 (2H, t, *J* = 7.1 Hz, H-6), 2.37 (3H, s, H-1), 1.58 (2H, m, H-7), 0.96 (3H, t, *J* = 7.2 Hz, H-8); δ_C (101 MHz, $CDCl_3$): 191.1 (C-2), 128.9 (C-4), 119.0 (C-3), 33.1 (C-6), 30.9 (C-5), 30.8 (C-1), 22.8 (C-7), 13.4 (C-8).

(*E*/*Z*)-1-(4-azidobutyl)-2-(3-(propylthio)prop-1-en-1-yl)disulfane, **(30)**

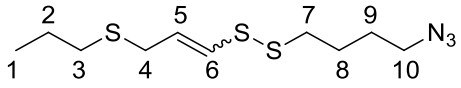

A solution of the thioacetate **29** (78 mg, 0.40 mmol) in dry degassed MeOH (1 mL) was prepared and cooled to -40 °C, under N_2. KOH (28 mg, 0.48 mmol) in MeOH (1 mL) was added and after 30 minutes, the solution was further cooled to -78 °C. The sulfenylating agent **27** (180 mg, 0.63 mmol) in anhydrous DCM (1 mL) was added. After two hours the reaction was quenched with sat. aq. NH_4Cl (5 mL), the solvent removed under vacuum

and the product was extracted into DCM (3 x 15 mL). The extracts were washed with sat. aq. NaCl (2 x 10 mL), dried ($MgSO_4$) and concentrated under vacuum. Silica-gel column chromatography (EtOAc:Hexane = 5:95) of the residue yielded the disulfide **30** as a pale yellow oil in 3:5 mixture of *E*/*Z*-isomers (61 mg, 55%).

E/Z mixture: R_f = 0.75 (EtOAc:Hex = 1:9);

E-isomer: δ_H (400 MHz, $CDCl_3$): 6.02 (1H, dt, *J* = 14.6, 1.0 Hz, H-6) 5.81 (1H, dt, *J* = 14.6, 7.3 Hz, H-5), 3.13 (2H, d, *J* = 7.3 Hz, H-4), 3.33 (2H, t, *J* = 6.3 Hz, H-10), 2.57 (2H, t, *J* = 6.9 Hz, H-7), 2.41 (2H, t, *J* = 7.4, H-3), 1.91-1.74 (2H, m, H-8/9), 1.57 (2H, m, H-2), 096 (3H, t, *J* = 7.4 Hz, H-1).
Z-isomer: δ_H (400 MHz, $CDCl_3$): 6.06 (1H, d, *J* = 9.2 Hz, H-6), 5.64 (1H, dt, *J* = 9.2, 7.8 Hz, H-5), 3.19 (2H, d, *J* = 7.8 Hz, H-4), 3.33 (2H, t, *J* = 6.3 Hz, H-10), 2.59 (2H, t, *J* = 6.9 Hz, H-7), 2.43 (2H, t, *J* = 7.4 Hz, H-3), 1.91-1.74 (2H, m, H-8/9), 1.57 (2H, m, H-2), 0.96 (3H, t, *J* = 7.4 Hz, H-1).

(*E*/*Z*)-1-(4-azidobutyl)-2-(3-(propylsulfinyl)prop-1-en-1-yl)disulfane, **(31)**

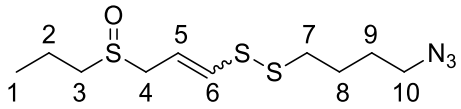

The sulfide **30** (31 mg, 0.11 mmol, 1 eq) was dissolved in DCM (0.5 mL) under N_2 and cooled to -78°C. *m*-CPBA (21 mg, 0.12 mmol, 1.1 eq) was added and the reaction was kept at -78°C, resulting in a more polar spot being observed on TLC (EtOAc:Hexane = 80:20). The reaction was allowed to warm to room temperature, and upon full consumption of the starting material by TLC the reaction was quenched with saturated aqueous sodium bicarbonate (2 mL). The product was extracted into DCM (3 x 3 mL) and the combined organic fractions were washed (2 x 2 mL water, 2 mL brine), dried over $MgSO_4$ and concentrated under reduced pressure. The purification via silica column chromatography afforded the azide-ajoene **31** as a 2:3 mixture of *E/Z*-isomers as a clear colourless oil (25 mg, 77%).

E/Z mixture: R_f = 0.4 (EtOAc:Hex = 1:1);

E-isomer: δ_H (400 MHz, $CDCl_3$): 6.38 (2H, d, *J* = 14.7 Hz, H-6), 5.95 (2H, dt, *J* = 14.7, 7.7 Hz, H-5), 3.68-3.55 (2H, m, H-4), 3.42 (2H, t, *J* = 6.4 Hz, H-10), 2.74 (2H, t, *J* = 9.8 Hz, H-7), 2.72-

2.56 (2H, m, H-3), 2.02-1.93 (2H, m, H-2), 1.90-1.75 (4H, m, H-8/9), 1.09 (2H, t, *J* = 7.4 Hz, H-1).

Z-isomer: δ_H (400 MHz, $CDCl_3$): 6.58 (2H, d, *J* = 9.4 Hz, H-6), 5.79 (2H, dt, *J* = 9.4, 8.0 Hz, H-5), 3.58-346 (2H, m, H-4), 3.42 (2H, t, *J* = 6.4 Hz, H-10), 2.77 (2H, t, *J* = 9.8 Hz, H-7), 2.72-.256 (2H, m, H-3), 2.02-1.93 (2H, m, H-2), 1.90-1.75 (4H, m, H-8/9), 1.09 (2H, t, *J* = 7.4 Hz, H-1).

5-((3a*S*,4*S*,6a*R*)-2-oxohexahydro-1*H*-thieno[3,4-*d*]imidazol-4-yl)-*N*-(prop-2-yn-1-yl)pentanamide, **(32)**[321]

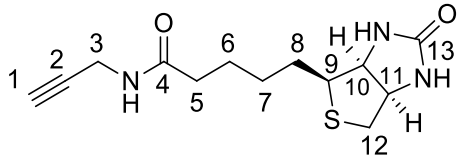

Triethylamine (119 µL, 0.856 mmol) was added to biotin hydroxysuccinimidyl ester **24** (146 mg, 0.428 mmol) and propargyl amine (42 µL, 0.655 mmol) in DMF (8.5 mL). After stirring for 24 hours, at room temperature, the reaction mixture was concentrated under vacuum. After addition of diethyl ether, the precipitate was filtered and dried under vacuum. The purification by silica gel column chromatography (MeOH:DCM = 2:8) afforded the amide **32** as white solid (96 mg, 80%).

R_f = 0.3 (MeOH:DCM = 1:9); δ_H (400 MHz, MeOD): 4.48 (1H, dd, *J* = 7.8, 48 Hz, H-10), 4.29 (1H, dd, *J* = 7.9, 4.5 Hz, H-11), 3.93 (2H, d, *J* = 2.5 Hz, H-3), 3.20-3.13 (1H, m, H-9), 2.90 (1H, dd, *J* = 12.8, 4.9 Hz, H-12a), 2.71 (1H, dd, *J* = 12.8, 2.8 Hz, H-12b), 2.37 (1H, t, *J* = 2.5 Hz, H-1), 2.20 (2H, t, *J* = 7.4 Hz, H-5), 1.77-1.38 (6H, m, H-6/7/8).

(*E*/*Z*)-5-((3a*S*,4*S*,6a*R*)-2-oxohexahydro-1*H*-thieno[3,4-*d*]imidazol-4-yl)-*N*-((1-(4-((3-(propylsulfinyl)prop-1-en-1-yl)disulfanyl)butyl)-1*H*-1,2,3-triazol-4-yl)methyl)pentanamide, **(33)**

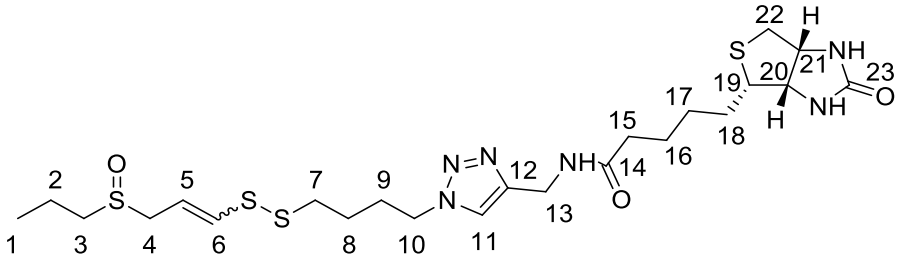

~~The reaction vessel was loaded with $CuSO_4.5H_2O$ (2.5 mg, 0.01 mmol, 0.1 eq) and sodium ascorbate (5.9 mg, 0.03 mmol, 0.3 eq) in H_2O (1 mL) under N_2. To the rapidly stirring solution the azide-ajoene **31** (30 mg, 0.10 mmol, 1 eq) in DMF (1 mL) and biotin-alkyne **32** (29 mg, 0.10 mmol, 1 eq) in DMF (1 mL) were added. The reaction was heated to 30°C and left to stir over-night for 18 hours. The solvents were removed via lyophilisation and the off-white solid residue was subjected to silica gel column chromatography (MeOH:DCM = 10:90) to afford biotin-ajoene **33** as an unstable light yellow oil (11 mg, ~20% by TLC).~~

~~*E/Z* mixture: R_f = 0.7 (EtOAc); Lack of ^{1}H-NMR spectrum due to instability during data acquisition.~~

S-prop-2-yn-1-yl 4-methylbenzenesulfonothioate, **(34)**[328]

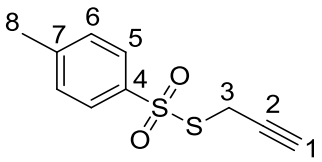

To a solution of potassium thiotosylate (1.30 g, 5.74 mmol, 1 eq) in DMF (7 mL) propargyl bromide (80% in toluene) (0.63 mL, 6.03 mmol,1.05 eq) was added dropwise and stirred under argon for 4 hours at rt. Upon reaction completion (TLC), the reaction mixture was diluted with diethyl ether (50 mL) and washed copiously with H_2O (5 x 15 mL). The organic layer was dried ($MgSO_4$), filtered, concentrated and the residue purified using flash column chromatography (EtOAc:Pet. Ether = 10:90) to yield the propargyl thiotosylate **34** (1. 10 g, 85%) as a colourless crystalline solid.

R_f = 0.5 (EtOAc:Hexane, = 15:85); IR ν_{max}/ cm^{-1} (ATR): 3270 (alkyne C-H stretch); Mp (EtOAc/Pet. Ether): 43-44 °C, Mp: 45-46 °C[328]; δ_H (300 MHz,$CDCl_3$): 7.84 (d, *J* = 8.2 Hz, 2H, **H-5**), 7.35 (d, *J* = 8.2 Hz, 2H, **H-6**), 3.79 (d, *J* = 2.7 Hz, 2H, **H-3**), 2.45 (s, 3H, **H-8**), 2.14 (t, *J* = 2.7 Hz, 1H, **H-1**). δ_C (101 MHz, $CDCl_3$) 145.1, 141.9, 129.8, 127.3, 76.4, 73.4, 24.2, 21.6; HRMS (ES): *m/z* found 249.0012 $[M + Na]^+$, $C_{10}H_{10}NaO_2S_2$ requires 249.0020.

(*E/Z*)-1-(3-((4-Methoxybenzyl)thio)prop-1-en-1-yl)-2-(prop-2-yn-1-yl)disulfane, **(35)**

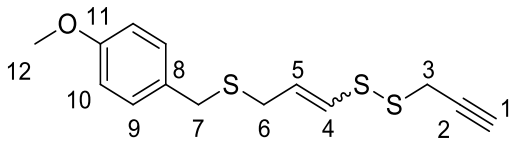

PMB-Thioacetate **2** (0.20 g, 0.75 mmol, 1 eq) was dissolved in anhydrous MeOH (0.75 mL, 1M) and cooled to -40 °C (CH_3CN/liquid nitrogen) under argon, then KOH in MeOH (43.9 mg 0.78 mmol, 1.05 eq, 1M) was added dropwise under vigorous stirring. The hydrolysis proceeded for 30 min. The mixture was then cooled to -78 °C and propargyl thiotosylate **34** in MeOH (176 mg, 0.78 mmol, 1.05 eq, 1M) was added dropwise. The solution was stirred at -78 °C for 1 hour and then warmed to rt. The reaction was quenched by the addition of ammonium chloride, diluted with H_2O (5 mL) and extracted with EtOAc (3 x 15 mL). The pooled organic fractions were washed with H_2O (2x 10 mL), sat. NaCl (10 mL), dried ($MgSO_4$), filtered and concentrated. The purification with flash column chromatography (EtOAc:Pet. Ether = 10:90) gave the vinyl disulfide **35** (129 mg, 58%) as a pungent-smelling, unstable light-yellow oil and a 1:2 mixture of *E/Z*-isomers.

E/Z mixture: R_f = 0.7 (EtOAc:Hexane, = 15:85); IR ν_{max}/ cm^{-1} (ATR): 3286 (alkyne C-H stretch), 1678 (C-C stretch);

E-isomer: δ_H (300 MHz, $CDCl_3$): 7.23 (d, *J* = 8.6 Hz, 2H, **H-9**), 6.86 (d, *J* = 8.7 Hz, 2H, **H-10**), 6.19 (dt, *J* = 14.7, 1.0 Hz, 1H, **H-4**), 5.93 (dt, *J* = 14.7, 7.3 Hz, 1H, **H-5**), 3.80 (s, 3H, **H-12**), 3.64 (s, 2H, **H-7**), 3.47 (d, *J* = 2.6 Hz, 2H, **H-3**), 3.08 (dd, *J* = 7.3, 1.1 Hz, 2H, **H-6**), 2.31 (t, *J* = 2.6 Hz, 1H, **H-1**); δ_C (101 MHz, $CDCl_3$): 158.7, 130.0, 129.8, 129.4, 127.3, 114.0, 79.1, 72.7, 55.3, 34.7, 32.6, 26.7.
Z-isomer: δ_H (300 MHz, $CDCl_3$): 7.22 (d, *J* = 8.6 Hz, 2H, **H-9**), 6.85 (d, *J* = 8.7 Hz, 2H, **H-10**), 6.37 (dt, *J* = 9.3, 1.0 Hz, 1H, **H-4**), 5.74 (dt, *J* = 9.3, 7.6 Hz, 1H, **H-5**), 3.80 (s, 1H, **H-12**), 3.68 (s, 2H, **H-7**), 3.47 (d, *J* = 2.6 Hz, 2H, **H-3**), 3.22 (dd, *J* = 7.6, 1.1 Hz, 2H, **H-6**), 2.30 (t, *J* = 2.6

Hz, 1H, **H-1**); δ_C (101 MHz, $CDCl_3$): 158.7, 131.0, 130.0, 129.8, 129.2, 114.0, 79.1, 72.7, 55.3, 35.3, 29.2, 27.3.

(*E/Z*)-1-(3-((4-Methoxybenzyl)sulfinyl)prop-1-en-1-yl)-2-(prop-2-yn-1-yl)disulfane, **(36)**

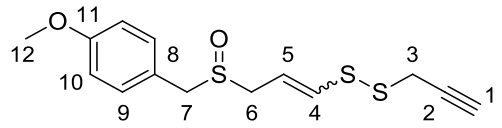

To a cooled solution (-78 °C) of vinyl disulfide **35** (100 mg, 0.34 mmol, 1 eq) in DCM (5 mL), *m*-CPBA (77%, 84 mg, 0.37 mmol, 1.1 eq) was added portion-wise, followed by stirring for 2 hours and then warmed to rt. The reaction was quenched with sat. aq. $NaHCO_3$ (2 mL), diluted with H_2O (3 mL) and extracted with EtOAc (3x 15 mL). The combined fractions were washed with H_2O (2x 10 mL) followed by sat. aq. NaCl (10 mL), then dried ($MgSO_4$), filtered and concentrated. Purification by flash column chromatography (EtOAc:Pet. Ether = 80:20) yielded the sulfoxide **36** (65 mg, 61%) as a clear light-yellow oil and a 3:5 mixture of *E/Z*-isomers.

E/Z mixture: R_f = 0.4 (EtOAc:Pet. Ether = 70:30); IR ν_{max}/ cm^{-1} (ATR): 3281 (alkyne C-H stretch), 1030 (sulfoxide S=O stretch); HRMS (ES): *m/z* found 313.0206 $[M+H]^+$, $C_{14}H_{16}NaO_2S_3$ requires 313.0210.

E-isomer: δ_H (400 MHz,$CDCl_3$):7.22 (d, 2H, *J* = 8.7 Hz, **H-9**), 6.91 (d, 2H, *J* = 8.7 Hz, **H-10**), 6.45 (d, 1H, *J* = 15.0 Hz, **H-4**), 6.00 (dt, 1H, *J* = 15.0, 7.8 Hz, **H-5**), 3.94 (s, 2H, **H-7**), 3.81 (s, 3H, **H-12**), 3.49 (d, 2H, *J* = 2.6 Hz, **H-3**), 3.48-3.28 (m, 2H, **H-6**), 2.33 (t, 1H, *J* = 2.6 Hz, **H-1**); δ_C (101 MHz, $CDCl_3$): 159.9, 133.8, 131.2, 121.5, 118.5, 114.5, 79.0, 73.1, 56.5, 55.3, 52.8, 26.8.
Z-isomer: δ_H (400 MHz, $CDCl_3$): 7.23 (d, 2H, *J* = 8.7 Hz, **H-9**), 6.91 (d, 2H, *J* = 8.7 Hz, **H-10**), 6.73 (d, 1H, *J* = 9.4 Hz, **H-4**), 5.85 (dt, 9.4, 7.8 1H, **H-5**), 3.94 (s, 2H, **H-7**), 3.81 (s, 3H, **H-12**), 3.60-3.42 (m, 2H, **H-6**), 3.50 (d, 2H, *J* = 2.6 Hz, **H-3**), 2.31 (t, 1H, *J* = 2.6 Hz, **H-1**); δ_C (101 MHz, $CDCl_3$): 159.9, 137.1, 131.3, 121.6, 119.5, 114.6, 79.0, 73.0, 57.0, 55.3, 49.4, 27.3.

tert-butyl (3-(2-(2-(3-azidopropoxy)ethoxy)ethoxy)propyl)carbamate, **(37)**[565]

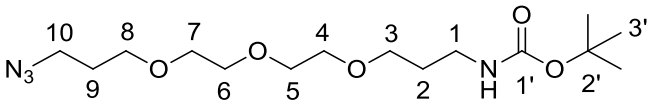

Imidazole-1-sulfonyl azide hydrogen sulfate (507 mg, 1.87 mmol, 1.2 eq) was added to the mono-Boc-protected diamine linker **20** (500 mg, 1.56 mmol, 1 eq) in MeOH (10 mL). K_2CO_3 (539 mg, 3.90 mmol, 2.5 eq) and $CuSO_4$ (3.9 mg, 15.6 µmol, 0.01 eq) was then added and the mixture stirred at rt for 3 hours. The mixture was concentrated, diluted with H_2O (30 mL), acidified with conc. HCl and extracted with EtOAc (3 x 30 mL). The combined organic layers were dried ($MgSO_4$), filtered and concentrated. Flash column chromatography (EtOAc:Pet. Ether = 60:40) gave the azide **37** (559 mg, 86%) as colourless oil.

R_f = 0.5 (EtOAc:Pet. Ether, = 50:50); IR ν_{max}/ cm^{-1} (ATR): 2097 (azide N≡N stretch);δ_H (300 MHz, $CDCl_3$): 4.92 (brs, 1H, **NH**), 3.91 (s, 1H, **NH**), 3.66 – 3.52 (m, 12H, **H-3/-4/-5/-6/-7/-8**), 3.39 (t, *J* = 6.0 Hz, 2H, **H-10**), 3.22 (q, *J* = 6.0 Hz, 2H, **H-1**), 1.86 (p, *J* = 6.0 Hz, 2H, **H-9**), 1.76 (p, *J* = 6.0 Hz, 2H, **H-2**), 1.44 (s, 9H, **H-3'**); δ_C (101 MHz, $CDCl_3$): 156.1, 79.0, 70.5, 70.5, 70.4, 70.2, 69.5, 67.9, 48.5, 38.5, 29.7, 29.1, 28.4; HRMS (ES): *m/z* found 347.2284 $[M + H]^+$, $C_{15}H_{31}N_4O_5$ requires 347.2294.

3-(2-(2-(3-azidopropoxy)ethoxy)ethoxy)propan-1-amine, **(38)**[565]

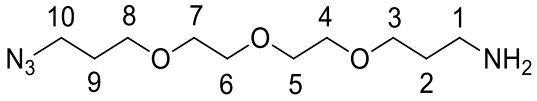

Trifluoroacetic acid (1.33 mL, 17.3 mmol, 15 eq) was added to a cooled (0 °C) solution of mono-Boc protected linker **20** (400 mg, 1.15 mmol, 1 eq) in DCM (15 mL) and stirred for 2 hours. The reaction mixture was concentrated, basified with sat. aq. $NaHCO_3$, extracted with DCM (3 x 30 mL), dried ($MgSO_4$), filtered and concentrated. Purification by flash column chromatography (MeOH:DCM = 20:80) gave the azide monoamine linker **38** (127 mg, 45%) as a colourless oil.

R_f = 0.2 (MeOH:DCM, = 10:90); IR ν_{max}/ cm^{-1} (ATR): 2097 (azide N≡N stretch); 1573 (1 ° amine NH_2 scissoring); δ_H (300 MHz, CD_3OD): 4.55 (s, 2H, **NH_2**) 3.64-3.57 (m, 10H, **H-4/-5/-6/-7/-8**),3.54 (t, J= 6.1 Hz, 2H, **H-3**), 3.38 (t, *J* = 6.7 Hz, 2H, **H-10**), 2.74 (t, *J* = 6.8 Hz, 2H, **H-1**), 1.83 (p, *J* = 6.4 Hz, 2H, **H-2**), 1.72 (p, *J* = 6.5 Hz, 2H, **H-9**); δ_C (101 MHz,

$CD_3OD:CDCl_3$ = 2:8): 71.1, 71.1, 70.8, 70.7, 70.1, 68.5, 49.0, 39.7, 33.0, 29.6; HRMS (ES): *m/z* found 247.1774 $[M + H]^+$, $C_{10}H_{23}N_4O_3$ requires 247.1770.

N-(3-(2-(2-(3-azidopropoxy)ethoxy)ethoxy)propyl)-5-((3aS,4S,6aR)-2-oxohexahydro-1H-thieno[3,4-d]imidazol-4-yl)pentanamide, **(39)**[327]

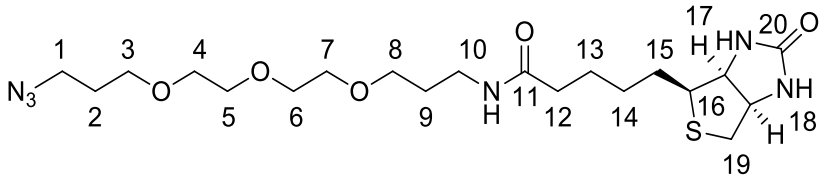

The azide linker **38** (240 mg, 0.97 mmol, 1 eq) was dissolved in DMF (5 mL), then biotin NHS ester **24** (333 mg, 0.97 mmol, 1eq) and DIPEA (186 uL, 1.07 mmol, 1.1 eq) were added and stirred at rt under argon for 2 hours. The reaction was neutralised with sat. NH_4Cl and then diluted with DCM (20 mL) and H_2O (3 mL). The mixture was extracted into DCM (3 x 20 mL) and the combined organic fractions were washed with H_2O (5 mL), dried ($MgSO_4$) and concentrated. Purification by flash column chromatography (MeOH:DCM = 20:80) gave the biotin-azide **39** (228 mg, 50%) as a colourless wax.

R_f = 0.6 (MeOH:DCM, = 15:85); IR ν_{max}/ cm^{-1} (ATR): 2092 (azide N≡N stretch), 1695 (ureido C=O stretch), 1640 (amide C=O stretch); δ_H (400 MHz, $(CD_3)_2SO$): 7.68 (t, *J* = 5.0 Hz, 1H, **NH**), 6.37 (s, 1H, **NH**), 6.31 (s, 1H, **NH**), 4.31 (dd, *J* = 7.4, 5.4 Hz, 1H, **H-17**), 4.15-4.11 (m, 1H, **H-18**), 3.54-3.44 (m, 10H, **H-4/-5/-6/-7/-8**), 3.39 (t, *J* = 7.0 Hz, 2H, **H-3**), 3.37 (t, *J* = 7.2 Hz, 2H, **H-1**), 3.28 (s, **H_2O**), 3.12-3.05 (m, 1H, **H-16**), 3.07 (q, *J* = 6.5 Hz, 2H, **H-10**), 2.82 (dd, *J* = 12.5, 5.0 Hz, 1H, **H-19a**), 2.58 (d, *J* = 12.5 Hz, 1H, **H-19b**), 2.05 (t, *J* = 7.4 Hz, 2H, **H-12**), 1.75 (p, *J* = 6.5 Hz, 2H, **H-2**), 1.64-1.42 (m, 4H, **H-13/-15**), 1.61 (p, *J* = 6.7 Hz, 2H, **H-9**), 1.38-1.24 (m, 2H, **H-14**); δ_C (101 MHz, $(CD_3)_2SO$): 171.8, 162.6, 69.7, 69.7, 69.5, 69.5, 68.1, 67.1 61.0, 59.2, 55.3, 47.8, 39.7, 35.7, 35.2, 29.4, 28.5, 28.1, 28.0, 25.2; HRMS (ES): *m/z* found 473.2538 $[M + H]^+$, $C_{20}H_{37}N_6O_5S$ requires 473.2546.

(*E/Z*)-*N*-(3-(2-(2-(3-(4-(((3-((4-methoxybenzyl)sulfinyl)prop-1-en-1-yl)disulfanyl)methyl)-1H-1,2,3-triazol-1-yl)propoxy)ethoxy)ethoxy)propyl)-5-((3aS,4S,6aR)-2-oxohexahydro-1H-thieno[3,4-d]imidazol-4-yl)pentanamide, **(40)**

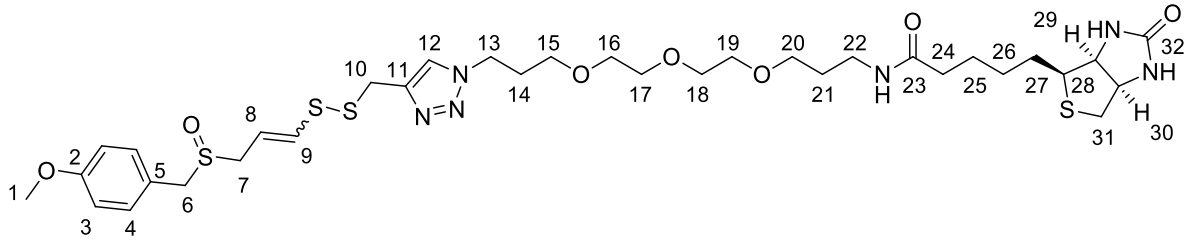

Prior to setting up the reaction, the "Click"-precatalyst, $CuSO_4$/THPTA, was pre-chelated for 10 min by mixing aq. $CuSO_4.5H_2O$ (20 µL, 8 µmol, 0.4 M, 0.05 eq) and aq. THPTA (40 µL, 8 µmol, 0.2 M, 0.05 eq). The ajoene alkyne **36** (50 mg, 0.16 mmol, 1eq) and biotin azide **39** (76 mg, 0.16 mmol, 1 eq) were dissolved in *t*BuOH:H_2O (1.4 mL as 1.3:1) and added to the reaction flask. Then the $CuSO_4$/THPTA solution (60 µL, 8 µmol, 0.13 M, 0.05 eq) was added. Lastly, aq. sodium ascorbate (40 µL, 32 µmol, 0.8 M, 0.2 eq) was added to the reaction mixture and it was stirred under argon at rt for 36 hours. The reaction was quenched by the addition of sat. aq. NH_4Cl (1 mL), extracted into DCM (3 x 25 mL), washed with sat. aq. NaCl, dried ($MgSO_4$) and concentrated. The flash column chromatography purification (MeOH:DCM = 25:75) afforded the biotin-ajoene **40** (80 mg, 64%) as a colourless wax in a 3:5 mixture of *E/Z*-isomers.

E/Z mixture: R_f = 0.4 (MeOH:DCM = 15:85); IR ν_{max}/ cm^{-1} (ATR): 1689 (ureido C=O stretch), 1642, 1462 (triazole C=C stretch, N=N stretch); HRMS (ES): *m/z* found 807.2662 $[M + Na]^+$, $C_{34}H_{52}N_6NaO_7S_4$ requires 807.2678;

E-isomer: δ_H (300 MHz, CD_3OD): 7.76 (s, 1H, **H-12**), 7.22 (d, *J* = 8.7 Hz, 2H, **H-4**), 6.90 (d, *J* = 8.7 Hz, 2H, **H-3**), 6.30 (d, *J* = 14.8 Hz, 1H, **H-9**), 5.87 (dt, *J* = 14.8, 7.8 Hz, 1H, **H-8**), 4.49-4.43 (m, 3H, **H-13/-29**), 4.33-4.25 (m, 1H, **H-30**),4.01 (s, 2H, **H-6**), 3.97-3.85 (m, 2H, **H-10**), 3.79 (s, 3H, **H-1**), 3.63-3.33 (m, 14H, **H-7/-15/-16/-17/-18/-19/-20**), 3.24 (t, *J* = 6.6 Hz, 2H, **H-22**), 3.17-3.11 (m, 1H, **H-28**), 2.89 (dd, *J* = 12.6 Hz, 5.0 Hz, 1H, **H-31a**), 2.70 (d, *J* = 12.6 Hz, 1H, **H-31b**), 2.17-2.11 (m, 2H, **H-14**), 2.15 (t, *J* = 7.4 Hz, 2H, **H-24**), 1.73 (p, *J* = 6.5 Hz, 2H, **H-21**), 1.78-1.52 (m, 4H, **H-25/-27**), 1.42-1.09 (m, 2H, **H-26**); δ_C (101 MHz, CD_3OD): 174.6, 164.9, 160.4, 143.8, 134.3, 131.8, 124.2, 121.8, 117.8, 114.9, 70.9, 70.8,

70.6, 70.5, 69.7, 67.7, 62.5, 60.7, 56.6, 56.0, 55.6, 53.1, 47.8, 40.6, 37.5, 36.3, 32.6, 30.0, 29.5, 28.9, 28.6, 26.0.

Z-isomer: δ_H (300 MHz, CD_3OD): 7.76 (s, 1H, **H-12**), 7.22 (d, *J* = 8.7 Hz, 2H, **H-4**), 6.89 (d, *J* = 8.7 Hz, 2H, **H-3**), 6.40 (d, *J* = 9.4 Hz, 1H, **H-9**), 5.69 (dt, *J* = 9.4, 7.8 Hz, 1H, **H-8**), 4.49 – 4.43 (m, 3H, **H-13/-29**), 4.33- 4.25 (m, 1H, **H-30**), 4.03 (s, 2H, **H-6**), 3.97-3.85 (m, 2H, **H-10**), 3.78 (s, 3H, **H-1**), 3.63-3.33 (m, 14H, **H-7/-15/-16/-17/-18/-19/-20**), 3.24 (t, *J* = 6.6 Hz, 2H, **H-22**), 3.17-3.11 (m, 1H, **H-28**), 2.89 (dd, *J* = 12.6 Hz, 5.0 Hz, 1H, **H-31a**), 2.70 (d, *J* = 12.6 Hz, 1H, **H-31b**), 2.17-2.11 (m, 2H, **H-14**), 2.15 (t, *J* = 7.4 Hz, 2H, **H-24**), 1.73 (p, *J* = 6.5 Hz, 2H, **H-21**), 1.78-1.52 (m, 4H, **H-25/-27**), 1.42-1.09 (m, 2H, **H-26**); δ_C (101 MHz, CD_3OD): 174.6, 164.9, 160.4, 143.8, 138.4, 131.8, 124.2, 121.9, 119.2, 114.9, 70.9, 70.8, 70.6, 70.5, 69.7, 67.7, 62.5, 60.7, 57.1, 56.0, 55.6, 49.9, 47.8, 40.6, 37.5, 36.3, 33.5, 30.6, 29.5, 28.9, 28.6, 26.0.

Biological Methods

The work on biological samples and specimens was performed in an appropriate biosafety-certified laboratory with temperature control, airflow regulation and filtration. All necessary precautions for handling, storage and disposal were followed. All samples were prepared in reverse-osmosis/deionised water (unless stated otherwise). All cell culture solutions were autoclaved or filtered through a 22 μm filter prior to use.

7.4 Animal Studies

All animal experiments were performed in accordance with the guidelines outlined by the Animal Ethics Research Committee. The protocol was approved by the committee (UCT protocol number 018/003). Authorisation for Daniel Kusza to perform specific procedures was given by the South African Council (Authorisation number AL17/16489). All mice were acclimatised from the SPF breeding labs to BSL2 for 3 days prior to the experiment. The SPF nude mice were exclusively handled and treated inside a laminar flow hood (F-10 sterilised) in the BSL2 procedure rooms of the UCT Animal Research Unit. All mice were numbered with ear clippings and no more than 5 mice were housed within a specific pathogen free cage. The welfare of the mice was monitored by myself daily and food, water and fresh nesting material was provided regularly by trained animal carers at the facility. The oesophageal cancer cell-line WHCO1 used, is derived from a biopsy of primary oesophageal squamous cell carcinoma of South African origin.[566]

7.4.1 Pilot Study 1: WHCO1 Tumour Implantation

On day 1, six eight-week old UCT21 nude mice were subcutaneously injected with $2.5x10^6$ WHCO1 cells in 100 μL sterile PBS into the right flank using a 25G needle (a well-localised bleb was considered a sign of a technically satisfactory injection). The mice were monitored daily and their body weight was measured every second day. Once tumours became palpable (around day 10), the tumour length and height were measured using a digital calliper (Tork Craft) every third day. The volume was calculated using the formula for an ellipsoid, where: volume = (length*width^2)/2.[258,567] At the end of the experiment (day 36), all animals were euthanised using 5% halothane inhalation in air (3 mL per 1 L per 5 mice). Death was confirmed by cervical dislocation and a post-mortem was performed. The tumours were excised, weighed and photographed.

7.4.2 Pilot Study 2: Testing of Ajoene Dosage

On day 1, six eight-week old UCT21 nude mice were divided into two subgroups (low and high dose). On day 2, *Z*-ajoene was dissolved in phospholipid stabilised soybean oil, Intralipid® (Sigma) and administered to the mice by oral gavage thrice weekly in a total volume of 0.1 mL for 2 weeks (= 6 doses). One group (low dose) received 25 mg/kg body weight, and other group (high dose) received 50 mg/kg body weight. The mice were monitored daily and their body weight was measured every second day. At the end of the experiment (day 14), all animals were euthanised using 5% halothane inhalation in air (3 mL per 1 L per 5 mice). Death was confirmed by cervical dislocation and a post-mortem was performed.

7.4.3 Oral Administration of DATS and Ajoene in WHCO1 Murine Xenograft Study

On day 1, thirty eight-week old UCT21 nude mice (15 males and 15 females) were divided into three subgroups (control, ajoene, DATS) and a baseline reading was taken. Each subgroup contained five females and five males, housed in separate cages according to sex. Every mouse received a subcutaneous injection of tumour cells (2.5×10^6 WHCO1 cells in 100 µL sterile PBS) into the right flank using a 25G needle. From Day 2 to Day 48, each mouse in the treated group was given 0.1 mL of 50 mg/kg garlic compound (*E/Z*-ajoene or DATS) in Intralipid® thrice weekly via oral gavage (total of 21 treatments in 7 weeks). The control group received an oral gavage of 0.1 mL Intralipid® (vehicle) alone. The mice were weighed the day after treatment. Once tumours became palpable, the tumour length and height was measured using a digital calliper as outlined before. On day 49, all animals were euthanised using 5% halothane inhalation in air (3 mL per 1 L per 5 mice). Death was confirmed by cervical dislocation and a post-mortem was performed. The tumours were excised, weighed and photographed.

7.4.4 Statistics

Statistical analysis was performed using Graph-Pad Prism 5 software (GraphPad Software, La Jolla, CA). A two-tailed, unpaired *t*-test was used to ascertain the statistically significant differences between untreated and treated groups when comparing the values of animal tumour volumes, tumour weights and growth rates (based on the regression lines of log(tumour volume) versus time). Statistical significance was defined as a *p*-value of less than 0.05, where * *p*-value < 0.05; ** *p*-value < 0.01; *** *p*-value < 0.005.

7.5 *In vitro* Blood-Stability Assay

Mouse (6-8 weeks old, BALB/c, female) blood was collected at the UCT animal facility and kept at 4°C in K_2EDTA coated tubes. Fresh whole mouse blood (400 uL) was transferred to a glass vial and heated to 37°C in a water bath under slow magnetic stirring. A timer was started, and the blood was spiked with 4 µL of 100 mM ajoene analogue (in DMSO) to give a final concentration of 1 mM ajoene and 1% DMSO. At specified time points (0, 5, 10, 15, 20, 60 and 120 min), 50 uL of blood was removed and added to 125 µL CH_3CN. The sample was sonicated for 10 minutes at 37°C, centrifuged for 10 min at 12500 rpm and filtered through a 22 µm (18 mm diameter) nylon syringe filter (Sigma) into a 2 mL HPLC vial with 0.2 mL glass insert (Supelco). Each ajoene compound was tested in triplicate where each repeat was done on blood from a different mouse. The samples were run on an Agilent 6410 TQ MS, with an Agilent 1200 HPLC using a Kinetex 1.7µm EVO C18 column (LC column 50x2.1 mm), 1 µL injection volume, flow 1.2 mL/min; gradient: t = 0 min: 95% A – 5% B; t = 0.2 min: 95% A – 5% B; t = 1.5 min: 0% A – 100% B; t = 1.9 min: 0% A – 100% B; t = 2.20 min: 95% A – 5% B; t = 2.70 min: 95% A – 5% B. Mobile phase A: Water, 0.1% formic acid; Mobile phase B: Acetonitrile, 0.1% formic acid ESI+, UV chromatogram (range 210-400 nm). The areas under the absorbance curve (as validated from the M^+ ion of the MS read-out) were normalised (where area of t_0 =100%) and plotted against time. The respective ajoene compound half-life was calculated using the one phase decay equation in Graph-Pad Prism 5 software (GraphPad Software, La Jolla, CA).

7.6 Mass-Spectrographic Analysis of Ajoene-Treated Haemoglobin

Purified human haemoglobin protein (Sigma-Aldrich) was suspended in PBS (1 mg/ mL) and treated with 100 µM *Z*-ajoene in DMSO or DMSO alone (control) and incubated at 37° C for 2 hours. The protein samples were then purified by SDS-PAGE, the gel was stained with Coomassie and the identified bands were excised. Gel pieces were treated with trypsin (Promega) at a final trypsin:protein ratio of 1:20 made up to 50 µL with 50 mM NH_4HCO_3 (Sigma-Aldrich). Samples were digested for 18 hours at 37 °C. Peptides were then dried by vacuum centrifugation and resuspended in 0.1% formic acid (Sigma-Aldrich) and 2.5% acetonitrile (Anatech) to a final concentration of 500 ng/µL. Samples were then stored at − 80 °C until analysis. Nano-RP LC chromatography was performed using a Dionex Ultimate 3000 nano-HPLC system. LC-MS/MS analysis was conducted

with a Q-Exactive quadrupole-Orbitrap mass spectrometer (Thermo Fisher Scientific) coupled with a Dionex Ultimate 3000 nano-HPLC system. The mobile phases consisted of solution A (0.1% formic acid in water) and solution B (100% CH_3CN, 0.1% formic acid). The HPLC fractionated peptides were dissolved in sample loading buffer (2.5% CH_3CN, 0.1% formic acid) and loaded onto a C18 trap column (100 µm × 20 mm × 5 µm). Chromatographic separation was performed using a C18 column (75 µm × 250 mm × 3.6 µm). The mass spectrometer was operated in positive ion mode with a capillary temperature of 250 °C and an applied electrospray voltage of 1.95 kV. Database interrogation was performed by the Centre for Proteomic and Genomic Research (CPGR, Cape Town, South Africa) with the Mascot algorithm using the MSDB database on a GPS workstation.

7.7 Cell Culture and Western Blots

7.7.1 Origin, Growing Conditions and Maintenance of Cell Lines

The MDA-MB-231 cell line was purchased from ATCC (ATCC CRL-2692) and the cells were cultured in Dulbecco's Modified Eagle medium (Gibco®, Life Technologies) supplemented with 10% foetal bovine serum (FBS) (HyClone™, GE Healthcare Life Sciences) and 100 µg/mL penicillin and 100 µg/mL streptomycin (Biochrom). The oesophageal cancer cell-line WHCO1 was derived from a biopsy of primary oesophageal squamous cell carcinoma of South African origin,[566] and the cells were cultured in Dulbecco's Modified Eagle medium (Gibco®, Life Technologies) supplemented with 10% foetal bovine serum (FBS) (HyClone™, GE Healthcare Life Sciences) and 100 µg/mL penicillin and 100 µg/mL streptomycin (Biochrom). The MCF-12A cell line was purchased from ATCC (ATCC CRL-10782) and the cells were cultured in special medium comprised of 1:1 of Dulbecco's Modified Eagle medium (Gibco®, Life Technologies) and Ham's F-12 Nutrient Mix (Gibco®, Life Technologies), supplemented with 10% foetal bovine serum (FBS) (HyClone™,GE Healthcare Life Sciences), 100 µg/mL penicillin, 100 µg/mL streptomycin (Biochrom), 10 ug/mL insulin (Novo Nordisk), 100 ng/mL cholera toxin (Sigma-Aldrich), 500 ng/mL hydrocortisone (Sigma-Aldrich) and 20 ng/mL EGF (BD Biosciences). Cells were incubated in a humidified 5% CO_2 at 37°C incubator and split upon reaching 80% confluence. All experiments were performed on logarithmically growing cells. Upon splitting or plating, the cells were washed with sterile PBS and then lifted with Trypsin-EDTA in PBS according to standard protocols. The cells in the

suspension were stained with trypan blue (0.4% in PBS) and their number was quantified using a haemocytometer. For long term storage, the cells were grown to 80% confluence in their respective media on a 100 mm dish. To collect cells, the media was removed and cells were washed with 5 mL phosphate buffer saline (PBS) (pH 7.5), and then incubated with 3 mL trypsin (at 37 °C, 5% CO_2, 91% humidity) for 2 minutes to detach cells from the dish. After transfer of the cells to a 12 mL tube, the trypsin was neutralised by the addition of 4 mL media and centrifuged at 4000 rpm for 3 minutes (Hettich Zentrifuge). The supernatant was removed, and cells were re-suspended in 5 mL media. The cells were pelleted by centrifugation at 4000 rpm (1541 × g) and re-suspended in media and 10 % DMSO at a concentration of ~ 1×10^6 cells/mL. Cells were stored in 1 mL aliquots in cryotubes at - 80 °C for 48 hours, then transferred to liquid nitrogen for long term storage.

7.7.2 Cellular Viability Assays

Cytotoxicity of ajoene and its analogues was evaluated using the standard MTT cellular viability assay. Briefly, cells are seeded at a density of 2.5 x 10^3 cells per well in 90 µL growth media in a 96-well culture plate and allowed to attach overnight. The following day, a 2-fold stock dilution series of the test compound, ranging from 200 – 0 mM was prepared in DMSO. Each solution was then further diluted 100-fold into growth medium and 10 µL of this was added in triplicate to the cells (0.1% v/v DMSO) and incubated for 24 hours to give final concentrations of ajoene in the micromolar range and 0.1% DMSO. Thereafter, 10 µL of 5 mg/mL MTT (Sigma-Aldrich) was added and incubated with the cells for 4 h. The resulting formazan crystals were solubilised into 100 µL of 10% SDS in 0.01 M HCl (Merck) overnight at 37 °C. The absorbance of each well was read at 595 nm using a Multiscan FC multi-well reader (Thermo Scientific). The background absorbance of the media, test compound and MTT reagent (without cells) was then subtracted from each reading and data was analysed using Graphpad Prism 5, non-linear regression analysis fitted to sigmoidal dose-response curve with 595 nm baseline versus log(concentration) to obtain the IC_{50} at 95% confidence interval.

7.7.3 Western Blot Analysis

Lysis buffer: 0.15 M NaCl, 0.01 M EDTA, 0.01 M Tris pH 8, 1% IGEPAL CA-630, H_2O.
PBS buffer: 137 mM NaCl, 2.7 mM KCl, 10 mM Na_2HPO_4, 1.8 mM KH_2PO_4, pH 7.4, H_2O.
SDS-PAGE running buffer: 25 mM Tris, 190 mM glycine, 3.5 mM SDS, H_2O.
Transfer buffer: 25mM Tris, 190 mM glycine, 20% MeOH, H_2O.
PBS-Tween buffer: 0.1% Tween-20, PBS, pH 7.4

For detection of biotinylated protein from MDA-MB-231 and MCF-12A cells, whole cell lysate was prepared using standard protocols. Briefly, cells were seeded in 35 mm or 100 mm culture dishes at a density of 0.3 x 10^6 or 2.2 x 10^6 cells per dish, respectively, and allowed to attach overnight. Thereafter biotin-ajoene **40**, or related compounds at the indicated concentration in DMSO (0.1% v/v) or DMSO alone, were added for the indicated time. Culture media was removed, cells were washed with ice-cold PBS and then lysed using lysis buffer (150 µL for a 35 mm dish and 450 µL for a 100 mm dish) supplemented with 1 mM protease inhibitor (Roche). Total protein was quantified using the Pierce® Bradford Protein Assay kit (Thermo Fisher Scientific, Life Technologies) according to the manufacturer's instruction. Equal amounts of total protein lysates (10-20 µg with 20% loading buffer/lane marker) were separated by SDS-PAGE (10-well, 1.5 mm, 10% acrylamide gel) and transferred to a 0.2 µm nitrocellulose membrane (Bio-Rad) using conventional methods. The membranes were blocked using 3% BSA (Roche Diagnostics, Sigma-Aldrich) in PBS-Tween for one hour at rt. For the detection of biotinylation, the membranes were incubated overnight at 4°C with streptavidin (anti-Biotin)-horseradish peroxidase-conjugated antibody (1:2500, Thermo Scientific), washed three times (PBS-Tween) and treated with LumiGLO chemiluminescent reagent (KPL, Biocom Biotech). For the detection of specific proteins, the membranes were incubated with primary antibodies overnight at 4 °C: anti-vimentin (1:1000, Santa Cruz), anti-GSTP1 (1:1000, Thermo Fischer), anti-GAPDH (1:1000, Santa Cruz). The next day the membranes were washed three times (PBS-Tween), incubated using appropriate horseradish peroxidase-conjugated secondary antibodies (one hour at room temperature), washed (PBS-Tween) and treated with LumiGLO chemiluminescent reagent (KPL, Biocom Biotech). Proteins were visualised using the UVP BioSpectrum™500 Imaging System (UVP, LCC Upland, CA, USA), captured with a CCD camera (Canon Inc) and analysed with the VisionWorks LS Acquisition analysis software (UVP, LCC Upland, USA). A protein ladder (Thermo Fisher

Scientific, Life Technologies) was used to estimate the molecular weight of proteins. Protein loading control was quantified by colloidal silver staining.

7.7.4 Colloidal Silver Staining

The nitrocellulose membrane was washed with H_2O (3 x 20 mL) for 5 min. For 20 mL staining solution (for 1-2 nitrocellulose membranes): 1 mL aq. trisodium citrate (40% w/v) and freshly prepared 0.8 mL aq. $FeSO_4.7H_2O$ (20% w/v) were combined in 18 mL H_2O and 0.2 mL of aq. $AgNO_3$ (20% w/v) was added drop-wise over 1-2 min to form a suspension (in a glass tray). The solution was immediately used on the membrane, stained for 2-5 min under shaking, then rinsed with H_2O (3 x 10 mL) and air-dried. The silver-stained membranes were captured using the UVP BioSpectrum™500 Imaging System (UVP, LCC Upland, CA, USA) fitted with a CCD camera (Canon Inc) and analysed with the VisionWorks LS Acquisition analysis software (UVP, LCC Upland, USA).

7.7.5 Dose Response Assay

For the detection of the change in lysate protein biotinylation, MDA-MB-231 and MCF-12A cells were seeded in a 6-well (35 mm) plate at 0.3 x 10^6 cells per well. The following day, the cells were treated for 24 hours with 2-fold dilutions of biotin-ajoene **40** (80, 40, 20, 10, 5 and 0 μM), and whole cell lysate was prepared according to the protocol described above. Total protein was quantified using the Pierce® Bradford Protein Assay kit (Thermo Fisher Scientific, Life Technologies) according to the manufacturer's instruction. Equal amounts (15 μg) of total protein lysates were separated by SDS-PAGE and transferred onto a 0.2 μm nitrocellulose membrane (Bio-Rad) using conventional methods. Proteins were then analysed by western blot according to the method outlined in **section 7.7.3**.

7.7.6 Cleaving of Biotin Label from Proteins

The removal of the biotin label was performed by incubating 15 ug of biotin-ajoene **40** (40 μM) treated lysate protein with 100 mM DTT (in H_2O) for 10 min at 37°C. The proteins were separated and analysed by western blot according to the method in **section 7.7.3**.

7.7.7 Competition Assay

MDA-MB-231 and MCF-12A cells were seeded in a 6-well (35 mm) plate at 0.3 x 10^6 cells per well. Thereafter, cells were pre-treated with *E/Z*-ajoene (20, 40 and 60 μM) for 2 hours, followed by the addition of biotin-ajoene **40** (40 μM), and incubated for a further 6 hours. Control cells were either untreated (negative control) or treated (positive control) with biotin-ajoene (40 μM) alone (no ajoene). Lysate was collected for western blot analysis according to the method in **section 7.7.3**.

7.7.8 Biotinylation of Recombinant Proteins

To confirm biotinylation of known protein targets, aliquots of 5 μL of recombinant protein (1 μg/μL) (Vimentin (Peprotech), GSTP1 (Sigma-Aldrich)) in 7 μL PBS were incubated with 1.5 μL biotin-ajoene **40** in DMSO (200, 100, 50, 25 and 0 μM) for 1 hour 30 min at 37°C. Certain aliquots were also incubated with 15 uL of 200 mM DTT in water, or water alone (30min and 37C). All proteins were separated by SDS-PAGE and analysed by western blot according to the method in **section 7.7.3**.

7.8 Proteomics

All reagents used were MS- or HPLC-grade. The buffers were prepared using milliQ H_2O, then filtered using a 22 μm syringe filter (Sigma) and adjusted to the desired pH (see section 7.2.6.2). Sample handling involved non-autoclaved microcentrifuge tubes and filtered pipette tips. Cell lysates were prepared using the previous method (see section 7.2.5) and their total protein concentration was quantified using the Pierce® Bradford Protein Assay kit (Thermo Fisher Scientific, Life Technologies) according to the manufacturer's instruction. The method for the affinity purification and digestion of biotinylated proteins is an adaptation of the protocol by Dr. Muneerah Smith.[389]

7.8.1 Buffers and Solutions

Wash buffer 1 (WB1): 500 mM NaCl, 50 mM Tris HCl, 0.1 % Triton X-100, pH 7.5.

Wash Buffer 2 (WB2): 60% CH_3CN, ddH_2O

Wash Buffer 3 (WB3): 50 mM Tris HCl, pH 7

Elution Buffer (EB): 50 mM Tris HCl, 5 mM DTT, pH 8

Desalting Solutions: Solution A: 2% CH_3CN, 0.1% formic acid

Solution B: 100% MeOH

Solution C: 60% CH_3CN, 0.1% formic acid

7.8.2 Magnetic Bead Equilibration and Incubation

NB: After addition of buffer to the magnetic beads (e.g. for wash or elution steps), the containing sample tube was closed and agitated (by vortex) for 2 min and then placed into the magnetic separator. Time (approx. 1 min) was given for the magnetic microparticles to clear, the supernatant was removed by careful aspiration using a micropipette and then discarded (unless otherwise stated).

A streptavidin-coated magnetic bead slurry (1 mg in 100 µL from MagReSyn®, Separations) was added to a microcentrifuge tube, diluted with 1 mL WB1 and the supernatant was removed. The beads were then washed with WB1 (2 x 1 mL). The lysate protein (500 µg) was diluted with WB1 to a total volume of 1 mL and incubated with the beads at 4 °C on a shaker overnight. The next day, the beads were washed with WB1 (3 x 1 mL), WB2 (1 mL) and WB3 (3 x 1 mL). To denature the proteins, the beads were then incubated with 20 uL of EB and shaken on a vortex mixer for 30 min at rt. The proteins were then alkylated using iodoacetamide (2 µL 100 mM) and stored in the dark for 10 min at rt.

7.8.3 On-Bead Digest and Peptide Elution

Following alkylation, trypsin (1 µL, 0.5 µg/µL – Promega) was added to each sample tube and they were placed into shaking incubator for 18 hours at 37 °C. After the tryptic digest, the supernatant was collected and the beads were washed with 60 µL EB (no DTT). The supernatant and washes of the individual samples were pooled into a new microcentrifuge tube, 1 µL trypsin was added and the mixture was shaken at 37 °C for 2

hours. The digestion was stopped by the addition of 1.7 µL formic acid (= 2% concentration overall).

7.8.4 Detergent removal and desalting

The residual detergents were removed using a HiPPR detergent removal resin (Thermo Fischer) and the procedure was followed according to the manufacturer's instruction. Briefly, 160 uL of resin slurry (for 80 µL peptide sample) was added to a spin column and equilibrated with WB3 (3 x 80 µL, centrifuge at 1500 RCF for 1 min to elute). The peptides were then incubated with the resin on a shaker for 10 min at rt and then the column was centrifuged for 2 min at 1500 RCF to elute the detergent-free peptides into a fresh microcentrifuge tube.

The peptides were then desalted using an SOP provided by the team of the IDM Proteomics & Metabolomics Platform (UCT). The C18 resin inside a 200 µL stage-tip was activated by adding 100 µL of solution B (see 7.2.6.2) and centrifuged at 1000 rpm for 1 min to elute. Then the C18 resin was equilibrated with 200 µL solution A and centrifuged at 2000 rpm for 1 min. The peptide sample was added to the C18 stage tip and centrifuged at 4000 rpm for 1 min. The C18 resin was washed with 200 µL solution A and centrifuged at 2000 rpm for 1 min. Finally, the peptides were eluted into a glass vial insert by adding 100 µL of solution C to the C18 resin and centrifuging at 6000 rpm for 2 min. The vial inserts containing the eluted peptides were dried on a speedyVac concentrator (Eppendorf), inserted into a 2 mL HPLC screw top sample vial and stored at -20 °C until further processing.

7.8.5 Peptide analysis

The peptide analysis was performed at the IDM Proteomics & Metabolomics Platform (UCT), according to their protocol.

The desalted peptides were resuspended in 10 µL of solution A, of which 1 µL was measured on an Thermo Scientific™ UltiMate™ 3000 RSLC system (Thermo Fisher) coupled to a Thermo Scientific™ Q Exactive™ Hybrid Quadrupole-Orbitrap™ mass spectrometer (Thermo Fisher). Peptides were chromatographically separated using a 75 µm (ID), 30 cm column packed in-house with reversed-phase 3 µm solid core C18 resin (Dr Maisch) at a flow rate of 600 nL/min at 40°C. The gradient consisted of 7% solution B (0.1% FA, CH_3CN) increased to 29% solution B over 55 minutes followed by a washout

at 80% solution B for 4 minutes at 1200 nl/min. MS1 spectra were acquired between 300-1,750 Thompson at a resolution of 70,000 with an AGC target of 3×10^6 within 30 ms. Using a dynamic exclusion window of 90 sec, 15 most intense ions were selected for HCD fragmentation with an NCE of 28. MS2 spectra were acquired at a resolution of 17,500 and a minimum AGC of 1×10^3 within 80 ms.

7.8.6 Mass Spectrometry Data Analysis

All raw files were analysed together using the MaxQuant software, version 1.6.14.0.[393,394] The derived peak list was searched with its built-in Andromeda search engine against the human FASTA database that was downloaded from Uniprot on the 9th of August 2020. Trypsin/P was set as the digestion enzyme (cleavage C-terminal after K or R), with allowance for 2 missed cleavages. The minimum required peptide length was set to seven amino acids and the maximum peptide weight was set to 4600 Da. Protein N-terminal acetylation and methionine oxidation were set as variable modifications and carbamidomethylation of cysteine as set as a fixed modification. As no labelling was performed, the multiplicity was set to 1. During the main search, parent masses were allowed an initial mass deviation of 4.5 ppm and fragment ions were allowed a mass deviation of 0.5 Da. PSM and protein identifications were filtered using a target-decoy approach at a false discovery rate (FDR) of 1%. The "match between runs" and "find dependent peptides" features were turned off. Relative, label-free quantification of proteins was done using the MaxLFQ algorithm integrated into MaxQuant.[399]

7.8.7 Data Analysis

Further analysis of the MaxQuant-processed data was performed using Perseus (version 1.6.15.0).[400,401] The "proteingroups.txt" file produced by MaxQuant was loaded into Perseus. First, hits to the reverse database, contaminants and proteins identified only with modified peptides were filtered from the main data frame. Then the LFQ intensities were logarithmised (base 2), column annotations were added and the samples were grouped according to their experimental condition (untreated and treated), which gave two groups of five technical replicates. The proteins were filtered based on valid representation in the data set, where proteins lacking at least 4 valid values in at least one of the replicate groups were eliminated. After this, missing values were imputed with values representing a normal distribution around the detection limit of the mass

spectrometer. Here, mean and standard deviation of the distribution of the real intensities were determined, then a new distribution with a downshift of 1.8 standard deviation and a width of 0.3 standard deviations was created. The total matrix was imputed using these values to enable statistical analysis Next a student's *t*-test was performed comparing the treated group to the untreated group (S_0 = 3, permutation-based FDR = 1% with 250 randomisations). Using the "volcano plot" tool in Perseus, the resulting differences between the logarithmised means of the two group ("$\log_2$(treated-untreated") and the negative logarithmised *p* values ("-log *p*") were plotted against each other, on the y and x axes, respectively. The cut-off was set at a *p* value of 0.01 (FDR) and an 8-fold difference (S_0 = 3) to visualise and identify the proteins that were enriched and also statistically significant (*t*-test) in the treated group. Pathway analyses were performed using the KEGG Mapper (https://www.genome.jp/kegg/mapper.html),[568] the DAVID Functional Annotation Tool (DAVID Bioinformatics Resources 6.8; https://david.ncifcrf.gov/home.jsp),[569,570] the UniProt Retrieve/ID mapping tool and search function (https://www.uniprot.org/) and the iCysMod database (http://icysmod.omicsbio.info/).[418] KEGG pathway diagrams were downloaded from the results page of the Search&Color Pathway mapping tool on the KEGG Mapper website. The Voronoi treemaps were generated by uploading the UniProt ascension numbers and enrichment scores (fold-change) of all significantly enriched proteins into Proteomaps webtool (https://proteomaps.net/methods.html).[471] Venn diagrams were generated using Venny 2.1.[571] Graphs and figures were either directly exported from Perseus or generated using Microsoft Excel or Graph-Pad Prism 5. The list of all identified protein targets of biotin-ajoene **40** can be found in the **Appendix**.

7.9 Appendix

Tables

#	Gene	Protein name(s)	*p*-value	fold-change (T vs UT)
1	**AARS**	Alanine--tRNA ligase, cytoplasmic	1.41E-06	17.82
2	**ABCE1**	ATP-binding cassette sub-family E member 1	1.93E-07	6.80
3	**ABCF2**	ATP-binding cassette sub-family F member 2	1.88E-08	6.17
4	**ACAA2**	3-ketoacyl-CoA thiolase, mitochondrial	1.94E-09	20.76
5	**ACADVL**	Very long-chain specific acyl-CoA dehydrogenase, mitochondrial	7.71E-07	20.37
6	**ACAT1**	Acetyl-CoA acetyltransferase, mitochondrial	1.30E-08	21.27
7	**ACAT2**	Acetyl-CoA acetyltransferase, cytosolic	5.02E-07	8.49
8	**ACLY**	ATP-citrate synthase	8.50E-04	38.46
9	**ACO1**	Cytoplasmic aconitate hydratase	2.03E-06	8.02
10	**ACOT9**	Acyl-coenzyme A thioesterase 9, mitochondrial	4.13E-06	2.88
11	**ACSL3**	Long-chain-fatty-acid--CoA ligase 3	9.86E-07	8.53
12	**ACSL4**	Long-chain-fatty-acid--CoA ligase 4	1.58E-07	14.24
13	**ACTA1; ACTC1; ACTG2; ACTA2**	Actin, alpha skeletal muscle; Actin, alpha cardiac muscle 1; Actin, gamma-enteric smooth muscle; Actin, aortic smooth muscle	1.81E-06	77.32
14	**ACTB**	Actin, cytoplasmic 1; Actin, cytoplasmic 1, N-terminally processed	5.53E-10	120.15
15	**ACTG1**	Actin, cytoplasmic 2; Actin, cytoplasmic 2, N-terminally processed	1.10E-05	2.78
16	**ACTN1**	Alpha-actinin-1	4.11E-08	126.49
17	**ACTN4**	Alpha-actinin-4	1.46E-11	95.38
18	**ACTR1A**	Alpha-centractin	1.74E-04	3.35
19	**ACTR2**	Actin-related protein 2	1.47E-07	24.80
20	**ACTR3**	Actin-related protein 3	5.53E-05	23.53
21	**ADH5**	Alcohol dehydrogenase class-3	1.20E-05	6.90
22	**ADSL**	Adenylosuccinate lyase	1.45E-03	3.39
23	**AGPS**	Alkyldihydroxyacetonephosphate synthase, peroxisomal	1.07E-04	5.72
24	**AHSA1**	Activator of 90 kDa heat shock protein ATPase homolog 1	3.26E-08	20.13
25	**AIFM1**	Apoptosis-inducing factor 1, mitochondrial	1.74E-04	3.93
26	**AIMP1**	Aminoacyl tRNA synthase complex-interacting multifunctional protein 1; Endothelial monocyte-activating polypeptide 2	3.00E-05	7.00
27	**AIMP2**	Aminoacyl tRNA synthase complex-interacting multifunctional protein 2	1.44E-02	3.83
28	**AKAP12**	A-kinase anchor protein 12	8.37E-08	17.25
29	**AKR1B1**	Aldose reductase	2.26E-05	6.70
30	**ALDH18A1**	Delta-1-pyrroline-5-carboxylate synthase;Glutamate 5-kinase;Gamma-glutamyl phosphate reductase	7.31E-05	3.40
31	**ALDH1A3**	Aldehyde dehydrogenase family 1 member A3	1.09E-03	4.32
32	**ALDH7A1**	Alpha-aminoadipic semialdehyde dehydrogenase	5.63E-07	4.30
33	**ALDH9A1**	4-trimethylaminobutyraldehyde dehydrogenase	3.34E-05	5.19
34	**ALDOA**	Fructose-bisphosphate aldolase A;Fructose-bisphosphate aldolase	5.09E-10	5.71
35	**ANLN**	Actin-binding protein anillin	1.55E-04	6.37

36	**AP2A1**	AP-2 complex subunit alpha-1	2.34E-05	3.63
37	**AP2B1**	AP-2 complex subunit beta	4.15E-08	16.85
38	**APEH**	Acylamino-acid-releasing enzyme	2.90E-04	4.08
39	**API5**	Apoptosis inhibitor 5	1.30E-07	14.34
40	**APMAP**	Adipocyte plasma membrane-associated protein	1.09E-05	4.79
41	**APRT**	Adenine phosphoribosyltransferase	3.46E-04	6.84
42	**ARCN1**	Coatomer subunit delta	6.19E-07	12.40
43	**ARF1; ARF3; ARF5**	ADP-ribosylation factor 1; ADP-ribosylation factor 3;ADP-ribosylation factor 5	1.94E-07	32.36
44	**ARF4**	ADP-ribosylation factor 4	6.09E-09	37.89
45	**ARHGAP1**	Rho GTPase-activating protein 1	5.12E-05	4.75
46	**ARHGAP29**	Rho GTPase-activating protein 29	6.00E-08	7.19
47	**ARHGEF1**	Rho guanine nucleotide exchange factor 1	8.65E-04	2.98
48	**ARPC2**	Actin-related protein 2/3 complex subunit 2	9.69E-07	17.11
49	**ARPC3**	Actin-related protein 2/3 complex subunit 3	2.41E-05	3.74
50	**ARPC4-TTLL3; ARPC4**	Actin-related protein 2/3 complex subunit 4	9.61E-08	20.49
51	**ASNS**	Asparagine synthetase [glutamine-hydrolyzing]	3.00E-04	3.11
52	**ATIC**	Bifunctional purine biosynthesis protein PURH;Phosphoribosylaminoimidazolecarboxamide formyltransferase; IMP cyclohydrolase	1.43E-07	50.30
53	**ATL3**	Atlastin-3	1.19E-05	4.33
54	**ATP1A1**	Sodium/potassium-transporting ATPase subunit alpha-1	2.78E-04	18.55
55	**ATP2A2**	Sarcoplasmic/endoplasmic reticulum calcium ATPase 2	1.11E-07	9.52
56	**ATP5A1**	ATP synthase subunit alpha, mitochondrial	1.75E-02	5.28
57	**ATP5B**	ATP synthase subunit beta, mitochondrial; ATP synthase subunit beta	9.19E-07	33.67
58	**ATP5O**	ATP synthase subunit O, mitochondrial	4.10E-02	3.56
59	**ATP6V1A**	V-type proton ATPase catalytic subunit A	5.88E-05	6.96
60	**BLVRA**	Biliverdin reductase A	3.98E-02	3.44
61	**CACYBP**	Calcyclin-binding protein	1.41E-04	8.75
62	**CAND1**	Cullin-associated NEDD8-dissociated protein 1	3.01E-07	30.43
63	**CAP1**	Adenylyl cyclase-associated protein 1	2.31E-08	28.92
64	**CAPG**	Macrophage-capping protein	1.06E-05	2.93
65	**CAPN1**	Calpain-1 catalytic subunit	9.69E-03	6.46
66	**CAPN2**	Calpain-2 catalytic subunit	3.68E-05	34.13
67	**CAPNS1**	Calpain small subunit 1	3.47E-06	13.58
68	**CAPZA1**	F-actin-capping protein subunit alpha-1	1.83E-07	20.91
69	**CAPZA2**	F-actin-capping protein subunit alpha-2	1.10E-04	3.70
70	**CAPZB**	F-actin-capping protein subunit beta	2.36E-06	19.25
71	**CASK**	Peripheral plasma membrane protein CASK	1.67E-03	3.22
72	**CAT**	Catalase	7.13E-09	17.08
73	**CBR1**	Carbonyl reductase [NADPH] 1	5.62E-08	10.63
74	**CBS**	Cystathionine beta-synthase	1.13E-05	9.17
75	**CCT2**	T-complex protein 1 subunit beta	1.10E-06	53.75
76	**CCT3**	T-complex protein 1 subunit gamma	9.08E-07	74.65
77	**CCT4**	T-complex protein 1 subunit delta	1.72E-06	48.24

78	**CCT5**	T-complex protein 1 subunit epsilon	2.76E-08	53.75
79	**CCT6A**	T-complex protein 1 subunit zeta	5.77E-02	3.80
80	**CCT7**	T-complex protein 1 subunit eta	6.54E-04	45.24
81	**CCT8**	T-complex protein 1 subunit theta	7.13E-11	117.70
82	**CD44**	CD44 antigen	1.77E-05	5.97
83	**CDC2; CDK1**	Cyclin-dependent kinase 1	1.26E-03	8.52
84	**CDC37**	Hsp90 co-chaperone Cdc37; Hsp90 co-chaperone Cdc37, N-terminally processed	1.26E-02	5.22
85	**CDCP1**	CUB domain-containing protein 1	2.14E-05	4.09
86	**CFL1**	Cofilin-1	1.32E-03	61.30
87	**CHORDC1**	Cysteine and histidine-rich domain-containing protein 1	7.36E-08	5.90
88	**CKAP5**	Cytoskeleton-associated protein 5	4.57E-07	11.22
89	**CLIC1**	Chloride intracellular channel protein 1	3.44E-05	57.09
90	**CLIC4**	Chloride intracellular channel protein 4	1.04E-08	17.84
91	**CLTC**	Clathrin heavy chain; Clathrin heavy chain 1	4.19E-08	7.09
92	**CLUH**		3.86E-05	8.92
93	**CMPK1**	UMP-CMP kinase	8.01E-06	4.20
94	**CNDP2**	Cytosolic non-specific dipeptidase	6.57E-06	9.26
95	**CNN2**	Calponin; Calponin-2	9.51E-02	3.77
96	**CNN3**	Calponin-3; Calponin	3.18E-02	9.83
97	**COPA**	Coatomer subunit alpha;Xenin; Proxenin	2.70E-02	5.34
98	**COPB1**	Coatomer subunit beta	1.52E-05	21.22
99	**COPG1**	Coatomer subunit gamma-1	1.52E-06	18.02
100	**CORO1B**	Coronin-1B	1.08E-07	15.10
101	**CPNE1**	Copine-1	1.57E-07	15.65
102	**CPNE3**	Copine-3	1.22E-03	5.85
103	**CS**	Citrate synthase, mitochondrial; Citrate synthase	3.03E-07	26.69
104	**CSDE1**	Cold shock domain-containing protein E1	6.18E-06	3.31
105	**CSE1L**	Exportin-2	4.89E-07	68.01
106	**CSNK2A1; CSNK2A3**	Casein kinase II subunit alpha 3; Casein kinase II subunit alpha	1.14E-06	3.19
107	**CSRP1**	Cysteine and glycine-rich protein 1	1.04E-09	46.98
108	**CSTB**	Cystatin-B	5.32E-07	25.07
109	**CTNNA1**	Catenin alpha-1	5.69E-04	4.04
110	**CTPS1**	CTP synthase 1; CTP synthase	2.57E-07	19.65
111	**CTTN**	Src substrate cortactin	1.76E-02	5.22
112	**CUL2**	Cullin-2	5.74E-05	7.17
113	**CYFIP1**	Cytoplasmic FMR1-interacting protein 1	4.03E-09	7.50
114	**DARS**	Aspartate--tRNA ligase, cytoplasmic	6.80E-06	25.64
115	**DDB1**	DNA damage-binding protein 1	1.16E-04	3.93
116	**DDOST**	Dolichyl-diphosphooligosaccharide--protein glycosyltransferase 48 kDa subunit	4.03E-03	3.23
117	**DDX1**	ATP-dependent RNA helicase DDX1	2.04E-08	3.85
118	**DDX19A**	ATP-dependent RNA helicase DDX19A	2.73E-07	7.76
119	**DDX21**	Nucleolar RNA helicase 2	1.06E-10	13.34
120	**DDX39B**	Spliceosome RNA helicase DDX39B	5.51E-07	18.33

121	**DDX6**	Probable ATP-dependent RNA helicase DDX6	2.26E-03	3.70
122	**DHRS7**	Dehydrogenase/reductase SDR family member 7	2.51E-04	3.16
123	**DHX15**	Pre-mRNA-splicing factor ATP-dependent RNA helicase DHX15	8.12E-04	3.60
124	**DHX9**	ATP-dependent RNA helicase A	4.74E-02	4.66
125	**DIAPH1**	Protein diaphanous homolog 1	1.06E-05	8.52
126	**DLAT**	Acetyltransferase component of pyruvate dehydrogenase complex; Dihydrolipoyllysine-residue acetyltransferase component of pyruvate dehydrogenase complex, mitochondrial	2.24E-04	3.93
127	**DNAJA1**	DnaJ homolog subfamily A member 1	4.60E-08	23.09
128	**DNAJA2**	DnaJ homolog subfamily A member 2	1.95E-07	6.96
129	**DNAJC9**	DnaJ homolog subfamily C member 9	3.90E-05	4.53
130	**DNM1L**	Dynamin-1-like protein	1.80E-06	23.40
131	**DNM2**	Dynamin-2	8.16E-04	3.40
132	**DPP3**	Dipeptidyl peptidase 3	7.71E-06	3.65
133	**DPYSL2**	Dihydropyrimidinase-related protein 2	7.16E-05	5.29
134	**DRG1**	Developmentally-regulated GTP-binding protein 1	2.13E-05	7.32
135	**DSP**	Desmoplakin	5.37E-05	4.39
136	**DSTN**	Destrin	8.37E-07	20.76
137	**DYNC1H1**	Cytoplasmic dynein 1 heavy chain 1	1.16E-09	132.20
138	**ECHS1**	Enoyl-CoA hydratase, mitochondrial	2.31E-07	9.66
139	**EEF1A1; EEF1A1P5**	Elongation factor 1-alpha 1; Putative elongation factor 1-alpha-like 3;Elongation factor 1-alpha	4.18E-06	3.35
140	**EEF1A2**	Elongation factor 1-alpha 2	4.13E-06	29.55
141	**EEF1B2**	Elongation factor 1-beta	8.45E-07	22.14
142	**EEF1D**	Elongation factor 1-delta	3.81E-03	5.34
143	**EEF1G**	Elongation factor 1-gamma	7.94E-04	16.15
144	**EEF2**	Elongation factor 2	6.37E-08	9.18
145	**EFTUD2**	116 kDa U5 small nuclear ribonucleoprotein component	2.42E-04	5.52
146	**EHD1**	EH domain-containing protein 1	3.26E-09	13.52
147	**EIF2A**	Eukaryotic translation initiation factor 2A; Eukaryotic translation initiation factor 2A, N-terminally processed	1.17E-04	3.32
148	**EIF2S1**	Eukaryotic translation initiation factor 2 subunit 1	1.23E-02	6.56
149	**EIF2S3; EIF2S3L**	Eukaryotic translation initiation factor 2 subunit 3; Putative eukaryotic translation initiation factor 2 subunit 3-like protein	9.61E-07	16.35
150	**EIF3A**	Eukaryotic translation initiation factor 3 subunit A	5.66E-02	4.02
151	**EIF3B**	Eukaryotic translation initiation factor 3 subunit B	2.37E-07	14.98
152	**EIF3C; EIF3CL**	Eukaryotic translation initiation factor 3 subunit C; Eukaryotic translation initiation factor 3 subunit C-like protein	1.16E-09	17.93
153	**EIF3D**	Eukaryotic translation initiation factor 3 subunit D	3.24E-05	10.94
154	**EIF3E**	Eukaryotic translation initiation factor 3 subunit E	3.27E-07	16.10
155	**EIF3F**	Eukaryotic translation initiation factor 3 subunit F	2.84E-08	12.78
156	**EIF3G**	Eukaryotic translation initiation factor 3 subunit G	6.98E-05	4.10
157	**EIF3I**	Eukaryotic translation initiation factor 3 subunit I	3.80E-05	4.66
158	**EIF3K**	Eukaryotic translation initiation factor 3 subunit K	1.47E-03	3.68
159	**EIF3L**	Eukaryotic translation initiation factor 3 subunit L	2.19E-04	8.30
160	**EIF3M**	Eukaryotic translation initiation factor 3 subunit M	2.27E-06	8.55
161	**EIF4A1**	Eukaryotic initiation factor 4A-I	1.73E-03	6.24

162	**EIF4A3**	Eukaryotic initiation factor 4A-III; Eukaryotic initiation factor 4A-III, N-terminally processed	1.28E-05	6.66
163	**EIF4G1**	Eukaryotic translation initiation factor 4 gamma 1	3.40E-05	30.20
164	**EIF4G2**	Eukaryotic translation initiation factor 4 gamma 2	7.00E-05	6.66
165	**EIF5B**	Eukaryotic translation initiation factor 5B	4.26E-06	5.36
166	**EIF6**	Eukaryotic translation initiation factor 6	1.18E-06	42.32
167	**ELAC2**	Zinc phosphodiesterase ELAC protein 2	6.35E-05	3.62
168	**ENO1**	Alpha-enolase	3.64E-07	5.11
169	**ENO2**	Gamma-enolase; Enolase	2.83E-04	3.12
170	**EPHA2**	Ephrin type-A receptor 2	9.13E-05	5.62
171	**EPRS**	Bifunctional glutamate/proline--tRNA ligase; Glutamate--tRNA ligase; Proline--tRNA ligase	8.24E-08	33.59
172	**ERO1L**	ERO1-like protein alpha	1.30E-03	4.13
173	**ESYT1**	Extended synaptotagmin-1	1.47E-05	6.23
174	**ETF1**	Eukaryotic peptide chain release factor subunit 1	2.55E-07	5.44
175	**ETFA**	Electron transfer flavoprotein subunit alpha, mitochondrial	5.09E-07	3.89
176	**ETFB**	Electron transfer flavoprotein subunit beta	3.50E-06	6.95
177	**EXOSC2**	Exosome complex component RRP4	2.24E-08	4.37
178	**FAM129A**	Protein Niban	2.11E-05	3.48
179	**FAM129B**	Niban-like protein 1	2.20E-09	18.78
180	**FAM49B**	Protein FAM49B	6.71E-04	4.39
181	**FARSA**	Phenylalanine--tRNA ligase alpha subunit	3.13E-03	4.13
182	**FARSB**	Phenylalanine--tRNA ligase beta subunit	1.79E-04	3.05
183	**FDPS**	Farnesyl pyrophosphate synthase	2.66E-06	12.78
184	**FH**	Fumarate hydratase, mitochondrial	1.33E-05	2.80
185	**FHL1**	Four and a half LIM domains protein 1	4.97E-06	5.93
186	**FKBP4**	Peptidyl-prolyl cis-trans isomerase FKBP4; Peptidyl-prolyl cis-trans isomerase FKBP4, N-terminally processed	7.78E-07	22.39
187	**FLII**	Protein flightless-1 homolog	6.07E-04	4.51
188	**FLNA**	Filamin-A	6.45E-05	4.32
189	**FLNB**	Filamin-B	1.18E-05	10.39
190	**FUBP1**	Far upstream element-binding protein 1	6.00E-06	8.73
191	**FUBP3**	Far upstream element-binding protein 3	1.58E-05	8.56
192	**FUS**	RNA-binding protein FUS	4.66E-07	11.40
193	**FXR1**	Fragile X mental retardation syndrome-related protein 1	1.17E-02	5.43
194	**G6PD**	Glucose-6-phosphate 1-dehydrogenase	3.66E-07	39.01
195	**GANAB**	Neutral alpha-glucosidase AB	3.85E-03	9.79
196	**GAPDH**	Glyceraldehyde-3-phosphate dehydrogenase	1.08E-06	3.14
197	**GARS**	Glycine--tRNA ligase	4.79E-06	21.69
198	**GART**	Trifunctional purine biosynthetic protein adenosine-3;Phosphoribosylamine--glycine ligase; Phosphoribosylformylglycinamidine cyclo-ligase; Phosphoribosylglycinamide formyltransferase	4.15E-07	24.87
199	**GCN1L1**	Translational activator GCN1	2.33E-05	6.66
200	**GDI1**	Rab GDP dissociation inhibitor alpha	8.50E-07	14.70
201	**GDI2**	Rab GDP dissociation inhibitor beta	1.17E-04	35.17
202	**GFPT1**	Glutamine--fructose-6-phosphate aminotransferase [isomerizing] 1	2.62E-08	19.14

203	**GLS**	Glutaminase kidney isoform, mitochondrial	1.29E-06	12.39
204	**GMPS**	GMP synthase [glutamine-hydrolyzing]	4.66E-05	5.91
205	**GNAI2**	Guanine nucleotide-binding protein G(i) subunit alpha-2	7.58E-07	18.47
206	**GNAS**	Guanine nucleotide-binding protein G(s) subunit alpha isoforms XLas;Guanine nucleotide-binding protein G(s) subunit alpha isoforms short	1.25E-04	2.99
207	**GNB1**	Guanine nucleotide-binding protein G(I)/G(S)/G(T) subunit beta-1	4.02E-06	6.88
208	**GNB2**	Guanine nucleotide-binding protein G(I)/G(S)/G(T) subunit beta-2	2.13E-03	8.28
209	**GOT2**	Aspartate aminotransferase, mitochondrial	4.24E-05	12.80
210	**GPI**	Glucose-6-phosphate isomerase	3.83E-05	26.55
211	**GRHPR**	Glyoxylate reductase/hydroxypyruvate reductase	3.45E-05	7.53
212	**GSN**	Gelsolin	1.48E-05	6.90
213	**GSTO1**	Glutathione S-transferase omega-1	2.21E-07	9.28
214	**GSTP1**	Glutathione S-transferase P	6.58E-04	22.24
215	**GTF2I**	General transcription factor II-I	9.11E-05	4.45
216	**HADHA**	Trifunctional enzyme subunit alpha, mitochondrial; Long-chain enoyl-CoA hydratase; Long chain 3-hydroxyacyl-CoA dehydrogenase	1.22E-05	13.13
217	**HADHB**	Trifunctional enzyme subunit beta, mitochondrial;3-ketoacyl-CoA thiolase	2.47E-04	3.37
218	**HDLBP**	Vigilin	5.51E-06	4.17
219	**HIST1H4A**	Histone H4	3.54E-03	6.94
220	**HK1**	Hexokinase-1	1.92E-07	19.50
221	**HLA-A; HLA-B; HLA-H; HLA-C**	HLA class I histocompatibility antigen, A-3 alpha chain; Putative HLA class I histocompatibility antigen, alpha chain H	3.80E-03	3.14
222	**HM13**	Minor histocompatibility antigen H13	4.48E-07	10.58
223	**HMGCS1**	Hydroxymethylglutaryl-CoA synthase, cytoplasmic	7.96E-10	14.65
224	**HNRNPC**	Heterogeneous nuclear ribonucleoproteins C1/C2	1.26E-04	3.77
225	**HNRNPDL**	Heterogeneous nuclear ribonucleoprotein D-like	4.88E-04	3.47
226	**HNRNPF**	Heterogeneous nuclear ribonucleoprotein F;Heterogeneous nuclear ribonucleoprotein F, N-terminally processed	5.29E-02	5.18
227	**HNRNPL**	Heterogeneous nuclear ribonucleoprotein L	9.66E-08	16.30
228	**HNRNPR**	Heterogeneous nuclear ribonucleoprotein R	1.62E-06	12.82
229	**HNRNPU**	Heterogeneous nuclear ribonucleoprotein U	1.12E-02	13.82
230	**HPRT1**	Hypoxanthine-guanine phosphoribosyltransferase	1.16E-05	16.44
231	**HSD17B10**	3-hydroxyacyl-CoA dehydrogenase type-2	2.12E-03	14.23
232	**HSD17B12**	Very-long-chain 3-oxoacyl-CoA reductase	2.27E-03	5.15
233	**HSD17B4**	Peroxisomal multifunctional enzyme type 2;(3R)-hydroxyacyl-CoA dehydrogenase; Enoyl-CoA hydratase 2	9.73E-05	5.62
234	**HSP90AA1**	Heat shock protein HSP 90-alpha	6.67E-04	38.10
235	**HSP90AB1**	Heat shock protein HSP 90-beta	1.80E-08	4.98
236	**HSP90B1**	Endoplasmin	3.44E-06	38.08
237	**HSPA1B; HSPA1A**	Heat shock 70 kDa protein 1B; Heat shock 70 kDa protein 1A	8.22E-05	16.73
238	**HSPA4**	Heat shock 70 kDa protein 4	2.39E-09	36.89
239	**HSPA9**	Stress-70 protein, mitochondrial	1.42E-05	29.90

240	**HSPB1**	Heat shock protein beta-1	1.48E-01	3.97
241	**HSPD1**	60 kDa heat shock protein, mitochondrial	9.87E-05	40.78
242	**HSPH1**	Heat shock protein 105 kDa	7.49E-10	62.41
243	**HUWE1**	E3 ubiquitin-protein ligase HUWE1	1.85E-05	5.28
244	**HYOU1**	Hypoxia up-regulated protein 1	1.45E-05	5.69
245	**IARS**	Isoleucine--tRNA ligase, cytoplasmic	2.00E-08	9.93
246	**IDH1**	Isocitrate dehydrogenase [NADP] cytoplasmic	1.17E-06	28.37
247	**IL13RA2**	Interleukin-13 receptor subunit alpha-2	2.83E-03	4.50
248	**ILF2**	Interleukin enhancer-binding factor 2	8.04E-07	7.36
249	**IMMT**	MICOS complex subunit MIC60	8.73E-07	7.45
250	**IMPDH2**	Inosine-5-monophosphate dehydrogenase 2	8.08E-07	12.73
251	**IPO4**	Importin-4	1.69E-07	8.13
252	**IPO5**	Importin-5	2.69E-11	57.58
253	**IPO7**	Importin-7	1.66E-07	17.72
254	**IQGAP1**	Ras GTPase-activating-like protein IQGAP1	4.24E-06	87.46
255	**ITCH**	E3 ubiquitin-protein ligase Itchy homolog	1.15E-06	4.99
256	**KARS**	Lysine--tRNA ligase	3.82E-08	27.40
257	**KHDRBS1**	KH domain-containing, RNA-binding, signal transduction-associated protein 1	3.45E-07	13.52
258	**KHSRP**	Far upstream element-binding protein 2	1.11E-09	23.40
259	**KIF5B**	Kinesin-1 heavy chain	2.82E-04	10.07
260	**KLC1**	Kinesin light chain 1	1.41E-05	10.03
261	**KPNA2**	Importin subunit alpha-1	4.91E-07	57.29
262	**KPNB1**	Importin subunit beta-1	2.27E-09	68.70
263	**KTN1**	Kinectin	4.04E-03	3.77
264	**LARS**	Leucine--tRNA ligase, cytoplasmic	5.36E-05	8.74
265	**LDHA**	L-lactate dehydrogenase A chain	1.01E-04	3.01
266	**LDHB**	L-lactate dehydrogenase B chain; L-lactate dehydrogenase	2.72E-07	4.23
267	**LGALS1**	Galectin-1	2.28E-04	31.41
268	**LMAN1**	Protein ERGIC-53	1.02E-04	4.54
269	**LPCAT1**	Lysophosphatidylcholine acyltransferase 1	1.43E-04	4.81
270	**LRPPRC**	Leucine-rich PPR motif-containing protein, mitochondrial	2.44E-08	32.15
271	**LTA4H**	Leukotriene A-4 hydrolase	9.38E-04	4.32
272	**MACF1**	Microtubule-actin cross-linking factor 1, isoforms 1/2/3/5	2.88E-05	8.08
273	**MAP1B**	Microtubule-associated protein 1B; MAP1B heavy chain; MAP1 light chain LC1	7.27E-05	12.22
274	**MAP4**	Microtubule-associated protein; Microtubule-associated protein 4	3.09E-06	10.30
275	**MAPK1**	Mitogen-activated protein kinase 1	1.14E-07	19.94
276	**MAPRE1**	Microtubule-associated protein RP/EB family member 1	1.31E-07	5.51
277	**MARS**	Methionine--tRNA ligase, cytoplasmic	8.03E-09	10.70
278	**MAT2A**	S-adenosylmethionine synthase isoform type-2	3.69E-05	9.65
279	**MBOAT7**	Lysophospholipid acyltransferase 7	1.55E-05	3.30
280	**MCCC2**	Methylcrotonoyl-CoA carboxylase beta chain, mitochondrial	3.13E-06	2.96
281	**MCM2**	DNA replication licensing factor MCM2	6.46E-06	12.36
282	**MCM3**	DNA replication licensing factor MCM3	4.60E-07	18.59
283	**MCM4**	DNA replication licensing factor MCM4	2.95E-08	11.58

284	**MCM5**	DNA replication licensing factor MCM5; DNA helicase	5.26E-07	10.29
285	**MCM6**	DNA replication licensing factor MCM6	3.51E-08	9.96
286	**ME2**	NAD-dependent malic enzyme, mitochondrial	1.13E-06	5.69
287	**MGST1**	Microsomal glutathione S-transferase 1	3.09E-09	8.69
288	**MIF**	Macrophage migration inhibitory factor	1.04E-02	16.69
289	**MMS19**	MMS19 nucleotide excision repair protein homolog	3.82E-04	3.65
290	**MSH2**	DNA mismatch repair protein Msh2	5.06E-06	5.32
291	**MSH6**	DNA mismatch repair protein Msh6	1.76E-06	3.24
292	**MTCH2**	Mitochondrial carrier homolog 2	1.01E-09	6.58
293	**MT-CO2**	Cytochrome c oxidase subunit 2	1.38E-03	5.10
294	**MTHFD1**	C-1-tetrahydrofolate synthase, cytoplasmic; Methylenetetrahydrofolate dehydrogenase; Methenyltetrahydrofolate cyclohydrolase; Formyltetrahydrofolate synthetase; C-1-tetrahydrofolate synthase, cytoplasmic, N-terminally processed	2.25E-04	5.49
295	**MYH10**	Myosin-10	5.74E-04	4.33
296	**MYH9**	Myosin-9	2.33E-04	21.33
297	**MYL6**	Myosin light polypeptide 6	7.42E-04	22.71
298	**MYO1C**	Unconventional myosin-Ic	5.87E-08	8.70
299	**MYOF**	Myoferlin	1.14E-06	12.84
300	**N/A**	Uncharacterized actin-binding protein	4.95E-08	22.45
301	**NAA15**	N-alpha-acetyltransferase 15, NatA auxiliary subunit	6.70E-08	12.27
302	**NAGK**	N-acetyl-D-glucosamine kinase	8.57E-05	11.51
303	**NAMPT**	Nicotinamide phosphoribosyltransferase	1.27E-06	14.22
304	**NAP1L1**	Nucleosome assembly protein 1-like 1	3.20E-05	8.55
305	**NAPA**	Alpha-soluble NSF attachment protein	2.09E-06	8.17
306	**NARS**	Asparagine--tRNA ligase, cytoplasmic	3.12E-06	13.21
307	**NASP**	Nuclear autoantigenic sperm protein	9.37E-04	3.22
308	**NCAPD2**	Condensin complex subunit 1	1.12E-06	6.53
309	**NCEH1**	Neutral cholesterol ester hydrolase 1	1.65E-05	9.18
310	**NCKAP1**	Nck-associated protein 1	6.68E-06	6.37
311	**NCL**	Nucleolin	1.58E-05	4.82
312	**NHP2L1**	NHP2-like protein 1; NHP2-like protein 1, N-terminally processed	4.95E-03	10.10
313	**NME1**	Nucleoside diphosphate kinase A	5.11E-03	3.86
314	**NME1-NME2; NME2; NME1**	Nucleoside diphosphate kinase; Nucleoside diphosphate kinase B	1.26E-04	68.78
315	**NNMT**	Nicotinamide N-methyltransferase	2.39E-05	4.16
316	**NNT**	NAD(P) transhydrogenase, mitochondrial	9.64E-06	6.90
317	**NPEPPS**	Puromycin-sensitive aminopeptidase	8.44E-09	32.63
318	**NPM1**	Nucleophosmin	3.30E-06	20.88
319	**NQO1**	NAD(P)H dehydrogenase [quinone] 1	1.00E-02	14.83
320	**NSDHL**	Sterol-4-alpha-carboxylate 3-dehydrogenase, decarboxylating	1.25E-06	4.75
321	**NSUN2**	tRNA (cytosine(34)-C(5))-methyltransferase	3.96E-07	10.35
322	**NUDC**	Nuclear migration protein nudC	1.91E-08	14.63
323	**NUDCD1**	NudC domain-containing protein 1	5.07E-06	3.23
324	**NUP155**	Nuclear pore complex protein Nup155	1.37E-08	6.63

325	**NUP93**	Nuclear pore complex protein Nup93	1.53E-06	4.84
326	**OAT**	Ornithine aminotransferase, mitochondrial; Ornithine aminotransferase, hepatic form; Ornithine aminotransferase, renal form	3.94E-07	9.12
327	**OGDH**	2-oxoglutarate dehydrogenase, mitochondrial	5.15E-08	13.26
328	**OLA1**	Obg-like ATPase 1	2.97E-08	5.97
329	**OTUB1**	Ubiquitin thioesterase OTUB1	5.35E-06	5.22
330	**OXCT1**	Succinyl-CoA:3-ketoacid coenzyme A transferase 1, mitochondrial	2.76E-06	7.97
331	**P4HB**	Protein disulfide-isomerase	4.56E-06	9.27
332	**PA2G4**	Proliferation-associated protein 2G4	1.17E-07	14.87
333	**PAFAH1B1**	Platelet-activating factor acetylhydrolase IB subunit alpha	1.80E-05	7.96
334	**PAFAH1B2**	Platelet-activating factor acetylhydrolase IB subunit beta	9.93E-04	4.05
335	**PAFAH1B3**	Platelet-activating factor acetylhydrolase IB subunit gamma	2.14E-07	7.81
336	**PAICS**	Multifunctional protein ADE2; Phosphoribosylaminoimidazole-succinocarboxamide synthase; Phosphoribosylaminoimidazole carboxylase	2.51E-09	28.69
337	**PAIP1**	Polyadenylate-binding protein-interacting protein 1	2.26E-05	8.10
338	**PAPSS2**	Bifunctional 3-phosphoadenosine 5-phosphosulfate synthase 2; Sulfate adenylyltransferase; Adenylyl-sulfate kinase	7.98E-03	6.79
339	**PARK7**	Protein deglycase DJ-1	1.62E-07	19.36
340	**PARP1**	Poly [ADP-ribose] polymerase 1	3.31E-06	12.30
341	**PCBP1**	Poly(rC)-binding protein 1	7.08E-03	5.77
342	**PCBP2**	Poly(rC)-binding protein 2	2.73E-08	29.38
343	**PCMT1**	Protein-L-isoaspartate O-methyltransferase; Protein-L-isoaspartate(D-aspartate) O-methyltransferase	3.44E-03	3.06
344	**PCNA**	Proliferating cell nuclear antigen	2.46E-03	10.56
345	**PDCD6IP**	Programmed cell death 6-interacting protein	1.22E-05	17.71
346	**PDHB**	Pyruvate dehydrogenase E1 component subunit beta, mitochondrial	3.74E-05	5.25
347	**PDIA3**	Protein disulfide-isomerase A3	1.13E-07	8.65
348	**PDIA4**	Protein disulfide-isomerase A4	9.14E-07	4.22
349	**PDIA6**	Protein disulfide-isomerase A6	1.42E-07	6.82
350	**PDLIM7**	PDZ and LIM domain protein 7	3.27E-04	4.67
351	**PEBP1**	Phosphatidylethanolamine-binding protein 1; Hippocampal cholinergic neurostimulating peptide	1.34E-03	3.55
352	**PFAS**	Phosphoribosylformylglycinamidine synthase	2.63E-10	21.86
353	**PFKL**	ATP-dependent 6-phosphofructokinase, liver type	4.87E-05	4.33
354	**PFKP**	ATP-dependent 6-phosphofructokinase, platelet type	6.21E-06	62.59
355	**PFN1**	Profilin-1	1.41E-04	93.06
356	**PGD**	6-phosphogluconate dehydrogenase, decarboxylating	3.39E-12	56.54
357	**PGK1**	Phosphoglycerate kinase 1	1.48E-04	67.99
358	**PGRMC2**	Membrane-associated progesterone receptor component 2	1.63E-07	4.76
359	**PHB**	Prohibitin	5.23E-02	5.74
360	**PHB2**	Prohibitin-2	9.96E-02	4.70
361	**PHGDH**	D-3-phosphoglycerate dehydrogenase	7.44E-08	12.97
362	**PICALM**	Phosphatidylinositol-binding clathrin assembly protein	1.04E-03	3.46
363	**PITPNB**	Phosphatidylinositol transfer protein beta isoform	4.43E-08	6.64
364	**PKM**	Pyruvate kinase PKM; Pyruvate kinase	4.70E-06	6.32

365	**PLAA**	Phospholipase A-2-activating protein	2.34E-06	4.80
366	**PLIN3**	Perilipin-3	1.14E-06	19.82
367	**PLS3**	Plastin-3	3.83E-08	38.54
368	**PPA1**	Inorganic pyrophosphatase	7.22E-05	7.06
369	**PPIA**	Peptidyl-prolyl cis-trans isomerase A; Peptidyl-prolyl cis-trans isomerase A, N-terminally processed; Peptidyl-prolyl cis-trans isomerase	1.12E-06	14.49
370	**PPME1**	Protein phosphatase methylesterase 1	8.39E-03	7.82
371	**PPP1CA**	Serine/threonine-protein phosphatase PP1-alpha catalytic subunit; Serine/threonine-protein phosphatase	2.24E-06	9.14
372	**PPP2R1A**	Serine/threonine-protein phosphatase 2A 65 kDa regulatory subunit A alpha isoform	2.13E-07	39.68
373	**PPP2R4; DKFZp781M17165**	Serine/threonine-protein phosphatase 2A activator	2.68E-07	10.24
374	**PRDX1**	Peroxiredoxin-1	3.73E-07	6.65
375	**PRDX2**	Peroxiredoxin-2	2.59E-05	5.22
376	**PRDX3**	Thioredoxin-dependent peroxide reductase, mitochondrial	4.25E-09	12.78
377	**PRDX6**	Peroxiredoxin-6	2.03E-03	10.61
378	**PRKDC**	DNA-dependent protein kinase catalytic subunit	1.27E-08	43.15
379	**PRMT1**	Protein arginine N-methyltransferase 1	5.97E-09	47.51
380	**PRMT5**	Protein arginine N-methyltransferase 5; Protein arginine N-methyltransferase 5, N-terminally processed	5.06E-06	6.35
381	**PRPF8**	Pre-mRNA-processing-splicing factor 8	2.81E-07	13.14
382	**PRPS1**	Ribose-phosphate pyrophosphokinase 1	2.06E-05	4.48
383	**PSAT1**	Phosphoserine aminotransferase	1.13E-07	11.04
384	**PSMA6**	Proteasome subunit alpha type; Proteasome subunit alpha type-6	2.87E-03	3.73
385	**PSMA7; PSMA8**	Proteasome subunit alpha type-7; Proteasome subunit alpha type-7-like	9.21E-07	5.42
386	**PSMC1**	26S protease regulatory subunit 4	1.83E-07	12.69
387	**PSMC2**	26S protease regulatory subunit 7	2.62E-05	19.55
388	**PSMC3**	26S protease regulatory subunit 6A	6.66E-08	15.88
389	**PSMC4**	26S protease regulatory subunit 6B	4.92E-07	8.05
390	**PSMC5**	26S protease regulatory subunit 8	3.61E-05	18.21
391	**PSMC6**	26S protease regulatory subunit 10B	7.62E-09	19.84
392	**PSMD1**	26S proteasome non-ATPase regulatory subunit 1	9.48E-07	11.30
393	**PSMD11**	26S proteasome non-ATPase regulatory subunit 11	2.81E-04	2.87
394	**PSMD12**	26S proteasome non-ATPase regulatory subunit 12	1.29E-04	4.20
395	**PSMD13**	26S proteasome non-ATPase regulatory subunit 13	3.45E-07	11.94
396	**PSMD14**	26S proteasome non-ATPase regulatory subunit 14	4.45E-03	5.13
397	**PSMD2**	26S proteasome non-ATPase regulatory subunit 2	7.85E-08	47.25
398	**PSMD3**	26S proteasome non-ATPase regulatory subunit 3	7.20E-06	5.96
399	**PSMD5**	26S proteasome non-ATPase regulatory subunit 5	1.39E-06	9.00
400	**PSMD6**	26S proteasome non-ATPase regulatory subunit 6	2.42E-06	14.54
401	**PSME1**	Proteasome activator complex subunit 1	2.15E-05	4.32
402	**PTBP1**	Polypyrimidine tract-binding protein 1	1.24E-02	5.31
403	**PTGES3**	Prostaglandin E synthase 3	2.25E-09	39.25

404	**PUF60**	Poly(U)-binding-splicing factor PUF60	3.80E-06	6.99
405	**PXN**	Paxillin	8.06E-07	5.83
406	**PYCR1**	Pyrroline-5-carboxylate reductase 1, mitochondrial;	8.67E-06	4.60
407	**PYGB**	Glycogen phosphorylase, brain form	3.94E-05	35.13
408	**PYGL**	Glycogen phosphorylase, liver form; Alpha-1,4 glucan phosphorylase	1.94E-10	40.56
409	**QARS**	Glutamine--tRNA ligase	4.69E-07	10.10
410	**RAB11A; RAB11B**	Ras-related protein Rab-11A; Ras-related protein Rab-11B	7.54E-03	4.67
411	**RAB14**	Ras-related protein Rab-14	9.60E-06	12.61
412	**RAB1B; RAB1C**	Ras-related protein Rab-1B; Putative Ras-related protein Rab-1C	3.02E-04	19.76
413	**RAB32**	Ras-related protein Rab-32	5.29E-04	3.28
414	**RAB5C**	Ras-related protein Rab-5C	3.08E-06	23.20
415	**RAB7A**	Ras-related protein Rab-7a	1.41E-07	34.63
416	**RAC1; RAC3; RAC2**	Ras-related C3 botulinum toxin substrate 1; Ras-related C3 botulinum toxin substrate 3; Ras-related C3 botulinum toxin substrate 2	4.57E-09	17.14
417	**RAE1**	mRNA export factor	1.14E-04	9.30
418	**RANGAP1**	Ran GTPase-activating protein 1	3.28E-08	34.99
419	**RARS**	Arginine--tRNA ligase, cytoplasmic	2.27E-08	15.46
420	**RBM39**	RNA-binding protein 39	5.96E-06	6.08
421	**RCC1**	Regulator of chromosome condensation	2.66E-04	4.91
422	**RECQL**	ATP-dependent DNA helicase Q1	2.15E-09	30.89
423	**RHEB**	GTP-binding protein Rheb	2.65E-05	4.40
424	**RHOC; RHOA**	Rho-related GTP-binding protein RhoC	5.51E-03	11.57
425	**RNH1**	Ribonuclease inhibitor	1.85E-07	25.78
426	**RNPEP**	Aminopeptidase B	3.42E-04	3.45
427	**RPL12**	60S ribosomal protein L12	7.24E-08	40.01
428	**RPL13A; RPL13a**	60S ribosomal protein L13a	6.52E-02	4.79
429	**RPL17; RPL17-C18orf32**	60S ribosomal protein L17	1.50E-09	25.35
430	**RPL19**	Ribosomal protein L19; 60S ribosomal protein L19	3.67E-06	8.94
431	**RPL21**	60S ribosomal protein L21	8.06E-03	5.69
432	**RPL23**	60S ribosomal protein L23	3.61E-02	3.87
433	**RPL23A**	60S ribosomal protein L23a	3.52E-03	4.68
434	**RPL24**	60S ribosomal protein L24	6.60E-06	20.47
435	**RPL27A**	60S ribosomal protein L27a	1.49E-02	14.14
436	**RPL30**	60S ribosomal protein L30	1.05E-10	24.74
437	**RPL38**	60S ribosomal protein L38	1.27E-05	4.81
438	**RPL5**	60S ribosomal protein L5	3.43E-07	18.73
439	**RPL7**	60S ribosomal protein L7	1.42E-01	5.41
440	**RPL9**	60S ribosomal protein L9	1.15E-08	21.26
441	**RPLP0; RPLP0P6**	60S acidic ribosomal protein P0; 60S acidic ribosomal protein P0-like	3.15E-03	9.81

442	**RPLP1**	60S acidic ribosomal protein P1	1.94E-02	3.36
443	**RPLP2**	60S acidic ribosomal protein P2	3.97E-02	6.93
444	**RPN1**	Dolichyl-diphosphooligosaccharide-protein glycosyltransferase subunit 1	1.75E-04	12.67
445	**RPN2**	Dolichyl-diphosphooligosaccharide-protein glycosyltransferase subunit 2	1.49E-03	5.87
446	**RPS12**	40S ribosomal protein S12	4.92E-03	11.16
447	**RPS13**	40S ribosomal protein S13	2.62E-07	11.50
448	**RPS14**	40S ribosomal protein S14	8.77E-02	3.66
449	**RPS15A**	40S ribosomal protein S15a	5.82E-08	30.39
450	**RPS17**	40S ribosomal protein S17	4.35E-06	8.35
451	**RPS23**	40S ribosomal protein S23	2.40E-06	7.95
452	**RPS24**	40S ribosomal protein S24	2.02E-06	7.53
453	**RPS5**	40S ribosomal protein S5; 40S ribosomal protein S5, N-terminally processed	3.68E-07	31.72
454	**RPS6**	40S ribosomal protein S6	1.82E-07	20.51
455	**RPS6KA1**	Ribosomal protein S6 kinase; Ribosomal protein S6 kinase alpha-1	1.84E-03	3.25
456	**RPS7**	40S ribosomal protein S7	1.37E-05	3.57
457	**RPSA**	40S ribosomal protein SA	1.62E-02	6.75
458	**RRAS2**	Ras-related protein R-Ras2	1.03E-05	4.96
459	**RTCB**	tRNA-splicing ligase RtcB homolog	8.60E-06	9.33
460	**RUVBL1**	RuvB-like 1	5.31E-08	18.65
461	**RUVBL2**	RuvB-like 2	4.14E-06	12.40
462	**S100A10**	Protein S100-A10	2.17E-05	13.26
463	**S100A11**	Protein S100-A11; Protein S100-A11, N-terminally processed	2.86E-06	14.17
464	**SAE1**	SUMO-activating enzyme subunit 1; SUMO-activating enzyme subunit 1, N-terminally processed	3.90E-09	3.84
465	**SAMHD1**	Deoxynucleoside triphosphate triphosphohydrolase SAMHD1	1.44E-08	4.61
466	**SAR1A**	GTP-binding protein SAR1a	2.27E-05	9.69
467	**SCFD1**	Sec1 family domain-containing protein 1	6.74E-05	3.72
468	**SCRN1**	Secernin-1	3.14E-04	4.56
469	**SDHA**	Succinate dehydrogenase [ubiquinone] flavoprotein subunit, mitochondrial	7.88E-03	9.45
470	**SEC13**	Protein SEC13 homolog	1.67E-07	14.48
471	**SEC24C**	Protein transport protein Sec24C	8.89E-04	3.73
472	**SEC31A**	Protein transport protein Sec31A	1.75E-05	6.22
473	**SEPT2**	Septin-2	7.48E-06	13.96
474	**SEPT7**	Septin-7	1.89E-05	8.70
475	**SERPINB6**	Serpin B6	4.11E-06	6.68
476	**SERPINH1**	Serpin H1	9.52E-08	31.41
477	**SF3A1**	Splicing factor 3A subunit 1	1.09E-04	4.68
478	**SF3A3**	Splicing factor 3A subunit 3	1.35E-04	3.17
479	**SF3B1**	Splicing factor 3B subunit 1	3.89E-04	8.80
480	**SF3B2**	Splicing factor 3B subunit 2	3.32E-04	4.28
481	**SF3B3**	Splicing factor 3B subunit 3	6.44E-06	16.95
482	**SFN**	14-3-3 protein sigma	1.27E-08	11.68
483	**SHMT1**	Serine hydroxymethyltransferase, cytosolic	1.05E-06	6.60

484	**SHMT2**	Serine hydroxymethyltransferase, mitochondrial; Serine hydroxymethyltransferase	2.48E-05	25.55
485	**SLC16A3**	Monocarboxylate transporter 4	2.01E-05	4.07
486	**SLC25A1**	Tricarboxylate transport protein, mitochondrial	1.53E-07	9.32
487	**SLC25A3**	Phosphate carrier protein, mitochondrial	2.83E-07	19.61
488	**SLC25A5**	ADP/ATP translocase 2; ADP/ATP translocase 2, N-terminally processed	2.95E-02	9.17
489	**SLC25A6; SLC25A4**	ADP/ATP translocase 3; ADP/ATP translocase 3, N-terminally processed; ADP/ATP translocase 1	3.50E-07	6.28
490	**SLC3A2**	4F2 cell-surface antigen heavy chain	5.59E-08	22.51
491	**SLC7A5**	Large neutral amino acids transporter small subunit 1	2.98E-03	5.62
492	**SMC2**	Structural maintenance of chromosomes protein 2	6.85E-06	4.35
493	**SMC4**	Structural maintenance of chromosomes protein 4;	1.09E-02	3.10
494	**SMS**	Spermine synthase	2.63E-03	3.68
495	**SMTN**	Smoothelin	5.10E-07	10.49
496	**SND1**	Staphylococcal nuclease domain-containing protein 1	1.99E-05	28.53
497	**SNRNP200**	U5 small nuclear ribonucleoprotein 200 kDa helicase	1.32E-04	5.59
498	**SNRNP70**	U1 small nuclear ribonucleoprotein 70 kDa	5.57E-05	2.84
499	**SORD**	Sorbitol dehydrogenase	3.31E-05	3.80
500	**SPR**	Sepiapterin reductase	4.94E-05	5.46
501	**SPTAN1**	Spectrin alpha chain, non-erythrocytic 1	8.61E-11	68.96
502	**SPTBN1**	Spectrin beta chain, non-erythrocytic 1	1.03E-09	69.53
503	**SQSTM1**	Sequestosome-1	1.99E-05	4.34
504	**SRM**	Spermidine synthase	1.62E-06	9.52
505	**SRP68**	Signal recognition particle subunit SRP68	2.25E-07	4.64
506	**SRP72**	Signal recognition particle subunit SRP72	1.73E-05	10.43
507	**SRPR**	Signal recognition particle receptor subunit alpha	2.24E-05	3.04
508	**SRPRB**	Signal recognition particle receptor subunit beta	2.94E-04	3.69
509	**SRSF6; SRSF4**	Serine/arginine-rich splicing factor 6;Serine/arginine-rich splicing factor 4	4.05E-05	4.59
510	**SRSF7**	Serine/arginine-rich splicing factor 7	3.29E-09	7.48
511	**SSB**	Lupus La protein	2.69E-03	3.10
512	**SSRP1**	FACT complex subunit SSRP1	4.43E-05	8.15
513	**ST13; ST13P5; ST13P4**	Hsc70-interacting protein; Putative protein FAM10A5; Putative protein FAM10A4	2.12E-06	10.92
514	**STAT1**	Signal transducer and activator of transcription 1-alpha/beta; Signal transducer and activator of transcription	1.00E-04	3.76
515	**STAT3**	Signal transducer and activator of transcription 3;	6.46E-07	2.84
516	**STIP1**	Stress-induced-phosphoprotein 1	3.72E-08	58.88
517	**STK26; STK25**	Serine/threonine-protein kinase 26; Serine/threonine-protein kinase 25	1.14E-03	3.80
518	**STOML2**	Stomatin-like protein 2, mitochondrial	9.68E-05	3.22
519	**STRAP**	Serine-threonine kinase receptor-associated protein	4.62E-05	13.21
520	**SUGT1**	Suppressor of G2 allele of SKP1 homolog	4.23E-10	11.70
521	**SUPT16H**	FACT complex subunit SPT16	2.00E-06	9.07
522	**SYNCRIP**	Heterogeneous nuclear ribonucleoprotein Q	7.06E-04	21.40

523	**TAGLN2**	Transgelin-2	5.35E-04	27.54
524	**TARDBP; TDP43**	TAR DNA-binding protein 43	3.72E-04	3.80
525	**TARS**	Threonine--tRNA ligase, cytoplasmic	1.84E-03	25.21
526	**TCP1**	T-complex protein 1 subunit alpha	1.17E-02	10.78
527	**TFRC**	Transferrin receptor protein 1; Transferrin receptor protein 1, serum form	2.05E-09	29.33
528	**TGM2**	Protein-glutamine gamma-glutamyltransferase 2	5.69E-06	3.61
529	**TIGAR**	Fructose-2,6-bisphosphatase TIGAR	1.88E-03	4.19
530	**TK1**	Thymidine kinase; Thymidine kinase, cytosolic	2.04E-06	10.02
531	**TKT**	Transketolase	2.55E-04	3.96
532	**TLN1**	Talin-1	3.98E-12	162.03
533	**TMPO**	Lamina-associated polypeptide 2, isoform alpha; Thymopoietin; Thymopentin	5.49E-06	3.66
534	**TNPO1**	Transportin-1	2.56E-08	19.58
535	**TNPO3**	Transportin-3	1.46E-05	4.82
536	**TOMM34**	Mitochondrial import receptor subunit TOM34	3.23E-06	3.96
537	**TOMM70A**	Mitochondrial import receptor subunit TOM70	4.81E-07	9.06
538	**TOP1**	DNA topoisomerase 1	2.85E-04	12.79
539	**TOP2A**	DNA topoisomerase 2-alpha	6.44E-06	5.56
540	**TPI1**	Triosephosphate isomerase	6.71E-07	27.13
541	**TPM3**	Tropomyosin alpha-3 chain	3.40E-08	69.95
542	**TPM3**	Tropomyosin alpha-3 chain	6.43E-03	3.70
543	**TPT1**	Translationally-controlled tumor protein	9.33E-08	16.43
544	**TPX2**	Targeting protein for Xklp2	5.29E-04	3.15
545	**TRAP1**	Heat shock protein 75 kDa, mitochondrial	4.66E-05	7.33
546	**TRIM25**	E3 ubiquitin/ISG15 ligase TRIM25	1.38E-06	5.96
547	**TRIM28**	Transcription intermediary factor 1-beta	7.22E-07	23.43
548	**TRIP13**	Pachytene checkpoint protein 2 homolog	3.03E-07	20.73
549	**TRPV1; SHPK**	Sedoheptulokinase	1.50E-03	3.20
550	**TSN**	Translin	1.17E-05	5.19
551	**TTLL12**	Tubulin--tyrosine ligase-like protein 12	1.13E-07	7.05
552	**TUBA1C; TUBA1B**	Tubulin alpha-1C chain	1.48E-07	34.36
553	**TUBA4A**	Tubulin alpha-4A chain	7.03E-04	4.03
554	**TUBB6**	Tubulin beta-6 chain	1.66E-07	19.42
555	**TUFM**	Elongation factor Tu, mitochondrial	3.54E-02	3.93
556	**TWF1**	Twinfilin-1	4.81E-06	5.85
557	**TWF2**	Twinfilin-2	3.53E-07	4.33
558	**TXN**	Thioredoxin	2.20E-08	29.50
559	**TXNDC17**	Thioredoxin domain-containing protein 17	3.75E-06	5.95
560	**U2AF1; U2AF1L4**	Splicing factor U2AF 35 kDa subunit; Splicing factor U2AF 26 kDa subunit	2.77E-03	4.20
561	**UAP1**	UDP-N-acetylhexosamine pyrophosphorylase; UDP-N-acetylgalactosamine pyrophosphorylase; UDP-N-acetylglucosamine pyrophosphorylase	2.50E-08	67.36

562	**UBA1**	Ubiquitin-like modifier-activating enzyme 1	4.17E-08	130.47
563	**UBA6**	Ubiquitin-like modifier-activating enzyme 6	1.99E-04	3.35
564	**UBE2L3**	Ubiquitin-conjugating enzyme E2 L3	6.39E-03	8.70
565	**UBE2S**	Ubiquitin-conjugating enzyme E2 S	5.28E-04	4.34
566	**UBR4**	E3 ubiquitin-protein ligase UBR4	1.31E-05	4.79
567	**UGDH**	UDP-glucose 6-dehydrogenase	2.62E-07	11.19
568	**UGP2**	UTP--glucose-1-phosphate uridylyltransferase	1.16E-02	4.26
569	**UMPS**	Uridine 5-monophosphate synthase; Orotate phosphoribosyltransferase; Orotidine 5-phosphate decarboxylase	6.07E-07	3.35
570	**UPF1**	Regulator of nonsense transcripts 1	2.01E-04	5.30
571	**UPP1**	Uridine phosphorylase 1	4.41E-05	14.27
572	**UQCRC1**	Cytochrome b-c1 complex subunit 1, mitochondrial	2.01E-06	23.93
573	**UQCRC2**	Cytochrome b-c1 complex subunit 2, mitochondrial	1.23E-06	8.32
574	**USO1**	General vesicular transport factor p115	2.22E-04	4.02
575	**USP10**	Ubiquitin carboxyl-terminal hydrolase 10	2.05E-05	3.75
576	**USP14**	Ubiquitin carboxyl-terminal hydrolase; Ubiquitin carboxyl-terminal hydrolase 14	7.29E-04	2.91
577	**USP5**	Ubiquitin carboxyl-terminal hydrolase 5	3.23E-07	16.74
578	**VARS**	Valine--tRNA ligase	2.89E-08	17.39
579	**VASP**	Vasodilator-stimulated phosphoprotein	1.26E-05	14.84
580	**VAT1**	Synaptic vesicle membrane protein VAT-1 homolog	1.77E-08	30.01
581	**VCL**	Vinculin	8.54E-08	86.64
582	**VCP**	Transitional endoplasmic reticulum ATPase	2.35E-05	62.97
583	**VDAC2**	Voltage-dependent anion-selective channel protein 2	1.51E-08	29.29
584	**VPS29**	Vacuolar protein sorting-associated protein 29	7.36E-04	3.36
585	**VPS35**	Vacuolar protein sorting-associated protein 35	9.16E-06	24.00
586	**WDR1**	WD repeat-containing protein 1	2.13E-08	49.86
587	**WDR77**	Methylosome protein 50	4.61E-04	3.71
588	**XPO1**	Exportin-1	2.52E-08	34.76
589	**XRCC5**	X-ray repair cross-complementing protein 5	2.63E-08	28.21
590	**XRCC6**	X-ray repair cross-complementing protein 6	9.79E-09	35.09
591	**YARS**	Tyrosine--tRNA ligase, cytoplasmic; Tyrosine--tRNA ligase, cytoplasmic, N-terminally processed; Tyrosine--tRNA ligase	6.04E-06	7.61
592	**YBX1**	Nuclease-sensitive element-binding protein 1	5.02E-02	3.64
593	**YWHAB**	14-3-3 protein beta/alpha;14-3-3 protein beta/alpha, N-terminally processed	1.62E-03	19.42
594	**YWHAE**	14-3-3 protein epsilon	1.99E-06	185.15
595	**YWHAG**	14-3-3 protein gamma;14-3-3 protein gamma, N-terminally processed	1.52E-07	25.03
596	**YWHAH**	14-3-3 protein eta	6.97E-08	31.85
597	**YWHAQ**	14-3-3 protein theta	2.28E-08	69.63
598	**YWHAZ**	14-3-3 protein zeta/delta	1.22E-06	244.37
599	**ZC3HAV1**	Zinc finger CCCH-type antiviral protein 1	3.93E-03	4.93
600	**ZNF185**	Zinc finger protein 185	1.38E-04	5.14

Table 7.1: Biotin-ajoene 40 interactome isolated from MDA-MB-231 cancer cells.

Gene	Protein name	Fold-change	R-value
PFKP	ATP-dependent 6-phosphofructokinase, platelet type	62.6	2.18
PRMT1	Protein arginine N-methyltransferase 1	47.5	1.92
CAPN2	Calpain-2 catalytic subunit	34.1	1.50
EPRS	Bifunctional glutamate/proline--tRNA ligase	33.6	2.52
RPS5	40S ribosomal protein S5;40S ribosomal protein S5	31.7	1.63
TXN	Thioredoxin	29.5	1.05
IDH1	Isocitrate dehydrogenase [NADP] cytoplasmic	28.4	1.37
GSTP1	Glutathione S-transferase P	22.2	2.38
ACAT1	Acetyl-CoA acetyltransferase, mitochondrial	21.3	1.06
CLIC4	Chloride intracellular channel protein 4	17.8	1.45
PDCD6IP	Programmed cell death 6-interacting protein	17.7	3.00
HMGCS1	Hydroxymethylglutaryl-CoA synthase, cytoplasmic	14.7	1.14
IMPDH2	Inosine-5-monophosphate dehydrogenase 2	12.7	2.60
GSTO1	Glutathione S-transferase omega-1	9.3	0.84
P4HB	Protein disulfide-isomerase	9.3	1.09
PDIA3	Protein disulfide-isomerase A3	8.7	1.06
OXCT1	Succinyl-CoA:3-ketoacid coenzyme A transferase 1	8.0	2.84
ATP6V1A	V-type proton ATPase catalytic subunit A	7.0	0.86
PDIA6	Protein disulfide-isomerase A6	6.8	1.59
NCAPD2	Condensin complex subunit 1	6.5	2.11
TXNDC17	Thioredoxin domain-containing protein 17	6.0	0.95
EIF5B	Eukaryotic translation initiation factor 5B	5.4	2.34
HUWE1	E3 ubiquitin-protein ligase HUWE1	5.3	2.35

ALDH9A1	4-trimethylaminobutyraldehyde dehydrogenase	5.2	0.92
NUP93	Nuclear pore complex protein Nup93	4.8	1.81
PDIA4	Protein disulfide-isomerase A4	4.2	1.75
TUBA4A	Tubulin alpha-4A chain	4.0	2.65
TKT	Transketolase	4.0	2.37
MMS19	MMS19 nucleotide excision repair protein homolog	3.6	2.22
ADSL	Adenylosuccinate lyase	3.4	2.01
EEF1A1	Elongation factor 1-alpha 1	3.3	2.30
CASK	Peripheral plasma membrane protein CASK	3.2	1.76

Table 7.2: Protein targets of the biotin-ajoene interactome containing known hyper-reactive cysteine sites.
"Cysteine ligandability", R-value < 3; Weerapana *et al.*[413]

Gene	Protein name	Protein class	Fold-change
ALDOA	Fructose-bisphosphate aldolase A	aldolase	5.7
PFKP	ATP-dependent 6-phosphofructokinase; platelet type	carbohydrate kinase	62.6
FKBP4	Peptidyl-prolyl cis-trans isomerase FKBP4	chaperone	22.4
NASP	Nuclear autoantigenic sperm protein	chaperone	3.2
PPIA	Peptidyl-prolyl cis-trans isomerase A	chaperone	14.5
PTGES3	Prostaglandin E synthase 3	chaperone	39.3
VCP	Transitional endoplasmic reticulum ATPase	chaperone-like protein	63.0
CCT4	T-complex protein 1 subunit delta	chaperonin	48.2
CCT5	T-complex protein 1 subunit epsilon	chaperonin	53.7
CCT8	T-complex protein 1 subunit theta	chaperonin	117.7
TCP1	T-complex protein 1 subunit alpha	chaperonin	10.8
SUPT16H	FACT complex subunit SPT16	chromatin/chromatin-binding, or -regulatory protein	9.1

HNRNPU	Heterogeneous nuclear ribonucleoprotein U	chromatin/chromatin-binding, or -regulatory protein	13.8
STIP1	Stress-induced-phosphoprotein 1	co-chaperone	58.9
MIF	Muellerian-inhibiting factor	cytokine	16.7
SEPT7	Septin-7	cytoskeletal protein	8.7
DIAPH1	Protein diaphanous homolog 1	cytoskeletal protein	8.5
EEF1G	Elongation factor 1-gamma	cytoskeletal protein	16.2
FLNA	Filamin-A	cytoskeletal protein	4.3
FLNB	Filamin-B	cytoskeletal protein	10.4
MYH9	Myosin-9	cytoskeletal protein	21.3
TLN1	Talin-1	cytoskeletal protein	162.0
ALDH18A1	Delta-1-pyrroline-5-carboxylate synthase	dehydrogenase	3.4
GAPDH	Glyceraldehyde-3-phosphate dehydrogenase	dehydrogenase	3.1
IMPDH2	Inosine-5'-monophosphate dehydrogenase 2	dehydrogenase	12.7
LDHA	L-lactate dehydrogenase A chain	dehydrogenase	3.0
PHGDH	D-3-phosphoglycerate dehydrogenase	dehydrogenase	13.0
MCM6	DNA replication licensing factor MCM6	DNA metabolism protein	10.0
HPRT1	Hypoxanthine-guanine phosphoribosyltransferase	glycosyltransferase	16.4
ARF4	ADP-ribosylation factor 4	G-protein	37.9
ARF5	ADP-ribosylation factor 5	G-protein	32.4
OLA1	Obg-like ATPase 1	G-protein	6.0
HSPA4	Heat shock 70 kDa protein 4	heat shock protein	36.9
HSPD1	60 kDa heat shock protein; mitochondrial	heat shock protein	40.8
HSPH1	Heat shock protein 105 kDa	heat shock protein	62.4
HSP90AB1	Heat shock protein HSP 90-beta	heat shock protein	5.0

CLIC4	Chloride intracellular channel protein 4	ion channel	17.8
TPI1	Triosephosphate isomerase	isomerase	27.1
GMPS	GMP synthase [glutamine-hydrolyzing]	ligase	5.9
PFAS	Phosphoribosylformylglycinamidine synthase	ligase	21.9
DNM1L	Dynamin-1-like protein	membrane traffic protein	23.4
NPEPPS	Puromycin-sensitive aminopeptidase	metalloprotease	32.6
NUDC	Nuclear migration protein nudC	microtubule or microtubule-binding cytoskeletal protein	14.6
MAP4	Microtubule-associated protein 4	microtubule or microtubule-binding cytoskeletal protein	10.3
TUBA1C	Tubulin alpha-1C chain	microtubule or microtubule-binding cytoskeletal protein	34.4
GART	Trifunctional purine biosynthetic protein adenosine-3	Multifunctional protein	24.9
MTHFD1	C-1-tetrahydrofolate synthase; cytoplasmic	Multifunctional protein	5.5
PAICS	Multifunctional protein ADE2	Multifunctional protein	28.7
PARK7	Parkinson disease protein 7	Multifunctional protein	19.4
CAPZB	F-actin-capping protein subunit beta	non-motor actin binding protein	19.3
CFL1	Cofilin-1	non-motor actin binding protein	61.3
CNN2	Calponin-2	non-motor actin binding protein	3.8
DSTN	Destrin	non-motor actin binding protein	20.8
WDR1	WD repeat-containing protein 1	non-motor actin binding protein	49.9
HSD17B10	3-hydroxyacyl-CoA dehydrogenase type-2	oxidoreductase	14.2
TXN	Thioredoxin	oxidoreductase	29.5
PRDX1	Peroxiredoxin-1	peroxidase	6.7
PRDX3	Thioredoxin-dependent peroxide reductase; mitochondrial	peroxidase	12.8
PPP2R1A	Serine/threonine-protein phosphatase 2A 65 kDa regulatory subunit A alpha isoform	phosphatase modulator	39.7

PRMT1	Protein arginine N-methyltransferase 1	protein modifying enzyme	47.5
PPA1	Inorganic pyrophosphatase	pyrophosphatase	7.1
RPLP0	60S acidic ribosomal protein P0	ribosomal protein	9.8
RPS5	40S ribosomal protein S5	ribosomal protein	31.7
KHSRP	Far upstream element-binding protein 2	RNA metabolism protein	23.4
PCBP1	Poly(rC)-binding protein 1	RNA metabolism protein	5.8
PCBP2	Poly(rC)-binding protein 2	RNA metabolism protein	29.4
STRAP	Tetratricopeptide repeat protein 5	RNA metabolism protein	13.2
MMS19	MMS19 nucleotide excision repair protein homolog	scaffold/adaptor protein	3.6
YWHAG	14-3-3 protein gamma	scaffold/adaptor protein	25.0
YWHAH	14-3-3 protein eta	scaffold/adaptor protein	31.8
YWHAQ	14-3-3 protein theta	scaffold/adaptor protein	69.6
YWHAZ	14-3-3 protein zeta/delta	scaffold/adaptor protein	244.4
CAP1	Prostasin	serine protease	28.9
GSTP1	Glutathione S-transferase P	transferase	22.2
GSTO1	Glutathione S-transferase omega-1	transferase	9.3
TKT	Transketolase	transketolase	4.0
EEF2	Elongation factor 2	translation elongation factor	9.2
EEF1A1	Elongation factor 1-alpha 1	translation factor	3.3
EIF3C	Eukaryotic translation initiation factor 3 subunit C	translation initiation factor	17.9
EIF4G1	Eukaryotic translation initiation factor 4 gamma 1	translation initiation factor	30.2
HPRT1	Eukaryotic translation initiation factor 3 subunit B	translation initiation factor	16.4
IPO4	Importin-4	transporter	8.1
KPNA2	Importin subunit alpha-1	transporter	57.3

NUP93	Nuclear pore complex protein Nup93	transporter	4.8
SEC13	Protein SEC13 homolog	transporter	14.5
XPO1	Exportin-1	transporter	34.8
HUWE1	E3 ubiquitin-protein ligase HUWE1	ubiquitin-protein ligase	5.3
CLTC	Clathrin heavy chain 1	vesicle coat protein	7.1

Table 7.3: Protein targets overlapping between the datasets of Weerapana *et al.*, Gruhlke *et al.*, and this study.

Figures

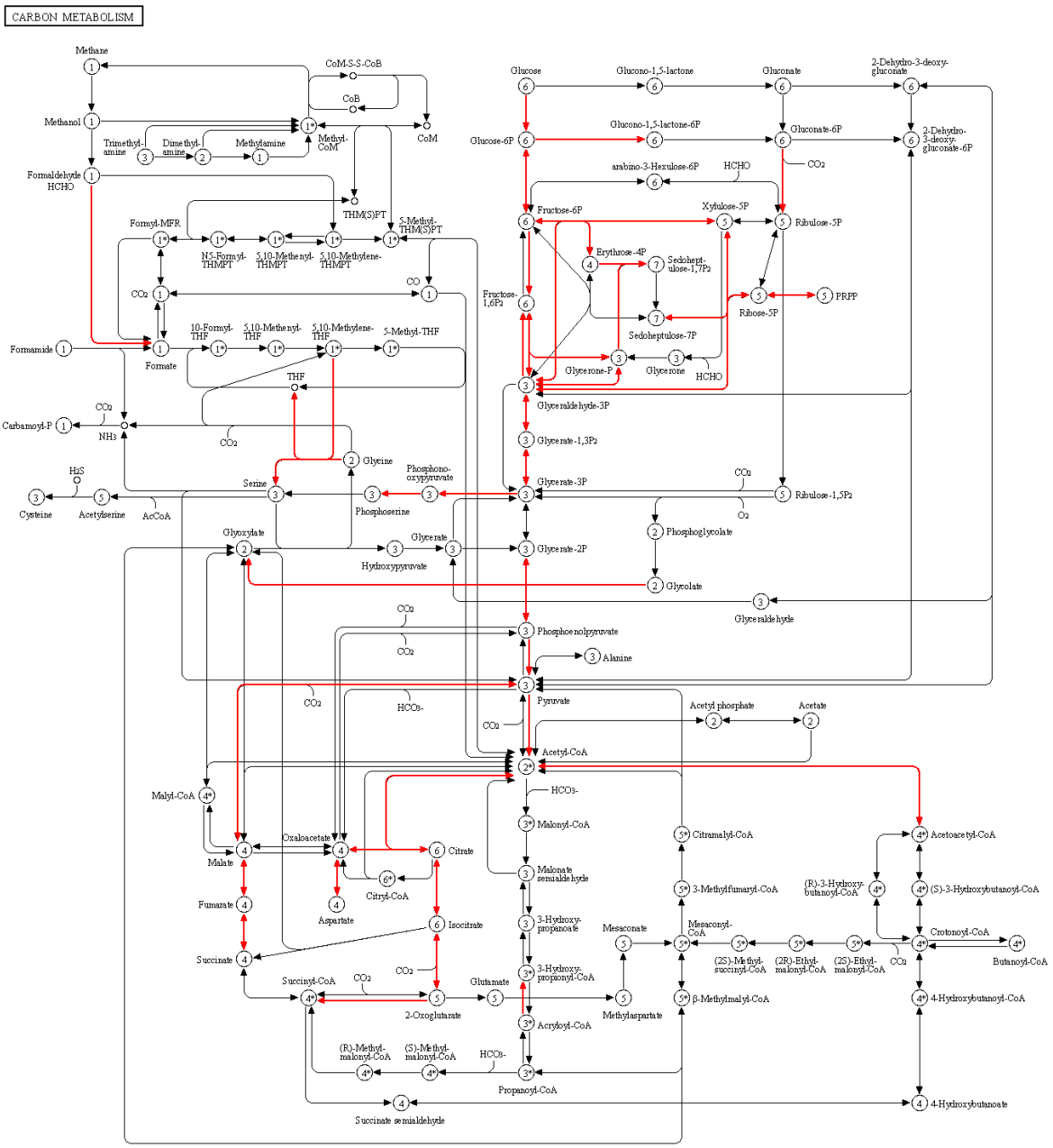

Figure 7.1: Targets of ajoene involved in carbon metabolism.
(highlighted in red)

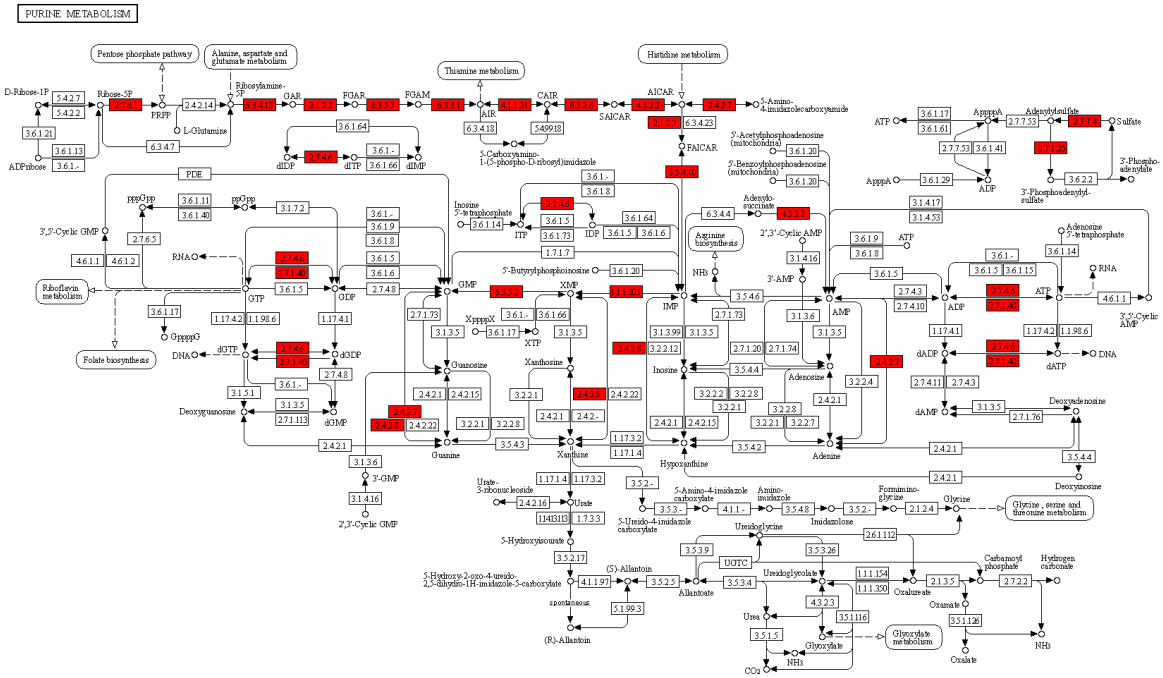

Figure 7.2: Targets of ajoene involved in purine metabolism.
(highlighted in red)

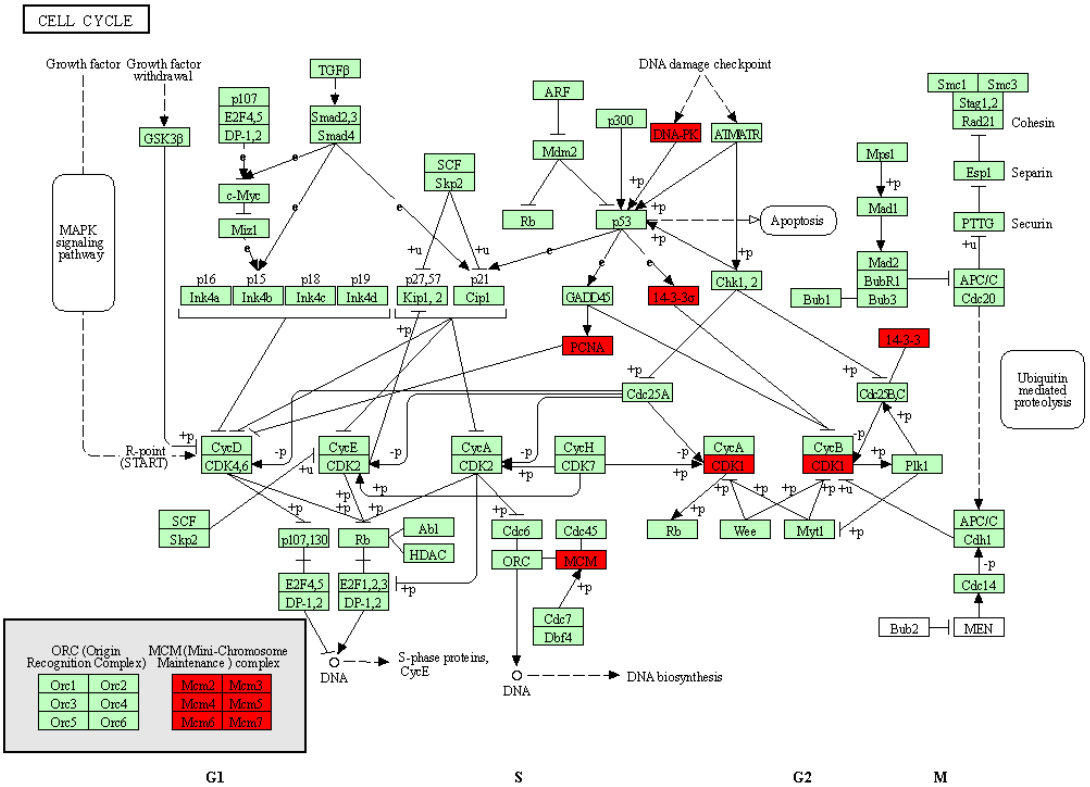

Figure 7.3: Targets of ajoene involved in the regulation of the cell cycle.
(highlighted in red)

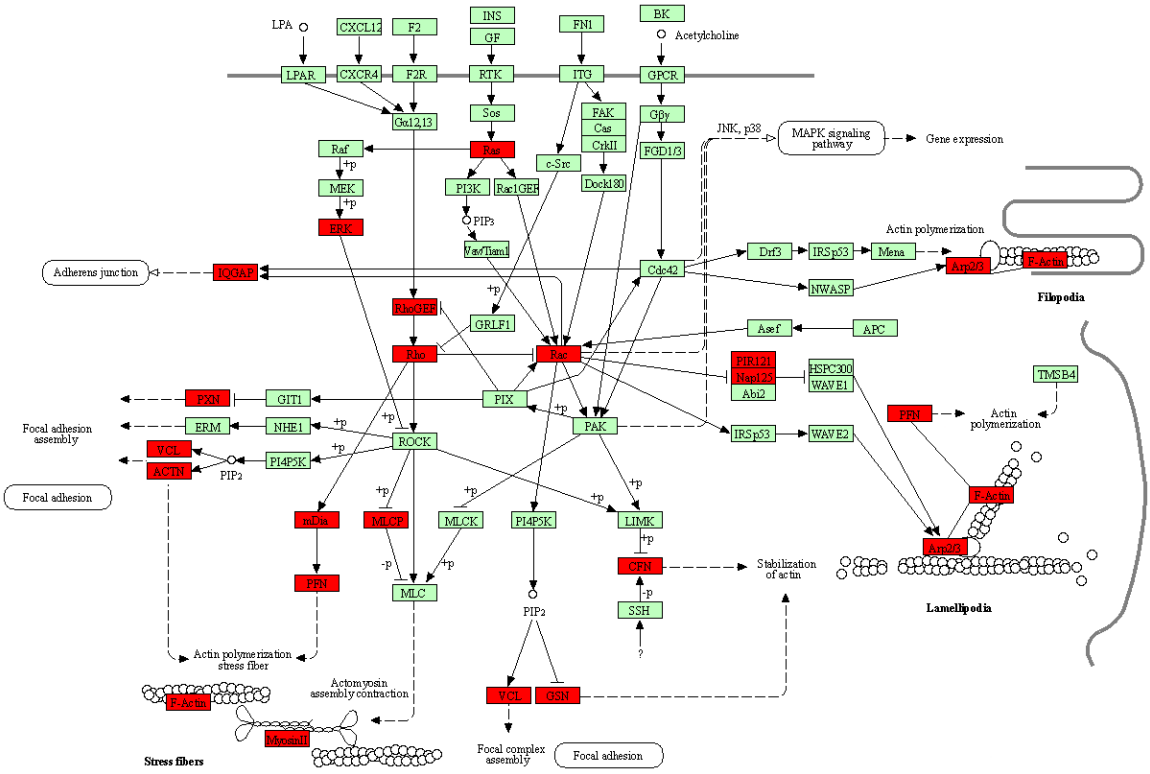

Figure 7.4: Targets of ajoene involved in the regulation of the actin cytoskeleton.
(highlighted in red)

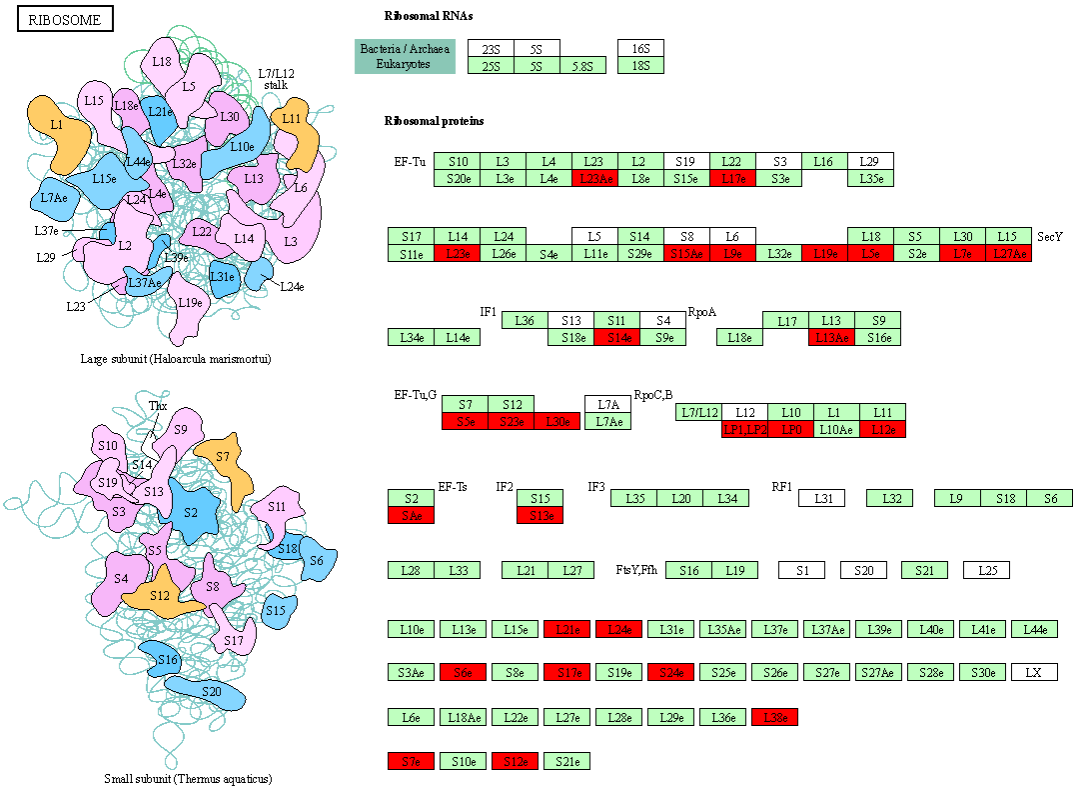

Figure 7.5: Targets of ajoene within the ribosome.
(highlighted in red)

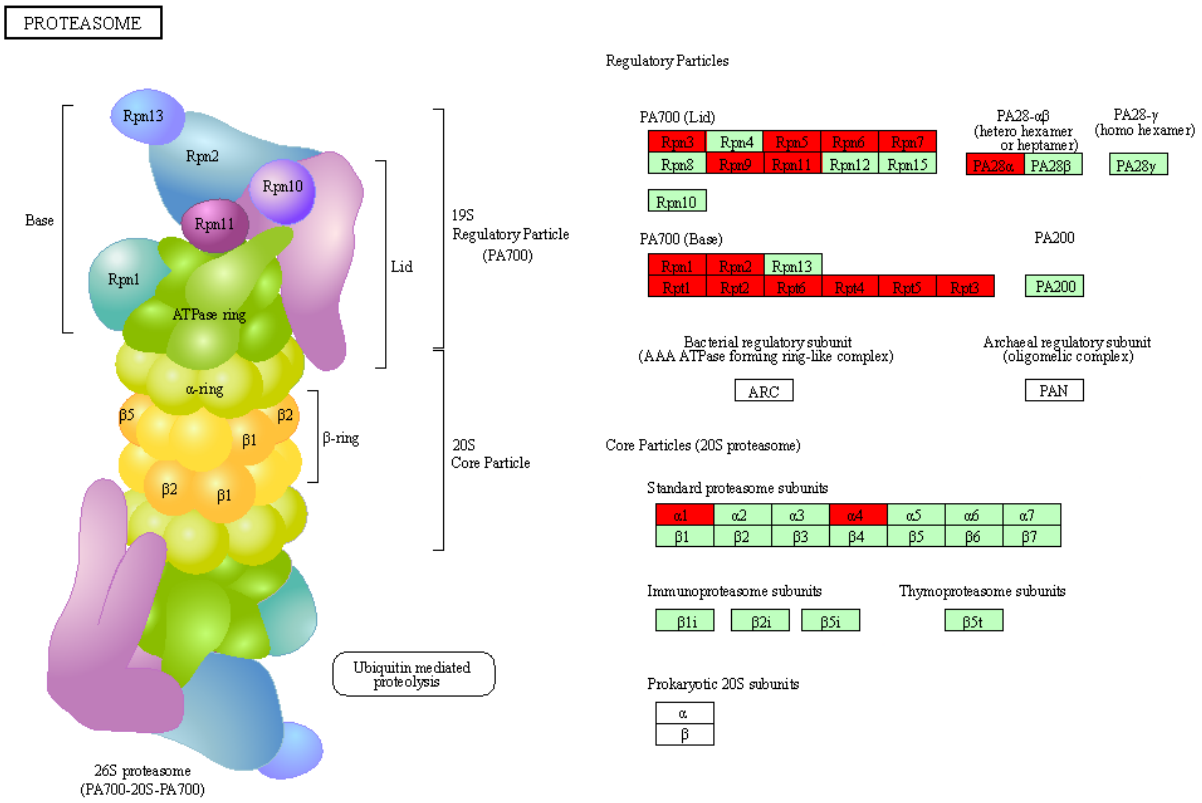

Figure 7.6: Targets of ajoene within the proteasome.
(highlighted in red)

References

(1) Cancer Research UK. Worldwide cancer statistics | Cancer Research UK https://www.cancerresearchuk.org/health-professional/cancer-statistics/worldwide-cancer#heading-One (accessed Apr 7, 2020).

(2) Higginson, J. International Agency for Research on Cancer. https://www.iarc.fr/ (accessed Apr 7, 2020).

(3) Lifetime Risk of Developing or Dying From Cancer https://www.cancer.org/cancer/cancer-basics/lifetime-probability-of-developing-or-dying-from-cancer.html (accessed Apr 7, 2020).

(4) Parkin, D.; Ferlay, J.; Jemal, A.; Borok, M.; Manraj, S. S.; N'da, G.; Ogunbiyi, J.; Liu, B.; Bray, F. *Cancer in Sub-Saharan Africa. IARC Scientific Publication 167*; 2018.

(5) CANSA. » Prevalence Cancer | CANSA – The Cancer Association of South Africa https://www.cansa.org.za/south-african-cancer-statistics/ (accessed Apr 7, 2020).

(6) Made, F.; Wilson, K.; Jina, R.; Tlotleng, N.; Jack, S.; Ntlebi, V.; Kootbodien, T. *Cancer Epidemiol.* **2017**, *51*, 56–61.

(7) Wu, S.; Powers, S.; Zhu, W.; Hannun, Y. A. *Nature* **2016**, *529* (7584), 43–47.

(8) Marnett, L. *Trends Genet.* **2001**, *17* (4), 214–221.

(9) Tubbs, A.; Nussenzweig, A. *Cell* **2017**, *168* (4), 644–656.

(10) Roos, W. P.; Thomas, A. D.; Kaina, B. *Nat. Rev. Cancer* **2016**, *16* (1), 20–33.

(11) Aggarwal, B. B.; Van Kuiken, M. E.; Iyer, L. H.; Harikumar, K. B.; Sung, B. *Exp. Biol. Med.* **2009**, *234* (8), 825–849.

(12) Benigni, R.; Bossa, C. *Chem. Rev.* **2011**, *111* (4), 2507–2536.

(13) IARC. List of Classifications – IARC Monographs on the Identification of Carcinogenic Hazards to Humans https://monographs.iarc.fr/list-of-classifications/ (accessed Apr 7, 2020).

(14) Słoczyńska, K.; Powroźnik, B.; Pękala, E.; Waszkielewicz, A. M. *J. Appl. Genet.* **2014**, *55* (2), 273–285.

(15) Brower, V. *Nat. Biotechnol.* **1998**, *16* (8), 728–731.

(16) Kotecha, R.; Takami, A.; Espinoza, J. L. *Oncotarget* **2016**, *7* (32), 52517–52529.

(17) Rivlin, R. S. *J. Nutr.* **2001**, *131* (3), 951S-954S.

(18) Petrovska, B. B.; Cekovska, S. *Pharmacogn. Rev.* **2010**, *4* (7), 106–110.

(19) Harris, J. C.; S., C.; S., P.; D., L.; Cottrell, S. L.; Plummer, S.; Lloyd, D. *Appl. Microbiol. Biotechnol.* **2001**, *57* (3), 282–286.

(20) Khatua, T. N.; Adela, R.; Banerjee, S. K. *Can. J. Physiol. Pharmacol.* **2013**, *91* (6), 448–458.

(21) WEISBERGER, A. S.; PENSKY, J. *Cancer Res.* **1958**, *18* (11), 1301–1308.

(22) Fleischauer, A. T.; Poole, C.; Arab, L. *Am. J. Clin. Nutr.* **2000**, *72* (4), 1047–1052.

(23) Fleischauer, A. T.; Arab, L. *J. Nutr.* **2001**, *131* (3s), 1032S-40S.

(24) González, C. A.; Pera, G.; Agudo, A.; Bueno-de-Mesquita, H. B.; Ceroti, M.; Boeing, H.; Schulz, M.; Del Giudice, G.; Plebani, M.; Carneiro, F.; Berrino, F.; Sacerdote, C.; Tumino, R.; Panico, S.; Berglund, G.; Simán, H.; Hallmans, G.; Stenling, R.; Martinez, C.; Dorronsoro, M.; Barricarte, A.; Navarro, C.; Quiros, J. R.; Allen, N.; Key, T. J.; Bingham, S.; Day, N. E.; Linseisen, J.; Nagel, G.; Overvad, K.; Jensen, M. K.; Olsen, A.; Tjønneland, A.; Büchner, F. L.; Peeters, P. H. M. H.; Numans, M. E.; Clavel-Chapelon, F.; Boutron-Ruault, M.-C. C.; Roukos, D.; Trichopoulou, A.; Psaltopoulou, T.; Lund, E.; Casagrande, C.; Slimani, N.; Jenab, M.; Riboli, E. *Int. J. Cancer* **2006**, *118* (10), 2559–2566.

(25) Ngo, S. N. T.; Williams, D. B.; Cobiac, L.; Head, R. J. *J. Nutr.* **2007**, *137* (10), 2264–2269.

(26) Shukla, Y.; Kalra, N. *Cancer Lett.* **2007**, *247* (2), 167–181.

(27) Zhou, Y.; Zhuang, W.; Hu, W.; Liu, G.; Wu, T.; Wu, X. *Gastroenterology* **2011**, *141* (1), 80–89.

(28) Zhu, B.; Zou, L.; Qi, L.; Zhong, R.; Miao, X. *Clin. Gastroenterol. Hepatol.* **2014**, *12* (12), 1991-2001.e4.

(29) Nicastro, H. L.; Ross, S. A.; Milner, J. A. *Cancer Prev. Res.* **2015**, *8* (3), 181–189.

(30) Turati, F.; Rossi, M.; Pelucchi, C.; Levi, F.; La Vecchia, C. *Br. J. Nutr.* **2015**, *113* (S2), S102–S110.

(31) Kim, H.; Keum, N. N.; Giovannucci, E. L.; Fuchs, C. S.; Bao, Y. *Int. J. Cancer* **2018**, *143* (5), 1047–1053.

(32) Pourzand, A.; Tajaddini, A.; Pirouzpanah, S.; Asghari-Jafarabadi, M.; Samadi, N.; Ostadrahimi, A.-R.; Sanaat, Z. *J. Breast Cancer* **2018**, *21* (2), 231.

(33) Kim, J. Y.; Kwon, O. *Am. J. Clin. Nutr.* **2009**, *89* (1), 257–264.

(34) Pittler, M. H.; Ernst, E. *Mol. Nutr. Food Res.* **2007**, *51* (11), 1382–1385.

(35) Suleria, H. A. R.; Butt, M. S.; Khalid, N.; Sultan, S.; Raza, A.; Aleem, M.; Abbas, M. *Asian*

Pacific J. Trop. Dis. **2015**, *5* (4), 271–278.

(36) Oosthuizen, C. B.; Reid, A.-M.; Lall, N. In *Medicinal Plants for Holistic Health and Well-Being*; Elsevier, 2018; pp 277–295.

(37) Block, E. *Sci. Am.* **1985**, *252* (3), 114–119.

(38) Becker-Rose, H. *Zeitschrift für Angew. Chemie* **1931**, *44* (17), 301–302.

(39) Cavallito, C. J.; Bailey, J. H. *J. Am. Chem. Soc.* **1944**, *66* (11), 1950–1951.

(40) Borlinghaus, J.; Albrecht, F.; Gruhlke, M. C. H.; Nwachukwu, I. D.; Slusarenko, A. J.; Borlinghaus, J.; Albrecht, F.; Gruhlke, M. C. H.; Nwachukwu, I. D.; Slusarenko, A. J. *Molecules* **2014**, *19* (8), 12591–12618.

(41) Stoll, A.; Seebeck, E. *Helv. Chim. Acta* **1948**, *31* (1), 189–210.

(42) Staba, E. J.; Lash, L.; Staba, J. E. *J. Nutr.* **2001**, *131* (3), 1118S--1119S.

(43) Lawson, L.; Wang, Z.-Y.; Hughes, B. *Planta Med.* **1991**, *57* (04), 363–370.

(44) Tocmo, R.; Liang, D.; Lin, Y.; Huang, D. *Front. Nutr.* **2015**, *2*, 1.

(45) Cavallito, C. J.; Buck, J. S.; Suter, C. M. *J. Am. Chem. Soc.* **1944**, *66* (11), 1952–1954.

(46) Freeman, G. G. *J. Sci. Food Agric.* **1975**, *26* (4), 471–481.

(47) Iberl, B.; Winkler, G.; Muller, B.; Knobloch, K.; Müller, B.; Knobloch, K.; Muller, B.; Knobloch, K.; Müller, B.; Knobloch, K. *Planta Med.* **1990**, *56* (3), 320–326.

(48) Locatelli, D. A.; Nazareno, M. A.; Fusari, C. M.; Camargo, A. B. *Food Chem.* **2017**, *220*, 219–224.

(49) Haina Wang, X. J. *J. Drug Metab. Toxicol.* **2013**, *04* (05).

(50) Block, E.; Dethier, B.; Bechand, B.; Cotelesage, J. J. H.; George, G. N.; Goto, K.; Pickering, I. J.; Mendoza Rengifo, E.; Sheridan, R.; Sneeden, E. Y.; Vogt, L. *J. Agric. Food Chem.* **2018**, *66* (39), 10193–10204.

(51) Block, E.; Ahmad, S. *J. Am. Chem. SOC* **1984**, *106*, 8295–8296.

(52) Harjai, K.; Kumar, R.; Singh, S. *FEMS Immunol. Med. Microbiol.* **2010**, *58* (2), 161–168.

(53) Fong, J.; Yuan, M.; Jakobsen, T. H.; Mortensen, K. T.; Delos Santos, M. M. S.; Chua, S. L.; Yang, L.; Tan, C. H.; Nielsen, T. E.; Givskov, M. *J. Med. Chem.* **2017**, *60* (1), 215–227.

(54) Go, Y. M.; Chandler, J. D.; Jones, D. P. *Free Radic. Biol. Med.* **2015**, *84*, 227–245.

(55) Jacob, C. *Nat. Prod. Rep.* **2006**, *23* (6), 851.

(56) Wills, E. D. *Biochem. J.* **1956**, *63* (3), 514–520.

(57) Nagahara, N. *J. Amino Acids* **2011**, *2011*, 709404.

(58) Yang, J.; Carroll, K. S.; Liebler, D. C. *Mol. Cell. Proteomics* **2016**, *15* (1), 1–11.

(59) Denicola, G. M.; Karreth, F. A.; Humpton, T. J.; Gopinathan, A.; Wei, C.; Frese, K.; Mangal, D.; Yu, K. H.; Yeo, C. J.; Calhoun, E. S.; Scrimieri, F.; Winter, J. M.; Hruban, R. H.; Iacobuzio-Donahue, C.; Kern, S. E.; Blair, I. A.; Tuveson, D. A. *Nature* **2011**, *475* (7354), 106–110.

(60) Go, Y. M.; Jones, D. P. *J. Biol. Chem.* **2013**, *288* (37), 26512–26520.

(61) Yang, H.-Y.; Lee, T.-H. *BMB Rep.* **2015**, *48* (4), 200–208.

(62) Baba, S. P.; Bhatnagar, A. *Curr. Opin. Toxicol.* **2018**, *7* (2018), 133–139.

(63) Dalle–Donne, I.; Milzani, A.; Gagliano, N.; Colombo, R.; Giustarini, D.; Rossi, R. *Antioxid. Redox Signal.* **2008**, *10* (3), 445–474.

(64) Niwa, T. *J. Chromatogr. B* **2007**, *855* (1), 59–65.

(65) Sosa, V.; Moliné, T.; Somoza, R.; Paciucci, R.; Kondoh, H.; LLeonart, M. E. *Ageing Res. Rev.* **2013**, *12* (1), 376–390.

(66) Asaduzzaman Khan, M.; Tania, M.; Zhang, D.; Chen, H. *Chinese J. Cancer Res.* **2010**, *22* (2), 87–92.

(67) Winterbourn, C. C.; Hampton, M. B. *Free Radic. Biol. Med.* **2008**, *45* (5), 549–561.

(68) Forman, H. J.; Zhang, H.; Rinna, A. *Mol. Aspects Med.* **2009**, *30* (1–2), 1–12.

(69) Hayes, J. D.; Flanagan, J. U.; Jowsey, I. R. *Annu. Rev. Pharmacol. Toxicol.* **2005**, *45* (1), 51–88.

(70) Tew, K. D.; Manevich, Y.; Grek, C.; Xiong, Y.; Uys, J.; Townsend, D. M. *Free Radic. Biol. Med.* **2011**, *51* (2), 299–313.

(71) Barrett, W. C.; DeGnore, J. P.; König, S.; Fales, H. M.; Keng, Y. F.; Zhang, Z. Y.; Yim, M. B.; Chock, P. B. *Biochemistry* **1999**, *38* (20), 6699–6705.

(72) Townsend, D. M. *Mol. Interv.* **2007**, *7* (6), 313–324.

(73) Regazzoni, L.; Panusa, A.; Yeum, K. J.; Carini, M.; Aldini, G. *J. Chromatogr. B Anal. Technol. Biomed. Life Sci.* **2009**, *877* (28), 3456–3461.

(74) Dalle-Donne, I.; Colombo, G.; Gagliano, N.; Colombo, R.; Giustarini, D.; Rossi, R.; Milzani, A. *Free Radic. Res.* **2011**, *45* (1), 3–15.

(75) Wu, J. H.; Batist, G. *Biochim. Biophys. Acta - Gen. Subj.* **2013**, *1830* (5), 3350–3353.

(76) Traverso, N.; Ricciarelli, R.; Nitti, M.; Marengo, B.; Furfaro, A. L.; Pronzato, M. A.; Marinari, U. M.; Domenicotti, C. **2013**, *2013*.

(77) Hu, Y.; Urig, S.; Koncarevic, S.; Wu, X.; Fischer, M.; Rahlfs, S.; Mersch-Sundermann, V.; Becker, K. *Biol. Chem.* **2007**, *388* (10), 1069–1081.

(78) Pinto, J. T.; Krasnikov, B. F.; Cooper, A. J. L. *J. Nutr.* **2006**, *136* (3), 835–841.

(79) Zhang, G.; Li, B.; Lee, C.-H.; Parkin, K. L. *J. Agric. Food Chem.* **2010**, *58* (3), 1564–1571.

(80) Kaschula, C. H.; Hunter, R.; Hassan, H. T.; Stellenboom, N.; Cotton, J.; Zhai, X. Q.; Parker, M. I. *Anticancer. Agents Med. Chem.* **2011**, *11* (3), 260–266.

(81) Smith, M.; Hunter, R.; Stellenboom, N.; Kusza, D. A.; Parker, M. I. I.; Hammouda, A. N. H.; Jackson, G.; Kaschula, C. H. *Biochim. Biophys. Acta - Gen. Subj.* **2016**, *1860* (7), 1439–1449.

(82) Hosono, T.; Fukao, T.; Ogihara, J.; Ito, Y.; Shiba, H.; Seki, T.; Ariga, T. *J. Biol. Chem.* **2005**, *280* (50), 41487–41493.

(83) Herman-Antosiewicz, A.; Powolny, A. A.; Singh, S. V. *Acta Pharmacol. Sin.* **2007**, *28* (9), 1355–1364.

(84) Rabinkov, A.; Miron, T.; Mirelman, D.; Wilchek, M.; Glozman, S.; Yavin, E.; Weiner, L. *Biochim. Biophys. Acta - Mol. Cell Res.* **2000**, *1499* (1–2), 144–153.

(85) Nagy, P. *Antioxid. Redox Signal.* **2013**, *18* (13), 1623–1641.

(86) Gruhlke, M. C. H.; Antelmann, H.; Bernhardt, J.; Kloubert, V.; Rink, L.; Slusarenko, A. J. *Free Radic. Biol. Med.* **2019**, *131* (September 2018), 144–153.

(87) Das, A.; Banik, N. L.; Ray, S. K. *Cancer* **2007**, *110* (5), 1083–1095.

(88) Wu, X.-J.; Kassie, F.; Mersch-Sundermann, V. *Mutat. Res.* **2005**, *579* (1–2), 115–124.

(89) Wang, Y.; Sun, Z.; Chen, S.; Jiao, Y.; Bai, C. *Tumor Biol.* **2016**, *37* (3), 3727–3738.

(90) Simon, H. U.; Haj-Yehia, A.; Levi-Schaffer, F. *Apoptosis* **2000**, *5* (5), 415–418.

(91) Zhang, W.; Hu, X.; Shen, Q.; Xing, D. *Nat. Commun.* **2019**, *10* (1), 1–14.

(92) Deavall, D. G.; Martin, E. A.; Horner, J. M.; Roberts, R. *J. Toxicol.* **2012**, *2012*, 645460.

(93) Munday, R.; Munday, J. S.; Munday, C. M. *Free Radic. Biol. Med.* **2003**, *34* (9), 1200–1211.

(94) Prütz, W. A.; Sies, H. *Free Radic. Res.* **1993**, *18* (3), 159–165.

(95) Iciek, M.; Kwiecień, I.; Włodek, L.; Kwiecień, I.; Włodek, L.; Kwiecień, I.; Włodek, L. *Environ. Mol. Mutagen.* **2009**, *50* (3), 247–265.

(96) Yagdi, E.; Cerella, C.; Dicato, M.; Diederich, M. *Food Chem. Toxicol.* **2016**, *95*, 219–233.

(97) Bhuiyan, A. I.; Papajani, V. T.; Paci, M.; Melino, S. *Molecules* **2015**, *20* (1), 1731–1750.

(98) Kiesel, V. A.; Stan, S. D. *Biochem. Biophys. Res. Commun.* **2017**, *484* (4), 833–838.

(99) Olson, K. R. *Free Radic. Biol. Med.* **2019**.

(100) De Doncker, S.; Ali, D.; Kaschula, C. H.; Hunter, R.; Rees-Jones, S. C. M. *J. Org. Chem.* **2019**.

(101) Greaves, M.; Maley, C. C. *Nature* **2012**, *481* (7381), 306–313.

(102) Hanahan, D.; Weinberg, R. A. *Cell* **2011**, *144* (5), 646–674.

(103) Hanahan, D.; Weinberg, R. A. *Cell* **2000**, *100* (1), 57–70.

(104) Petrovic, V.; Nepal, A.; Olaisen, C.; Bachke, S.; Hira, J.; Søgaard, C. K.; Røst, L. M.; Misund, K.; Andreassen, T.; Melø, T. M.; Bartsova, Z.; Bruheim, P.; Otterlei, M. *Nutrients* **2018**, *10* (4), 1–14.

(105) Banerjee, S. K.; Mukherjee, P. K.; Maulik, S. K. *Phyther. Res.* **2003**, *17* (2), 97–106.

(106) Khanum, F.; Anilakumar, K. R.; Viswanathan, K. R. *Crit. Rev. Food Sci. Nutr.* **2004**, *44* (6), 479–488.

(107) Penning, T. M. *Curr. Cancer Res.* **2011**, *6*, 135–158.

(108) Wargovich, M. J. *J. Nutr.* **2006**, *136* (3), 832S-834S.

(109) Kay, H. Y.; Won Yang, J.; Kim, T. H.; Lee, D. Y.; Kang, B.; Ryu, J.-H.; Jeon, R.; Kim, S. G. *J. Nutr.* **2010**, *140* (7), 1211–1219.

(110) Zhang, M.; Pan, H.; Xu, Y.; Wang, X.; Qiu, Z.; Jiang, L. *Cell. Physiol. Biochem.* **2017**, *41* (6), 2255–2267.

(111) Xu, X. H.; Li, G. L.; Wang, B. A.; Qin, Y.; Bai, S. R.; Rong, J.; Deng, T.; Li, Q. *Brain Res.* **2015**, *1614*, 38–50.

(112) Yun, H.-M. M.; Ban, J. O.; Park, K.-R. R.; Lee, C. K.; Jeong, H.-S. S.; Han, S. B.; Hong, J. T. *Pharmacol. Ther.* **2014**, *142* (2), 183–195.

(113) Herman-Antosiewicz, A.; Singh, S. V. *Mutat. Res. Mol. Mech. Mutagen.* **2004**, *555* (1–2), 121–131.

(114) Shang, A.; Cao, S.-Y.; Xu, X.-Y.; Gan, R.-Y.; Tang, G.-Y.; Corke, H.; Mavumengwana, V.; Li, H.-B. *Foods* **2019**, *8* (7), 246.

(115) Dirsch, V. M.; Gerbes, A. L.; Vollmar, A. M. *Mol. Pharmacol.* **1998**, *53* (3), 402–407.

(116) Kelkel, M.; Cerella, C.; Mack, F.; Schneider, T.; Jacob, C.; Schumacher, M.; Dicato, M.; Diederich, M. *Carcinogenesis* **2012**, *33* (11), 2162–2171.

(117) Venkatesh, Y. P. In *Immunology*; Elsevier, 2018; Vol. 1, pp 203–224.

(118) Lee, D. Y.; Li, H.; Lim, H. J.; Lee, H. J.; Jeon, R.; Ryu, J.-H. *J. Med. Food* **2012**, *15* (11), 992–999.

(119) Jeong, Y.; Ryu, J.; Shin, J.-H.; Kang, M.; Kang, J.; Han, J.; Kang, D. *Molecules* **2016**, *21*

(4), 430.

(120) Hsiao-Pei Chang; Shih-Yi Huang, and; Chen*, Y.-H. **2005**.

(121) Rodrigues, C.; Percival, S. S. *Nutrients* **2019**, *11* (2), 295.

(122) Percival, S. S. *J. Nutr.* **2016**, *146* (2), 433S-436S.

(123) Kuttan, G. *J. Ethnopharmacol.* **2000**, *72* (1–2), 93–99.

(124) Ebrahimpour, S.; Tabari, M. A.; Youssefi, M. R.; Aghajanzadeh, H.; Behzadi, M. Y. *Pharmacognosy Res.* **2013**, *5* (3), 189–194.

(125) Schäfer, G.; Kaschula, C. H. *Anticancer. Agents Med. Chem.* **2014**, *14* (2), 233–240.

(126) Arreola, R.; Quintero-Fabián, S.; López-Roa, R. I.; Flores-Gutiérrez, E. O.; Reyes-Grajeda, J. P.; Carrera-Quintanar, L.; Ortuño-Sahagún, D. *J. Immunol. Res.* **2015**, *2015*, 1–13.

(127) Filén, S.; Lahesmaa, R. *J. Signal Transduct.* **2010**, *2010*, 268589.

(128) Hotchkiss, R. S.; Strasser, A.; McDunn, J. E.; Swanson, P. E. *N. Engl. J. Med.* **2009**, *361* (16), 1570–1583.

(129) Jiang, X.; Zhu, X.; Huang, W.; Xu, H.; Zhao, Z.; Li, S.; Li, S.; Cai, J.; Cao, J. *Int. Immunopharmacol.* **2017**, *48*, 135–145.

(130) Xiao, D.; Pinto, J. T.; Soh, J.-W.; Deguchi, A.; Gundersen, G. G.; Palazzo, A. F.; Yoon, J.-T.; Shirin, H.; Weinstein, I. B. *Cancer Res.* **2003**, *63* (20), 6825–6837.

(131) Xiao, D.; Choi, S.; Johnson, D. E.; Vogel, V. G.; Johnson, C. S.; Trump, D. L.; Lee, Y. J.; Singh, S. V. *Oncogene* **2004**, *23* (33), 5594–5606.

(132) Filomeni, G.; Aquilano, K.; Rotilio, G.; Ciriolo, M. R. *Cancer Res.* **2003**, *63* (18), 5940–5949.

(133) De Gianni, E.; Fimognari, C. In *Enzymes*; Elsevier Inc., 2015; Vol. 37, pp 167–192.

(134) Wei, Z.; Shan, Y.; Tao, L.; Liu, Y.; Zhu, Z.; Liu, Z.; Wu, Y.; Chen, W.; Wang, A.; Lu, Y. *Mol. Carcinog.* **2017**, *56* (10), 2317–2331.

(135) Huang, J.; Yang, B.; Xiang, T.; Peng, W.; Qiu, Z.; Wan, J.; Zhang, L.; Li, H. H.; Li, H. H.; Ren, G. **2015**, *59* (6), 1063–1075.

(136) Ng, K. T. P.; Guo, D. Y.; Cheng, Q.; Geng, W.; Ling, C. C.; Li, C. X.; Liu, X. B.; Ma, Y. Y.; Lo, C. M.; Poon, R. T. P.; Fan, S. T.; Man, K. *PLoS One* **2012**, *7* (2), 1–9.

(137) Kaschula, C. H.; Tuveri, R.; Ngarande, E.; Dzobo, K.; Barnett, C.; Kusza, D. A.; Graham, L. M.; Katz, A. A.; Rafudeen, M. S.; Parker, M. I. I.; Hunter, R.; Schäfer, G. *BMC Cancer* **2019**, *19* (1), 248.

(138) Howard, E. W.; Ling, M. T. M.-T. M. T.; Chee, W. C.; Hiu, W. C.; Wang, X.; Yong, C. W.;

Chua, C. W.; Cheung, H. W.; Wang, X.; Wong, Y. C.; Chee, W. C.; Hiu, W. C.; Wang, X.; Yong, C. W. *Clin. Cancer Res.* **2007**, *13* (6), 1847–1856.

(139) Xiao, X.; Chen, B.; Liu, X.; Liu, P.; Zheng, G.; Ye, F.; Tang, H.; Xie, X. *PLoS One* **2014**, *9* (11), e112720.

(140) Liu, Y.; Zhu, P.; Wang, Y.; Wei, Z.; Tao, L.; Zhu, Z.; Sheng, X.; Wang, S.; Ruan, J.; Liu, Z.; Cao, Y.; Shan, Y.; Sun, L.; Wang, A.; Chen, W.; Lu, Y. *PLoS One* **2015**, *10* (4).

(141) Zhang, Q.; Li, X. T.; Chen, Y.; Chen, J. Q.; Zhu, J. Y.; Meng, Y.; Wang, X. Q.; Li, Y.; Geng, S. S.; Xie, C. F.; Wu, J. S.; Zhong, C. Y.; Han, H. Y. *Cancer Chemother. Pharmacol.* **2018**, *81* (6), 969–977.

(142) Lee, C. G.; Lee, H. W.; Kim, B. O.; Rhee, D. K.; Pyo, S. *J. Funct. Foods* **2015**, *15*, 172–185.

(143) Ried, K. *J. Nutr.* **2016**, *146* (2), 389S-396S.

(144) Wang, J.; Zhang, X.; Lan, H.; Wang, W. *Food Nutr. Res.* **2017**, *61* (1), 1377571.

(145) Powolny, A. A.; Singh, S. V. *Cancer Lett.* **2008**, *269* (2), 305–314.

(146) Zhang, Y.; Liu, X.; Ruan, J.; Zhuang, X.; Zhang, X.; Li, Z. *Biomed. Pharmacother.* **2020**, *123*, 109730.

(147) Fodale, V.; Pierobon, M.; Liotta, L.; Petricoin, E. *Cancer J.* **2011**, *17* (2), 89–95.

(148) Hassan, H. T. *Leuk. Res.* **2004**, *28* (7), 667–671.

(149) Suddek, G. M. *Pharm. Biol.* **2014**, *52* (8), 1009–1014.

(150) Li, S.; Guang, Y.; Zhu, X.; Lin, C.; Sun, Y.; Zhao, Z. *Oncol. Rep.* **2017**, *38* (3), 1637–1644.

(151) Wang, Z.; Xia, Q.; Cui, J.; Diao, Y.; Li, J. *Oncol. Rep.* **2014**, *31* (6), 2720–2726.

(152) Hwang, J. W.; Cho, H.; Lee, J. Y.; Jeon, Y.; Kim, S. N.; Lee, S. J.; Bae, G. U.; Yoon, S.; Jeon, R.; Kim, Y. K. *Food Chem. Toxicol.* **2016**, *96*, 35–42.

(153) Kaschula, C. H.; Hunter, R.; Cotton, J.; Tuveri, R.; Ngarande, E.; Dzobo, K.; Schäfer, G.; Siyo, V.; Lang, D.; Kusza, D. A.; Davies, B.; Katz, A. A.; Parker, I.; Parker, M. I. *Mol. Carcinog.* **2016**, *55* (8), 1213–1228.

(154) Giordano, S.; Petrelli, A. *Curr. Med. Chem.* **2008**, *15* (5), 422–432.

(155) Naznin, M. T.; Akagawa, M.; Okukawa, K.; Maeda, T.; Morita, N. *Food Chem.* **2008**, *106* (3), 1113–1119.

(156) Yoo, M.; Lee, S.; Kim, S.; Shin, D. *Food Sci. Nutr.* **2014**, *2* (5), 605–611.

(157) Block, E.; Ahmad, S.; Catalfamo, J. L.; Jain, M. K.; Apitz-Castro, R.; Eric Block, Saleem Ahmad, James L. Catalfamo, Mahendra K. Jain, and R. A.-C. *J. Am. Chem. Soc.* **1986**, *108* (22), 7045–7055.

(158) Perez, H. A.; De la Rosa, M.; Apitz, R. *Antimicrob. Agents Chemother.* **1994**, *38* (2), 337–339.

(159) Yang, J.-Y.; Della-fera, M. A.; Nelson-dooley, C.; Baile, C. A. *Apoptosis* **2006**, *14* (3), 388–397.

(160) Rayalam, S.; Della-Fera, M. A.; Baile, C. A. *J. Nutr. Biochem.* **2008**, *19* (11), 717–726.

(161) Han, C. Y.; Ki, S. H.; Kim, Y. W.; Noh, K.; Lee, D. Y.; Kang, B.; Ryu, J. H.; Jeon, R.; Kim, E. H.; Hwang, S. J.; Kim, S. G. *Antioxidants Redox Signal.* **2011**, *14* (2), 187–202.

(162) Naganawa, R.; Iwata, N.; Ishikawa, K.; Fukuda, H.; Fujino, T.; Suzuki, A. *Appl. Envir. Microbiol.* **1996**, *62* (11), 4238–4242.

(163) Jakobsen, T. H.; Van Gennip, M.; Phipps, R. K.; Shanmugham, M. S.; Christensen, L. D.; Alhede, M.; Skindersoe, M. E.; Rasmussen, T. B.; Friedrich, K.; Uthe, F.; Jensen, P. Ø.; Moser, C.; Nielsen, K. F.; Eberl, L.; Larsen, T. O.; Tanner, D.; Høiby, N.; Bjarnsholt, T.; Givskov, M.; Jensen, P. Ø.; Eberl, L.; Givskov, M.; Uthe, F.; Christensen, L. D.; Bjarnsholt, T.; Van Gennip, M.; Rasmussen, T. B.; Skindersoe, M. E.; Larsen, T. O.; Alhede, M.; Shanmugham, M. S.; Moser, C.; Friedrich, K.; Phipps, R. K.; Tanner, D.; Shanmugham, M. S.; Christensen, L. D.; Alhede, M.; Skindersoe, M. E.; Rasmussen, T. B.; Friedrich, K.; Uthe, F.; Jensen, P. Ø.; Moser, C.; Nielsen, K. F.; Eberl, L.; Larsen, T. O.; Tanner, D.; Høiby, N.; Bjarnsholt, T.; Givskov, M.; Jensen, P. Ø.; Eberl, L.; Givskov, M.; Uthe, F.; Christensen, L. D.; Bjarnsholt, T.; Van Gennip, M.; Rasmussen, T. B.; Skindersoe, M. E.; Larsen, T. O.; Alhede, M.; Shanmugham, M. S.; Moser, C.; Friedrich, K.; Phipps, R. K.; Tanner, D. *Antimicrob. Agents Chemother.* **2012**, *56* (5), 2314–2325.

(164) Yoshida, S.; Kasuga, S.; Hayashi, N.; Ushiroguchi, T.; Matsuura, H.; Nakagawa, S. *Appl. Envir. Microbiol.* **1987**, *53* (3), 615–617.

(165) San-Blas, G.; San-Blas, F.; Gil, F.; Marino, L.; Apitz-Castro, R. *Antimicrob. Agents Chemother.* **1989**, *33* (9), 1641–1644.

(166) Davis, S. R. *J. Antimicrob. Chemother.* **2003**, *51* (3), 593–597.

(167) Li, M.; Ciu, J.-R. R.; Ye, Y.; Min, J.-M. M.; Zhang, L.-H. H.; Wang, K.; Gares, M.; Cros, J.; Wright, M.; Leung-Tack, J. *Carcinogenesis* **2002**, *23* (4), 573–579.

(168) Taylor, P.; Noriega, R.; Farah, C.; Abad, M.-J. J.; Arsenak, M.; Apitz, R. *Cancer Lett.* **2006**, *239* (2), 298–304.

(169) Arora, A.; Tripathi, C.; Shukla, Y. *Curr. Cancer Ther. Rev.* **2005**, *1* (2), 199–205.

(170) Hunter, R.; Kaschula, C. H.; Parker, I. M.; Caira, M. R.; Richards, P.; Travis, S.; Taute,

F.; Qwebani, T. *Bioorganic Med. Chem. Lett.* **2008**, *18* (19), 5277–5279.

(171) Li, H.; Jeong, J. H.; Kwon, S. W.; Lee, S. K.; Lee, H. J.; Ryu, J.-H. H. *Molecules* **2020**, *25* (3), 703.

(172) Apitz-Cȧstro, R.; Cabrera, S.; Cruz, M. R.; Ledezma, E.; Jain, M. K. *Thromb. Res.* **1983**, *32* (2), 155–169.

(173) Dressinandt, G.; Rockinger, H.; Prigge, H. Process For Preparation Of Ajoene. DE19500863A1, 1995.

(174) Overberger, C. G.; Biletch, H.; Finestone, A. B.; Lilker, J.; Herbert, J. *J. Am. Chem. Soc.* **1953**, *75* (9), 2078–2082.

(175) Kaschula, C. H.; Hunter, R.; Parker, I. M. Organosulfur Compounds, A Method Of Making Organosulfur Compounds And Their Use For Inhibiting The Growth Of Tumour Cells. WO 2010/016011 A1, 2010.

(176) Raok, J.; Jae-ha, R.; Hyewon, C.; Yoon-jung, K.; Sang-hyun, M.; Ji-hoon, Y.; JEON, R.; RYU, J.-H.; CHO, H.; KIM, Y.-J.; MIN, S.-H.; YU, J.-H. Novel Organic Sulfur Compound, Method For Preparing Same, And Pharmaceutical Composition For Preventing Or Treating Cancer Or An Inflammatory Disease, Containing Same As Active Ingredient. WO 2018/012947 A1, 2018.

(177) Alun, S. R. Process For Producing Ajoene. US 10131629 B2, 2018.

(178) Bjarnsholt, T.; Høiby, N.; Givskov, M. Process For The Manufacture Of Ajoene Derivatives. US 2014/0303070 A1, 2014.

(179) Silva, F.; Khokhar, S. S.; Williams, D. M.; Saunders, R.; Evans, G. J. S. S.; Graz, M.; Wirth, T. *Angew. Chemie - Int. Ed.* **2018**.

(180) Raynbird, M. Y.; Silva, F.; Smallman, H.; Khokhar, S. S.; Neef, D.; Evans, G. J. S.; Wirth, T. *Chem. – A Eur. J.* **2020**, chem.202001598.

(181) Yamamoto Raynbird, M.; Khokhar, S. S.; Neef, D.; Evans, G. J. S.; Wirth, T. *Chem. – A Eur. J.* **2021**.

(182) Hunter*, R.; Kaschula, C.; Stellenboom, N.; Cotton, J.; Parker, M. I. *Phosphorus. Sulfur. Silicon Relat. Elem.* **2013**, *188* (11), 1497–1507.

(183) Kaschula, C. H.; Hunter, R.; Stellenboom, N.; Caira, M. R.; Winks, S.; Ogunleye, T.; Richards, P.; Cotton, J.; Zilbeyaz, K.; Wang, Y.; Siyo, V.; Ngarande, E.; Parker, M. I. *Eur. J. Med. Chem.* **2012**, *50*, 236–254.

(184) Lee, H. J.; Jeong, J. H.; Ryu, J. H. *J. Funct. Foods* **2019**, *56*, 102–109.

(185) Ledezma, E.; Apitz-Castro, R.; Cardier, J. *Cancer Lett.* **2004**, *206* (1), 35–41.

(186) Scharfenberg, K.; Wagner, R.; Wagner, K. G. *Cancer Lett.* **1990**, *53* (2–3), 103–108.
(187) Agarwal, K. C. *Med. Res. Rev.* **1996**, *16* (1), 111–124.
(188) Cho, S.-J.; Ryu, J.; Surh, Y. *J. Cancer Prev.* **2019**, *24* (2), 112–122.
(189) Gallwitz, H.; Bonse, S.; Martinez-Cruz, A.; Schlichting, I.; Schumacher, K.; Krauth-Siegel, R. L. *J. Med. Chem.* **1999**, *42* (3), 364–372.
(190) Scharfenberg, K.; Ryll, T.; Wagner, R.; Wagner, K. G. *J. Cell. Physiol.* **1994**, *158* (1), 55–60.
(191) Ghezzi, P. *Free Radic. Res.* **2005**, *39* (6), 573–580.
(192) Forman, H. J.; Fukuto, J. M.; Torres, M. *Am. J. Physiol. Physiol.* **2004**, *287* (2), C246–C256.
(193) Townsend, D. M.; Tew, K. D.; Tapiero, H. *Biomed. Pharmacother.* **2003**, *57* (3), 145–155.
(194) Poole, L. B. *Free Radic. Biol. Med.* **2015**, *80*, 148–157.
(195) Bednar, R. A. *Biochemistry* **1990**, *29* (15), 3684–3690.
(196) Awoonor-Williams, E.; Rowley, C. N. *J. Chem. Theory Comput.* **2016**, *12* (9), 4662–4673.
(197) Singh, R.; Whitesides, G. M. *J. Am. Chem. Soc.* **1990**, *112* (3), 1190–1197.
(198) Roos, G.; Foloppe, N.; Messens, J. *Antioxid. Redox Signal.* **2013**, *18* (1), 94–127.
(199) Wilson, J. M.; Bayer, R. J.; Hupe, D. J. *J. Am. Chem. Soc.* **1977**, *99* (24), 7922–7926.
(200) Singh, R.; Whitesides, G. M. *Chem. Sulphur-Containing Funct. Groups* **2010**, 633–658.
(201) Ferrer-Sueta, G.; Manta, B.; Botti, H.; Radi, R.; Trujillo, M.; Denicola, A. *Chem. Res. Toxicol.* **2011**, *24* (4), 434–450.
(202) Szajewski, R. P.; Whitesides, G. M. *J. Am. Chem. Soc.* **1980**, *102* (6), 2011–2026.
(203) DeCollo, T. V.; Lees, W. J. *J. Org. Chem.* **2001**, *66* (12), 4244–4249.
(204) Gilbert, B. H. F.; Mclean, M. *Adv. Enzymol. Relat. Areas Mol. Biol.* **1963**, *63*, 69–172.
(205) Bach, R. D.; Dmitrenko, O.; Thorpe, C.; Robert D. Bach, *; Olga Dmitrenko, and; Thorpe, C.; Bach, R. D.; Dmitrenko, O.; Thorpe, C. *J. Org. Chem.* **2008**, *73* (1), 12–21.
(206) Kemp, M.; Go, Y.-M.; Jones, D. P. *Free Radic. Biol. Med.* **2008**, *44* (6), 921–937.
(207) Cooper, N. J. In *Comprehensive Organic Functional Group Transformations II*; Elsevier, 2005; Vol. 3, pp 355–396.
(208) Fernandes, P. A.; Ramos, M. J. *Chem. - A Eur. J.* **2004**, *10* (1), 257–266.
(209) Sundaram, S.; Milner, J. *J. Nutr.* **1996**, *126* (May), 1355–1361.

(210) Shirin, H.; Pinto, J. T.; Kawabata, Y.; Soh, J.-W.; Delohery, T.; Moss, S. F.; Murty, V.; Rivlin, R. S.; Holt, P. R.; Weinstein, I. B. *Cancer Res.* **2001**, *61* (2), 725–731.

(211) Torres-Palazzolo, C.; Ramirez, D.; Locatelli, D.; Manucha, W.; Castro, C.; Camargo, A. *J. Food Compos. Anal.* **2018**, *70* (December 2017), 49–53.

(212) Salehi, B.; Zucca, P.; Orhan, I. E.; Azzini, E.; Adetunji, C. O.; Mohammed, S. A.; Banerjee, S. K.; Sharopov, F.; Rigano, D.; Sharifi-Rad, J.; Armstrong, L.; Martorell, M.; Sureda, A.; Martins, N.; Selamoğlu, Z.; Ahmad, Z. *Trends Food Sci. Technol.* **2019**, *86*, 502–516.

(213) Borrelli, F.; Capasso, R.; Izzo, A. A. *Mol. Nutr. Food Res.* **2007**, *51* (11), 1386–1397.

(214) Kamel, A.; Saleh, M. *Stud. Nat. Prod. Chem.* **2000**, *23* (C), 455–485.

(215) Block, E. *Garlic and Other Alliums*; The Royal Society of Chemistry, 2010.

(216) Rybak, M. E.; Calvey, E. M.; Harnly, J. M. *J. Agric. Food Chem.* **2004**, *52* (4), 682–687.

(217) Reuter, H. D.; Koch, H. P.; Lawson, L. D. *Williams Wilkins, Balt. MD* **1996**.

(218) Bat-Chen, W.; Golan, T.; Peri, I.; Ludmer, Z.; Schwartz, B. *Nutr. Cancer* **2010**, *62* (7), 947–957.

(219) Horev-Azaria, L.; Eliav, S.; Izigov, N.; Pri-Chen, S.; Mirelman, D.; Miron, T.; Rabinkov, A.; Wilchek, M.; Jacob-Hirsch, J.; Amariglio, N.; Savion, N. *Eur. J. Nutr.* **2009**, *48* (2), 67–74.

(220) Taucher, J.; Hansel, A.; Jordan, A.; Lindinger, W. *J. Agric. Food Chem.* **1996**, *44* (12), 3778–3782.

(221) Lawson, L. D.; Wang, Z. J. *J. Agric. Food Chem.* **2005**, *53* (6), 1974–1983.

(222) Nagae, S.; Ushijima, M.; Hatono, S.; Imai, J.; Kasuga, S.; Matsuura, H.; Itakura, Y.; Higashi, Y. *Planta Med.* **1994**, *60* (03), 214–217.

(223) Egen-Schwind, C.; Eckard, R.; Kemper, F. H. *Planta Med.* **1992**, *58* (4), 301–305.

(224) Germain, E.; Auger, J.; Ginies, C.; Siess, M. H.; Teyssier, C. *Xenobiotica* **2002**, *32* (12), 1127–1138.

(225) Minami, T.; Boku, T.; Inada, K.; Morita, M.; Okazaki, Y. *J. Food Sci.* **1989**, *54* (3), 763–763.

(226) Ahmad, J. I. *Nutr. Food Sci.* **1996**, *96* (1), 32–35.

(227) Lawson, L.; Hughes, B. *Planta Med.* **1992**, *58* (04), 345–350.

(228) Freeman, F.; Kodera, Y. *J. Agric. Food Chem.* **1995**, No. 9, 2332–2338.

(229) Wang, H.; Li, X.; Liu, X.; Shen, D.; Qiu, Y.; Zhang, X.; Song, J. *J. Sci. Food Agric.* **2015**, *95* (9), 1838–1844.

(230) Miron, T.; Rabinkov, A.; Mirelman, D.; Wilchek, M.; Weiner, L. *Biochim. Biophys. Acta - Biomembr.* **2000**, *1463* (1), 20–30.

(231) Lawson, L. D. **1993**, *1960* (December 1992), 306–330.

(232) Rosen, R. T. T.; Hiserodt, R. D.; Fukuda, E. K.; Ruiz, R. J.; Zhou, Z.; Lech, J.; Rosen, S. L.; Hartman, T. G. *BioFactors* **2000**, *13* (1–4), 241–249.

(233) Lawson, L. D. (Murdock H. S. U. (USA)); Wang, Z. J. In *41st Annual Congress on Medicinal Plant Research, Duesseldorf (Germany), 31 Aug - 4 Sep 1993*; 1993.

(234) Rossi, R.; Milzani, A.; Dalle-Donne, I.; Giustarini, D.; Lusini, L.; Colombo, R.; Di Simplicio, P. *Clin. Chem.* **2002**, *48* (5), 742–753.

(235) Mansoor, M. A.; Svardal, A. M.; Ueland, P. M. *Anal. Biochem.* **1992**, *200* (2), 218–229.

(236) Gao, C.; Jiang, X.; Wang, H.; Zhao, Z.; Wang, W. *J Drug Metab Toxicol* **2013**, *4* (5), 1–10.

(237) Brady, J. F.; Ishizaki, H.; Fukuto, J. M.; Lin, M. C.; Fadel, A.; Gapac, J. M.; Yang, C. S. *Chem. Res. Toxicol.* **1991**, *4* (6), 642–647.

(238) Halliwell, B.; Zhao, K.; Whiteman, M. *Free Radic. Res.* **2000**, *33* (6), 819–830.

(239) Li, X.; Ni, J.; Tang, Y.; Wang, X.; Tang, H.; Li, H.; Zhang, S.; Shen, X. *Nat. Prod. Res.* **2018**, *6419* (18), 1–4.

(240) Saud, S. M.; Li, W.; Gray, Z.; Matter, M. S.; Colburn, N. H.; Young, M. R.; Kim, Y. S. *Cancer Prev. Res.* **2016**, *9* (7), 607–615.

(241) Lee, H.-J.; Lee, H. G.; Choi, K.-S.; Surh, Y.-J.; Na, H.-K. *Biochem. Biophys. Res. Commun.* **2013**, *437* (2), 267–273.

(242) Sun, X.; Guo, T.; He, J.; Zhao, M.; Yan, M.; Cui, F.; Deng, Y. *Pharmazie* **2006**, *61* (12), 985–988.

(243) Ramirez, D. A.; Locatelli, D. A.; González, R. E.; Cavagnaro, P. F.; Camargo, A. B. *J. Food Compos. Anal.* **2017**, *61*, 4–19.

(244) Bayan, L.; Koulivand, P. H.; Gorji, A. *Avicenna J. phytomedicine* **2014**, *4* (1), 1–14.

(245) Mikaili, P.; Maadirad, S.; Moloudizargari, M.; Aghajanshakeri, S.; Sarahroodi, S. *Iran. J. Basic Med. Sci.* **2013**, *16* (10), 1031–1048.

(246) Behnam, A. Herpes Treatment. US 9089597 B2, 2015.

(247) Li, Z.; Le, W.; Cui, Z. *Cell Death Discov.* **2018**, *4* (1), 108.

(248) Amagase, H.; Petesch, B. L.; Matsuura, H.; Kasuga, S.; Itakura, Y. *J. Nutr.* **2001**, *131* (3), 955S – 962.

(249) Shashikant, K. N.; Basappa, S. C.; Sreenivasamurthy, V. **1985**.

(250) Turner, P. V; Brabb, T.; Pekow, C.; Vasbinder, M. A. *J. Am. Assoc. Lab. Anim. Sci.* **2011**, *50* (5), 600–613.

(251) Xiong, T.; Liu, X. W.; Huang, X. L.; Xu, X. F.; Xie, W. Q.; Zhang, S. J.; Tu, J. *Oncol. Lett.* **2018**, *15* (5), 7817–7827.

(252) Yin, X.; Zhang, J.; Li, X.; Liu, D.; Feng, C.; Liang, R.; Zhuang, K.; Cai, C.; Xue, X.; Jing, F.; Wang, X.; Wang, J.; Liu, X.; Ma, H. *Int. J. Mol. Sci.* **2014**, *15* (7), 12422–12441.

(253) Jiang, X. Y.; Zhu, X. S.; Xu, H. Y.; Zhao, Z. X.; Li, S. Y.; Li, S. Z.; Cai, J. H.; Cao, J. M. *Acta Pharmacol. Sin.* **2017**, *38* (7), 1048–1058.

(254) Lai, K.-C.; Hsu, S.-C.; Yang, J.-S.; Yu, C.-C.; Lein, J.-C.; Chung, J.-G. *J. Cell. Mol. Med.* **2015**, *19* (2), 474–484.

(255) Xiao, D.; Lew, K. L.; Kim, Y. A.; Zeng, Y.; Hahm, E. R.; Dhir, R.; Singh, S. V. *Clin. Cancer Res.* **2006**, *12* (22), 6836–6843.

(256) Pai, M. H.; Kuo, Y. H.; Chiang, E. P. I.; Tang, F. Y. *Br. J. Nutr.* **2012**, *108* (1), 28–38.

(257) van Meerloo, J.; Kaspers, G. J. L.; Cloos, J. Humana Press, 2011; pp 237–245.

(258) Tomayko, M. M.; Reynolds, C. P. *Cancer Chemother. Pharmacol.* **1989**, *24* (3), 148–154.

(259) Delgado San Martin, J. A.; Worthington, P.; Yates, J. W. T. *Lab. Anim.* **2015**, *49* (2), 168–171.

(260) Venkateswarlu, S.; Panchagnula, G. K. **2006**, *45* (April), 1063–1066.

(261) Menichetti, R.; Kanekal, K. H.; Bereau, T. *ACS Cent. Sci.* **2019**, *5* (2), 290–298.

(262) Nagano, N.; Ota, M.; Nishikawa, K. *FEBS Lett.* **1999**, *458* (1), 69–71.

(263) Chi, B. K.; Huyen, N. T. T.; Loi, V. Van; Gruhlke, M. C. H.; Schaffer, M.; Mäder, U.; Maaß, S.; Becher, D.; Bernhardt, J.; Arbach, M.; Hamilton, C. J.; Slusarenko, A. J.; Antelmann, H. *Antioxidants* **2019**, *8* (12), 605.

(264) Horn, T.; Bettray, W.; Slusarenko, A.; Gruhlke, M. *Antioxidants* **2018**, *7* (7), 86.

(265) Khramtsov, V. V.; Yelinova (Popova), V. I.; Weiner, L. M.; Berezina, T. A.; Martin, V. V.; Volodarsky, L. B. *Anal. Biochem.* **1989**, *182* (1), 58–63.

(266) Yun, J.; Oliynyk, S.; Lee, Y.; Kim, J.; Yun, K.; Jeon, R.; Ryu, J. H.; Oh, S. *Arch. Pharm. Res.* **2017**, *40* (1), 106–111.

(267) Zinellu, A.; Sotgia, S.; Mangoni, A. A.; Sotgiu, E.; Arru, D.; Paliogiannis, P.; Sengupta, S.; Carru, C. *Int. J. Pept. Res. Ther.* **2019**, *25* (1), 187–194.

(268) Simmons, D.; Hlaing, T. *Diabet. Med.* **2014**, *31* (11), 1387–1392.

(269) Bonaventura, J.; Rodriguez, E. N.; Beyley, V.; Vega, I. E. *J. Med. Food* **2010**, *13* (4),

943–949.

(270) Dybas, J.; Bokamper, M. J.; Marzec, K. M.; Mak, P. J. *Spectrochim. Acta - Part A Mol. Biomol. Spectrosc.* **2020**, *239*, 118530.

(271) Vandegriff, K. D.; Malavalli, A.; Minn, C.; Jiang, E.; Lohman, J.; Young, M. A.; Samaja, M.; Winslow, R. M. *Biochem. J.* **2006**, *399* (3), 463–471.

(272) Dayer, M.; Moosavi-Movahedi, A. *Protein Pept. Lett.* **2010**, *17* (4), 473–479.

(273) Minetti, M.; Malorni, W. *Antioxid. Redox Signal.* **2006**, *8* (7–8), 1165–1169.

(274) Mathew, B.; Srinivasan, K.; Johnson, P.; Thomas, T.; Mandal, A. *Indian J. Med. Res.* **2019**, *149* (4), 497–502.

(275) Yi, L.; Ragsdale, S. W. *J. Biol. Chem.* **2007**, *282* (29), 21056–21067.

(276) Vitturi, D. A.; Sun, C. W.; Harper, V. M.; Thrash-Williams, B.; Cantu-Medellin, N.; Chacko, B. K.; Peng, N.; Dai, Y.; Wyss, J. M.; Townes, T.; Patel, R. P. *Free Radic. Biol. Med.* **2013**, *55*, 119–129.

(277) Storz, J. F.; Weber, R. E.; Fago, A. *Comp. Biochem. Physiol. - A Mol. Integr. Physiol.* **2012**, *161* (2), 265–270.

(278) Craescu, C. T.; Poyart, C.; Schaeffer, C.; Garel, M. C.; Kister, J.; Beuzard, Y. *J. Biol. Chem.* **1986**, *261* (31), 14710–14716.

(279) Alayash, A. I. *Lab. Investig.* **2021**, *101* (1), 4–11.

(280) Mitra, A.; Muralidharan, M.; Srivastava, D.; Das, R.; Bhat, V.; Mandal, A. K. *Hemoglobin* **2017**, *41* (4–6), 300–305.

(281) Zhang, R.; Hess, D. T.; Reynolds, J. D.; Stamler, J. S. *J. Clin. Invest.* **2016**, *126* (12), 4654–4658.

(282) Nakagawa, A.; Ferrari, M.; Schleifer, G.; Cooper, M. K.; Liu, C.; Yu, B.; Berra, L.; Klings, E. S.; Safo, R. S.; Chen, Q.; Musayev, F. N.; Safo, M. K.; Abdulmalik, O.; Bloch, D. B.; Zapol, W. M. *Mol. Pharm.* **2018**, *15* (5), 1954–1963.

(283) Zhang, R.; Hess, D. T.; Qian, Z.; Hausladen, A.; Fonseca, F.; Chaube, R.; Reynolds, J. D.; Stamler, J. S. *Proc. Natl. Acad. Sci. U. S. A.* **2015**, *112* (20), 6425–6430.

(284) Wodak, S.; De Coen, J.; Edelstein, S.; Demarne, H.; Beuzard, Y. *J. Biol. Chem.* **1986**, *261* (31), 14717–14724.

(285) Nohl, H.; Stolze, K. *Gen. Pharmacol. Vasc. Syst.* **1998**, *31* (3), 343–347.

(286) Amrolia, P.; Sullivan, S. G.; Stern, A.; Munday, R. *J. Appl. Toxicol.* **1989**, *9* (2), 113–118.

(287) Altinok-Yipel, F.; Yipel, M.; Tekeli, I. O. *Acta Hortic.* **2016**, *1143* (1143), 311–314.

(288) Robertson, J. E.; Christopher, M. M.; Rogers, Q. R. *J. Am. Vet. Med. Assoc.* **1998**, *212* (8), 1260–1266.

(289) Saastamoinen, M.; Särkijärvi, S.; Hyyppä, S. *Animals* **2019**, *9* (1), 13.

(290) Salgado, B.; Monteiro, L.; Rocha, N. *J. Venom. Anim. Toxins Incl. Trop. Dis.* **2011**, *17* (1), 4–11.

(291) Lee, K. W.; Yamato, O.; Tajima, M.; Kuraoka, M.; Omae, S.; Maede, Y. *Am. J. Vet. Res.* **2000**, *61* (11), 1446–1450.

(292) Cope, R. B. *Vet. Med.* **2005**, *100* (8), 562.

(293) Augusti, K. T. *Indian J. Exp. Biol.* **1996**, *34* (7), 634–640.

(294) Nakagawa, S.; Masamoto, K.; Sumiyoshi, H.; Kunihiro, K.; Fuwa, T. *J. Toxicol. Sci.* **1980**, *5* (1), 91–112.

(295) Moriguchi, T.; Takasugi, N.; Itakura, Y. *J. Nutr.* **2001**, *131* (3), 1016S-1019S.

(296) Chan, K. chi; Yin, M. chin; Chao, W. ju. *Food Chem. Toxicol.* **2007**, *45* (3), 502–507.

(297) Rossi, R.; Milzani, A.; Dalle-Donne, I.; Giannerini, F.; Giustarini, D.; Lusini, L.; Colombo, R.; Di Simplicio, P. *J. Biol. Chem.* **2001**, *276* (10), 7004–7010.

(298) Shokeer, A.; Mannervik, B. *Biochim. Biophys. Acta - Gen. Subj.* **2010**, *1800* (4), 466–473.

(299) Guengerich, F. P. In *Methods in Enzymology*; Academic Press Inc., 2005; Vol. 401, pp 342–353.

(300) Kaschula, C. H.; Hunter, R.; Iqbal Parker, M. *BioFactors* **2010**, *36* (1), 78–85.

(301) Chen, X.; Wang, Y.; Ma, N.; Tian, J.; Shao, Y.; Zhu, B.; Wong, Y. K.; Liang, Z.; Zou, C.; Wang, J. *Signal Transduct. Target. Ther.* **2020**, *5* (1), 72.

(302) Niphakis, M. J.; Cravatt, B. F. *Annu. Rev. Biochem.* **2014**, *83* (1), 341–377.

(303) Pichler, C. M.; Krysiak, J.; Breinbauer, R. *Bioorganic Med. Chem.* **2016**, *24* (15), 3291–3303.

(304) Elia, G. *Proteomics* **2008**, *8* (19), 4012–4024.

(305) Diamandis, E. P.; Christopoulos, T. K. *Clin. Chem.* **1991**, *37* (5), 625–636.

(306) Hermanson, G. T. In *Bioconjugate Techniques*; Elsevier, 2013; Vol. 11, pp 465–505.

(307) Rybak, J.-N.; Scheurer, S. B.; Neri, D.; Elia, G. *Proteomics* **2004**, *4* (8), 2296–2299.

(308) Cheah, J. S.; Yamada, S. *Biochem. Biophys. Res. Commun.* **2017**, *493* (4), 1522–1527.

(309) Pike, C. Strategies towards the Design and Synthesis of a Biotinylated-Ajoene Analogue for the Identification of Ajoene Drug Targets, University of Cape Town, 2013.

(310) Kusza, D. A. Mechanistic Insights into the Cancer Cell Cytotoxicity and Blood Stability of the Garlic Compound Ajoene, University of Cape Town, 2016.

(311) Jezowska, M.; Romanowska, J.; Bestas, B.; Tedebark, U.; Honcharenko, M. *Molecules* **2012**, *17*, 14174–14185.

(312) Stewart, S. G.; Braun, C. J.; Polomska, M. E.; Karimi, M.; Abraham, L. J.; Stubbs, K. A. *Org. Biomol. Chem.* **2010**, *8* (18), 4059–4062.

(313) Kayushin, A.; Demekhina, A.; Korosteleva, M.; Miroshnikov, A.; Azhayev, A. *Nucleosides. Nucleotides Nucleic Acids* **2012**, *30* (7–8), 490–502.

(314) Kolb, H. C.; Finn, M. G.; Sharpless, K. B. *Angew. Chem. Int. Ed. Engl.* **2001**, *40* (11), 2004–2021.

(315) Hein, C. D.; Liu, X.-M.; Wang, D. *Pharm. Res.* **2008**, *25* (10), 2216–2230.

(316) Liang, L.; Astruc, D. *Coord. Chem. Rev.* **2011**, *255* (23–24), 2933–2945.

(317) Walker, J. M. Humana Press, Totowa, NJ, 2009; pp 11–15.

(318) Veitch, N. C. *Phytochemistry* **2004**, *65* (3).

(319) Fosang, A. J.; Colbran, R. J. *J. Biol. Chem.* **2015**, *290* (50), 29692–29694.

(320) Lowe, A. B. *Polymer (Guildf).* **2014**, *55* (22), 5517–5549.

(321) Villemin, E.; Gravel, E.; Izard, N.; Filoramo, A.; Vivien, L.; Doris, E. *Chem. - A Eur. J.* **2015**, *21* (51), 18649–18653.

(322) Henthorn, H. A.; Pluth, M. D. *J. Am. Chem. Soc.* **2015**, *137* (48), 15330–15336.

(323) Speers, A. E.; Cravatt, B. F. *Chem. Biol.* **2004**, *11* (4), 535–546.

(324) Veronese, F. M.; Pasut, G. *Drug Discov. Today* **2005**, *10* (21), 1451–1458.

(325) Ren, W. X.; Han, J.; Uhm, S.; Jang, Y. J.; Kang, C.; Kim, J. H.; Kim, J. S. *Chem. Commun.* **2015**, *51* (52), 10403–10418.

(326) Alconcel, S. N. S.; Baas, A. S.; Maynard, H. D. *Polym. Chem.* **2011**, *2* (7), 1442–1448.

(327) Chambers, J. M.; Lindqvist, L. M.; Webb, A.; Huang, D. C. S. S.; Savage, G. P.; Rizzacasa, M. A. *Org. Lett.* **2013**, *15* (6), 1406–1409.

(328) Weidner, J. P.; Block, S. S. *J. Med. Chem.* **1964**, *7*, 671–673.

(329) Potter, G. T.; Jayson, G. C.; Miller, G. J.; Gardiner, J. M. *J. Org. Chem.* **2016**, *81* (8), 3443–3446.

(330) Díez-González, S. *Curr. Org. Chem.* **2011**, *44* (I), 2830–2845.

(331) Goldman, A.; Harper, S.; Speicher, D. W. *Curr. Protoc. Protein Sci.* **2016**, *86* (1), 10.8.1-10.8.11.

(332) Grant, M. K. O.; Shapiro, S. L.; Ashe, K. H.; Liu, P.; Zahs, K. R. *Biol. Proced. Online* **2019**,

21 (1), 6.

(333) Chapman-Smith, A.; Cronan, J. E. *J. Nutr.* **1999**, *129*, 477–484.

(334) Pacheco-Alvarez, D.; Solórzano-Vargas, R. S.; Gravel, R. A.; Cervantes-Roldán, R.; Velázquez, A.; León-Del-Río, A. *J. Biol. Chem.* **2004**, *279* (50), 52312–52318.

(335) Ferri, N.; Yokoyama, K.; Sadilek, M.; Paoletti, R.; Apitz-Castro, R.; Gelb, M. H.; Corsini, A. *Br. J. Pharmacol.* **2003**, *138* (5), 811–818.

(336) Xu, B.; Monsarrat, B.; Gairin, J. E.; Girbal-Neuhauser, E. *Fundam. Clin. Pharmacol.* **2004**, *18* (2), 171–180.

(337) Dirsch, V.; Antlsperger, D.; Hentze, H.; Vollmar, A. *Leukemia* **2002**, *16* (1), 74–83.

(338) Antlsperger, D. S. M.; Dirsch, V. M.; Ferreira, D.; Su, J.-L.; Kuo, M.-L.; Vollmar, A. M. *Oncogene* **2003**, *22* (4), 582–589.

(339) Jung, Y.; Park, H.; Zhao, H.-Y.; Jeon, R.; Ryu, J.-H.; Kim, W.-Y. *Mol. Cells* **2014**, *37* (7), 547–553.

(340) Siyo, V.; Schäfer, G.; Hunter, R.; Grafov, A.; Grafova, I.; Nieger, M.; Katz, A. A.; Parker, M. I.; Kaschula, C. H. *Molecules* **2017**, *22* (6), 892.

(341) Lee, H.; Heo, J.-W.; Kim, A.-R.; Kweon, M.; Nam, S.; Lim, J.-S.; Sung, M.-K.; Kim, S.-E.; Ryu, J.-H. *Nutrients* **2019**, *11* (11), 2724.

(342) Dirsch, V. M.; Vollmar, A. M. *Biochem. Pharmacol.* **2001**, *61* (5), 587–593.

(343) Hitchcock, J. K.; Mkwanazi, N.; Barnett, C.; Graham, L. M.; Katz, A. A.; Hunter, R.; Schäfer, G.; Kaschula, C. H. *Mol. Nutr. Food Res.* **2020**, 2000854.

(344) Chung, H. S.; Wang, S.-B.; Venkatraman, V.; Murray, C. I.; Van Eyk, J. E. *Circ. Res.* **2013**, *112* (2), 382–392.

(345) Nietzel, T.; Mostertz, J.; Hochgräfe, F.; Schwarzländer, M. *Mitochondrion* **2017**, *33*, 72–83.

(346) Long, M. J. C.; Aye, Y. *Cell Chem. Biol.* **2017**, *24* (7), 787–800.

(347) Cooper, A. J.; Pinto, J. T.; Callery, P. S. *Expert Opin. Drug Metab. Toxicol.* **2011**, *7* (7), 891–910.

(348) Dalle-Donne, I.; Rossi, R.; Colombo, G.; Giustarini, D.; Milzani, A. *Trends Biochem. Sci.* **2009**, *34* (2), 85–96.

(349) Klatt, P.; Lamas, S. *Eur. J. Biochem.* **2000**, *267* (16), 4928–4944.

(350) Chaikuad, A.; Koch, P.; Laufer, S. A.; Knapp, S. *Angew. Chemie Int. Ed.* **2018**, *57* (16), 4372–4385.

(351) Wu, S.; Luo (Howard), H.; Wang, H.; Zhao, W.; Hu, Q.; Yang, Y. *Biochem. Biophys. Res.*

Commun. **2016**, *478* (3), 1268–1273.

(352) Gould, N. S.; Evans, P.; Martínez-Acedo, P.; Marino, S. M.; Gladyshev, V. N.; Carroll, K. S.; Ischiropoulos, H. *Chem. Biol.* **2015**, *22* (7), 965–975.

(353) Mnatsakanyan, R.; Shema, G.; Basik, M.; Batist, G.; Borchers, C. H.; Sickmann, A.; Zahedi, R. P. *Expert Rev. Proteomics* **2018**, *15* (6), 515–535.

(354) Kuljanin, M.; Mitchell, D. C.; Schweppe, D. K.; Gikandi, A. S.; Nusinow, D. P.; Bulloch, N. J.; Vinogradova, E. V.; Wilson, D. L.; Kool, E. T.; Mancias, J. D.; Cravatt, B. F.; Gygi, S. P. *Nat. Biotechnol.* **2021**, 1–12.

(355) Van Der Reest, J.; Lilla, S.; Zheng, L.; Zanivan, S.; Gottlieb, E. *Nat. Commun.* **2018**, *9* (1), 1–16.

(356) Fra, A.; Yoboue, E. D.; Sitia, R. *Front. Mol. Neurosci.* **2017**, *10* (June), 1–9.

(357) Meng, J.; Fu, L.; Liu, K.; Tian, C.; Wu, Z.; Jung, Y.; Ferreira, R. B.; Carroll, K. S.; Blackwell, T. K.; Yang, J. *Nat. Commun.* **2021**, *12* (1), 1415.

(358) Huang, J.; Willems, P.; Wei, B.; Tian, C.; Ferreira, R. B.; Bodra, N.; Martínez Gache, S. A.; Wahni, K.; Liu, K.; Vertommen, D.; Gevaert, K.; Carroll, K. S.; Van Montagu, M.; Yang, J.; Van Breusegem, F.; Messens, J. *Proc. Natl. Acad. Sci. U. S. A.* **2019**, *116* (42), 20256–20261.

(359) Akter, S.; Fu, L.; Jung, Y.; Conte, M. Lo; Lawson, J. R.; Lowther, W. T.; Sun, R.; Liu, K.; Yang, J.; Carroll, K. S. *Nat. Chem. Biol.* **2018**, *14* (11), 995–1004.

(360) Petrova, B.; Liu, K.; Tian, C.; Kitaoka, M.; Freinkman, E.; Yang, J.; Orr-Weaver, T. L. *Proc. Natl. Acad. Sci. U. S. A.* **2018**, *115* (34), E7978–E7986.

(361) Fu, L.; Liu, K.; Sun, M.; Tian, C.; Sun, R.; Betanzos, C. M.; Tallman, K. A.; Porter, N. A.; Yang, Y.; Guo, D.; Liebler, D. C.; Yang, J. *Mol. Cell. Proteomics* **2017**, *16* (10), 1815–1828.

(362) Xiao, H.; Jedrychowski, M. P.; Schweppe, D. K.; Huttlin, E. L.; Yu, Q.; Heppner, D. E.; Li, J.; Long, J.; Mills, E. L.; Szpyt, J.; He, Z.; Du, G.; Garrity, R.; Reddy, A.; Vaites, L. P.; Paulo, J. A.; Zhang, T.; Gray, N. S.; Gygi, S. P.; Chouchani, E. T. *Cell* **2020**, *180* (5), 968-983.e24.

(363) Backus, K. M. In *Current Topics in Microbiology and Immunology*; Springer Verlag, 2018; Vol. 420, pp 375–417.

(364) Müller, A.; Eller, J.; Albrecht, F.; Prochnow, P.; Kuhlmann, K.; Bandow, J. E.; Slusarenko, A. J.; Leichert, L. I. O. *J. Biol. Chem.* **2016**, *291* (22), 11477–11490.

(365) Loi, V. Van; Huyen, N. T. T.; Busche, T.; Tung, Q. N.; Gruhlke, M. C. H.; Kalinowski, J.;

Bernhardt, J.; Slusarenko, A. J.; Antelmann, H. *Free Radic. Biol. Med.* **2019**, *139*, 55–69.

(366) Rabinkov, A.; Miron, T.; Konstantinovski, L.; Wilchek, M.; Mirelman, D.; Weiner, L. *Biochim. Biophys. Acta - Gen. Subj.* **1998**, *1379* (2), 233–244.

(367) Boroughs, L. K.; DeBerardinis, R. J. *Nat. Cell Biol.* **2015**, *17* (4), 351–359.

(368) Prasad, S.; Gupta, S. C.; Tyagi, A. K. *Cancer Lett.* **2017**, *387*, 95–105.

(369) Harris, I. S.; Treloar, A. E.; Inoue, S.; Sasaki, M.; Gorrini, C.; Lee, K. C.; Yung, K. Y.; Brenner, D.; Knobbe-Thomsen, C. B.; Cox, M. A.; Elia, A.; Berger, T.; Cescon, D. W.; Adeoye, A.; Brüstle, A.; Molyneux, S. D.; Mason, J. M.; Li, W. Y.; Yamamoto, K.; Wakeham, A.; Berman, H. K.; Khokha, R.; Done, S. J.; Kavanagh, T. J.; Lam, C. W.; Mak, T. W. *Cancer Cell* **2015**, *27* (2), 211–222.

(370) Hopkins, B. L.; Neumann, C. A. *Redox Biol.* **2019**, *21* (January), 101–104.

(371) Oka, O. B. V.; Yeoh, H. Y.; Bulleid, N. J. *Biochem. J.* **2015**, *469* (2), 279–288.

(372) Hatahet, F.; Ruddock, L. W. *Antioxid. Redox Signal.* **2009**, *11* (11), 2807–2850.

(373) Appenzeller-Herzog, C. *J. Cell Sci.* **2011**, *124* (6), 847–855.

(374) Bass, R.; Ruddock, L. W.; Klappa, P.; Freedman, R. B. *J. Biol. Chem.* **2004**, *279* (7), 5257–5262.

(375) Schubert, U.; Antón, L. C.; Gibbs, J.; Norbury, C. C.; Yewdell, J. W.; Bennink, J. R. *Nature* **2000**, *404* (6779), 770–774.

(376) Karagöz, G. E.; Acosta-Alvear, D.; Walter, P. *Cold Spring Harb. Perspect. Biol.* **2019**, *11* (9).

(377) Tabas, I.; Ron, D. *Nat. Cell Biol.* **2011**, *13* (3), 184–190.

(378) Kim, H.; Bhattacharya, A.; Qi, L. *Semin. Cancer Biol.* **2015**, *33*, 25–33.

(379) Cao, S. S.; Kaufman, R. J. *Antioxid. Redox Signal.* **2014**, *21* (3), 396–413.

(380) Laskay, Ü. A.; Lobas, A. A.; Srzentić, K.; Gorshkov, M. V.; Tsybin, Y. O. *J. Proteome Res.* **2013**, *12* (12), 5558–5569.

(381) Petrovic, V.; Olaisen, C.; Sharma, A.; Nepal, A.; Bugge, S.; Sundby, E.; Hoff, B. H.; Slupphaug, G.; Otterlei, M. *Anal. Biochem.* **2017**, *523*, 10–16.

(382) Duncan, J. S.; Whittle, M. C.; Nakamura, K.; Abell, A. N.; Midland, A. A.; Zawistowski, J. S.; Johnson, N. L.; Granger, D. A.; Jordan, N. V.; Darr, D. B.; Usary, J.; Kuan, P. F.; Smalley, D. M.; Major, B.; He, X.; Hoadley, K. A.; Zhou, B.; Sharpless, N. E.; Perou, C. M.; Kim, W. Y.; Gomez, S. M.; Chen, X.; Jin, J.; Frye, S. V.; Earp, H. S.; Graves, L. M.; Johnson, G. L. *Cell* **2012**, *149* (2), 307–321.

(383) Fonslow, B. R.; Carvalho, P. C.; Academia, K.; Freeby, S.; Xu, T.; Nakorchevsky, A.; Paulus, A.; Yates, J. R. *J. Proteome Res.* **2011**, *10* (8), 3690–3700.

(384) Piran, U.; Riordan, W. J. *J. Immunol. Methods* **1990**, *133* (1), 141–143.

(385) Dundas, C. M.; Demonte, D.; Park, S. *Appl. Microbiol. Biotechnol.* **2013**, *97* (21), 9343–9353.

(386) Scheurer, S. B.; Roesli, C.; Neri, D.; Elia, G. *Proteomics* **2005**, *5* (12), 3035–3039.

(387) Schiapparelli, L. M.; McClatchy, D. B.; Liu, H. H.; Sharma, P.; Yates, J. R.; Cline, H. T. *J. Proteome Res.* **2014**, *13* (9), 3966–3978.

(388) Schäfer, G.; Hitchcock, J. K.; Shaw, T. M.; Katz, A. A.; Parker, M. I. *J. Cell. Biochem.* **2015**, *116* (3), 408–417.

(389) Smith, M. An Immunoproteomic Approach to Identifying Cancer-Associated Autoantibody Biomarkers, University of Cape Town, 2018.

(390) Fukuyama, H.; Ndiaye, S.; Hoffmann, J.; Rossier, J.; Liuu, S.; Vinh, J.; Verdier, Y. *J. Proteomics* **2012**, *75* (15), 4610–4619.

(391) Choi, E.; Loo, D.; Dennis, J. W.; O'Leary, C. A.; Hill, M. M. *Electrophoresis* **2011**, *32* (24), 3564–3575.

(392) Kinter, M.; Sherman, N. E. In *Protein Sequencing and Identification Using Tandem Mass Spectrometry*; John Wiley & Sons, Inc.: Hoboken, NJ, USA, 2005; Vol. 9, pp 1–5.

(393) Cox, J.; Mann, M. *Nat. Biotechnol.* **2008**, *26* (12), 1367–1372.

(394) Cox, J.; Neuhauser, N.; Michalski, A.; Scheltema, R. A.; Olsen, J. V.; Mann, M. *J. Proteome Res.* **2011**, *10* (4), 1794–1805.

(395) Tamvakopoulos, C. *Mass Spectrom. Rev.* **2007**, *26* (3), 389–402.

(396) Olsen, J. V.; Mann, M. *Proc. Natl. Acad. Sci. U. S. A.* **2004**, *101* (37), 13417–13422.

(397) Elias, J. E.; Gygi, S. P. *Nat. Methods* **2007**, *4* (3), 207–214.

(398) Käll, L.; Storey, J. D.; MacCoss, M. J.; Noble, W. S. *J. Proteome Res.* **2008**, *7* (1), 40–44.

(399) Cox, J.; Hein, M. Y.; Luber, C. A.; Paron, I.; Nagaraj, N.; Mann, M. *Mol. Cell. Proteomics* **2014**, *13* (9), 2513–2526.

(400) Tyanova, S.; Cox, J. In *Methods in Molecular Biology*; Humana Press Inc., 2018; Vol. 1711, pp 133–148.

(401) Tyanova, S.; Temu, T.; Sinitcyn, P.; Carlson, A.; Hein, M. Y.; Geiger, T.; Mann, M.; Cox, J. *Nat. Methods* **2016**, *13* (9), 731–740.

(402) Lazar, C.; Gatto, L.; Ferro, M.; Bruley, C.; Burger, T. *J. Proteome Res.* **2016**, *15* (4), 1116–1125.

(403) Tytgat, H. L. P. P.; Schoofs, G.; Driesen, M.; Proost, P.; Van Damme, E. J. M. M.; Vanderleyden, J.; Lebeer, S. *Microb. Biotechnol.* **2015**, *8* (1), 164–168.

(404) Keller, B. O.; Sui, J.; Young, A. B.; Whittal, R. M. *Anal. Chim. Acta* **2008**, *627* (1), 71–81.

(405) Chen, X.; Zhou, H.; Li, X.; Duan, N.; Hu, S.; Liu, Y.; Yue, Y.; Song, L.; Zhang, Y.; Li, D.; Wang, Z. *EBioMedicine* **2018**, *30*, 129–137.

(406) Pavao, M.; Huang, Y.-H.; Hafer, L. J.; Moreland, R. B.; Traish, A. M. *BMC Cancer* **2001**, *1* (1), 15.

(407) Buxade, M.; Morrice, N.; Krebs, D. L.; Proud, C. G. *J. Biol. Chem.* **2008**, *283* (1), 57–65.

(408) Karhumaa, P.; Parkkila, S.; Waheed, A.; Parkkila, A. K.; Kaunisto, K.; Tucker, P. W.; Huang, C. J.; Sly, W. S.; Rajaniemi, H. *J. Biol. Chem.* **2000**, *275* (21), 16044–16049.

(409) Arai, M.; Kawachi, T.; Kotoku, N.; Nakata, C.; Kamada, H.; Tsunoda, S.; Tsutsumi, Y.; Endo, H.; Inoue, M.; Sato, H.; Kobayashi, M. *ChemBioChem* **2016**, *17* (2), 181–189.

(410) Bak, D. W.; Bechtel, T. J.; Falco, J. A.; Weerapana, E. *Curr. Opin. Chem. Biol.* **2019**, *48*, 96–105.

(411) Yuan, K.; Liu, Y.; Chen, H.-N.; Zhang, L.; Lan, J.; Gao, W.; Dou, Q.; Nice, E. C.; Huang, C. *Proteomics* **2015**, *15* (2–3), 287–299.

(412) Edfeldt, F. N. B.; Folmer, R. H. A.; Breeze, A. L. *Drug Discov. Today* **2011**, *16* (7–8), 284–287.

(413) Weerapana, E.; Wang, C.; Simon, G. M.; Richter, F.; Khare, S.; Dillon, M. B. D. D.; Bachovchin, D. A.; Mowen, K.; Baker, D.; Cravatt, B. F. *Nature* **2010**, *468* (7325), 790–795.

(414) Maurais, A. J.; Weerapana, E. *Curr. Opin. Chem. Biol.* **2019**, *50* (1), 29–36.

(415) Duan, J.; Gaffrey, M. J.; Qian, W.-J. *Mol. Biosyst.* **2017**, *13* (5), 816–829.

(416) Vinogradova, E. V.; Zhang, X.; Remillard, D.; Lazar, D. C.; Suciu, R. M.; Wang, Y.; Bianco, G.; Yamashita, Y.; Crowley, V. M.; Schafroth, M. A.; Yokoyama, M.; Konrad, D. B.; Lum, K. M.; Simon, G. M.; Kemper, E. K.; Lazear, M. R.; Yin, S.; Blewett, M. M.; Dix, M. M.; Nguyen, N.; Shokhirev, M. N.; Chin, E. N.; Lairson, L. L.; Melillo, B.; Schreiber, S. L.; Forli, S.; Teijaro, J. R.; Cravatt, B. F. *Cell* **2020**, *182* (4), 1009-1026.e29.

(417) Backus, K. M.; Correia, B. E.; Lum, K. M.; Forli, S.; Horning, B. D.; González-Páez, G. E.; Chatterjee, S.; Lanning, B. R.; Teijaro, J. R.; Olson, A. J.; Wolan, D. W.; Cravatt, B. F. *Nature* **2016**, *534* (7608), 570–574.

(418) Wang, P.; Zhang, Q.; Li, S.; Cheng, B.; Xue, H.; Wei, Z.; Shao, T.; Liu, Z.-X.; Cheng, H.; Wang, Z. *Brief. Bioinform.* **2021**.

(419) Acuner Ozbabacan, S. E.; Engin, H. B.; Gursoy, A.; Keskin, O. *Protein Eng. Des. Sel.* **2011**, *24* (9), 635–648.

(420) Groitl, B.; Jakob, U. *Biochim. Biophys. Acta - Proteins Proteomics* **2014**, *1844* (8), 1335–1343.

(421) Held, J. M. *Antioxid. Redox Signal.* **2020**, *32* (10), 659–676.

(422) Dalle-Donne, I.; Rossi, R.; Giustarini, D.; Colombo, R.; Milzani, A. *Free Radic. Biol. Med.* **2007**, *43* (6), 883–898.

(423) Fowler, N. J.; Blanford, C. F.; De Visser, S. P.; Warwicker, J. *Sci. Rep.* **2017**, *7* (1), 1–12.

(424) Nakamura, F.; Osborn, T. M.; Hartemink, C. A.; Hartwig, J. H.; Stossel, T. P. *J. Cell Biol.* **2007**, *179* (5), 1011–1025.

(425) Wang, M.; Herrmann, C. J.; Simonovic, M.; Szklarczyk, D.; von Mering, C. *Proteomics* **2015**, *15* (18), 3163–3168.

(426) Noguchi, M.; Takata, T.; Kimura, Y.; Manno, A.; Murakami, K.; Koike, M.; Ohizumi, H.; Hori, S.; Kakizuka, A. *J. Biol. Chem.* **2005**, *280* (50), 41332–41341.

(427) Mizuno, Y.; Hori, S.; Kakizuka, A.; Okamoto, K. *Neurosci. Lett.* **2003**, *343* (2), 77–80.

(428) Kobayashi, T.; Tanaka, K.; Inoue, K.; Kakizuka, A. *J. Biol. Chem.* **2002**, *277* (49), 47358–47365.

(429) Liu, C.; Wei, J.; Xu, K.; Sun, X.; Zhang, H.; Xiong, C. *Cell Prolif.* **2019**, *52* (2), e12549.

(430) Tung, M. C.; Tsai, C. S. S.; Tung, J. N.; Tsao, T. Y.; Chen, H. C.; Yeh, K. T.; Liao, C. F.; Jiang, M. C. *Cancer Epidemiol. Biomarkers Prev.* **2009**, *18* (5), 1570–1577.

(431) Tsai, C. S. S.; Chen, H. C.; Tung, J. N.; Tsou, S. S.; Tsao, T. Y.; Liao, C. F.; Chen, Y. C.; Yeh, C. Y.; Yeh, K. T.; Jiang, M. C. *Am. J. Pathol.* **2010**, *176* (4), 1619–1628.

(432) Tai, C. J.; Shen, S. C.; Lee, W. R.; Liao, C. F.; Deng, W. P.; Chiou, H. Y.; Hsieh, C. I.; Tung, J. N.; Chen, C. S.; Chiou, J. F.; Li, L. T.; Lin, C. Y.; Hsu, C. H.; Jiang, M. C. *Exp. Cell Res.* **2010**, *316* (17), 2969–2981.

(433) Tian, C.; Sun, R.; Liu, K.; Fu, L.; Liu, X.; Zhou, W.; Yang, Y.; Yang, J. *Cell Chem. Biol.* **2017**, *24* (11), 1416-1427.e5.

(434) Groen, E. J. N.; Gillingwater, T. H. *Trends Mol. Med.* **2015**, *21* (10), 622–632.

(435) Yang, U.; Yang, H. Y.; Kim, J. S.; Lee, T. H. *Biochem. Biophys. Res. Commun.* **2012**, *427* (3), 587–592.

(436) Xu, W.; Lukkarila, J. L.; da Silva, S. R.; Paiva, S.-L.; Gunning, P. T.; Schimmer, A. D. *Curr. Pharm. Des.* **2013**, *19* (18), 3201–3209.

(437) Dirsch, V. M.; Kiemer, A. K.; Wagner, H.; Vollmar, A. M. *Atherosclerosis* **1998**, *139* (2), 333–339.

(438) Marino, S. M.; Gladyshev, V. N. *J. Biol. Chem.* **2012**, *287* (7), 4419–4425.

(439) Wang, H.; Chen, X.; Li, C.; Liu, Y.; Yang, F.; Wang, C. *Biochemistry* **2018**, *57* (4), 451–460.

(440) Wang, C.; Weerapana, E.; Blewett, M. M.; Cravatt, B. F. *Nat. Methods* **2014**, *11* (1), 79–85.

(441) Abo, M.; Li, C.; Weerapana, E. *Mol. Pharm.* **2018**, *15* (3), 743–749.

(442) Topf, U.; Suppanz, I.; Samluk, L.; Wrobel, L.; Böser, A.; Sakowska, P.; Knapp, B.; Pietrzyk, M. K.; Chacinska, A.; Warscheid, B. *Nat. Commun.* **2018**, *9* (1), 1–17.

(443) Shcherbik, N.; Pestov, D. G. *Cells* **2019**, *8* (11), 1379.

(444) Antalis, C. J.; Arnold, T.; Rasool, T.; Lee, B.; Buhman, K. K.; Siddiqui, R. A. *Breast Cancer Res. Treat.* **2010**, *122* (3), 661–670.

(445) Goudarzi, A. *Life Sci.* **2019**, *232*, 116592.

(446) Storr, S. J.; Carragher, N. O.; Frame, M. C.; Parr, T.; Martin, S. G. *Nat. Rev. Cancer* **2011**, *11* (5), 364–374.

(447) Zhang, J.; Li, X.; Han, X.; Liu, R.; Fang, J. *Trends Pharmacol. Sci.* **2017**, *38* (9), 794–808.

(448) Aryal, B.; Rao, V. A. *PLoS One* **2018**, *13* (3), e0194164.

(449) Louie, S. M.; Grossman, E. A.; Crawford, L. A.; Ding, L.; Camarda, R.; Huffman, T. R.; Miyamoto, D. K.; Goga, A.; Weerapana, E.; Nomura, D. K. *Cell Chem. Biol.* **2016**, *23* (5), 567–578.

(450) Melino, S.; Sabelli, R.; Paci, M. *Amino Acids* **2011**, *41* (1), 103–112.

(451) DeLaBarre, B.; Hurov, J.; Cianchetta, G.; Murray, S.; Dang, L. *Chem. Biol.* **2014**, *21* (9), 1143–1161.

(452) Shen, J.; Jin, Z.; Lv, H.; Jin, K.; Jonas, K.; Zhu, C.; Chen, B. *Cell. Oncol.* **2020**, *43* (4), 617–629.

(453) Lang, L.; Chemmalakuzhy, R.; Shay, C.; Teng, Y. In *Advances in Experimental Medicine and Biology*; Springer New York LLC, 2019; Vol. 1134, pp 243–258.

(454) Li, Z.; Wang, D.; Lu, J.; Huang, B.; Wang, Y.; Dong, M.; Fan, D.; Li, H.; Gao, Y.; Hou, P.; Li, M.; Liu, H.; Pan, Z. Q.; Zheng, J.; Bai, J. *Cell Death Differ.* **2020**, *27* (12), 3226–3242.

(455) Liu, L. M.; Sun, W. Z.; Fan, X. Z.; Xu, Y. L.; Cheng, M. Bin; Zhang, Y. *Cancer Res.* **2019**, *79* (11), 2865–2877.

(456) Brandes, N.; Schmitt, S.; Jakob, U. *Antioxid. Redox Signal.* **2009**, *11* (5), 997–1014.

(457) Qin, W.; Qin, K.; Zhang, Y.; Jia, W.; Chen, Y.; Cheng, B.; Peng, L.; Chen, N.; Liu, Y.; Zhou, W.; Wang, Y. L.; Chen, X.; Wang, C. *Nat. Chem. Biol.* **2019**, *15* (10), 983–991.

(458) Xu, I. M. J.; Lai, R. K. H.; Lin, S. H.; Tse, A. P. W.; Chiu, D. K. C.; Koh, H. Y.; Law, C. T.; Wong, C. M.; Cai, Z.; Wong, C. C. L.; Ng, I. O. L. *Proc. Natl. Acad. Sci. U. S. A.* **2016**, *113* (6), E725–E734.

(459) Xu, R.; Pelicano, H.; Zhou, Y.; Carew, J. S.; Feng, L.; Bhalla, K. N.; Keating, M. J.; Huang, P. *Cancer Res.* **2005**, *65* (2), 613–621.

(460) Ganapathy-Kanniappan, S.; Geschwind, J.-F. H. *Mol. Cancer* **2013**, *12* (1), 152.

(461) White-Gilbertson, S.; Kurtz, D. T.; Voelkel-Johnson, C. *Mol. Oncol.* **2009**, *3* (5–6), 402–408.

(462) Pelletier, J.; Thomas, G.; Volarević, S. *Nat. Rev. Cancer* **2018**, *18* (1), 51–63.

(463) Yamaguchi, H.; Condeelis, J. *Biochim. Biophys. Acta - Mol. Cell Res.* **2007**, *1773* (5), 642–652.

(464) Jiang, X.; Qin, Y.; Kun, L.; Zhou, Y. *Front. Oncol.* **2021**, *11*, 333.

(465) Lipinski, C. A. *J. Pharmacol. Toxicol. Methods* **2000**, *44* (1), 235–249.

(466) Pajouhesh, H.; Lenz, G. R. *NeuroRx* **2005**, *2* (4), 541–553.

(467) Requejo, R.; Hurd, T. R.; Costa, N. J.; Murphy, M. P. *FEBS J.* **2010**, *277* (6), 1465–1480.

(468) Spadaro, D.; Yun, B.-W.; Spoel, S. H.; Chu, C.; Wang, Y.-Q.; Loake, G. J. *Physiol. Plant.* **2010**, *138* (4), 360–371.

(469) Kanehisa, M. *Nucleic Acids Res.* **2000**, *28* (1), 27–30.

(470) Kanehisa, M. *Protein Sci.* **2019**, *28* (11), 1947–1951.

(471) Liebermeister, W.; Noor, E.; Flamholz, A.; Davidi, D.; Bernhardt, J.; Milo, R. *Proc. Natl. Acad. Sci. U. S. A.* **2014**, *111* (23), 8488–8493.

(472) Ferreira, L. M. R. *Exp. Mol. Pathol.* **2010**, *89* (3), 372–380.

(473) Spitz, D. R.; Sim, J. E.; Ridnour, L. A.; Galoforo, S. S.; Lee, Y. J. *Ann. N. Y. Acad. Sci.* **2000**, *899* (1), 349–362.

(474) Lord-Fontaine, S.; Averill-Bates, D. A. *Free Radic. Biol. Med.* **2002**, *32* (8), 752–765.

(475) Aykin-Burns, N.; Ahmad, I. M.; Zhu, Y.; Oberley, L. W.; Spitz, D. R. *Biochem. J.* **2009**, *418* (1), 29–37.

(476) Li, L.; Fath, M. A.; Scarbrough, P. M.; Watson, W. H.; Spitz, D. R. *Redox Biol.* **2015**, *4*,

127–135.

(477) Luo, M.; Wicha, M. S. *Semin. Radiat. Oncol.* **2019**, *29* (1), 42–54.

(478) Rashmi, R.; Huang, X.; Floberg, J. M.; Elhammali, A. E.; McCormick, M. L.; Patti, G. J.; Spitz, D. R.; Schwarz, J. K. *Cancer Res.* **2018**, *78* (6), 1392–1403.

(479) Shenton, D.; Grant, C. M. *Biochem. J.* **2003**, *374* (Pt 2), 513–519.

(480) Li, M.; Min, J. M.; Cui, J. R.; Zhang, L. H.; Wang, K.; Valette, A.; Davrinche, C.; Wright, M.; Leung-Tack, J. *Nutr. Cancer* **2002**, *42* (2), 241–247.

(481) Zachara, N. E. *FEBS Lett.* **2018**, *592* (23), 3950–3975.

(482) Büll, C.; Stoel, M. A.; den Brok, M. H.; Adema, G. J. *Cancer Res.* **2014**, *74* (12), 3199–3204.

(483) Teoh, S. T.; Ogrodzinski, M. P.; Ross, C.; Hunter, K. W.; Lunt, S. Y. *Front. Oncol.* **2018**, *8*, 174.

(484) Puttamallesh, V. N.; Deb, B.; Gondkar, K.; Jain, A.; Nair, B.; Pandey, A.; Chatterjee, A.; Gowda, H.; Kumar, P. *Genes (Basel).* **2020**, *11* (7), 1–17.

(485) Raimi, O. G.; Hurtado-Guerrero, R.; Borodkin, V.; Ferenbach, A.; Urbaniak, M. D.; Ferguson, M. A. J.; van Aalten, D. M. F. *RSC Chem. Biol.* **2020**, *1* (1), 13–25.

(486) Yin, J.; Ren, W.; Huang, X.; Deng, J.; Li, T.; Yin, Y. *Front. Immunol.* **2018**, *9*, 1697.

(487) Liu, X.; Paila, U. D.; Teraoka, S. N.; Wright, J. A.; Huang, X.; Quinlan, A. R.; Gatti, R. A.; Concannon, P. *Int. J. Radiat. Oncol. Biol. Phys.* **2018**, *100* (1), 162–173.

(488) Szabados, E.; Hindmarsh, E. J.; Phillips, L.; Duggleby, R. G.; Christopherson, R. I. *Biochemistry* **1994**, *33* (47), 14237–14245.

(489) Almatroodi, S. A.; Alsahli, M. A.; Almatroudi, A.; Rahmani, A. H. *Anticancer. Agents Med. Chem.* **2019**, *19* (11), 1314–1324.

(490) Kalra, S.; Joshi, G.; Munshi, A.; Kumar, R. *Eur. J. Med. Chem.* **2017**, *142*, 424–458.

(491) Go, N. Cysteine 119 of Cdk1, a potential target of ROS, is crucial for the association of Cdk1 with Cyclin B1, Graduate School of Ajou University, 2017.

(492) Brunet, A.; Kanai, F.; Stehn, J.; Xu, J.; Sarbassova, D.; Frangioni, J. V.; Dalal, S. N.; Decaprio, J. A.; Greenberg, M. E.; Yaffe, M. B. *J. Cell Biol.* **2002**, *156* (5), 817–828.

(493) Kim, H. S.; Ullevig, S. L.; Nguyen, H. N.; Vanegas, D.; Asmis, R. *Arterioscler. Thromb. Vasc. Biol.* **2014**, *34* (7), 1514–1521.

(494) Zang, L.; Toy, D. P.; Hancock, W. S.; Sgroi, D. C.; Karger, B. L. *J. Proteome Res.* **2004**, *3* (3), 604–612.

(495) Bergamaschi, A.; Christensen, B. L.; Katzenellenbogen, B. S. *Breast Cancer Res.* **2011**,

13 (3), 1–14.

(496) Yan, Y.; Xu, Y.; Gao, Y. Y.; Zong, Z. H.; Zhang, Q.; Li, C.; Wang, H. Q. *Cancer Sci.* **2013**, *104* (1), 55–61.

(497) Wang, B.; Liu, K.; Lin, H.-Y.; Bellam, N.; Ling, S.; Lin, W.-C. *Mol. Cell. Biol.* **2010**, *30* (6), 1508–1527.

(498) Chang, C. C.; Zhang, C.; Zhang, Q.; Sahin, O.; Wang, H.; Xu, J.; Xiao, Y.; Zhang, J.; Rehman, S. K.; Li, P.; Hung, M. C.; Behbod, F.; Yu, D. *Oncotarget* **2016**, *7* (23), 35270–35283.

(499) Li, Z.; Zhao, J.; Du, Y.; Hae, R. P.; Sun, S. Y.; Bernal-Mizrachi, L.; Aitken, A.; Khuri, F. R.; Fu, H. *Proc. Natl. Acad. Sci. U. S. A.* **2008**, *105* (1), 162–167.

(500) Terman, J. R.; Kashina, A. *Curr. Opin. Cell Biol.* **2013**, *25* (1), 30–38.

(501) Eke, I.; Cordes, N. *Semin. Cancer Biol.* **2015**, *31*, 65–75.

(502) Fife, C. M.; McCarroll, J. A.; Kavallaris, M. *Br. J. Pharmacol.* **2014**, *171* (24), 5507–5523.

(503) Olson, M. F.; Sahai, E. *Clin. \& Exp. metastasis* **2009**, *26* (4), 273.

(504) White, C. D.; Brown, M. D.; Sacks, D. B. *FEBS Lett.* **2009**, *583* (12), 1817–1824.

(505) Briggs, M. W.; Sacks, D. B. *EMBO Rep.* **2003**, *4* (6), 571–574.

(506) Krishnamurthy, N.; Kurzrock, R. *Cancer Treat. Rev.* **2018**, *62*, 50–60.

(507) Casteel, D. E.; Turner, S.; Schwappacher, R.; Rangaswami, H.; Su-Yuo, J.; Zhuang, S.; Boss, G. R.; Pilz, R. B. *J. Biol. Chem.* **2012**, *287* (45), 38367–38378.

(508) Zhu, Z. C.; Liu, J. W.; Li, K.; Zheng, J.; Xiong, Z. Q. *Oncogene* **2018**, *37* (22), 2936–2952.

(509) Miluzio, A.; Ricciardi, S.; Manfrini, N.; Alfieri, R.; Oliveto, S.; Brina, D.; Biffo, S. *Biochem. Soc. Trans.* **2016**, *44* (6), 1667–1673.

(510) Miluzio, A.; Oliveto, S.; Pesce, E.; Mutti, L.; Murer, B.; Grosso, S.; Ricciardi, S.; Brina, D.; Biffo, S. *Oncotarget* **2015**, *6* (35), 37471–37485.

(511) Brina, D.; Miluzio, A.; Ricciardi, S.; Biffo, S. *Biochim. Biophys. Acta - Gene Regul. Mech.* **2015**, *1849* (7), 830–835.

(512) Silvera, D.; Formenti, S. C.; Schneider, R. J. *Nat. Rev. Cancer* **2010**, *10* (4), 254–266.

(513) Robichaud, N.; Sonenberg, N.; Ruggero, D.; Schneider, R. J. *Cold Spring Harb. Perspect. Biol.* **2019**, *11* (7), a032896.

(514) Simsek, D.; Barna, M. *Curr. Opin. Cell Biol.* **2017**, *45*, 92–101.

(515) Fels, D. R.; Koumenis, C. *Cancer Biol. Ther.* **2006**, *5* (7), 723–728.

(516) Marciniak, S. J.; Yun, C. Y.; Oyadomari, S.; Novoa, I.; Zhang, Y.; Jungreis, R.; Nagata,

K.; Harding, H. P.; Ron, D. *Genes Dev.* **2004**, *18* (24), 3066–3077.

(517) Ling, J.; Söll, D. *Proc. Natl. Acad. Sci. U. S. A.* **2010**, *107* (9), 4028–4033.

(518) Soares Moretti, A. I.; Martins Laurindo, F. R. *Arch. Biochem. Biophys.* **2017**, *617*, 106–119.

(519) Xu, S.; Sankar, S.; Neamati, N. *Drug Discov. Today* **2014**, *19* (3), 222–240.

(520) Popielarski, M.; Ponamarczuk, H.; Stasiak, M.; Watała, C.; Świątkowska, M. *Am. J. Cancer Res.* **2019**, *9* (8), 1554–1582.

(521) Gestaut, D.; Limatola, A.; Joachimiak, L.; Frydman, J. *Curr. Opin. Struct. Biol.* **2019**, *55*, 50–58.

(522) Rüßmann, F.; Stemp, M. J.; Moñkemeyer, L.; Etchells, S. A.; Bracher, A.; Hartl, F. U. *Proc. Natl. Acad. Sci. U. S. A.* **2012**, *109* (52), 21208–21215.

(523) Araki, K.; Suenaga, A.; Kusano, H.; Tanaka, R.; Hatta, T.; Natsume, T.; Fukui, K. *Biochem. Biophys. Res. Commun.* **2016**, *481* (3–4), 232–238.

(524) Guest, S. T.; Kratche, Z. R.; Bollig-Fischer, A.; Haddad, R.; Ethier, S. P. *Exp. Cell Res.* **2015**, *332* (2), 223–235.

(525) Xu, W. X.; Song, W.; Jiang, M. P.; Yang, S. J.; Zhang, J.; Wang, D. D.; Tang, J. H. *Front. Genet.* **2021**, *12*, 342.

(526) Santoro, M. G. *Biochem. Pharmacol.* **2000**, *59* (1), 55–63.

(527) Saibil, H. *Nat. Rev. Mol. Cell Biol.* **2013**, *14* (10), 630–642.

(528) Delaunay-Moisan, A.; Appenzeller-Herzog, C. *Free Radic. Biol. Med.* **2015**, *83*, 341–351.

(529) Oakes, S. A. *Am. J. Pathol.* **2020**, *190* (5), 934–946.

(530) Yadav, R. K.; Chae, S.-W.; Kim, H.-R.; Chae, H. J. *J. Cancer Prev.* **2014**, *19* (2), 75–88.

(531) Hazari, Y. M.; Bashir, A.; Haq, E. ul; Fazili, K. M. *Tumor Biol.* **2016**, *37* (11), 14381–14390.

(532) Eletto, D.; Chevet, E.; Argon, Y.; Appenzeller-Herzog, C. *J. Cell Sci.* **2014**, *127* (17), 3649–3658.

(533) Hwang, J.; Qi, L. *Trends Biochem. Sci.* **2018**, *43* (8), 593–605.

(534) Livnat-Levanon, N.; Kevei, É.; Kleifeld, O.; Krutauz, D.; Segref, A.; Rinaldi, T.; Erpapazoglou, Z.; Cohen, M.; Reis, N.; Hoppe, T.; Glickman, M. H. *Cell Rep.* **2014**, *7* (5), 1371–1380.

(535) Park, J. E.; Miller, Z.; Jun, Y.; Lee, W.; Kim, K. B. *Transl. Res.* **2018**, *198*, 1–16.

(536) Tax, G.; Lia, A.; Santino, A.; Roversi, P. *J. Oncol.* **2019**, *2019*, 1–14.

(537) Lieu, E. L.; Nguyen, T.; Rhyne, S.; Kim, J. *Exp. Mol. Med.* **2020**, *52* (1), 15–30.

(538) Röhrig, F.; Schulze, A. *Nat. Rev. Cancer* **2016**, *16* (11), 732–749.

(539) Tong, X.; Zhao, F.; Thompson, C. B. *Curr. Opin. Genet. Dev.* **2009**, *19* (1), 32–37.

(540) Wu, W.; Zhao, S. *Acta Biochim. Biophys. Sin. (Shanghai).* **2013**, *45* (1), 18–26.

(541) Arora, R.; Schmitt, D.; Karanam, B.; Tan, M.; Yates, C.; Dean-Colomb, W. *Oncotarget* **2015**, *6* (2), 662–678.

(542) Seki, T.; Hosono, T.; Hosono-Fukao, T.; Inada, K.; Tanaka, R.; Ogihara, J.; Ariga, T. *Asia Pac. J. Clin. Nutr.* **2008**, *17* (SUPPL. 1), 249–252.

(543) Heng, Y.-W.; Koh, C.-G. *Int. J. Biochem. Cell Biol.* **2010**, *42* (10), 1622–1633.

(544) Kedrin, D.; van Rheenen, J.; Hernandez, L.; Condeelis, J.; Segall, J. E. *J. Mammary Gland Biol. Neoplasia* **2007**, *12* (2–3), 143–152.

(545) Kovac, B.; Mäkela, T. P.; Vallenius, T. *PLoS One* **2018**, *13* (5), e0196986.

(546) Desai, S.; Barai, A.; Bukhari, A. B.; De, A.; Sen, S. *Biochim. Biophys. Acta - Mol. Cell Res.* **2018**, *1865* (1), 196–208.

(547) Yang, P.; Yang, Y.; Sun, P.; Tian, Y.; Gao, F.; Wang, C.; Zong, T.; Li, M.; Zhang, Y.; Yu, T.; Jiang, Z. *Int. J. Biol. Sci.* **2020**, *17* (1), 32–49.

(548) Fernald, K.; Kurokawa, M. *Trends Cell Biol.* **2013**, *23* (12), 620–633.

(549) Mullarky, E.; Cantley, L. C. In *Innovative Medicine*; Springer Japan: Tokyo, 2015; pp 3–23.

(550) Gan, Y.; Ye, F.; He, X.-X. *J. Cancer* **2020**, *11* (8), 2252–2264.

(551) Xing, H.; Zhang, S.; Weinheimer, C.; Kovacs, A.; Muslin, A. J. *EMBO J.* **2000**, *19* (3), 349–358.

(552) Okamura, T.; Antoun, G.; Keir, S. T.; Friedman, H.; Bigner, D. D.; Ali-Osman, F. *J. Biol. Chem.* **2015**, *290* (52), 30866–30878.

(553) Wang, K.; Jiang, J.; Lei, Y.; Zhou, S.; Wei, Y.; Huang, C. *Trends Biochem. Sci.* **2019**, *44* (5), 401–414.

(554) Jones, L. H.; Neubert, H. *Sci. Transl. Med.* **2017**, *9* (386), eaaf7951.

(555) Manzoni, C.; Kia, D. A.; Vandrovcova, J.; Hardy, J.; Wood, N. W.; Lewis, P. A.; Ferrari, R. *Brief. Bioinform.* **2018**, *19* (2), 286–302.

(556) Vasaikar, S. V.; Straub, P.; Wang, J.; Zhang, B. *Nucleic Acids Res.* **2018**, *46* (D1), D956–D963.

(557) Chakraborty, S.; Hosen, M. I.; Ahmed, M.; Shekhar, H. U. *Biomed Res. Int.* **2018**, *2018*.

(558) Gottlieb, H. E.; Kotlyar, V.; Nudelman, A. *J. Org. Chem.* **1997**, *62* (21), 7512–7515.

(559) Cheng, C.-S.; Ferber, C.; Bashford, R. I.; Grillot, G. F. *J. Am. Chem. Soc.* **1951**, *73* (9), 4081–4084.

(560) Mabunda, M. Synthesis and Biological Activity of Ajoenes, University of Cape Town, 2013.

(561) Biwi, J. A Structure-Activity Relationship Study of Dihydroajoenes as Anti-Cancer Agents, University of Cape Town, 2014.

(562) Yang, Y. Y.; Ascano, J. M.; Hang, H. C. *J Am Chem Soc* **2010**, *132* (11), 3640–3641.

(563) Braun, M.; Hartnagel, U.; Ravanelli, E.; Schade, B.; Böttcher, C.; Vostrowsky, O.; Hirsch, A. *European J. Org. Chem.* **2004**, *2004* (9), 1983–2001.

(564) Wenska, M.; Alvira, M.; Steunenberg, P.; Stenberg, Å.; Murtola, M.; Strömberg, R. *Nucleic Acids Res.* **2011**, *39* (20), 9047–9059.

(565) Wang, T.; Wu, Y.; Kuan, S. L.; Dumele, O.; Lamla, M.; Ng, D. Y. W.; Arzt, M.; Thomas, J.; Mueller , J. O.; Barner-Kowollik , C.; Weil, T. *Chem. - A Eur. J.* **2015**, *21* (1), 228–238.

(566) Veale, A. L.; others. *S. Afr. J. Sci.* **1984**, *80* (6), 260.

(567) Euhus, D. M.; Hudd, C.; Laregina, M. C.; Johnson, F. E. *J. Surg. Oncol.* **1986**, *31* (4), 229–234.

(568) Kanehisa, M.; Sato, Y. *Protein Sci.* **2020**, *29* (1), 28–35.

(569) Huang, D. W.; Sherman, B. T.; Lempicki, R. A. *Nat. Protoc.* **2009**, *4* (1), 44–57.

(570) Huang, D. W.; Sherman, B. T.; Lempicki, R. A. *Nucleic Acids Res.* **2009**, *37* (1), 1–13.

(571) Oliveros, J. C. Venny. An interactive tool for comparing lists with Venn's diagrams. https://bioinfogp.cnb.csic.es/tools/venny/index.html.

The End?